DOC.20080129.0008

QA: QA

MDL-NBS-HS-000020 REV 02

August 2005

BECHTEL SAIC COMPANY LLC

Particle Tracking Model and Abstraction of Transport Processes

THIS DOCUMENT CONTAINS THE FOLLOWING, LOCATED AT THE BACK OF THE DOCUMENT:
1) ADDENDUM 001, DATED 08/17/2007
2) ADDENDUM 002, DATED 01/24/2008

NOTICE OF OPEN CHANGE DOCUMENTS - THIS DOCUMENT IS IMPACTED BY THE LISTED CHANGE DOCUMENTS AND CANNOT BE USED WITHOUT THEM.

---

1) ACN-001, DATED 09/17/2007

Prepared for:
U.S. Department of Energy
Office of Civilian Radioactive Waste Management
Office of Repository Development
1551 Hillshire Drive
Las Vegas, Nevada 89134-6321

Prepared by:
Bechtel SAIC Company, LLC
1180 Town Center Drive
Las Vegas, Nevada 89144

Under Contract Number
DE-AC28-01RW12101

DISCLAIMER

This report was prepared as an account of work sponsored by an agency of the United States Government. Neither the United States Government nor any agency thereof, nor any of their employees, nor any of their contractors, subcontractors or their employees, makes any warranty, express or implied, or assumes any legal liability or responsibility for the accuracy, completeness, or any third party's use or the results of such use of any information, apparatus, product, or process disclosed, or represents that its use would not infringe privately owned rights. Reference herein to any specific commercial product, process, or service by trade name, trademark, manufacturer, or otherwise, does not necessarily constitute or imply its endorsement, recommendation, or favoring by the United States Government or any agency thereof or its contractors or subcontractors. The views and opinions of authors expressed herein do not necessarily state or reflect those of the United States Government or any agency thereof.

QA: QA

Particle Tracking Model and Abstraction of Transport Processes

MDL-NBS-HS-000020 REV 02

August 2005

BSC

Model Signature Page/Change History

Complete only applicable items.

2. Type of Mathematical Model

☐ Process Model ☒ Abstraction Model ☐ System Model

Describe Intended Use of Model

The purpose of this report is to document the abstraction model being used in Total System Performance Assessment model calculations for radionuclide transport in the unsaturated zone.

3. Title

Particle Tracking Model and Abstraction of Transport Processes

4. DI (including Rev. No.):

MDL-NBS-HS-000020 REV 02

	Printed Name	Signature	Date
5. Originator	B. Robinson		8/2/2005
6. Independent Technical Reviewer	R. Andrews		8/2/05
7. Checker	L. Pan		8/2/05
8. QER	J. Gebhart		8/3/05
9. Responsible Manager/Lead	J. Houseworth		8/3/05
10. Responsible Manager for	M. Zhu		8/3/05

11. Remarks ROGER HENDING

L. Concors supported checking of the DIRS and P. Rogers supported checking SAR

Change History

12. Revision No.	13. Description of Change
Rev 00	Initial Issue
Rev 01	Entire model document revised to incorporate evaluation comments by the Regulatory Integration Team. Changes too extensive to use Step 5.8Q1) from AP-SIII.10Q, Rev 2, ICN 7.
Rev 02	Entire model document revised to incorporate new base-case model results and sensitivity analyses related to flow and transport model parameters, change bars not used. In response to CR 5185, Table 6-22 has changed citation from Table 6-6 of the source AMR to the AMR output DTN: SN0306T0504103.006.

INTENTIONALLY LEFT BLANK

CONTENTS

Page

1. PURPOSE 1-1

2. QUALITY ASSURANCE 2-1

3. USE OF SOFTWARE 3-1
   3.1 SOFTWARE TRACKED BY CONFIGURATION MANAGEMENT 3-1
   3.2 EXEMPT SOFTWARE 3-3

4. INPUTS 4-1
   4.1 DIRECT INPUT 4-1
      4.1.1 Data 4-1
      4.1.2 Parameters and Parameter Uncertainty 4-2
   4.2 CRITERIA 4-12
   4.3 CODES, STANDARDS, AND REGULATIONS 4-15

5. ASSUMPTIONS 5-1

6. MODEL DISCUSSION 6-1
   6.1 MODELING OBJECTIVES AND APPROACH 6-1
   6.2 FEATURES, EVENTS, AND PROCESSES INCLUDED IN THE MODEL 6-2
   6.3 THE UZ TRANSPORT ABSTRACTION MODEL 6-4
   6.4 THE NUMERICAL REPRESENTATION OF THE UZ TRANSPORT ABSTACTION MODEL 6-7
      6.4.1 Basic Methods 6-9
      6.4.2 Dispersion 6-12
      6.4.3 Fracture/Matrix Interaction Submodel 6-14
      6.4.4 Multiple Radionuclides with Decay/Ingrowth 6-18
      6.4.5 Colloid Transport 6-21
      6.4.6 Particle Sources and Sinks 6-24
      6.4.7 EBS Random Release Model for Radionuclide Source Terms 6-25
      6.4.8 Climate Change and Water Table Rise 6-29
      6.4.9 Interface with GoldSim 6-31
   6.5 UZ TRANSPORT ABSTRACTION MODEL INPUTS 6-32
      6.5.1 Pregenerated Flow Fields 6-35
      6.5.2 Dispersivity 6-36
      6.5.3 Matrix Porosity and Rock Density 6-37
      6.5.4 Matrix Sorption Coefficient (mL/g) 6-40
      6.5.5 Matrix Diffusion Coefficient (m^2/sec) 6-41
      6.5.6 Fracture Residual Saturation and Active Fracture Model Gamma Parameters (Unitless) 6-46
      6.5.7 Fracture Porosity, Fracture Spacing (m), and Fracture Aperture (m) 6-50
      6.5.8 Fracture Surface Retardation Factor (Unitless) 6-56
      6.5.9 Colloid Filtration at Matrix Interface 6-57

CONTENTS (Continued)

Page

6.5.10 Colloid Size Exclusion 6-58
6.5.11 Colloid Size Distribution 6-59
6.5.12 Colloid Concentration and Colloid K_c 6-60
6.5.13 Fractions of Colloids Traveling Unretarded and Colloid Retardation Factor 6-64
6.5.14 Radionuclide Half Lives (Years) and Daughter Products 6-65
6.5.15 Repository Radionuclide Release Bins 6-66
6.5.16 Radionuclide Collecting Bins at UZ/SZ Interface 6-67
6.6 BASE-CASE MODEL 6-71
6.6.1 Overview 6-71
6.6.2 Base-Case Model Results 6-75
6.6.3 Sensitivity to Flow Parameter Uncertainty 6-84
6.6.4 Sensitivity to AFM and Diffusion Parameter Uncertainty 6-94
6.7 EVALUATION OF ALTERNATIVE MODELS AND MODEL UNCERTAINTY 6-100
6.8 DESCRIPTION OF BARRIER CAPABILITY 6-106
6.8.1 Analyses of Barrier Capability 6-107
6.8.2 Summary of Barrier Capability 6-110
6.9 OTHER TSPA IMPLEMENTATION CONSIDERATIONS 6-113
6.9.1 FEHM Code Issues 6-113
6.9.2 Model Input Issues 6-114

7. VALIDATION 7-1
7.1 CONFIDENCE BUILDING DURING MODEL DEVELOPMENT TO ESTABLISH THE SCIENTIFIC BASIS AND ACCURACY FOR INTENDED USE 7-1
7.2 POSTDEVELOPMENT MODEL VALIDATION TO SUPPORT THE SCIENTIFIC BASIS OF THE MODEL 7-2
7.2.1 COMPARISONS WITH DISCRETE FRACTURE MODEL 7-4
7.2.1.1 Test of Advective Transport Between Continua 7-5
7.2.1.2 Comparisons with Diffusion for Fracture-Dominated Flow 7-5
7.2.1.3 Comparisons with Diffusion and Sorption for Intermediate Flow Case 7-7
7.2.1.4 Summary of Validation Tests for a Discrete Fracture Model 7-13
7.2.2 Comparison with the Dual-k and MINC Model Formulations on a Two-Dimensional Cross-Section Model 7-13
7.2.3 Comparison with T2R3D Process Model for the Three-Dimensional System 7-16
7.2.3.1 Comparisons of FEHM and T2R3D for the Dual-k Conceptual Model 7-17
7.2.3.2 Influence of Diffusion Coefficient and f/m Interaction ACM 7-17
7.2.3.3 Tests of the Active Fracture Model Implementation 7-19

CONTENTS (Continued)

Page

7.3 SUMMARY OF VALIDATION ACTIVITIES 7-22

8. CONCLUSIONS 8-1
8.1 SUMMARY OF MODELING ACTIVITY 8-1
8.2 MODEL OUTPUTS 8-2
8.2.1 Developed Output 8-2
8.2.2 Output Uncertainty 8-5
8.3 HOW THE APPLICABLE ACCEPTANCE CRITERIA ARE ADDRESSED 8-6

9. INPUTS AND REFERENCES 9-1
9.1 DOCUMENTS CITED 9-1
9.2 CODES, STANDARDS, REGULATIONS, AND PROCEDURES 9-8
9.3 SOURCE DATA, LISTED BY DATA TRACKING NUMBER 9-9
9.4 OUTPUT DATA, LISTED BY DATA TRACKING NUMBER 9-11
9.5 SOFTWARE CODES 9-11

APPENDIX A – DERIVATION OF THE DISTRIBUTION OF WATER CONTENT AND EFFECTIVE PERMEABILITY FOR SAMPLING MATRIX DIFFUSION COEFFICIENT A-1
APPENDIX B – DERIVATION OF WATER TABLE COLLECTING BINS B-1
APPENDIX C – DERIVATION OF FRACTURE-MATRIX INTERACTION SUBMODEL AND GENERATION OF TRANSFER FUNCTIONS C-1

INTENTIONALLY LEFT BLANK

FIGURES

Page

6-1. Overview Schematic of the GoldSim-FEHM Coupling 6-2
6-2. Schematic of Water Movement and Radionuclide Transport Through the UZ 6-6
6-3. Schematic of the Cell-Based Particle-Tracking Technique 6-10
6-4. Schematic of the RTTF Technique for Determining Particle Residence Time in a Cell 6-10
6-5. Schematic of the Fracture Transport Submodel 6-18
6-6. Comparison of Software CHAIN and FEHM Transport Results for a Case with a 4-Member Decay-Ingrowth CHAIN and a Retardation Factor of 1.9 for Species 3 6-21
6-7. Flow Chart of FEHM EBS Random Release Model 6-28
6-8. Detailed Schematic Flow Chart of GoldSim-FEHM Coupling 6-32
6-9. Cumulative Probability for Matrix Diffusion Under Saturated Conditions 6-44
6-10. Comparison of Cation/Anion Distributions with Reimus High/Low Distributions for Unsaturated Conditions 6-44
6-11. Comparison of the Distributions with Diffusion Data 6-45
6-12. Relationship Between Fracture Frequency and Standard Deviation 6-54
6-13. Relationship Between Fracture Porosity and Frequency 6-56
6-14. SMT Repository Release Nodes 6-68
6-15. FEHM Repository Release Nodes Transformed Based on SMT Release Nodes (Shown in Figure 6-14) 6-69
6-16. Source Regions for Radionuclide Release in the SZ Transport Abstraction Model 6-70
6-17. Base-Case Model Normalized Mass Flux at the Water Table for 36 Radionuclide Species, Present-Day Mean Infiltration Scenario, Representative Parameter Values, and Present-Day Water Table 6-76
6-18. Base-Case Model Normalized Mass Flux at the Water Table for 36 Radionuclide Species, Glacial-Transition Mean Infiltration Scenario, Representative Parameter Values, and Elevated Water Table 6-77
6-19. Base-Case Model Normalized Mass Flux at the Water Table for Irreversible Fast and Irreversible Slow Colloids, Glacial-Transition Mean Infiltration Scenario, Representative Parameter Values, and Elevated Water Table 6-79
6-20. Base-Case Model Normalized Mass Flux at the Water Table for Conservative Radionuclides and ^{90}Sr, Glacial-Transition Mean Infiltration Scenario, Representative Parameter Values, and Elevated Water Table 6-80
6-21. Base-Case Model Normalized Mass Flux at the Water Table for Moderately Sorbing Radionuclides, Glacial-Transition Mean Infiltration Scenario, Representative Parameter Values, and Elevated Water Table 6-81
6-22. Base-Case Model Normalized Mass Flux at the Water Table for Aqueous Species of Americium and Plutonium, Glacial-Transition Mean Infiltration Scenario, Representative Parameter Values, and Elevated Water Table 6-82
6-23. Base-Case Model Normalized Mass Flux at the Water Table for Aqueous Species of Cesium and Americium, Glacial-Transition Mean Infiltration Scenario, Representative Parameter Values, and Elevated Water Table 6-83

FIGURES (Continued)

Page

6-24. Base-Case Model Normalized Mass Flux at the Water Table for Various Moderately to Strongly Sorbing Radionuclides, Glacial-Transition Mean Infiltration Scenario, Representative Parameter Values, and Elevated Water Table 6-84
6-25. Base-Case Model Normalized Mass Flux at the Water Table for ^{99}Tc and ^{237}Np, Glacial-Transition Mean Infiltration Scenario, for Different Values (Plus and Minus One Standard Deviation (σ) from the Base Case) of the van Genuchten α Parameter for the Fracture Continuum, and Elevated Water Table 6-87
6-26. Base-Case Model Normalized Mass Flux at the Water Table for Different Species of ^{242}Pu, Glacial-Transition Mean Infiltration Scenario, for Different Values (Plus and Minus One Standard Deviation (σ) from the Base Case) of the van Genuchten α Parameter for the Fracture Continuum, and Elevated Water Table 6-88
6-27. Base-Case Model Normalized Mass Flux at the Water Table for ^{99}Tc and ^{237}Np, Glacial-Transition Mean Infiltration Scenario, for Different Values (Plus and Minus One Standard Deviation (σ) from the Base Case) of the van Genuchten α Parameter for the Matrix Continuum, and Elevated Water Table 6-89
6-28. Base-Case Model Normalized Mass Flux at the Water Table for different species of ^{242}Pu, Glacial-Transition Mean Infiltration Scenario, for Different Values (Plus and Minus One Standard Deviation (σ) from the Base Case) of the van Genuchten α Parameter for the Matrix Continuum, and Elevated Water Table 6-90
6-29. Base-Case Model Normalized Mass Flux at the Water Table for ^{99}Tc and ^{237}Np, Glacial-Transition Mean Infiltration Scenario, for Different Values (Plus and Minus One Standard Deviation (σ) from the Base Case) of the Absolute Permeabilities of the Fracture Continuum, and Elevated Water Table 6-91
6-30. Base-Case Model Normalized Mass Flux at the Water Table for Different Species of ^{242}Pu, Glacial-Transition Mean Infiltration Scenario, for Different Values (Plus and Minus one Standard Deviation (σ) from the Base Case) of the Absolute Permeabilities of the Fracture Continuum, and Elevated Water Table 6-92
6-31. Base-Case Model Normalized Mass Flux at the Water Table for ^{99}Tc and ^{237}Np, Glacial-Transition Mean Infiltration Scenario, for Different Values (Plus and Minus One Standard Deviation (σ) from the Base Case) of the Permeabilities of the Matrix Continuum, and Elevated Water Table 6-93
6-32. Base-Case Model Normalized Mass Flux at the Water Table for Different Species of ^{242}Pu, Glacial-Transition Mean Infiltration Scenario, for Different Values (Plus and Minus one Standard Deviation (σ) from the Base Case) of the Permeabilities of the Matrix Continuum, and Elevated Water Table 6-94
6-33. Base-Case Model Normalized Mass Flux at the Water Table for ^{99}Tc, Glacial-Transition Mean Infiltration Scenario, for Different Values of the AFM γ Parameter, and Elevated Water Table 6-96
6-34. Base-Case Model Normalized Mass Flux at the Water Table for ^{237}Np, Glacial-Transition Mean Infiltration Scenario, for Different Values of the AFM γ Parameter, and Elevated Water Table 6-97

FIGURES (Continued)

Page

6-35. Base-Case Model Normalized Mass Flux at the Water Table for ^{242}Pu, Glacial-Transition Mean Infiltration Scenario, for Different Values of the AFM γ Parameter, and Elevated Water Table 6-98
6-36. Base-Case Model Normalized Mass Flux at the Water Table for ^{99}Tc, Glacial-Transition Mean Infiltration Scenario, with the AFM γ Parameter Changed in all Units Versus only in the TSw Units, and Elevated Water Table 6-99
6-37. Base-Case Model Normalized Mass Flux at the Water Table for ^{99}Tc, Glacial-Transition Mean Infiltration Scenario, for Different Values of the effective area available for diffusion, and Elevated Water Table 6-100
6-38. Base-Case Model Normalized Mass Flux at the Water Table for ^{99}Tc, Glacial-Transition Mean Infiltration Scenario, for Different Values of the AFM γ Parameter and Different Fracture-Matrix Diffusion Conceptual Model (Dual-k versus DFM), and Elevated Water Table 6-104
6-39. Base-Case Model Normalized Mass Flux at the Water Table for ^{237}Np, Glacial-Transition Mean Infiltration Scenario, for Different Values of the AFM γ Parameter and Different Fracture-Matrix Diffusion Conceptual Model (Dual-k versus DFM), and Elevated Water Table 6-105
6-40. Base-Case Model Normalized Mass Flux at the Water Table for ^{242}Pu, Glacial-Transition Mean Infiltration Scenario, for Different Values of the AFM γ Parameter and Different Fracture-Matrix Diffusion Conceptual Model (Dual-k versus DFM), and Elevated Water Table 6-106
6-41. Normalized Cumulative Breakthrough Curves of the 11 Radionuclides Under Present-Day Mean Infiltration Condition, Representative Parameter Values, and Present-Day Water Table 6-112
6-42. Normalized Cumulative Breakthrough Curves of the 11 Species of Radionuclides Under Glacial-Transition Mean Infiltration Condition, Representative Parameter Values, and Elevated Water Table 6-113
6-43. Base-Case Model Normalized Mass Flux at the Water Table for species irreversibly sorbed to colloids, Glacial-Transition Mean Infiltration Scenario, Representative Parameter Values, Elevated Water Table, Comparing the Impact of Including the Size-Exclusion Process in the Fault Zones (Base-Case Model, Solid Curves) versus Assuming No Size Exclusion in Faults (TSPA Model, Dotted Curves) 6-116
6-44. Base-Case Model Normalized Mass Flux at the Water Table for Species Irreversibly Sorbed to Colloids, Glacial-Transition Mean Infiltration Scenario, Representative Parameter Values, Elevated Water Table, Comparing the Impact of Including the Size-Exclusion Process in the Fault Zones (Base Case Model, Solid Curves) versus Assuming No Size Exclusion in Faults (TSPA Model, Dotted Curves) 6-117
7-1. Particle-Tracking Abstraction Model Behavior for Advective Transport Between the Fracture and Matrix Continua: No Diffusion or Sorption, Solute Injected into the Fracture, Compared to Theoretical Results 7-6

FIGURES (Continued)

Page

7-2. Comparison of Discrete Fracture Model and Particle-Tracking Abstraction Model: Non-Sorbing Solute Injected into the Fracture for Different Values of Diffusion Coefficient, f_f = 0.99 7-7
7-3. Comparison of Discrete Fracture Model and Particle-Tracking Abstraction Model: Non-Sorbing Solute Injected into the Fracture for Different Values of Diffusion Coefficient, f_f = 0.6 7-8
7-4. Comparison of Discrete Fracture Model and Particle-Tracking Abstraction Model: Sorbing Solute Injected into the Fracture for Different Values of Diffusion Coefficient 7-10
7-5. Comparison of Discrete Fracture Model and Particle-Tracking Abstraction Model: Solute Injected into the Fracture for Different Values of Sorption Coefficient, D_m = 1.e-11 7-10
7-6. Comparison of Discrete Fracture Model and Particle-Tracking Abstraction Model: Solute Injected into the Fracture for Different Values of Sorption Coefficient, D_m = 1.e-10 7-11
7-7. Comparison of Discrete Fracture Model and Particle-Tracking Abstraction Model: Non-sorbing Solute Injected into the Matrix for Different Values of Diffusion Coefficient 7-12
7-8. Comparison of Discrete Fracture Model and Particle-Tracking Abstraction Model: Sorbing Solute Injected into the Fracture for Different Numbers of Grid Cells in the Flow Path 7-13
7-9. Comparison of Particle-Tracking Model with T2R3D Models for a Two-Dimensional, Mountain-Scale Model: with (and without) Diffusion, for Dual-k and DFM Formulations for the f/m Interaction Model, Present-Day Mean Infiltration, Representative Parameter Values, and Present-Day Water Table 7-15
7-10. Comparison of Breakthrough Curves for ^{99}Tc for T2R3D and the UZ Transport Abstraction Model: Simulations for Different Present-Day Infiltration Rate Scenarios (Lower, Mean, and Upper), Representative Parameter Values, and Present-Day Water Table 7-18
7-11. Comparison of Breakthrough Curves for ^{99}Tc for T2R3D and the UZ Transport Abstraction Model: Present-Day Mean Infiltration Scenario, Diffusion in FEHM Ranging from No Diffusion to High Values, Representative Parameter Values, and Present-Day Water Table 7-19
7-12. Breakthrough Curves for ^{99}Tc Using the UZ Transport Abstraction Model to Investigate the Role f/m Interaction Conceptual Model: Simulations for Different Present-Day Infiltration Rate Scenarios (Lower, Mean, and Upper), Representative Parameter Values, and Present-Day Water Table 7-20
7-13. Breakthrough Curves for Conservative Solute Using the UZ Transport Abstraction Model to Investigate the Role of AFM Parameter Gamma: Dual-k ACM, Simulation for Different Values of Gamma in Rock Units Beneath the Repository, Present-Day Mean Infiltration, Representative Parameter Values, and Present-Day Water Table 7-21

FIGURES (Continued)

Page

7-14. Breakthrough Curves for Conservative Solute Using the UZ Transport Abstraction Model to Investigate the Role of AFM Parameter Gamma: Discrete Fracture ACM, Simulation for Different Values of Gamma in Rock Units Beneath the Repository, Present-Day Mean Infiltration, Representative Parameter Values, and Present-Day Water Table 7-22
B-1. Listing of Files Used to Develop the Water Table Binning B-3
C-1. Transfer Function Computed for the Discrete Fracture Model Formulation: Solute Injection in Fracture, Breakthrough in Fracture, Diffusion Coefficients Given in Table C-2 ..... C-7
C-2. Transfer Function Computed for the Dual-k Model Formulation: Solute Injection in Fracture, Breakthrough in Fracture, Diffusion Coefficients Given in Table C-2 ..... C-7

INTENTIONALLY LEFT BLANK

TABLES

Page

3-1. Qualified Software Used in This Report 3-2
3-2. Exempt Software 3-3

4-1. Input Data Associated with Model Setup and Flow Fields 4-2
4-2. Transport Input Parameters for the UZ Transport Abstraction Model 4-3
4-3. Project Requirements and YMRP Acceptance Criteria Applicable to this Report 4-12

6-1. Included FEPs for This Model Report and Their Disposition in the TSPA-LA 6-3
6-2. The Structure of the in[ ] Array Passed to FEHM from GoldSim 6-27
6-3. UZ Model Units Correlated to Hydrogeologic Units 6-34
6-4. Dispersivity Used in UZ Transport Abstraction Model 6-36
6-5. Matrix Porosities Used in the Transport Model 6-37
6-6. Matrix Rock Density Values 6-39
6-7. Sorption-Coefficient Distributions for Unsaturated Zone Units 6-41
6-8. Distribution of Water Content and Effective Permeability 6-46
6-9. Fracture Residual Saturation Values 6-46
6-10. Fracture Gamma Parameter for Lower-Bound Infiltration Scenario 6-48
6-11. Fracture Gamma Parameter for Mean Infiltration Scenario 6-49
6-12. Fracture Gamma Parameter for Upper-Bound Infiltration Scenario 6-50
6-13. Fracture Porosity and Frequency Data 6-52
6-14. Fracture Porosity and Frequency in Each Model Layer, and Grouping of Fracture Rock Layers Below the Repository 6-53
6-15. Fracture Porosity and Frequency Distribution Data for Layers Below the Repository 6-55
6-16. Fracture Surface Retardation Factor 6-56
6-17. Cumulative Probabilities for Colloid Transport at Matrix Interfaces 6-57
6-18. Colloid Size Exclusion Factor Used in FEHM 6-59
6-19. Colloid Size Distribution 6-60
6-20. Kc for Irreversible Colloid 6-60
6-21. Colloid Concentration Distribution 6-61
6-22. Radionuclide Sorption Coefficient (mL/g) onto Colloids 6-63
6-23. Fractions of Colloids Traveling Unretarded 6-64
6-24. Colloid Retardation Factors 6-65
6-25. Radionuclide Half-Lives and Daughter Products Used in the TSPA-LA 6-66
6-26. Definition of Repository Release Bins 6-67
6-27. Radionuclides Simulated in Base-Case Run 6-72
6-28. Selected Parameter Values for Base-case UZ Model 6-73
6-29. Scenarios for UZ Base-Case and TSPA Model Flow Simulations 6-75
6-30. Summary of Alternative Conceptual Model Processes and Their Dispositions for the TSPA-LA 6-101
6-31. Radionuclide Transport Times in Years to the Water Table for Instantaneous Release 6-108

TABLES (Continued)

Page

6-32. Radionuclide Transport Times in Years to the Water Table for Continuous Release 6-109
6-33. Colloid Transport Times in Years to the Water Table for Continuous Release 6-110

7-1. Parameter Values for Discrete Fracture Model Test Suite 7-4

8-1. List of Uncertain Parameters to be Sampled in the TSPA-LA Runs 8-2
8-2. Computer Files Necessary to Run the Base-Case UZ Transport Abstraction Model 8-3

A-1. Crosswalk between Rock Groups and Model Units A-2
A-2. Porosity and Permeability of Model Units and Associated Rock Group A-2
C-1. List of Parameter Values Used to Compute Transfer Function Curves C-5
C-2. Diffusion Coefficients Used in Simulations C-6

ACRONYMS AND ABBREVIATIONS

ACM	alternative conceptual model
AFM	active fracture model
CML	carboxylate modified polystyrene latex
DCPT	Dual Continuum Particle Tracking Computer Code
DFM	discrete fracture model
dll	dynamic link library
dual-k	dual permeability
EBS	engineered barrier system
FEHM	finite element heat and mass model
FEP	feature, event, and process
f/m	fracture/matrix
LA	license application
MINC	matrix-fracture system - multiple interactive continua
PTn	Paintbrush nonwelded vitric tuff
RTTF	residence time transfer function
SMT	Smeared-source, mountain-scale thermal model (part of Multiscale model)
SZ	saturated zone
TDMS	technical data management system
TSPA	total system performance assessment
TSPA-LA	total system performance assessment for the license application
TSw	Topopah Spring welded unit
TWP	technical work plan
UTM	Universal Transverse Mercator (map type)
UZ	unsaturated zone
YMRP	*Yucca Mountain Review Plan, Final Report*

INTENTIONALLY LEFT BLANK

1. PURPOSE

The purpose of this report is to document the abstraction model being used in total system performance assessment (TSPA) model calculations for radionuclide transport in the unsaturated zone (UZ). The UZ transport abstraction model uses the particle-tracking method that is incorporated into the finite element heat and mass model (FEHM) computer code (Zyvoloski et al. 1997 [DIRS 100615]) to simulate radionuclide transport in the UZ. This report outlines the assumptions, design, and testing of a model for calculating radionuclide transport in the UZ at Yucca Mountain. In addition, methods for determining and inputting transport parameters are outlined for use in the TSPA for license application (LA) analyses.

This report relies on many different sources as listed in Section 4. The direct inputs for the UZ transport model setup and flow fields are taken primarily from those developed in *UZ Flow Models and Submodels* (BSC 2004 [DIRS 169861]). An additional set of flow fields with adjusted hydrologic parameters were created for the study analysis in this report and were provided by *Parameter Sensitivity Analysis for Unsaturated Zone Flow* (BSC 2005 [DIRS 174116]). Transport input parameters for rock properties include inputs from the reports: *Analysis of Hydrologic Properties Data* (BSC 2004 [DIRS 170038]); *Calibrated Properties Model* (BSC 2004 [DIRS 169857]); *Saturated Zone Flow and Transport Model Abstraction* (BSC 2005 [DIRS 174012]), and active fracture parameters from *UZ Flow Models and Submodels* (BSC 2004 [DIRS 169861]). Radionuclide transport properties and colloid parameters are from *Waste Form and In-drift Colloids-Associated Radionuclide Concentrations: Abstract and Summary* and *Saturated Zone Colloid Transport* (BSC 2005 [DIRS 174290]); Repository location data are from *Multiscale Thermohydrologic Model* (BSC 2005 [DIRS 173944]); Process-level transport model calculations are documented in another report for the UZ, *Radionuclide Transport Models Under Ambient Conditions* (BSC 2004 [DIRS 164500]).

The TSPA-LA report, *Total System Performance Assessment Model/Analysis for the License Application* is considered the sole user of output from this report.

The technical scope, content, and management of this report are described in the planning document *Technical Work Plan for Unsaturated Zone Transport Model Report Integration* (BSC 2004 [DIRS 171282]). Additional scope for update of the base case transport calculations that addresses sensitivity to key flow and transport parameters is described in the revised *Technical Work Plan for Unsaturated Zone Flow, Drift Seepage, and Unsaturated ZoneTransport Modeling* (BSC 2005 [DIRS 173951], Section 2.1). There are no deviations from the technical work plan. This report:

- Conducts UZ transport abstraction model sensitivity analyses for variations in hydrologic properties for a given infiltration rate using flow fields prepared by *Parameter Sensitivity Analysis for Unsaturated Zone Flow* (BSC 2005 [DIRS 174116]). See Section 6.6.3 on sensitivity to flow parameter uncertainty.

- Conducts UZ transport abstraction model sensitivity analyses for the calibrated gamma value of the Active Fracture Model by sampling the gamma within a range supported by the field transport tests. See Section 6.6.4 on sensitivity to active fracture model (AFM) parameter uncertainty.

- Conducts analyses to assess the conservatism in the treatment of matrix diffusion involving uncertainty in the effective surface area. See Section 6.6.4 on diffusion parameter uncertainty.

- The modeling software, FEHM, is modified and qualified as V2.23 (LANL 2005 [DIRS 174121]) for the particle tracking simulations and analyses used in this report. Modifications and the versions of FEHM (versions 2.20 and higher) used for data development and model simulations are described in Section 3.1.

- The output DTN: LA0506BR831371.001 from this report is an update to DTN: LA0407BR831371.001 from Rev 01 and corrects FEHM model parameters so base case results are consistent with the TSPA model for comparisons with the new sensitivity analysis as presented in this document. The base case simulations are updated to correspond with the TSPA model by using an elevated water table rise for the glacial-transition infiltration scenario, colloid filtration at unit interfaces, and dual-k transfer function curves instead of DFM transfer function curves.

Three-dimensional, dual-permeability flow fields generated to characterize UZ flow (documented by BSC 2004 [DIRS 169861]; DTN: LB03023DSSCP9I.001 [DIRS 163044]) are converted to make them compatible with the FEHM code for use in this abstraction model. This report establishes the numerical method and demonstrates the use of the model that is intended to represent UZ transport in the TSPA-LA. Capability of the UZ barrier for retarding the transport is demonstrated in this report, and by the underlying process model (BSC 2004 [DIRS 164500]).

Note that Section 7.2.3.3 presents the technical justification that the abstraction model properly implements the AFM with matrix diffusion.

The particle-tracking technique presented in this report, called the residence time transfer function (RTTF) particle-tracking technique (Robinson et al. 2003 [DIRS 171674]), uses a cell-based approach that sends particles from node to node on a finite difference or finite element grid, after keeping each particle at the cell for a prescribed period of time. To incorporate transport mechanisms such as dispersion and matrix diffusion, the residence time of a particle at a cell is computed using a transfer function that ensures that the correct distribution of residence times at the cell is reproduced. This procedure is computationally very efficient, enabling large-scale transport simulations of several million particles to be completed rapidly on modern workstations. This requirement was needed for complex, three-dimensional simulation involving multiple radionuclides. Furthermore, since the cell-based approach directly uses mass flow rate information generated from a numerical fluid flow solution; complex, unstructured computational grids; and the dual-permeability flow model, formulation poses no additional complications. For the present application, the technique was adapted for use in unsaturated, dual-permeability transport simulations. For such systems, numerical techniques are required to allow accurate simulation of dual-permeability systems in which there is a vast disparity in the transport times depending upon whether the transport is in the fractures or the matrix. This report outlines the approach and defines the proper use of that approach. Furthermore, colloid-facilitated radionuclide transport can be simulated, and complex source terms and decay chain/ingrowth capabilities have been included in the model.

Like all numerical methods, the particle-tracking technique has limitations that must be considered when deciding whether its use is appropriate for a given application. The key physical and chemical assumptions are advection-dominated transport and linear, equilibrium sorption. Also, the accuracy of the method for dual-permeability flow systems was investigated in detail by performing comparisons to analytical solutions and alternate numerical methods, including the UZ transport process models documented by *Radionuclide Transport Models Under Ambient Conditions* (BSC 2004 [DIRS 164500]) and *UZ Flow Models and Submodels* (BSC 2004 [DIRS 169861]), and testing of the FEHM code presented in the software documentation (LANL 2003 [DIRS 166306]). Given these results, this report demonstrates that the particle-tracking model can be used in three-dimensional radionuclide transport simulations of the Yucca Mountain UZ as long as the limits on the model are recognized and parameters and inputs are chosen accordingly. Discussion of the limits and applicability are provided in this report. Inputs used in the calculations presented are representative of those to be used in TSPA model calculations, but it may be expected that exercising the model in TSPA multiple realizations may uncover simulation cases in which further examination and updating of the UZ transport abstraction model might be necessary.

INTENTIONALLY LEFT BLANK

2. QUALITY ASSURANCE

Development of this report and the supporting modeling activities have been determined to be subject to the Office of Civilian Radioactive Waste Management's quality assurance program as indicated by *Technical Work Plan for Unsaturated Zone Flow, Drift Seepage and Unsaturated Zone Transport Modeling* (BSC 2005 [DIRS 173951]). Approved quality assurance procedures identified in the TWP (BSC 2005 [DIRS 173951]) have been used to conduct and document the activities described in this report. The TWP also identifies the methods used to control the electronic management of data during the modeling and documentation activities.

This report discusses ambient radionuclide transport through hydrogeologic units below the repository, which constitute a natural barrier that is classified in the *Q-List* (BSC 2005 [DIRS 171190]) as "Safety Category" because it is important to waste isolation, as defined in AP-2.22Q, *Classification Analyses and Maintenance of the Q-List*. The results of this report are important to the demonstration of compliance with the postclosure performance objectives prescribed in 10 CFR 63.113 [DIRS 173273]. The report contributes to the analysis data used to support performance assessment; the conclusions do not directly impact engineered features important to preclosure safety, as defined in AP-2.22Q.

INTENTIONALLY LEFT BLANK

3. USE OF SOFTWARE

3.1 SOFTWARE TRACKED BY CONFIGURATION MANAGEMENT

The computer codes used directly in this modeling activity are summarized in Table 3-1. The computer software code on which the UZ transport abstraction model is based is FEHM V2.21 (LANL 2003 [DIRS 165741]). The qualification status of this and other software is indicated in the electronic Document Input Reference System database. All software was obtained from Software Configuration Management and is appropriate for the application. Qualified codes were used only within the range of validation as required by LP-SI.11Q-BSC, *Software Management*. Computer files for this report are located in data tracking numbers and identified in the respective discussions in Section 6; the outputs are listed in Section 8.2.

The FEHM V2.21 (LANL 2003 [DIRS 165741]) and FEHM V2.23 (LANL 2005 [DIRS 174121]) programs are the primary software used to represent physical processes for the UZ transport abstraction model. The FEHM V2.20 (LANL 2003 [DIRS 161725]) was used to develop repository zone location data for use in the GoldSim system model and was not used for any other purpose. The range of use for FEHM V2.21 and higher, as presented in this report, is for tracer transport in unsaturated, isothermal flow through fractured, porous rock. The routine ppptrk V1.0 (LANL 2003 [DIRS 165753]) was used to post-process transport results to obtain cumulative mass breakthrough curves at the water table. The routine discrete_tf V1.1 (LANL 2003 [DIRS 165742]) was used to convert discrete fracture model (DFM) results to transfer functions. The routine fehm2post V1.0 (LANL 2003 [DIRS 165754]) was used to execute multiple FEHM simulations along with pre- and post-processing runs. The range of use for ppptrk V1.0, discrete_tf V1.1, fehm2post V1.0 are for any range of output generated by FEHM V2.21 or FEHM V2.23. FEHM V2.21 and V2.23 are coupled with the software GoldSim V7.50.100 (BSC 2003 [DIRS 161572]) for total system performance simulations. There are no restrictions on the range of use of GoldSim V7.50.100 relative to the dynamically linked FEHM. No software was used prior to qualification.

The particle tracking method, as implemented in FEHM V2.21 and V2.23, was selected for use because this method allows for a numerically efficient calculation of radionuclide transport in the UZ, as required for multiple-realizations of this process in TSPA-LA. In addition, model validation exercises presented in this report show that the transport calculation methodology used in both versions of FEHM are compatible with other transport methods that have been successfully used to analyze transport processes in field tests at Yucca Mountain (Section 7). FEHM V2.23 adds to the previous release of FEHM V2.21 by allowing the user control of particle tracking problem size and better control of the random seed and a decay-ingrowth particle release factor. The software routines ppptrk V1.0, discrete_tf V1.1, and fehm2post V1.0 were selected because they have been specifically developed to be used with FEHM V2.21. GoldSim V7.50.100 was selected because FEHM V2.21 was dynamically linked to this software for total system performance dose calculations. A more recent version of GoldSim V8.02 (BSC 2004 [DIRS 169844]) has been implemented for TSPA-LA. However, both versions of GoldSim only act as an input/output interface for the dynamically linked FEHM module for UZ transport. No modifications to FEHM were required for linking with GoldSim V8.02. Therefore, use of the older version in this report has no impact on the results presented. There are no limitations on the use of this software within the range of use identified above.

Table 3-1. Qualified Software Used in This Report

Software Title/Version (v)	Software Tracking Number	Platform/Operating System	Code Usage	DIRS
FEHM V2.20	10086-2.20-00	PC/Windows 2000 and SUN/OS 5.7 and 5.8	Used in extracting repository coordinate locations for nodes for use in the GoldSim system model.	[DIRS 161725]
FEHM V2.21	10086-2.21-00	PC/Windows 2000, and SUN/OS 5.8	Generation of transfer function curve information using a discrete fracture model. Simulation of particle tracking validation runs. Abstraction model simulations.	[DIRS 165741]
FEHM V2.23	10086-2.23-01	SUN/OS 5.9	Simulation of particle tracking base case runs. Abstraction model simulations.	[DIRS 174121]
GoldSim V7.50.100	10344-7.50.100-00	PC/Windows 2000	Abstraction model simulations.	[DIRS 161572]
ppptrk V1.0	11030-1.0-00	SUN/OS 5.8 and 5.9	Post-processing of particle breakthrough curve information.	[DIRS 165753]
discrete_tf V1.1	11033-1.1-00	PC/Windows 2000	Post-processing of discrete fracture model results to convert results to transfer functions.	[DIRS 165742]
fehm2post V1.0	11031-1.0-00	PC/Windows 2000 and SUN/OS 5.8 and 5.9	Executes multiple FEHM simulations along with pre- and post-processing runs. Used to execute the individual simulations and generation of transfer function curves used in the TSPA-LA UZ transport abstraction model.	[DIRS 165754]

DIRS = Document Input Reference System; FEHM = finite element heat and mass (model); TSPA-LA = Total System Performance Assessment for the License Application; UZ = unsaturated zone.

3.2 EXEMPT SOFTWARE

Commercial, off-the-shelf software used in support of this report is listed in Table 3-2. This software is exempt from the requirements of LP-SI.11Q-BSC.

Table 3-2. Exempt Software

Software Name and Version (V)	Software Tracking Number	Description	Computer and Platform Identification
Fortner Plot	N/A	The commercial software, Fortner Plot, was used for plotting the results of breakthrough curve simulations. Only built-in standard functions in this software were used. No software routines or macros were used with this software to prepare this report. The output was visually checked for correctness.	SUN Workstation
Microsoft Excel 97	N/A	This standard spreadsheet package is used to perform simple spreadsheet calculations using built-in formulas and functions.	IBM PC, Window 2000 Operating System
Techplot 10	N/A	The commercial software, Techplot 10, was used for plotting the results of breakthrough curve simulations. Only built-in standard functions in this software were used. No software routines or macros were used with this software to prepare this report. The output was visually checked for correctness.	IBM PC, Window 2000 Operating System

INTENTIONALLY LEFT BLANK

4. INPUTS

4.1 DIRECT INPUT

Data and parameters used in this report as direct inputs to the UZ transport abstraction model include:

- Numerical grid for the UZ transport abstraction model
- UZ flow field for the prevailing climate
- UZ rock properties
  - Porosity
  - Fracture spacing and frequency
  - AFM parameter γ
  - Fracture residual saturation
  - Rock density
- UZ radionuclide transport parameters
  - Matrix diffusion coefficient
  - Radionuclide matrix sorption coefficient
  - Colloid size distribution
  - Colloid size exclusion factor at fracture-matrix interface
  - Colloid filtration factor at matrix interface
  - Colloid concentration
  - Radionuclide sorption coefficient onto colloid
  - Colloid retardation factor
- Repository release locations.

These data and parameters are discussed in greater detail in the next sections.

4.1.1 Data

In TSPA simulations, flow fields are pregenerated and saved for use in the UZ transport abstraction model to be used in TSPA analyses. At run time, FEHM reads in the pregenerated flow fields and associated water saturations and uses them in transport simulations. The site-scale UZ flow model grid and flow field for the prevailing climate are used in this report as input to FEHM to illustrate the set-up of UZ transport abstraction model. The effects of flow field uncertainty on TSPA are investigated through multiple realizations with different climate scenarios and corresponding flow fields.

Data on UZ flow in the repository were developed using the site-scale UZ flow model. The site-scale model incorporates the entire UZ in the vicinity of Yucca Mountain UZ; it accounts for the main stratigraphic units using layer-averaged rock properties, and represents the major faults. Relevant rock properties of each hydrogeologic unit (for fractures, matrix, and fault zones) have been calibrated against water saturation data, water-potential data, pneumatic-pressure data, perched-water data, and temperature data (BSC 2004 [DIRS 169857], Section 6.2; BSC 2004 [DIRS 169861], Sections 6.2 through 6.4). The flow results also include the effects of

preferential flow in the fracture network as implemented in the active fracture model (AFM) (BSC 2004 [DIRS 169861], Section 6.1.2). The calibrations are conducted for lower, mean, and upper infiltration scenarios for the present-day climate to include this key uncertainty in the parameterization. These data, converted for use in the particle tracking algorithm and include the fracture and matrix flux and the fracture and matrix water saturations, are available in DTN: LB0305TSPA18FF.001 [DIRS 165625] and in *UZ Flow Models and Submodels* (BSC 2004 [DIRS 169861]).

Repository location data are used to select repository nodes in the three-dimensional site scale model for releasing radionuclides into the UZ. There is no uncertainty related to this data.

The data in Table 4-1 are used as inputs to FEHM for constructing the UZ transport abstraction model. The remainder of this section describes in detail the data sources and rationale for their selection.

Table 4-1. Input Data Associated with Model Setup and Flow Fields

Data Name	Data Source	DTN
Site-scale UZ flow model grid and nine base-case flow fields; preqlA.ini, preqmA.ini, prequA.ini, monqla.ini, monqmA.ini, monqua.ini, glaqlA.ini, glaqmA.ini, glaquA.ini, fehmn.zone, fehmn.zone2, fehmn.grid, fehmn.stor, and glaqmA_wtrise.ini, glaq_lA.dat, glaq_mA.dat, glaq_uA.dat	BSC 2004 [DIRS 169861] *UZ Flow Models and Submodels* (MDL-NBS-HS-000006 REV 02)	LB0305TSPA18FF.001 [DIRS 165625] LB0312TSPA06FF.001 [DIRS 166671]
Eight UZ flow fields for site scale sensitivity study.	BSC 2005 [DIRS 174116] *Parameter Sensitivity Analysis for Unsaturated Zone Flow* (ANL-NBS-HS-000049 REV 00)	LB0506TSPA08FF.001 [DIRS 174117]
Repository release bin location	BSC 2005 [DIRS 173944] *Multiscale Thermohydrologic Model* (ANL-EBS-MD-000049 REV 03)	LL030610323122.029 [DIRS 164513]
Water saturation	BSC 2004 [DIRS 169861] *UZ Flow Models and Submodels* (MDL-NBS-HS-000006 REV 02)	LB03023DSSCP9I.001 [DIRS 163044]

DTN = data tracking number; UZ = unsaturated zone

4.1.2 Parameters and Parameter Uncertainty

The parameters listed in Table 4-2 are inputs to the UZ transport abstraction model. The values of those parameters affect the strength of the transport mechanism to which those parameters are related. The values of the parameters vary from layer to layer, as do the distributions. Rock properties (rock density, fracture porosity, fracture spacing, fracture aperture, AFM parameter, and fracture residual saturation) are used as inputs to the FEHM UZ transport abstraction model. The validity and uncertainty of those parameters are documented in the corresponding reports, *Analysis of Hydrologic Properties Data* (BSC 2004 [DIRS 170038]), *Calibrated Properties Model* (BSC 2004 [DIRS 169857]), and *UZ Flow Models and Submodels* (BSC 2004 [DIRS 169861]). In this report, the mean values of those parameters are used to demonstrate the abstraction of the UZ transport abstraction model. In addition, selected parameter sensitivity analyses are conducted in this report at the subsystem level. The influence of these and other

parameter uncertainties on system performance will be studied in TSPA multiple realization runs.

Radionuclide transport properties are used in FEHM for simulating the transport processes of radionuclides in the unsaturated fracture media from repository downward to the water table.

Colloid size distribution, concentration, sorption coefficient, size exclusion, filtration factors, and retardation factors are input parameters to FEHM for simulating colloid-facilitated radionuclide transport in fractured media. Those data are functions of colloid and rock properties and vary from layer to layer.

The uncertainty and validity of each parameter are addressed in the corresponding documents listed in the parameter source column in Table 4-2 and are also discussed below and in the various subsections of Section 6.5 of this report as indicated in the parameter name column of Table 4-2.

Table 4-2. Transport Input Parameters for the UZ Transport Abstraction Model

Parameter Name (Section Discussed)	Parameter Source	DTN	Parameter Value(s)	Units	Distribution (or Single Value if Fixed)
Matrix porosity Section 6.5.3	BSC 2003* [DIRS 161773] *Analysis of Hydrologic Properties Data* (MDL-NBS-HS-000014 REV 00)	LB0210THRMLPRP.001 [DIRS 160799]	Varies from layer to layer	None	Fixed
Rock density Section 6.5.3	BSC 2003* [DIRS 161773] *Analysis of Hydrologic Properties Data* (MDL-NBS-HS-000014 REV 00)	LB0210THRMLPRP.001 [DIRS 160799]	Varies from layer to layer	kg/m^3	Single value
Fracture porosity Section 6.5.7	BSC 2004 [DIRS 170038] *Analysis of Hydrologic Properties Data* (ANL-NBS-HS-000042 REV00)	LB0205REVUZPRP.001 [DIRS 159525] LB0207REVUZPRP.001 [DIRS 159526]	Varies from layer to layer	None	Beta distribution. Layers are grouped together based on similar rock properties
Fracture frequency Section 6.5.7	BSC 2004 [DIRS 170038] *Analysis of Hydrologic Properties Data* (ANL-NBS-HS-000042 REV 00)	LB0205REVUZPRP.001 [DIRS 159525] LB0207REVUZPRP.001 [DIRS 159526]	Varies from layer to layer	m^{-1}	Log-normal distribution
Active fracture model parameters Section 6.5.6	BSC 2004 [DIRS 169861] *UZ Flow Models and Submodels* (MDL-NBS-HS-000006 REV02)	LB0305TSPA18FF.001 [DIRS 165625]	Varies from layer to layer and with infiltration scenario	None	Fixed value for a specific infiltration

Table 4-2. Transport Input Parameters for the UZ Transport Abstraction Model (Continued)

Parameter Name (Section Discussed)	Parameter Source	DTN	Parameter Value(s)	Units	Distribution (or Single Value if Fixed)
Fracture residual saturation Section 6.5.6	BSC 2004 [DIRS 169857] *Calibrated Properties Model* (MDL-NBS-HS-000003 REV02)	LB0208UZDSCPMI.002 [DIRS 161243] LB0208UZDSCPLI.002 [DIRS 161788] LB0302UZDSCPUI.002 [DIRS 161787]	0.01	None	Fixed
Matrix permeability Section 6.5.6	BSC 2004 [DIRS 169857] *Calibrated Properties Model* (MDL-NBS-HS-000003 REV02)	LB0208UZDSCPMI.002 [DIRS 161243] LB0208UZDSCPLI.002 [DIRS 161788] LB0302UZDSCPUI.002 [DIRS 161787]	Varies from layer to layer and with infiltration scenario	m^2	Log-normal distribution Layers are grouped together based on similar rock properties
Matrix porosity (for matrix diffusion) Section 6.5.5	BSC 2004 [DIRS 170038] *Analysis of Hydrologic Properties Data* (ANL-NBS-HS-000042 REV00)	LB0207REVUZPRP.002 [DIRS 159672] LB03023DSSCP9I.001 [DIRS 163044]	Varies from layer to layer	None	Beta distribution Layers are grouped together based on similar rock properties
Colloid concentration distribution Section 6.5.12	BSC 2005 [DIRS 174290] *Waste Form and In-Drift Colloids-Associated Radionuclide Concentrations: Abstract and Summary* (MDL-EBS-PA-000004 REV 02)	SN0306T0504103.005 [DIRS 164132]	Concentration will be sampled based on the given distribution	mg/L	Cumulative distribution
Radionuclide sorption coefficient onto colloid Section 6.5.12	BSC 2005 [DIRS 174290] *Waste Form and In-drift Colloids-Associated Radionuclide Concentrations: Abstract and Summary* (MDL-EBS-PA-000004 REV 02)	SN0306T0504103.006 [DIRS 164131]	Values will be sampled based on the given distribution	mL/g	Uniform distribution parameter range depends on the type of radionuclides
Colloid size distribution Section 6.5.11	N/A	LL000122051021.116 [DIRS 142973]	Parameter values are sampled at run time	None	Cumulative distribution
Colloid filtration factors Section 6.5.9	N/A	LA0003MCG12213.002 [DIRS 147285]	Cumulative Probabilities of a particle being filtered at matrix interface. Varies from layer to layer	None	Fixed values but varies with layers

Table 4-2. Transport Input Parameters for the UZ Transport Abstraction Model (Continued)

Parameter Name (Section Discussed)	Parameter Source	DTN	Parameter Value(s)	Units	Distribution (or Single Value if Fixed)
Colloid size exclusion factors Section 6.5.10	N/A	LA0003MCG12213.002 [DIRS 147285]	Probability of a colloid being excluded at fracture-matrix interface. Varies from layer to layer	None	Fixed values but vary from layer to layer
Fractions of colloid traveling unretarded Section 6.5.13	BSC 2004 [DIRS 170006] *Saturated Zone Colloid Transport* (ANL-NBS-HS-000031 REV 02)	LA0303HV831352.003 [DIRS 165624]	Varies with transport time	None	Fractions of colloids traveling unretarded are given.
Colloid retardation factor Section 6.5.13	BSC 2004 [DIRS 170006] *Saturated Zone Colloid Transport* (ANL-NBS-HS-000031 REV 02)	LA0303HV831352.002 [DIRS 163558]	Sampled statistical values	None	Cumulative distribution
Matrix diffusion coefficient Section 6.5.5	BSC 2005 [DIRS 174012] *Saturated Zone Flow and Transport Model Abstraction* (MDL-NBS-HS-000021 REV 03)	SN0306T0502103.006 [DIRS 163944]	Sampled parameter values	m^2/s	Layers are grouped together based on similar rock properties and parameters are sampled for estimating matrix diffusion coefficient
Fracture dispersivity	N/A	LA0303PR831231.005 [DIRS 166259]	10.	m	Fixed
Matrix sorption coefficient Section 6.5.4	BSC 2004 [DIRS 164500] *Radionuclide Transport Models Under Ambient Conditions* (MDL-NBS-HS-000008 REV 02)	LA0408AM831341.001 [DIRS 171584]	Parameter values are sampled based on the given distribution	mL/g	Distributions defined in DTN by rock type and radionuclide
Radionuclide half-lives Section 6.5.14	Parrington et al. 1996 [DIRS 103896]	N/A: Accepted data	Varies for each radionuclide	Yr	Fixed value for each radionuclide

DTN = data tracking number.

This report is cited because it is the source of DTN: LB0210THRMLPRP.001 [DIRS 160799]. Justification for using an output DTN from a source to be superseded by BSC 2004 [DIRS 170038] *Analysis of Hydrologic Properties Data* (ANL-NBS-HS-000042 REV00) is given in the text of this Section (4.1.2) under the heading "Matrix Porosity".

Unsaturated Zone Flow Parameters

The UZ flow fields and property sets provide the information needed to calculate the flowing fracture spacing based on the AFM (Liu et al. 1998 [DIRS 105729], Equation 17). The ratio of the geometric fracture spacing to the flowing fracture spacing is equated to the normalized

fracture water saturation raised to an exponent that is the active fracture parameter (Liu et al. 1998 [DIRS 105729], Equation 17). The active fracture parameter is given in DTN: LB0305TSPA18FF.001 [DIRS 165625] and fracture residual saturation is a uniform value of 0.01 for all climate scenarios as given in DTNs: LB0208UZDSCPLI.002 [DIRS 161788], LB0208UZDSCPMI.002 [DIRS 161243], and LB0302UZDSCPUI.002 [DIRS 161787]. Because the flow model computes water flux using the normalized water saturation (BSC 2004 [DIRS 169861], Appendix E), the uniform value with no uncertainty is appropriate.

Fracture Frequency and Fracture Porosity

Data for the mean and standard deviation of fracture frequency and fracture porosity for the hydrologic units in and beneath the repository are given in Table 6-5 of the report, *Analysis of Hydrologic Properties Data* (BSC 2004 [DIRS 170038]; DTN: LB0205REVUZPRP.001 [DIRS 159525]). Fracture frequency is determined from qualified fracture property data developed from field data (BSC 2004 [DIRS 170038], Section 6.1.2). These include detailed line survey fracture data (collected from the Exploratory Studies Facility North and South Ramps, Main Drift, and Enhanced Characterization of the Repository Block Cross Drift, providing spatially varying frequency, length, and fracture dips and strikes) and fracture frequency data from boreholes. A combination of fracture porosity data derived from gas tracer tests in the Exploratory Studies Facility, fracture frequency data, fracture aperture estimates, and the geometry of fracture networks are used to develop representative fracture porosities for the UZ model layers (BSC 2004 [DIRS 170038], Section 6.1.3). Fracture aperture is calculated within this report based on these direct input parameters, fracture porosity and fracture frequency. See Section 6.5.7 for a complete discussion of the uncertainty treatment for fracture frequency and fracture porosity. Fracture frequency data in the repository host rock provides estimates for the standard deviation of fracture frequency in some, but not all, of the model units. Data from units having standard deviations are used to develop uncertainty data for those without such data.

Matrix Porosity

Matrix water content is needed to determine the advective transport velocity from the water flux provided by the flow model. Water content is the product of the porosity and the water saturation. Water saturation is an output of the flow model. Matrix porosity is also used by the flow model, although steady-state flow fields are insensitive to this parameter. The two site-specific data sets for matrix porosity are the thermal property set (DTN: LB0210THRMLPRP.001 [DIRS 160799]) and the hydrologic property set (DTN: LB0207REVUZPRP.002 [DIRS 159672]).

Flint (1998 [DIRS 100033], pp. 11 to 19) and Rousseau et al. (1999 [DIRS 102097], pp. 125 to 153) describe sample collection and laboratory measurement methodologies, as well as estimates of core uncertainty for the hydrologic properties set. Core samples are grouped and analyzed according to the hydrogeologic units characterized by Flint (1998 [DIRS 100033], pp. 19 to 46) and detailed in a scientific notebook (Wang 2003 [DIRS 161654], SN-LBNL-SCI-003-V2, pp. 57–83). See Table 6-3 for a correlation of hydrogeologic units to the UZ model layers.

The thermal properties set matrix porosities are based on DTNs: SN0206T0503102.005 [DIRS 160258] and SN0208T0503102.007 [DIRS 160257]. These data were derived from petrophysical measurements. The first of these two DTNs supplies properties for most of the lithostratigraphic layers except those in the proposed repository horizon. The second DTN deals with thermal properties of the lithostratigraphic layers in the repository horizon, namely the upper lithophysal, the middle nonlithophysal, the lower lithophysal, and the lower nonlithophysal stratigraphic units of Topopah Spring welded tuff. Borehole petrophysical measurements of bulk density and neutron porosity are used to make quantitative estimates of matrix porosity (BSC 2004 [DIRS 169854], Section 4).

The UZ flow and UZ transport process models selected the thermal property set for matrix porosity and for consistency, this property set is implemented here, with the exception of porosity values used for matrix diffusion (discussed below). For units below the repository, the matrix porosity differences between the two property sets are not large, ranging from 22 percent to –9 percent difference between the thermal property set and the hydrologic property set in the different hydrologic units, with an average difference of about 3 percent.

The thermal properties set DTN: LB0210THRMLPRP.001 [DIRS 160799] is output from Rev 00 of *Analysis of Hydrologic Properties Data* (BSC 2003 [DIRS 161773]), which has since been superceded. The associated DTN now requires justification to qualify for use as a direct input (Section 5.2.1 of LP-SIII.10Q-BSC). As recommended, a comparison of the original data set to the corrected data set in DTN: LB0402THRMLPRP.001 [DIRS 168481] is also made. There are three reasons why the original data set is being used for radionuclide transport:

1. For most applications, other UZ models supporting TSPA-LA use the properties given in DTN: LB0210THRMLPRP.001 [DIRS 160799]. Therefore, these properties are needed for consistency with other models implemented in TSPA-LA. Those applications that do not use DTN: LB0210THRMLPRP.001 [DIRS 160799] use DTN: LB0207REVUZPRP.002 [DIRS 159672] (not DTN: LB0402THRMLPRP.001 [DIRS 168481]) because this data set contains additional statistical information (standard deviations) for hydrologic properties.

2. The errors in DTN: LB0210THRMLPRP.001 [DIRS 160799] have negligible effect on transport times through the UZ. Profiles along three boreholes between the repository and the water table (BSC 2004 [DIRS 164500], Appendix C) were checked for total porosity (for nonsorbing radionuclides) and total "storage capacity" (porosity plus sorptive storage fraction) using properties from DTN: LB0210THRMLPRP.001 [DIRS 160799] and from DTN: LB0402THRMLPRP.001 [DIRS 168481]. The differences were less than 5% in all but one case and less than 11% in the exceptional case, using a matrix water saturation of 0.9 and a sorption coefficient (K_d) of 1 mL/g for the sorbing cases. These differences are insignificant compared with the order of magnitude uncertainties in transport times shown in *Radionuclide Transport Models Under Ambient Conditions* (BSC 2004 [DIRS 164500], Figures 6-8, 6-33, 6-34, 6-36, 6-38, and 6-39). In addition, sensitivity studies conducted with the mountain-scale THC model using the two thermal property data sets found that the differences in thermal properties and matrix porosity have negligible effects on temperatures, gas compositions, and water chemistry (BSC 2005 [DIRS 174101], Appendix VI).

3. The differences in all cases give smaller total porosities and sorptive storage fractions, leading to faster radionuclide transport through the UZ using DTN: LB0210THRMLPRP.001 [DIRS 160799] instead of DTN: LB0402THRMLPRP.001 [DIRS 168481].

Diffusion in Fractured Rock

Site-specific diffusion cell data were used to develop a correlation between the matrix diffusion coefficient, and the porosity and permeability of the rock matrix under saturated conditions, as discussed in (Reimus et al. 2002 [DIRS 163008]) and *Saturated Zone Flow and Transport Model Abstraction* (BSC 2005 [DIRS 174012], Section 6.5.2.6, Equation 6-19).

The diffusing species ^3HHO, Br^-, and I^- were used in the experiments to define the correlation. Samples of welded and nonwelded volcanic tuffs were taken from Pahute Mesa and the C-holes near Yucca Mountain. The ranges in porosity and permeability of these samples are approximately 0.05 to 0.3 and 10^{-18} m^2 to 10^{-14} m^2, respectively. The porosity and permeability of rock units in the repository horizon are in approximately the same range (porosity ranges from 0.11 to 0.15 (BSC 2004 [DIRS 170038], Table 6-6) and permeability from 10^{-19} m^2 to 10^{-17} m^2 (BSC 2004 [DIRS 169861], Table A-1). Reimus et al. (2002 [DIRS 163008], Section 4) found that differences in rock type account for the largest variability in the effective diffusion coefficients, rather than variability between diffusing species, size, and charge. The highest predictability in determining a value of the matrix diffusion coefficient occurs when both matrix porosity and log permeability are known, with log permeability as the most important predictive variable. The correlation, given in Section 6.5.5, accounts for effects of changes in water saturation on diffusion through an adjustment of a correlation derived for saturated conditions to one applicable to unsaturated conditions. The correlation involves matrix porosity and permeability.

Data for matrix porosity and permeability are used to evaluate matrix diffusion. Matrix porosity is taken from the hydrologic parameter set presented in *Analysis of Hydrologic Properties Data* (BSC 2004 [DIRS 170038], Table 6-6; DTN: LB0207REVUZPRP.002 [DIRS 159672]). The porosity data set selected for use in the TSPA is the thermal properties data set presented in intial version of *Analysis of Hydrologic Properties Data* (BSC 2003 [DIRS 161773], Table 9; DTN: LB0210THRMLPRP.001 [DIRS 160799]). Use of this data for matrix porosity is justified in the previous discussion under *Matrix Porosity*. However, the differences in values within and below the repository are, on average, about 3% lower for the hydrologic parameter set. The reason for using the hydrologic property set is because this data set provides an estimate of the variance of the porosity, which is used to statistically sample matrix porosity. See Section 6.5.5 for a complete discussion of the uncertainty treatment.

Matrix permeability is taken from the drift-scale calibrated property sets (BSC 2004 [DIRS 169857], Tables 6-8, 6-9, and 6-10; DTNs: LB0208UZDSCPLI.002 [DIRS 161788]; LB0208UZDSCPMI.002 [DIRS 161243]; and LB0302UZDSCPUI.002 [DIRS 161787]). These permeability values are calibrated against water saturation and water potential values for the lower, mean, and upper bound present-day infiltration cases using one-dimensional models and inverse modeling methods (BSC 2004 [DIRS 169857], Section 6.3.2). These cases represent the uncertainty in flux through the UZ and therefore the property sets calibrated to these different

infiltration cases represent the uncertainty in the properties that are consistent with the calibration. The subsequent calibrations with the site-scale 3D model did not affect the values of matrix permeability (BSC 2004 [DIRS 169861], Appendix A, Tables A-1, A-2, and A-3).

Fracture Dispersivity

The fracture dispersivity is set at a fixed value of 10 m. There are few data available on dispersivity distributions at Yucca Mountain site. Neuman (1990 [DIRS 101464]) showed that field dispersivity varied with the scale of study. Field tracer tests at the C-holes at Yucca Mountain also showed that on a 100 m scale, field dispersivity had a range of approximately 3 to 63 m (BSC 2004 [DIRS 170010], Table 6.3-3). The 10 m value is toward the lower end of the value from field studies and available in DTN: LA0303PR831231.005 [DIRS 166259]. The influence of dispersion on radionuclide transport is not expected to be important because the spreading of radionuclides due to matrix diffusion effects have a much greater impact on transport times than longitudinal dispersion over the expected range of longitudinal dispersivities. Although the impact of dispersivity should be very small, the value chosen should be conservative, as higher dispersivity tends to spread the radionuclide plume and reduce the peak value. While it can be argued that for a decaying species, higher dispersivity can allow a greater fraction of the mass to arrive downstream before decaying, the point here is that in comparison to diffusion and large scale heterogeneities, dispersivity effects have a very small influence on the breakthrough curves. This justifies the use of a fixed value for dispersivity rather than treating it as a stochastic parameter (Table 6-4).

Sorption

The derivation of sorption coefficient probability distributions for the elements of interest on the major rock types in Yucca Mountain involves both an evaluation of available experimental data and sorption modeling. Sorption data have been obtained in laboratory experiments in which crushed rock samples from the Yucca Mountain site were contacted with groundwaters (or simulated groundwaters) representative of the site, spiked with one or more of the elements of interest (BSC 2004 [DIRS 164500], Section A.1). Experimental data were used to evaluate the impact of variations in rock sorption properties within each of the rock types, radionuclide concentrations, sorption kinetics, and water chemistry on sorption coefficients for the elements of interest. The radioisotopes of americium, cesium, neptunium, protactinum, plutonium, radium, strontium, thorium, and uranium are treated as sorbing. The radioisotopes of carbon, iodine, and technetium are treated as nonsorbing.

The modeling of sorption in the TSPA-LA is based on the linear sorption model, which is characterized by the same lumped parameter for the sorption coefficient K_d that is used in the process models. All aqueous radionuclides that travel in fractures are conservatively assumed not to be absorbed by the fracture walls (BSC 2004 [DIRS 164500], Section 6.4.2). For radionuclides that travel in the matrix, the partitioning of radionuclides between the solute and the matrix is described by the sorption coefficient for each radionuclide. The matrix sorption coefficients that have been developed for different rock types (zeolitic, devitrified, and vitric) are listed in Table 6-7 with their statistical distributions. These distributions are sampled to represent the uncertainty in sorption in the TSPA-LA. The influence of expected variations in water chemistry, radionuclide concentrations, and variations in rock surface properties within

each of the major rock types were incorporated into the probability distributions. Effective K_d values, obtained from batch experiments involving high-concentration solutions, will tend to underestimate the field K_d values if the expected field concentrations are low and nonlinear sorption prevails (BSC 2004 [DIRS 164500], Section 6.1.2.3).

The evaluation of the effects of sorption on transport also requires specification of the rock bulk density, matrix water content, as shown in Equation 6-2. Matrix water content is the product of the water saturation times the porosity. The matrix porosity used for determining the retardation of sorbing solutes is from the thermal property set, DTN: LB0210THRMLPRP.001 [DIRS 160799], which is the same value of matrix porosity used to determine the advective transport velocity in the matrix, as discussed above. Bulk rock density is computed from grain densities given in DTN: LB0210THRMLPRP.001 [DIRS 160799] by multiplying by the ratio of the grain volume to the bulk volume, which is equal to one minus the porosity. See also the discussion under *Matrix Porosity* (this section) concerning the use of DTN: LB0210THRMLPRP.001 [DIRS 160799] rather than DTN: LB0402THRMLPRP.001 [DIRS 168481] for grain density.

Radionuclide Sorption onto Colloids

Colloid transport is represented through radionuclide attachment to colloids that are either reversible or irreversible. For reversible attachment, the degree of partitioning onto colloids is a function of both the colloid concentration and the sorption coefficient for a given radioelement onto the colloid (Section 6.5.12). The groundwater colloid size distribution that was developed for use in the TSPA-LA model was based on data from 79 groundwater samples collected in the vicinity of Yucca Mountain and 11 samples collected from the Idaho National Engineering and Environmental Laboratory (INEEL). The INEEL groundwater colloid data (DTN: LA0002SK831352.003 [DIRS 161771]) were deemed appropriate for inclusion in the data analysis among the groundwater data from the Yucca Mountain area because the climate in Idaho Falls is similarly arid and the field sampling and analytical techniques used at both locations were similar (DTN: SN0306T0504103.005 [DIRS 164132]). Note that the distributions for two ionic strength conditions are presented, however, only the lower ionic strength distribution was used for TSPA because the lower ionic strength distribution results in greater colloid concentrations leading to greater colloid-facilitated radionuclide transport.

Sorption partition coefficients (K_d values) have been developed for selected radionuclides onto smectite and iron oxyhydroxides (DTN: SN0306T0504103.006 [DIRS 164131]). Smectite is representative of defense high-level waste glass degradation product colloids and natural groundwater colloids. Iron oxyhydroxides are representative of steel corrosion-generated colloids (assumed to be iron oxyhydroxides). These colloidal constituents may act as pseudocolloids that sorb radionuclides and subsequently be transported from the engineered barrier system (EBS) by seepage waters moving through the repository. The K_d values for the radioelements Pu, Am, Th, Pa, and Cs are drawn from both project-supported experimental work, government publications, and the open literature. For a given radionuclide (except Cs) the maximum value of each K_d value range is the same to allow for the possibility that iron oxyhydroxide will occur both as iron oxyhydroxides colloids and as coatings on, or microcrystalline aggregates in association with, smectite colloids in the iron-rich waste package environment. For Cs, which attaches more strongly to smectite (by ion exchange) than iron

oxyhydroxides, the upper value of the K_d value range is different for iron oxyhydroxides and smectite.

For irreversible attachment, the parameter K_c is set to a fixed value of 10^{20} that practically ensures that radioelements remain permanently attached to the colloid (Section 6.5.12).

Colloid Filtration and Size Exclusion

Colloid size exclusion is treated in the model for colloid movement from fractures into the rock matrix. Size exclusion is treated on the basis of effective colloid and matrix pore diameters, where a colloid is excluded from entry into a pore that is smaller than the colloid. The matrix pore size distributions for different rock types were developed from moisture retention curve measurements on rock matrix samples taken from 16 different hydrogeologic units between the repository host rock and the water table at Yucca Mountain (DTN: LA0003MCG12213.002 [DIRS 147285]). The pore size distribution data were used for the average effective colloid diameter of 0.1 μm, giving the expected fraction of colloids excluded from entering the rock matrix in each hydrogeologic unit.

Colloid filtration is treated in the model for colloid transport between successive rock matrix hydrogeologic units. This is based on physical straining, in which filtration will occur if a colloid attempts to pass though a pore with an effective diameter that is smaller than the colloid effective diameter. Pore size distributions are based on the data discussed above. Colloid size distribution data is available from measurements colloids generated from high-level waste glass corrosion using a dynamic light-scattering method (DTN: LL000122051021.116 [DIRS 142973], MOL.20010216.0003 Section 6.3; see also DTN: LL991109751021.094 [DIRS 142910], MOL.20000124.0207 p. 32 and 34).

Colloid Retardation in Transport Through Fractures

Colloid retardation in transport through fractures in volcanic tuffs has been investigated in field tests conducted in the saturated zone (SZ) at Yucca Mountain (BSC 2004 [DIRS 170006], Section 6.4). These retardation factors represent the chemical and physical filtration of colloids in the SZ. The field measurements were conducted using fluorescent carboxylate modified polystyrene latex (CML) microspheres ranging in diameter from 280 nm to 830 nm. Results from laboratory fracture experiments conducted using silica, montmorillonite, and clinoptilolite colloids in addition to CML microspheres suggest that colloid filtration and retardation parameters derived from CML microsphere responses in field tracer tests should be conservative if used to predict natural inorganic colloid transport in fractured systems. The retardation factors have been derived in terms of a cumulative probability distribution representing the uncertainty in retardation factors applied to colloid transport through fractures (DTN: LA0303HV831352.002 [DIRS 163558]). The application of these results to the UZ is based on the similar geologic units (fractured volcanic rocks) and transport processes at the scale governing colloid transport processes. Furthermore, colloid transport in the UZ is expected to be less favorable than in the SZ as a result of the smaller fractures (or possibly water films) in which water flows through unsaturated fractures, leading to a conservative representation of colloid transport in the UZ. In addition to colloid retardation, a fraction of unretarded colloid transport is developed based on the attachment rates derived from the colloid transport field test data

(DTN: LA0303HV831352.003 [DIRS 165624]). This distribution is tied to the transport time distributions experienced by the colloids (BSC 2004 [DIRS 170006], Section 6.6). Rather than incorporating the full distribution as a function of transport time, a single conservative value for unretarded colloid transport is used as discussed in Section 6.5.13.

4.2 CRITERIA

Technical requirements to be satisfied by performance assessment are based on 10 CFR 63.114 [DIRS 173273] and identified in *Project Requirements Document* (Canori and Leitner 2003 [DIRS 166275]). The acceptance criteria that will be used by the U.S. Nuclear Regulatory Commission to determine whether the technical requirements have been met are identified in *Yucca Mountain Review Plan, Final Report* (YMRP) (NRC 2003 [DIRS 163274]). The pertinent requirements and criteria for this report are summarized in Table 4-3.

Table 4-3. Project Requirements and YMRP Acceptance Criteria Applicable to this Report

Requirement Number[a]	Requirement Title[a]	10 CFR 63 Link	YMRP Acceptance Criteria
PRD -002/T-016	Requirements for performance assessment	10 CFR 63.114 (a)-(c), (e), (g) [DIRS 173273]	2.2.1.3.7.3, Criteria 1 to 5

[a] From Canori and Leitner (2003 [DIRS 166275]).

[b] From NRC (2003 [DIRS 163274]).

YMRP = *Yucca Mountain Review Plan, Final Report*

The pertinent requirements and acceptance criteria for this report are identified in Section 2.2.1.3.7.3 of the YMRP (NRC 2003 [DIRS 163274]). As presented in Section 1.0, the TWP governing the work presented REV 01 of this report is *Technical Work Plan for: Unsaturated Zone Transport Model Report Integration* (BSC 2004 [DIRS 171282]). Rev 02, the current revision, updates this document with work involving sensitivity studies: the work is outlined in the planning document, *Technical Work Plan for: Unsaturated Zone Flow, Drift Seepage and Unsaturated Zone Transport Modeling* (BSC 2005 [DIRS 173951]). Rev 1 requires Criteria 1-5, whereas Rev 2 requires Criteria 1-4. All five acceptance criteria and subcriteria are included here for completeness and identified in the discussion below, followed by a short description of their applicability to this report. Where a subcriterion includes several components, only some of those components may be addressed. How these components are addressed is summarized in Section 8.3 of this report.

Acceptance Criteria 1: System Description and Model Integration Are Adequate.

(1) Total system performance assessment adequately incorporates important design features, physical phenomena, and couplings, and uses consistent and appropriate assumptions throughout the radionuclide transport in the unsaturated zone abstraction process;

(2) The description of the aspects of hydrology, geology, geochemistry, design features, physical phenomena, and couplings that may affect radionuclide transport in the unsaturated zone is adequate. For example, the description includes changes in

transport properties in the unsaturated zone, from water-rock interaction. Conditions and assumptions in the total system performance assessment abstraction of radionuclide transport in the unsaturated zone are readily identified, and consistent with the body of data presented in the description;

(3) The abstraction of radionuclide transport in the unsaturated zone uses assumptions, technical bases, data, and models that are appropriate and consistent with other related U.S. Department of Energy abstractions. For example, assumptions used for radionuclide transport in the unsaturated zone are consistent with the abstractions of radionuclide release rates and solubility limits and flow paths in the unsaturated zone (Sections 2.2.1.3.4 and 2.2.1.3.6 of the Yucca Mountain Review Plan, respectively). The descriptions and technical bases provide transparent and traceable support for the abstraction of radionuclide transport in the unsaturated zone;

(4) Boundary and initial conditions used in the abstraction of radionuclide transport in the unsaturated zone are propagated throughout its abstraction approaches. For example, the conditions and assumptions used to generate transport parameter values are consistent with other geological, hydrological, and geochemical conditions in the total system performance assessment abstraction of the unsaturated zone;

(5) Sufficient data and technical bases for the inclusion of features, events, and processes related to radionuclide transport in the unsaturated zone in the total system performance assessment abstraction are provided;

(6) Guidance in NUREG–1297 and NUREG–1298 (Altman et al. 1988 [DIRS 103597]; Altman et al. 1988 [DIRS 103750]), or other acceptable approaches, is followed for peer review and data qualification.

Acceptance Criteria 2: Data Are Sufficient for Model Justification.

(1) Geological, hydrological, and geochemical values used in the license application are adequately justified (e.g., flow-path length, sorption coefficients, retardation factors, colloid concentrations, etc.). Adequate descriptions of how the data were used, interpreted, and appropriately synthesized into the parameters are provided;

(2) Sufficient data have been collected on the characteristics of the natural system to establish initial and boundary conditions for the total system performance assessment abstraction of radionuclide transport in the unsaturated zone;

(3) Data on the geology, hydrology, and geochemistry of the unsaturated zone, including the influence of structural features, fracture distributions, fracture properties, and stratigraphy, used in the total system performance assessment abstraction are based on appropriate techniques. These techniques may include laboratory experiments, site-specific field measurements, natural analog research, and process-level modeling studies. As appropriate, sensitivity or uncertainty analyses used to support the U.S. Department of Energy total system performance assessment abstraction are adequate to determine the possible need for additional data.

Acceptance Criteria 3: Data Uncertainty Is Characterized and Propagated Through the Model Abstraction.

(1) Models use parameter values, assumed ranges, probability distributions, and bounding assumptions that are technically defensible, reasonably account for uncertainties and variabilities, and do not result in an under-representation of the risk estimate;

(2) For those radionuclides where the total system performance assessment abstraction indicates that transport in fractures and matrix in the unsaturated zone is important to waste isolation: (i) estimated flow and transport parameters are appropriate and valid based on techniques that may include laboratory experiments, field measurements, natural analog research, and process-level modeling studies conducted under conditions relevant to the unsaturated zone at Yucca Mountain; and (ii) models are demonstrated to adequately reproduce field transport test results. For example, if a sorption coefficient approach is used, the assumptions implicit in that approach are verified;

(4) Uncertainty is adequately represented in parameter development for conceptual models, process-level models, and alternative conceptual models considered in developing the abstraction of radionuclide transport in the unsaturated zone. This may be done either through sensitivity analyses or use of conservative limits;

Acceptance Criteria 4: Model Uncertainty Is Characterized and Propagated Through the Model Abstraction.

(1) Alternative modeling approaches of features, events, and processes are considered and are consistent with available data and current scientific understanding, and the results and limitations are appropriately considered in the abstraction;

(2) Conceptual model uncertainties are adequately defined and documented, and effects on conclusions regarding performance are properly assessed;

(3) Consideration of conceptual model uncertainty is consistent with available site characterization data, laboratory experiments, field measurements, natural analog information and process-level modeling studies; the treatment of conceptual mode uncertainty does not result in an under-representation of the risk estimate;

(4) Appropriate alternative modeling approaches are consistent with available data and current scientific knowledge, and appropriately consider their results and limitations, using tests and analyses that are sensitive to the processes modeled. For example, for radionuclide transport through fractures, the U.S. Department of Energy adequately considers alternative modeling approaches to develop its understanding of fracture distributions and ranges of fracture flow and transport properties in the unsaturated zone.

Acceptance Criteria 5: Model Abstraction Output Is Supported by Objective Comparisons.

(1) The models implemented in this total system performance assessment abstraction provide results consistent with output from detailed process-level models and/or empirical observations (laboratory and field testings and/or natural analogs);

(2) Outputs of radionuclide transport in the unsaturated zone abstractions reasonably produce or bound the results of corresponding process-level models, empirical observations, or both. The U.S. Department of Energy abstracted models for radionuclide transport in the unsaturated zone are based on the same hydrological, geological, and geochemical assumptions and approximations shown to be appropriate for closely analogous natural systems or experimental systems;

(3) Well-documented procedures that have been accepted by the scientific community to construct and test the mathematical and numerical models are used to simulate radionuclide transport through the unsaturated zone;

(4) Sensitivity analyses or bounding analyses are provided to support the total system performance assessment abstraction of radionuclide transport in the unsaturated zone that cover ranges consistent with site data, field or laboratory experiments and tests, and natural analog research.

4.3 CODES, STANDARDS, AND REGULATIONS

No codes, standards, or regulations, other than those identified in the *Project Requirements Documents* (Canori and Leitner 2003 [DIRS 166275], Table 2-3) and determined to be applicable in Table 4-3, were used in this analysis/model report.

INTENTIONALLY LEFT BLANK

5. ASSUMPTIONS

In this section, the assumptions taken to develop the UZ radionuclide transport abstraction model are outlined as the first step toward developing the computational and mathematical models needed in radionuclide transport calculations for the TSPA-LA model. In Section 6.4, the mathematical basis for this algorithm is outlined, and theory is developed to incorporate the effects of sorption, dispersion, and matrix diffusion into this new particle-tracking framework. In the remainder of this section, the fundamental assumptions of the techniques itself and the specific implementation for the UZ transport abstraction model are listed and justified.

Assumption 1: The AFM (Liu et al. 1998 [DIRS 105729]) appropriately accounts for reduced fracture/matrix (f/m) interaction.

Rationale: The reduction in f/m contact area is a result of flow focusing. This flow focusing is represented using the active fracture unsaturated flow model. Model validation for the AFM was carried out in *Conceptual Model and Numerical Approaches for Unsaturated Zone Flow and Transport* (BSC 2004 [DIRS 170035], Section 7.4.1), through a comparison of a one-dimensional, AFM-based model with ^{14}C data. The analysis showed that the AFM could be used to explain the transport times implied by the ^{14}C data in boreholes USW UZ-1 and USW SD-12. On the basis of this agreement, it can be assumed that the AFM is a suitable model for addressing fracture-matrix interactions for radionuclides simulated in the abstraction model. A sensitivity analysis is presented in this report to examine the impact of uncertainty in these parameters on the transport predictions.

Confirmation Status: This assumption does not require further verification, as the model has been validated for use, as discussed above.

Where Used: Section 6.4.3.

Assumption 2: The influence of matrix diffusion in a dual-permeability system can be handled with a subgrid-block model consisting of parallel flow in a discrete fracture and connected matrix.

Rationale: Although the submodel consisting of a repeating system of parallel, equally spaced fractures and parallel flow in the fractures and matrix is an idealization; it captures one of the key features in the UZ system, namely the influence of radionuclide diffusion between fractures and matrix. Furthermore, the influence of sharp concentration gradients in the matrix is implicitly accounted for in the model by incorporating results from a discrete fracture model designed to handle these effects accurately. Therefore, systems with relatively small amounts of matrix diffusion can be simulated, in contrast to implementations of dual-permeability transport that represent the matrix with a single grid block. In numerical modeling, this type of idealization, commonly referred to as "upscaling," is a technique for capturing the essential features of a physical system, even though it is understood that the actual system contains

geometric complexities not simulated in the model. For example, Table 6-13 shows that the distribution of fracture spacings of mapped fractures is not uniform. However, the important spacing of interest for transport is the spacing of flowing fractures, which adds significant additional uncertainty. Given this situation, an appropriate assumption for the purpose of capturing the impact of matrix diffusion is to assume the model geometry of equally spaced flowing fractures.

Confirmation Status: This assumption does not require verification.

Where Used: Section 6.4.3.

Assumption 3: Dispersion of both aqueous and colloidal species in the UZ can be approximated as consisting only of longitudinal dispersion, characterized by a constant value of the dispersivity α_l.

Rationale: When dispersivity is used to model solute spreading in porous media, it is introduced to capture variability in the flow velocity existing at smaller scales than are modeled in the numerical grid. Large-scale spreading caused by features explicitly present in the flow simulation is captured directly, and is not considered to be dispersion in the sense being used here. Because the use of this model is to predict transport time distributions of radionuclides to the water table, longitudinal dispersion is potentially important to capture a dispersed solute front arriving at the water table. By contrast, transverse dispersion, omitted in this model, will tend to allow mass to migrate short distances in the horizontal direction. For example, as a rule of thumb, assume that a transverse dispersivity of one-tenth the longitudinal dispersivity of 10 m (see Table 6-2), a value of 1 m is representative. The characteristic distance of spreading of a dispersing plume resulting from a point source is given by Freeze and Cherry (1979 [DIRS 101173], p. 395) $\sqrt{2D_t t} = \sqrt{2\alpha_t v(L/v)} = \sqrt{2\alpha_t L}$, where D_t is the transverse dispersion coefficient, α_t is the transverse dispersivity, and t is the characteristic time equal to the velocity, v, divided by the length, L. For a radionuclide point source traveling vertically to the water table ($L \approx 350$ m), the transverse spreading of the plume at the water table is approximately $\sqrt{2(1)(350)} = 26$ m. This amount of lateral spreading is small compared to the width of the repository, or even the width of a grid block in the UZ model. Therefore, the velocity field encountered by the plume is not expected to be significantly different than if no transverse dispersion is assumed. On this basis, lateral transverse dispersion is insignificant and can be neglected. Finally, to a first approximation, this variability will act similarly on aqueous and colloidal components. As a result, the same dispersivity should be used for both.

Confirmation Status: This assumption does not require verification.

Where Used: Section 6.4.2.

Assumption 4: Radionuclide releases at the location of the repository can be represented stochastically by identifying regions on the basis of the predicted water flux through the medium, and placing particles randomly within this region to represent the release.

Rationale: Water flux through the repository region is known to be a key factor controlling waste package degradation and waste mobilization. By partitioning the finite difference grid cells in the UZ model into groups based on flux, radionuclides will preferentially enter the system at locations where the flux is highest. This approach preserves this known relationship, and does not artificially introduce radionuclides into the model at locations where transport times are extremely long. This approximation fulfills the goal of ensuring that release locations are correlated to percolation flux at the repository, while simplifying in an appropriate way the method for selecting the release location, allowing the binning to remain constant during a given simulation.

Confirmation Status: This assumption does not require verification.

Where Used: Section 6.5.15.

Assumption 5: For the purposes of computing radionuclide transport, flow through the UZ can be approximated assuming that the system (rock mass and flow conditions) has not been influenced by repository waste heat effects or drift shadow effects. Durable changes to the rock mass hydrologic properties are also assumed to be negligible.

Rationale: Numerical modeling shows that the flow conditions around the repository will change after waste emplacement due to thermal-hydrologic effects, and these effects are expected to last for a few thousand years (BSC 2005 [DIRS 172232], Section 8.1). As long as the radionuclide releases occur after the main part of this perturbation takes place, the system should have bounced back to its ambient flow conditions. Regarding the potential for durable changes to the rock mass properties, a range of hydrologic flow conditions (in the form of different flow fields imported to the model) are assumed. It is assumed that this range will encompass the possibility of changes to the far-field rock conditions from repository waste heat.

Confirmation Status: This assumption does not require verification.

Where Used: Section 6.5.1.

Assumption 6: Climate changes can be considered in an approximate way by imparting an instantaneous jump from one steady state flow field to another, with a corresponding rise or fall in the water table representing the bottom of the UZ

model. Shorter-term transients (wet and dry years, individual storm events, etc.) are assumed to be adequately captured with a model that assumes such transients can be averaged to obtain a long-term, effective steady state.

Rationale: In simulations of system performance lasting 10,000 to 20,000 years, long-term changes in climatic conditions are expected to change the UZ flow field from its present-day condition. In the Yucca Mountain UZ, water transport times of hundreds to thousands of years through the entire system are likely, although this process is obviously uncertain. Assuming that the jump from one steady state flow field to another occurs instantaneously is a reasonable approximation, given the uncertainties and the inability to observe this process directly. When the climate changes from drier to wetter during the regulatory compliance period (BSC 2004 [DIRS 170002], Section 7), transport velocities will immediately be greater and the flow path length to the water table will be shorter; imposing both of these changes immediately will ensure that the approach will not artificially delay the imposition of the more rapid transport conditions. Regarding short-term transients, the relatively unfractured portions of the rock, such as the Paintbrush nonwelded vitric tuff (PTn), will dampen such transients, allowing a long-term steady state model to be used (BSC 2004 [DIRS 169861], Appendix G).

Confirmation Status: This assumption does not require verification.

Where Used: Section 6.4.8.

6. MODEL DISCUSSION

6.1 MODELING OBJECTIVES AND APPROACH

This report documents the UZ transport abstraction model to be used in TSPA-LA simulations. The UZ transport abstraction model studies the movement of radionuclides released from the EBS into the unsaturated fractured geological media downward to the water table. Radionuclide mass flux versus time exiting the UZ is transferred to the SZ model in the TSPA-LA system model.

Processes affecting radionuclide transport in the UZ include advection, dispersion, fracture-matrix interaction, sorption, colloid-facilitated transport, climate change and water table rises, and radionuclide decay/ingrowth. The numerical representation of those processes is described in Section 6.4.

The pregenerated flow fields are simulated in the documents by *UZ Flow Models and Submodels* (BSC 2004 [DIRS 169861]) and *Parameter Sensitivity Analysis for Unsaturated Zone Flow* (BSC 2005 [DIRS 174116]) and saved for TSPA-LA use. The use of pregenerated flow fields increases the efficiency of transport simulations.

In TSPA runs, GoldSim (BSC 2003 [DIRS 161572]) initiates a call to the FEHM (V2.21 or higher) external dynamic link library (dll) to start UZ transport simulations (Figure 6-1). GoldSim (BSC 2003 [DIRS 161572]) passes the following data to FEHM through the interface:

- Simulation time
- Flow fields to be used
- Coordinates for early failed packages and number of repository subregions
- Number of radionuclide species
- Radionuclide mass release from EBS to UZ in each designated subregion for each species.

At the end of each FEHM UZ transport run, FEHM passes the simulated mass output at the water table back for input to SZ.

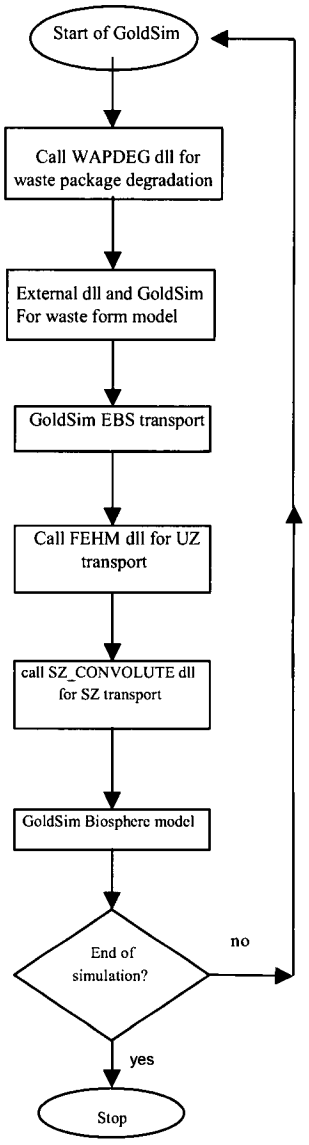

Figure 6-1. Overview Schematic of the GoldSim-FEHM Coupling

6.2 FEATURES, EVENTS, AND PROCESSES INCLUDED IN THE MODEL

The development of a comprehensive list of FEPs potentially relevant to postclosure performance of the Yucca Mountain repository is an ongoing, iterative process based on site-specific information, design, and regulations. The list of FEPS relevant to this AMR was initially identified in the TWP (BSC 2004 [DIRS 171282]) and has been further refined based on subsequent review of the LA FEP List as documented in DTN: MO0407SEPFEPLA.000 [DIRS 170760]. The FEP 1.2.02.01.0A, Fractures, has been added to the list identified in the TWP (BSC 2004 [DIRS 171282]) because fractures are included in the UZ transport abstraction model that supports TSPA-LA. Table 6-1 provides a list of FEPs that are specifically addressed in this report and identifies the sections of this AMR that addresses those FEPs. The rationale for excluding a FEP from the TSPA-LA model is given in the Scientific Analysis Report, *Features, Events, and Processes in UZ Flow and Transport* (BSC 2005 [DIRS 174191]).

Table 6-1. Included FEPs for This Model Report and Their Disposition in the TSPA-LA

FEP Number	FEP Name	Section Where FEP is Addressed*
1.2.02.01.0A	Fractures	Sections 6.4.3, 6.5.1, 6.5.6, 6.5.7, 6.6.4, 6.6.2, and 7.2.3.3
1.2.02.02.0A	Faults	Sections 6.5.1, 6.5.7, and 6.6.2.
1.3.01.00.0A	Climate change	Sections 6.4.8 and 6.6.2
1.3.07.02.0B	Water table rise affects UZ	Section 6.4.8
1.4.01.01.0A	Climate modification increases recharge	Sections 6.5.1 and 6.6.2
2.1.08.01.0A	Water influx at the repository	Section 6.5.15
2.2.03.01.0A	Stratigraphy	Section 6.5.1.
2.2.03.02.0A	Rock properties of host rock and other units	Sections 6.5.3, 6.5.7, and 6.6.2.
2.2.07.02.0A	Unsaturated groundwater flow in the geosphere	Sections 6.5.1 and 6.6.2.
2.2.07.04.0A	Focusing of unsaturated flow (fingers, weeps)	Sections 6.5.1, 6.6.2, and C5.
2.2.07.06.0B	Long-term release of radionuclides from the repository	Sections 6.4.6 and 6.4.7
2.2.07.07.0A	Perched water develops	Section 6.5.1
2.2.07.08.0A	Fracture flow in the UZ	Sections 6.5.1 and 6.5.6
2.2.07.09.0A	Matrix imbibition in the UZ	Section 6.5.1
2.2.07.15.0B	Advection and dispersion in the UZ	Sections 6.4.1, 6.4.2, 6.5.1, 6.5.2, 6.6.2, and 7.2.1.1.
2.2.08.01.0B	Chemical characteristics of groundwater in the UZ	Sections 6.5.4 and 6.5.8
2.2.08.06.0B	Complexation in the UZ	Sections 6.5.4 and 6.5.8
2.2.08.08.0B	Matrix diffusion in the UZ	Sections 6.4.3, 6.5.5, 6.5.6, 6.6.2, 6.6.4, 7.2.1.2, 7.2.1.3, 7.2.3.3, and Appendix C.
2.2.08.09.0B	Sorption in the UZ	Sections 5., 6.4.3, 6.4.5, 6.5.4, 6.5.8, 6.6.2, and 7.2.1.3
2.2.08.10.0B	Colloidal transport in the UZ	Sections 6.4.5, 6.5.9, 6.5.10, 6.5.11, 6.5.12, 6.5.13, and 6.6.2
2.2.09.01.0B	Microbial activity in the UZ	Section 6.5.4
3.1.01.01.0A	Radioactive decay and ingrowth	Sections 6.4.4, 6.5.14, and 6.6.2

NOTE: *For FEPs requiring additional explanation as to the manner in which they have been treated, see the text. FEP = feature, event, and process; UZ = unsaturated zone

The following descriptions elaborate on several of the FEPs listed in Table 6-1. Those not included below do not require additional explanation.

- 1.2.02.01.0A—Elements of this FEP are implicitly included through the use of the pregenerated flow fields (Section 6.5.1. DTNs: LB0305TSPA18FF.001 [DIRS 165625] and LB0312TSPA06FF.001 [DIRS 166671]).

- 1.2.02.02.0A—Elements of this FEP are implicitly included through the use of the pregenerated flow fields (Section 6.5.1; DTNs: LB0305TSPA18FF.001 [DIRS 165625] and LB0312TSPA06FF.001 [DIRS 166671]).

- 1.3.01.00.0A—Elements of this FEP are implicitly included through the use of the pregenerated flow fields under different climates (DTNs: LB0305TSPA18FF.001 [DIRS 165625] and LB0312TSPA06FF.001 [DIRS 166671]).

- 1.3.07.02.0B—Elements of this FEP are implicitly included through the use of the pregenerated flow fields under different climates, with water table rise built into the flow fields (DTN: LB0312TSPA06FF.001 [DIRS 166671]).

- 1.4.01.01.0A—Elements of this FEP are implicitly included through the use of the pregenerated flow fields under different climates (DTNs: LB0305TSPA18FF.001 [DIRS 165625] and LB0312TSPA06FF.001 [DIRS 166671]).

- 2.2.03.01.0A—Elements of this FEP are implicitly included through the use of the pregenerated flow fields (Section 6.5.1; DTNs: LB0305TSPA18FF.001 [DIRS 165625] and LB0312TSPA06FF.001 [DIRS 166671]).

- 2.2.07.02.0A—Elements of this FEP are implicitly included through the use of the pregenerated flow fields (Section 6.5.1; DTNs: LB0305TSPA18FF.001 [DIRS 165625] and LB0312TSPA06FF.001 [DIRS 166671]).

- 2.2.07.04.0A—Elements of this FEP are implicitly included through the use of the pregenerated flow fields (Section 6.5.1; DTNs: LB0305TSPA18FF.001 [DIRS 165625] and LB0312TSPA06FF.001 [DIRS 166671]). In addition, this FEP is more fully addressed in *UZ Flow Models and Submodels* (BSC 2004 [DIRS 169861]).

- 2.2.07.07.0A—Elements of this FEP are implicitly included through the use of the pregenerated flow fields (Section 6.5.1; DTN: LB0305TSPA18FF.001 [DIRS 165625] and DTN: LB0312TSPA06FF.001 [DIRS 166671]). In addition, more detailed information on the treatment of perched water in the UZ can be found in the model report, *UZ Flow Models and Submodels* (BSC 2004 [DIRS 169861]).

- 2.2.07.08.0A—Elements of this FEP are implicitly included through the use of the pregenerated flow fields (Section 6.5.1; DTN: LB0305TSPA18FF.001 [DIRS 165625] and DTN: LB0312TSPA06FF.001 [DIRS 166671]) and implementation of the active fracture model in the transport abstraction. In addition, this FEP is more fully addressed in *UZ Flow Models and Submodels* (BSC 2004 [DIRS 169861]).

- 2.2.07.09.0A—Elements of this FEP are implicitly included through the use of the pregenerated flow fields (Section 6.5.1; DTN: LB0305TSPA18FF.001 [DIRS 165625] and DTN: LB0312TSPA06FF.001 [DIRS 166671]). In addition, this FEP is more fully addressed in *UZ Flow Models and Submodels* (BSC 2004 [DIRS 169861]).

- 2.2.09.01.0B—The parameter distributions for sorption coefficient were developed with microbial effects considered. See the process model report (BSC 2004 [DIRS 164500], Section 6.4.2) for a discussion of this issue.

6.3 THE UZ TRANSPORT ABSTRACTION MODEL

The UZ transport component of the total system model tracks the movement of radionuclides released from the EBS down to the water table (Figure 6-2).

The top boundary of the site-scale UZ flow model is the ground surface, with prescribed infiltration rates, and the bottom boundary is the water table, modeled with constant pressure. The side boundaries are no flow (BSC 2004 [DIRS 169861], Section 6.1.3).

The UZ flow fields are pregenerated and saved for use by FEHM. During TSPA simulation runs, the FEHM dll reads in the pregenerated flow fields and then carries out transport simulations. The impact of climate change is investigated by using the UZ flow fields corresponding to different climate scenarios. The FEHM-compatible flow field files developed for the TSPA-LA model are in DTNs: LB0305TSPA18FF.001 [DIRS 165625] and LB0312TSPA06FF.001 [DIRS 166671].

The UZ transport abstraction model is based on the dual-k formulation for fluid flow, with additional transport considerations to incorporate the influence of sorption and fracture-matrix interactions on radionuclide transport. The influence of spatial variability is included through a three-dimensional model that incorporates the appropriate geometry and geology.

For the UZ transport abstraction model, radionuclides are released at the repository where failed waste packages release radionuclides into the system. Any radionuclide that reaches the water table is removed from the UZ transport system and put into the SZ system.

Once a radionuclide particle is released from the EBS into the UZ, the particle is carried by water traveling through the fractured media downward to the water table. The following transport mechanisms can affect the movement of a radionuclide particle and are considered in the UZ transport abstraction model:

- Advection
- Dispersion
- Sorption
- Fracture-matrix interaction, including matrix diffusion
- Colloid-facilitated transport
- Radioactive decay/ingrowth
- Climate change and water table rise.

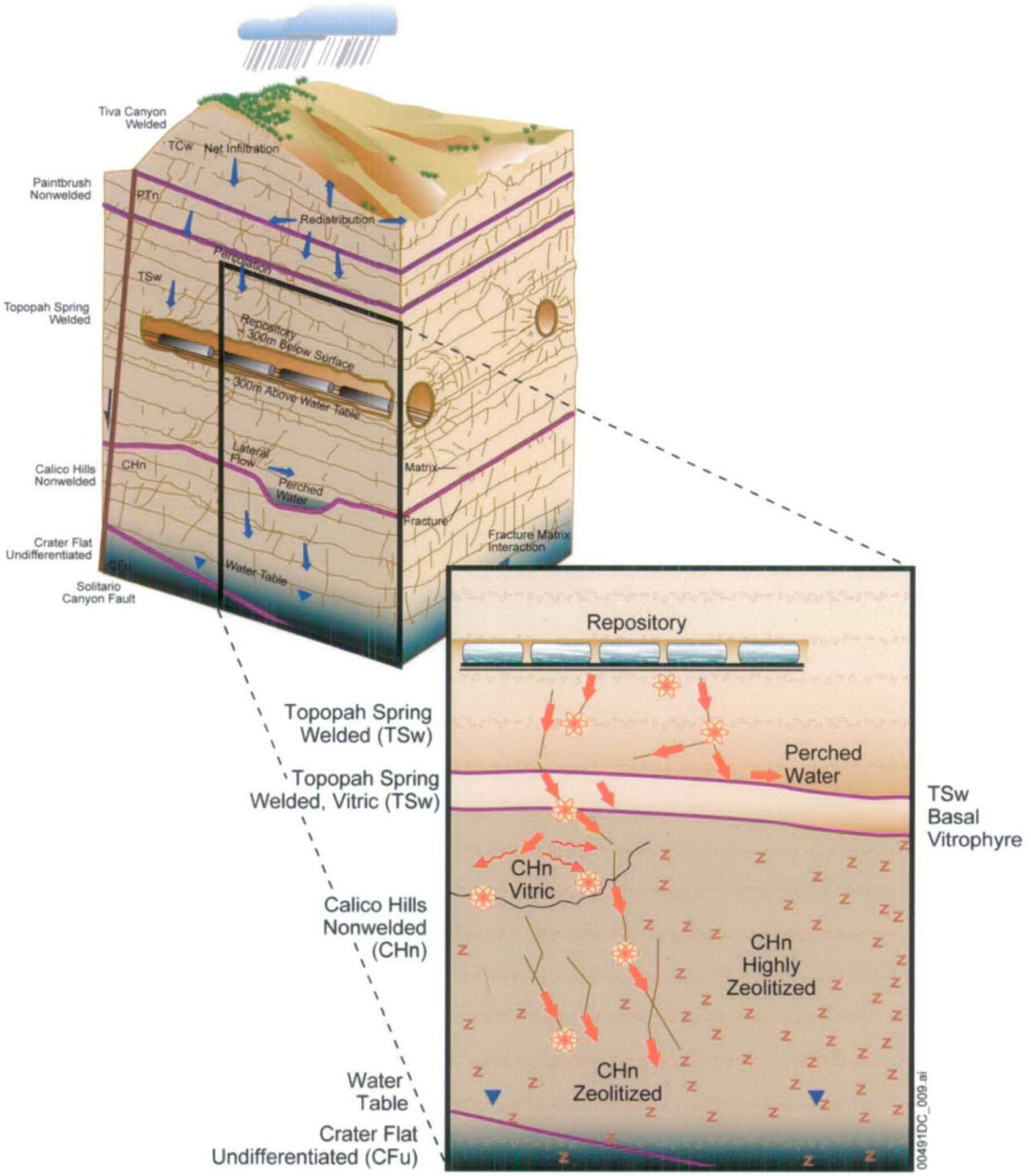

Figure 6-2. Schematic of Water Movement and Radionuclide Transport Through the UZ

Implementation of the above transport mechanisms inside FEHM are described in Section 6.4 of this report. The abstraction model is designed to facilitate parameter uncertainty analyses in TSPA. This is done by running multiple realizations with different parameter values based on parameter distributions.

Performing multiple realizations (numbering in the hundreds) for such a complex system requires that the software used for simulating radionuclide transport in the system be efficient

while also being able to handle complex physical and chemical processes with sufficient accuracy. FEHM (Zyvoloski et al. 1997 [DIRS 100615]) was selected for simulating radionuclide transport in the system because of the efficiency of the particle tracking method and its ability to handle advection, dispersion, sorption, matrix-diffusion, and multiple-species radionuclide decay/ingrowth in the system.

6.4 THE NUMERICAL REPRESENTATION OF THE UZ TRANSPORT ABSTACTION MODEL

This section outlines the development of the general transport methods used for the RTTF particle-tracking model and issues specific to the use of this model to simulate radionuclide transport for the Yucca Mountain UZ.

Prediction of solute transport is a critical element of many groundwater flow studies, including contaminant transport and the movement of dissolved species in solution. Modeling efforts typically are motivated by the need to predict the movement of a pollutant or dissolved chemical in the subsurface to answer practical questions concerning the rate and direction of contaminant movement and the predicted concentration in solution. In a typical solute transport simulation, a dissolved chemical is introduced into a steady-state or time-varying flow field, and the fate of the chemical is tracked while undergoing physical and chemical processes such as advection, dispersion, chemical and biological reaction, or diffusion into dead-end pore space. Often, a concentration front is established that must be tracked accurately. In addition, many field investigations employ natural or introduced tracers to study the flow and transport system. These studies also require models to simulate the movement of dissolved species.

Traditional solutions to the advection-dispersion equation, such as those used in most finite-element or finite-difference flow and transport codes, are versatile and allow the simultaneous solution of multiple interacting species. One drawback of a finite-difference or finite-element solution to the advection-dispersion equation is that significant numerical dispersion may arise in the portion of a computational domain occupied by a front of rapidly varying concentration. Reducing the numerical dispersion requires either increased grid resolution or higher-order approximation methods, both of which may lead to prohibitive computational costs. Numerical dispersion affects the migration of a contaminant in a manner similar to that of actual dispersion, so it is often difficult to separate numerical from actual dispersion in complex transport simulations.

Approaches to cope with this problem include front-tracking algorithms with multiple grids (e.g., Yeh 1990 [DIRS 101501]; Wolfsberg and Freyberg 1994 [DIRS 101498]), the method of characteristics (e.g., Chiang et al. 1989 [DIRS 101384]), hybrid Eulerian-Lagrangian solution techniques (Neuman 1984 [DIRS 101463]), and particle-tracking techniques (e.g., Tompson and Gelhar 1990 [DIRS 101490]). Front-tracking algorithms solve the advection-dispersion equation in integrated form on a numerical grid while tailoring the mesh to increase the resolution of the calculation at fronts. In contrast, an Eulerian-Lagrangian technique casts the advection-dispersion equation using the total derivative, so that the advection portion of transport can be solved accurately using particle-tracking techniques or the method of characteristics, while the dispersion component of transport is solved on a finite-difference or finite-element grid using standard techniques.

Particle-tracking transport models take a fundamentally different approach. The trajectory of individual molecules or packets of fluid containing molecules are tracked through the model domain. When the fluid path lines are the model result of interest (Pollack 1988 [DIRS 101466]; Lu 1994 [DIRS 101413]), a relatively small number of particles can be used to trace the streamlines. Particle tracking is also used to simulate solute transport, such as the migration of a contaminant plume (Akindunni et al. 1995 [DIRS 101378]) or the prediction of breakthrough curves in interwell tracer experiments (Johnson et al. 1994 [DIRS 101400]). For these applications, a relatively large number of such particles must be used to obtain accurate solutions to the transport problem. Particle tracking has also been used to solve the advective portion of complex reactive transport models that simulate chemical reactions among multiple species (Fabriol et al. 1993 [DIRS 101387]).

In a typical particle-tracking algorithm, a particle is sent to a new position assuming that the magnitude and direction of the velocity vector are constant during a time step. If small enough time steps are taken, particle pathways can be tracked accurately. Dispersion is treated as a random process that diverts the particle a random distance from its dispersion-free, deterministic path. In these so-called "random walk" models (e.g., Kinzelbach 1988 [DIRS 101402]), dispersion is usually calculated stochastically, subject to a Gaussian model to reproduce the specified dispersion coefficient. The technique has also been extended by employing non-Gaussian random walk functions to represent scale-dependent dispersion (Scheibe and Cole 1994 [DIRS 101477]). Linear equilibrium sorption can be handled through the use of a retardation factor to correct the magnitude of the particle velocity.

A crucial component of most random-walk particle-tracking algorithms developed to date is the need to accurately estimate the velocity at every position in the model domain. In the context of a finite-difference or finite-element numerical code, this means that velocities at positions other than the node points of the fluid flow grid must be computed using an interpolation scheme. Many studies have proposed and studied the accuracy of different interpolation schemes, including methods developed for regular, two-, or three-dimensional finite difference grids (Schafer-Perini and Wilson 1991 [DIRS 101476]; Zheng 1993 [DIRS 101502]), for two- and three-dimensional finite-element grids (Cordes and Kinzelbach 1992 [DIRS 101385]), and for codes that employ the boundary element method for computing fluid flow (Latinopoulos and Katsifarakis 1991 [DIRS 101408]). Special techniques have been developed to handle complexities such as point fluid sources and sinks, and abrupt changes in the conductivity of the medium (Zheng 1994 [DIRS 101503]).

Unfortunately, many of the velocity interpolation schemes used in conventional particle-tracking techniques are computationally intensive, thus limiting the number of particles that can practically be used. Another drawback to traditional particle-tracking approaches is that spatial and temporal discretization often results in numerical inaccuracy in the fluid flow solution upon which velocity determinations are based. Thus, precise and time-consuming velocity interpolation schemes may not be justified in finite-difference or finite-element models. Finally, and most important for the simulation of transport in the UZ at Yucca Mountain, dual-permeability models employ overlapping continua to represent fracture and matrix flow (Zyvoloski et al. 1992 [DIRS 101026]; Zimmerman et al. 1993 [DIRS 100614]). To develop a streamline-based particle-tracking method for dual-permeability models, velocity interpolations on each continuum would have to be coupled to a transfer term that allows particles to move

from one medium to the other. This additional complexity, along with the inherent approximations associated with the dual-permeability method itself, may make precise velocity interpolation calculations of limited validity.

In this model, a particle-tracking technique is employed that can be used for transient, multidimensional finite-difference or finite-element codes. The algorithm is designed for computing solute concentration fields quickly and easily with structured or unstructured numerical grids of arbitrary complexity. Both continuum and dual-permeability formulations can be simulated. This flexibility is accomplished by extending the cell-based strategy of Desbarats (1990 [DIRS 101386]) for mapping out the path of the particle. In this method, the calculation of an "exact" pathline is replaced with a cell-to-cell migration of the particle. The mass flux from cell to cell is used directly, and no velocity interpolations are required. Since numerical solutions for fluid flow are typically mass conservative (though not necessarily accurate) the particle-tracking method automatically conserves mass.

6.4.1 Basic Methods

The particle-tracking method developed in the present study views the fluid flow computational domain as an interconnected network of fluid storage volumes. Particles travel only from cell to cell, requiring no greater resolution of the particle pathways. In this sense, the method is similar to the node-to-node routing method of Desbarats (1990 [DIRS 101386], p. 156). This simple starting point has been extended to include many different transport submodels and complex flow domains. Even though some aspects of the development that follows would appear to be applicable for steady-state, single-porosity flow fields, the extensions to the method for treating transient flow systems and dual-porosity model formulations are discussed in Section 6.4.3. The two steps in the particle-tracking approach are: 1) determine the time a particle spends in a given cell; and 2) determine which cell the particle travels to next. These two steps are detailed below.

The residence time for a particle in a cell is governed by a transfer function describing the probability of the particle spending a given length of time in the cell. Thus, this particle-tracking approach is called the RTTF method (Robinson et al. 2003 [DIRS 171674]). The schematic plots shown in Figures 6-3 and 6-4 illustrate the basis of the RTTF approach. For a cumulative probability distribution function of particle residence times, the residence time of a particle in a cell is computed by generating a random number between 0 and 1 to determine the corresponding residence time from the distribution function. In the simplest case of advective transport through the cell, there is only one possible transport time through the cell, and the function is the Heaviside function (a unit step function). However, dispersion and diffusion give rise to a distribution of transport times through the cell that must be reproduced in order to simulate these mechanisms. In the example in Figure 6-4, the advection-dispersion equation was used to generate the RTTF curve, but other transport mechanisms can be incorporated as well.

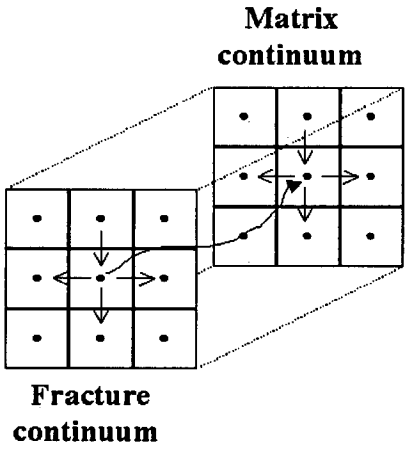

Figure 6-3. Schematic of the Cell-Based Particle-Tracking Technique

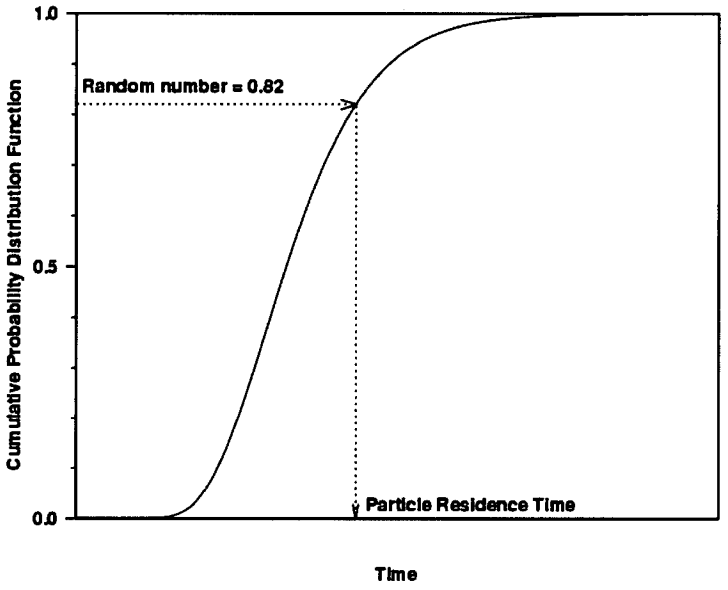

NOTE: The time axis represents the probabilistically determined residence time of a particle in the cell.

Figure 6-4. Schematic of the RTTF Technique for Determining Particle Residence Time in a Cell

If a large number of particles pass through the cell, the cumulative residence time distribution of particles in the cell will be reproduced. Particle-tracking models of single-fracture transport (Yamashita and Kimura 1990 [DIRS 101499]) have employed this approach to simulate fracture transport with diffusion into the rock matrix. From the solution of the flow field in a numerical model, the mass of fluid in the computational cell and the mass flow rate to or from each adjacent cell is computed. In the simplest case, the residence time of a particle in a cell, τ_{part}, is given by:

$$\tau_{part} = \tau_{fl} = \frac{M_{fl}}{\sum \dot{m}_{out}} \qquad \text{(Eq. 6-1)}$$

where M_{fl} is the fluid mass in the cell and the summation term in the denominator refers to the outlet fluid mass flow rates from the cell to adjacent cells. In the absence of dispersion or other transport mechanisms, the transfer function describing the distribution of particle residence times is a Heaviside function (unit step function) that is unity at the fluid residence time τ_{fl}, because for this simple case, particles entering the cell will possess this residence time. Equilibrium, linear sorption is included by correcting the particle-residence time by a retardation factor, R. Thus, $\tau_{part} = R\,\tau_{fl}$, and R is given by:

$$R = 1 + \frac{\rho_b K_d}{\theta_{fl}} \qquad \text{(Eq. 6-2)}$$

where:

K_d is the equilibrium sorption coefficient (mL fluid/g rock)

ρ_b is the bulk rock density (g rock/mL total)

θ_{fl} is the volumetric water content (mL fluid/mL total).

The use of a linear, equilibrium sorption model warrants further discussion. It is well known that the effective sorption coefficient in porous media is a function of many factors, including mineralogy, groundwater aqueous chemistry (including redox conditions), and heterogeneity at scales smaller than are considered in numerical models. Furthermore, the kinetics of the sorption reaction must be considered to ensure that the reactions are effectively at equilibrium. Despite these limitations, the K_d model is by far the most widely used sorption model in performance assessment calculations due to its simplicity and ease of use. The factors listed above do not preclude the use of this model. However, they must be considered when establishing the parameter uncertainty distribution for K_d. As long as the range of sorption coefficients used in performance assessment calculations takes into account uncertainties arising due to the factors listed here, then this approach is valid for the intended use of this model. As was the case for advection, in the particle tracking model formulation, in the absence of other transport processes, the transfer function for sorption is also a Heaviside function. Note that the method is applicable for either liquid or gas phase transport, so the generic term "fluid" is used in the definition above. However, in this report, only liquid phase transport is simulated.

Before discussing more complex transfer functions for the RTTF method, the method for determining which cell a particle travels to after completing its stay at a given cell is discussed. The approach that is consistent with the RTTF method is that the probability of traveling to a neighboring cell is proportional to the mass flow rate to that cell. Only outflows are included in this calculation; the probability of traveling to an adjacent node is 0 if fluid flows from that node to the current node. In summary, the particle-tracking algorithm is: 1) compute the residence time of a particle at a cell using the RTTF method; and 2) at the end of its stay, send the particle to an adjacent cell randomly, with the probability of traveling to a given cell proportional to the mass flow rate to that cell.

6.4.2 Dispersion

Transport processes such as dispersion can be incorporated into the RTTF particle-tracking algorithm through the use of transfer functions. For dispersion, within a computational cell, the equation for one-dimensional, axial dispersion is applied. The solution desired is the concentration-time breakthrough curve at the outlet of the one-dimensional model for a unit step change in inlet concentration. This solution represents the cumulative distribution of transport times for transport with dispersion, which is what is desired for the transfer function. The transport equation and boundary conditions for the one-dimensional, advective-dispersion equation are (Freeze and Cherry 1979 [DIRS 101173], from equation 9.9):

$$R\,\frac{\partial C}{\partial t} = D_{eff}\,\frac{\partial^2 C}{\partial z^2} - v\frac{\partial C}{\partial z} \qquad \text{(Eq. 6-3)}$$

$$C(z,t) = 0, \qquad t = 0 \qquad \text{(Eq. 6-4)}$$

$$C(z,t) = C_0, \qquad z = 0 \qquad \text{(Eq. 6-5)}$$

$$C(z,t) = 0, \qquad z \to \infty \qquad \text{(Eq. 6-6)}$$

where

C is the concentration (moles/kg fluid)

C_0 is the injection concentration (moles/kg fluid)

v is the flow velocity (m/s)

D_{eff} is the effective dispersion coefficient (m^2/s), given by $D_{eff} = \alpha v$, where α is the dispersivity of the medium (m).

Here the molecular diffusion coefficient is ignored, since in general it is much smaller than the flow dispersion component of D_{eff}. A nondimensional version of Equation 6-3 can be obtained by the following transformations: $\hat{C} = C/C_0$, $\hat{z} = z/L$, and $\hat{t} = vt/R\,L$, where L is the flow path length. The solution to Equations 6-3 to 6-6 is obtained after manipulation of Freeze and Cherry (1979 [DIRS 101173], p. 391, Equation 9.5), yielding:

$$\hat{C} = \frac{1}{2}\left[erfc\left(\frac{\sqrt{Pe}\left(1-\hat{t}\right)}{2\sqrt{\hat{t}}}\right) + e^{Pe}\,erfc\left(\frac{\sqrt{Pe}\left(1+\hat{t}\right)}{2\sqrt{\hat{t}}}\right)\right] \qquad \text{(Eq. 6-7)}$$

where Pe is the Peclet number (dimensionless), $Pe = vL/D_{eff} = L/\alpha$. This solution was obtained from Freeze and Cherry by substituting the definitions of Pe and $\hat{t}$ into the corresponding terms of the Freeze and Cherry equation and performing the needed algebra.

The use of this solution in the RTTF particle-tracking method requires that the transport problem be advection-dominated, such that during the time spent in a computational cell, solute would not tend to spread a significant distance away from that cell. Then, the approximate use of a distribution of times within a single cell will be adequate. Quantitatively, the criterion for applicability is based on the grid Peclet number $Pe_g = \Delta x / \alpha$, where Δx is the characteristic length scale of the computational cell. Specifically, for cells where the Peclet number would be less then one, the code performs the calculation assuming a value of 1, which effectively reduces dispersivity for these cells. Note that in contrast to conventional numerical solutions of the advective-dispersion equation, coarse spatial discretization is helpful for satisfying this criterion. Of course, the mesh spacing must still be small enough to provide an accurate flow solution. Highly dispersive transport invalidates the assumptions of the RTTF particle-tracking technique. When dispersion coefficients are large, accurate solutions to the advective-dispersion equation are easily obtained by conventional finite-difference or finite-element techniques, so these techniques should be used instead under these circumstances.

For multidimensional flow systems, the dispersion model developed for one-dimensional systems can be extended to include dispersion coefficient values aligned with the coordinate axes. For this case, the flow direction is determined by the vector drawn from the nodal position of the previous cell to the current cell, and the dispersivity for this flow direction is computed from the equation for an ellipsoid:

$$\alpha = \frac{L}{\sqrt{\Delta x^2 / \alpha_x^2 + \Delta y^2 / \alpha_y^2 + \Delta z^2 / \alpha_z^2}} \qquad \text{(Eq. 6-8)}$$

where L now represents the distance from the previous cell to the current cell, Δx, Δy, and Δz are the distances from one grid point to the other in the three coordinate directions, and α_x, α_y, and α_z are the longitudinal dispersivities in the three coordinate directions. The RTTF particle-tracking technique cannot be simply formulated with a longitudinal and transverse dispersion coefficient model with the tensor aligned with the flow direction because the flow rates between cells are defined rather than the actual flow velocity at a position. For a dispersion model aligned with the flow direction, a random-walk particle-tracking method such as that of Tompson and Gelhar (1990 [DIRS 101490]), also implemented in the SZ particle-tracking algorithm of FEHM, or a conventional finite-element or finite-difference solution to the advection-dispersion equation, such as the reactive transport solution module in FEHM, should be used instead.

The numerical implementation of this technique requires the determination of the dimensionless time $\hat{t}$ in Equation 6-7 for a randomly determined value of the dimensionless concentration $\hat{C}$. This determination is accomplished numerically in the particle-tracking code by fitting Equation 6-7 at selected values of Pe between 1 and 1,000 using a piecewise continuous series of straight lines spanning the entire range of values. Then, the value of $\hat{t}$ at an arbitrary value of Pe is computed by linear interpolation between values determined at the Peclet numbers that bracket the actual value. This technique, involving a simple search for the correct type curves, followed by the calculation of two values of $\hat{t}$ and an interpolation, is much more

computationally efficient (about a factor of two in CPU time) and robust than an iterative approach to the exact solution using Newton's method. Solutions of adequate accuracy (less than 1% root mean squared error; see LANL 2003 [DIRS 166306] tests titled "Tests of Cell-Based Particle Tracking Model") are easily obtained using this linear-interpolation method. This error is trivial compared to the uncertainties being propagated through the model. Therefore, this implementation is adequate for the purposes of the model.

6.4.3 Fracture/Matrix Interaction Submodel

In a dual-permeability system, the transfer of solute mass between fractures and matrix can occur via advection, where fluid movement carries solute from one medium to the other, and matrix diffusion, where molecular diffusion transports mass. Matrix diffusion has been recognized as an important transport mechanism in fractured porous media (e.g., Neretnieks 1980 [DIRS 101148]; Robinson 1994 [DIRS 101154]). For many hydrologic flow systems, fluid flow is dominated by fractures because of the orders-of-magnitude larger permeabilities in the fractures compared to the surrounding rock matrix. However, even when fluid in the matrix is completely stagnant, solute can migrate into the matrix via molecular diffusion, resulting in a physical retardation of solute compared to pure fracture transport. This effect has recently been demonstrated on the laboratory scale by Reimus (1995 [DIRS 101474]), and on the field scale both by Maloszewski and Zuber (1991 [DIRS 146957]) and in the SZ at Yucca Mountain by Reimus et al. (1999 [DIRS 126243]). In the UZ at Yucca Mountain, dual-permeability models allow fluid to migrate in both fractures and the matrix. An additional process that allows solute to transport between the continua is molecular diffusion. The distribution of transport times through such a system is a complex function of the relative velocities in the two media, the advective flux between the media, the spacing between flowing fractures, matrix diffusion coefficients, and sorption. This section describes the submodel developed to obtain transfer functions suitable for use in dual-permeability systems.

For transport in a dual-permeability system at the field scale, it is important to recognize that the flow model consists of one matrix grid cell for each fracture cell. However, important processes associated with flow and transport occur at scales smaller than those considered in the mountain-scale UZ model, particularly in the immediate region of the matrix adjacent to each flowing fracture. Therefore, the incorporation of fracture-matrix interactions into the model is in essence an upscaling problem. The goal of this development is to utilize a suitable idealized system that captures, at the small scale, important transport processes, and allows this small-scale behavior to be simply upscaled for inclusion in the large-scale model. This model report will demonstrate that this upscaling method will allow testing of ACMs for the f/m interaction model for transport.

To accomplish the upscaling within the particle tracking transport model, the transfer function approach is used to construct an idealized transport model at the small scale that allows the transfer functions to be tabulated. In a dual-permeability system, transport behavior is vastly different depending on whether solute starts in the fracture or in the matrix. Therefore, the transfer function method is adapted in the UZ transport abstraction model to accommodate dual-permeability behavior. The approach consists of using transfer functions to determine both the residence time in a cell, and to determine whether the particle enters the next cell in the fractures or the matrix. In this way, the combined fracture and matrix system will be treated as a unified

medium in which there is a distribution of transport times depending on whether the particle enters the cells in the fracture versus the matrix. The transfer functions themselves (described below and in Appendix C) are computed based on an idealized f/m transport model with parallel flow in the fractures and matrix. The choice of a parallel fracture model for developing the matrix diffusion submodel is for convenience and due to the fact that information does not exist to warrant more complex fracture geometries. The steps of the algorithm are as follows (the algorithm starts with a known particle location, either in the fracture or matrix continuum):

Step 1. Determine probabilistically whether the particle should move to the other medium due to advective flux to that medium

Step 2. Determine probabilistically whether the particle will leave this cell via the current medium or the other medium

Step 3. Use the conditional transfer function to determine probabilistically the residence time of the particle

Step 4. Determine probabilistically using the relative total flux to adjacent nodes which cell the particle moves to next (whether it starts in the fracture or matrix continuum in the next cell has been determined previously in Step 2).

This approach handles the combined fracture and matrix continua as a single porous medium through which mass travels, and apportions the particles to each continuum according to the diffusive and advective fluxes defined by the flow field and the transport parameters. In the most general case, the dual-permeability flow model at the mountain scale prescribes a net flow through the fracture continuum, a net flow through the matrix continuum, and a fracture to matrix (or matrix to fracture) fluid flux. To implement this algorithm and allow the transfer function to be computed readily, Step 1 takes the fracture-matrix advective flux term and applies it immediately when the particle enters the cell. Then, after potentially shifting the particle from one medium to the other via advection (with no increase to the transport time), the subsequent transfer functions are based on parallel flow in the two continua with no flux between the continua. This approach, which amounts to a form of upwinding of the fracture-matrix fluid flux term, simplifies the transfer function process by eliminating the need for an additional variable, the fracture-matrix advective flux, in the construction of the transfer function curves. Instead, a probability p_{fm} of the particle transferring to the other medium (Step 1) is assigned:

$p_{fm} = 0$ if the fracture-matrix flux term f_{fm} is into the medium in which the particle already resides, or

$p_{fm} = f_{fm} / f_{out}$, where f_{out} is the total flux out of the continuum in which the particle currently resides, either to adjacent cells within that continuum or to the other continuum.

Step 2 accounts for the fact that there is a finite probability that, due to matrix diffusion, the particle will leave the cell through the other medium regardless of where it starts. In the transfer function approach, solute mass is introduced in the model system (the two-dimensional) in either

the fracture fluid or the matrix fluid. For the general case of water flow through both the fracture and matrix, mass leaves the DFM via either medium. Therefore, conditional transfer functions must be generated to obtain the probabilities in Step 2. That is, for mass injected with the fracture fluid entering the discrete fracture submodel, there is a breakthrough curve for mass leaving the model via the fracture fluid, and a similar breakthrough curve for mass leaving via the matrix fluid. Similarly, there are two breakthrough curves for mass injected with the matrix fluid. The plateau values attained for a given transfer function curve represents the probability of leaving via a particular medium in Step 2. In other words, the probability of a particle leaving via a given continuum equals the steady state solute mass flux (the plateau of the transfer function curve) divided by the total mass flux through the DFM. This step provides a way to assign probabilities for moving particles between the media via diffusion in a system in which water flows through both continua.

Once Step 2 is completed using the steady state solute mass flux derived from the conditional transfer functions, the selection of the transfer function to apply to obtain the residence time for Step 3 is also determined. This part of the method is identical to that described previously, which is to generate a random number between 0 and 1 and determine the particle residence time from the transfer function.

Finally, Step 4 routes the particle to the appropriate connecting cell in the finite volume domain, as described earlier. If the particle is determined to enter an adjoining cell via the fracture continuum, then the internodal fluxes associated with the fractures are used to define the probabilities of traveling to each connected fracture cell. Similarly, for transport to an adjoining matrix cell, matrix fluxes are used.

The process employed in this model to obtain the transfer functions for the dual-k transport submodel consists of a series of numerical simulations on the idealized model system shown in Figure 6-5. Because each grid block in the mountain-scale model possesses different hydrologic and transport parameters, a procedure for deriving a nondimensional form of the submodel is required to make the method practical. Appendix C presents the derivation of the nondimensional model, and presents the method for generating the transfer function curves. In summary, there are three nondimensional groups that, if specified, fully capture the range of behavior of the submodel:

$$p_1 = \frac{D_m \tau_f R_f}{B^2 R_m} \qquad \text{(Eq. 6-9)}$$

$$p_2 = \frac{D_m \tau_f \theta_m}{bB\theta_f} \qquad \text{(Eq. 6-10)}$$

$$p_3 = \frac{\tau_f R_f}{\tau_m R_m} \qquad \text{(Eq. 6-11)}$$

In these equations, D_m is the effective diffusion coefficient; τ_f and τ_m are the fluid transport times in the fracture and matrix, respectively; R_f and R_m are the retardation factors in the

fracture and matrix, respectively; B is the half-spacing between flowing fractures; b is the fracture half-aperture; and θ_f and θ_m are the volumetric water contents of the fracture and matrix, respectively. For a given parameter vector (p_1, p_2, p_3), there is a unique set of conditional transfer function curves of the form $\hat{C}$ versus $\hat{t}$, where $\hat{C}$ is the normalized breakthrough curve for the nondimensional time $\hat{t}$ given by

$$\hat{t} = \frac{t}{R_f \tau_f} \qquad \text{(Eq. 6-12)}$$

The set of conditional transfer function curves consists of a total of four normalized curves for each (p_1, p_2, p_3): mass input in fracture, output in fracture; mass input in fracture, output in matrix; mass input in matrix, output in fracture; and mass input in matrix, output in matrix. This capability for sampling conditional transfer functions associated with the fracture-matrix interaction dual-k submodel of the UZ transport abstraction model has been implemented and documented in FEHM V2.21 (LANL 2003 [DIRS 165741]). For details on the generation of the transfer function curves and other important implementation details, see Appendix C.

The final issue associated with implementing the transfer function approach is the means by which the idealized model of Figure 6-5 is simulated. In this abstraction model, two ACMs are implemented to simulate different types of f/m interaction conceptualizations. In the first ACM, called the DFM formulation, a two-dimensional numerical grid is used with fine discretization in the matrix close to the fracture. This allows sharp gradients in concentration close to the fracture to be captured. The second ACM, called the dual-k formulation, uses a numerical grid with one finite volume cell that is paired with each fracture grid cell. This type of discretization is identical to that used in the dual-k transport formulation of the T2R3D process model (BSC 2004 [DIRS 164500]). It could be argued that the DFM formulation more accurately captures the small-scale transport processes. However, the dual-k formulation has the advantage of consistency with the model formulation on which the flow simulations are based. Furthermore, as a practical matter, the three-dimensional process model uses a dual-k formulation for transport, so, for benchmarking purposes, the dual-k approach is more likely to yield comparable results.

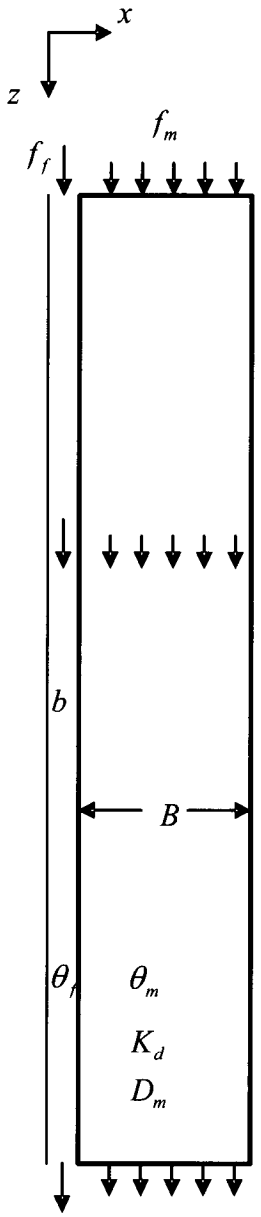

Figure 6-5. Schematic of the Fracture Transport Submodel

The advantage of the transfer function approach used in the particle tracking abstraction model is that both conceptualizations can be implemented easily by using either the DFM or dual-k model grid to generate the transfer function curves. Then, when running the abstraction model, the user selects one or the other set of transfer function curves, and all other input remains the same. However, due to the fact that process model validation activities were performed based on a dual-k model, the dual-k transfer functions should be used in TSPA analyses. Additional details on the behavior of these two f/m interaction submodels are presented in Appendix C.

6.4.4 Multiple Radionuclides with Decay/Ingrowth

The FEHM code (Zyvoloski et al. 1997 [DIRS 100615]) allows particles to decay with or without the production of the daughter product. For multiple species with decay chains, the code

uses the approach outlined below to determine the number of decayed particles, and the code performs the bookkeeping needed to keep track of the locations and numbers of each type of radionuclide. These multiple species can each have their own transport parameters such as sorption and diffusion coefficients.

For decay-ingrowth simulations with time-dependent release of tracer particles, the computational burden increases dramatically with the number of particles in the field. For example, the decay-ingrowth calculation for species *i* decaying into species *j* at a decay rate λ is:

$$N_j = \sum_{m=1}^{N_i} \{1 - \exp[-\lambda(t - t_m)]\} \qquad \text{(Eq. 6-13)}$$

where N_j is the number of particles of species *j* decayed from species *i*, N_i is the number of particles of species *i*, and t_m is the time at which the *m th* particle is injected into the system. If 500,000 particles of species *i* are injected into the system, then at each time step, the number of mathematical operations for ingrowth calculations alone are around 2.5 million. For a simulation time period of 1 million years, the typical calculation requires about 100 time steps. Therefore, the total number of operations for ingrowth calculations will reach 0.25 billion, and for site-scale simulations, the use of Equation 6-13 would be extremely inefficient.

To reduce the computational burden in simulations, the decay-ingrowth calculation in Equation 6-13 is approximated with an integral by assuming that particles are injected into the system uniformly in time domain. Multiplying both sides of Equation 6-13 by Δt, the average injection time interval between particles, and approximating Equation 6-13 with respect to $t - t_m$:

$$N_j \approx \left\{(\tau_1 - \tau_2) + \frac{1}{\lambda} \bullet [\exp(-\lambda\tau_1) - \exp(-\lambda\tau_2)]\right\} \Big/ \Delta t \qquad \text{(Eq. 6-14)}$$

where $\tau_1 = t - t_1$ and $\tau_2 = t - t_{Ni}$, t_1 is the time at which particle injection starts, t_{Ni} is the time of the Nth injected particle, and t is the time at which the decay-ingrowth calculation is carried out. The use of Equation 6-14 reduces the number of operations within one time step from millions of operations to just 10, which greatly increases the speed of simulations. Validity of this approach is demonstrated in Figure 6-6.

The accuracy of the integral approach depends on the number of particles and their release history. In general, the use of a greater number of particles increases the accuracy. With respect to release, for the same number of particles, a simulation with a constant release rate will exhibit less error than a time-varying release such as a shorter pulse. If the release rate changes with time, the release period is divided into segments so that within each segment the release rate can be treated as a constant.

Validity of this approach was demonstrated in detail by *Validation Test Plan (VTP) for the FEHM Application Version 2.21* (LANL 2003 [DIRS 166306]). A FEHM test run from the cited document is summarized in this report to demonstrate the capability of FEHM decay-ingrowth model. Simulation results from the FEHM particle-tracking model with decay and ingrowth

were verified against results from a semi-analytical solutions for a 4 species chain decay-ingrowth model, CHAIN (van Genuchten 1985 [DIRS 146961]). The method of comparison for the run is a visual comparison of the plotted results.

For all comparisons of FEHM with the semi-analytical solution for decay-ingrowth simulations, a flow system was developed with the following attributes (LANL 2003 [DIRS 166306]):

- Saturated steady-state flow in a one-dimensional system
- Porosity of 0.3
- Average pore-water velocity was 1.05192×10^{-4} m/year
- Solute with constant injection concentration of 1.0 mol/L released from 0 to 5,000 years at origin x=0. Breakthrough data were collected at x=1 m down stream
- FEHM grid resolution: 0.005 m
- Longitudinal dispersivity of 0.005 m.

In the test case, a pseudosequential decay chain is simulated with species $1 \rightarrow 2 \rightarrow 3 \rightarrow 4$, with half lives for species 1 through species 4 of 10,000 years, 3,000 years, 10,000 years, and 4,000 years, respectively. The transport process was dominated by advection and dispersion only with a grid Peclet number of 1.0. In the FEHM simulations, the 5,000-year release period was divided into 50 segments so that each segment corresponds to 100 years. Within each segment, 10,000 particles were injected into the system uniformly over the 100-year period for species 1. There was no source release for the other species, which are generated by the decay-ingrowth model. The retardation factors for species 1 through species 4 were 1.0, 1.0, 1.9, and 1.001, respectively.

The FEHM and CHAIN breakthrough curves are plotted in Figure 6-6. In general, good agreement was observed between FEHM and CHAIN curves. Combined with the suite of validation runs documented in Section 7 of this report, this simulation demonstrates that the particle tracking model accurately handles decay chains and, thus, is suitable for use in simulating multiple radionuclides in the UZ transport abstraction model.

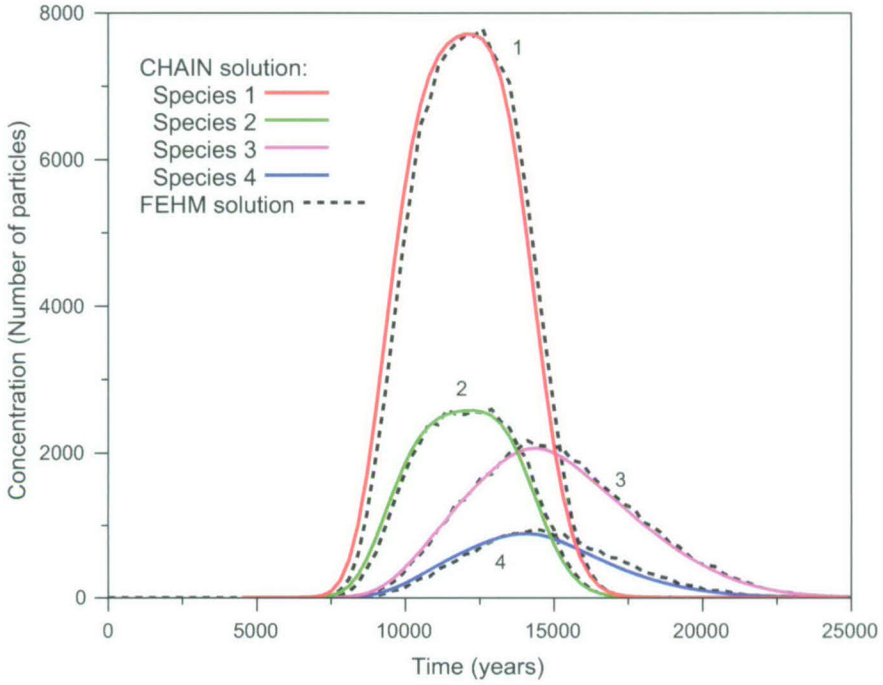

NOTE: Peclet Number = 1.0 (used for comparative purposes only; taken from Figure 59 in LANL 2003 [DIRS 166306].

Figure 6-6. Comparison of Software CHAIN and FEHM Transport Results for a Case with a 4-Member Decay-Ingrowth CHAIN and a Retardation Factor of 1.9 for Species 3

6.4.5 Colloid Transport

Colloids are divided into three basic types: true colloids, primary colloids, and pseudocolloids:

True colloids—originate from the hydrolysis and polymerization of actinide ions dissolved in solution. Degradation of commercial SNF may form true colloids (e.g., plutonium oxides and hydroxides) consisting of americium, plutonium, and rare earths, but these are anticipated to sorb to iron oxide/oxyhydroxides, forming a "pseudocolloid". However, the solution chemistry and temperature in the waste package and EBS prevents significant introduction of true colloids to the environment (BSC 2005 [DIRS 174290], Section 6.3.1).

Waste form colloids—originate from the nucleation of corrosion products of defense high-level glass waste. These colloids are composed of smectite (clay) and have plutonium and americium embedded in the colloid structure (BSC 2005 [DIRS 174290], Section 6.3.1). Colloids with embedded radionuclides will be termed "irreversible colloids" for the purposes of radionuclide transport due to the strong, permanent association between the colloid and the radionuclides.

Pseudocolloids—consist of nonradioactive particles that may sorb radionuclides. Colloids with radionuclides sorbed to their surfaces will be called "reversible colloids" for the purposes of radionuclide transport because the radionuclides can attach and detach from the colloid. Note that clay colloids formed from defense high-level waste glass may interact with radionuclides as irreversible and/or reversible colloids. Pseudocolloids are distinguished as either natural groundwater colloids or corrosion product colloids. Corrosion product colloids originate from

the corrosion of steel components in the engineered barrier system and defense high-level waste glass. Colloids formed from steel corrosion products are composed of a mixture of hydrous ferric oxides that are modeled as hematite (BSC 2005 [DIRS 174290], Section 6.3.1). Defense high-level waste glass corrosion produces colloidal smectite, as discussed for waste form colloids. Natural groundwater colloids are generated by natural geochemical processes in the rock that transform rock minerals into clay minerals. For the purposes of modeling colloid transport, these clays are treated as smectite (BSC 2005 [DIRS 174290], Section 6.3.1).

Irreversible colloids—are treated in the UZ transport abstraction model as a particle with zero diffusion (discussed below and in Section 6.5.5). In addition, due to colloid size, these particles preferentially move through fractures as a result of the size exclusion model (see below and Section 6.5.10). Because the radionuclides are permanently attached to the colloids, colloid filtration effectively removes the associated radionuclides from the system (see below and Section 6.5.9). Transport of these colloids in the fractures are retarded as a result of colloid interactions with the rock which is described with a retardation factor (see below and Section 6.5.13). Finally, a fraction of the irreversible colloid component will not be retarded; this fraction is termed the "irreversible fast colloids" (Section 6.5.13). Isotopes of plutonium and americium are affected by irreversible colloid transport (BSC 2005 [DIRS 174290], Section 6.3.1).

Reversible colloids—differ from irreversible colloids in the UZ transport abstraction model because the radionuclide may detach from a colloid, becoming an aqueous species, and subsequently may reattach to a different colloid. Because of this, colloid filtration is not included in the processes affecting reversible colloids. As for irreversible colloids, reversible colloids have zero diffusion and preferentially move through the fractures due to size exclusion. The effective strength of radionuclide associations with reversible colloids is a function of both the intrinsic sorptive capacity of a given radionuclide on a colloid surface, expressed as a sorption coefficient, and the mass density of colloids in the water (see below and Section 6.5.12). Isotopes of plutonium, americium, thorium, protactinium, and cesium are affected by reversible colloid transport (BSC 2005 [DIRS 174290], Section 6.3.3.1).

For colloid-facilitated transport involving reversible colloid species, the transport equations for matrix diffusion, with either the semi-infinite or finite fracture spacings, can be simply revised. The expression for transport for contaminant on colloids is analogous to Equation 6-3 earlier (Freeze and Cherry 1979 [DIRS 101173], from equation 9.9):

$$R_{coll}\frac{\partial C_{coll}}{\partial t} = D_{eff}\frac{\partial^2 C_{coll}}{\partial z^2} - v\frac{\partial C_{coll}}{\partial z} \qquad \text{(Eq. 6-15)}$$

where D_{eff} is the same as for an aqueous solute and R_{coll} is the colloid retardation factor. The basis for not including colloid matrix diffusion is that the estimated values for diffusion coefficient of colloids from *Radionuclide Transport Models Under Ambient Conditions* (BSC 2004 [DIRS 164500], Table 6-8) are significantly lower than values for aqueous species presented in Section 6.5.5 of this report. Rather than incorporating an additional parameter in the model, it is conservatively assumed that colloids travel via advection and reversible retardation without matrix diffusion.

To estimate retardation of colloids in the fracture continuum, field experiments at the C-wells complex near Yucca Mountain were examined, in which transport of microspheres was used as an analogue for colloids. The microsphere breakthrough curves were fit to forward and reverse filtration rates (DTN: LA0002PR831231.003 [DIRS 144462]). These rate constants were then used to calculate a retardation factor for colloid transport through saturated fractured rock (BSC 2004 [DIRS 170006]; DTN: LA0303HV831352.002 [DIRS 163558]). For compatibility with this analysis of field data, this approach is adopted in the numerical model as well. The governing equation for the corresponding dissolved contaminant moving in fractures with interactions with matrix blocks but without decay can be derived from Equation (1) of (Sudicky and Frind 1982 [DIRS 105043]) and re-written as:

$$R_f \frac{\partial C}{\partial t} = D_{eff} \frac{\partial^2 C}{\partial z^2} - v \frac{\partial C}{\partial z} - \frac{q}{b} \qquad \text{(Eq. 6-15a)}$$

where R_f is the retardation factor of the dissolved contaminant, b is half of the fracture aperture, and q (mass per time per unit area) is the mass exchange rate through fracture-matrix interface.

At this stage, a relation between C_{coll} and C is required. Most measurements of sorption onto bulk rock and colloids are interpreted using an equilibrium sorption model. For compatibility with the data collected on sorption, this approach is adopted in the numerical model as well. Therefore, the parameter used in the model to capture this behavior is the equilibrium sorption parameter $K_c = C_{coll} / C_{fluid}$, where C_{coll} is the radionuclide concentration residing on the colloids (moles radionuclide on colloid per kg fluid), and C_{fluid} is the corresponding concentration in the fluid phase (moles aqueous radionuclide per kg fluid). Combining Equations 6-15 and 6-15a, and making use of the relation $K_c = C_{coll} / C$:

$$\left(\frac{R_f + K_c R_{coll}}{1 + K_c} \right) \frac{\partial C}{\partial t} = D_{eff} \frac{\partial^2 C}{\partial z^2} - v \frac{\partial C}{\partial z} - \frac{q}{b(1 + K_c)} \qquad \text{(Eq. 6-16)}$$

This equation can be recognized as being analogous to the matrix diffusion model of Sudicky and Frind (1982 [DIRS 105043], Eq. 1), with the exception of a different term preceding the time derivative and a modified denominator of the term involving diffusive flux, q. Mathematically, this implies that the transport equation for matrix diffusion can be revised to include colloid facilitated transport by replacing the half-aperture, b, by:

$$b_{coll} = (1 + K_c) b \qquad \text{(Eq. 6-17)}$$

and the retardation factor in the fracture by:

$$R_{f,coll} = \frac{R_f + K_c R_{coll}}{1 + K_c} \qquad \text{(Eq. 6-18)}$$

These relationships are built into the FEHM particle-tracking code, so that the additional terms K_c and R_{coll} are provided as inputs. Note that to simulate a radionuclide irreversibly attached to

colloids, one should set a large value of K_c (say, 10^{20}). Thus, for $R_f = 1$, the value used in UZ abstraction model simulations (Section 6.5.8), the effective retardation factor reduces to R_{coll}. In the more general case, either a retarded or unretarded colloidally bound radionuclide may be simulated by setting R_{coll} to a number greater than or equal to 1, and the model uses Equation 6-18 to compute the effective retardation factor in the presence of colloids.

In addition to the transport of radionuclides bound to colloids, there are several mechanisms related to the migration of the colloids themselves that can be simulated in the model. Above, the retardation factor for colloid migration R_{coll} was introduced. In addition, the model parameterization provides a means for accounting for colloid size and surface charge effects. When the colloid size and/or surface properties preclude their transport into a porous medium, size exclusion and/or filtration can occur. In the particle-tracking module, models have been implemented for these processes. For advective flow from fracture to matrix in the dual-permeability model, a size-exclusion model is implemented whereby colloids can remain in the fracture in proportions greater than the relative flow rate entering the matrix. A size exclusion parameter $f_{coll} \leq 1$ is defined such that the probability of particles entering the matrix due to advective transport is multiplied by this factor. Therefore, complete exclusion from the matrix is obtained by setting $f_{coll} = 0$, whereas aqueous solute behavior is retained by setting $f_{coll} = 1$. Filtration, resulting in complete immobilization of the particle, can also be simulated at specified interfaces within either the fracture or matrix continua. To invoke this mechanism, a filtration factor f_{filt} at an interface (the finite element connections between two specified zones in an FEHM simulation) is defined. If a particle is slated to pass from one zone to the other via advective transport, f_{filt} is the probability the particle continues moving, $(1 - f_{filt})$ is the probability that it is irreversibly removed by filtration.

When using the size exclusion and filtration options, a word of caution is warranted. Colloid simulations are typically used to provide a mechanism for radionuclides to travel in the water bound to colloids. Filtration renders the colloids immobile, which, in reality, only renders the radionuclide immobile if it is irreversibly bound to the colloid. When the radionuclide is only weakly sorbed to the colloid, the filtration option will artificially remove radionuclide mass from the system, resulting in a nonconservative simulation. In addition, size exclusion is not used for reversible colloid-facilitated radionuclide transport because this transport method relies on a constant colloid concentration throughout the fractures and matrix (see Equation 6-27). If size exclusion were included, the effects on colloid concentrations between the fractures and matrix would need to be addressed. Therefore, the size exclusion and filtration options must only be invoked for irreversibly bound radionuclides or when simulating colloid tracer experiments.

6.4.6 Particle Sources and Sinks

There are two methods for introducing particles into the flow system: particles are (1) either injected with the source fluid entering the model domain or (2) released at a particular cell or set of cells. The first method is used to track source fluid as it passes through the system. The number of particles entering with the source fluid at each cell is proportional to the source flow rate at that cell, which is equivalent to injecting fluid with a constant solute concentration. For

Method 2, an arbitrary number of particles are released at each specified cell, regardless of the source flow rate. In the present application, Method 2 is used to input particles, which are used to represent radionuclide mass into the system at the repository level.

Within Method 2, there are various ways to input a time-varying source of particles. For stand-alone simulations, the particles are inserted at a constant rate for a specified duration. There is also an option, used when the FEHM code is coupled with GoldSim (BSC 2003 [DIRS 161572]), to input a time-varying and spatially varying source mass flux into the model. The details of the method for accepting complex sources of multiple radionuclides from the EBS model are discussed in the next section.

When fluid exits the model domain at a sink, the model treats this flow as another outlet flow from the cell. The decision of whether the particle leaves the system or travels to an adjacent cell is then made on a probabilistic basis, just as though the fluid sink were another connected cell. Thus, the complexities discussed by Zheng (1994 [DIRS 101503]) for handling a so-called weak sink are avoided in the RTTF particle-tracking model.

6.4.7 EBS Random Release Model for Radionuclide Source Terms

This section discusses the implementation of the interface between the EBS and the UZ transport abstraction models, describing the way in which released radionuclide mass from the EBS enters the UZ. In broad overview, the radionuclides that are released from the EBS are represented in the FEHM abstraction model as particles. Each particle introduced in FEHM represents a given mass. FEHM converts the mass from the GoldSim EBS abstraction model to a specific number of particles, with a mass conversion factor that allows for the translation from mass to particles. At each time step, the mass to particle conversion factor is computed based on the remaining simulation time and the available memory, so that a sufficient number of particles can be applied to each radionuclide, subject to total memory constraints on the computer. The code uses the selected conversion factor to calculate the number of particles to be injected at the current time step. The conversion factor times the input mass in moles gives the number of particles to be tracked. The molecular weight for each species is also tracked. The code uses the molecular weight and the conversion factor to convert between mass and particles. During transport through the model, each particle has an attribute that specifies the radionuclide mass associated with each particle, so that when that particle leaves the model, the correct mass is recorded. Particles for radionuclides that decay to stable isotopes are removed from the simulation after decay. Particles that decay to a daughter radionuclide being tracked in the simulation are converted to the decay product by tracking the species identifier asssociated with the decay product. When a particle leaves the UZ, it is converted back to radionuclide mass before being returned to GoldSim. In this way, mass is conserved exactly at the EBS-UZ and UZ-SZ interfaces of the TSPA-LA model. The algorithm for determining the conversion factor is based on input that the user adjusts to effectively use the available memory on a particular computer. Details on the inputs available to adjust the memory utilization are presented in *Software Code: FEHM* (LANL 2003 [DIRS 165741]).

The remainder of this section describes the algorithm for apportioning the particles to different locations within the repository domain to simulate the spatial and temporal distribution of radionuclide releases from the EBS. The development of "bins" of similar release behavior for

the TSPA-LA model is presented in Section 6.5.15. If waste packages containing high-level radionuclide material in the repository eventually fail due to corrosion, the process will almost certainly be variable in both space and time. At early times, a few packages may fail, releasing radionuclides into the UZ. At later times, a greater number of packages may fail. In Viability Assessment calculations (DOE 1998 [DIRS 100547], Figure 4-10), releases from the EBS to UZ were spread over the entire repository subregions. Such treatment of the EBS release could result in significant artificial dilution of the UZ transport source term. In reality, waste packages may not fail uniformly in space and time. Rather, a few waste packages may fail at early times, while others may fail gradually over longer time periods. An EBS random release model was developed in FEHM to allow the model to simulate early failed packages and time- and spatially-variable radionuclide releases.

To begin, a repository is defined consisting of N_large subregions. Each subregion contains certain number of waste packages. Initially, M_fine packages fail at locations designated by package x-y locations (x,y). The M_fine failed packages release radionuclides at a mass flow rate of M_flux_i, where i is the i^{th} failed package.

With time, packages fail in the subregions of the repository. At each time step, there are a certain number of failed packages in each subregion i. The mass flux released from those packages is denoted as N_large_flux for the i^{th} subregion. In this model, the release nodes in the numerical grid for the failed packages are randomly selected from the available repository nodes within that subregion to mimic the failure process of the waste packages. The mass release of M_fine packages is separated from those of the other failed packages.

To simulate the impact of the EBS random release on system performance at the Yucca Mountain site, the FEHM EBS random release model was developed to perform the following tasks:

- Locate the M_fine early failed package nodes in repository subregions based on given failed package coordinates. If no node matches a given coordinate, then select the nearest node to the given coordinate. Note that in the current version of the TSPA-LA model, the M_fine user option is not used. However, because it is still in the code, the GoldSim (BSC 2003 [DIRS 161572]) calling program passes M_fine = 0 to FEHM. This situation (where the M_fine option is not used) is discussed in more detail in the following paragraphs.

- Randomly select the failed package nodes in the designated subregion i.

- Release particle into the selected fracture or matrix nodes based on the fracture flow fraction data passed from EBS.

For a species, a particle can be released into a fracture node or a matrix node. The probability of the particle being released into the fracture node is proportional to the fracture fractional flow data from EBS. At run time, a random number is generated for each particle, if the random number is smaller than the fracture fractional flow data, then the particle will be released into the selected fracture node. Otherwise, the particle will be injected into the matrix node corresponding to the selected fracture node.

From FEHM particle-tracking subroutine *part_track*, subroutine *getrip* is called to determine the particle release locations. First, the subroutine obtains information passed by GoldSim (BSC 2003 [DIRS 161572]) in an input one-dimensional array called in[ ]. The structure of the in[ ] array is shown in Table 6-2.

The algorithm used in FEHM EBS random release model is summarized in Figure 6-7, the flow chart of the EBS random release model.

Table 6-2. The Structure of the in[ ] Array Passed to FEHM from GoldSim

Array Index	Index Variable	Array Data	Data Length
1		Time	1
2		Flow field index	1
3		Parameter index	1
4		rseed – random number seed for the particle tracking residence time calculations	1
5		rseed_release – random number seed for the release location determination	1
6		Flag for fractional flow data – if 1, then fractional fracture data are provided to partition particles probabilistically in either the fracture or matrix	1
7		M_fine, number of early failed packages	1
8		Coordinates (x,y values) of early failed packages	M_fine * 2
8+(2*M_fine)	index_N_large	N_large, number of repository sub-regions	1
index_N_large + 1		List number of failed packages in each sub-region	N_large
index_N_large + N_large + 1	index_N_species	Number of species or the product of number of species and N_large	1
index_N_species + 1		nflow_frac, fraction of the releases into the fractures for each species. Optional input default value: 1	N_large * N_species
index_N_species + N_large*N_species+1[(a)]	index_in_flag	Flag for mass input, 0 = no mass input, 1 = mass input	1
index_in_flag + 1	index_in_buffers	Number of input buffers (M_fine + N_large)	1
index_in_flag + 2	index_out_buffers	Number of output buffers	1
index_out_buffers + 1	index_mass	Mass release for each species during the current time step. Values are passed first for the early failed packages for all species from the first releasing node to the M_fine th node. Then, from the first sub-region in the N_large th sub-region (M_fine + N_large) * N_species.	(N_large+ M_fine)* N_species

NOTE: Array Index is the numbered start position of data in[ ] variable sized array for GoldSim [DIRS 161572]. Array Variable contains the appropriate value pointing to the start position of the indicated Array Data.

[(a)] This array index formula assumes array in[6]=1. If not (i.e., if fractional releases into the fractures are not being input), this array index is index_N_species + 1

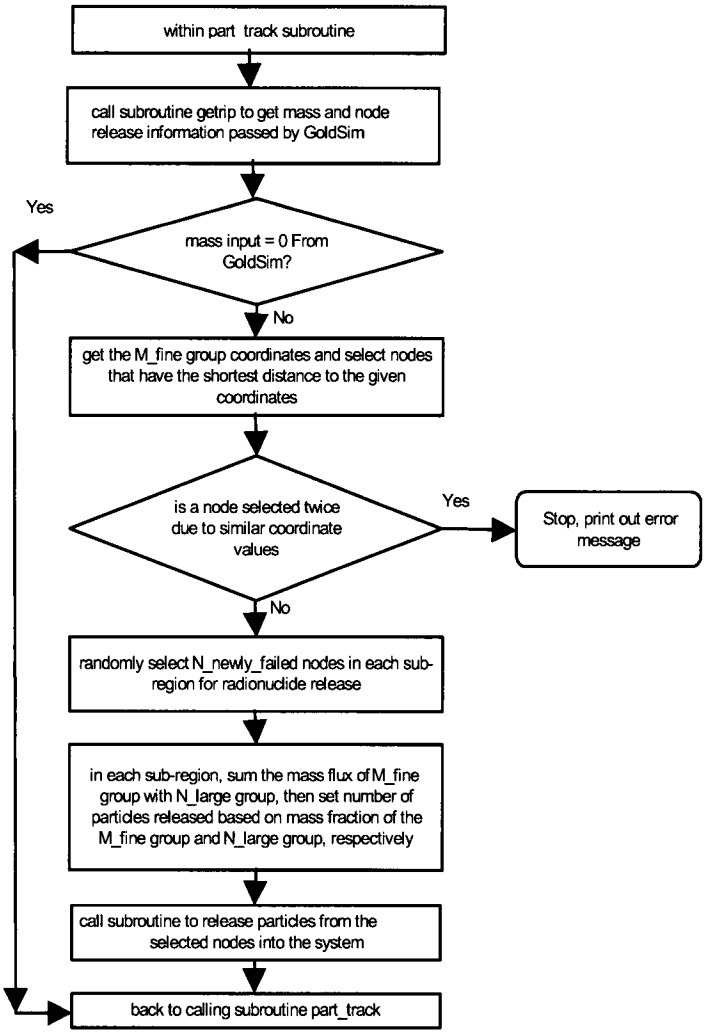

Figure 6-7. Flow Chart of FEHM EBS Random Release Model

Starting with the M_fine early failed packages, *getrip* extracts the (x,y) coordinates of the early failed packages and loops through each repository subregion node to select the one that is closest to the given coordinates. To prevent a node being selected more than once for two or more given coordinates, getrip checks the selected nodes for overlapping. If overlapping is found, *getrip* prints out error messages to the error file *fehmn.err*, then stops the program.

When the selection of M_fine nodes is complete, *getrip* extracts the number of failed packages in each subregion for the N_large subregions. The number of failed packages at the current time step is compared with the values at the previous time step to determine the number of newly failed packages, N_newly_failed, within the current time step in each subregion. Then, *getrip* randomly selects N_newly_failed nodes within the corresponding subregion. The selected failed nodes are stored in the memory for use in releasing radionuclides and are removed from the base of available repository nodes. If the number of failed packages is larger than the number of nodes in a subregion, then radionuclides will be released from all nodes within the subregion. Once all nodes of failed packages are determined, *getrip* allocates the number of released

particles proportionally to the mass flux values of each failed package. Then, subroutine *setmptr* is called to inject particles into the system for each species.

When the locations/coordinates of M_fine early failed packages are unknown, the user can simulate the effect of early failed packages on UZ transport by passing the number of early failed packages in the N_large subregions to FEHM. FEHM then randomly selects the locations of the early failed packages and releases particles into the UZ as described in the paragraph above. Using this option, the user will pass M_fine=0 to FEHM and omit the coordinates of the early failed packages (the 8th data block in Table 6-2 is not needed).

To investigate the influence of matrix diffusion on UZ transport behavior, a radionuclide can be released from either a fracture node or a matrix node. For a given release location and time, the probability of the releases occurring in the fractures is an input to FEHM in the form of data passed from GoldSim to FEHM in the input array in[ ] (Table 6-2). At run time, a random number is generated; when the generated random number is smaller than the fractional releases into the fractures, the particle is released from a selected fracture node. Otherwise, the particle is released through a selected matrix node.

In the case of radionuclide release as gas phase and transport through geosphere, TSPA treats the released mass as aqueous phase. This is expected to bound any dose effects of gas-phase release due to the large dilution of gas-phase release in the atmosphere (BSC 2005 [DIRS 174191]).

6.4.8 Climate Change and Water Table Rise

One important factor that could affect the performance of the repository is future climate changes. As it is difficult and time consuming to simulate the transition of flow fields from one climate to another, in TSPA several pregenerated flow fields are used to represent the corresponding climates. These flow fields are developed in *UZ Flow Models and Submodels* (BSC 2004 [DIRS 169861]), and are converted to FEHM-compatible flow fields in DTN: LB0305TSPA18FF.001 [DIRS 165625]. This approach treats flow in the system as a sequence of steady states. For TSPA simulations, those pregenerated flow fields are read in by FEHM at run time and whenever the GoldSim (BSC 2003 [DIRS 161572]) model signals to FEHM that the climate is changing. From that point until the climate changes again, the flow field is taken to be steady. The following discussion details the numerical approach for handling varying flow fields.

The RTTF particle-tracking method for a time-varying fluid flow system as compared with a steady flow system is more complex but still tractable. Consider a numerical simulation in which a discrete time step is taken at time t and a new fluid flow field is computed. In this model, the new fluid flow time $t_{new} = t + \Delta t$ is treated as an intermediate time at which the particle-tracking calculation must stop. The time is intermediate because if the flow field is at steady state, there is no reason to stop at any time before the end of the simulation except to record particle information for output or processing purposes. The fate of all particles is tracked from time t to time t_{new}; assuming that the flow field is constant over this time interval. When the simulation reaches t_{new}, the position (cell number) of the particle is recorded, along with its fractional time remaining at the cell and the randomly generated y-coordinate of the transfer

function used for that particle in the cell. When the new fluid flow solution is established, the remaining residence time for a particle is determined from the following steps:

1. Compute a new fluid residence time τ_f.

2. Using the y-coordinate of the transfer function previously computed and the new transfer function, calculate a new particle residence time.

3. Multiply this time by the fractional time remaining in the cell to obtain the remaining time in the cell.

This method approximates the behavior in a transient system, while reducing to the behavior that would be obtained in an unchanging flow field had the calculation not been forced to stop at the intermediate time.

Another transient effect that must be considered is that the sum of the outlet mass flow rates $\sum \dot{m}_{out}$ in Equation 6-1 does not necessarily equal the sum of the inlet mass flow rates. When there is net fluid flow into a cell, the particle-tracking algorithm uses the sum of the inlet flow rates in Equation 6-1, whereas Equation 6-1 itself is used when there is net outflow from a cell. Finally, with respect to the transfer function methodology outlined in Section 6.4.3, when the climate changes, the code redefines the parameters in Equations 6-9, 6-10, and 6-11, and uses these parameters and the new flow field to continue the transport simulation.

It is expected that the water table will be higher in future climates. One issue related to climate change is water table rise. In the UZ transport abstraction model, the water table is switched instantaneously from one climate to another when climate changes. Any radionuclides (in the form of particles in the particle tracking model) below the new water table are immediately removed from the UZ and sent to SZ within the TSPA. This approach is conservative as both the flow field and water table are immediately switched to the wetter climate at time of climate change, which not only accelerates the movement of radionuclides in the system but also tends to result in instantaneous pulses of radionuclides into the SZ.

To set the water table elevation to a higher value than that used for the development of the flow fields in DTN: LB0305TSPA18FF.001 [DIRS 165625], the flow field files are postprocessed using the software WTRISE (LBNL 2003 [DIRS 163453]) and are available in DTN: LB0312TSPA06FF.001 [DIRS 166671]. The use of WTRISE requires the specification of a water table elevation under the future climate scenarios. The code adjusts the flow field for all grid blocks beneath this elevation to force particles to immediately leave when reaching any of these grid blocks. Therefore, an elevation for the higher water table must be selected.

The magnitude of the rise in the water table beneath the repository at Yucca Mountain under previous glacial-transition climatic conditions is uncertain, but estimates are available from several independent lines of evidence (Forester et al. 1999 [DIRS 109425], pp. 56 and 57). Early groundwater flow modeling of the response to a doubling of the mean annual precipitation indicated a maximum increase of 130 m of the water table in the vicinity of Yucca Mountain (Czarnecki 1984 [DIRS 101043], p. 21). Analysis of mineralogic alteration (zeolitization and tridymite distribution) in the UZ at Yucca Mountain showed that the water table has probably not

risen more than 60 m above its present position in the geologic past (Levy 1991 [DIRS 100053], p. 477). Analyses of $^{87}Sr/^{86}Sr$ ratios in calcite veins of the UZs and SZs at Yucca Mountain indicated previous water table positions of 85 m higher than present (Marshall et al. 1993 [DIRS 101142], p. 1948). Groundwater flow modeling of the regional flow system under projected future climate conditions simulated water levels of 60 m to 150 m higher than present beneath Yucca Mountain (D'Agnese et al. 1999 [DIRS 120425], p. 2).

Given this set of estimates from multiple, independent sources, (Forester et al. 1999 [DIRS 109425], p. 56) suggests that site data are consistent with past water table elevations up to 120 m higher than present day elevations. This value of 120 m is therefore adopted in this report for the purpose of establishing the water table under future, wetter climates. Because the water table is not flat, a nominal elevation for the present-day water table must be selected and the future water table must then be based on that selection. For the typical water table elevation under present day conditions beneath the repository of 730 m (BSC 2004 [DIRS 170037], Section 6.4.5.1), a rise of 120 m results in an elevation of 850 m. As a comparison, *Saturated Zone Site-Scale Flow Model* (BSC 2004 [DIRS 170037], Section 6.4.5.1) performed an analysis in which the water table was assumed to be 100 m higher than present-day, but processed the water table to parallel the present-day water table. Figure 6-11 in *Saturated Zone Site-Scale Flow Model* (BSC 2004 [DIRS 170037]) shows that for the future water table analysis used to investigate the impact on SZ processes, the 850-m elevation contours passes through the repository footprint. Therefore, choosing an elevation of 850 m for processing the UZ flow fields for the future climate cases is consistent with available site data, and is consistent with SZ studies. Furthermore, since there is no site data or numerical modeling available to form a basis for selecting different water table elevations for the various future climate states, the 850-m elevation is used for future climate flow fields. With respect to UZ transport to the water table, this approximation should be conservative because a reasonable maximum elevation, resulting in a minimum for the UZ flow path length, is used for future climates, even though some of the site data mentioned above yielded estimates of smaller water table rise. The flow fields processed to incorporate the higher water table for the future, wetter climates are available in DTN: LB0312TSPA06FF.001 [DIRS 166671].

6.4.9 Interface with GoldSim

The interface between GoldSim and FEHM establishes a protocol for defining the radionuclide sources to the UZ transport abstraction model provided by GoldSim (BSC 2003 [DIRS 161572]), the definition of a particular flow field for FEHM to use, and exit mass fluxes of radionuclides from the UZ model (from FEHM to GoldSim based on the particle-tracking simulation). This protocol is quite flexible, allowing an arbitrary number of source regions, radionuclides, exit regions, and flow fields to be defined and passed between GoldSim and FEHM through the FEHM subroutine call statement. Figure 6-8 shows a simplified flow chart of the GoldSim-FEHM coupling.

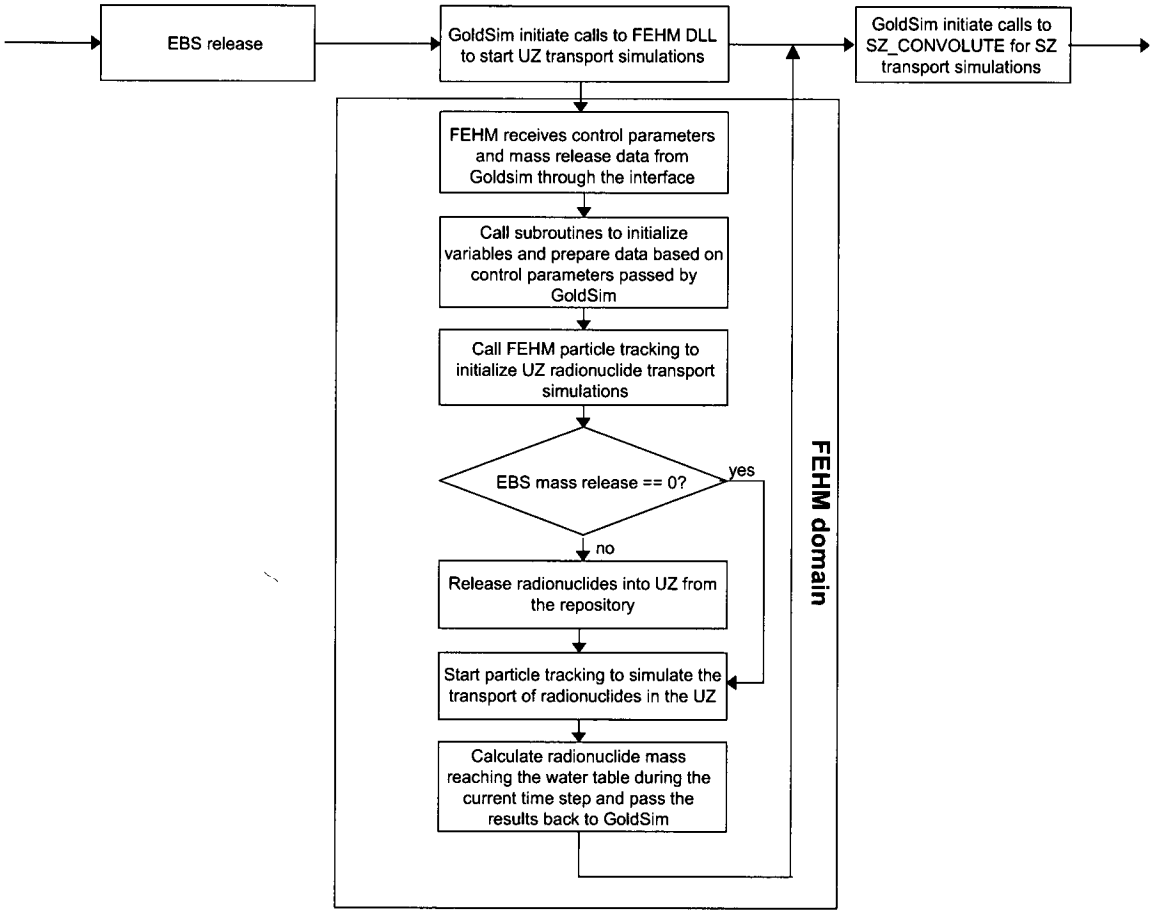

Figure 6-8. Detailed Schematic Flow Chart of GoldSim-FEHM Coupling

During a GoldSim simulation, FEHM cedes control of the time step to GoldSim. At each time, GoldSim provides a flag defining the flow field and the mass flux inputs of radionuclides. By changing the flow field during a simulation, the model can simulate the impact of a climate-induced change in the UZ system. When this occurs, FEHM reads in the new flow field and proceeds with the transport simulation (see Section 6.4.8). Since each flow field is a steady state flow field, the implicit assumption is a quasi-steady one, that is, the system establishes a new steady state rapidly in comparison to transport velocities through the UZ. At the end of each time step, FEHM returns to GoldSim the exiting mass flux values from the UZ transport abstraction model.

6.5 UZ TRANSPORT ABSTRACTION MODEL INPUTS

This section describes the input parameters and their uncertainties. The importance of different transport mechanisms depends on the values of the corresponding parameters that are inputs to the UZ transport abstraction model. Parameters read in by the FEHM abstraction as input to the UZ transport abstraction model include the model's layer units and associated values of

- Dispersivity (m)
- Matrix porosity and rock density (kg/m^3)
- Matrix sorption coefficient (mL/g)

- Matrix diffusion coefficient (m^2/sec)
- Fracture residual saturation and fracture gamma parameters (unitless)
- Fracture porosity, fracture spacing (m), and fracture aperture (m)
- Fracture surface retardation factor (unitless)
- Colloid size distribution, colloid K_c, colloid R_{coll}, and colloid filtration factor
- Radionuclide half lives (years) and daughter products.

For layers above the repository (see Table 6-3), placeholder values for these transport parameters are used in the input files for the model, but these values are not germane to the model results because radionuclide particles do not pass through these units. Beyond the transport parameters, at run time, FEHM also reads in the pregenerated flow fields, model layers (FEHM node zone lists), and node properties associated with the defined zones. These data are inputs from the site-scale UZ flow model to the UZ transport abstraction model. Finally, boundary and initial conditions comprise the remaining model inputs required to perform a transport simulation. In this model, the top boundary is the repository, where radionuclides are released from the EBS into the system. The strength of the source release varies with time and depends on the failure rate of the waste packages. At the bottom boundary (the water table), radionuclides are removed from the UZ system and become the source term for the SZ transport abstraction model. The side boundaries of the UZ transport abstraction model are no-flow boundaries defined as the outer surfaces of the model domain. Finally, the initial condition of the UZ transport abstraction model is set to a concentration of zero for all radionuclides because the model simulations are initiated before any radionuclides have escaped the EBS.

Note that for some parameters, such as longitudinal dispersivity, colloid transport parameters, and matrix diffusion parameters, different values and ranges are developed in this report when compared to *Radionuclide Transport Models Under Ambient Conditions* (BSC 2004 [DIRS 164500]). The values and ranges developed in the following sections are the values to be used in TSPA calculations; whereas in *Radionuclide Transport Models Under Ambient Conditions* (BSC 2004 [DIRS 164500]), the parameters are set to explore the sensitivity of the model to the parameter uncertainties. Note also that fracture aperture is calculated within this report based on the direct input parameters, fracture porosity and fracture frequency as discussed in Section 6.5.7 and shown in Table 6-15. It is also important to note that for the purposes of comparing the process and abstraction models in Section 7, consistent parameters were used.

The following Table 6-3 lists the UZ model units (FEHM zones) and correlates these layers to their representative hydrogeologic units. The sub-sections below give a more detailed discussion about each parameter.

Table 6-3. UZ Model Units Correlated to Hydrogeologic Units

Hydrogeologic Units	UZ Unit	UZ Unit Names	Nodes in Unit	UZ Unit	UZ Unit Names	Nodes in Unit
Layers above repository						
CCR, CUC	1	tcwM1	915	47	tcwF1	736
CUL, CW	2	tcwM2	7077	48	tcwF2	5747
CMW	3	tcwM3	1787	49	tcwF3	1505
CNW	4	ptnM1	3588	50	ptnF1	3319
BT4	5	ptnM2	2954	51	ptnF2	2453
TPY	6	ptnM3	2414	52	ptnF3	2065
BT3	7	ptnM4	6905	53	ptnF4	5473
TPP	8	ptnM5	11483	54	ptnF5	9183
BT2	9	ptnM6	5215	55	ptnF6	4378
TC	10	tswM1	1561	56	tswF1	1432
TR	11	tswM2	6457	57	tswF2	5025
Layers below repository						
TUL	12	tswM3	9002	58	tswF3	7408
TMN	13	tswM4	5023	59	tswF4	4215
TLL	14	tswM5	13929	60	tswF5	11568
TM2	15	tswM6	3856	61	tswF6	3152
TM1	16	tswM7	2344	62	tswF7	1889
PV3	17	tswM8*	1714	63	tswF8*	862
PV2 (tsw9 is split into tswv and tswz)	18	tswMz*	273	64	tswFz*	24
	19	tswMv*	564	65	tswFv*	466
BT1a	20	ch1Mz*	496	66	ch1Fz*	0
	21	ch1Mv	1712	67	ch1Fv	1464
CHV	22	ch2Mv	512	68	ch2Fv	390
	23	ch3Mv	465	69	ch3Fv	358
	24	ch4Mv	400	70	ch4Fv	315
	25	ch5Mv	285	71	ch5Fv	227
CHZ	26	ch2Mz*	1061	72	ch2Fz*	0
	27	ch3Mz	4072	73	ch3Fz	3204
	28	ch4Mz	3214	74	ch4Fz	2595
	29	ch5Mz*	1987	75	ch5Fz*	1612
BT	30	ch6Mz*	1524	76	ch6Fz*	1169
	31	ch6Mv	83	77	ch6Fv	64
PP4 (zeolitic)	32	pp4Mz*	932	78	pp4Fz*	823
PP3 (devitrified)	33	pp3Md	1886	79	pp3Fd	1498
PP2 (devitrified)	34	pp2Md	1436	80	pp2Fd	1123
PP1 (zeolitic)	35	pp1Mz	2076	81	pp1Fz	1609
BF3 (welded)	36	bf3Md	1412	82	bf3Fd	980
BF2 (nonwelded)	37	bf2Mz	224	83	bf2Fz	112

Table 6-3. UZ Model Units Correlated to Hydrogeologic Units (Continued)

Hydrogeologic Units	UZ Unit	UZ Unit Names	Nodes in Unit	UZ Unit	UZ Unit Names	Nodes in Unit
Layers below repository						
Not available, use BF3	38	tr3Md	1	84	tr3Fd	0
Not available, use BF2	39	tr2Mz	0	85	tr2Fz	0
Use PP3, replace tsw8 for perched	40	pcM38	1826	86	pcF38	1826
Use PV2, replace tsw9 for perched	41	pcM39	1324	87	pcF39	1324
Use BT1a, replace ch1z for perched	42	pcM1z	3207	88	pcF1z	3207
Use CHZ, replace ch[2,5]z for perched	43	pcM2z	3490	89	pcF2z	3490
	44	pcM5z	9	90	pcF5z	9
Use BT, replace ch6z for perched	45	pcM6z	8	91	pcF6z	8
Use PP4, replace pp4 for perched	46	pcM4p	8	92	pcF4p	8
Fault Fracture Zones						
Faults in Tiva Canyon welded hydrogeologic units				93	tcwFf	1791
Faults in Paintbrush nonwelded hydrogeologic units				94	ptnFf	5688
Faults in Topopah Spring welded hydrogeologic units				95	tswFf	8682
Faults in Calico Hills nonwelded hydrogeologic units				96	chnFf	6235

Source for Hydrogeologic Unit (HGU) assignments for the UZ layers and faults: *UZ Flow Models and Submodels* (BSC 2004 [DIRS 169861], Tables 6.1-1 and F-1).

* Model zones 40-46 and 86-92 labeled with "pc" are used to represent the perched-water conceptual model and replace previously defined zones as noted in the table and discussed in *UZ Flow Models and Submodels* (BSC 2004 [DIRS 169861], Section 6.2.3).

6.5.1 Pregenerated Flow Fields

In TSPA runs, a total of 9 base-case flow fields corresponding to 9 climate scenarios: present day [lower-bound, mean, and upper-bound], monsoon [lower-bound, mean, and upper-bound], and glacial transition [lower-bound, mean, and upper-bound], , were pregenerated with the TOUGH2 software code (LBNL 1999 [DIRS 113943]) and fed into FEHM. The climate scenarios are converted to 6 future wetter climates with a water table rise by converting saturation and flux at previously unsaturated nodes.

The flow fields are based on the dual-k model formulation that allows water flow in both fractures and the corresponding matrix blocks. A total of 120,711 physical nodes were used to discretize the Yucca Mountain Project site. For the dual-k model, at any physical node, there is a fracture node and a corresponding matrix node. Thus, the flow model has a total of 241,422 flow nodes (DTNs: LB0305TSPA18FF.001 [DIRS 165625] and LB0312TSPA06FF.001 [DIRS 166671]).

The site-scale UZ flow model is characterized by potential lateral flow in the PTn unit, the occurrence of perched water within low-permeability zeolites in the Calico Hills nonwelded unit or the densely welded basal vitrophyre of the Topopah Spring welded (TSw) unit, and the effects of faults on the UZ flow system (BSC 2004 [DIRS 169861]).

In TSPA-LA runs, the 3 present-day flow fields plus 6 flow fields with water table rise corresponding to future climate will be used. The name of the flow fields and corresponding files are listed in Table 4-1.

The influence of hydrologic flow parameter uncertainty on radionuclide transport is investigated using sensitivity analyses in Section 6.6.3 of this report. The sensitivity simulations use 8 pregenerated flow fields in which parameters are individually varied plus and minus one standard deviation from the best-fit value. These 8 flow fields are available in LB0506TSPA08FF.001 [DIRS 174117] and are output from *Parameter Sensitivity Analysis for Unsaturated Zone Flow* (BSC 2005 [DIRS 174116]).

6.5.2 Dispersivity

The site-scale UZ flow model has indicated that flow in the fractured rock system is dominated by fracture flow. In such a system, radionuclide transport is primarily advection dominated, and the influence of dispersion on radionuclide transport is not expected to be important. The reason for this is that when compared to the spreading of radionuclides due to matrix diffusion effects, the impact on transport times of longitudinal dispersion is likely to be small.

There are few data available on dispersivity distributions at Yucca Mountain site. Neuman (1990 [DIRS 101464]) showed that field dispersivity varied with the scale of study. Field tracer tests at the C-holes at Yucca Mountain also showed that on a 100-m scale, field dispersivity had a range of approximately 3 m to 63 m (BSC 2004 [DIRS 170010], Table 6.3-3).

In the UZ transport abstraction model, the fracture dispersivity is set at 10 m, except as discussed in Section 6.4.2. This is toward the lower end of values from field studies and are available in DTN: LA0303PR831231.005 [DIRS 166259]. Although the impact of dispersivity should be very small, the value chosen should be conservative, as higher dispersivity tends to spread the radionuclide plume and reduce the peak concentration. While it can be argued that for a decaying species, higher dispersivity can allow a greater fraction of the mass to arrive downstream before decaying, the point here is that in comparison to diffusion and large scale heterogeneities, dispersivity effects have a very small influence on the breakthrough curves. This justifies the use of a fixed value for dispersivity rather than treating it as a stochastic parameter (Table 6-4).

Table 6-4. Dispersivity Used in UZ Transport Abstraction Model

Input Name	Input Description	Input Sources	Value (Units)	Type of Uncertainty
Fracture dispersivity	Input to FEHM for simulating dispersion effect	DTN: LA0303PR831231.005 [DIRS 166259]	10 m	Fixed value

FEHM = finite element heat and mass (model)

Because the dual-k abstraction model treats the combined fracture-matrix system as a unified continuum, this dispersivity applies to the medium as a whole. Therefore, the model does not distinguish between fracture dispersivity and matrix dispersivity.

6.5.3 Matrix Porosity and Rock Density

Matrix porosity is used to calculate the matrix pore volume associated with each matrix block. The pore volume data are then multiplied by the corresponding water saturation data to determine the fluid volume in a cell.

Matrix porosity and rock density values combined with rock sorption coefficient and water saturation are used for calculating matrix retardation factors used in simulating the sorption effect on radionuclide transport.

Values of matrix porosity are from the Technical Data Management System (TDMS) (DTN: LB0210THRMLPRP.001 [DIRS 160799]) and are listed in Table 6-5.

Table 6-5. Matrix Porosities Used in the UZ Transport Abstraction Model

Matrix Layer	Matrix Porosity	Input Description	Input Source	Type of Uncertainty
tcwM1	1.18E-01	Matrix porosity values are used in determining matrix pore volume, simulating matrix diffusion effects, and calculating matrix sorption retardation factors.	LB0210THRMLPRP.001 [DIRS 160799] *"Thermal Properties of UZ Model Layers: Data Summary"*	Fixed values for each layer but varies from layer to layer
tcwM2	1.18E-01			
tcwM3	4.57E-02			
ptnM1	3.54E-01			
ptnM2	3.54E-01			
ptnM3	3.54E-01			
ptnM4	3.54E-01			
ptnM5	3.54E-01			
ptnM6	2.51E-01			
tswM1	4.57E-02			
tswM2	1.18E-01			
tswM3	1.43E-01			
tswM4	1.29E-01			
tswM5	1.49E-01			
tswM6	1.06E-01			
tswM7	1.06E-01			
tswM8	4.57E-02			
tswMv	4.57E-02			
tswMz	4.57E-02			
ch1Mv	3.54E-01			
ch2Mv	3.28E-01			
ch3Mv	3.28E-01			
ch4Mv	3.28E-01			
ch5Mv	3.28E-01			

Table 6-5. Matrix Porosities Used in the UZ Transport Abstraction Model (Continued)

Matrix Layer	Matrix Porosity	Input Description	Input Source	Type of Uncertainty
ch6Mv	3.28E-01	Matrix porosity values are used in determining matrix pore volume, simulating matrix diffusion effects, and calculating matrix sorption retardation factors.	LB0210THRMLPRP.001 [DIRS 160799] *"Thermal Properties of UZ Model Layers: Data Summary"*	Fixed values for each layer but varies from layer to layer
ch1Mz	3.54E-01			
ch2Mz	3.28E-01			
ch3Mz	3.28E-01			
ch4Mz	3.28E-01			
ch5Mz	3.28E-01			
ch6Mz	3.28E-01			
pp4Mz	2.97E-01			
pp3Md	2.97E-01			
pp2Md	2.33E-01			
pp1Mz	2.73E-01			
bf3Md	1.88E-01			
bf2Mz	2.62E-01			
tr3Md	2.80E-01			
tr2Mz	3.35E-01			
pcM38	4.57E-02			
pcM39	4.57E-02			
pcM1z	3.54E-01			
pcM2z	3.28E-01			
pcM5z	3.28E-01			
pcM6z	3.28E-01			
pcM4p	2.97E-01			

NOTE: Layers defining the perched water units are assigned porosity values that are the same as those of the corresponding geologic unit in which they reside.

Rock density values are from the TDMS (DTN: LB0210THRMLPRP.001 [DIRS 160799]) and are listed in Table 6-6. These densities are bulk rock densities, obtained from the grain density in the cited DTN, multiplied by one minus the porosity, using the porosities listed in Table 6-5.

Table 6-6. Matrix Rock Density Values

Matrix Layer	Rock Density (kg/m^3)	Rock Type	Input Description	Input Source	Type of Uncertainty
tcwM1	2.217 E+03	–	Rock density data are used by FEHM in the calculation of matrix sorption retardation factors. These densities are bulk rock densities obtained from the grain density in the cited DTN, multiplied by one minus the porosity, using the porosities listed in Table 6-5.	LB0210THRMLPRP.001 [DIRS 160799] *"Thermal Properties of UZ Model Layers: Data Summary"*	Fixed values for each layer but varies from layer to layer
tcwM2	2.217 E+03	–			
tcwM3	2.170 E+03	–			
ptnM1	1.478 E+03	–			
ptnM2	1.478 E+03	–			
ptnM3	1.478 E+03	–			
ptnM4	1.478 E+03	–			
ptnM5	1.478 E+03	–			
ptnM6	1.709 E+03	–			
tswM1	2.170 E+03	–			
tswM2	2.217 E+03	–			
tswM3	2.022 E+03	D			
tswM4	2.149 E+03	D			
tswM5	1.980 E+03	D			
tswM6	2.211 E+03	D			
tswM7	2.211 E+03	D			
tswM8/pcM38	2.170 E+03	D			
tswMv (tsw9)	2.170 E+03	V			
tswMz (tsw9)	2.170 E+03	Z			
pcM39	2.170 E+03	D			
ch1Mv	1.478 E+03	V			
ch2Mv	1.516 E+03	V			
ch3Mv	1.516 E+03	V			
ch4Mv	1.516 E+03	V			
ch5Mv	1.516 E+03	V			
ch6Mv*	1.516 E+03	V			
ch1Mz/pcM1z	1.478 E+03	Z			
ch2Mz/pcM2z	1.516 E+03	Z			
ch3Mz	1.516 E+03	Z			
ch4Mz	1.516 E+03	Z			
ch5Mz/pcM5z	1.516 E+03	Z			
ch6Mz/pcM6z	1.516 E+03	Z			
pp4Mz/pcM4p	1.478 E+03	Z			
pp3Md	1.478 E+03	D			
pp2Md	1.829 E+03	D			
pp1Mz	1.481 E+03	Z			
bf3Md	1.709 E+03	D			
bf2Mz	1.486 E+03	Z			
tr3Md	1.707 E+03	D			
tr2Mz	1.478 E+03	Z			

Table 6-6. Matrix Rock Density Values (Continued)

Matrix Layer	Rock Density (kg/m^3)	Rock Type	Input Description	Input Source	Type of Uncertainty
Fault Zone Rock Density Data					
tcwFf	2.198 E+03	–			
ptnFf	1.577 E+03	–			
tswFf	2.125 E+03	D			
chnFf	1.550 E+03	Z			

NOTES: Layers defining the perched water units (pc) are assigned porosity values that are the same as those of the corresponding model unit which they replace.

*Rock density not given for layer ch6mv in the cited DTN. Value taken to be the same as ch5mv.

D = Devitrified, Z = Zeolitic, V = Vitric, DTN = data tracking number; FEHM = finite element heat and mass (model)

6.5.4 Matrix Sorption Coefficient (mL/g)

Dissolved radionuclide waste traveling through the matrix can be retarded due to sorption on to the surface of the porous matrix material. In TSPA-LA runs, the linear sorption model is used to describe the partitioning of radionuclides between the solute and the matrix through the UZ system. Matrix sorption coefficients can be read in by FEHM at run time. The values are then used to calculate matrix rock retardation factors of different radionuclides. The validity of the linear equilibrium model and the derivation of sorption coefficient distributions based on laboratory experiment data are documented in *Radionuclide Transport Models Under Ambient Conditions* (BSC 2004 [DIRS 164500]).

The strength of matrix sorption depends on the properties of the rock material, aqueous composition, and the radionuclides. Matrix sorption coefficients for different rock types (zeolitic, devitrified, and vitric) are taken from the TDMS (DTN: LA0408AM831341.001 [DIRS 171584]). Values of the sorption coefficient are divided into three groups based on rock type (e.g., devitrified, vitric, and zeolitic). In addition, the parameter distributions for sorption coefficient were developed with microbial effects taken into consideration. See the process model report (BSC 2004 [DIRS 164500], Section 6.4.2) for a discussion of this issue. Table 6-7 lists the statistical distribution of matrix sorption coefficient for different radionuclide types.

To address the influence of the sorption coefficient uncertainty on system performance, the matrix sorption coefficients of each species are presampled for each rock type (based on the listed distribution values in Table 6-7) for each TSPA realization. *Radionuclide Transport Models Under Ambient Conditions* (BSC 2004 [DIRS 164500], Appendix B) discusses the method of correlating sorption coefficients to one another in the stochastic sampling of parameters.

Table 6-7. Sorption-Coefficient Distributions for Unsaturated Zone Units

Species	Rock Type	Type of Uncertainty Distribution	Coefficients Describing Distribution (K_d: mL/g)	Input Description
U	Zeolitic	Cumulative	(K_d value, probability) (0, 0) (0.5, 0.5) (30, 1.0)	The matrix sorption coefficient data are read in at runtime by FEHM for simulating the effect of matrix sorption on radionuclide transport.
	Devitrified	Cumulative	(K_d value, probability) (0, 0) (0.2, 0.5) (4., 1.0)	
	Vitric	Cumulative	(K_d value, probability) (0, 0) (0.2, 0.5) (3., 1.0)	
Np	Zeolitic	Cumulative	(K_d value, probability) (0, 0) (0.5, 0.5) (6., 1.0)	
	Devitrified	Cumulative	(K_d value, probability) (0, 0) (0.5, 0.5) (6., 1.0)	
	Vitric	Cumulative	(K_d value, probability) (0, 0) (1.0, 0.5) (3., 1.0)	
Pu	Zeolitic	Cumulative	(K_d value, probability) (10., 0) (100., 0.5) (200., 1.0)	
	Devitrified	Cumulative	(K_d value, probability) (10., 0) (70., 0.5) (200., 1.0)	
	Vitric	Cumulative	(K_d value, probability) (10., 0) (100., 0.5) (200., 1.0)	
Am	Zeolitic	Truncated Normal	Range = 1000 – 10000, Mean=5500, Std Dev=1500	
	Devitrified	Truncated Normal	Range = 1000 – 10000, Mean=5500, Std Dev=1500	
	Vitric	Cumulative	(K_d value, probability) (100., 0) (400., 0.5) (1000., 1.0)	
Pa	Zeolitic	Truncated Normal	Range = 1000 – 10000, Mean=5500, Std Dev=1500	
	Devitrified	Truncated Normal	Range = 1000 – 10000, Mean=5500, Std Dev=1500	
	Vitric	Truncated Normal	Range = 1000 – 10000, Mean=5500, Std Dev=1500	
Cs	Zeolitic	Cumulative	(K_d value, probability) (425., 0) (5000., 0.5) (20000., 1.0)	
	Devitrified	Uniform	Range = 1 – 15	
	Vitric	Cumulative	(K_d value, probability) (0., 0) (2., 0.5) (100., 1.0)	
Sr	Zeolitic	Uniform	Range = 50 – 2000	
	Devitrified	Uniform	Range = 10 – 70	
	Vitric	Uniform	Range = 0 – 50	
Ra	Zeolitic	Uniform	Range = 1000 – 5000	
	Devitrified	Uniform	Range = 100 – 1000	
	Vitric	Uniform	Range = 50 – 600	
Th	Zeolitic	Uniform	Range = 1000 – 30000	
	Devitrified	Uniform	Range = 1000 – 10000	
	Vitric	Uniform	Range = 1000 - 10000	

DTN: LA0408AM831341.001 [DIRS 171584].
FEHM = finite element heat and mass (model)

NOTE: The radioisotopes of carbon, iodine, and technetium are treated as nonsorbing and are not included in the source DTN. These species are assigned 0.0 K_d values for all three rock types. The values used for the base-case model are median values of these distributions and are listed in Section 6.6.1

6.5.5 Matrix Diffusion Coefficient (m^2/sec)

It has been shown that matrix diffusion combined with matrix sorption can play an important role in slowing the movement of radionuclides in fractured rocks (Sudicky and Frind 1982 [DIRS 105043]).

A matrix diffusion coefficient is used in FEHM for simulating the effect of matrix diffusion on radionuclide transport in the fractured media. Values of matrix diffusion coefficient affect the strength of fracture-matrix interaction due to diffusion of radionuclides.

In the radionuclide transport process model documented in *Radionuclide Transport Models Under Ambient Conditions* (BSC 2004 [DIRS 164500], p. 6-9), the diffusive flux is defined in terms of the concentration gradient and the effective diffusion coefficient, which is the product of the free-water diffusion coefficient, the water content, and the tortuosity. *Radionuclide Transport Models Under Ambient Conditions* (BSC 2004 [DIRS 164500], p. 6-9) shows, based on work by Grathwohl (2000 [DIRS 141512]), that it is a reasonable approximation to set tortuosity equal to the matrix porosity. The abstraction model calls for the effective diffusion coefficient as a direct parameter input, rather than separately defining tortuosity and free-water diffusion coefficient. In the development below, correlations between effective diffusion coefficient, water content, and matrix permeability are proposed based on available experimental data. The end result of this development is a range of effective diffusion coefficients that in effect capture the uncertainty in the mechanisms associated with diffusion through tortuous pore spaces. Therefore, even though the tortuosity is not a direct model input, its impact on matrix diffusion, and the correlation between diffusion and matrix porosity, is implicitly captured in the abstraction model.

In current TSPA simulations, unsaturated matrix diffusion coefficients are based on the correlation between matrix diffusion, porosity, and saturated permeability developed for the SZ (Reimus et al. 2002 [DIRS 163008]). To adapt the relationship for the UZ, the porosity is replaced with water content and the permeability is replaced with effective permeability. The equation is re-written as:

$$\log(D_m) = -3.49 + 1.38\theta_m + 0.165\log(k_m) \qquad \text{(Eq. 6-19)}$$

where D_m is the matrix diffusion coefficient in cm^2/s, θ_m is the matrix water content, and k_m is the effective permeability to water in m^2.

The data from Reimus et al. (2002 [DIRS 163008]) suggests that the range of diffusion coefficients for tritium, bicarbonate, and pertechnetate individually are roughly similar to the range of mean values for each. This suggests that a single broad distribution scaled by the range of values between cations and anions from DTN: LA0003JC831362.001 [DIRS 149557] would provide a better representation of the uncertainty in matrix diffusion. To capture this with the correlation given by Reimus et al. (2002 [DIRS 163008]), consider the following transformation:

$$X = \log\left(\frac{D_0}{D_m}\right) \qquad \text{(Eq. 6-20)}$$

where D_0 is the limiting upper value for D_m. This value is given in DTN: LA0003JC831362.001 [DIRS 149557] as 10^{-9} m^2/s. The average for X is

$$\mu_X = \log(D_0) - \overline{\log(D_m)} \qquad \text{(Eq. 6-21)}$$

where the second term on the right hand side is the mean of $\log(D_m)$. Stipulating that the variable X ranges from 0 to infinity, D_m is constrained to be less than 10^{-9} m^2/s.

Given the semi-infinite range for X, it can be sampled as a lognormal distribution. This introduces the second logarithmic transformation, Y,

$$Y = \ln(X) \quad \text{(Eq. 6-22)}$$

the mean for Y is taken to be

$$\mu_Y = \ln(\mu_X) \quad \text{(Eq. 6-23)}$$

such that the mean for the Reimus correlation is unchanged by the transformation to a lognormal distribution. In this case, note that μ_x is the median of X, not the mean. Distribution parameters may be obtained by setting $\overline{\log(D_m)}$ to be the log of the geometric mean of the mean values in DTN: LA0003JC831362.001 [DIRS 149557] and then adjust the standard deviation for Y such that it covers the range of values represented by cations and anions in DTN: LA0003JC831362.001 [DIRS 149557]. The standard deviation of 0.3 for Y results in a spread for the distribution that is representative of the spread of values in DTN: LA0003JC831362.001 [DIRS 149557], as shown in Figure 6-9.

The range of values for the UZ may be examined using 5th and 95th percentile values for water content and effective matrix permeability. Doing this, the "low" distribution may be computed based on the Reimus correlation (Reimus et al. 2002 [DIRS 163008]) by assigning the mean using the 5th percentile water content and effective matrix permeability and a "high" distribution based on the 95th percentile of values of these quantities. The results are shown in Figure 6-10.

Figure 6-10 shows that most of the matrix diffusion coefficients estimated using Equation 6-19 will fall within the range of the "Reimus low" and "Reimus high" curves. The data used to develop the distributions in DTN: LA0003JC831362.001 [DIRS 149557] were from diffusion measurements under saturated conditions. Therefore, the generally lower values represented by the Reimus distributions are expected. The comparison with measured diffusion coefficients for tritium, technetium, and carbon is given in Figure 6-11. Again, the correlations for the UZ are lower than the measured values, which were performed under saturated conditions.

The groups of model units for sampling matrix diffusion shown in Table 6-8 were selected based on similarity in properties of porosity, permeability, and water content. Distributions for the water content and (log) effective permeability to water for each group are derived from the 9 flow fields used for TSPA calculations (BSC 2004 [DIRS 169861]; DTN: LB03023DSSCP9I.001 [DIRS 163044]).

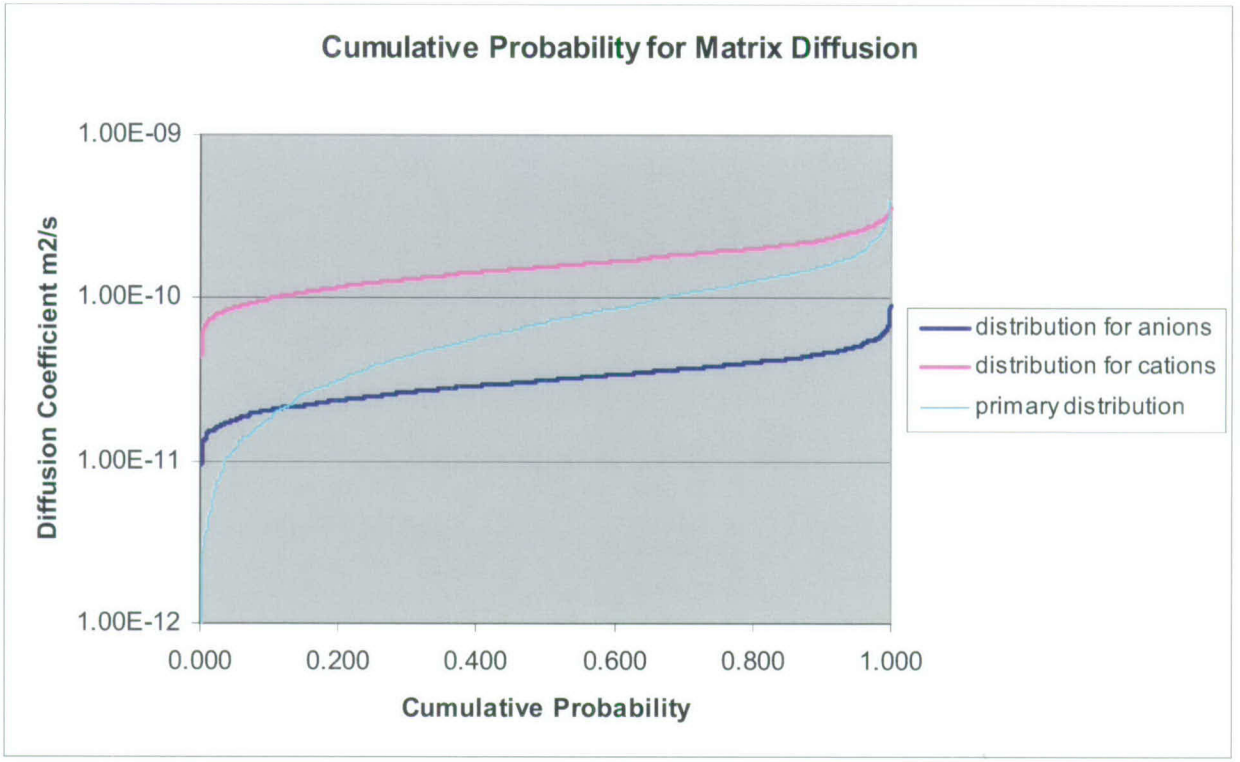

Output DTN: LA0506BR831371.001.

Figure 6-9. Cumulative Probability for Matrix Diffusion Under Saturated Conditions

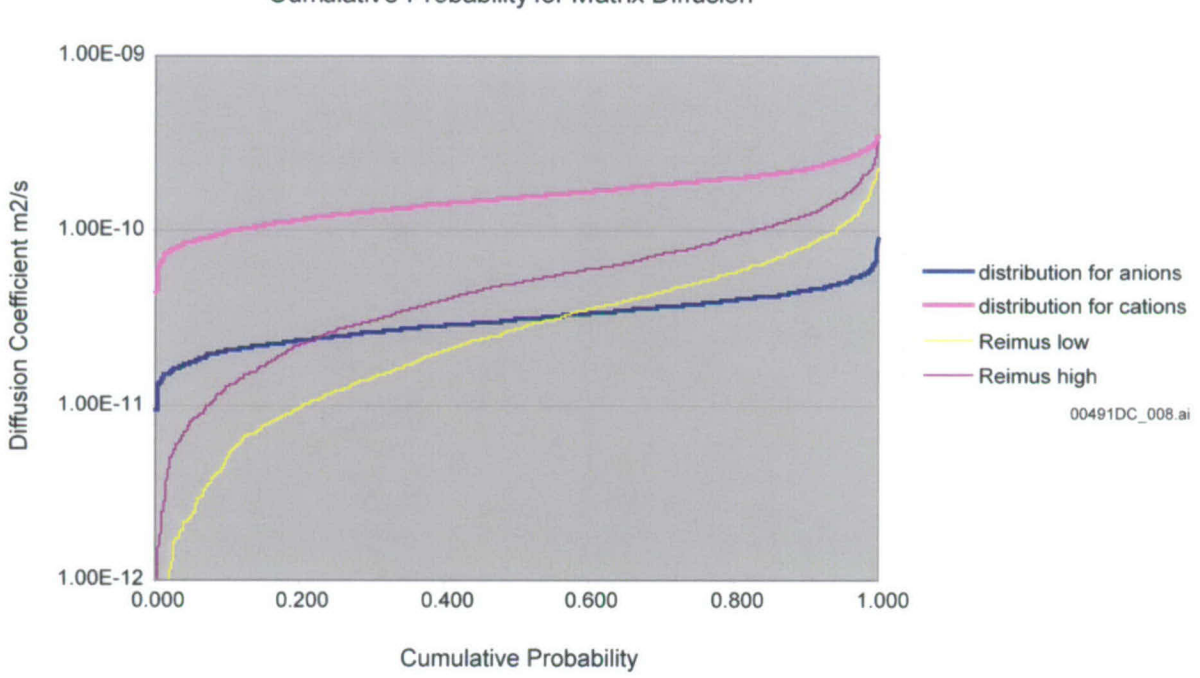

Output DTN: LA0506BR831371.001.

Figure 6-10. Comparison of Cation/Anion Distributions with Reimus High/Low Distributions for Unsaturated Conditions

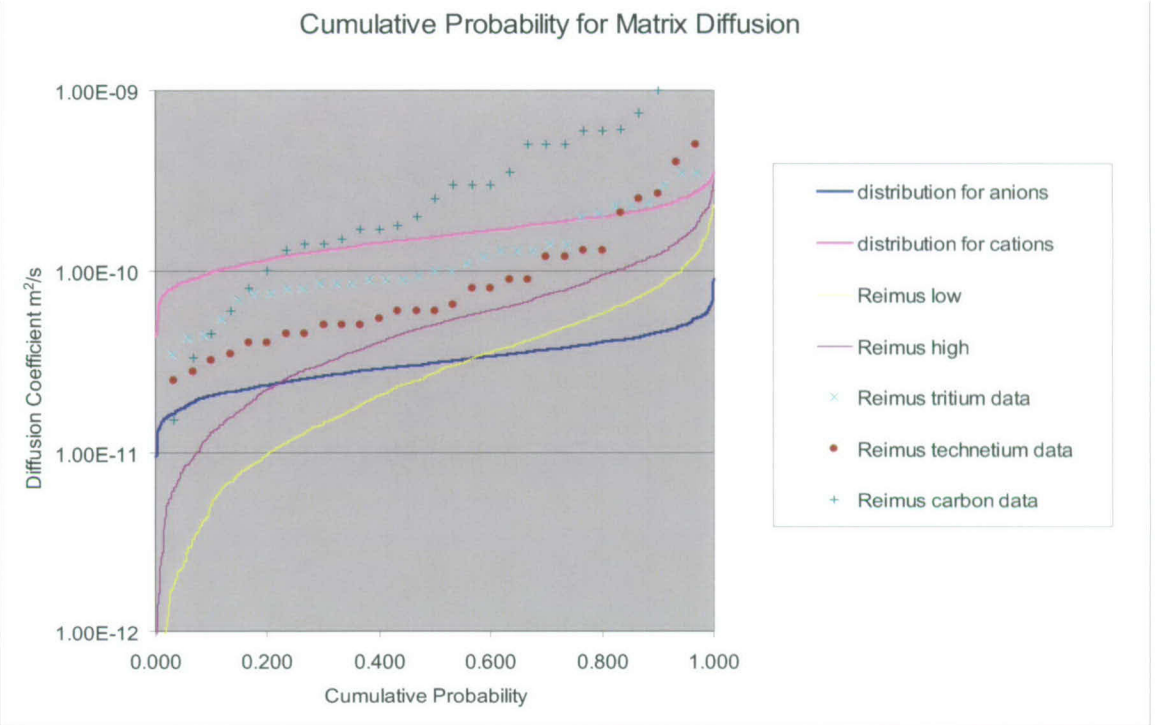

Output DTN: LA0506BR831371.001.

Figure 6-11. Comparison of the Distributions with Diffusion Data

The influence of matrix diffusion coefficient uncertainty on radionuclide transport is investigated by independently sampling water content and permeability for each rock group (Table 6-8; techniques for deriving the numerical values are presented in Appendix A). The water content and (log) effective permeability are independently sampled from these cumulative distributions. A matrix diffusion coefficient is then computed from Equation 6-19.

In all TSPA simulations, colloid matrix diffusion (diffusion of a colloid from the fracture to the matrix) is neglected because of lack of data and because diffusion coefficients for colloidal particles are expected to be small. This is conservative with respect to the TSPA calculation of transport times through the UZ.

Table 6-8. Distribution of Water Content and Effective Permeability

Group Index	Unit	Mean Water Content (-)	Standard Deviation Water Content	Maximum Water Content	Minimum Water Content	Mean Log Effective Permeability (m^2)	Standard Deviation Log Effective Permeability (m^2)	D_m Calculated Using Listed Mean Values and Eq. 6-19 (m^2/s)
1	bf2Mz, ch1Mz, ch[1,2,3,4,5, 6]Mv, tswMv, tswMz, pp3Md, pp2Md, pp1Mz, pp4Mz, bf3Md, tr3Md	2.06E-01	8.41E-02	5.33E-01	6.81E-03	-1.62E+01	5.50E-01	1.33E-10
2	ch[2,3,4,5,6]Mz, pcm[1,2,5,6]Mz, pcM39, pcM4p	3.00E-01	5.12E-02	5.78E-01	7.73E-02	-1.83E+01	4.20E-01	8.10E-11
3	tswM[3,4,5,6,7,8], pcM38	1.12E-01	3.43E-02	3.19E-01	7.75E-5	-1.89E+01	4.62E-01	3.47E-11

Output DTN: LA0506BR831371.001.

NOTE: A beta distribution was used for the matrix water content, and a lognormal distribution was used for the matrix effective permeability.

6.5.6 Fracture Residual Saturation and Active Fracture Model Gamma Parameters (Unitless)

Fracture residual saturation and fracture γ parameter values are used by FEHM to calculate the fracture spacing based on the AFM (Liu et al. 1998 [DIRS 105729]).

In TSPA-LA, a constant fracture residual saturation of 0.01 is used for all layers (DTN: LB0208UZDSCPMI.002 [DIRS 161243]). Note that this DTN also lists values for the matrix. These are not directly used in the UZ transport abstraction model. Currently, there are no data from Yucca Mountain that could be used to assess the uncertainty in fracture residual saturation (Table 6-9).

Table 6-9. Fracture Residual Saturation Values

Input Name	Input Value	Input Description	Input Source	Type of Uncertainty
Fracture residual saturation	0.01	Fracture residual saturation is used to calculate active fracture spacing	LB0208UZDSCPMI.002 [DIRS 161243]	Fixed value. The fracture residual saturation is constant over all layers and does not change with climate.

Values of fracture γ parameter vary with infiltration rates in each rock layer. Tables 6-10 through 6-12 list the fracture γ parameter values used in TSPA-LA for different infiltration scenarios (DTN: LB0305TSPA18FF.001 [DIRS 165625]). The basic input parameter sets of fractures and matrix rocks were estimated through a series of one-dimensional model inversions

provided by *Calibrated Properties Model* (BSC 2004 [DIRS 169857]). Note that according to Tables 6-8, 6-9, and 6-10 of the Calibrated Properties report, the flow models were developed assuming that there is no fracture flow in the vitric Calico Hills units; instead, matrix flow is assumed. In these units, the γ value of 0.25 is used as a placeholder in the abstraction model. The value used is immaterial because the flow occurs only in the matrix, and the transport reverts to a matrix-only transport model for this situation.

The one-dimensional inverted property sets were used by *UZ Flow Models and Submodels* (BSC 2004 [DIRS 169861]) to develop three-dimensional model and calibrated parameter sets considered as base case scenario parameter sets for use in generating three-dimensional flow fields. The use of a three-dimensional model enabled further parameter adjustment to match field observation data in which lateral flow, perched water, and capillary barrier effects can be simulated. Adjusted parameters include fracture-matrix properties of the top the PTn units and perched water zones. The adjusted PTn unit properties provide a better match of liquid saturation and observed field data and the active-fracture γ parameter is set to zero for perched-water zones. The parameter adjustments are shown and discussed in Section 6.2.3 of (BSC 2004 [DIRS 169861]). The final calibrated γ parameter from these three-dimensional model studies are used for the base case studies of this report and are listed in the following Tables 6-10 through 6-12 and are available in TOUGH2 files in DTN: LB0305TSPA18FF.001 [DIRS 165625].

The influence of γ parameter uncertainty on radionuclide transport is investigated using sensitivity analyses in *UZ Flow Models and Submodels* (BSC 2004 [DIRS 169861], Section 6.8; Section 7.2.3.3). Section 6.4.4 of this report investigates the uncertainty range of 0.2 to 0.6 for the γ parameter (BSC 2004 [DIRS 169861], Sections 7.4.1 and 7.4.2).

Table 6-10. Fracture Gamma Parameter for Lower-Bound Infiltration Scenario

Model Layer	Fracture γ	Model Layer	Fracture γ	Input Description	Input Source	Type of Uncertainty
tcwF1	0.4834	ch1Fz	2.759 E-01	This value is read in by FEHM and used in calculating fracture spacing values based on the active fracture model.	LB0305TSPA18FF.001 [DIRS 165625] *"Eighteen 3-D Site Scale UZ Flow Fields Converted from TOUGH2 to T2FEHM Format."* TOUGH2 File: *glaq_IA.dat*.	Fixed value for each layer but varies from layer to layer. The values also depend on climate.
tcwF2	0.4834	ch2Fz	2.759 E-01			
tcwF3	0.4834	ch3Fz	2.759 E-01			
ptnF1	0.1032E-01	ch4Fz	2.759 E-01			
ptnF2	0.1032E-01	ch5Fz	2.759 E-01			
ptnF3	0.1032E-01	ch6Fz	2.759 E-01			
ptnF4	0.1032E-01	pp4Fz	2.759 E-01			
ptnF5	0.1032E-01	pp3Fd	2.476 E-01			
ptnF6	0.1032E-01	pp2Fd	2.476 E-01			
tswF1	0.3741E-01	pp1Fz	2.759 E-01			
tswF2	0.5284	bf3Fd	2.476 E-01			
tswF3	0.5284	bf2Fz	2.759 E-01			
tswF4	0.4764	tr3Fd	2.476 E-01			
tswF5	0.4764	tr2Fz	2.759 E-01			
tswF6	0.4764	pcF38	0.000 E-01			
tswF7	0.4764	pcF39	0.000 E-01			
tswF8	0.4764	pc1Fz	0.000 E-01			
tswFz	0.2759	pc2Fz	0.000 E-01			
tswFv	0.2500	pc5Fz	0.000 E-01			
ch1Fv	0.2500	pc6Fz	0.000 E-01			
ch2Fv	0.2500	pc4Fp	0.000 E-01			
ch3Fv	0.2500	tcwFf (fault)	4.000 E-01			
ch4Fv	0.2500	ptnFf (fault)	1.138 E-01			
ch5Fv	0.2500	tswFf (fault)	3.000 E-01			
ch6Fv	0.2500	chnFf (fault)	3.000 E-01			

3-D = three-dimensional; FEHM = finite element heat and mass (model); UZ = unsaturated zone

Table 6-11. Fracture Gamma Parameter for Mean Infiltration Scenario

Model Layer	Fracture γ	Model Layer	Fracture γ	Input Description	Input Source	Type of Uncertainty
tcwF1	0.5866	ch1Fz	3.704 E-01	This value is read in by FEHM and used in calculating fracture spacing values based on the active fracture model.	LB0305TSPA18FF.001 [DIRS 165625] *"Eighteen 3-D Site Scale UZ Flow Fields Converted from TOUGH2 to T2FEHM Format"*. TOUGH2 File : glaq_mA.dat.	Fixed value for each layer but varies from layer to layer. The values also depend on climate.
tcwF2	0.5866	ch2Fz	3.704 E-01			
tcwF3	0.5866	ch3Fz	3.704 E-01			
ptnF1	0.9051E-01	ch4Fz	3.704 E-01			
ptnF2	0.9051E-01	ch5Fz	3.704 E-01			
ptnF3	0.9051E-01	ch6Fz	3.704 E-01			
ptnF4	0.9051E-01	pp4Fz	3.704 E-01			
ptnF5	0.9051E-01	pp3Fd	1.989 E-01			
ptnF6	0.9051E-01	pp2Fd	1.989 E-01			
tswF1	0.1289	pp1Fz	3.704 E-01			
tswF2	0.6000	bf3Fd	1.989 E-01			
tswF3	0.6000	bf2Fz	3.704 E-01			
tswF4	0.5686	tr3Fd	1.989 E-01			
tswF5	0.5686	tr2Fz	3.704 E-01			
tswF6	0.5686	pcF38	0.000 E-01			
tswF7	0.5686	pcF39	0.000 E-01			
tswF8	0.5686	pcF1z	0.000 E-01			
tswFz	0.3704	pcF2z	0.000 E-01			
tswFv	0.2500	pcF5z	0.000 E-01			
ch1Fv	0.2500	pcF6z	0.000 E-01			
ch2Fv	0.2500	pcF4p	0.000 E-01			
ch3Fv	0.2500	tcwFf (fault)	4.000 E-01			
ch4Fv	0.2500	ptnFf (fault)	1.138 E-01			
ch5Fv	0.2500	tswFf (fault)	3.000 E-01			
ch6Fv	0.2500	chnFf (fault)	3.000 E-01			

3-D = three-dimensional; FEHM = finite element heat and mass (model); UZ = unsaturated zone

Table 6-12. Fracture Gamma Parameter for Upper-Bound Infiltration Scenario

Model Layer	Fracture γ	Model Layer	Fracture γ	Input Description	Input Source	Type of Uncertainty
tcwf1	0.5000	ch1fz	5.000 E-01	This value is read in by FEHM and used in calculating fracture spacing values based on the active fracture model.	LB0305TSPA18FF.001 [DIRS 165625] "Eighteen 3-D Site Scale UZ Flow Fields Converted from TOUGH2 to T2FEHM Format." TOUGH2 File: glaq_uA.dat.	Fixed value for each layer but varies from layer to layer. The values also depend on climate.
tcwF2	0.5000	ch2Fz	5.000 E-01			
tcwF3	0.5000	ch3Fz	5.000 E-01			
ptnF1	0.8319E-01	ch4Fz	5.000 E-01			
ptnF2	0.8319E-01	ch5Fz	5.000 E-01			
ptnF3	0.8319E-01	ch6Fz	5.000 E-01			
ptnF4	0.8319E-01	pp4Fz	5.000 E-01			
ptnF5	0.8319E-01	pp3Fd	5.000 E-01			
ptnF6	0.8319E-01	pp2Fd	5.000 E-01			
tswF1	0.1000	pp1Fz	5.000 E-01			
tswF2	0.5606	bf3Fd	5.000 E-01			
tswF3	0.5606	bf2Fz	5.000 E-01			
tswF4	0.5700	tr3Fd	5.000 E-01			
tswF5	0.5700	tr2Fz	5.000 E-01			
tswF6	0.5700	pcF38	0.000 E-01			
tswF7	0.5700	pcF39	0.000 E-01			
tswF8	0.5700	pcF1z	0.000 E-01			
tswFz	0.5000	pcF2z	0.000 E-01			
tswFv	0.2500	pcF5z	0.000 E-01			
ch1Fv	0.2500	pcF6z	0.000 E-01			
ch2Fv	0.2500	pcF4p	0.000 E-01			
ch3Fv	0.2500	tcwFf (fault)	4.000 E-01			
ch4Fv	0.2500	ptnFf (fault)	1.138 E-01			
ch5Fv	0.2500	tswFf (fault)	3.000 E-01			
ch6Fv	0.2500	chnFf (fault)	3.000 E-01			

3-D = three-dimensional; FEHM = finite element heat and mass (model); UZ = unsaturated zone

6.5.7 Fracture Porosity, Fracture Spacing (m), and Fracture Aperture (m)

Fracture porosity is used in FEHM to calculate the fracture pore volume of the corresponding fracture node block for determining the resident time of radionuclides within each fracture cell.

Fracture spacing and aperture data are used by FEHM in estimating the effect of matrix diffusion on radionuclide transport. In the abstraction model, aperture and spacing based on geometric considerations are adjusted before use in the transport calculations to conform to the assumptions of the AFM of Liu et al. (1998 [DIRS 105729]). This section describes the geometric parameters. For a discussion of how the model implements the AFM for transport, see Appendix C, Section C5.

The fracture porosity and fracture spacing data are sampled to address the uncertainty of fracture properties on radionuclide transport in TSPA calculations. The data sets (DTNs: LB0205REVUZPRP.001 [DIRS 159525] and LB0207REVUZPRP.001 [DIRS 159526]) list fracture spacing data in terms of fracture frequency, defined as the inverse of fracture spacing. Thus, the fracture frequency is first sampled, and the inverse of the sampled data are taken to derive sampled fracture spacing data.

Table 6-13 lists the uncalibrated fracture porosity and frequency data based on field information. Among them, data for the fault zone are from DTN: LB0207REVUZPRP.001 [DIRS 159526]. Those are the uncalibrated properties as developed in *Calibrated Properties Model* (BSC 2004 [DIRS 169857]). However, fracture porosity and frequency data are not subject to adjustment in the calibration in *Calibrated Properties Model* (BSC 2004 [DIRS 169857]), therefore, these properties are carried forward into the calibrated property set without modification.

Among the listed geological rock layers, only those below the repository (tswf3 and below) could affect the transport of radionuclides downward toward the water table. Therefore, the sampling of properties in TSPA-LA is limited to these layers. Nevertheless, the use of this model in TSPA analyses requires further simplification to reduce to a manageable level the number of transport parameters that are varied stochastically in the TSPA realizations. For the purpose of assigning stochastic values of the fracture aperture, rock layers below the repository are grouped together based on similarity in the fracture porosity and frequency characteristics. The stochastic parameter values for aperture define the inherent level of uncertainty that needs to be propogated through the UZ transport abstraction model. This procedure and the uncertainty assessment for aperture are for the purposes of defining input to the UZ transport abstraction model. There are no results from the flow model that constrain the value of aperture suitable for use in the UZ transport abstraction model. Therefore, no assumptions of upstream models are violated, and the grouping and averaging procedure is valid for this purpose.

The nine groups identified are shown in Table 6-14. For groups with multiple units having different parameter values, an arithmetic average value is used for the group. An arithmetic average is sufficient because the variation of mean values between members of any group are insignificant relative to the standard deviation, as can be seen from Table 6-13. There is only one standard deviation for fracture porosity, so the other groups are assigned a fracture porosity standard deviation such that the ratio of the standard deviation to the mean is constant for all the groups. Group 9 (tswf3) has its own standard deviation for fracture frequency, which is used. For the other groups, the standard deviation is set equal to 0.831 times the mean. This is based on the relationship between fracture frequency and the standard deviation of fracture frequency found for model units above the proposed repository (see Figure 6-12). In this way, the mean and standard deviation for each parameter in each group were computed.

As porosity must lie within the finite range of 0 to 1, a beta distribution with these bounds is suitable for studying the influence of porosity uncertainty on radionuclide transport. Table 6-15 lists the distribution data for fracture porosity.

Given that fracture frequency can theoretically span values from zero to infinity, the lognormal distribution is suitable. The mean and standard deviation for $\ln(f)$ are given in terms of the

mean and standard deviation for f by the following relationships from the document by Hogg and Craig (1978 [DIRS 163236], pp. 180 and 432):

$$\mu_{\ln(f)} = \ln(\mu_f) - \frac{1}{2}\ln\left(1 + \frac{\sigma_f^2}{\mu_f^2}\right) \quad \text{(Eq. 6-24)}$$

$$\sigma_{\ln(f)} = \sqrt{\ln\left(1 + \frac{\sigma_f^2}{\mu_f^2}\right)} \quad \text{(Eq. 6-25)}$$

For further information on this derivation, see Appendices A and K in *Drift-Scale Radionuclide Transport* (BSC 2004 [DIRS 170040]), Equations A-1, A-2, and K-4 through K-7. Values for $\mu_{\ln(f)}$ and $\sigma_{\ln(f)}$ are given in Table 6-15.

Table 6-13. Fracture Porosity and Frequency Data

Model Layer	ϕ_f	Std. Dev.	f (1/m)	σ_f	Input Description	Input Source	Type of Uncertainty
tcwF1	2.4E-2	-	0.92	0.94	ϕ_f is the fracture porosity and f is fracture frequency. σ_f is the standard deviation for the fracture frequency. Data are uncalibrated. However, the fracture porosity and fracture frequency data are not subject to adjustment in calibration; therefore, those properties are carried forward into the calibrated property set without modification.	LB0205REVUZPRP.001 [DIRS 159525] Fault zone fracture porosity data are from LB0207REVUZPRP.001 [DIRS 159526].	As porosity must fall in the range of 0 and 1, a beta distribution is suitable to describe the uncertainty of the porosity values.
tcwF2	1.7E-2	-	1.91	2.09			
tcwF3	1.3E-2	-	2.79	1.43			
ptnF1	9.2E-3	-	0.67	0.92			
ptnF2	1.0E-2	-	0.46	-			
ptnF3	2.1E-3	-	0.57	-			
ptnF4	1.0E-2	-	0.46	0.45			
ptnF5	5.5E-3	-	0.52	0.6			
ptnF6	3.1E-3	-	0.97	0.84			
tswF1	5.0E-3	-	2.17	2.37			
tswF2	8.3E-3	-	1.12	1.09			
tswF3	5.8E-3	-	0.81	1.03			
tswF4	8.5E-3	2.50E-03	4.32	3.42			
tswF5	9.6E-3	-	3.16	-			
tswF6	1.3E-2	-	4.02	-			
tswF7	1.3E-2	-	4.02	-			
tswF8/pcF38	1.1E-2	-	4.36	-			
tswFz/tswFv/pcF39 (tswf9)	4.3E-3	-	0.96	-			
ch1Fv	6.1E-4	-	0.10	-			
ch2Fv	7.7E-4	-	0.14	-			
ch3Fv	7.7E-4	-	0.14	-			

Table 6-13. Fracture Porosity and Frequency Data (Continued)

Model Layer	ϕ_f	Std. Dev.	f (1/m)	σ_f	Input Description	Input Source	Type of Uncertainty
ch4Fv	7.7E-4	-	0.14	-	ϕ_f is the fracture porosity and f is fracture frequency. σ_f is the standard deviation for the fracture frequency. Data are uncalibrated. However, the fracture porosity and fracture frequency data are not subject to adjustment in calibration; therefore, those properties are carried forward into the calibrated property set without modification.	LB0205REVUZPRP.001 [DIRS 159525] Fault zone fracture porosity data are from LB0207REVUZPRP.001 [DIRS 159526].	As porosity must fall in the range of 0 and 1, a beta distribution is suitable to describe the uncertainty of the porosity values.
ch5Fv	7.7E-4	-	0.14	-			
ch6Fv	7.7E-4	-	0.14	-			
ch1Fz/pcF1z	1.6E-4	-	0.04	-			
ch2Fz/pcF2z	3.7E-4	-	0.14	-			
ch3Fz	3.7E-4	-	0.14	-			
ch4Fz	3.7E-4	-	0.14	-			
ch5Fz/pcF5z	3.7E-4	-	0.14	-			
ch6Fz/pcF6z	1.6E-4	-	0.04	-			
pp4Fz/pcF4p	3.7E-4	-	0.14	-			
pp3Fd	9.7E-4	-	0.20	-			
pp2Fd	9.7E-4	-	0.20	-			
pp1zF	3.7E-4	-	0.14	-			
bf3Fd	9.7E-4	-	0.20	-			
bf2Fz	3.7E-4	-	0.14	-			
tr3Fd	9.7E-4	-	0.20	-			
tr2Fz	3.7E-4	-	0.14	-			
tcwFf fault	2.9E-2	-	1.90	-			
ptnFf fault	1.1E-2	-	0.54	-			
tswFf fault	2.5E-2	-	1.70	-			
chnFf fault	1.0E-3	-	0.13	-			

Table 6-14. Fracture Porosity and Frequency in Each Model Layer, and Grouping of Fracture Rock Layers Below the Repository

Group	Units	Porosity	Frequency (m^{-1})
1	chnFf	1.0E-3	0.13
2	tswFf	2.5E-2	1.7
3	ch[2,3,4,5]Fz	3.7E-4	0.14
	pc[2,5]Fz	3.7E-4	0.14
	pp4Fz/pcF4p	3.7E-4	0.14
	pp1Fz	3.7E-4	0.14
	bf2Fz	3.7E-4	0.14
	tr2Fz	3.7E-4	0.14
4	pp3Fd	9.7E-4	0.20
	pp2Fd	9.7E-4	0.20
	bf3Fd	9.7E-4	0.20
	tr3Fd	9.7E-4	0.20
5	ch1Fz/pcF1z	1.6E-4	0.04
	ch6Fz/pcF6z	1.6E-4	0.04
6	ch1Fv	6.1E-4	0.10
	ch[2,3,4,5,6]Fv	7.7E-4	0.14

Table 6-14. Fracture Porosity and Frequency in Each Model Layer, and Grouping of Fracture Rock Layers Below the Repository (Continued)

Group	Units	Porosity	Frequency (m^{-1})
7	tswF9/pcF39/ tswFz/tswFv	4.3E-3	0.96
8	tswF4	8.5E-3	4.32
	tswF5	9.6E-3	3.16
	tswF[6,7]	1.3E-2	4.02
	tswF8/pcF38	1.1E-2	4.36
9	tswF3	5.8E-3	0.81

DTNs: LB0205REVUZPRP.001 [DIRS 159525];
LB0207REVUZPRP.001 [DIRS 159526].

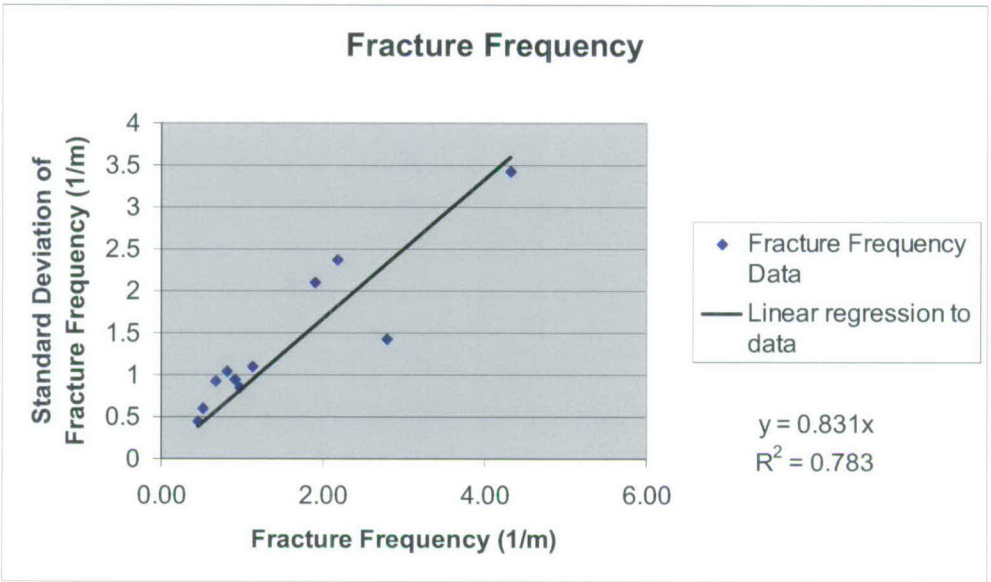

Output DTN: LA0506BR831371.001.

Figure 6-12. Relationship Between Fracture Frequency and Standard Deviation

Table 6-15. Fracture Porosity and Frequency Distribution Data for Layers Below the Repository

		Porosity (-) Beta Distribution min = 0; max = 1		Fracture Frequency (m^{-1})		Fracture Frequency (m^{-1}) Lognormal Distribution		Aperture (m) 2b Derived from Eq. 6-26: $2b = \frac{\phi_f}{f}$
Group	Units	Mean	Std Dev	Mean	Std Dev	Mean For ln (f)	Std Dev For ln (f)	
1	chnFf	1.0E-03	3.09E-04	1.26E-01	1.05E-01	-2.33E+00	7.24E-01	7.94E-03
2	tswFf	2.5E-02	7.25E-03	1.75E+00	1.45E+00	2.96E-01	7.24E-01	1.43E-02
3	ch[3,4]Fz	3.7E-4	1.09E-04	1.40E-01	1.16E-01	-2.23E+00	7.24E-01	2.64E-03
	ch[2,5]Fz/pcF[2,5]z							
	pp4Fz/pcf4p							
	pp1Fz							
	bf2Fz							
	tr2Fz							
4	pp3Fd	9.7E-4	2.85E-04	2.00E-01	1.66E-01	-1.87E+00	7.24E-01	4.85E-03
	pp2Fd							
	bf3Fd							
	tr3Fd							
5	ch1Fz/pcF1z ch6Fz/pcF6z	1.6E-4	4.71E-05	4.00E-02	3.32E-02	-3.48E+00	7.24E-01	4.00E-03
6	ch[1,2,3,4,5,6]Fv	6.9E-4	2.03E-04	1.20E-01	9.96E-02	-2.38E+00	7.24E-01	5.75E-03
7	tswFv,tswFz /pcF39 (tswF9)	4.3E-3	1.26E-03	9.60E-01	7.97E-01	-3.03E-01	7.24E-01	4.48E-03
8	tswF[4,5]	1.05E-02	3.10E-03	3.97E+00	3.29E+00	1.12E+00	7.24E-01	2.64E-03
	tswF[6,7]							
	tswF8/pcF38							
9	tswF3	5.8E-3	1.71E-03	8.10E-01	1.03E+00	-6.92E-01	9.81E-01	7.16E-03

Output DTN: LA0506BR831371.001.

In TSPA-LA calculations, the fracture porosity and fracture frequency are sampled independently. The basis for this approximation is that there is only a very weak correlation between fracture porosity and frequency (Figure 6-13). Therefore, correlating these two parameters is not warranted.

The sampled fracture porosity and frequency data are used in deriving the fracture spacing and aperture based on the following relationship:

$$\phi_f = (2b)f \qquad \text{(Eq. 6-26)}$$

where $2b$ is the fracture aperture (m), f is the fracture frequency (m^{-1}), and ϕ_f is the fracture porosity (-). Fracture frequency is the inverse of the fracture spacing.

As a final comment, there is some indication from published studies that there may be a scale dependence of the effective area available for diffusion between the fractures and matrix. Liu

et al. (2004 [DIRS 169948]) propose that the effective diffusion term increases by several orders of magnitude over the range of scales of interest for mountain-scale trasnport, perhaps due the effect of increased surface area as a greater number of fractures are involved in the flow and transport system. To explore this possibility, a sensitivity analysis is presented (Section 6.6.4) in which the parameter range consistent with the correlation presented in the journal article by Liu et al. (2004 [DIRS 169948], Figure 2) is tested.

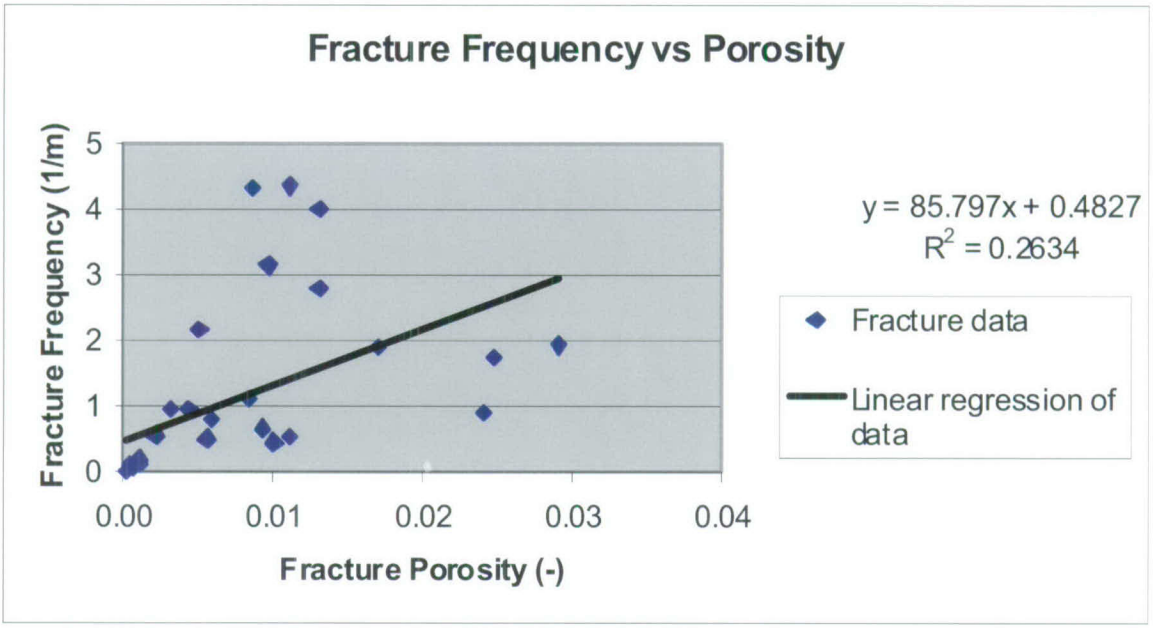

Output DTN: LA0506BR831371.001.

Figure 6-13. Relationship Between Fracture Porosity and Frequency

6.5.8 Fracture Surface Retardation Factor (Unitless)

Because few data are available on fracture surface retardation factors, no fracture surface retardation is simulated in the TSPA-LA model. In current TSPA simulations, the fracture surface retardation factors are set to 1.0 (no fracture surface retardation) to be conservative. Values of fracture surface retardation factors are included in FEHM input data file and are read in at run time (Table 6-16).

Table 6-16. Fracture Surface Retardation Factor

Rock Layers	Fracture Surface Retardation Factor	Input Description	Input Source	Type of Uncertainty
All layers	1.0	Parameter used to simulate the effect of fracture surface retardation on radionuclide transport.	N/A – conservative assumption used to assign this parameter	Fixed value

N/A = not applicable

6.5.9 Colloid Filtration at Matrix Interface

Matrix pore size distribution combined with colloid size distribution is used in FEHM for determining colloid filtration at the interfaces between matrix units. Each time step at a matrix unit interface FEHM compares a colloid's size against the sampled pore size of the matrix unit it is entering. If the colloid size is bigger than the pore size, then the colloid cannot enter the matrix and is removed from the simulation (permanently filtered). In TSPA simulations the cumulative probabilities for pore size distribution for each matrix unit are taken from DTN: LA0003MCG12213.002 [DIRS 147285] and listed in Table 6-17 (only colloid size data beneath the repository level are listed). In FEHM the matrix pore size data are sampled based on the cumulative pore size distribution probability data in Table 6-17 and the sampled data are used in simulating colloid filtration at matrix interfaces. Colloid filtration is only implemented for colloids with irreversibly bound radionuclides (see Section 6.4.5).

Table 6-17. Cumulative Probabilities for Colloid Transport at Matrix Interfaces

HGU (Group names)	UZ Model Units (entry layer)	Effective Pore Size to be Compared to Colloid Size (nm)						
		2,000	1,000	450	200	100	50	6
TMN / TSW4	Not used.	1.00	0.92	0.87	0.81	0.71	0.55	0.31
TLL / TSW5	tswM5	1.00	0.80	0.79	0.70	0.61	0.51	0.19
TM2 / TSW6	tswM6	1.00	0.94	0.90	0.82	0.65	0.51	0.21
TM1 / TSW7	tswM7	1.00	0.99	0.99	0.99	0.93	0.68	0.36
PV3 / TSW8	tswM8/pcM38	1.00	0.98	0.96	0.94	0.90	0.89	0.68
PV2 / TSW9	tswMz,tswMv (tswM9) / pcM39	1.00	0.72	0.57	0.47	0.39	0.35	0.22
BT1a / CH1	ch1Mv, ch1Mz/pcM1z	1.00	0.91	0.89	0.87	0.85	0.83	0.53
CHV	ch[2,3,4,5,6]Mv	1.00	0.58	0.49	0.43	0.39	0.36	0.07
CHZ	ch[3,4,]Mz, ch[2,5,6]Mz / pcM[2,5,6]z	1.00	0.79	0.76	0.73	0.68	0.56	0.30
BT / CH6	Not used.	1.00	0.95	0.94	0.92	0.92	0.85	0.40
PP1	pp1Mz	1.00	0.79	0.68	0.63	0.57	0.48	0.21
PP2	pp2Md	1.00	0.91	0.86	0.81	0.65	0.53	0.22
PP3	pp3Md	1.00	0.49	0.34	0.26	0.21	0.16	0.07
PP4	pp4Mz / pcM4p	1.00	0.99	0.99	0.98	0.98	0.96	0.32
BF2	bf2Mz	1.00	0.98	0.97	0.96	0.96	0.83	0.25
BF3	bf3Md	1.00	0.97	0.94	0.83	0.74	0.66	0.14
Type of Uncertainty		Fixed values						
Input Description		Data are used by FEHM in combination with colloid-size distribution data for simulating the effect of colloid filtration at matrix interface.						

Source DTN: LA0003MCG12213.002 [DIRS 147285].

FEHM = finite element heat and mass (model)

HGU = Hydrogeologic Units or layers as defined in Section 6.1 of *UZ Flow Models and Submodels* (BSC 2004 [DIRS 169861]), see Table 6-3 for correlation of HGU units and list of all UZ Model layers (FEHM zones).

6.5.10 Colloid Size Exclusion

Due to flow exchange between fractures and the corresponding matrix block, colloids may be carried into matrix from fractures by advection. The amount of colloids that can enter into matrix depends on the size of the colloids and the size of the matrix pores. At the fracture-matrix interface, when a colloid's size is larger than the matrix pore size, this colloid will stay in the fracture. On the other hand, when a particle size is smaller than the matrix pore size, the colloid will enter into the matrix through advection. The colloid size exclusion effect in the current FEHM model is simulated with a size exclusion factor f_c based on the percentage of the pores that are greater than the expected colloid size of 100 nm (DTN: LA0003MCG12213.002 [DIRS 147285]). Size exclusion is only implemented for colloids with irreversibly bound radionuclides (see Section 6.4.5). Table 6-18 lists the values used in FEHM. There is no site-specific transport data available to validate this aspect of the colloid transport model. The incorporation of this feature is intended to avoid a nonphysical situation in which colloids are allowed to enter the matrix even when they are larger than the typical pore size. This aspect of the model is conservative, in that it will tend to exclude some colloids from the slower moving matrix fluid and keep them in the fractures.

Table 6-18. Colloid Size Exclusion Factor Used in FEHM

HGU Groups	UZ Model Units	Size Exclusion Factor	Input Description	Input Source	Type of Uncertainty
TMN / TSW4	tswF4	0.29	Parameters are used by FEHM for simulating the effect of colloid size exclusion on radionuclide transport at the fracture-matrix interface.	LA0003MCG12213.002 [DIRS 147285]	Fixed value. In TSPA-LA simulations, a random number generator is used to determine the probability of a colloid entering into matrix from the corresponding fractures.
TLL / TSW5	tswF5	0.39			
TM2 / TSW6	tswF6	0.35			
TM1 / TSW7	tswF7	0.07			
PV3 / TSW8	tswF8/pcF38	0.10			
PV2 / TSW9	tswFz, tswFv (tswF9) / pcF39	0.61			
BT1a / CH1	ch1Fv, ch1Fz/pcF1z	0.15			
CHV	ch[2,3,4,5]Fv	0.61			
CHZ	ch[3,4]Fz, ch[2,5,6]Fz/ pcF[2,5,6]z	0.27			
BT / CH6	ch6Fv	0.08			
PP4	pp4Fz/pcF4p	0.02			
PP3	pp3Fd	0.79			
PP2	pp2Fd	0.35			
PP1	pp1Fz	0.43			
BF3	bf3Fd, tr3Fd	0.26			
BF2	bf2Fz, tr2Fz	0.04			
	tswFf	0.29			
	chnFf	0.27			

FEHM = finite element heat and mass (model); TSPA-LA = Total System Performance Assessment for the License Application. HGU = Hydrogeologic Units or layers as defined in Section 6.1 of *UZ Flow Models and Submodels* (BSC 2004 [DIRS 169861]), see Table 6-3 for correlation of HGU units and list of all UZ Model layers (FEHM zones) and their hydrogeologic associations.

NOTE: The tram and fault model units are not part of the TSPA-LA HGU groupings. The size exclusion factors for tr3Fd and tr2Fz used values from units in their associated rock groups. The units tswFf and chnFf represent faults in the Topopah Spring welded and Calico Hills nonwelded hydrogeologic units respectively. Their size exclusion factors were chosen from the highest associated unit under the repository.

6.5.11 Colloid Size Distribution

A colloid size distribution is used by FEHM to get the interpolated colloid size of each colloid particle. The colloid size information is then combined with pore size data to simulate filtration effects at matrix unit interfaces.

The colloid size range of 6 nm to 450 nm is based on *Colloid-Associated Radionuclide Concentration Limits: ANL* (CRWMS M&O 2001 [DIRS 154071], Section 6.3); DTN: LL000122051021.116 [DIRS 142973]. However, because a specific distribution was not available, the following distribution (Table 6-19) was chosen (not developed) to be consistent with *Colloid-Associated Radionuclide Concentration Limits: ANL* (CRWMS M&O 2001 [DIRS 154071], Figure 23).

The same colloid size distribution data are used in this abstraction model. FEHM data files contain the colloid size input data under the macro "size."

Table 6-19. Colloid Size Distribution

Colloid Size (nm)	Cumulative Probability	Input Description	Input Source	Type of Uncertainty
1	0	Colloid-size distribution data are used in simulating colloid filtration effect at matrix interface.	LL000122051021.116 [DIRS 142973]	FEHM read in the cumulative distribution data at run time. Random colloid size data are generated on the fly to address the effect of colloid size uncertainty on filtration.
6	0.2			
50	0.4			
100	0.6			
200	0.8			
450	1.0			

FEHM = finite element heat and mass (model)

6.5.12 Colloid Concentration and Colloid K_c

The colloid equilibrium sorption parameter K_c is defined as $K_c=C_{coll}/C_{fluid}$, where C_{coll} is the radionuclide concentration residing on colloids and C_{fluid} is the radionuclide concentration in fluid. Colloid K_c is used in FEHM as an input parameter for calculating the retardation factors for colloid facilitated radionuclide transport in the media.

Radionuclide sorption to colloids is categorized as either reversible and irreversible (Section 6.4.3). When sorption to colloids is treated as an irreversible process, a very large number (1.0E20) is assigned for K_c (see Table 6-20).

Table 6-20. K_c for Irreversible Colloid

Irreversible Colloids	K_c	Input Description	Input Source	Type of Uncertainty
Irreversible colloids	1.0E20	Simulating the effect of irreversible sorption to colloid	A large value that ensures the sorption process to colloids be irreversible	Fixed value

NOTE: This input value is not data; rather, it is a recommended input value to allow irreversible sorption to colloids to be simulated in the abstraction model.

In TSPA-LA calculations, to reflect the influence of reversible colloid facilitated radionuclide transport on system performance, colloid K_d values $K_{d,coll}$ are sampled at run time and used in the calculation of K_c. The sampled radionuclide sorption coefficients are then multiplied by the colloid concentration C_{coll} to calculate the colloid K_c values:

$$K_c = C_{coll} K_{d,coll} \quad \text{(Eq 6-27)}$$

Field data and laboratory experiments have shown that colloid concentration in groundwater can vary several order of magnitudes and is also a function of ionic strength and groundwater pH (BSC 2005 [DIRS 174290]; DTN: SN0306T0504103.005 [DIRS 164132]). To address the uncertainty of colloid concentration on colloid facilitated radionuclide transport, in TSPA-LA, the colloid concentration is sampled at run time and provided to FEHM for the calculation of reversible colloid K_c. Table 6-21 lists the distribution of colloid concentration used in TSPA-LA

and Table 6-22 presents the distributions of sorption coefficients onto colloids. As shown in the table, a cumulative distribution with values ranging from 0.001 to 200 mg/L is used if the ionic strength of the fluid is low (<0.05 M). However, to account for the fact that high ionic strength results in colloid flocculation, and, hence, low colloid concentrations, a value of 1.E-6 mg/L is used for high ionic strength fluids (>=0.05 M). Median values in Tables 6-21 and 6-22 are used to calculate the distributions used for colloids in the base-case model (see Section 6.6).

Colloid concentrations are sampled from the same distribution for the EBS, UZ, and SZ components of the TSPA model because the available information does not distinguish concentration of colloids in the EBS, UZ, and SZ. The current implementation is based on uncorrelated sampling of colloid concentrations in each domain (BSC 2005 [DIRS 174227], Section 6.3.8.4.1). Because correlating these concentrations may lead to a wider range of dose response in the TSPA model, a sensitivity study using the TSPA model is recommended in which colloid concentrations are 100% correlated between the EBS, UZ, and SZ components of the TSPA model.

Sorption coefficients for radionuclides on smectite colloids are sampled from the same distributions for the EBS, UZ, and SZ components of the TSPA model because no other site-specific data are available. The current implementation is based on uncorrelated sampling of sorption coefficients on smectite colloids in each component model for each radionuclide and in each domain (BSC 2005 [DIRS 174227], Section 6.3.8.4.1). Independent sampling for radionuclide sorption onto smectite colloids between the UZ and SZ components of the TSPA model is supported by the fact that factors controlling sorption onto colloids in these two environements are believed to be relatively independent (BSC 2004 [DIRS 164500], Appendix B2). For UZ and EBS transport, it is recommended that the following sensitivities be performed using the TSPA model:

- Correlate the K_d values on smectite colloids for Am and Pa with a correlation coefficient of 0.75. No correlation will be used for Am and Th. These are based on the correlations presented in *Radionuclide Transport Models Under Ambient Conditions* (BSC 2004 [DIRS 164500], Table B-2) for sorption of these radionuclides onto tuff.

- Correlate K_d values on smectite colloids 100% between the EBS and UZ components of the TSPA model to investigate the uncertainty in the sorption behavior between these two domains.

Table 6-21. Colloid Concentration Distribution

Colloid Concentration (mg/L)	Cumulative Probability	Input Description	Input Source	Type of Uncertainty
0.001 to 0.1	50	Ionic strength less than 0.05. Data are used in the estimation of reversible colloid Kc.	BSC 2005 [DIRS 174290], Section 6.3.2.4, Table 6-4. SN0306T0504103.005 [DIRS 164132]	The cumulative distribution data listed in this table will be used to generate random colloid concentrations at TSPA-LA runtime to address the influence of colloid concentration uncertainty of radionuclide transport.
0.1 to 1.0	75			
1.0 to 10	90			
10 to 50	98			
50 to 200	100			
1.E-6	100	Ionic strength >= 0.05		

NOTE: The probability of occurrence values listed in the source Table 6-4 are summed up to generate the cumulative probability in this table.

TSPA-LA = Total System Performance Assessment for the License Application.

Table 6-22. Radionuclide Sorption Coefficient (mL/g) onto Colloids

Radionuclide	Colloid	Values (-)	K_d Value Intervals	K_d Value Interval Probability of Occurrence	K_d Value Interval Cumulative Probability of Occurrence
Pu	Iron-(hydr)oxide	10^4 to 10^6	$< 1 \times 10^4$	0.	0.
			1×10^4 to 5×10^4	0.15	0.15
			5×10^4 to 1×10^5	0.20	0.35
			1×10^5 to 5×10^5	0.50	0.85
			5×10^5 to 1×10^6	0.15	1.00
			$> 1 \times 10^6$	0.	
Pu	Smectite	10^3 to 10^6	$< 1 \times 10^3$	0.	0.
			1×10^3 to 5×10^3	0.04	0.04
			5×10^3 to 1×10^4	0.08	0.12
			1×10^4 to 5×10^4	0.25	0.37
			5×10^4 to 1×10^5	0.20	0.57
			1×10^5 to 5×10^5	0.35	0.92
			5×10^5 to 1×10^6	0.08	1.00
			$> 1 \times 10^6$	0.	
Am, Th, Pa	Iron-(hydr)oxide	10^5 to 10^7	$< 1 \times 10^5$	0.	0.
			1×10^5 to 5×10^5	0.15	0.15
			1×10^5 to 5×10^5	0.20	0.35
			1×10^6 to 5×10^6	0.55	0.90
			5×10^6 to 1×10^7	0.10	1.00
			$> 1 \times 10^7$	0.	
	Smectite	10^4 to 10^7	$< 1 \times 10^4$	0.	0.
			1×10^4 to 5×10^4	0.07	0.07
			5×10^4 to 1×10^5	0.10	0.17
			1×10^5 to 5×10^5	0.23	0.40
			5×10^5 to 1×10^6	0.20	0.60
			1×10^6 to 5×10^6	0.32	0.92
			5×10^6 to 1×10^7	0.08	1.00
			$> 1 \times 10^7$	0.	
Cs	Iron-(hydr)oxide	10^1 to 10^3	$< 1 \times 10^1$	0.	0.
			1×10^1 to 5×10^1	0.13	0.13
			5×10^1 to 1×10^2	0.22	0.35
			1×10^2 to 5×10^2	0.55	0.90
			5×10^2 to 1×10^3	0.10	1.00
			$> 1 \times 10^3$	0.	
	Smectite	10^2 to 10^4	$< 1 \times 10^2$	0.	0.
			1×10^2 to 5×10^2	0.20	0.20
			5×10^2 to 1×10^3	0.25	0.45
			1×10^3 to 5×10^3	0.50	0.95
			5×10^3 to 1×10^4	0.05	1.00
			$> 1 \times 10^4$	0.	

Source: DTN: SN0306TO504103.006 [DIRS 164131]

6.5.13 Fractions of Colloids Traveling Unretarded and Colloid Retardation Factor

Colloid retardation factor, R_{coll}, is used in FEHM to study the impact of colloid retardation in the fractured media on either reversibly or irreversibly sorbed radionuclide transport. In addition, field experiments have shown that a small percentage of colloids transport through the groundwater system essentially without retardation (BSC 2004 [DIRS 170006]). The fractions of unretarded colloids have been developed based on field data and are listed in Table 6-23.

This table, derived in *Saturated Zone Colloid Transport* (BSC 2004 [DIRS 170006]), postulates that the fraction of colloids escaping retardation due to physical and chemical processes is a function of the residence time of the colloid and progressively fewer colloids migrate unretarded with time. This poses a difficulty in simulating transport for the unretarded colloids – the transport times of the combined UZ and SZ system are not known a priori. Therefore, it is recommended that the fraction be chosen for a transport time that can be reasonably expected to be conservative, such as 100 years for the combined system. Therefore, from Table 6-23, the fraction of colloids traveling unretarded should be set at 1.68E-03. If simulations suggest that a different residence time is more representative, then this time should be changed, and a new unretarded fraction should be selected from Table 6-23. It should be noted that this aspect of the colloid transport model is relatively uncertain, so parameter sensitivity studies are advisable if it is determined that a colloidal radionuclide are important to performance. Nevertheless, using the transport time of 100 years as the basis for the fraction of colloids traveling unretarded will result in a conservative model that provides an upper bound on rapid colloid transport.

Colloids traveling unretarded are given a colloid retardation factor of 1.

Table 6-23. Fractions of Colloids Traveling Unretarded

Transport Time (Years)	Fraction of Colloids Unretarded	Input Description	Input Source	Type of Uncertainty
1	1.10 E-02	This parameter is used in determining fractions of colloids traveling unretarded in the UZ.	BSC 2004 [DIRS 170006]; DTN: LA0303HV831352.003 [DIRS 165624]	Fixed value
5	5.70 E-03			
10	4.30 E-03			
20	3.24 E-03			
30	2.74 E-03			
40	2.44 E-03			
50	2.23 E-03			
75	1.89 E-03			
100	1.68 E-03			
300	1.07 E-03			
600	8.08 E-04			
1,000	6.56 E-04			
2,000	4.94 E-04			
5,000	3.40 E-04			
10,000	2.56 E-04			

UZ = unsaturated zone

For colloids that are delayed relative to a conservative species, the retardation of colloids in groundwater system depends on colloid type; colloid size; groundwater pH, Eh, and ionic strength; and rock properties, etc. Field tests at the C-wells complex near Yucca Mountain and Nevada Test Site and laboratory experiments were carried out under saturated conditions to estimate colloid retardation factors (BSC 2004 [DIRS 170006]). Although these experimental studies were performed under saturated conditions, their use in the UZ model is justified based on the fact that the fundamental fluid flow conditions at the scale of the filtration processes should be similar. In particular, the C-wells experiments were carried out in fractured tuffs, and the colloid retardation process in the UZ is also expected to be taking place within fractures. To account for the relatively large uncertainty associated with these processes, a broad distribution of colloid retardation factors is warranted. Table 6-24 lists the cumulative distribution data of colloid retardation factors.

Table 6-24. Colloid Retardation Factors

Colloid Retardation Factor	Cumulative Probability	Input Description	Input Source	Type of Uncertainty
6.00	0	Colloid retardation factor is used by FEHM in simulation of the effects of colloid retardation in fractured rock on colloid facilitated radionuclide transport.	Section 6.4.3 of BSC 2004 [DIRS 170006]; LA0303HV831352.002 [DIRS 163558]	A cumulative distribution is used to describe the distribution of colloid retardation factor. In TSPA-LA, the colloid retardation factor will be sampled at runtime and used by FEHM in TSPA-LA calculations.
6.00	0.15			
10.23	0.25			
26.00	0.50			
59.98	0.80			
800.	1.00			

FEHM = finite element heat and mass (model); TSPA-LA = Total System Performance Assessment for the License Application

In TSPA-LA calculations, to investigate the uncertainty of colloid retardation factors on radionuclide transport, colloid retardation factors are sampled for each realization at run time based on the given cumulative distribution in Table 6-24.

Colloid retardation factors are sampled from the same distribution for the UZ and SZ component of the TSPA model because no other site-specific data are available. The current implementation is based on uncorrelated sampling of colloid retardation factors in each domain (BSC 2005 [DIRS 174227], Section 6.3.8.4.1). The available information does not distinguish retardation of colloids in the UZ and SZ. Because correlating the retardation factors may lead to a wider range of dose response in the TSPA model, a sensitivity study using the TSPA model is recommended in which colloid retardation factors are 100% correlated between the UZ and SZ.

6.5.14 Radionuclide Half Lives (Years) and Daughter Products

FEHM needs the radionuclide half lives and information on daughter products to simulate the influence of radionuclide decay and ingrowth on system performance. The radionuclide half life and daughter products for the following species are used in FEHM as input parameters (see Table 6-25).

6.5.15 Repository Radionuclide Release Bins

Radionuclides will be released from nodes corresponding to the repository location. These nodes were grouped into bins (zones) that shared common infiltration ranges, to be compatible with a conceptual model for radionuclide release in which releases are a strong function of the percolation rates at the repository horizon. This would help to categorize release points according to high or low percolation rates. Five bins were chosen based on the cumulative probability of percolation for the glacial-transition climate period. The glacial-transition period was selected to perform this binning because the majority of the simulation is performed under this climate state. The definition of the 5 bins is listed in Table 6-26.

Node coordinates within each bin are given in the multiscale thermal-hydrologic model (DTN: LL030610323122.029 [DIRS 164513]). As the grid resolution of the thermal-hydrologic model is much finer (file: *NEVADA_SMT_percolation_BIN_ma.txt.* DTN: LL030610323122.029 [DIRS 164513]) than the UZ transport abstraction model, the node coordinates of the thermal-hydrologic model are mapped onto the FEHM grid to derive the corresponding FEHM nodes.

Table 6-25. Radionuclide Half-Lives and Daughter Products Used in the TSPA-LA

Radionuclide	Half-Life (yr)	Daughter Product	Input Description	Input Source	Type of Uncertainty
^{14}C	5.715E+03		Radionuclide half-lives and daughter products. Those data will be used by FEHM in radionuclide decay and ingrowth calculations.	Parrington et al. 1996 [DIRS 103896] DTN: N/A established fact	Fixed values
^{135}Cs	2.3E6				
^{137}Cs	3.007E+1				
^{129}I	1.57E+7				
^{90}Sr	2.878E+1				
^{99}Tc	2.13E+5				
^{243}Am	7.37E+3	^{239}Pu			
^{239}Pu	2.410E+4	^{235}U			
^{235}U	7.04E+8	^{231}Pa			
^{231}Pa	3.28E+04				
^{241}Am	4.327E+2	^{237}Np			
^{237}Np	2.14E+06	^{233}U			
^{233}U	1.592E+5	^{229}Th			
^{229}Th	7.3E+3				
^{240}Pu	6.56E+3	^{236}U			
^{236}U	2.342E+7	^{232}Th			
^{232}Th	1.40E+10				
^{232}U	6.98E+1				
^{242}Pu	3.75E+5	^{238}U			
^{238}Pu	8.77E+1	^{234}U			
^{238}U	4.47E+9	^{234}U			
^{234}U	2.46E+5	^{230}Th			
^{230}Th	7.54E+4	^{226}Ra			
^{226}Ra	1.599E+3				

FEHM = finite element heat and mass (model); N/A = not applicable

NOTE: Irreversible and reversible colloid facilitated radionuclide has the same half-life and daughter products as corresponding dissolved species.

Table 6-26. Definition of Repository Release Bins

	Bin 1	Bin 2	Bin 3	Bin 4	Bin 5
Range of Cumulative Probability	0 – 0.05	0.05 – 0.30	0.30 – 0.70	0.70 – 0.95	0.95 – 1.00
Range of Percolation for Glacial-Transition Climate (mm/year)	0.73 – 6.71	6.71 – 11.77	11.77 – 21.22	21.22 – 38.48	38.48 – 76.67

Source: BSC 2005 [DIRS 173944], Appendix VIII, "Binning Calculations."

NOTE: For percolation values, see file *NEVADA_SMT_percolation_BIN_ma.txt* in DTN: LL030610323122.029 [DIRS 164513].

The mapping was done using FEHM V2.21 (LANL 2003 [DIRS 165741]) and Microsoft Excel. The smeared-sources mountain-scale thermal model (SMT) node coordinates from the thermal-hydrologic model were read in by FEHM using the "zone" macro. FEHM did a search to find the closest node to a given SMT coordinate. Once FEHM nodes corresponding to the given SMT coordinates were found, Excel was used to get the frequency of FEHM node within each bin. The following rules are applied during the mapping using Excel.

- As the FEHM grid is coarser than the thermal-hydrologic model grid, it is possible that some nodes in the thermal-hydrologic model within different bins may map onto a single FEHM node in the corresponding bins. In this case, the FEHM node with the most frequent appearance prevails. For example, FEHM 36189 appeared two times in bin 1 and four times in bin 4. Based on the rule, FEHM node 36189 was assigned to bin 4.

- When an FEHM node appears an equal number of times in different bins, this node will be assigned to the highest bin number. For example, FEHM node 39316 appeared three times in bin 2 and bin 3, respectively. Thus, node 39316 was assigned to bin 3.

A file containing a listing of these bins and the associated nodes was created and named*repo.zon.xls*. The bin data are incorporated into FEHM zone files in TSPA simulations and used to release radionuclides from the repository.

Figures 6-14 and 6-15 plot the location of SMT repository release nodes and the transformed FEHM repository release nodes, respectively. It is clear that the transformed FEHM release nodes corresponding to the SMT release nodes closely. But, because of the much coarser FEHM grid and the lack of a one-to-one transformation from one grid to the other, the FEHM repository release nodes does not capture the detail depicted in the SMT grid. Nevertheless, the transformation is sufficient for the purposes of depicting the role of percolation variability on radionuclide releases and transport.

6.5.16 Radionuclide Collecting Bins at UZ/SZ Interface

For the UZ/SZ interface, all nodes at (or below) the highest potential water table elevation of 850 m in the UZ transport abstraction model were grouped into four regions (or bins). The purpose of this process is for increased resolution to be captured in the TSPA-LA model with respect to the arrival location and its impact on transport times in the SZ. Radionuclide mass reaching the water table in one location may have a different SZ travel path and transport time

than mass arriving at some other location. The collecting bins are the means by which this potentially significant feature of the system can be quantified. As discussed in *Saturated Zone Flow and Transport Model Abstraction* (BSC 2005 [DIRS 174012], Section 6.5.2.13), these source regions were selected to be compatible with the overall repository extent and on the general pattern of groundwater flow within the UZ model domain. Then, within the SZ transport simulations described in *Saturated Zone Flow and Transport Model Abstraction* (BSC 2005 [DIRS 174012]), the total radionuclide mass flow rate in each of these four bins will be focused at a random point (within each of the four bins), which is appropriate for a single leaking waste package or for highly focused groundwater flow along a fault or single fracture in the UZ. A more diffuse source of radionuclides at the water table may be more physically realistic for later times when numerous leaking waste packages occur, however, the use of a point source in the SZ is an approach that overestimates the concentration of radionuclides near the source (BSC 2005 [DIRS 174012], Section 6.5.2.13). The four regions (Figure 6-16) are defined by an east-west boundary at a Universal Transverse Mercator (UTM) easting coordinate of 548,50 m and a north-south boundary at a UTM northing coordinate at 4,078,63 m (BSC 2005 [DIRS 174012], Table 6-8).

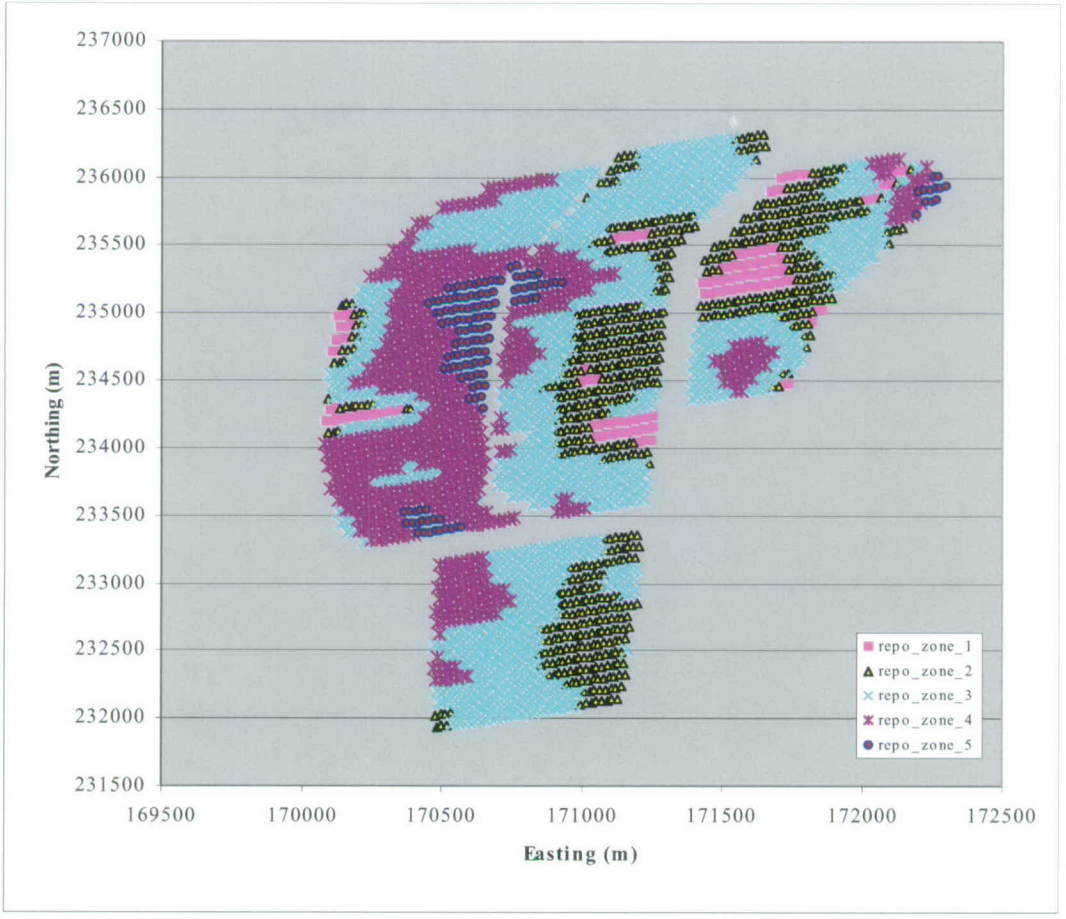

Output DTN: LA0506BR831371.001.

Figure 6-14. SMT Repository Release Nodes

All nodes at or beneath the water table in the UZ transport abstraction model were grouped into one of the four regions based on data listed in *Saturated Zone Flow and Transport Model Abstraction* (BSC 2005 [DIRS 174012], Table 6-8). All particles falling into each FEHM water table collecting bin are used to compute the input to the appropriate SZ source release bin. Since the FEHM water table collecting bins are larger than the SZ source release bins (defined in Figure 6-16), it is assured that no particles fall outside of the four SZ release zones and go uncounted. The FEHM water table collecting bin nodes were extracted from the ELEME data from TOUGH2 site scale flow model package (DTN: LB0323DSSCP9I.001 [DIRS 163044]). The data contain the cell name and coordinates for each node in the site scale UZ flow model. As the UZ transport abstraction model uses the Nevada State Plane coordinates, the given UTM coordinates are converted into Nevada State Plane coordinates during the extraction of the water table collect bins. The extraction was done in an Excel spreadsheet through several conditional if statements (see Appendix B for details).

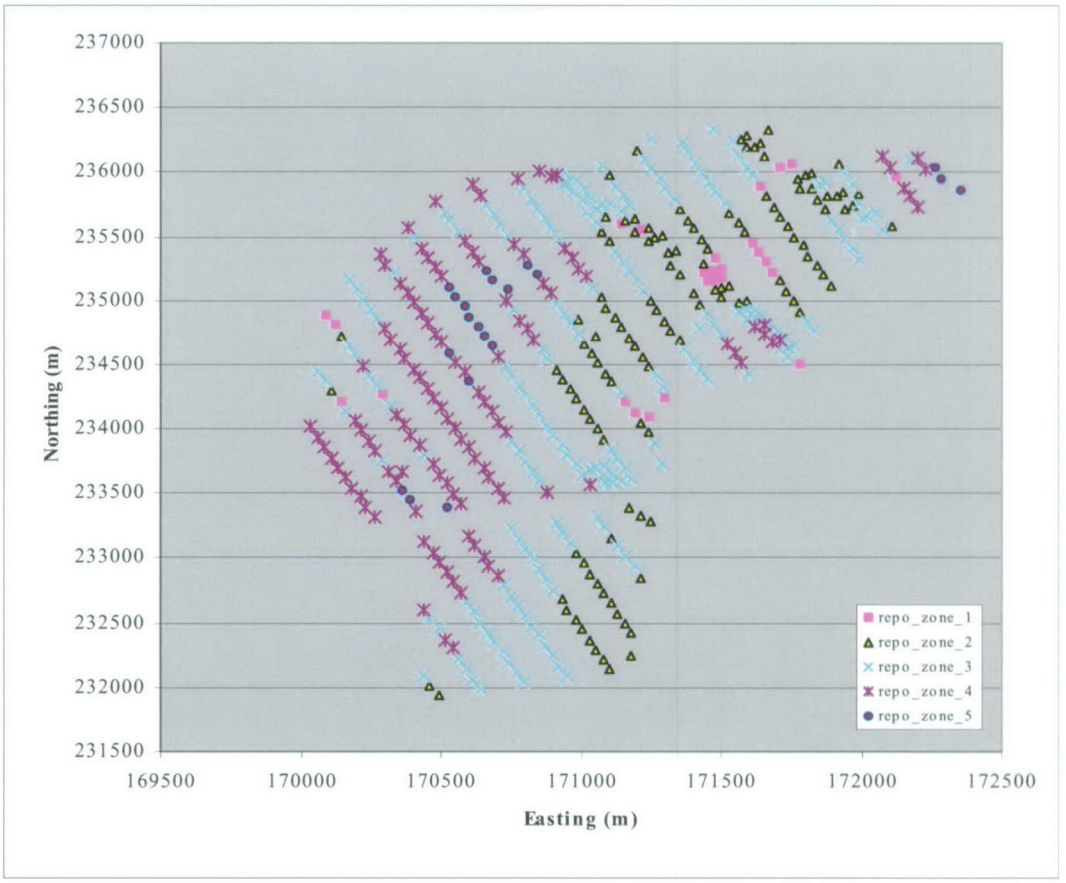

Output DTN: LA0506BR831371.001.

Figure 6-15. FEHM Repository Release Nodes Transformed Based on SMT Release Nodes (Shown in Figure 6-14)

The four collecting bins in FEHM are named 701, 702, 703, and 704, containing SZ source release regions 1, 2, 3, and 4, respectively. Among them, zone 701 contains all nodes beneath the water table with a UTM easting coordinate less than 548500 m (NSP: 171189.79 m) and a

UTM northing coordinate greater than 4078630 m (NSP: 233459.87 m); zone 702 contains all water table nodes with a UTM easting coordinate greater than 548500 m (NSP: 171189.79 m) and a UTM northing coordinate greater than 4078630 m (NSP: 233459.87 m); zone 703 contains all water table nodes with a UTM easting coordinate less than 548500 m (NSP: 171189.79 m) and a UTM northing coordinate less than 4078630 m (NSP: 233459.87 m); and zone 704 contains water table nodes with a UTM easting coordinate greater than 548500 m (NSP: 171189.79 m) and a UTM northing coordinate less than 4078630 m (NSP: 233459.87 m).

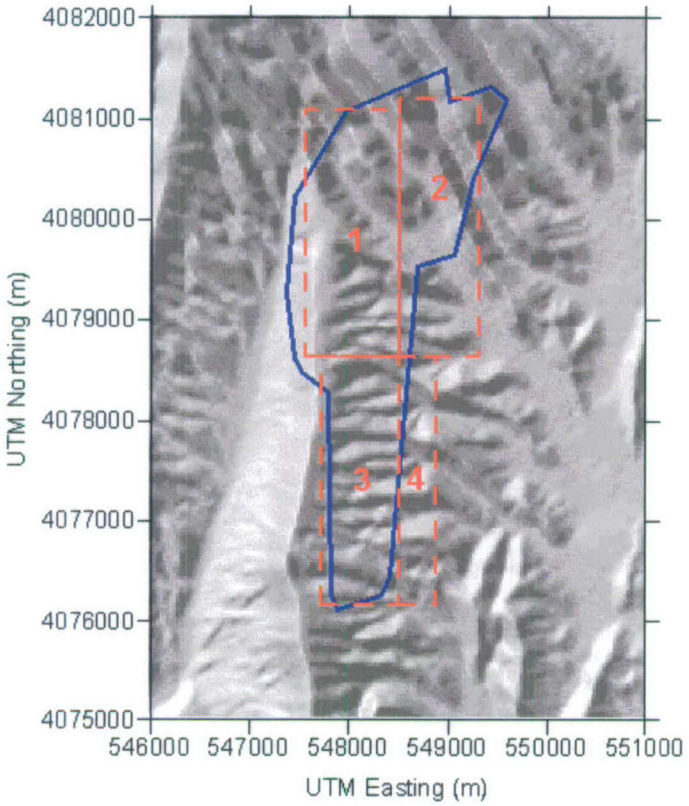

Source: BSC 2005 [DIRS 174012], Figure 6-27.

NOTE: Dashed lines represent the boundaries of the SZ release regions and the solid lines represent the boundary of the repository release region.

Figure 6-16. Source Regions for Radionuclide Release in the SZ Transport Abstraction Model

Nodes contained in each of the collection bins were stored in file *wt.zone* and defined in the corresponding FEHM zone file. These nodes are contained in the output DTN: LA0506BR831371.001. Once a particle reaches the water table, the particle is removed from the UZ transport system. Inside FEHM, the code records mass leaving the system within each bin/zone (FEHM V2.21 Users Manual, LANL 2003 [DIRS 165741]). As climate change can cause water table rise or fall, the defined collection bins/zones contain all nodes between the lowest and the highest water tables, up to an elevation of 850 m (see Section 6.4.8 for details). Note that for the simulations in this report, the present day water table is used for all simulation results to maintain consistency and allow comparison to the process model simulation results.

At the end of each simulation time step, FEHM collects the total radionuclide mass leaving each water table collection bin/zone and then passes the data to GoldSim (BSC 2003 [DIRS 161572]) for use as input for SZ transport simulations.

6.6 BASE-CASE MODEL

In this report, the base case is taken to be a case using either median or mean values (referred to as "representative" below) of radionuclide transport parameters and present day mean infiltration or glacial-transition mean infiltration. The results from this run will not be used directly by TSPA. Rather, this simulation activity illustrates the possible transport behavior of radionuclides within the UZ under the conditions of present-day or glacial-transition mean infiltration condition and representative transport parameter values. In TSPA-LA, the abstracted model will be used with different parameter combinations to study the uncertainty of parameters and flow fields on radionuclide transport through the UZ and its impacts on system performance. However, the base case represents typical behavior of the UZ transport abstraction model for the purposes of understanding the role of the UZ in the overall repository transport system.

6.6.1 Overview

The simulations were carried out using FEHM V2.23 (LANL 2005 [DIRS 174121]). Data used in these simulations are the radionuclides in Table 6-27 and the representative parameter values listed in Table 6-28. The flow fields used in the simulations are the present-day and glacial-transition mean infiltration. The objective of this run is to study the movement of radionuclides released from EBS into unsaturated fractured geological media downward to the water table.

A total of 36 species (Table 6-27) were simulated to study the transport of radionuclides in the UZ. This list of radionuclides is modified from the list given in *Initial Radionuclide Inventories* (BSC 2004 [DIRS 170022], Table 7-1). The list in Table 6-27 does not include radionuclides ^{227}Ac, ^{36}Cl, ^{245}Cm, ^{210}Pb, ^{241}Pu, ^{228}Ra, ^{79}Se, and ^{126}Sn identified in Table 7-1 of (BSC 2004 [DIRS 170022]). ^{36}Cl, ^{210}Pb, ^{79}Se, and ^{126}Sn are identified in Table 7-1 of (BSC 2004 [DIRS 170022]) as being included only for potential use in longer-term performance assessment calculations beyond the regulatory period. The half-life of ^{227}Ac is only 22 years (BSC 2002 [DIRS 160059], Table 2). Therefore, if released from the repository, this radionuclide will decay substantially before reaching the accessible environment. ^{227}Ac is only included as a decay product in secular equilibrium with ^{231}Pa in TSPA. ^{245}Cm, ^{241}Pu, and ^{228}Ra are not simulated in the UZ transport abstraction model, consistent with *Radionuclide Screening* (BSC 2002 [DIRS 160059], Table 13), but are included in total-systems models as part of the radionuclide inventory to allow for ingrowth of decay products in the inventory.

As shown in Table 6-27, the decay products associated with irreversible colloids are treated as either remaining with the colloid or entering the aqueous phase. If the decay product is a radionuclide associated with irreversible colloids (i.e. isotopes of americium and plutonium), then the decay product remains associated with an irreversible colloid. If the decay product is a radionuclide not associated with irreversible colloids (i.e. isotopes of uranium and neptunium, then the decay product enters the aqueous phase).

Table 6-27. Radionuclides Simulated in Base-Case Run

Index	Species Name	Half-Life (days)	Daughter Species
1	^{14}C	2.09E+06	Simple decay
2	^{135}Cs (rev)	8.4E+08	Simple decay
3	^{137}Cs (rev)	1.10E+04	Simple decay
4	^{129}I	5.73E+09	Simple decay
5	^{90}Sr	1.05E+04	Simple decay
6	^{99}Tc	7.78E+07	Simple decay
7	^{243}Am (rev)	2.69E+06	10
8	^{243}Am Ic	2.69E+06	11
9	^{243}Am If	2.69E+06	12
10	^{239}Pu (rev)	8.80E+06	13
11	^{239}Pu Ic	8.80E+06	13
12	^{239}Pu If	8.80E+06	13
13	^{235}U	2.57E+11	14
14	^{231}Pa (rev)	1.20E+07	Simple decay
15	^{241}Am (rev)	1.58E+05	18
16	^{241}Am Ic	1.58E+05	18
17	^{241}Am If	1.58E+05	18
18	^{237}Np	7.82E+08	19
19	^{233}U	5.81E+07	20
20	^{229}Th (rev)	2.7E+06	Simple decay
21	^{240}Pu (rev)	2.40E+06	24
22	^{240}Pu Ic	2.40E+06	24
23	^{240}Pu If	2.40E+06	24
24	^{236}U	8.55E+09	25
25	^{232}Th (rev)	5.11E+12	Simple decay
26	^{232}U	2.55E+04	Simple decay
27	^{242}Pu (rev)	1.37E+08	33
28	^{242}Pu Ic	1.37E+08	33
29	^{242}Pu If	1.37E+08	33
30	^{238}Pu (rev)	3.20E+04	34
31	^{238}Pu Ic	3.20E+04	34
32	^{238}Pu If	3.20E+04	34
33	^{238}U	1.63E+12	34
34	^{234}U	8.99E+07	35
35	^{230}Th (rev)	2.75E+07	36
36	^{226}Ra	5.84E+05	Simple decay

Source: BSC 2004 [DIRS 170022], Table 7-1.

NOTE: Half-life data are from Table 6-25. The second column shows the species name of the radionuclides. Species with names Ic represent irreversible colloids traveling retarded. Species with names If represent irreversible colloids traveling unretarded. The notation "(rev)" denotes a species in which reversible sorption onto colloids is applied. The "Index" column refers to the numbering scheme used for the radionuclide species in the FEHM input files used for the model simulations.

In tables of Section 6.5 where values for certain parameters are shown within a range of uncertainty, the basecase model uses a selected value within the defined range. Table 6-28 gives the selected values for the base-case runs. In most cases, the value for a parameter is represented by a "key" value that provides an index into a range of values appropriate for the particular parameter. The base-case model uses the median value of these keyed value ranges. For other parameters a median value is calculated given the values listed in Section 6.5.

Table 6-28. Selected Parameter Values for Base-case UZ Model

Key	Parameter Type	Value	Comments
Aperture (m) 2b Derived from Eq. 6-26 in Table 6-15			
-1	Group 1 Units	7.94E-03	
-2	Group 2 Units	1.43E-02	
-3	Group 3 Units	2.64E-03	
-4	Group 4 Units	4.85E-03	
-5	Group 5 Units	4.00E-03	
-6	Group 6 Units	5.75E-03	
-7	Group 7 Units	4.48E-03	
-8	Group 8 Units	2.64E-03	
-9	Group 9 Units	7.16E-03	
	tcwFf (faults in tcw units)	1.53E-02	calculated using 2b = porosity /frequency based on DTN:LB0207REVUZPRP.001
	ptnFf (faults in ptn units)	2.04E-02	
D_m Calculated Using Listed Mean Values and Eq. 6-19 (m^2/s) in Table 6-8			
-10	Group 1 Units	1.33E-10	
-11	Group 2 Units	8.10E-11	
-12	Group 3 Units	3.47E-11	
Representative Value Sorption Coefficients (Kd: mL/g) in Table 6-7			
-13	Am Zeolitic	5,500.0	
-14	Am Devitrified	5,500.0	
-15	Am Vitric	400.0	
-16	C Zeolitic	0.0	
-17	C Devitrified	0.0	
-18	C Vitric	0.0	
-19	Cs Zeolitic	5,000.0	
-20	Cs Devitrified	8.0	
-21	Cs Vitric	2.0	
-22	I Zeolitic	0.0	
-23	I Devitrified	0.0	
-24	I Vitric	0.0	
-25	Np Zeolitic	0.5	
-26	Np Devitrified	0.5	
-27	Np Vitric	1.0	
-28	Pa Zeolitic	5,500.0	
-29	Pa Devitrified	5,500.0	
-30	Pa Vitric	5,500.0	
-31	Pu Zeolitic	100.0	

Table 6-28. Selected Parameter Values for Base-case UZ Model (Continued)

Key	Parameter Type	Value	Comments
Representative Value Sorption Coefficients (Kd: mL/g) in Table 6-7			
-32	Pu Devitrified	70.0	
-33	Pu Vitric	100.0	
-34	Ra Zeolitic	3,000.0	
-35	Ra Devitrified	550.0	
-36	Ra Vitric	325.0	
-37	SR Zeolitic	1,025.0	
-38	SR Devitrified	40.0	
-39	SR Zeolitic	25.0	
-40	Tc Zeolitic	0.0	
-41	Tc Devitrified	0.0	
-42	Tc Vitric	0.0	
-43	Th Zeolitic	15,500.0	
-44	Th Devitrified	5,500.0	
-45	Th Vitric	5,500.0	
-46	U Zeolitic	0.5	
-47	U Devitrified	0.2	
-48	U Vitric	0.2	
Colloid Distribution Factors from Tables 6-21 and 6-22 Calculated using Eq. 6-27 with median values of each parameter(Base-case model uses smectite values)			
-49, -51,-53	Am, Th, Pa for smectite	0.075	Example calculation for Am on smectite:
	Am, Th, Pa for iron-hydroxide	0.21	Median C_{coll} = 0.1 mg/L = 0.1e-6 kg/L from Table 6-21
-50	Cs for smectite	1.4E-4	
	Cs for iron-hydroxide	2.09E-5	Median $K_{d,coll}$ = 7.5e5 mL/g = 7.5e5 L/kg (interpolated from Table 6-22)
-52	Pu for smectite	0.00825	
	Pu for iron-hydroxide	0.022	K_c = 0.1e-6 kg/L*7.5e5 L/kg = .075
-54	Retardation factor	25.98	Does not apply to the If (irreversible fast colloids)
Mean Value Fracture Frequency (m^{-1}) from Table 6-15			
	Group 1 Units	1.26E-01	
	Group 2 Units	1.75E+00	
	Group 3 Units	1.40E-01	
	Group 4 Units	2.00E-01	
	Group 5 Units	4.00E-02	
	Group 6 Units	1.20E-01	
	Group 7 Units	9.60E-01	
	Group 8 Units	3.97E+00	
	Group 9 Units	8.10E-01	

NOTE: The key values represent a file input location for a distribution of values that are sampled to represent the uncertainty parameters in runs for TSPA-LA.

6.6.2 Base-Case Model Results

The UZ Base-case simulations presented in this report are for present-day mean infiltration and glacial-transition mean infiltration with a raised water table. Table 6-29 shows the position in the 3 × 3 "matrix" of TSPA flow simulations for which model results are presented. In Section 6.7, these results are compared to others in which various flow and transport model parameters and conceptualizations are assumed.

In the figures of this section and others in which the term "normalized" is used, the simulation consists of a pulse input of particles, and the plot is the cumulative number of particles reaching the water table. Therefore, if all particles released from the repository reach the water table, the value will reach unity. Under the conditions of steady state flow, this integral plot represents the mass flux (normalized by the input mass flux) that would have been obtained if a constant mass flux had been input, even though the actual input was a pulse. For breakthrough curves that exceed unity, a source input at the repository is augmented by mass produced by ingrowth from the decay of a parent species. Note that for the colloid simulations, neither colloid filtration at matrix interfaces (Section 6.5.9) for irreversible colloids nor colloid retardation for reversible colloid species (Secrion 6.5.13) were included in earlier calculations, but both have been included in this revision.

Table 6-29. Scenarios for UZ Base-Case and TSPA Model Flow Simulations

	Lower Bound Infiltration	Mean Infiltration	Upper Bound Infiltration
Present Day	preq_lA	preq_mA Base-Case Present Day	preq_uA
Monsoon	monq_lA	preq_mA	preq_uA
Glacial Transition	glaq_lA	preq_mA Base-Case Glacial with Raised Water Table	preq_uA

Source: *UZ Flow Models and Submodels* (BSC 2004 [DIRS 169861], Table 6.2-9)

Figure 6-17 shows the normalized cumulative breakthrough curves at the water table for the 36 species simulated under the present-day mean infiltration condition, and Figure 6-18 shows the results for the glacial-transition mean infiltration condition.

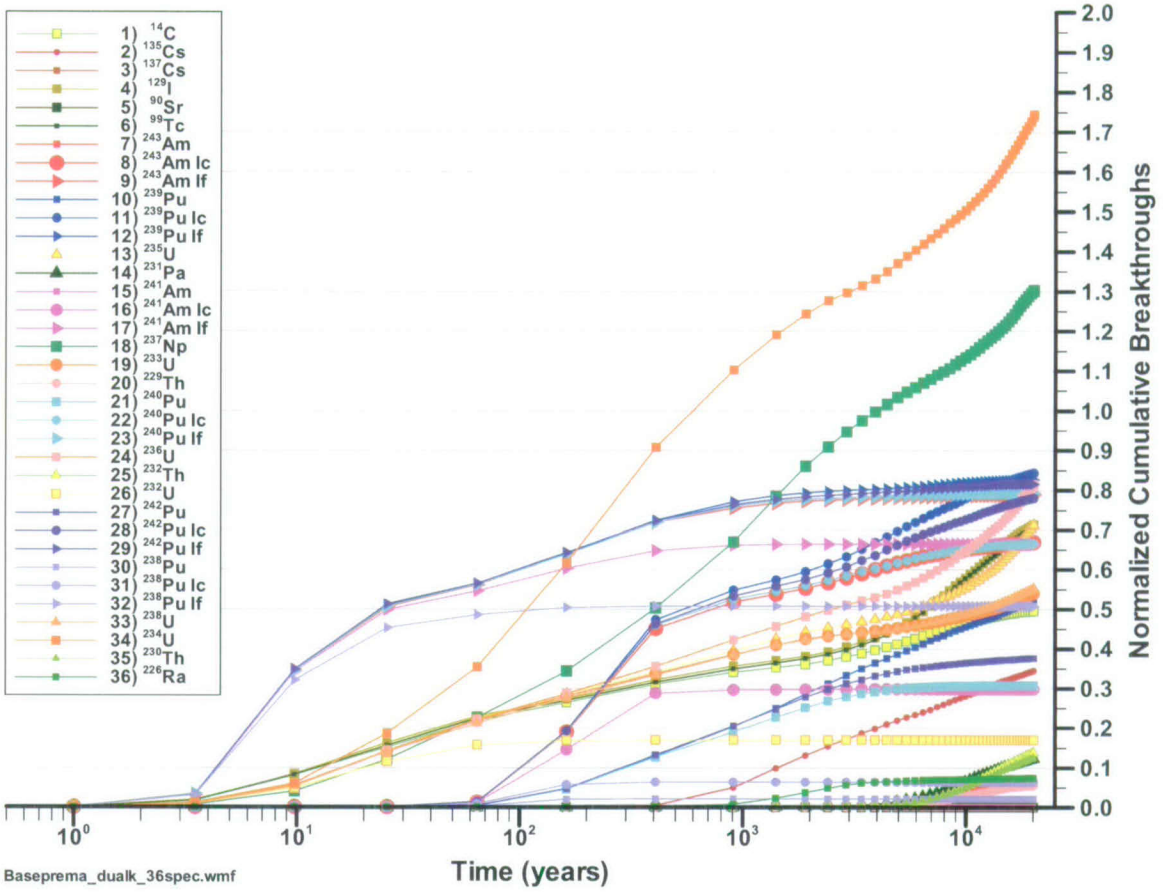

Output DTN: LA0506BR831371.001.

Figure 6-17. Base-Case Model Normalized Mass Flux at the Water Table for 36 Radionuclide Species, Present-Day Mean Infiltration Scenario, Representative Parameter Values, and Present-Day Water Table

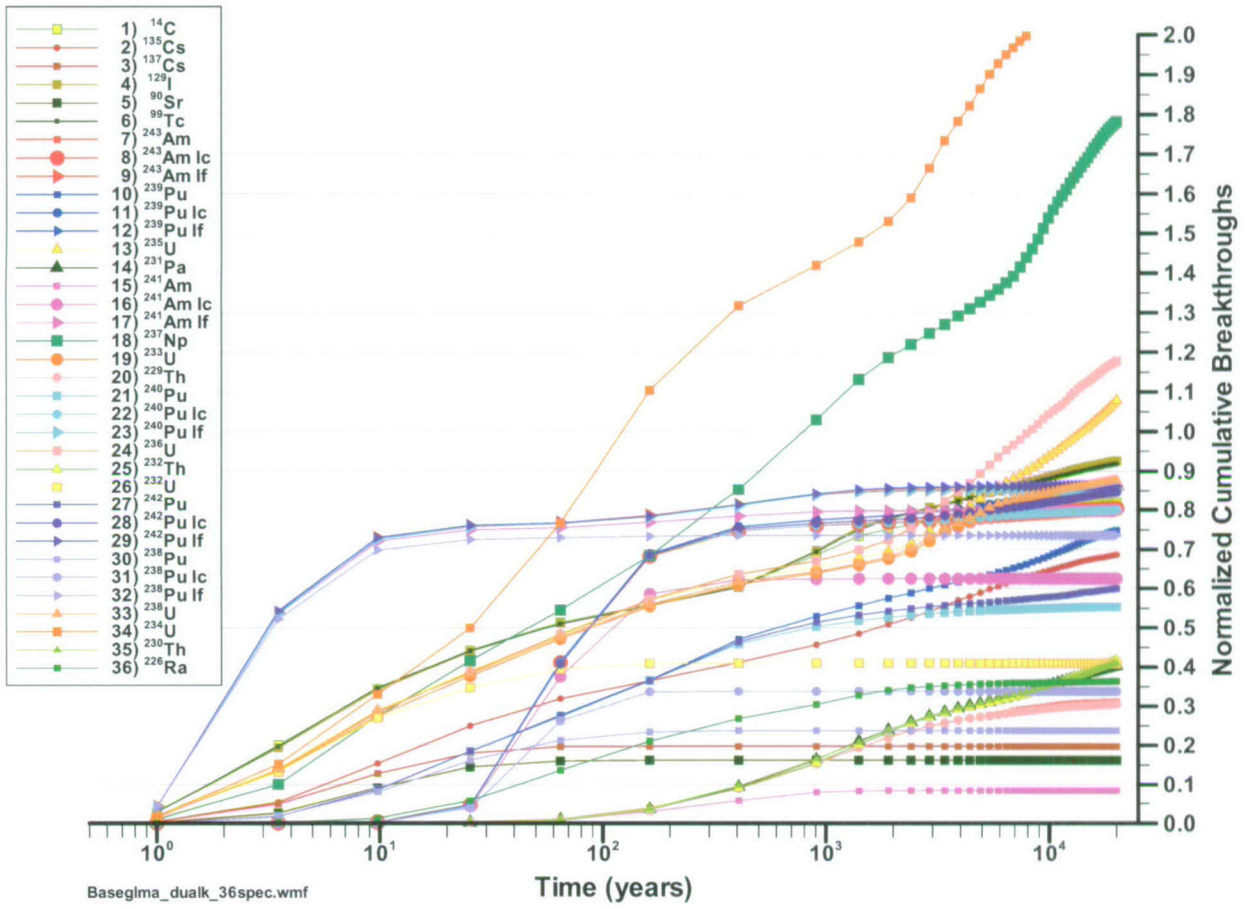

Output DTN: LA0506BR831371.001.

Figure 6-18. Base-Case Model Normalized Mass Flux at the Water Table for 36 Radionuclide Species, Glacial-Transition Mean Infiltration Scenario, Representative Parameter Values, and Elevated Water Table

For the detailed discussion of these results, the glacial-transition climate case is used to illustrate the type of transport mechanism most influencing the behavior. Beginning with colloidal species, the simulation results reveal that irreversible fast colloids (^{239}Pu, ^{241}Am, ^{242}Pu, and ^{243}Am in curves labeled If239, If241, If242, and If243, respectively), which are not affected by matrix diffusion and retardation, have the shortest breakthrough times. Within a time period of less than 100 years, over 50 percent of the irreversible fast colloids traveled through the UZ.

Irreversible slow colloids, which undergo retardation move more slowly than their corresponding fast colloids but faster than their corresponding dissolved species. The transport time of the irreversible slow colloids depends on their retardation factor. In TSPA-LA simulations, the retardation factors of the slow colloids will be sampled and its impact on system performance will be evaluated. For illustrative purposes, Figure 6-19 shows the breakthrough of the colloidal species that transport via either the "fast" ("If" species) or "slow" ("Ic" species) mechanisms. In the TSPA model, the fraction of irreversible fast colloids of 1.68E-03 (derived in Section 6.5.13) will be applied to the releases, and the remaining fraction (9.98E-01) will travels via the slow mechanism. The differences in travel times of these two classes of colloidal species are

controlled by the retardation factor of the colloids in the "Ic" category. However, in the context of the regulatory time period of 10,000 years, both types of colloids travel rapidly through the UZ.

Dissolved species have a broader distribution of breakthrough times than either irreversible fast colloids or irreversible slow colloids due to matrix diffusion and matrix sorption. The results for the glacial-transition mean infiltration scenario (Figure 6-20) show that for nonsorbing species, like Tc-99, C-14, and I-129, first arrivals at the water table begin within about one year, and about 50 percent of the mass travels through fast flow paths and arrives at the water table within roughly 60 years. The remainder of the mass travels at much lower velocities due to matrix diffusion. Dissolved species with moderate matrix sorption, like Np-237 and the isotopes of uranium (Figure 6-21), travel slightly more slowly through the UZ than the nonsorbing species ^{99}Tc, ^{14}C, and ^{129}I. For example, within the first 80 years under the glacial-transition mean infiltration conditions, about 50 percent of the total ^{233}U mass passed through the UZ. U-234 exhibits a relatively fast transport process with higher mass output than the other dissolved uranium radionuclides because it is produced by the decay of a colloid facilitated species (^{238}Pu). Strongly sorbing species like ^{242}Pu (median K_d of 100 mL/g in zeolitic, 70 mL/g in devitrified, and 100 mL/g in vitric layers) exhibit longer first arrival times, and transport of roughly 60%of the input through the UZ within the 20,000 year simulation period (Figure 6-22). The most strongly sorbing species (Figures 6-23 and 6-24) have the longest travel times: for example, ^{230}Th (mean K_d of 15,500 mL/g in zeolitic, 5,500 mL/g in devitrified, and 5,500 mL/g in vitric layers) has first arrivals at about 100 years, and 40% breaks through the UZ within the 20,000-year period. Finally, note that ^{234}U and ^{237}Np have normalized cumulative breakthrough values greater than 1 at 20,000 years due to the decay of ^{238}Pu (Pu238, If238, and Ic238) and ^{241}Am (Am241, If241, and Ic241), respectively. For completeness, several species not presented in other plots are also shown in Figure 6-24.

For comparison, the case run under the present-day mean infiltration condition (Figure 6-18) reveals that, for example, less ^{99}Tc breaks through at the water table after the 20,000-year simulation period under the present-day infiltration condition. This indicates that fast water flow under wetter infiltration conditions reduces the effect of matrix diffusion and transport radionuclides through the UZ within the simulation time period, whereas transport times are expected to be longer under present-day conditions.

With regard to colloid transport, the simulation results suggest that colloids can play an important role in accelerating the transport of radionuclides in the UZ, especially the irreversible fast colloids. Of course, if the quantity of colloids is low, the impact on dose would not be expected to be important. In TSPA-LA calculations, a conservative percentage of colloids will be selected to study its impact on dose. For irreversible slow colloids, the retardation factor should be sampled to investigate parameter uncertainty on system performance.

Matrix diffusion and matrix sorption can play an important role in retarding the movement of dissolved radionuclides and could significantly impact dose predictions. The strength of fracture-matrix interaction due to matrix diffusion and sorption depends on matrix diffusion coefficient, matrix sorption coefficient, fracture spacing, and fracture aperture. In TSPA-LA calculations, those parameters will be sampled based on uncertainty distributions, and the impact on system performance of these uncertainties will be quantified. Furthermore, the conceptual

model of fracture-matrix interactions has a strong influence on the model results. Parameter uncertainties are investigated further in the next section, and the influence of the conceptual model uncertainty is illustrated in Section 6.7. Another important factor that controls the transport process is infiltration rate. The impact of climate changes on system performance will be investigated using different flow fields developed in *UZ Flow Models and Submodels* (BSC 2004 [DIRS 169861]); DTN: LB0305TSPA18FF.001 [DIRS 165625]. These flow fields have different amounts of fracture and matrix flow, and water table elevation changes will also be included (see Section 6.4.8). Based on the results presented here, radionuclide transport velocities will increase during the wetter climates due to increased infiltration, greater fracture flow, and less pervasive matrix diffusion.

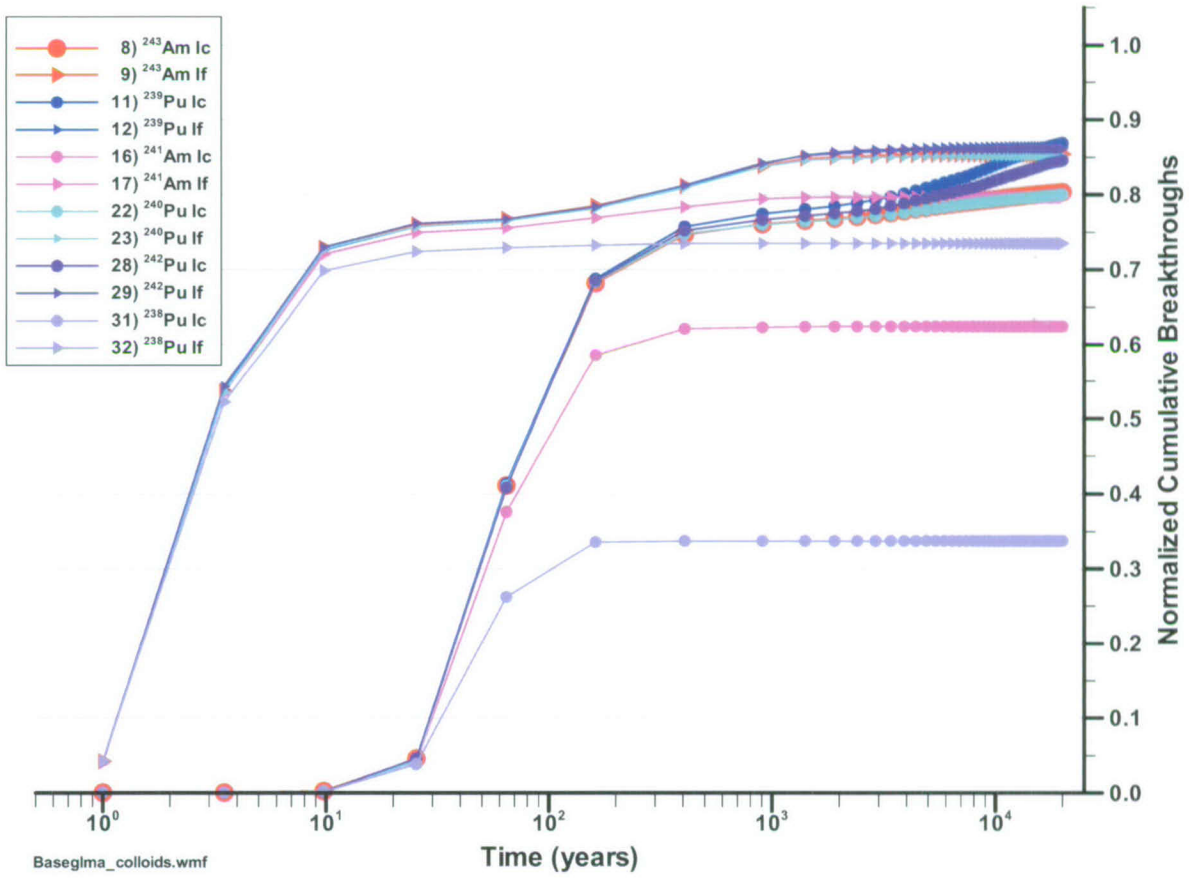

Output DTN: LA0506BR831371.001.

NOTE: These results are for comparison purposes only. Actual radionuclide mass flux reaching the water table will depend on release rates and locations, and will be simulated in the TSPA-LA model.

Figure 6-19. Base-Case Model Normalized Mass Flux at the Water Table for Irreversible Fast and Irreversible Slow Colloids, Glacial-Transition Mean Infiltration Scenario, Representative Parameter Values, and Elevated Water Table

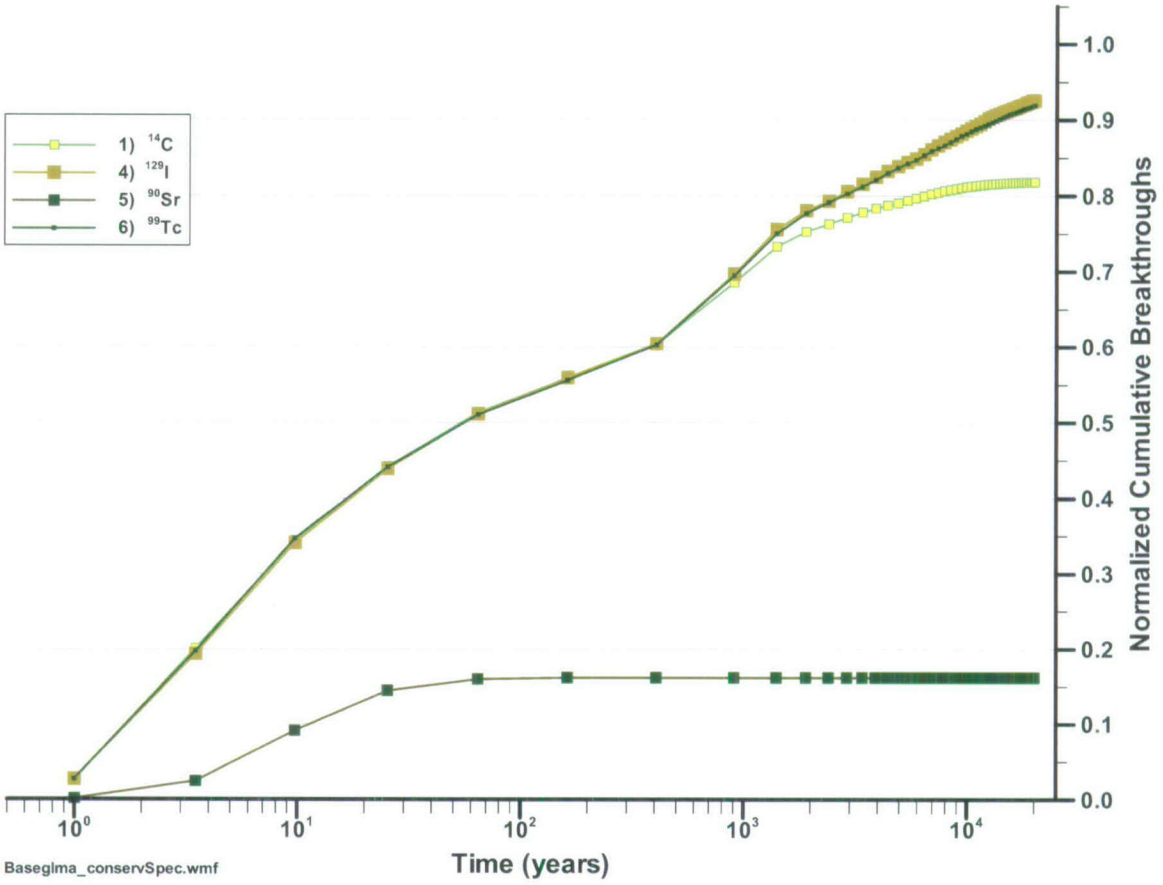

Output DTN: LA0506BR831371.001.

NOTE: These results are for comparison purposes only. Actual radionuclide mass flux reaching the water table will depend on release rates and locations, and will be simulated in the TSPA-LA model.

Figure 6-20. Base-Case Model Normalized Mass Flux at the Water Table for Conservative Radionuclides and ^{90}Sr, Glacial-Transition Mean Infiltration Scenario, Representative Parameter Values, and Elevated Water Table

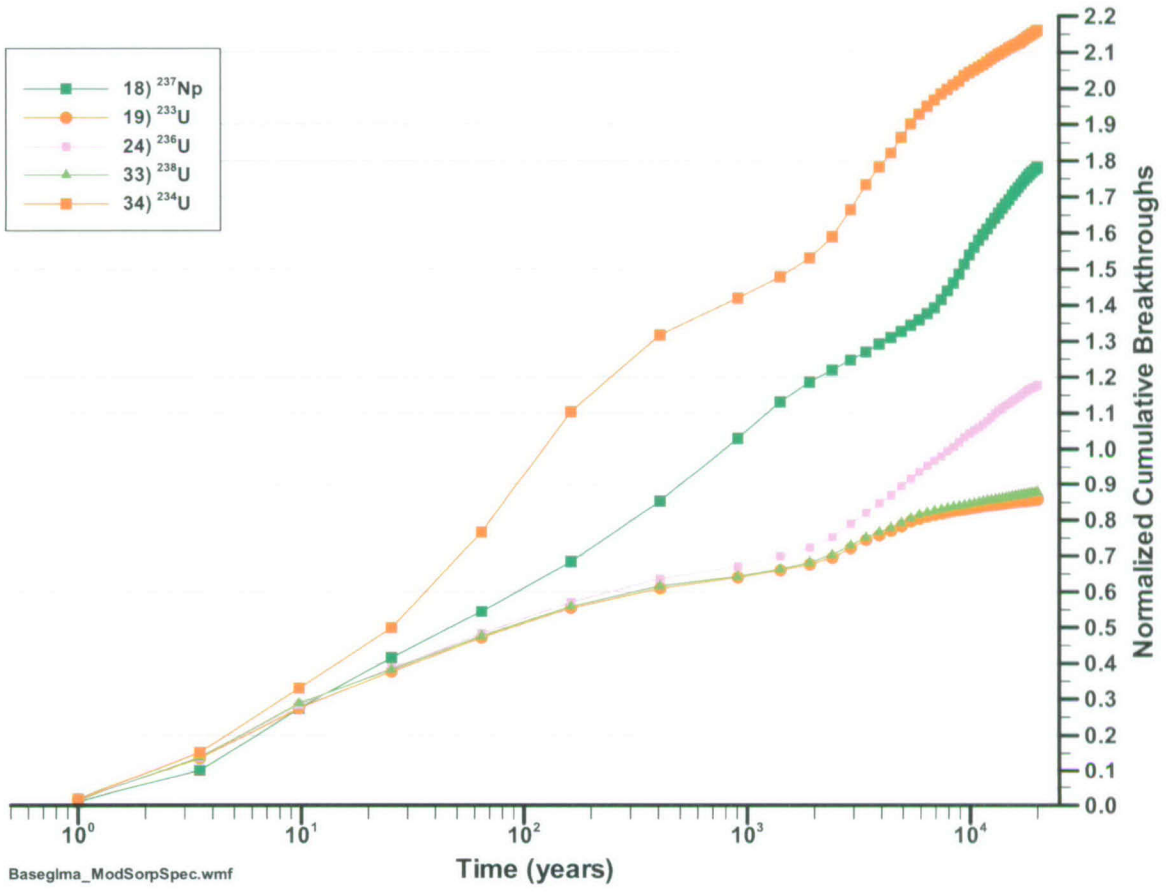

Output DTN: LA0506BR831371.001.

NOTE: These results are for comparison purposes only. Actual radionuclide mass flux reaching the water table will depend on release rates and locations, and will be simulated in the TSPA-LA model.

Figure 6-21. Base-Case Model Normalized Mass Flux at the Water Table for Moderately Sorbing Radionuclides, Glacial-Transition Mean Infiltration Scenario, Representative Parameter Values, and Elevated Water Table

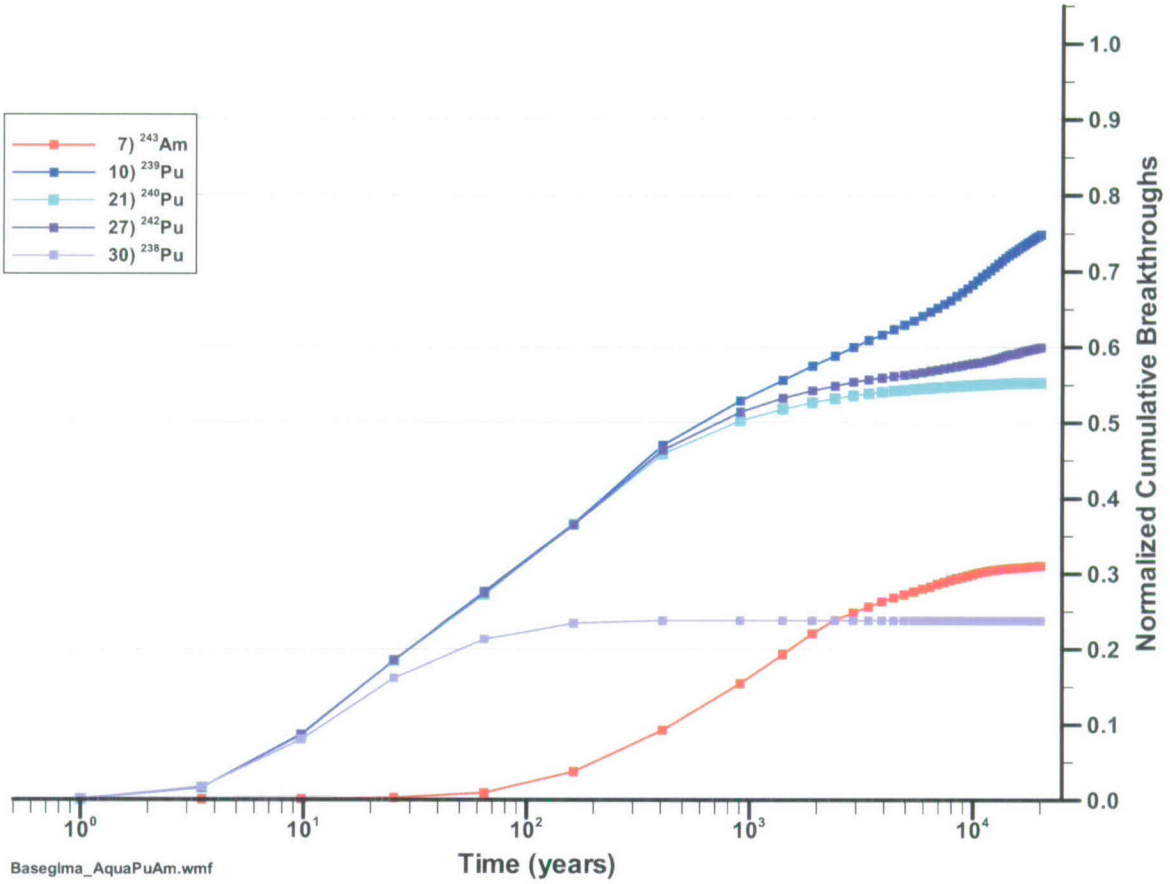

Output DTN: LA0506BR831371.001.

NOTE: These results are for comparison purposes only. Actual radionuclide mass flux reaching the water table will depend on release rates and locations, and will be simulated in the TSPA-LA model.

Figure 6-22. Base-Case Model Normalized Mass Flux at the Water Table for Aqueous Species of Americium and Plutonium, Glacial-Transition Mean Infiltration Scenario, Representative Parameter Values, and Elevated Water Table

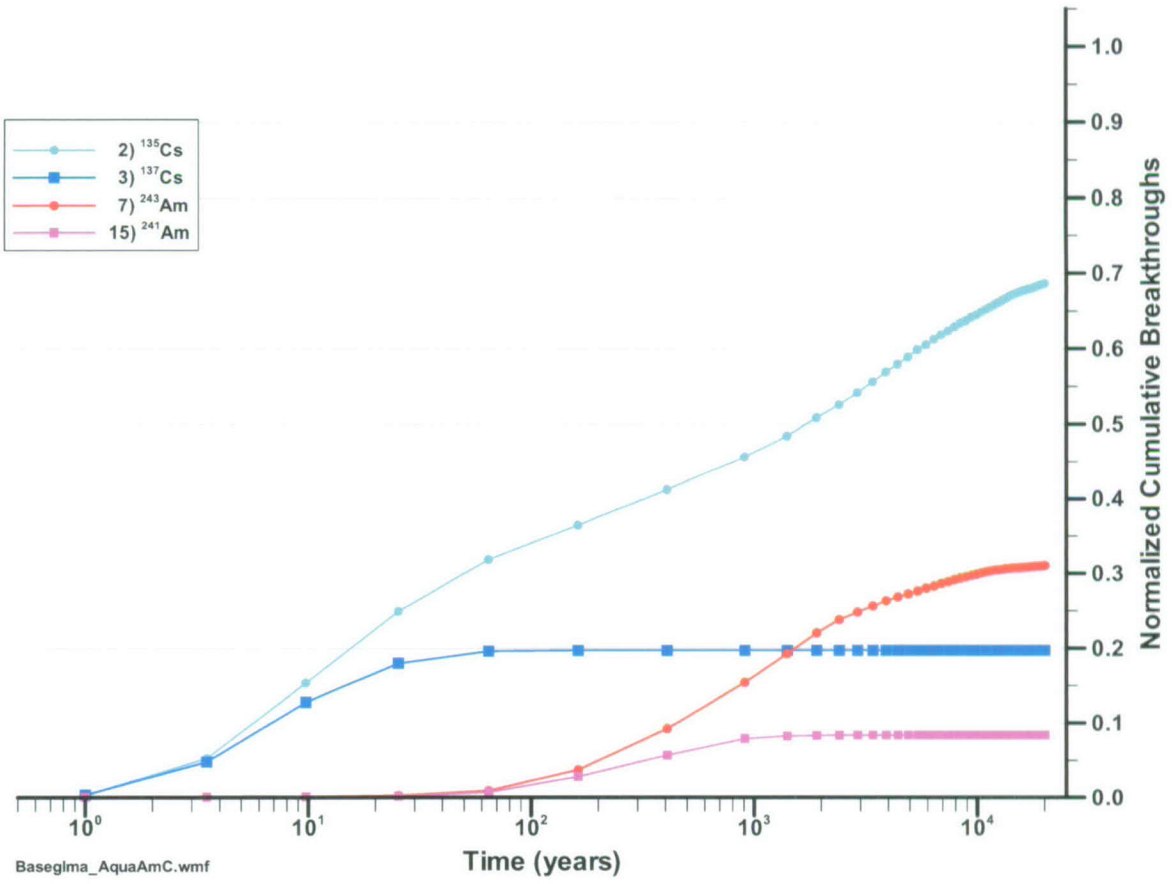

Output DTN: LA0506BR831371.001.

NOTE: These results are for comparison purposes only. Actual radionuclide mass flux reaching the water table will depend on release rates and locations, and will be simulated in the TSPA-LA model.

Figure 6-23. Base-Case Model Normalized Mass Flux at the Water Table for Aqueous Species of Cesium and Americium, Glacial-Transition Mean Infiltration Scenario, Representative Parameter Values, and Elevated Water Table

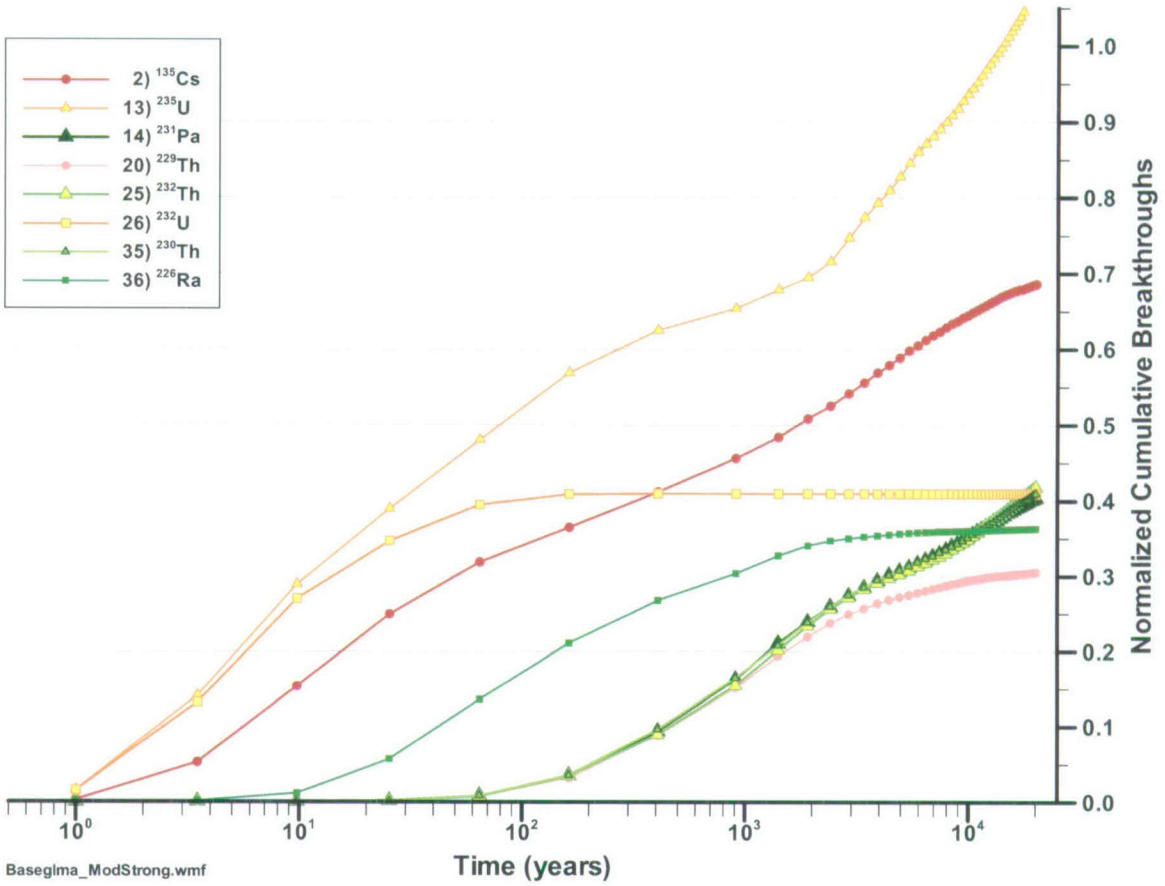

Output DTN: LA0506BR831371.001.

NOTE: These results are for comparison purposes only. Actual radionuclide mass flux reaching the water table will depend on release rates and locations, and will be simulated in the TSPA-LA model.

Figure 6-24. Base-Case Model Normalized Mass Flux at the Water Table for Various Moderately to Strongly Sorbing Radionuclides, Glacial-Transition Mean Infiltration Scenario, Representative Parameter Values, and Elevated Water Table

6.6.3 Sensitivity to Flow Parameter Uncertainty

The development of flow fields for use in TSPA models is based on a steady state model assumption in which the best calibrated parameter values are used for computing the fluxes through the UZ. However, *Analysis of Hydrologic Properties Data* (BSC 2004 [DIRS 170038], Section 6.4) showed that there is uncertainty in the values of hydrologic parameters used in the calibration of the flow model. This uncertainty means that essentially equivalent fits to the data can be obtained within specified ranges of these parameters. It is desirable to examine the impact of these uncertainties on the model predictions. This section presents sensitivity analysis results for radionuclide transport to various hydrologic property uncertainties. This analysis is conducted by incorporating into the UZ transport abstraction model steady state flow fields for cases in which each parameter in question is individually varied plus and minus one standard deviation σ from the best-fit value (BSC 2005 [DIRS 174116], Section 6.4.2). No recalibration is performed during this step because the parameters are considered to still be within their

uncertainty range given the available calibration data. For transport, simulations of radionuclide travel times to the water table are conducted and compared to the simulation results presented earlier for the flow field to be used in the TSPA model. For all simulations, the base-case transport parameters listed in Table 6-28 are assumed, and the glacial-transition mean infiltration scenario with elevated water table is used for the comparisons. Flow fields assuming the changed hydrologic parameter values are obtained from DTN: LB0506TSPA08FF.001 [DIRS 174117] and documented in *Parameter Sensitivity Analysis for Unsaturated Zone Flow* (BSC 2005 [DIRS 174116], Section 6.4.2).

Figures 6-25 and 6-26 show the results of simulations varying the value of the van Genuchten parameter α for the fracture continuum. The suite of radionuclides selected for comparison covers the range of conservative and weakly sorbing radionuclides (^{99}Tc and ^{237}Np, respectively; Figure 6-25), a more strongly sorbing radionuclide (^{242}Pu; Figure 6-26), and a colloidal radionuclide (^{242}Pu If; Figure 6-26). Note that ^{242}Pu If is selected to cover the end-member case of no diffusion or colloid retardation, so that the full range of potential transport parameters is captured in this sensitivity analysis. The sensitivity to the α parameter in the fracture continuum is very small: very subtle differences between the breakthrough curves for the different flow fields are observed in the figure.

Similarly, Figures 6-27 and 6-28 show that varying the value of the van Genuchten parameter α for the matrix continuum has very little impact on the predicted transport of conservative, sorbing or colloidal radionuclides. In this range, these parameters do little to change the relative flow fractions of water in the fracture and matrix continua and, therefore, the predicted transport times to the water table are not impacted significantly.

The impact of changing the absolute permeability of the fracture continuum is shown in Figures 6-29 (^{99}Tc and ^{237}Np) and 6-30 (^{242}Pu and ^{242}Pu If). There is moderate sensitivity to the permeability of the fracture continuum. Higher values of the permeability in this range of the parameter space result in a somewhat higher relative flow rate in the fractures, and thus more rapid breakthroughs. The magnitude of the effect is still relatively small, and appears to impact conservative, sorbing, and colloidal species in an equivalent way.

Of the hydrologic parameters varied in this sensitivity study, the absolute permeability of the matrix rocks has the greatest impact on UZ radionuclide transport, as shown in Figures 6-31 and 6-32. Increasing the matrix permeabilities from the best-fit values results in significantly longer travel times to the water table, a consequence of an increased relative flow fraction in the matrix. Interestingly, decreasing the matrix permeability has virtually no impact on the breakthrough curves. Apparently, the flow fractions are unchanged by this parameter variation. This is probably due to the fact that at very high fracture flow fractions, reducing the matrix permeability changes this situation very little because virtually all of the water is already flowing in the fractures. Conversely, in regions such as the vitric Calico Hills formation, flow is assumed to be matrix dominated, so changing the matrix permability affects the matrix saturation slightly, but not the flow regime. The implication of this sensitivity analysis to the TSPA model is that the flow simulations selected for the analyses are conservative with respect to the choice of the matrix permeability: lowering the permeabilities from their best-fit values has no impact on breakthrough times, whereas raising the permeabilities results in longer travel times.

In summary, the sensitivity of uncertain hydrologic parameters on UZ performance is small to moderate for the parameters tested for the glacial-transition mean infiltration scenario selected for study. The parameter sensitivity analyses presented in this section conformed to the scope of work specified in *Technical Work Plan for Unsaturated Zone Flow, Drift Seepage, and Unsaturated Zone Transport Modeling* (BSC 2005 [DIRS 173951], Section 2.1). Therefore, the sensitivity analyses represent the behavior of the model within a limited range of parameter variations. Therefore, an important subtlety of this analysis is that the conclusions should not be interpreted as an absolute statement on the influence of any parameter, but rather reflect the propogation of uncertainty in a model parameter within the range estimated based on inverse modeling using the available data. These results are specific to the parameter ranges selected, and could be different in a different portion of the parameter space of hydrologic, transport, and infiltration parameters. Given this caveat, the results indicate that the van Genuchten α parameter for either the fracture or matrix continua has the smallest impact on the results. Somewhat larger sensitivities were found for the fracture permeabilities, and the largest influence (for the parameters studied) was identified for the matrix permeabilities. For the latter, the best-fit flow fields selected for TSPA model analyses appear to yield a conservative result with respect to this parameter.

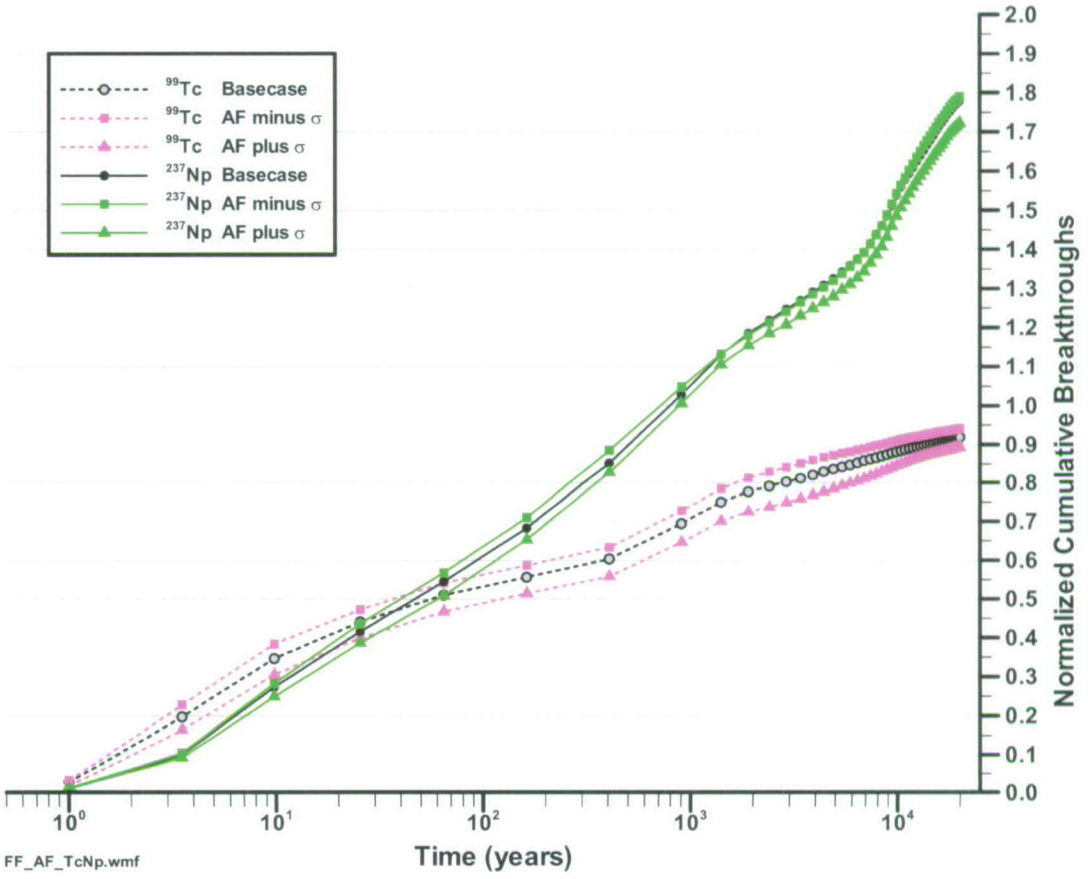

Output DTN: LA0506BR831371.002.

NOTE: These results are for comparison purposes only. Actual radionuclide mass flux reaching the water table will depend on release rates and locations, and will be simulated in the TSPA-LA model.

Figure 6-25. Base-Case Model Normalized Mass Flux at the Water Table for ^{99}Tc and ^{237}Np, Glacial-Transition Mean Infiltration Scenario, for Different Values (Plus and Minus One Standard Deviation (σ) from the Base Case) of the van Genuchten α Parameter for the Fracture Continuum, and Elevated Water Table

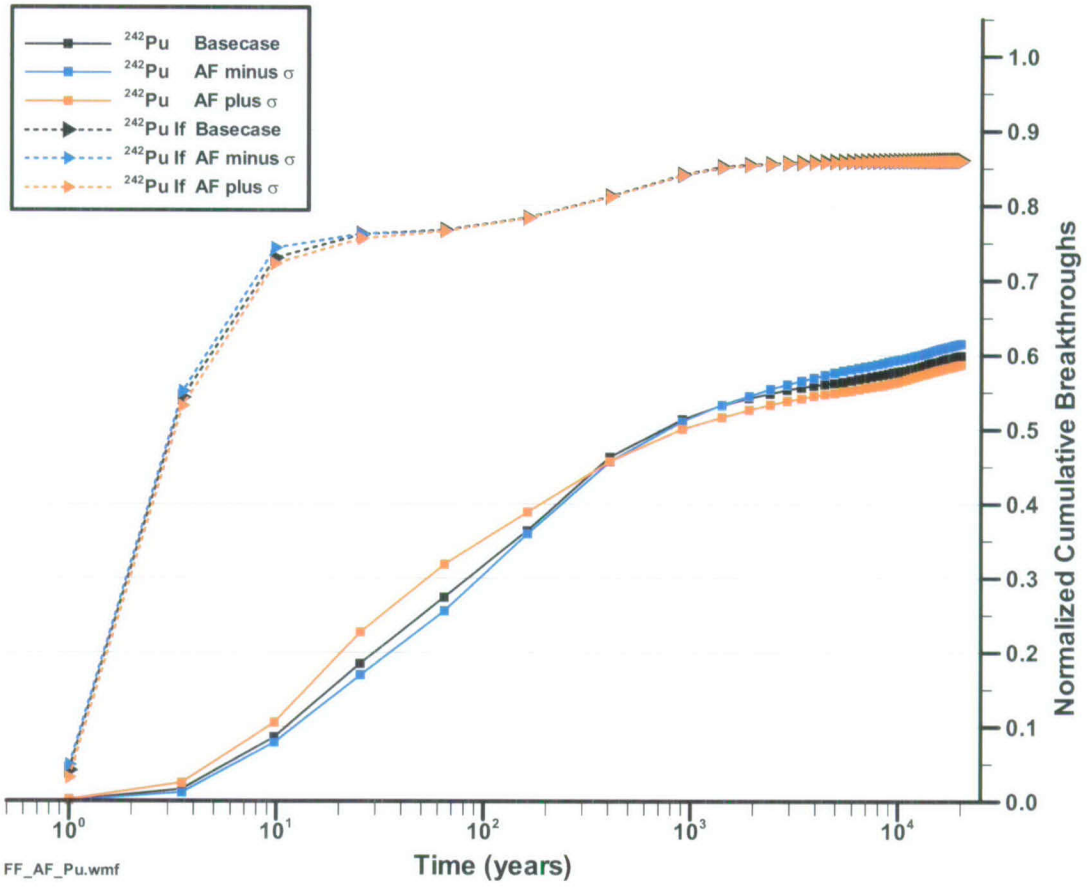

Output DTN: LA0506BR831371.002.

NOTE: These results are for comparison purposes only. Actual radionuclide mass flux reaching the water table will depend on release rates and locations, and will be simulated in the TSPA-LA model.

Figure 6-26. Base-Case Model Normalized Mass Flux at the Water Table for Different Species of ^{242}Pu, Glacial-Transition Mean Infiltration Scenario, for Different Values (Plus and Minus One Standard Deviation (σ) from the Base Case) of the van Genuchten α Parameter for the Fracture Continuum, and Elevated Water Table

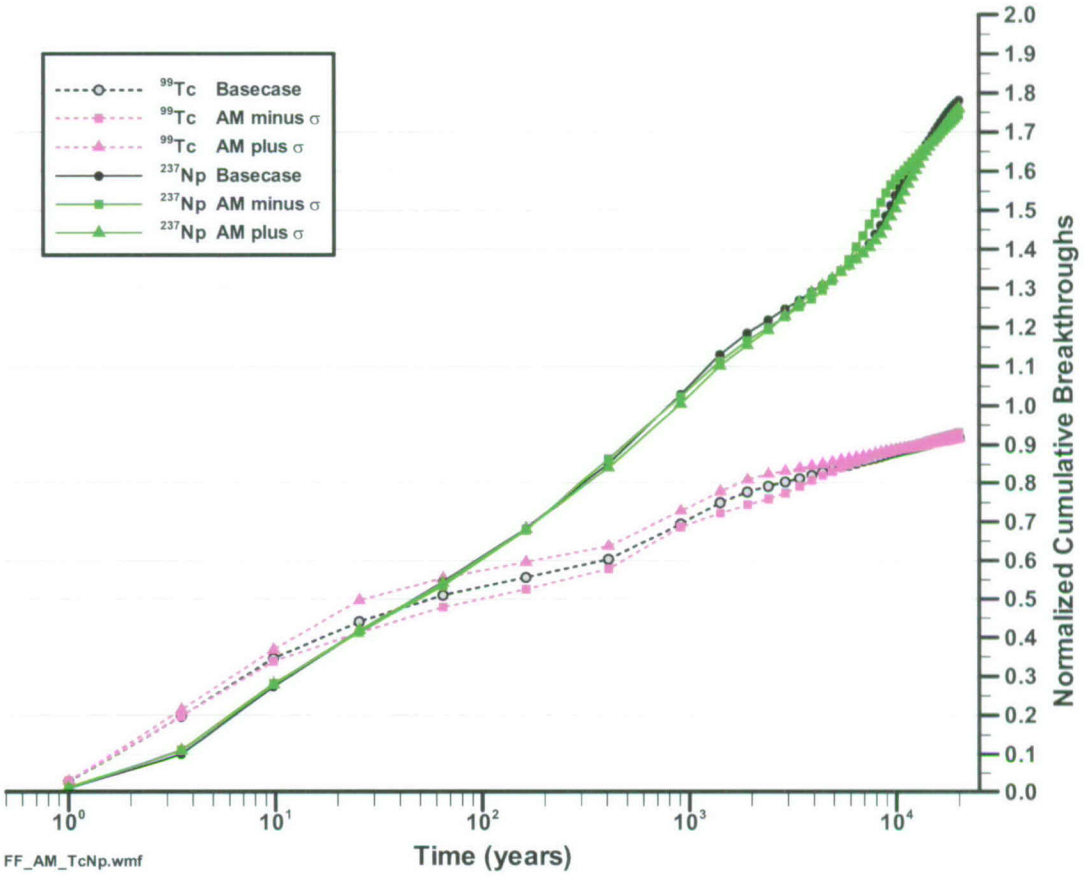

Output DTN: LA0506BR831371.002.

NOTE: These results are for comparison purposes only. Actual radionuclide mass flux reaching the water table will depend on release rates and locations, and will be simulated in the TSPA-LA model.

Figure 6-27. Base-Case Model Normalized Mass Flux at the Water Table for ^{99}Tc and ^{237}Np, Glacial-Transition Mean Infiltration Scenario, for Different Values (Plus and Minus One Standard Deviation (σ) from the Base Case) of the van Genuchten α Parameter for the Matrix Continuum, and Elevated Water Table

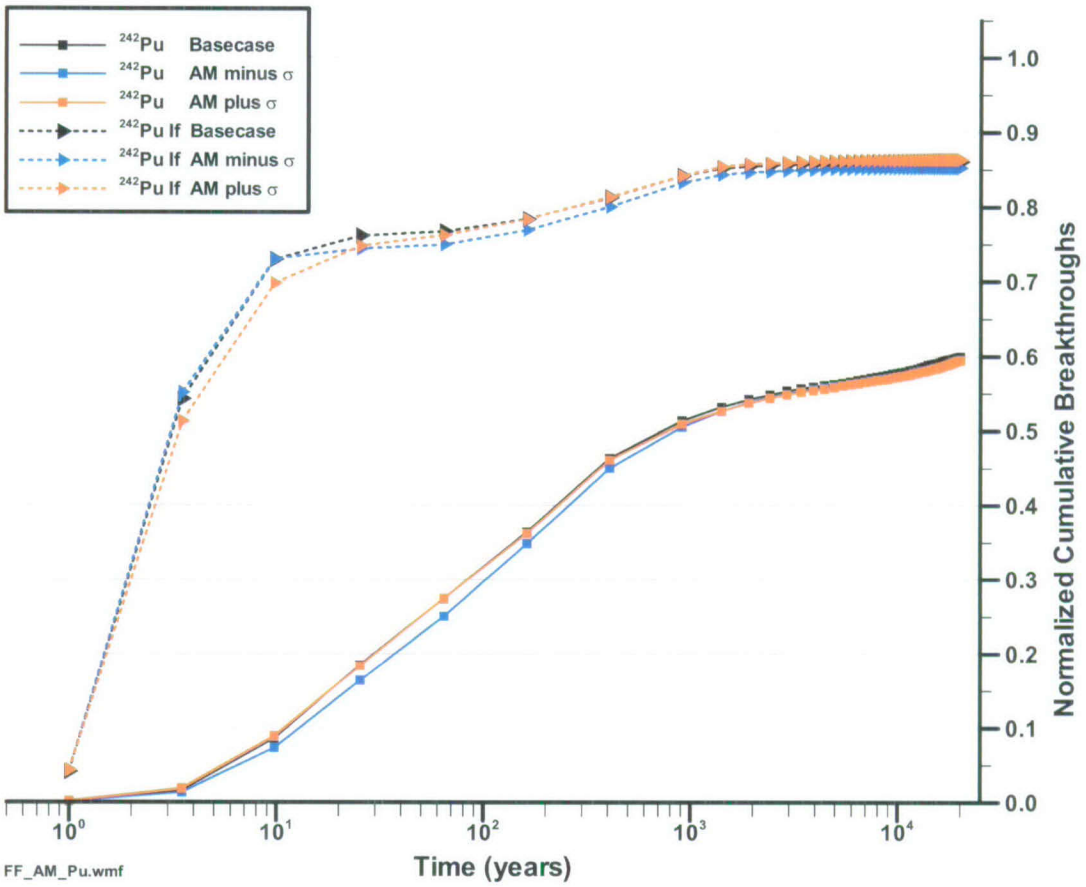

Output DTN: LA0506BR831371.002.

NOTE: These results are for comparison purposes only. Actual radionuclide mass flux reaching the water table will depend on release rates and locations, and will be simulated in the TSPA-LA model.

Figure 6-28. Base-Case Model Normalized Mass Flux at the Water Table for different species of ^{242}Pu, Glacial-Transition Mean Infiltration Scenario, for Different Values (Plus and Minus One Standard Deviation (σ) from the Base Case) of the van Genuchten α Parameter for the Matrix Continuum, and Elevated Water Table

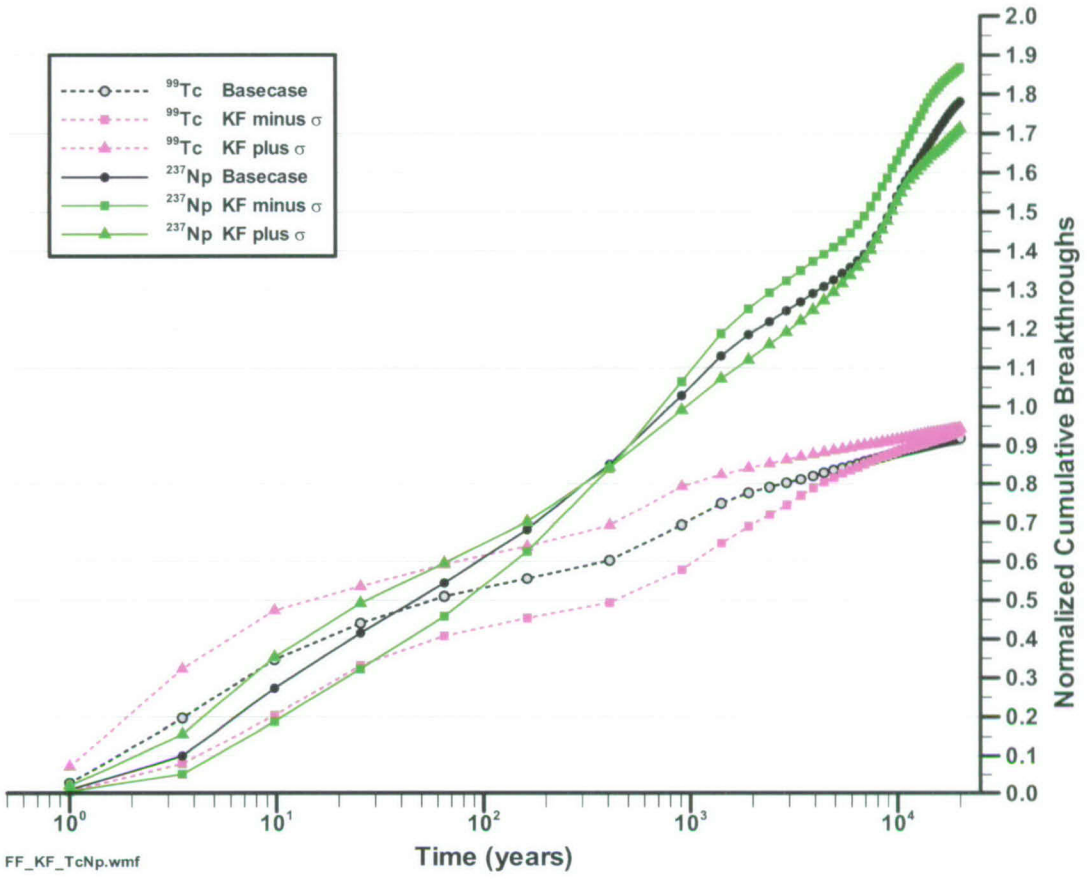

Output DTN: LA0506BR831371.002.

NOTE: These results are for comparison purposes only. Actual radionuclide mass flux reaching the water table will depend on release rates and locations, and will be simulated in the TSPA-LA model.

Figure 6-29. Base-Case Model Normalized Mass Flux at the Water Table for ^{99}Tc and ^{237}Np, Glacial-Transition Mean Infiltration Scenario, for Different Values (Plus and Minus One Standard Deviation (σ) from the Base Case) of the Absolute Permeabilities of the Fracture Continuum, and Elevated Water Table

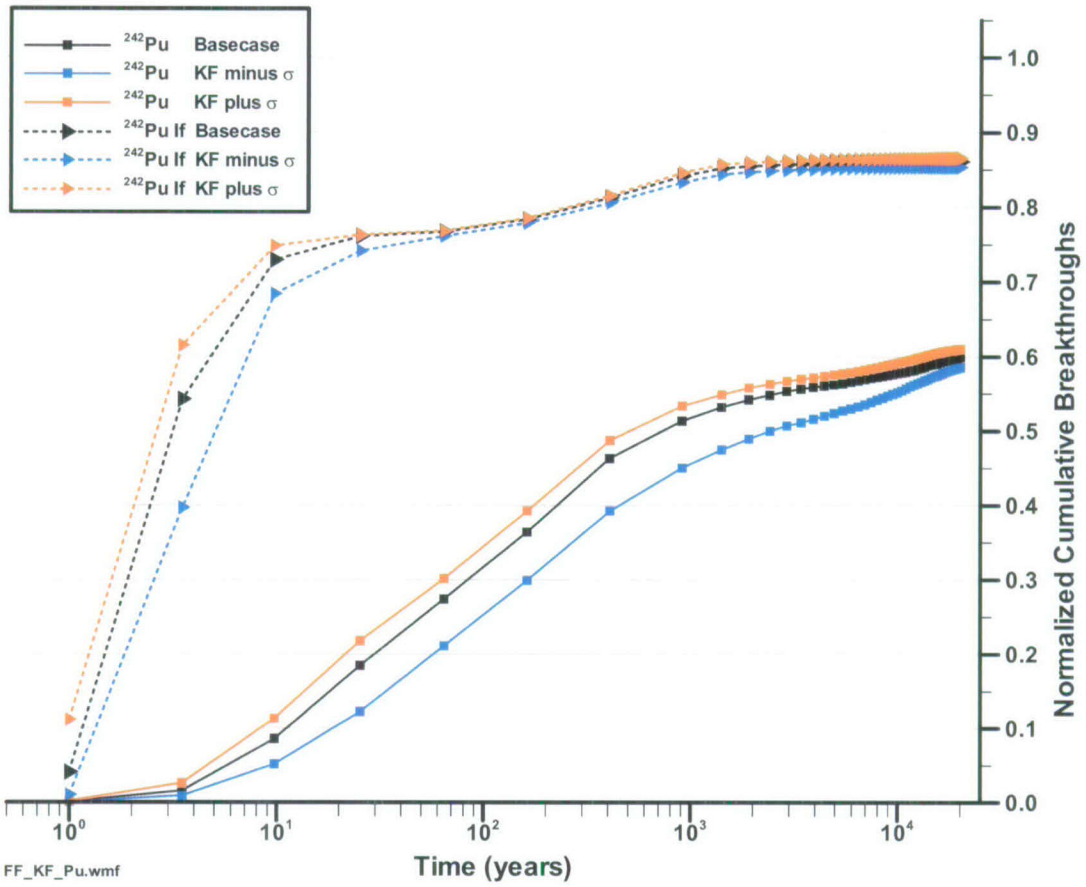

Output DTN: LA0506BR831371.002.

NOTE: These results are for comparison purposes only. Actual radionuclide mass flux reaching the water table will depend on release rates and locations, and will be simulated in the TSPA-LA model.

Figure 6-30. Base-Case Model Normalized Mass Flux at the Water Table for Different Species of ^{242}Pu, Glacial-Transition Mean Infiltration Scenario, for Different Values (Plus and Minus one Standard Deviation (σ) from the Base Case) of the Absolute Permeabilities of the Fracture Continuum, and Elevated Water Table

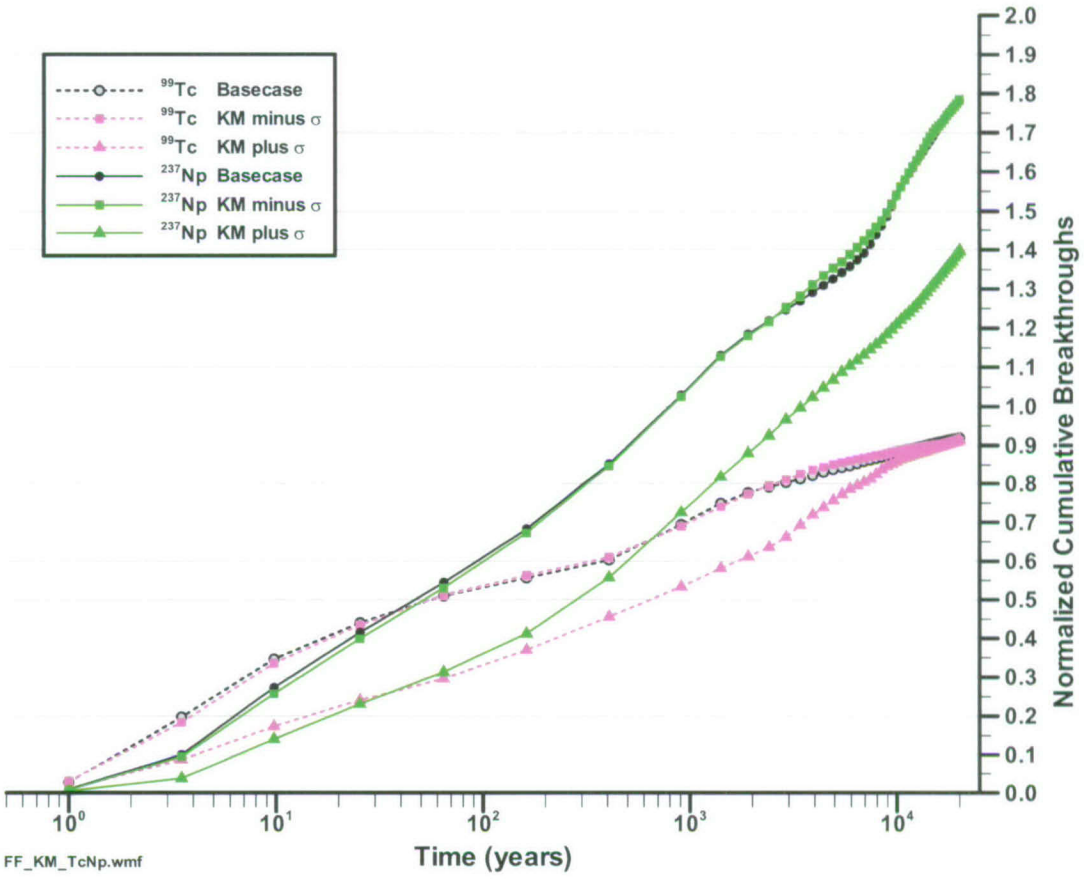

Output DTN: LA0506BR831371.002.

NOTE: These results are for comparison purposes only. Actual radionuclide mass flux reaching the water table will depend on release rates and locations, and will be simulated in the TSPA-LA model.

Figure 6-31. Base-Case Model Normalized Mass Flux at the Water Table for ^{99}Tc and ^{237}Np, Glacial-Transition Mean Infiltration Scenario, for Different Values (Plus and Minus One Standard Deviation (σ) from the Base Case) of the Permeabilities of the Matrix Continuum, and Elevated Water Table

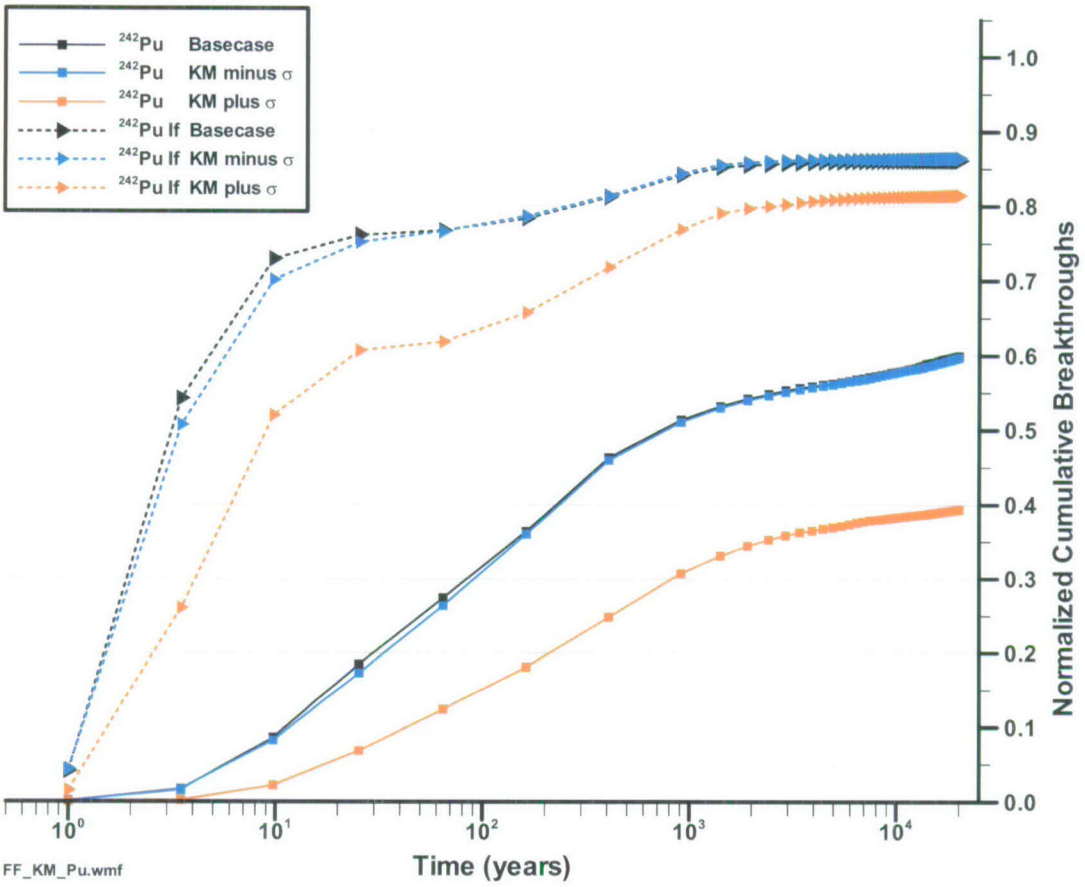

Output DTN: LA0506BR831371.002.

NOTE: These results are for comparison purposes only. Actual radionuclide mass flux reaching the water table will depend on release rates and locations, and will be simulated in the TSPA-LA model.

Figure 6-32. Base-Case Model Normalized Mass Flux at the Water Table for Different Species of ^{242}Pu, Glacial-Transition Mean Infiltration Scenario, for Different Values (Plus and Minus one Standard Deviation (σ) from the Base Case) of the Permeabilities of the Matrix Continuum, and Elevated Water Table

6.6.4 Sensitivity to AFM and Diffusion Parameter Uncertainty

Parameters related to the diffusion of radionuclides between the fracture and matrix continua are uncertain and, therefore, the sensitivity of these parameters must be examined. The magnitude of the diffusive flux is controlled by the surface area-to-fracture volume available for diffusion, and the diffusion coefficient itself. In this section, the focus is on exploring the uncertainty in the geometric and hydrologic parameters related to the surface area term, as these are the most uncertain terms controlling the diffusion rates.

The first set of sensitivity analyses are ones in which the γ parameter AFM model is varied within the uncertainty range of 0.2 to 0.6. This range bounds the uncertainty of this parameter for hydrologic model units below the repository as shown in Tables 6-10, 6-11, and 6-12 and as provided in DTN: LB0305TSPA18FF.001 ([DIRS 165625], TOUGH2 files glaq_1A.dat,

galq_mA.dat, and glaq_uA.dat). Furthermore analyses using ^{14}C data and fracture coating data indicate that this range in γ bounds the uncertainty of this parameter (BSC 2004 [DIRS 170035], Sections 7.4.1 and 7.4.2). The base-case model employed values of the γ parameter that are close to the upper end of this range; therefore, the sensitivity analyses explore the impact of lowering the value of this parameter. To be completely rigorous, one would need to regenerate flow fields using the alternate AFM parameters because the AFM influences both flow and transport processes. However, process flow model results (BSC 2004 [DIRS 169861], Section 6.8.1) have demonstrated that the AFM parameters have very little influence on the relevant flow model parameters for transport, namely the fluid saturations and steady-state fracture to fracture and matrix to matrix flow. Therefore, using the base-case flow fields is an excellent approximation to model results obtained using changed AFM parameter values. Appendix C, Section C5 of this report describes how the AFM model parameters are used to adjust the geometrically defined aperture and spacing parameters describing the fracture-matrix diffusion term. Smaller values of the γ parameter reduce the effective size of the matrix block and, therefore, increase the strength of the fracture-matrix flux term.

The impact of uncertainty in the γ parameter is shown in Figure 6-33 for conservative radionuclide ^{99}Tc, whereas Figures 6-34 and 6-35 are similar plots for weakly sorbing ^{237}Np and more-strongly sorbing ^{242}Pu, respectively. In these simulations, the γ parameter is assigned to a constant value within the entire model. Other simulations confirmed that despite variability from unit to unit of this parameter, a uniform value of 0.6 produces breakthrough curves that are in close agreement with the base-case simulations. Lower values of γ result in later first arrivals, while later-time behavior (out to the 20,000-year simulation duration) is relatively insensitive to γ. The influence of changing the γ parameter in different hydrologic units of the UZ model was also investigated by performing a comparison in which the γ parameter was varied only in the TSw units, compared to changing the parameter in all units below the repository. Figure 6-36 shows that all of the differences in breakthrough curve results are attributable to changing γ in the TSw; the value of γ in the other units does not impact the model results appreciably (Section 7.2.3.3).

A different type of sensitivity analysis involving uncertainty in the effective surface area is possible if one assumes that the uncertainty is not in the γ parameter per se, but rather in the diffusion coefficient or surface area term itself. Liu et al. (2004 [DIRS 169948], Figure 2) present a correlation that shows that the diffusive flux may be a function of scale, such that at larger scales, the diffusive flux increases. Although they describe their results in terms of an increase in the diffusion coefficient, their explanation of potential physical causes for this scale dependence implies that the effective area available for diffusion between the fractures and matrix may increase with scale. Given this explanation, this report examines a sensitivity to effective surface area. For our numerical formulation, access to the surface area is through the effective fracture aperture, b, such that an increase in surface area is obtained by decreasing the fracture aperture by the same proportion. Figure 6-37 shows the sensitivity to a 10- and 100-fold increase in the effective surface area for diffusion, a parameter range that is consistent with the correlation presented in the report by Liu et al. (2004 [DIRS 169948], Figure 2). For the conservative ^{99}Tc, first arrival times are significantly larger for greater surface areas, whereas the curves cross over at later breakthrough times. This characteristic behavior is expected for transport in a fracture with diffusion into a matrix of finite dimension. For the more strongly

sorbing ^{242}Pu, much longer first arrival times are also predicted with increasing surface area. In this case, radioactive decay and very long travel times result in lower late-time arrivals with increasing surface area as well.

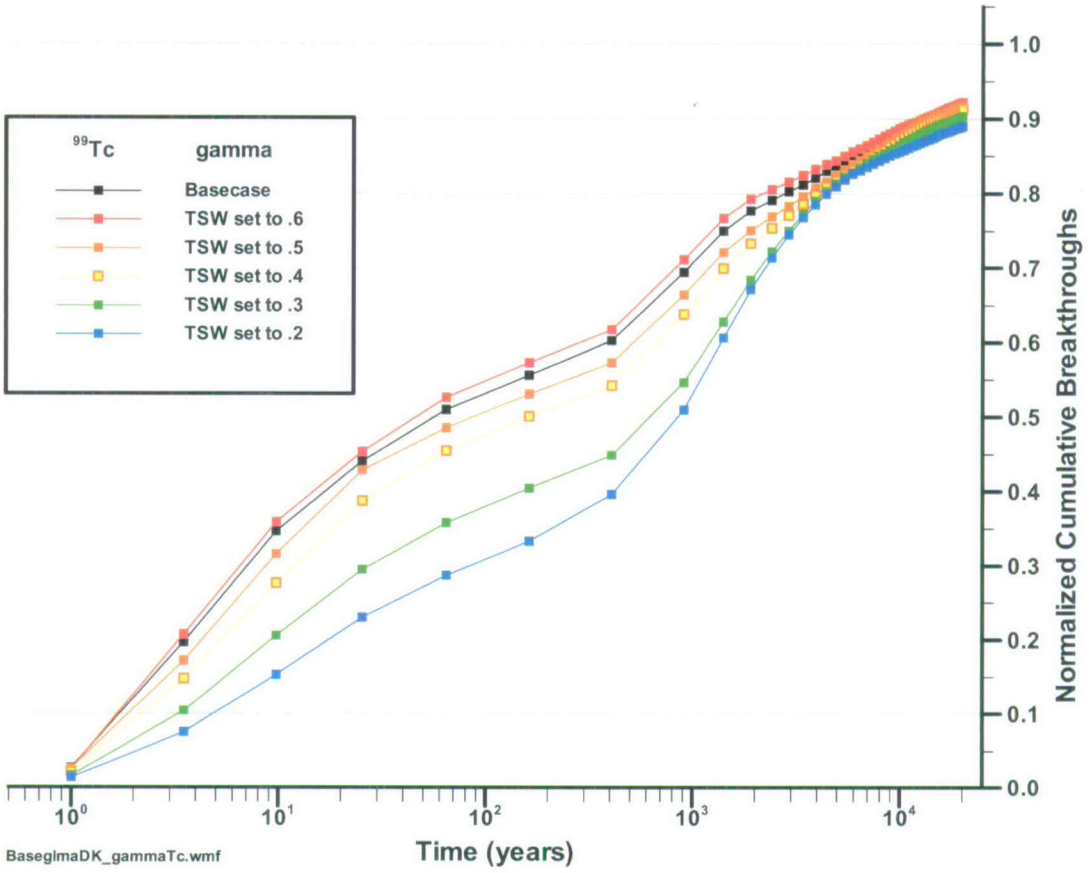

Output DTN: LA0506BR831371.003.

NOTE: These results are for comparison purposes only. Actual radionuclide mass flux reaching the water table will depend on release rates and locations, and will be simulated in the TSPA-LA model.

Figure 6-33. Base-Case Model Normalized Mass Flux at the Water Table for ^{99}Tc, Glacial-Transition Mean Infiltration Scenario, for Different Values of the AFM γ Parameter, and Elevated Water Table

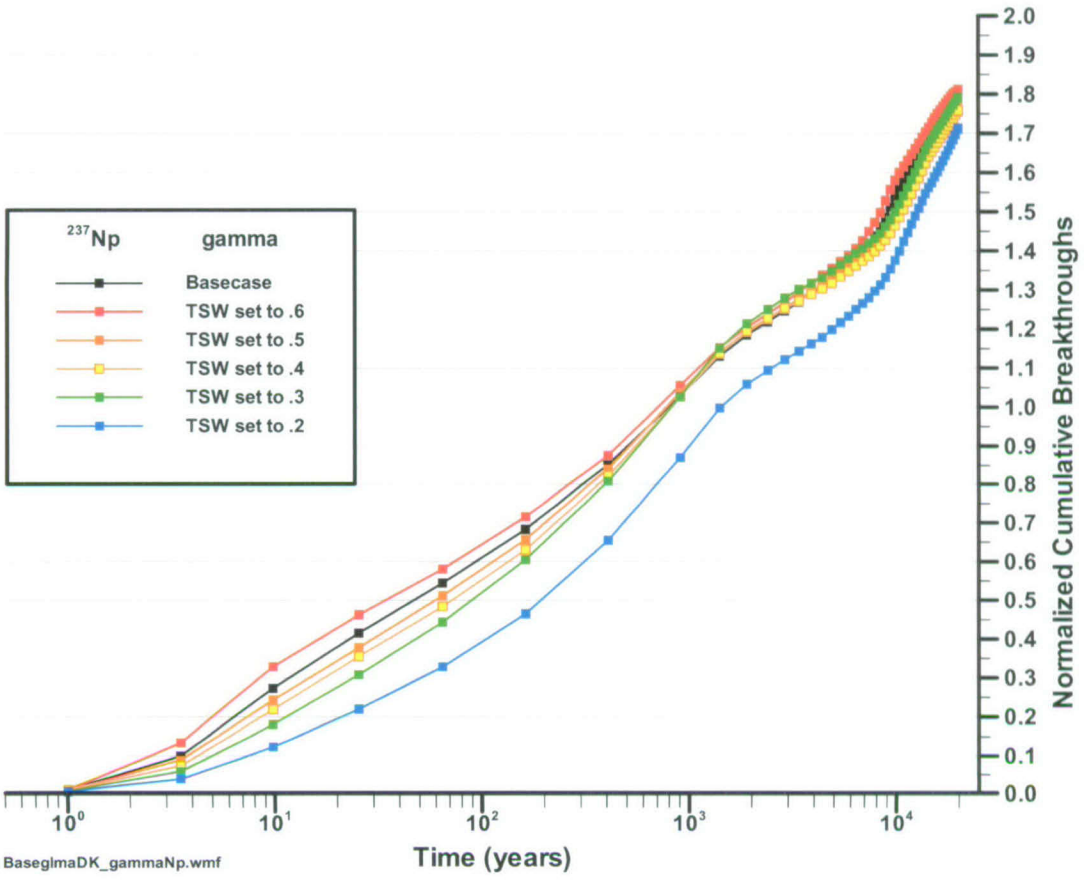

Output DTN: LA0506BR831371.003.

NOTE: These results are for comparison purposes only. Actual radionuclide mass flux reaching the water table will depend on release rates and locations, and will be simulated in the TSPA-LA model.

Figure 6-34. Base-Case Model Normalized Mass Flux at the Water Table for ^{237}Np, Glacial-Transition Mean Infiltration Scenario, for Different Values of the AFM γ Parameter, and Elevated Water Table

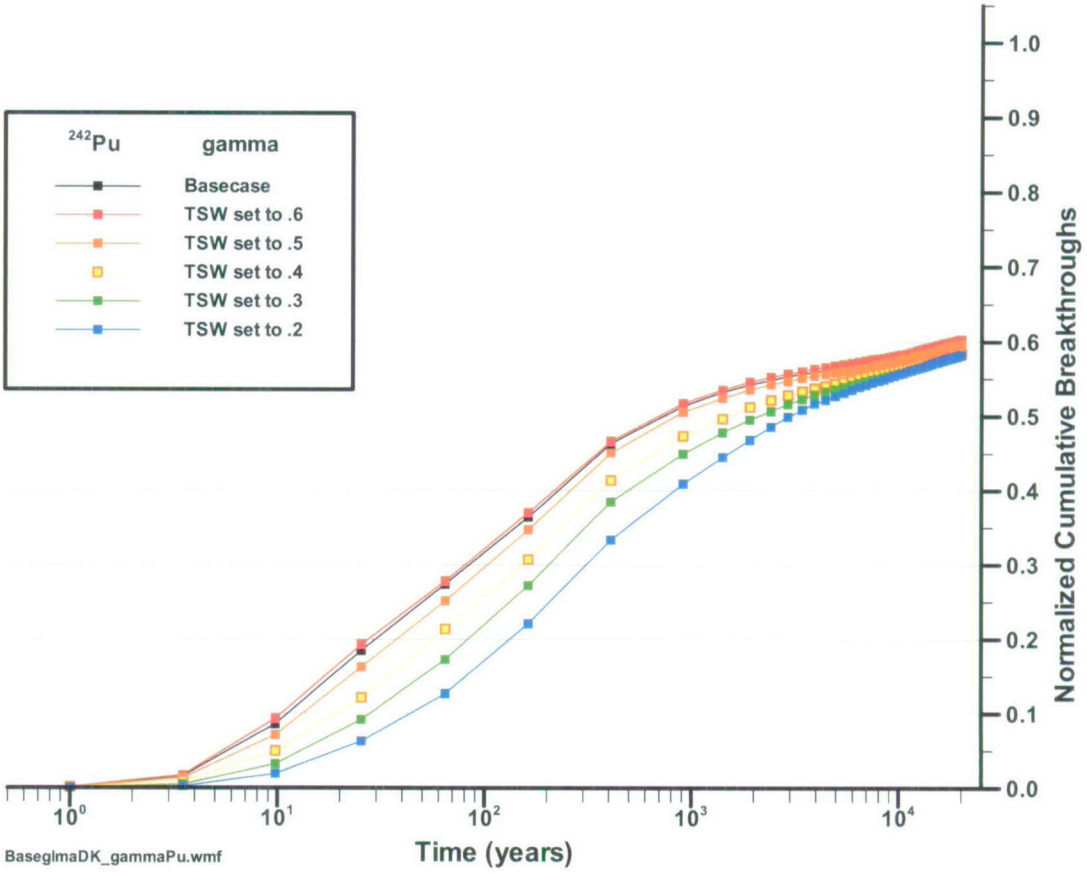

Output DTN: LA0506BR831371.003.

NOTE: These results are for comparison purposes only. Actual radionuclide mass flux reaching the water table will depend on release rates and locations, and will be simulated in the TSPA-LA model.

Figure 6-35. Base-Case Model Normalized Mass Flux at the Water Table for ^{242}Pu, Glacial-Transition Mean Infiltration Scenario, for Different Values of the AFM γ Parameter, and Elevated Water Table

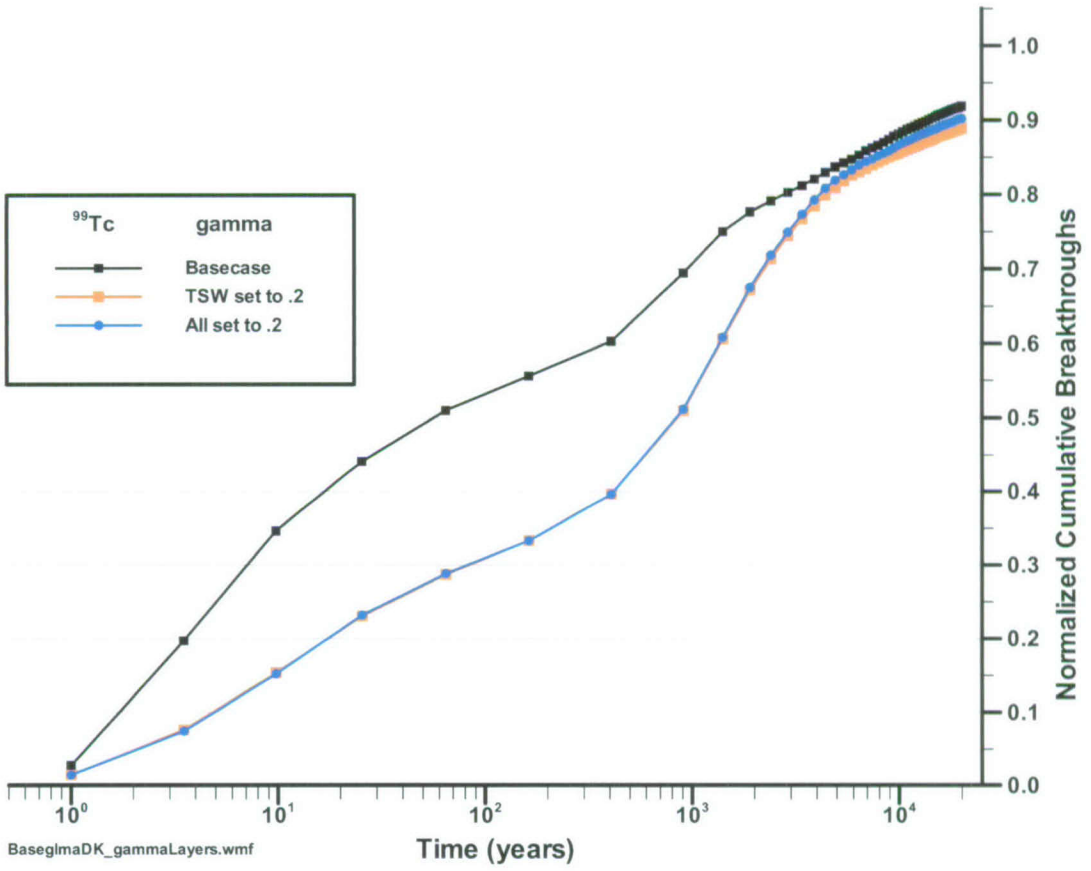

Output DTN: LA0506BR831371.003.

NOTE: These results are for comparison purposes only. Actual radionuclide mass flux reaching the water table will depend on release rates and locations, and will be simulated in the TSPA-LA model.

Figure 6-36. Base-Case Model Normalized Mass Flux at the Water Table for ^{99}Tc, Glacial-Transition Mean Infiltration Scenario, with the AFM γ Parameter Changed in all Units Versus only in the TSw Units, and Elevated Water Table

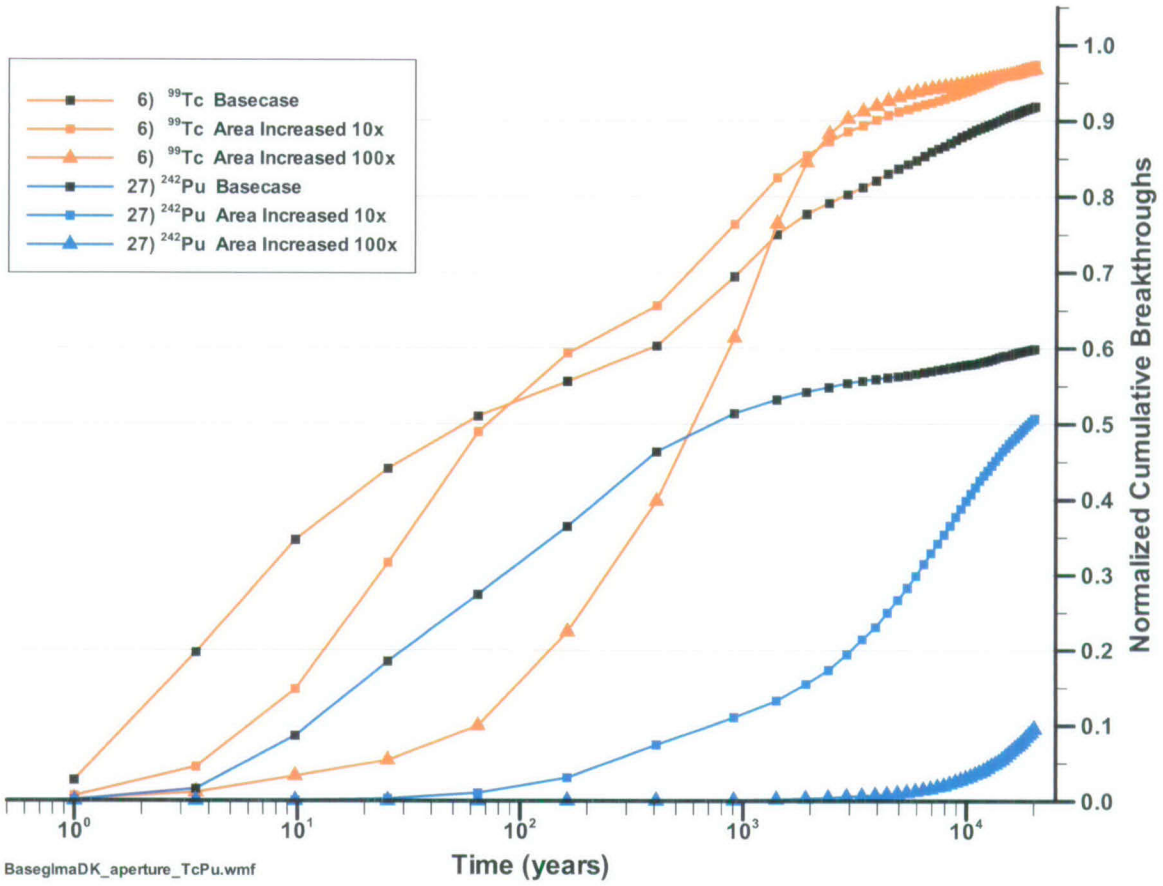

Output DTN: LA0506BR831371.003.

NOTE: These results are for comparison purposes only. Actual radionuclide mass flux reaching the water table will depend on release rates and locations, and will be simulated in the TSPA-LA model.

Figure 6-37. Base-Case Model Normalized Mass Flux at the Water Table for ^{99}Tc, Glacial-Transition Mean Infiltration Scenario, for Different Values of the Effective Area Available for Diffusion, and Elevated Water Table

In summary, the sensitivity of diffusion parameters in the UZ transport abstraction model is greater than the sensitivity to hydrologic parameters. Uncertainties applied directly to the surface area, or indirectly through the AFM model γ parameter result in significant differences in the predicted breakthrough curve at the water table for conservative and sorbing radionuclides. Colloidal radionuclides (the "If" and "Ic" species) have no sensitivity to diffusion model parameters because they are assumed to be non-diffusive.

6.7 EVALUATION OF ALTERNATIVE MODELS AND MODEL UNCERTAINTY

Geological, hydrological, and geochemical data have been used to support parameters used in conceptual models, process-level models, and alternative conceptual models considered in the abstraction of radionuclide transport in the UZ. These traceable, well-documented data have been used to support the technical bases for FEPs that have been included in the abstraction of radionuclide transport in the UZ (Table 6-1). As discussed in the radionuclide transport process

model (BSC 2004 [DIRS 164500]) on which this abstraction model is based, a conservative model approach has been used to address conceptual model or processes uncertainty (Table 6-30). The selected conceptual model of radionuclide transport in the UZ is consistent with the available data and current scientific understanding, and has employed conservative assumptions to treat processes for which data are lacking.

Table 6-30 gives a summary of alternative conceptual models and processes, and the recommended disposition for the TSPA-LA transport abstraction.

Table 6-30. Summary of Alternative Conceptual Model Processes and Their Dispositions for the TSPA-LA

Alternative Conceptual Model	Key Assumptions	Summary of Subsystem Evaluation	Recommend TSPA Evaluation
MINC model of UZ matrix, alternative to single matrix dual permeability model.	More accurately models concentration gradient at fracture-matrix interface, resulting in a more-accurate model of matrix diffusion.	Results in later break-through times when matrix diffusion is significant for long-lived radionuclides. MINC models not directly handled by particletracking codes.	MINC not directly used in TSPA because of large computation burden, but FEHM particle-tracking transport abstraction model exhibits behavior similar to that of the MINC formulation when the discrete fracture model for fracture/matrix interaction is used.
Finite difference numerical models EOS9nT, T2R3D, and DCPT particle tracking, alternative to FEHM particle tracking.	Provide a basis for modeling coupled flow and transport of single (T2R3D) or multiple radionuclides (EOS9nT).	Used primarily to provide validated models of UZ transport processes that form the basis for the abstraction models. These are calibrated against a variety of experimental and analytical models.	Large computational burden limits use for multiple realizations that can provide uncertainty estimates. FEHM particle tracking transport abstraction model can reproduce the results predicted by dual-k models by using transfer functions developed using a dual-k formulation.
Lateral flow diversion in UZ above repository, alternative to no PTn lateral diversion model flow fields.	Lateral flow in the PTn will divert percolating water to the faults and reduce percolation flux at repository.	Used in site-scale UZ flow model to provide evaluation of the impact of lateral flow on UZ flux. The steady state flow fields provide basis for transport simulations.	The base-case flow fields used provide a basis. Lateral diversion is not significant at infiltrations greater than 1 mm/yr and may be important only at lower bounds of infiltration ranges or in areas with low infiltration.
No radionuclide release into faults, alternative to radionuclide release into all repository level nodes including faults.	High fault permeability leads to fast advective transport of radionuclide directly released into faults to top of TSw and to water table.	No significant effects on overall transport to water table even for nonsorbing tracers, except for Np and Pu (which already has a high t_{10}, the time at which 10% of the mass arrives at the water table). There is no effect on t_{50} (the time for 50% arrival), because lateral diversion redirects advective flow to faults and other fast flow pathways	Conservative estimate of transport times, but has substantial effect on radionuclide arrival at top of CHn (TSw39). TSPA models should consider no release into faults by limiting the nodes into which radionuclides are released.

Table 6-30. Summary of Alternative Conceptual Model Processes and Their Dispositions for the TSPA-LA (Continued)

Alternative Conceptual Model	Key Assumptions	Summary of Subsystem Evaluation	Recommend TSPA Evaluation
Include drift shadow, a capillary diversion, alternative to no drift-shadow effects.	Capillary diversion even under ambient conditions may result in low fracture saturation below the drift (drift shadow) that may persist for years.	Drift shadow may develop and remain only under low infiltration. Seepage through fractures may be significant after climate change.	Ignoring drift shadow is a conservative assumption of transport in the UZ.
Perched water permeability barrier zones below the repository, alternative to no perched water permeability barrier (continuous and well-connected fractures).	Perched water may delay and dilute radionuclide concentration and reduce advective transport.	Continuous well-connected fractures are used to model transport processes using the particle-tracking method. The flow fields from the UZ account for perched water effects.	Perched water may only be present in the northern part of the repository. Treating perched water in a manner such that well-connected pathways exist is a conservative treatment.
Include TH, THC, and THM effects on UZ on flow and transport.	Vaporization due to repository heat will maintain the drift dry for several hundreds to a few thousand years. THC and THM effects may alter flow and transport properties of UZ rocks.	TH, THC, and THM effects are insignificant after change to Glacial-Transition climate, the period during which transport processes are dominant, following release of radionuclides by corrosion processes.	The impact of not including TH, THC, and THM effects has been treated in BSC 2005 [DIRS 174191], Section 6.9.

Source: BSC 2004 [DIRS 169861].

NOTES: CHn = Calico Hills nonwelded hydrogeologic; DCPT = Dual Continuum Particle Tracking Computer Code; FEHM = finite element heat and mass (model); MINC = matrix-fracture system - multiple interactive continua; TH = thermal-hydrologic; THC = thermal-hydrologic-chemical; THM = thermal-hydrologic-mechanical; TSPA = total system performance assessment; TSw = Topopah Spring welded unit; UZ = unsaturated zone.

Given the importance of the fracture-matrix diffusion model and parameter values illustrated in the previous section, in this section the conceptual model formulation for the diffusion term is selected for further examination. *Radionuclide Transport Models Under Ambient Conditions* (BSC 2004 [DIRS 164500]) discusses alternative conceptual radionuclide transport models involving:

- Different representations of the matrix-fracture system - multiple interactive continua, (MINC) versus dual-k systems
- Different conceptual methods of describing the transport problem (Particle tracking versus conventional representation in control-volume finite element codes).

Here the focus is on the first item, which is related to the fracture-matrix interchange term. In the MINC method, the steep gradients at the matrix fracture surface are resolved by including additional grids in the matrix in an appropriate number of nested shells. This is based on the concept that rapid changes at the fracture–matrix interface will propagate rapidly through the fracture system, while invading the tight matrix comparatively slowly (steep gradient to the inside of matrix block). Previous studies have shown that the MINC formulation results in later

breakthrough times (as the enhanced f/m interaction allows for increased diffusion), longer contact times, and more effective sorption (in sorbing media/solute systems). In *Radionuclide Transport Models Under Ambient Conditions* (BSC 2004 [DIRS 164500]), the MINC model response [using both T2R3D V1.4 (LBNL 1999 [DIRS 146654]) and TOUGH2 V1.11 MEOS9nTV1.0 (LBNL 1999 [DIRS 113943])] was compared to UZ transport models employing a particle-tracking-based numerical method, Dual Continuum Particle Tracking Computer Code (DCPT) V2.0 (LBNL 2002 [DIRS 154342]). The results of those simulations are presented in the context of model validation in Section 7 (Figure 7-9). The result with the MINC grid conforms to expectations, resulting in later breakthrough times, when matrix diffusion is significant.

Despite its conceptual appeal, the application of the MINC concept to the three-dimensional UZ site-scale model would incur a large computational burden because it necessitates replacement of the single matrix block in the current dual-k system with several MINC subdomains. The validation conducted in Section 7 shows that the FEHM particle-tracking code exhibits behavior similar to that of the MINC model when transfer functions developed using a DFM are used. By contrast, when transfer functions are developed with a dual-k formulation, behavior similar to that of the dual-k process model is obtained. In this section the impact of this ACM uncertainty is examined by performing a series of calculations for the glacial-transition mean infiltration scenario. The only difference in the models is that the DFM conceptualization (using transfer functions developed with the DFM) is used instead of the dual-k transfer functions. For the conservative radionuclides, represented by ^{99}Tc in Figure 6-38, the blue curves in the figure represent the DFM model formulation, whereas the orange curves (and the black base-case curve) represent the dual-k model. For comparison to parameter sensitivity results shown earlier, the impact of the AFM γ parameter is also included in the figure. Significantly later first arrival times are predicted with the DFM, whereas the breakthrough curves converge at later times. The conceptual uncertainty associated with diffusion into and out of the rock matrix is, in general, greater than parameter uncertainties related to the γ parameter. This is particularly true of sorbing radionuclides, as illustrated in Figure 6-39 for ^{237}Np and 6-40 for ^{242}Pu. Early arrivals are completely eliminated with the DFM formulation, and the separation in time between the dual-k and DFM model results increases with increasing sorption coefficient. Thus, the DFM formulation results in much longer travel times to the water table for sorbing radionuclides. The ability of diffusion to transport radionuclide into the matrix, which is enhanced in the DFM model, is particularly important for sorbing radionuclides. Further insight into the differences in these two ACMs may be gained from the discussion in Appendix C, Section C3.

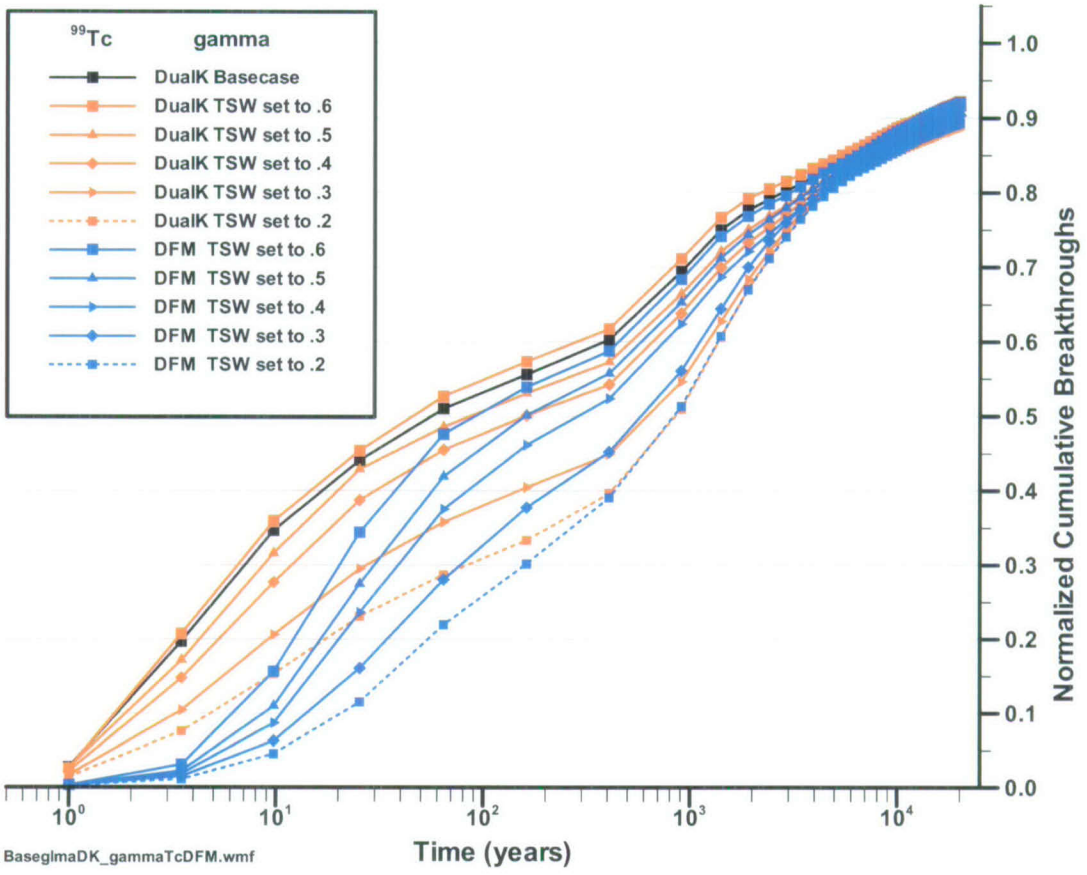

Output DTN: LA0506BR831371.003.

NOTE: These results are for comparison purposes only. Actual radionuclide mass flux reaching the water table will depend on release rates and locations, and will be simulated in the TSPA-LA model.

Figure 6-38. Base-Case Model Normalized Mass Flux at the Water Table for ^{99}Tc, Glacial-Transition Mean Infiltration Scenario, for Different Values of the AFM γ Parameter and Different Fracture-Matrix Diffusion Conceptual Model (Dual-k versus DFM), and Elevated Water Table

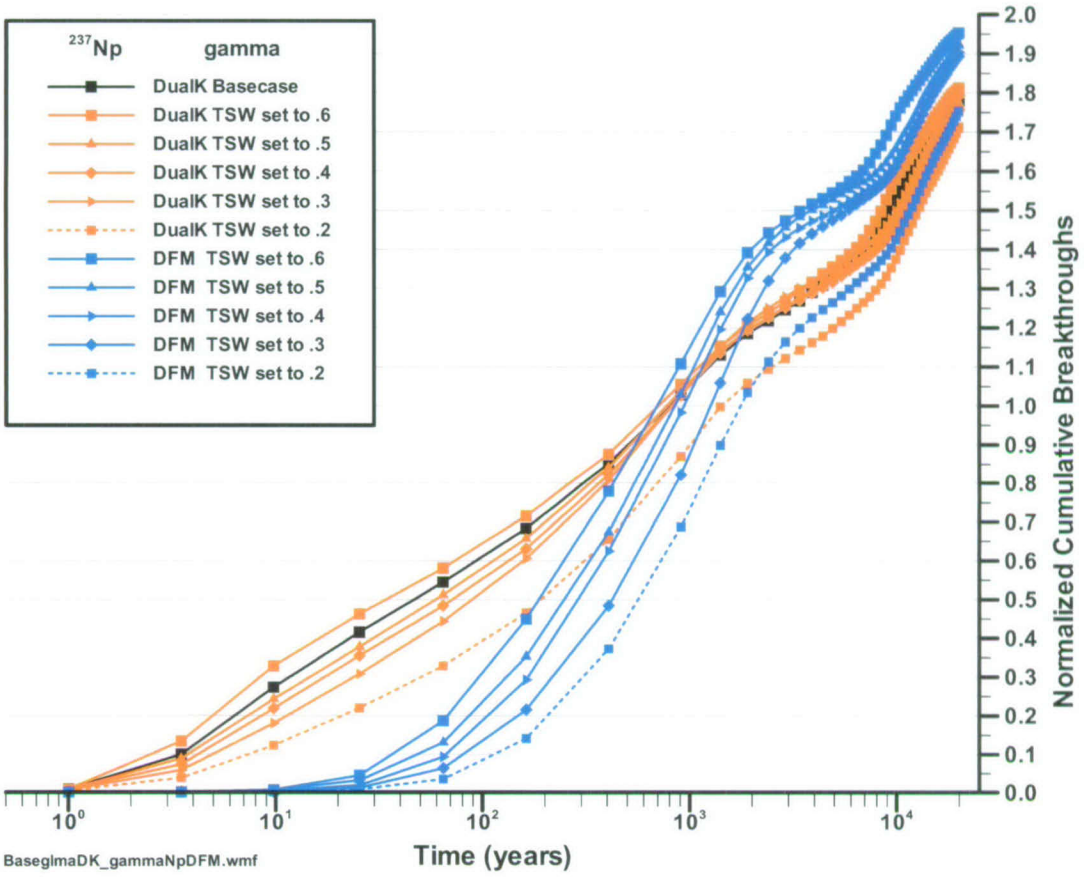

Output DTN: LA0506BR831371.003.

NOTE: These results are for comparison purposes only. Actual radionuclide mass flux reaching the water table will depend on release rates and locations, and will be simulated in the TSPA-LA model.

Figure 6-39. Base-Case Model Normalized Mass Flux at the Water Table for ^{237}Np, Glacial-Transition Mean Infiltration Scenario, for Different Values of the AFM γ Parameter and Different Fracture-Matrix Diffusion Conceptual Model (Dual-k versus DFM), and Elevated Water Table

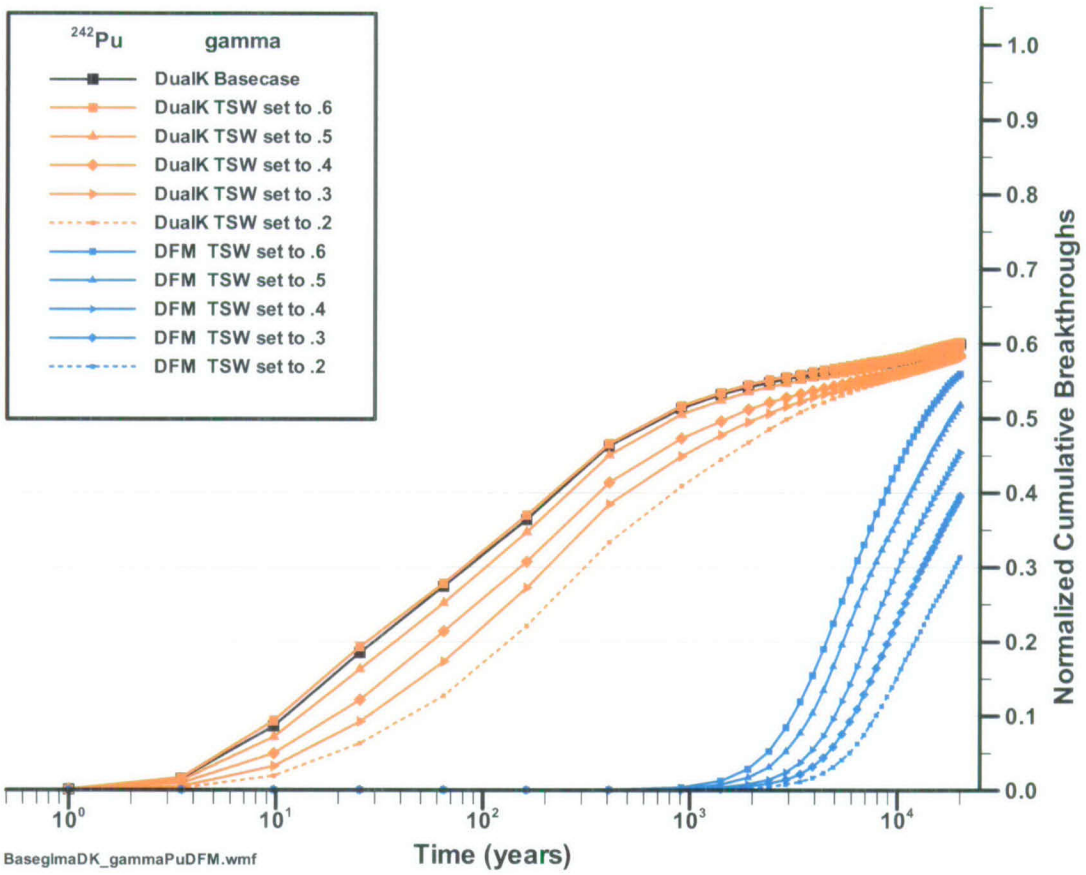

Output DTN: LA0506BR831371.003.

NOTE: These results are for comparison purposes only. Actual radionuclide mass flux reaching the water table will depend on release rates and locations, and will be simulated in the TSPA-LA model.

Figure 6-40. Base-Case Model Normalized Mass Flux at the Water Table for ^{242}Pu, Glacial-Transition Mean Infiltration Scenario, for Different Values of the AFM γ Parameter and Different Fracture-Matrix Diffusion Conceptual Model (Dual-k versus DFM), and Elevated Water Table

In summary, it is clear that the dual-k conceptual model is very conservative with respect to UZ transport performance, especially for sorbing radionuclides. The manner in which the UZ transport abstraction model is developed makes it possible to study the impact of this conceptual model uncertainty easily, by simply changing the transfer function curves used in the simulation. Therefore, these ACMs can both be examined at the total-system level using the UZ transport abstraction model.

6.8 DESCRIPTION OF BARRIER CAPABILITY

The UZ units below the repository are barriers that delay and limit radionuclide movement to the water table due to a variety of natural processes influenced by local hydrological, the intrinsic characteristics of the rocks, and by the repository design. A full treatment of the barrier capability is presented in *Radionuclide Transport Models Under Ambient Conditions* (BSC 2004

[DIRS 164500]); a condensed summary is given below. The major large-scale processes included in this TSPA abstraction model are:

1. The limited and low rate of flow of water through the UZ, which limits the rate at which radionuclides can move by advection out of the repository: included through the use of UZ model flow and transport properties and steady state flow fields (Section 6.5.1).

2. Sorption, which chemically binds radionuclides to minerals in the rock matrix: included by explicit modeling of sorption processes (Section 6.5.4).

3. Matrix diffusion, which physically traps and delays radionuclides within the rock matrix: included by explicit modeling of molecular diffusion in the abstraction of transport (Section 6.5.5).

Other processes that operate at a more local scale also contribute to UZ ability to limit water movement and radionuclide transport. Examples include the diversion of flowing water around drift openings in the UZ by capillary suction and the dryout zone of the region surrounding repository drifts by heat associated with emplacement waste. These processes are beyond the scope of this report, which treats only mountain-scale radionuclide transport.

On the other hand, colloidal transport of radionuclides has the potential to offset the effectiveness of both sorption and matrix diffusion by providing a mechanism for transport of radionuclides that have very low solubility limits. Radionuclides can be transported as intrinsic (true) colloids (fine particles 1 nm to 10,000 nm) of elemental particles (e.g., plutonium). They can also be transported as pseudo colloids (i.e., bound to naturally occurring fine particles). The size of the colloids determines their ability to be excluded or filtered by matrix pores, and transported by fracture advection and dispersion processes. The effect of colloidal transport is discussed in *Radionuclide Transport Models Under Ambient Conditions* (BSC 2004 [DIRS 164500]) and is accounted for in this TSPA abstraction of UZ transport (Sections 6.5.9 to 6.5.13).

6.8.1 Analyses of Barrier Capability

The breakthrough times provide a quantitative assessment of the ability of the UZ to delay (retard) the transport of radionuclides to the accessible environment. An example set of calculations from the UZ transport process model (BSC 2004 [DIRS 164500]) is reproduced in Tables 6-31, 6-32, and 6-33 for aqueous and colloidal radionuclide species. The sorption and diffusion parameters used in these simulations are given in *Radionuclide Transport Models Under Ambient Conditions* (BSC 2004 [DIRS 164500], Tables 6-3 and 6-4). The t_{10} (time for 10 percent arrival) and t_{50} (time for 50% arrival) values for solute and colloidal transport, are presented for representative radionuclides, and combinations of three climate states, three infiltration cases, and the two release scenarios (instantaneous and continuous). At repository closure, short-lived radionuclides such as ^{90}Sr and ^{137}Cs will be reduced to a small fraction of their initial inventory long before they could be transported through the UZ. For long-lived radionuclides, models provide a means for assessing the effectiveness of the UZ to delay and retard (by slow advection, sorption and diffusion) their transport through the UZ. For strongly

sorbing radionuclides like ^{239}Pu, the rate of movement is retarded so much that there is virtually no breakthrough before 10,000 years for the mean infiltration case. For weakly sorbing radionuclides such as ^{237}Np, radionuclide transport is retarded for at least 1,000 years (e.g., the glacial-transition mean scenario yields t_{50} time of 1,070 years). For the long-lived nonsorbing radionuclides like ^{99}Tc, the rate of transport is dictated by matrix diffusion and advective transport. These radionuclides require on the order of thousands of years under present-day mean infiltration conditions, and on the order of hundreds of years for the future-climate scenarios.

Table 6-31. Radionuclide Transport Times in Years to the Water Table for Instantaneous Release

Radionuclide	Climate/ Infiltration Case	Present-Day		Monsoon		Glacial-Transition	
		T_{10} (yrs)	T_{50} (yrs)	T_{10} (yrs)	T_{50} (yrs)	T_{10} (yrs)	T_{50} (yrs)
^{241}Am	Lower	-	-	-	-	-	-
	Mean	-	-	-	-	-	-
	Upper	12	-	3	-	1	-
^{237}Np	Lower	33,800	>1,000,000	15	6,160	185	34,400
	Mean	410	25,400	8	2,120	4	1,070
	Upper	4	1,600	2	714	1	336
^{231}Pa	Lower	-	-	-	-	-	-
	Mean	-	-	-	-	-	-
	Upper	13	-	4	-	2	-
^{239}Pu	Lower	-	-	86,000	-	-	-
	Mean	-	-	10,400	-	3,710	-
	Upper	1,530	-	4	-	2	-
^{226}Ra	Lower	-	-	-	-	-	-
	Mean	-	-	-	-	-	-
	Upper	-	-	-	-	3	-
^{90}Sr	Lower	-	-	-	-	-	-
	Mean	-	-	-	-	-	-
	Upper	-	-	-	-	3	-
^{99}Tc	Lower	13,900	>1,000,000	22	1,310	102	8,140
	Mean	83	6,640	9	417	6	164
	Upper	6	230	2	92	1	42
^{229}Th	Lower	-	-	-	-	-	-
	Mean	-	-	-	-	-	-
	Upper	-	-	4	-	2	-
^{233}U	Lower	65,200	>1,000,000	103	6,730	549	36,900
	Mean	433	29,100	34	2,130	16	893
	Upper	12	1,120	3	458	2	208

Table 6-31. Radionuclide Transport Times in Years to the Water Table for Instantaneous Release (Continued)

Radionuclide	Climate/ Infiltration Case	Present-Day		Monsoon		Glacial-Transition	
		T_{10} (yrs)	T_{50} (yrs)	T_{10} (yrs)	T_{50} (yrs)	T_{10} (yrs)	T_{50} (yrs)
^{235}U	Lower	55,300	>1,000,000	101	6,480	540	32,600
	Mean	430	26,500	34	2,080	15	882
	Upper	12	1,100	3	450	2	206
^{135}Cs	Lower	>1,000,000	>1,000,000	22,400	>1,000,000	150,000	>1,000,000
	Mean	52,500	>1,000,000	4,690	309,000	2,460	120,000
	Upper	2,170	71,200	753	24,500	305	990

DTN: LB0307MR0060R1.007 [DIRS 164752].

Source: BSC 2004 [DIRS 164500].

NOTE: Symbol "-" indicates breakthrough at this relative arrival (i.e., either 10% or 50%) was never achieved in simulations.

Table 6-32. Radionuclide Transport Times in Years to the Water Table for Continuous Release

Case (Mean Infiltration/ Present-Day Climate)	Species	t_{10} (years)	t_{50} (years)
Three-Parents	^{99}Tc	74	3,901
	^{237}Np	781	22,940
	^{235}Pu	-	-
^{239}Pu-Chain	$^{239}Pu+^{235}U+^{231}Pa$	6,419*	33,660*
^{241}Am-Chain	$^{241}Am+^{237}Np+^{233}U+^{229}Th$	1,027*	23,450*

DTN: LB0307MR0060R1.007 [DIRS 164752].

Source: BSC 2004 [DIRS 164500].

*Corresponds to the sum of the chain members.

NOTE: Symbol "-" indicates breakthrough at this relative arrival (i.e., either 10% or 50%) was never achieved in simulations.

Table 6-33. Colloid Transport Times in Years to the Water Table for Continuous Release

Case (Mean Infiltration/Present-Day Climate)	Colloid Size (nm)	t_{10} (years)	t_{50} (years)
1 (no declogging, in which colloids, once filtered, do not detach from the pore/fracture walls)	450	4.35	-
	200	4.39	-
	100	4.53	-
	6	-	-
2 (strong kinetic declogging, providing an estimate of maximum colloidal transport)	450	4.35	-
	200	4.39	-
	100	4.53	-
	6	-	-
3 (weak kinetic declogging, approaching equilibrium filtration behavior)	450	4.35	-
	200	4.39	-
	100	4.52	-
	6	-	-
4 (same as Case 2, but the fractures have the same colloidal transport properties as the corresponding matrix; provides an estimate of the importance of fractures in the transport of colloids)	450	32.4	243
	200	27.8	251
	100	27.6	-
	6	-	-

DTN: LB0307MR0060R1.007 [DIRS 164752].

Source: BSC 2004 [DIRS 164500].

Symbol "-" indicates breakthrough at this relative arrival (i.e. either 10% or 50%) was never achieved in simulations.

6.8.2 Summary of Barrier Capability

The radionuclide transport processes model (BSC 2004 [DIRS 164500]) demonstrates that even under the conservative approach in the three-dimensional site-scale models, the UZ of Yucca Mountain is an effective barrier to the transport of the strongly sorbing radionuclides (^{90}Sr, ^{226}Ra, ^{229}Th, ^{241}Am, ^{221}Pa, and ^{239}Pu). The variably sorbing ^{135}Cs (strongly on zeolites, much less on other rocks), the mildly sorbing ^{233}U, ^{235}U, ^{237}Np, and the nonsorbing ^{99}Tc arrive at the water table at times that are fractions of their respective half-lives. However, this is not necessarily an indication of a breached or ineffective UZ barrier, but can be a direct consequence of the conceptual model of UZ flow and of the conservative approach taken to model transport. Eliminating potential sources from the vicinity of the fault fractures appears to have a small effect on transport and arrivals at the water table. For instantaneous release, the breakthrough curves show a small increase in t_{10}, but t_{50} is practically unchanged.

In the previous section, results from the UZ transport process model were summarized. In this section the base-case UZ abstraction model results are discussed and compared to the results of the process model. Figures 6-41 and 6-42 plot the normalized cumulative breakthrough curves for the same 11 species listed in Table 6-31, which were simulated using the base-case abstraction model in this report. A comparison between the base-case results of this report

(Figures 6-41 and 6-42) and results from the process model (Table 6-31) reveals similar behavior for radionuclide transport through the UZ. The abstraction model shows that for the base-case model it takes the colloids far less time to travel through the UZ than the corresponding dissolved species. Due to matrix diffusion, the transport process for even nonsorbing species, like ^{99}Tc, are retarded, but transport times to the water table are nevertheless significantly shorter than the simulation time period of 20,000 years. Under the present day mean infiltration condition, 10 percent of the total mass travels through the UZ within roughly the first 12 years. By 6,000 years, about 50% of the ^{99}Tc arrives at the water table. Under the glacial-transition infiltration scenario, where the matrix diffusion effect is reduced by the fast flow in the fractures, 10% of the ^{99}Tc travels through the UZ in the first 2 years, and 50% arrives at the water table within approximately 60 years. These transport times are qualitatively similar to those for the process model presented in Table 6-31. The weakly adsorbed ^{237}Np had a relatively higher breakthrough value than ^{99}Tc due to the decay of ^{241}Am traveling in the form of dissolved species (^{241}Am), colloids with irreversible sorption but retardation (Ic241), and colloids traveling unretarded (If241). Species with short half-life (^{90}Sr and ^{241}Am) are significantly attenuated in the UZ due to decay. Clearly, these results are similar to the conclusions reached in *Radionuclide Transport Models Under Ambient Conditions* (BSC 2004 [DIRS 164500]), providing further confirmation that the abstraction model is in substantial agreement with the process model.

With regard to parameter uncertainties, sensitivity analyses presented in Sections 6.6.3 and 6.6.4 show the impact of uncertain hydrologic parameters on UZ performance is small to moderate for the parameters tested for the glacial-transition mean infiltration scenario selected for study, whereas somewhat greater sensitivities are observed with respect to diffusion and AFM parameters.

The largest uncertainty impact appears to be the ACM model uncertainty presented in Section 6.7, implying that uncertainties associated with the nature of diffusion from fracture to matrix are larger than the impact of parameter uncertainties. Because the TSPA model uses the dual-k ACM, the results are clearly conservative with respect to arrival times to the water table (Figures 6-38, 6-39, and 6-40). In all cases, the early arrivals at the water table are most affected by the choice of ACM. The degree of conservatism varies with the sorption coefficient of the radionuclide. Figure 6-38 shows a modest effect for nonsorbing species, in that the first arrivals are still short compared to the 20,000-year simulation period regardless of the ACM chosen. More dramatic impacts are found for the sorbing species, especially the strongly sorbing ones (Figure 6-40). The choice of the dual-k ACM dramatically impacts the arrival times at the water table for these species, resulting in first arrivals that are about three orders of magnitude shorter than for the DFM ACM.

In summary, the abstraction model results indicate that the UZ can act as an effective barrier to transport of the dissolved radionuclide species because of matrix diffusion and sorption. Fast fracture flow in the UZ can weaken the UZ barrier's capability by reducing the effectiveness of matrix diffusion. Given the current model assumptions, the UZ system is a weak barrier for the fraction of the radionuclide inventory that travels via colloid facilitated radionuclide transport, especially under the high-infiltration scenarios. Ultimately, the quality of the barrier with respect to colloids will depend on the quantity of colloids in groundwater, the sorption coefficient, matrix diffusion coefficient, and geological properties of rock layers. Monte Carlo simulations

to address the uncertainty of transport process on system performance are intended to be implemented in the TSPA-LA model.

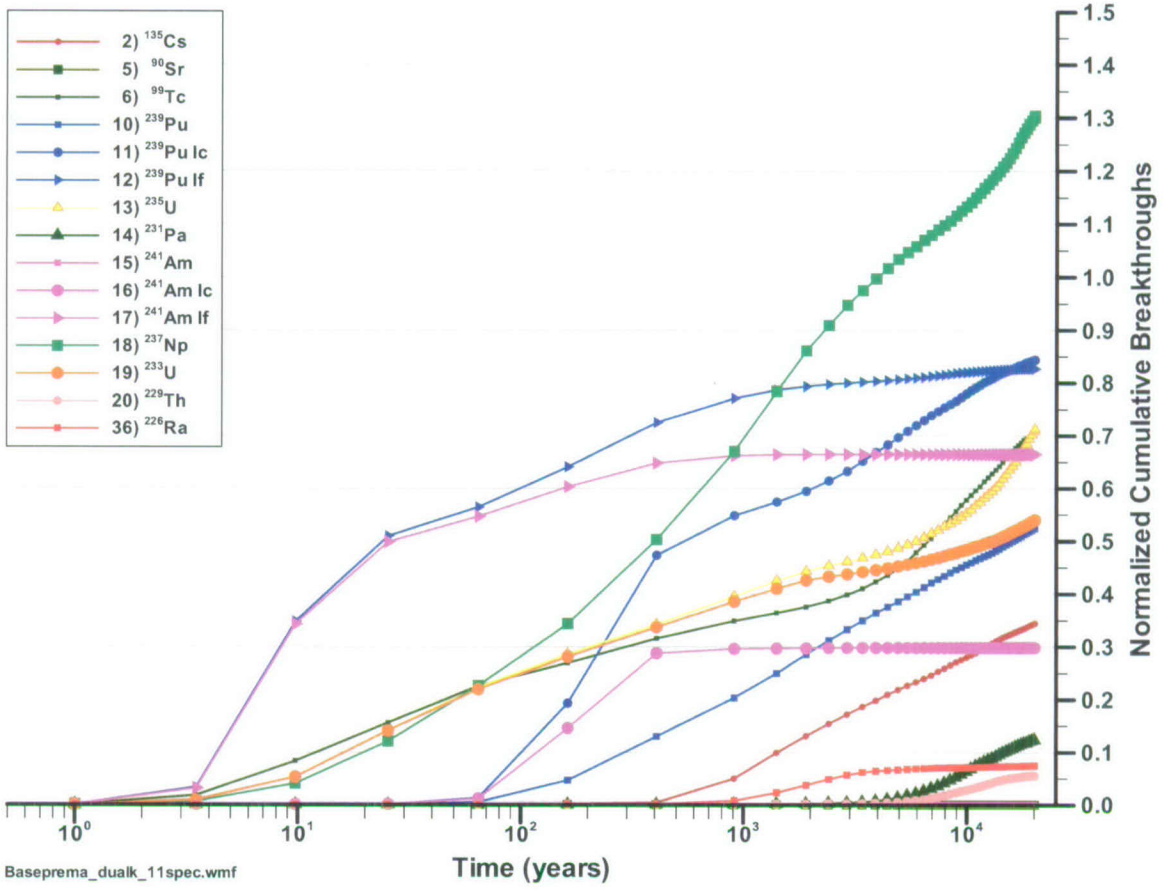

Output DTN: LA0506BR831371.001.

NOTE: Also shown are four breakthrough curves of colloidal forms of ^{239}Pu and ^{241}Am. Ic239 and If239 are colloid species of ^{239}Pu, and Ic241 and If241 are colloid species of Am-241.

Figure 6-41. Normalized Cumulative Breakthrough Curves of the 11 Radionuclides Under Present-Day Mean Infiltration Condition, Representative Parameter Values, and Present-Day Water Table

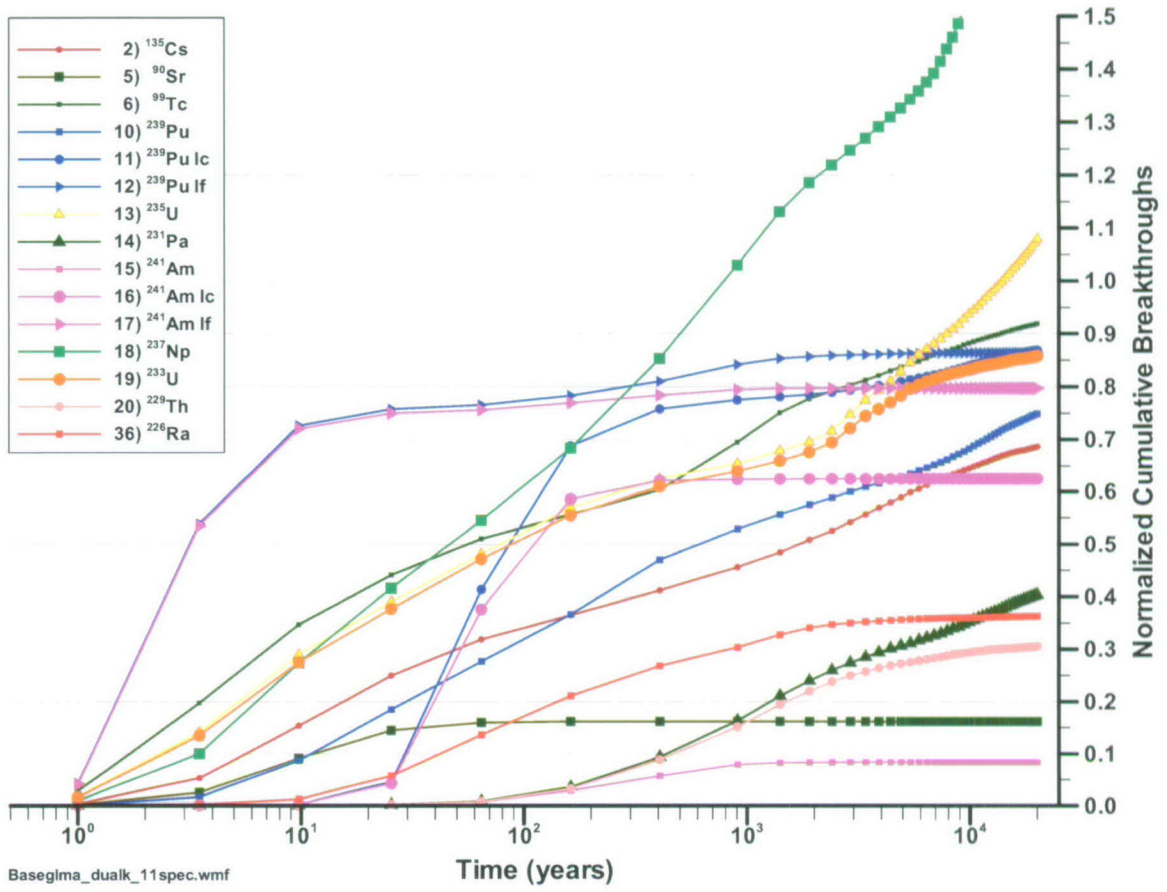

Output DTN: LA0506BR831371.001.

NOTE: Also shown are four breakthrough curves of colloidal forms of ^{239}Pu- and ^{241}Am. Ic239 and If239 are colloid species of ^{239}Pu, and Ic241 and If241 are colloid species of ^{241}Am.

Figure 6-42. Normalized Cumulative Breakthrough Curves of the 11 Species of Radionuclides Under Glacial-Transition Mean Infiltration Condition, Representative Parameter Values, and Elevated Water Table

6.9 OTHER TSPA IMPLEMENTATION CONSIDERATIONS

In the course of developing the revised UZ transport abstraction model documented herein, several minor inconsistencies were identified between the model results presented here and the TSPA model. This section documents and discusses the impact of these inconsistencies on the results presented herein and on the TSPA model results.

6.9.1 FEHM Code Issues

This report develops the base case UZ transport abstraction model for TSPA, and uses FEHM V2.23 to perform base-case analyses for the 36 species used in TSPA modeling. The calculations presented herein are a restricted set of calculations to demonstrate the performance of the model, compared to the TSPA model, which exercises the code over a wide range of parameters. Also, the TSPA model uses the GoldSim-FEHM interface to supply FEHM with

radionuclide mass input, which FEHM converts into particles. In contrast, this report performs representative travel time calculations in which a given number of particles are input directly into the entire repository footprint. For all of these reasons, inconsistencies in the TSPA simulations may result. This section outlines two code inconsistencies associated with FEHM V2.23. As is described below, the impacts of all of these inconsistencies on the results are investigated.

Code Issue 1. Neptunium released to the UZ rock matrix exits the UZ at an excessive rate.

Analysis of the inconsistency indicates that the differences arises only when particles are initiated in the matrix at a release node that has greater than 99% fracture flow at that location. Under these rare circumstances, the code does not, for some parameter combinations, find an appropriate transfer function to base the travel time calculation on. In a particular case neptunium, a weakly sorbing species, is conservatively predicted to diffuse from the matrix into the flowing fracture at higher rates than a nonsorbing species. In this report, no calculations using the base-case model are performed in which particles are released to the matrix. Even if these calculations had been performed, this inconsistency would only have been identified at those nodes in the repository domain that have greater than 99% of the flow in the fractures. The effect on the composite breakthrough curves from releases across the entire repository would, therefore, have been extremely small. It was noticed in the TSPA model results because the releases are often from a single node, and under certain rare conditions the node selected has more than 99% of the flow in the fractures. Therefore, this inconsistency has no impact in the report and the impact on the TSPA is insignificant conservative increase in unsaturated zone radionuclide transport (see SPR001420050614 as described in BSC 2005 [DIRS 174746]).

Code Issue 2. Code conservatively obtains a negative travel time in a cell.

This too is a very limited inconsistency that occurs in a small fraction of the total number of particle residence time computations. Specifically, it occurs occasionally when the actual time should be close to or equal to the minimum possible time in a cell, which is the travel time through the fracture continuum. This is related to the interpolation scheme used to determine the travel time. Because in most cases the total travel time of a particle is controlled by the much longer travel times that are encountered when a particle spends time in the matrix, the influence of a slightly negative travel time within a cell is small compared to the total time. Therefore, differences in the breakthrough curves are neglibly small in the calculations performed in this report, and the impact on the TSPA model is also insignificant.

6.9.2 Model Input Inconsistencies

In the development of the model parameter input for this version of the report, two inconsistencies were identified between the parameters used to generate the model results presented herein and the parameters used in the TSPA model. Both issues relate to colloid transport parameters. Because of the timing of the preparation of this report versus that of the TSPA model report, and based on the fact that the impacts on the results are small (see below), it was decided to document the differences, illustrate that the impacts are small, and proceed forward with TSPA model inputs that have these slight inconsistencies.

Input Inconsistency 1. Colloid-size exclusion factor values within the zones associated with faults in the model have been modified in this report but not in the TSPA model.

Until REV 02 of this report (the current version), the size-exclusion factors defined in Table 6-18 did not include values for the zones defined as faults in the UZ transport abstraction model. Model inputs for the size exclusion factor were set to the default value of 1.0 in these zones, implying that no size exclusion takes place in these zones. For consistency, this has been changed in this version of the report so that the size exclusion model applies to these fault zones as well (see Table 6-18 for the values used in these zones). The new model inputs for these zones (TswFf and ChnFf, the two such zones below the repository release locations in the model) have been changed to the values now cited in Table 6-18 for all colloidal species of the "irreversible" type, that is, the "Ic" and "If" species of Table 6-27. However, these changes make the input parameters reported in this report different than that of the TSPA model. The impact of this change on the results for all irreversible colloidal species is shown for the base case glacial-transitional climate in Figure 6-43. The dotted curves represent the results that will be obtained for these parameter values in the TSPA model, whereas the base case results with the modified size-exclusion parameters are shown in the solid curves. Although the difference caused by these changes is in the direction of shorter travel times, the differences are extremely slight and, thus, should have virtually no impact on TSPA results. This comparison justifies the use of the previously determined parameters for TSPA analyses.

Input Inconsistency 2. Colloid retardation factor parameter applied to the reversible colloidal radionuclides.

Until REV02 of this report (the current version), the only colloidal radionuclide for which colloid retardation was applied was the irreversible "Ic" species. The assumption of no colloid retardation for reversibly sorbed colloidal species was conservative, although not consistent with the model developed in Section 6.4.5. To address this difference, all species exhibiting reversible sorption onto colloids were changed from previous versions to include retardation of the colloids. Figure 6-44 shows the results of the comparison, with the solid curves representing the new abstraction model results, and the dotted curves representing the breakthrough for the TSPA model retardation values with the same values for all other input parameters. The results are very similar, with the model exhibiting slightly longer travel times when colloid retardation is included. TSPA model results are conservative with respect to UZ transport time for all combinations of model parameters. This may be confirmed by examination of Equation 6-18: any value of R_{coll} greater than 1 results in a larger effective retardation factor for the reversibly sorbed species. Recognizing that $R_f = 1$ for this model, values of $K_c >> 1$ result in the effective retardation factor approaching that of R_{coll}. In contrast, for the base case parameters applied in these simulations, $K_c << 1$ for all species except the isotopes of americium. Equation 6-18 shows that for $K_c << 1$ and $R_f = 1$, the effective retardation factor approaches $1 + K_c R_{coll}$, which is only marginally greater than 1 for all radionuclides except americium species, for which the effect is somewhat more pronounced.

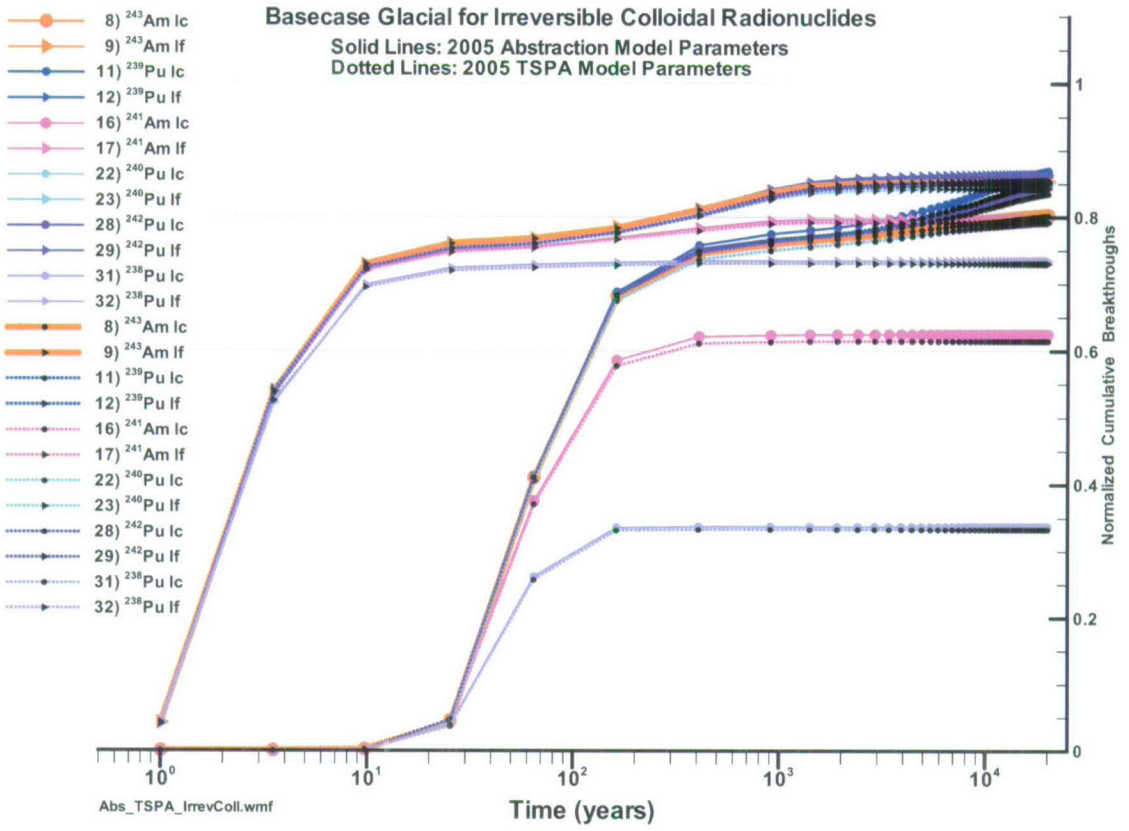

Output DTN: LA0506BR831371.001.

NOTE: These results are for comparison purposes only. Actual radionuclide mass flux reaching the water table will depend on release rates and locations, and will be simulated in the TSPA-LA model.

Figure 6-43. Base-Case Model Normalized Mass Flux at the Water Table for species irreversibly sorbed to colloids, Glacial-Transition Mean Infiltration Scenario, Representative Parameter Values, Elevated Water Table, Comparing the Impact of Including the Size-Exclusion Process in the Fault Zones (Base-Case Model, Solid Curves) versus Assuming No Size Exclusion in Faults (TSPA Model, Dotted Curves).

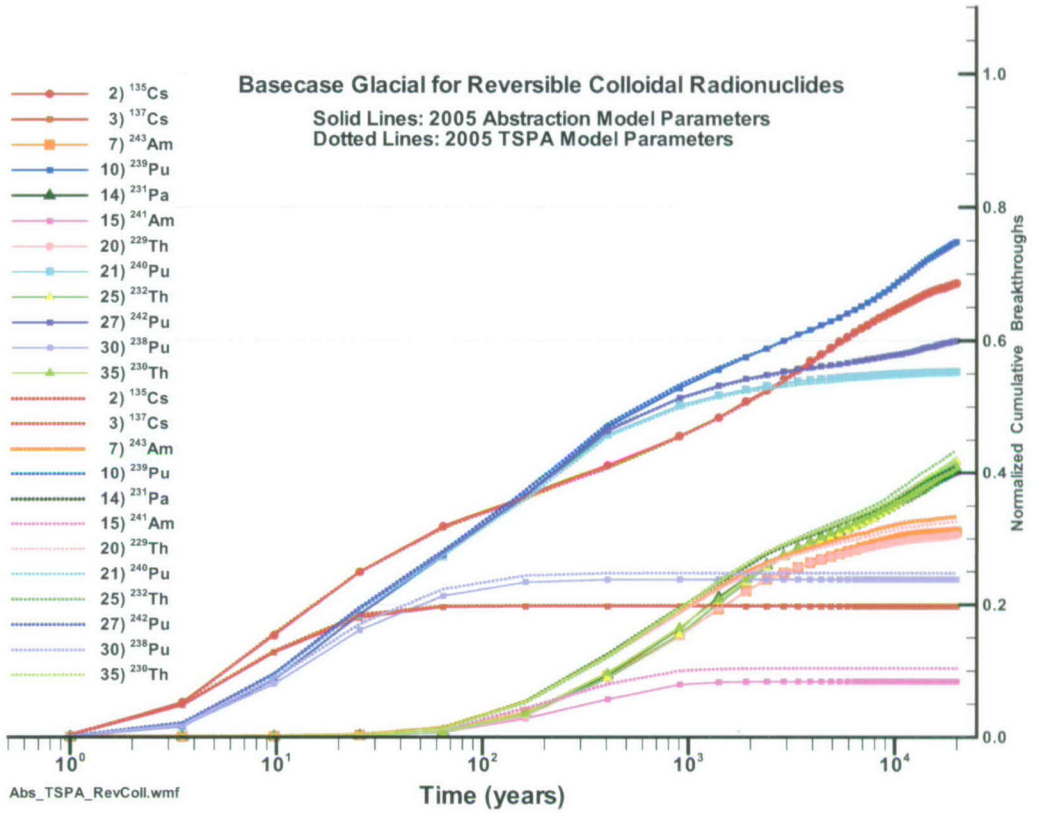

Output DTN: LA0506BR831371.001.

NOTE: These results are for comparison purposes only. Actual radionuclide mass flux reaching the water table will depend on release rates and locations, and will be simulated in the TSPA-LA model.

Figure 6-44. Base-Case Model Normalized Mass Flux at the Water Table for Species Irreversibly Sorbed to Colloids, Glacial-Transition Mean Infiltration Scenario, Representative Parameter Values, Elevated Water Table, Comparing the Impact of Including the Size-Exclusion Process in the Fault Zones (Base Case Model, Solid Curves) versus Assuming No Size Exclusion in Faults (TSPA Model, Dotted Curves).

This analysis is centered on the results for the base case (mean or median) values of these parameters. The result is that, by not including colloid retardation, the TSPA model is slightly conservative for the reversibly sorbed colloidal species when parameters near the midpoints of the ranges are selected. Based on the slight differences observed, the impact on TSPA model results would be insignificant. The TSPA model will be somewhat more conservative for parameter combinations leading to larger effective retardation in Equation 6-18, which will come about for larger values of either K_c or R_{coll}.

INTENTIONALLY LEFT BLANK

7. VALIDATION

This section describes the validation of the UZ radionuclide transport abstraction model. This model is intended to support TSPA calculations of radionuclide transport in the UZ. LP-2.29Q-BSC, *Planning for Science Activities* (Attachment 3, Table 1) requires Level II validation for models supporting that TSPA component. The criteria for confidence building during model development are given in *Technical Work Plan for: Unsaturated Zone Transport Model Report Integration* (BSC 2004 [DIRS 171282], Section 2.2.3). The general criteria for post-development model validation are given in LP-SIII.10Q-BSC, *Models*, Paragraph 5.3.2c). As specified in Attachment 3 of LP-2.29Q-BSC, the Level II postdevelopment model validation must implement a single, appropriate method from this list. Section 7.1 discusses confidence building during model development, which establishes the reasons for confidence in the UZ radionuclide transport abstraction model. Section 7.2 provides a detailed discussion of postdevelopment model validation activities based on corroboration with alternative models. Section 7.3 summarizes the model validation activities.

7.1 CONFIDENCE BUILDING DURING MODEL DEVELOPMENT TO ESTABLISH THE SCIENTIFIC BASIS AND ACCURACY FOR INTENDED USE

For confidence building during model development, Section 5.3.2(b) of LP-SIII.10Q-BSC specifies the following validation steps. Additional steps are listed in Attachment 3 of LP-2.29Q-BSC. The development of the UZ transport abstraction model has been conducted according to these specifications, as follows:

1. *Selection of input parameters and/or input data, and a discussion of how the selection process builds confidence in the model.*
   [LP-SIII.10Q-BSC 5.3.2(b) (1) and LP-2.29Q-BSC Attachment 3, Level I (a)].

The input parameters used in the abstraction process have been carefully selected from appropriate transport process models and from field and laboratory testing; they are reasonable and consistent with the data. Process model and parameter inputs to the abstraction have been discussed and evaluated in Sections 4.1 and 6.5. The process models supporting this abstraction have all been validated, typically in comparison with experimental data and through corroboration with alternative conceptual models. The boundary conditions and inputs used are appropriate; they sufficiently cover the expected conditions and ranges at Yucca Mountain, including temporal changes and spatial variability of processes and properties. Uncertainty in input parameters for this abstraction have been represented using appropriate probability distributions (Section 6.5). Percolation flux are provided through the results of the UZ flow model, where uncertainty is propagated through the lower, mean, and upper scenarios for each climate.

2. *Description of calibration activities, and/or initial boundary condition runs, and/or run convergences, simulation conditions set up to span the range of intended use and avoid inconsistent outputs, and a discussion of how the activity or activities build confidence in the model. Inclusion of a discussion of impacts of any non-convergence runs. [(LP-SIII.10Q-BSC 5.3.2(b)(2) and LP-2.29Q-BSC Attachment 3 Level I (e)].*

The fracture-matrix interaction submodel is developed through transfer functions that scale-up transport processes at the local scale such that they can be represented in the mountain-scale UZ transport abstraction (Section 6.4.3). This scale-up of processes helps build confidence in the model by incorporating finer-scale effects into the model results than can be directly represented in the processes operating on the mountain-scale grid. The particle tracking method is absolutely stable, so run nonconvergences are not applicable.

3. *Discussion of the impacts of uncertainties to the model results including how the model results represent the range of possible outcomes consistent with important uncertainties. [LP-SIII.10Q-BSC 5.3.2(b)(3) and LP-2.29Q-BSC Attachment 3 Level 1 (d) and (f)].*

Relevant sources of uncertainty related to transport parameters and flow simulation results have been characterized in and propagated through the UZ transport abstraction model (Section 6.5). Uncertainty in parameter values was identified and incorporated in the abstraction by use of probability distributions, including uncertainty identified in the upstream sources. For example, uncertainty in matrix diffusion is explicitly included by random sampling of the hydrologic characteristics that affect matrix diffusion as well as the uncorrelated uncertainty observed in measurements, while uncertainty in the future climates and percolation fluxes is accounted for by three different climate scenarios.

4. *Formulation of defensible assumptions and simplifications. [LP-2.29Q-BSC Attachment 3 Level I (b)].*

Discussion of assumptions and simplifications are provided in Section 5 and Section 6.4. The simplifications made are consistent with the purpose of this report (i.e., to develop an abstraction model that simplifies the complex process of radionuclide transport in the UZ for incorporation into the TSPA-LA). These simplifications are adequate and defensible.

5. *Consistency with physical principles, such as conservation of mass, energy, and momentum. [LP-2.29Q-BSC Attachment 3 Level I (c)].*

The process models that provide inputs to the abstraction have been discussed and evaluated in Sections 4.1 and 6.5. Results from these upstream models and the UZ transport abstraction model presented here are consistent with physical principles, such as conservation of mass.

7.2 POSTDEVELOPMENT MODEL VALIDATION TO SUPPORT THE SCIENTIFIC BASIS OF THE MODEL

Requirements and criteria for postdevelopment model validation of the UZ transport abstraction model have been developed in the TWP (BSC 2004 [DIRS 171282]), and discussed in general terms in Section 4.2, Acceptance Criterion 5. In essence, validation of this abstraction model consists of a series of visual comparisons of model results with both simple models and a full process model of the UZ. There are exceptions from the TWP (BSC 2004 [DIRS 171282], Section 2.2.3 and predecessors) in that it states that comparisons to the computer code DCPT V2.0 (LBNL 2002 [DIRS 154342]) and the analytical solution of Sudicky and Frind (1982 [DIRS 105043]) will be made. These comparisons are not included because it was determined that very similar comparisons could be made more efficiently that satisfy the criteria for validation. Therefore, the specific comparisons mentioned in the TWP (BSC 2004

[DIRS 171282] and predecessors) are in effect satisfied in this validation by performing comparisons equivalent to the ones cited in the TWP. In particular, the requirement of a comparison to the solution of Sudicky and Frind (1982 [DIRS 105043]) is satisfied by the comparison to the DFM in Section 7.2.1.1 below, and the requirement to compare to DCPT V2.0 (LBNL 2002 [DIRS 154342]) is satisfied in the comparisons to the process model in Sections 7.2.2 and 7.2.3. These simulations are designed to summarize and augment the code verification checks that have been performed and documented in the qualification of FEHM V2.21 (see verification and validation documentation of this code; LANL 2003 [DIRS 166306]), as well as the individual tests reported in other sections of this report (for example, the decay-chain example of Section 6.4.4). Tests in the verification and validation documentation but not reproduced here include additional tests for dispersion and matrix diffusion. Validation runs under the more complex situations of interest to TSPA, namely two-dimensional and three-dimensional model domains for which process model simulations are available, are also carried out in this report. This model validation strategy conforms with that required for Level II validation of models supporting the TSPA component (BSC 2004 [DIRS 171282], Section 2.2.1).

Three classes of comparisons are made in this validation section. The first, presented in Section 7.2.1, is a series of comparisons of the particle tracking model and a DFM. This comparison focuses on the ability of the model to adequately capture transport in a dual-permeability system under a variety of parameterizations. The series of tests is designed to demonstrate the validity of the underlying particle tracking method on a simple system. Simulations for this suite of runs can be thought of as representing the behavior of transport through an individual layer containing a small number of cells with uniform transport properties. Second, complexity is increased by comparing the particle-tracking model with simulations in a two-dimensional cross sectional model. For comparison purposes, results are available on this cross section from *Radionuclide Transport Models Under Ambient Conditions* (BSC 2004 [DIRS 164500]; DTN: LB03093RADTRNS.002 [DIRS 166071]), assuming both a dual-k and a MINC formulation to capture fracture-matrix interactions. The conceptual model for the f/m interactions has an impact on the predicted behavior, especially for the fastest traveling portion of the solute. By using different transfer function representations (the dual-k and discrete fracture conceptual models), the model is shown to exhibit behavior similar to that of the process models employing similar conceptualizations (dual-k and MINC, respectively). Finally, the third class of comparisons uses the full three-dimensional transport model very similar to that used in TSPA-LA, thereby representing the full complexity of the UZ in terms of heterogeneities in fluid flow conditions and properties. The radionuclide ^{99}Tc is released at the repository horizon, and the breakthrough at the water table is recorded and compared to results from T2R3D, documented in *Radionuclide Transport Models Under Ambient Conditions* (BSC 2004 [DIRS 164500]; DTN: LB0307MR0060R1.007 [DIRS 164752]). Results are available at the process model level only for the dual-k f/m interaction conceptualization, so direct comparisons to the particle tracking model are made for the dual-k transfer functions. Despite the fact that the dual-k formulation is ultimately recommended for use in the TSPA-LA model, the use of the DFM conceptualization in these validation studies allows a wider variety of benchmarking problems to be performed, thereby providing a more robust set of validation runs. In addition, if the DFM conceptualization is used at a later date in the TSPA model, this suite of tests confirms that the model is valid for those calculations. Finally, a sensitivity analysis shows the effect of

employing the DFM conceptualization in the particle-tracking model, and some qualitative tests of the implementation of the AFM in this abstraction model are presented.

In summary, for an abstraction model, the sole activity that applies for model validation is that the model reproduces the results of other models and the process model. Therefore, the benchmarking presented below constitutes proof of the correct functioning of the model.

7.2.1 COMPARISONS WITH DISCRETE FRACTURE MODEL

A DFM, in which transport in a dual-permeability medium is simulated directly, is an excellent test case of the computationally simpler transport model employed in the UZ abstraction model. In the most general case, water moves in both media, as well as between the media, and solute communicates between the media as it moves through the system via molecular diffusion and advection. First, a test case for the advective movement between the fracture and matrix in such a system is presented. Then, parallel flow and transport in the two media is tested, with solute introduced into either the fracture or the matrix. To investigate the ability of the model to span a range of hydrologic conditions, a fracture-dominated flow situation (essentially 100 percent fracture flow) and a case with a 60/40 f/m flow split are used for testing. Figure 6-5 represents the model system simulated with a DFM. Transport between the media occurs via molecular diffusion, so that the breakthrough curve at the outlet of such a model is a function of the relative and absolute velocities, and the degree of diffusive communication of solute between the media. Geometric, flow, and transport parameters, listed in Table 7-1 for this suite of tests, are selected to be representative of transport conditions in the UZ at Yucca Mountain, but do not constitute an actual model of the system, merely a testing setup to enable comparisons to be made. Therefore, data sources for these values are not required. Nevertheless, because the parameters are in general in the range likely to be encountered in TSPA-LA model analyses, the model comparisons provide a good test of the correct functioning of the model.

Table 7-1. Parameter Values for Discrete Fracture Model Test Suite

Parameter	Symbol	Value	
		Case 2 (Sect. 7.2.1.2)	Case 3 (Sect. 7.2.1.3)
Flow Path Length (m)	L	300	300
Fracture Half-Spacing (m)	B	0.5	0.5
Fracture Half-Aperture (m)	b	0.5e-3	0.5e-3
Fracture Saturation (unitless)	θ_f	0.2	0.2
Matrix Water Content (unitless)	θ_m	0.4	0.4
Fracture Water Flux (kg/s)	f_f	1.583e-5 (99% of total)	9.49e-6 (60% of total)
Matrix Water Flux (kg/s)	f_m	1.583e-7 (1% of total)	6.336e-6 (40% of total)
Diffusion Coefficient (m^2/s)	D_m	1.e-30, 1.e-12, 1.e-11, 1.e-10, 1.e-9	1.e-30, 1.e-12, 1.e-11, 1.e-10, 1.e-9
Matrix Sorption Coefficient (mL/g)	K_d	0	0 or 5

For this entire set of simulations, a two-dimensional DFM with these parameters was simulated using FEHM V2.21 (LANL 2003 [DIRS 165741]) in a manner similar to that used to generate the transfer functions (Appendix C), and the resulting breakthrough curves at the outlet were processed using the software routine discrete_tf V1.1 (LANL 2003 [DIRS 165742]). For the simulations using the particle-tracking model, a simple one-dimensional pathway is constructed consisting of ten dual-permeability cells (twenty total). The flow conditions (water contents, volumes, flow rates, etc.) were built into an FEHM restart flow field file by hand. These conditions, along with the grid files and the main FEHM input file, are read directly into the code and the transport particle tracking solution is obtained for the input flow field. This process was chosen to make this test as similar as possible to the way the code is to be used in TSPA calculations, in which flow fields are read in directly and transport is computed. Results are then postprocessed using software routine ppptrk V1.0 (LANL 2003 [DIRS 165753]).

7.2.1.1 Test of Advective Transport Between Continua

The initial test case (CASE 1) examines a situation with parallel flow in the two media, but with 90 percent fracture flux, 10% matrix flux for the first half of the flow path, transitioning abruptly to 60% fracture flux, 40% matrix flux for the second half of the path. Other geometric and storage parameters are the same as those listed in Table 7-1. Solute mass is input into the fracture. By turning off diffusion (which is tested separately in runs discussed later), it is trivial to determine the arrival times that the particle tracking code should produce. The early arrival represents mass that stays in the fracture, and later arrival represents the fracture transport for half of the path, and matrix transport for the remainder. In the results plotted in Figure 7-1, the vertical lines are the theoretical arrival times that the code should reproduce, and the horizontal line (at 2/3, or 0.67) is the theoretically determined proportion of mass that should take the fracture pathways all the way through the model. The particle tracking code reproduces the theoretical behavior for advective movement between the media, thereby confirming that the code correctly routes particles on the basis of advective flow between the fracture and matrix continua. The two simulation curves in the figure are: a simulation with the diffusion model turned off completely, and a simulation with the diffusion model invoked, but the diffusion coefficient set to a low value. Despite the fact that both means for performing the simulation yield acceptable results, it is advisable to completely turn off the diffusion model if the intention is to model a solute with no diffusion. Nevertheless, this result indicates that if diffusion coefficient is set low, the model yields the correct behavior.

7.2.1.2 Comparisons with Diffusion for Fracture-Dominated Flow

Figure 7-2 (Case 2) shows the results of simulations representative of fracture-dominated flow, with 99% of the flow occurring in the fracture. Solute is introduced into the fracture, and the breakthrough at the end of the model is simulated. The particle tracking simulations in this and the next subsection use the DFM formulation so that the direct comparison to the DFM can be made. The description of how those transfer functions are generated is described in Section 6.4.3 and Appendix C. The simulations show that over the range from fracture-dominated transport (D=1.e-30 m^2/s) to conditions corresponding to complete diffusive interchange between the two media (D=1.e-9 m^2/s), the particle tracking model provides very close agreement with the DFM of the same system. Although it is tempting to assume that the model is simply reproducing the same curve that was provided as input in the form of a transfer function, this is not the case. In

the particle-tracking model, the code executes a transfer function operation for each of the ten cells of the flow path. Each cell has a fracture transport time of one-tenth the total, meaning that the code correctly seeks the appropriate transfer function for that cell, and then predicts the overall breakthrough curve for a pathway consisting of multiple nodes. Deviations between the particle tracking model and the discrete fracture solution are due to the fact that the exact transfer functions for the test case are not available, and the model must find the curve with parameters closest to the desired values. This approach is therefore approximate, and relies on the code being supplied a family of transfer functions that covers the range of parameters encountered in a given simulation. Despite this limitation, this test demonstrates that the basic process for determining the transport times of individual particles through a series of connected cells is properly implemented. It also demonstrates the ability of the model to simulate the behavior for an important end-member condition, that of fracture-dominated flow.

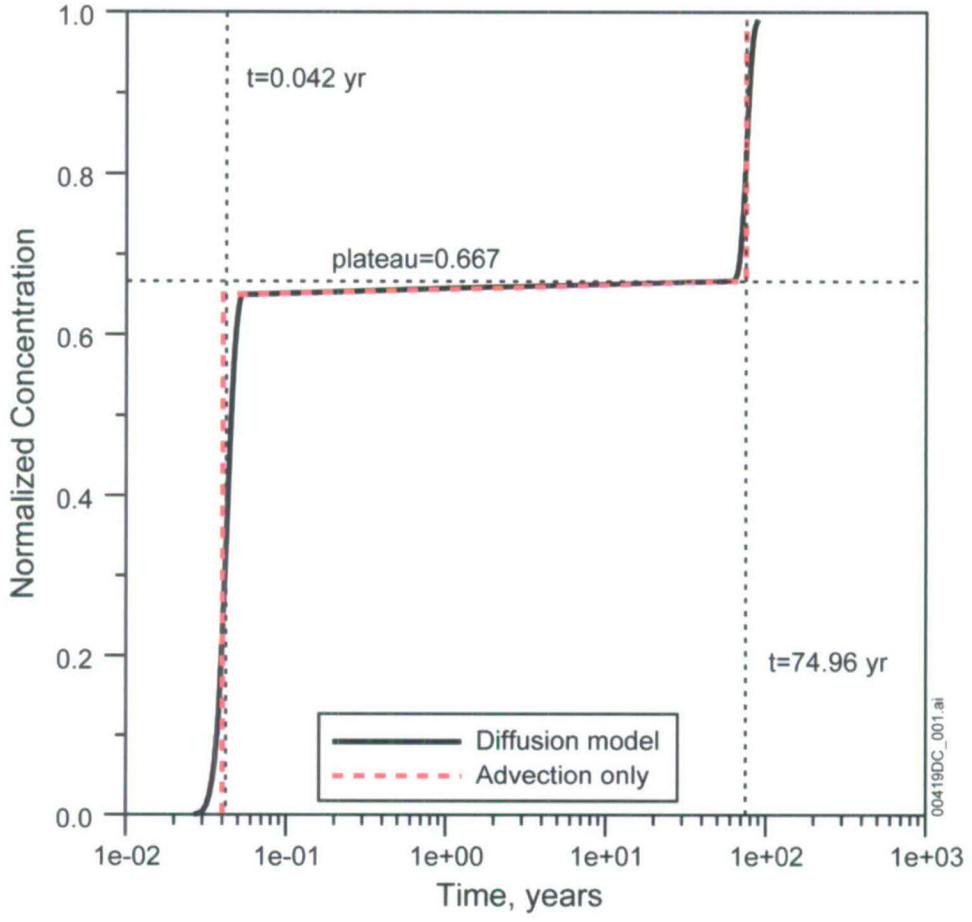

Output DTN: LA0311BR831371.001.

Figure 7-1. Particle-Tracking Abstraction Model Behavior for Advective Transport Between the Fracture and Matrix Continua: No Diffusion or Sorption, Solute Injected into the Fracture, Compared to Theoretical Results

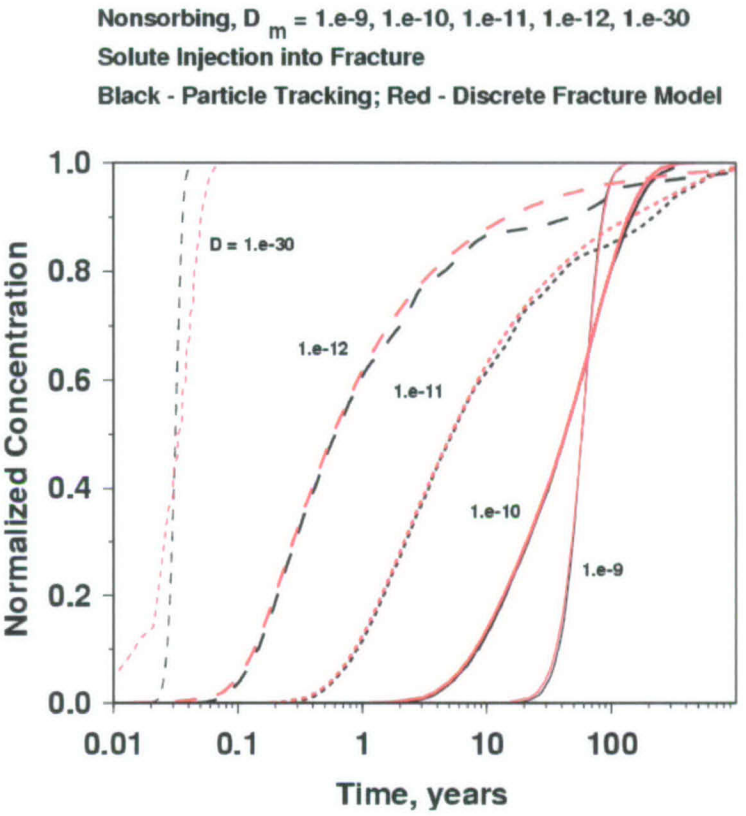

Output DTN: LA0311BR831371.001.

Figure 7-2. Comparison of Discrete Fracture Model and Particle-Tracking Abstraction Model: Non-Sorbing Solute Injected into the Fracture for Different Values of Diffusion Coefficient, f_f = 0.99

7.2.1.3 Comparisons with Diffusion and Sorption for Intermediate Flow Case

Figure 7-3 (Case 3) compares the DFM and the particle-tracking model for the case of more evenly divided flow in the two media (60/40 f/m flow split). Different diffusion coefficients are used, spanning the range from fracture-dominated transport to a diffusive regime in which the system is essentially behaving as a single continuum. The particle-tracking model replicates the behavior adequately over the entire range of parameters. At the lower diffusion coefficients (1.e-11 m^2/s and 1.e-12 m^2/s), there is a slight distortion in the breakthrough curve of the particle-tracking model at later times caused by the process by which particles are probabilistically shifted from one medium to the other due to the diffusive process. This is explained as follows. Consider the case in which a particle that enters a cell via the fracture is instructed by the algorithm to leave that cell via the matrix. This can occur in a low-diffusion regime for some of the solute mass. When the particle is placed in the matrix in the next cell, it is implicitly assumed to be randomly placed along the width of the matrix. In reality, for low diffusion, solute mass will reside preferentially near the fracture, so that the assumption of it being randomly placed along the matrix width is in error. This results in longer transport times for mass that shifts from fracture to matrix. The result is a tendency to predict longer transport times than is expected from a DFM. Despite this error, the initial breakthrough is captured very

well, and the overall trends of the DFM are reproduced. At higher diffusion coefficients, this problem does not occur because the assumption of randomly distributed solute mass along the matrix width is a good one. Therefore, the important end-member of single-continuum behavior, with breakthrough times controlled by the matrix storage volume, is reproduced as well. Finally, this phenomenon is less pronounced for the fracture-dominated flow case of the previous section because fewer particles leave via the matrix for the case of low matrix flow. Although this error is reasonably small compared to the robust fashion in which the model captures the transport behavior over orders of magnitude ranges in diffusion coefficient, and the error is fairly small for either fracture-dominated flow or highly diffusive transport, additional tests are conducted at the end of this section to investigate the nature of this error and document its magnitude.

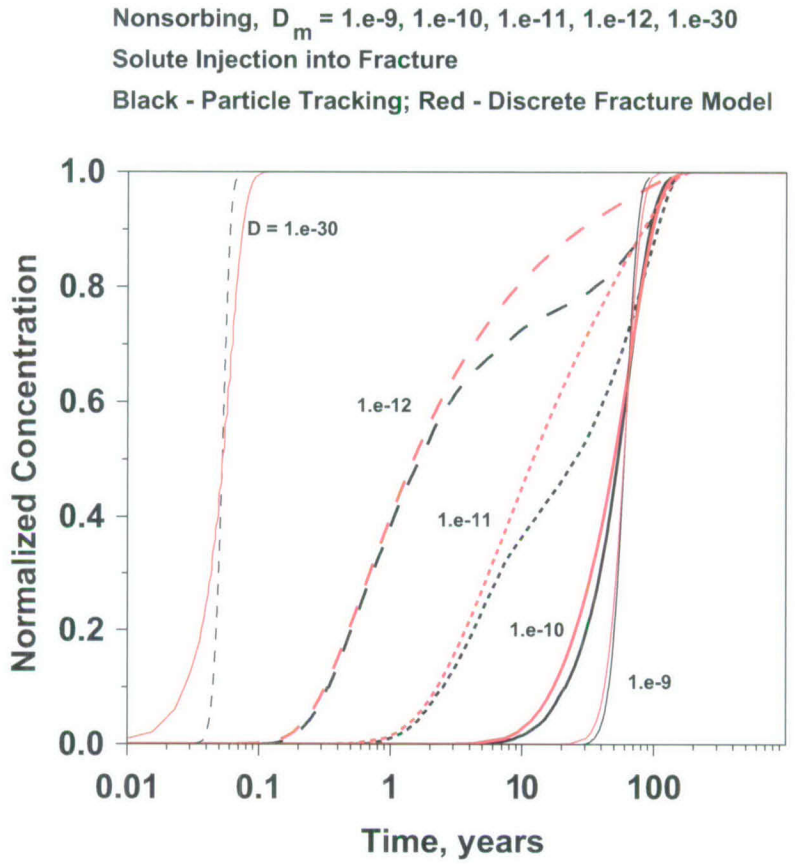

Output DTN: LA0311BR831371.001.

Figure 7-3. Comparison of Discrete Fracture Model and Particle-Tracking Abstraction Model: Non-Sorbing Solute Injected into the Fracture for Different Values of Diffusion Coefficient, f_f = 0.6

Figure 7-4 shows a set of breakthrough curves for Case 2 with a sorbing solute of $K_d = 5$ cc/g. Similar behavior is observed, with longer transport times caused by sorption of the mass that diffuses into the matrix. Similar to the nonsorbing solute comparisons, these comparisons illustrate that the model adequately captures the impact of sorption on the matrix rock. Differences similar to those observed in the nonsorbing cases are present, but the particle-

tracking model replicates the fracture-matrix interactions in the dual-k model over a broad range of diffusion coefficients with sorption included. Further verification of the correct implementation of the model for sorption is shown in Figures 7-5 and 7-6, which show the comparisons to the DFM for high values of K_d. At a diffusion coefficient of 1.e-11 (Figure 7-5) or 1.e-10 (Figure 7-6), the application of high values of K_d in the model are shown to reproduce the expected behavior for the DFM.

Next, Figure 7-7 replicates the conditions of the nonsorbing simulations, except that the solute mass is introduced into the matrix. Very important features of the transport behavior predicted by the DFM are replicated quite closely in these runs. The generally longer transport times are due to the introduction of mass into the slower moving matrix flow. The nature of these results in terms of first arrivals and mean behavior can be understood as follows. When diffusion is finite but relatively low, the small portion of the solute introduced close to the fracture can diffuse into the fracture and travel rapidly to the outlet, yielding a leading edge of the breakthrough curve at short times. This important aspect of the behavior for releases into the matrix is reproduced very accurately by the particle tracking code, as evidenced by the comparison to the DFM. This leading edge is not present for higher diffusion coefficients because mass diffuses readily between the continua, making the probability of rapid transport along the entire length of the model negligibly small. However, the rise in the breakthrough curve representing the bulk of the mass arrival occurs earlier for the high-diffusion case. This can be understood by recognizing that when diffusion is large enough to allow migration of solute over distances comparable to B, the system becomes essentially a composite medium with an effective flow rate equal to the sum of the fracture and matrix fluxes. By contrast, at low diffusion coefficients, transport times through the matrix are governed by the matrix flux, which in this example is only 40 percent of the total. Hence, arrival times for the matrix release case and low diffusion is later than for the high-diffusion case.

Of note in these comparisons is that the particle-tracking model reproduces these features quite well, with the following caveats. At later arrival times, the particle tracking and DFMs diverge, with particle tracking breakthroughs occurring earlier than the DFM breakthrough. The explanation described when explaining the differences for fracture releases applies in reverse for solute releases into the matrix. Nevertheless, the particle tracking simulations compare well overall with the DFM results, capturing the key features and the transport times for matrix releases. This comparison provides important assurance that the mass that enters the UZ transport abstraction model via EBS diffusive releases into the matrix will be properly simulated.

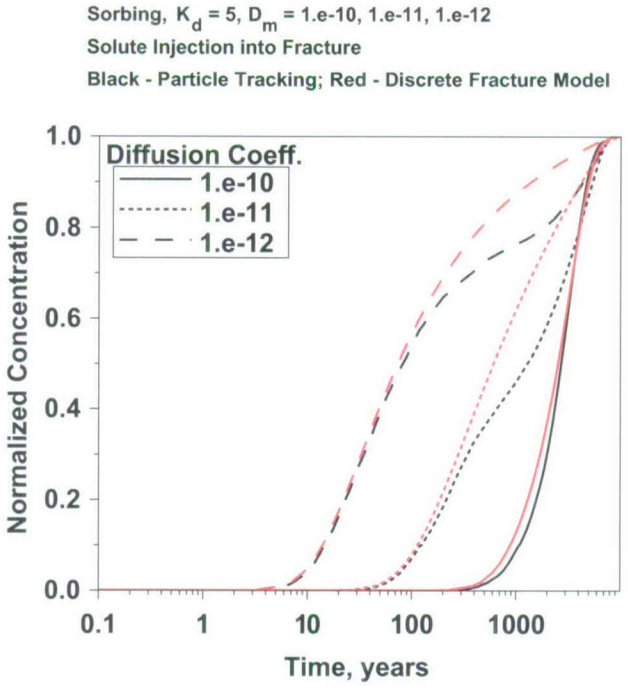

Output DTN: LA0311BR831371.001.

Figure 7-4. Comparison of Discrete Fracture Model and Particle-Tracking Abstraction Model: Sorbing Solute Injected into the Fracture for Different Values of Diffusion Coefficient

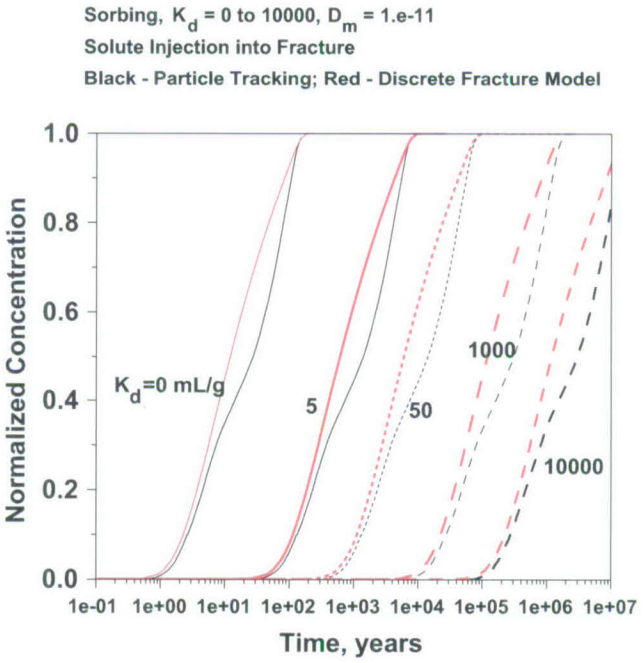

Output DTN: LA0311BR831371.001.

Figure 7-5. Comparison of Discrete Fracture Model and Particle-Tracking Abstraction Model: Solute Injected into the Fracture for Different Values of Sorption Coefficient, D_m = 1.e-11

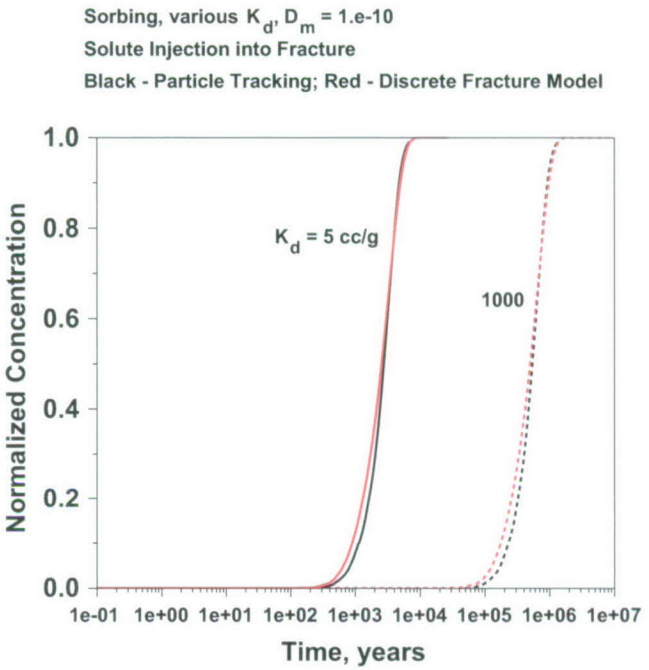

Output DTN: LA0311BR831371.001.

Figure 7-6. Comparison of Discrete Fracture Model and Particle-Tracking Abstraction Model: Solute Injected into the Fracture for Different Values of Sorption Coefficient, D_m = 1.e-10

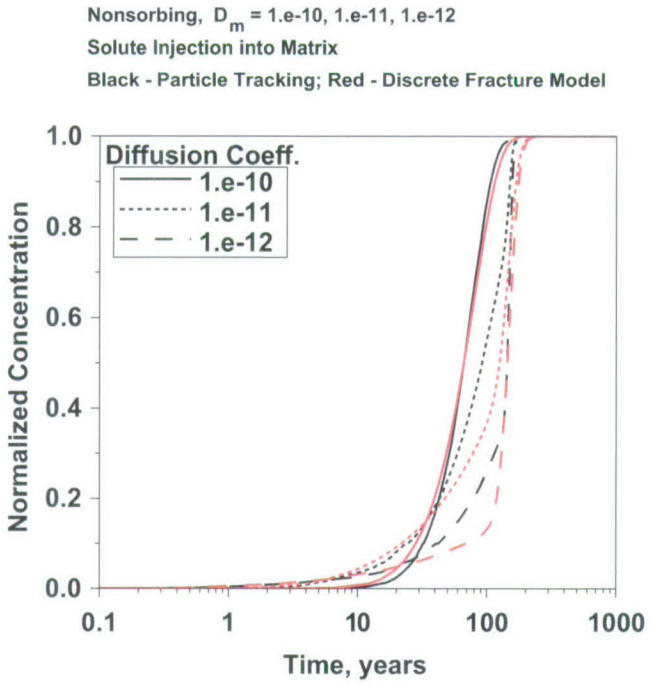

Output DTN: LA0311BR831371.001.

Figure 7-7. Comparison of Discrete Fracture Model and Particle-Tracking Abstraction Model: Non-sorbing Solute Injected into the Matrix for Different Values of Diffusion Coefficient

To further explore the discrepancies for cases with relatively even distribution of flow in the two media, a series of tests are conducted in which the number of grid cells in the path are varied. These tests were performed for D=1.e-11 m^2/s, no sorption, and solute introduced in the fracture. Figure 7-8 compares the breakthrough curves for different numbers of cells with the DFM results. In all cases the overall flow path characteristics are the same, but the discretization is varied. For one cell, the DFM is replicated virtually exactly, because this case simply reproduces a DFM result that was used to generate the transfer function itself. This curve merely shows that for a single cell, the code finds the correct transfer function and the stochastic particle-tracking method is implemented properly. As the number of cells in the path is increased to five or ten, the moderate error observed previously appears. An important point to consider in assessing this grid error is the fact that when flow transitions at interfaces of contrasting hydrologic properties, major transitions in particles from one medium to the other due to advection are likely to occur. Therefore, this type of test really replicates the behavior of the model within a single hydrogeologic unit. Since the number of grid cells within a unit tends to be rather small, the error within a unit is also likely to be small, perhaps of the magnitude shown in the five-cell curve.

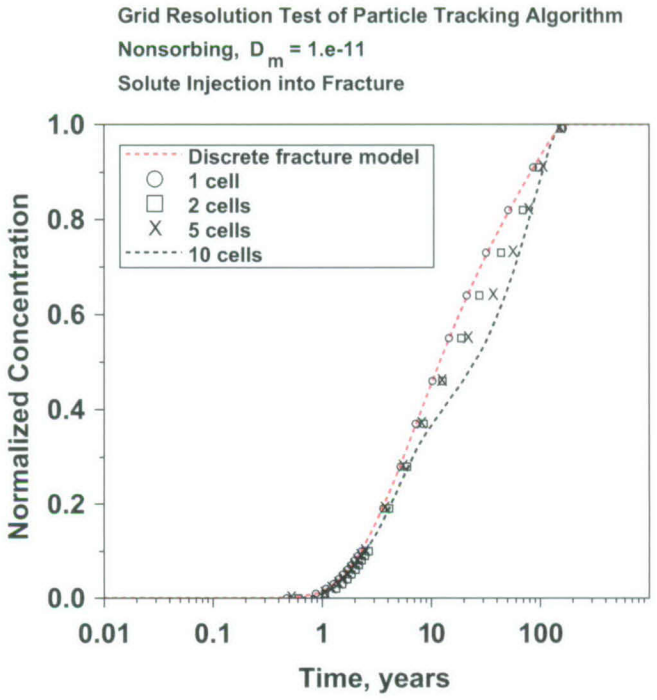

Output DTN: LA0311BR831371.001.

Figure 7-8. Comparison of Discrete Fracture Model and Particle-Tracking Abstraction Model: Sorbing Solute Injected into the Fracture for Different Numbers of Grid Cells in the Flow Path

7.2.1.4 Summary of Validation Tests for a Discrete Fracture Model

To summarize the results of this first validation test suite, the behavior of the particle-tracking model agrees well with a DFM over a very broad range of transport conditions. The deviations that have been observed between the two models are very unlikely to influence TSPA model predictions, and the cause of these differences is well understood. Furthermore, fracture-matrix advective transport has been demonstrated to be properly implemented, and the case of releases into the matrix is also shown to be properly implemented. Therefore these comparisons constitute an adequate demonstration of the effectiveness of the particle-tracking model for capturing the fracture-matrix interactions that the model is designed to simulate.

7.2.2 Comparison with the Dual-k and MINC Model Formulations on a Two-Dimensional Cross-Section Model

Multi-dimensional benchmarking simulations of the UZ transport system is the next step in the validation of the abstraction model. Of course, the system is too complex to enable comparison to analytical solutions. In fact, selecting a code to benchmark against is also difficult because all available codes formulate the transport problem differently. *Radionuclide Transport Models Under Ambient Conditions* (BSC 2004 [DIRS 164500]) showed that these formulations, which constitute ACMs for transport, can produce significantly different results. These differences must be understood to appreciate the differences in the benchmarking results, especially for a complex, multidimensional model. In this section, benchmarking is performing comparing the particle-tracking abstraction model developed here to simulations of the system performed using

T2R3D, documented by *Radionuclide Transport Models Under Ambient Conditions* (BSC 2004 [DIRS 164500]). Two ACMs have been developed on the two-dimensional cross section model using T2R3D. The simulations called "dual-k" use a finite-volume dual-permeability model formulation in which the fracture-matrix diffusion term is governed by a simple gradient calculated as the difference in concentration between the media divided by a characteristic distance, on the order of the flowing fracture spacing. In addition, in *Radionuclide Transport Models Under Ambient Conditions* (BSC 2004 [DIRS 164500]), the MINC conceptual model employs a series of grid blocks in the matrix. The UZ abstraction model implemented in FEHM is capable of simulating either situation. In the conceptualization called the DFM f/m interaction model, sharp concentration gradients are captured through use of a transfer function obtained using a DFM with fine discretization in the matrix, analogous to a MINC formulation. These are the transfer functions used in the comparisons to the DFM in Section 7.2.1. By contrast, a dual-k model can be used to generate transfer functions, and those results might be expected to resemble those of T2R3D when an analogous dual-k formulation is used. These comparisons are performed in this section. A final point on these alternative conceptual models is that in all abstraction model cases, the flow field on which the transport model is run is a dual-k flow field because the particle tracking abstraction model was formulated with the dual-k flow assumption. Therefore, the transport runs with the DFM formulation for the f/m interaction submodel employ a finely discretized matrix block for transport, but a single matrix block for the flow field. This approach should enable sharp gradients likely to be present for solute transport to be captured in the model.

Figure 7-9 plots the comparison results of the particle-tracking model and the two ACMs simulated with T2R3D. For the FEHM runs, the two-dimensional flow fields compatible with FEHM were obtained from the TDMS (DTN: LB0310T2FEHMFF.001 [DIRS 166060]). In all cases, particles are released uniformly across all nodes designated as repository nodes in the model. The first case assumes no diffusion, and the transfer function option to handle fracture-matrix interactions is not used. This comparison is performed to benchmark the particle tracking code in a mode in which particles are routed through the model with dispersion. There is excellent agreement between the particle tracking model and the dual-k, no-diffusion model using T2R3D. Slight differences may be attributable to subtle differences in model formulation, or due to the fact that one of the eleven nodes designated as a repository node in the T2R3D runs was omitted from the particle-tracking runs because it was found to be located in the PTn. Even with these possible sources for the difference, the agreement provides confidence that particle routing and transit times are properly implemented.

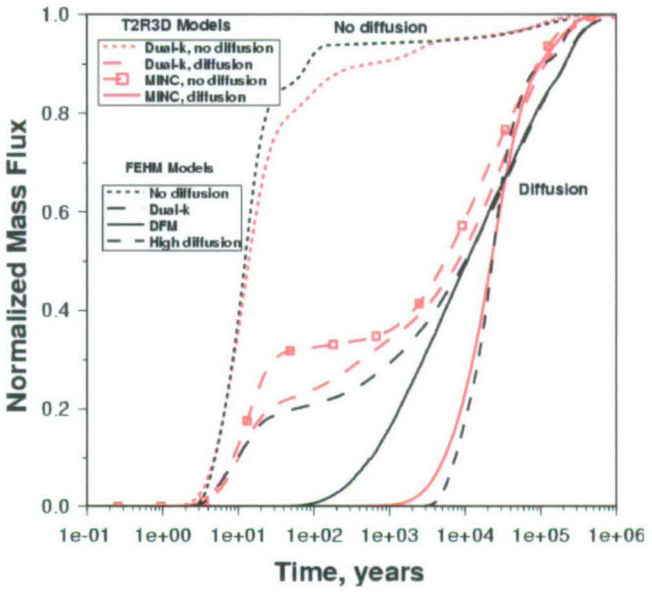

T2R3D Simulations DTN: LB03093RADTRNS.002 [DIRS 166071].

Output DTN: LA0311BR831371.002.

Figure 7-9. Comparison of Particle-Tracking Model with T2R3D Models for a Two-Dimensional, Mountain-Scale Model: with (and without) Diffusion, for Dual-k and DFM Formulations for the f/m Interaction Model, Present-Day Mean Infiltration, Representative Parameter Values, and Present-Day Water Table

Colloid transport model results in *Radionuclide Transport Models Under Ambient Conditions* (BSC 2004 [DIRS 164500], Section 6.18) indicate that breakthrough of radionuclides bound to colloids are dominated by fracture flow and the lack of diffusion into the matrix. The breakthrough times cited in Table 6-33 above illustrate this effect. Therefore, even though there are no direct comparisons of the abstraction model with T2R3D model results for colloid species, the no-diffusion comparison provides high confidence that colloid-facilitated transport of radionuclides is accurately reproduced in the abstraction model.

Before proceeding to the results with diffusion, a discussion of the MINC simulation with no diffusion is in order. Since transport runs without diffusion depend only on advective processes, it is apparent that the mismatch between the MINC, no diffusion, and the dual-k simulations (both T2R3D and particle tracking) indicates that there are differences in the flow regime for the MINC model. The reasons for this difference stem from the fact that the numerical discretization of this model is different than that of the dual-k model. This discussion does not imply that one model is correct and the other is not, but points out that because of differences in the flow regimes of the MINC and dual-k flow models, the particle tracking runs, which input the dual-k flow field rather than the MINC flow field, will not necessarily match the MINC results precisely. Nevertheless, similar breakthrough curve features should be predicted by the particle tracking and MINC models, when the former are computed with the DFM conceptual model transfer function curves. By contrast, diffusion in the dual-k transport model is expected to predict much earlier breakthrough of a portion of the solute mass.

The simulations with diffusion in Figure 7-9 confirm this result. In this figure, various FEHM particle-tracking simulations are benchmarked against simulations using a dual-k or MINC formulation for the two-dimensional cross section. For the FEHM models, the transfer functions for the various cases are those described in Appendix C. The difference in predicted behavior between the two conceptual models is reflected in the FEHM simulations in a manner similar to that of the T2R3D models. Comparing the MINC and FEHM DFM conceptual model, first arrivals in both cases occur much later in time than the dual-k models. For comparison, a high-diffusion case is also presented to illustrate the upper limit of breakthrough times for this flow field. Regarding the dual-k models, the characteristic feature of early arrival of a significant portion of the mass at times similar to that of pure fracture transport is produced in both the T2R3D and abstraction models. The fraction of the mass arriving early is lower in the FEHM model than in the T2R3D model, but qualitatively, the dual-k transfer function curves yield behavior quite similar to the model result using T2R3D. Also, both the T2R3D model and abstraction model results converge at longer transport times, regardless of the formulation of the f/m interaction model or the value of diffusion coefficient used. Finally, the high-diffusion FEHM simulation (run using the dual-k transfer functions) is shown to bracket the behavior of the breakthrough curves in the figure, with results that are very close to that of the MINC model.

These indicators show that the abstraction model compares adequately with the T2R3D models, and properly accounts for the role of conceptual model uncertainty in the f/m interaction model. The relatively minor differences of the models employing the dual-k f/m conceptual model are probably attributable to subtle differences in model formulation and mathematical techniques for solving the transport problem.

7.2.3 Comparison with T2R3D Process Model for the Three-Dimensional System

Full simulation of the three-dimensional UZ transport system is the last step in the validation of the abstraction model. Section 7.2.2 showed that on a system for which the dual-k and MINC f/m interaction model results were available for comparison, the FEHM particle tracking results can provide qualitatively similar behavior for these ACMs simply by choosing transfer functions developed for a given conceptualization. In this section, the particle tracking abstraction model is benchmarked against simulations of the system performed using T2R3D, documented in *Radionuclide Transport Models Under Ambient Conditions* (BSC 2004 [DIRS 164500]). The T2R3D simulations use a finite-volume dual-permeability model formulation in which the fracture-matrix diffusion term is governed by a simple gradient calculated as the difference in concentration between the media divided by a characteristic distance, on the order of the flowing fracture spacing. No results are available using a MINC or other formulation that captures sharp gradients into the matrix. Therefore, the principle FEHM benchmarking simulations will be those using the dual-k transfer functions. However, these results demonstrate that the code can effectively explore uncertainty associated with this conceptual model. Because these comparisons use similar flow model and flow parameters as will be used in the TSPA-LA model, the model comparison provides direct proof of the correct functioning of the model under conditions that will be present in the TSPA model. Because these validation simulation comparisons were performed before the latest parameter distributions were developed, there are small differences in the parameters used in these comparisons from those presented in Section 6. Furthermore, consistency with the process model required the use of the present-day water table to perform the comparison of the process and abstraction models. For these reasons, the actual

predictions presented below are slightly different than those presented earlier, but are adequate for validation purposes because they test the same model setup and very similar parameter values to those used in the TSPA model.

7.2.3.1 Comparisons of FEHM and T2R3D for the Dual-k Conceptual Model

These comparisons are conducted for a nonsorbing radionuclide Tc-99, since simulations in Section 7.2.1 above showed that sorption is handled appropriately. For model runs using either FEHM or T2R3D, breakthrough at the water table is simulated for a release function consisting of a pulse of radionuclide introduced uniformly across the entire repository. The comparisons between the models are for the cumulative, normalized arrival time distributions at the water table. Of course, these release functions are not realistic representations of how the actual engineered system will behave. Such a release function yields the distribution of transport times for the UZ as a whole for releases across the repository, and, as such, is a useful point of reference for how the UZ behaves, as well as being an appropriate benchmark for comparing the models. From the standpoint of model validation, the benchmarking is appropriate because each of the models uses the same source region. Parameters in the abstraction model are uncertain. For this comparison, values documented by *Radionuclide Transport Models Under Ambient Conditions* (BSC 2004 [DIRS 164500]) are used to perform this comparison, and the present-day climate flow fields are used to make the comparison throughout the entire simulation period. This approach allows testing the model over a significant range of infiltration scenarios, those spanning the uncertainty range for infiltration rate using the three present-day flow fields derived in *UZ Flow Models and Submodels* (BSC 2004 [DIRS 169861]).

Figure 7-10 shows the cumulative transport time distributions through the UZ for ^{99}Tcfor the two models for the three flow fields (lower, mean, and upper) developed to capture uncertainty in the present-day infiltration rates. The agreement between FEHM using the dual-k transfer functions and T2R3D is quite good, considering the vast range of infiltration conditions covered in these comparisons. For the lower infiltration scenario, the early arrival of a small fraction of the released mass, and the steepening breakthrough curve after 10,000 years, are observed in both models. The plateau at values between 0.4 and 0.5 at long times is due to radioactive decay of ^{99}Tc. For the mean infiltration flow field, the agreement of the process and abstraction models is also excellent at all transport times. For the upper infiltration scenario, FEHM predicts an earlier arrival for the fastest moving solute, indicating a difference in the way the two models handle diffusion in rapid fracture flow. Nevertheless, in benchmarking exercises of such a complex model, differences are the norm. Note that differences in travel times within the first 100 years of breakthrough are not likely to have a significant influence on predicted performance because the early breakthrough portion effectively bypasses the UZ barrier in either case. In summary, the benchmarking results are very successful, in that all significant features of the UZ transport system are captured with the abstraction model.

7.2.3.2 Influence of Diffusion Coefficient and f/m Interaction ACM

To amplify on the simulations presented in the previous section, Figure 7-11 brackets the behavior of the particle-tracking model as a function of diffusion. This figure shows the behavior of the FEHM model over the complete range of diffusion coefficients, from no diffusion to a case in which diffusion is set so high that it effectively yields a composite medium

behavior (D=1.e-8 m^2/s). The envelope of behavior as a function of diffusion is quite large, whereas the behavior of T2R3D is reproduced when the same parameters and conceptual model for f/m interactions is selected. This result, when combined with the 1D results of Figures 7-2, 7-3, and 7-4, and the two-dimensional results of Figure 7-9, illustrates that the abstraction model yields reasonable results over a wide range of diffusion coefficient, one of the key parameter uncertainties in the TSPA-LA model. Also shown in Figure 7-11 is the predicted behavior using the DFM formulation for the f/m interaction model. No process model results are available for comparison due to the computational limitations of simulating the full three-dimensional model using an MINC formulation.

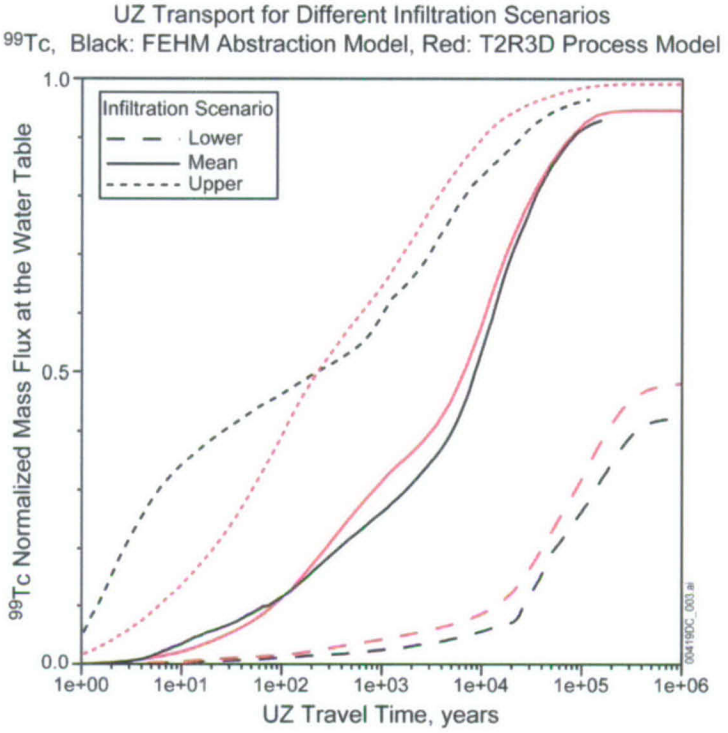

T2R3D Simulations: DTN: LB0307MR0060R1.007 [DIRS 164752].

Output DTN: LA0311BR831371.002.

Figure 7-10. Comparison of Breakthrough Curves for ^{99}Tc for T2R3D and the UZ Transport Abstraction Model: Simulations for Different Present-Day Infiltration Rate Scenarios (Lower, Mean, and Upper), Representative Parameter Values, and Present-Day Water Table

These limitations are not an issue for the abstraction model, which simply uses a different set of transfer functions as input. The results are reasonable, given the understanding of these models and the comparisons presented in Section 7.2.2 for the smaller two-dimensional cross section model. The main differences for these ACMs are at the earliest arrival times, where the dual-k model predicts much faster arrivals at the water table. For later transport times, the two curves track each other closely, showing that the results are insensitive to the conceptual model. Finally, all breakthrough curves with diffusion, including the high-diffusion case, converge at large transport times. This result is also reasonable, providing additional evidence for the correct functioning of the f/m interaction model.

The influence of f/m conceptual model is explored more fully in Figure 7-12, a comparison, using only the FEHM particle-tracking model, of the dual-k and DFM ACMs for all of the flow scenarios. The choice of ACM is particularly sensitive for the upper infiltration scenario, whereas differences become progressively more subtle for the mean and lower infiltration scenarios, respectively. As the fluid velocity is reduced, the characteristic diffusional distance into the matrix increases. For this situation, the dual-k model becomes more like the DFM in the sense that concentration gradients in the latter are not nearly as steep. With respect to the abstraction model, these comparisons have reasonable qualitative explanations. This result illustrates that the abstraction model can propagate conceptual model uncertainties for f/m interactions through the TSPA-LA model.

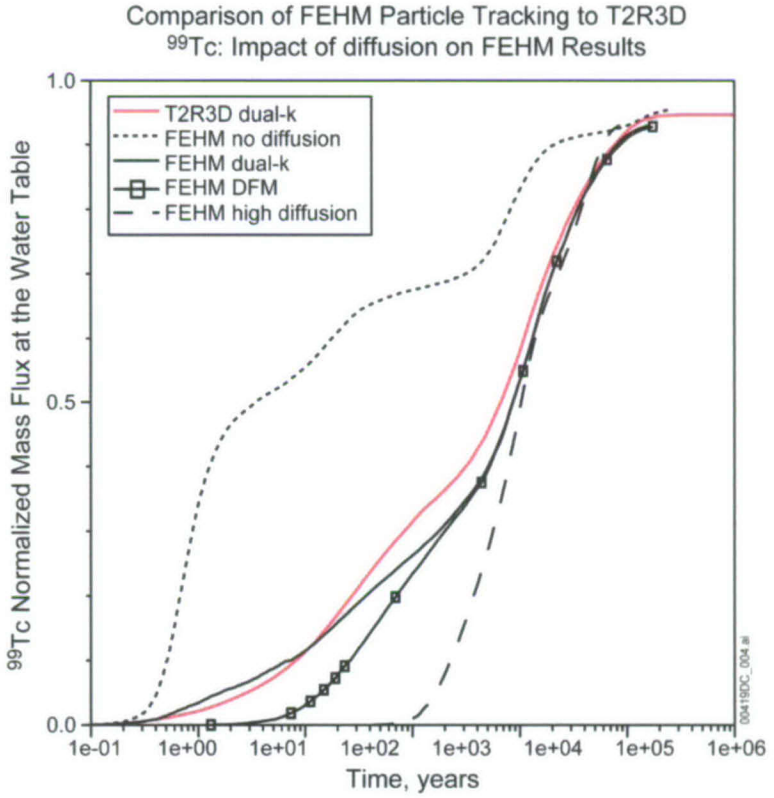

T2R3D Simulations: DTN: LB0307MR0060R1.007 [DIRS 164752].

Output DTN: LA0311BR831371.002.

Figure 7-11. Comparison of Breakthrough Curves for ^{99}Tc for T2R3D and the UZ Transport Abstraction Model: Present-Day Mean Infiltration Scenario, Diffusion in FEHM Ranging from No Diffusion to High Values, Representative Parameter Values, and Present-Day Water Table

7.2.3.3 Tests of the Active Fracture Model Implementation

The AFM has been identified in *Radionuclide Transport Models Under Ambient Conditions* (BSC 2004 [DIRS 164500] and *UZ Flow Models and Submodels* (BSC 2004 [DIRS 169861]) as a model whose parameters are quite uncertain, and potentially this uncertainty may significantly influence UZ performance predictions. Therefore, it is important to demonstrate that the sensitivity explored in the process model work can be represented in the abstraction model. This

section examines the impact of the gamma parameter in the AFM on the results. This set of simulations is intended to confirm that the AFM formulation in FEHM yields results similar to that of the process model, and to extend those results by performing the same analysis for the DFM model for f/m interactions.

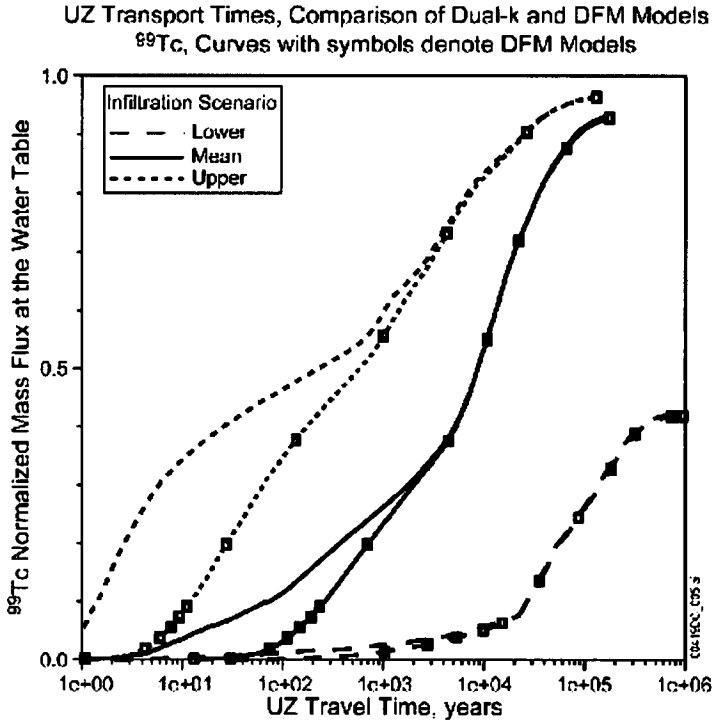

Output DTN: LA0311BR831371.002.

Figure 7-12. Breakthrough Curves for ^{99}Tc Using the UZ Transport Abstraction Model to Investigate the Role f/m Interaction Conceptual Model: Simulations for Different Present-Day Infiltration Rate Scenarios (Lower, Mean, and Upper), Representative Parameter Values, and Present-Day Water Table

Figure 7-13 illustrates the impact of lowering the gamma parameter in the same fashion as was done in *UZ Flow Models and Submodels* (BSC 2004 [DIRS 169861], Section 6.8.2). Note the close qualitative similarity of the simulation results with that of Figure 6.8-3 of that report. Lowering the gamma parameter in the TSw in the same manner as in *UZ Flow Models and Submodels* (BSC 2004 [DIRS 169861]) yields a trend toward longer arrival times for the earliest arriving solute. The curves converge at longer transport times. The fact that the lowering of gamma in additional units below the repository has no further effect indicates that the principle sensitivity is for the AFM parameters in the TSw. For the purposes of the abstraction model validation, this qualitative comparison to the results reported in *UZ Flow Models and Submodels* (BSC 2004 [DIRS 169861], Figure 6.8-3) provides strong evidence that the implementation in FEHM with respect to the AFM replicates the behavior of the process model.

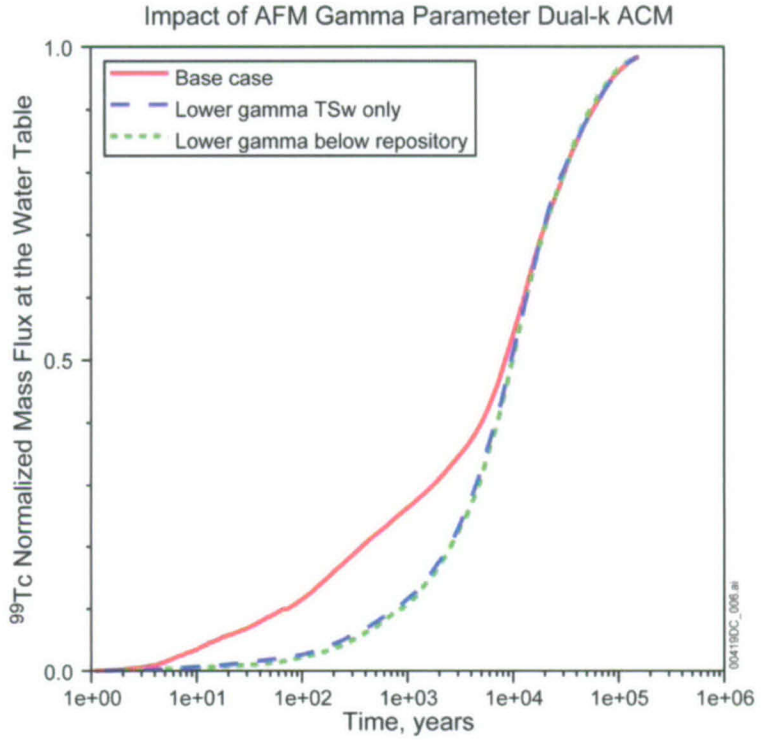

T2R3D Simulations: DTN: LB0307MR0060R1.007 [DIRS 164752].

Output DTN: LA0311BR831371.002.

NOTE: The colors, line types, and legend descriptors are chosen to facilitate a direct visual comparison to the simulation results presented in BSC 2004 [DIRS 169861], Figure 6.8-3.

Figure 7-13. Breakthrough Curves for Conservative Solute Using the UZ Transport Abstraction Model to Investigate the Role of AFM Parameter Gamma: Dual-k ACM, Simulation for Different Values of Gamma in Rock Units Beneath the Repository, Present-Day Mean Infiltration, Representative Parameter Values, and Present-Day Water Table

Finally, Figure 7-14 shows a similar investigation of the role of AFM model parameters for the DFM conceptualization. Note that in comparison to the dual-k DFM, gamma has smaller influence on the transport behavior. This result is a consequence of the way in which the two ACMs simulate the early-time behavior of the breakthrough curves. When a more refined grid is used to resolve gradients in the matrix, the role of flowing fracture spacing and interface area is less important than for the case in which a single matrix grid block is used to represent diffusion. The implication of this conclusion is that AFM model parameters will have a relatively smaller influence on predicted UZ behavior for the DFM conceptualization. By contrast, a larger sensitivity to AFM gamma parameter is predicted for the dual-k conceptual model. These differences must be recognized when interpreting sensitivity studies involving the AFM and the f/m interaction models. In general, the diffusion coefficient itself, rather than the AFM model parameters, is a much more sensitive parameter controlling the UZ performance.

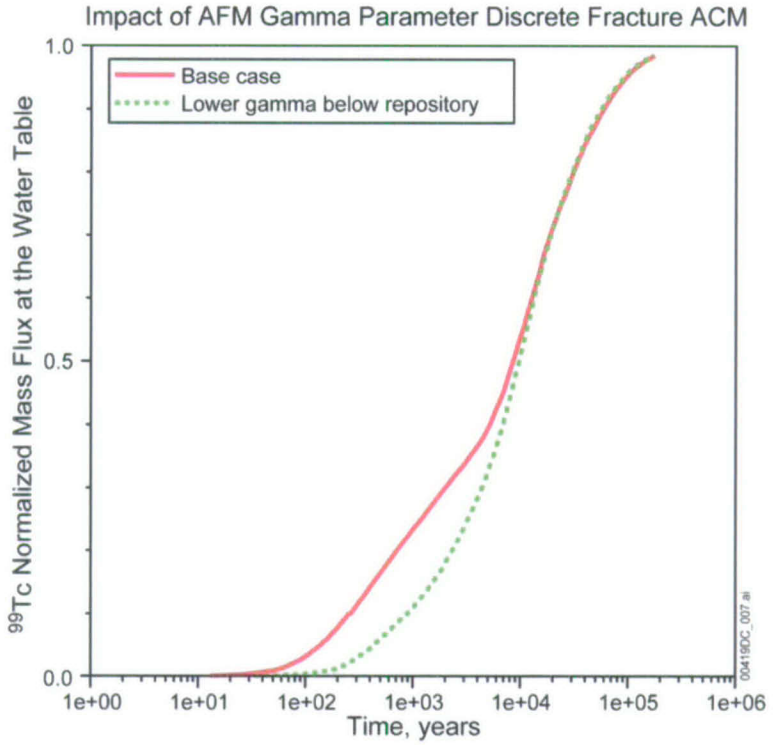

Output DTN: LA0311BR831371.002.

NOTE: The colors, line types, and legend descriptors are chosen to facilitate a direct visual comparison to the simulation results presented in BSC 2004 [DIRS 169861], Figure 6.8-3.

Figure 7-14. Breakthrough Curves for Conservative Solute Using the UZ Transport Abstraction Model to Investigate the Role of AFM Parameter Gamma: Discrete Fracture ACM, Simulation for Different Values of Gamma in Rock Units Beneath the Repository, Present-Day Mean Infiltration, Representative Parameter Values, and Present-Day Water Table

7.3 SUMMARY OF VALIDATION ACTIVITIES

As outlined in Section 7, the intended use of the radionuclide transport abstraction model calls for Level II validation activities that demonstrate that the basic physical principles are appropriately represented in the model and that a single post-development model validation method is implemented. In this case, the post-development model validation method used is corroboration with alternative mathematical models. Confidence building during model development is described in Section 7.1. Postdevelopment activities are discussed in Section 7.2 and summarized below. Postdevelopment model validation was conducted through a series of model comparison studies. Comparisons were made with a discrete fracture model, a dual-k and MINC model formulations on a two-dimensional, site-scale cross-sectional model, and a dual-k model for the three-dimensional site-scale model domain.

The series of simulations presented in this section, along with additional simulations performed to test the performance of the model in *Validation Test Plan (VTP) for the FEHM Application Version 2.21* (LANL 2003 [DIRS 166306]), provide assurance that the UZ transport system is adequately captured in the abstraction model that is the subject of this report. Direct numerical comparisons with quantitative criteria would be inappropriate for these comparisons because the

modeling approach is designed to capture the essential features of the transport behavior over an extremely broad range of conditions (flow rates, transport parameters, relative flow rates in the two media, and the conceptual model for f/m interactions). Furthermore, analytical solutions do not exist to perform the comparisons made in this study, so the issue of whether the model is "correct" is not answerable by simply comparing to another code. Rather, the sort of benchmarking performed in this section is designed to build confidence in the adequacy of the abstraction model through a series of comparisons designed to probe the key features of the model that will be exercised during its use in TSPA simulations. In addition to the lack of exact solutions to use as absolute benchmarks, there is no unique way to establish a suitable quantitative criterion that is guaranteed to be appropriate. The complete problem involves nine distinct flow fields and numerous different radioelements (some with chain decay) and two different colloid types. Releases can occur at different points in time relative to the sequence of climate changes. These complexities lead to the use of qualitative comparisons.

Adequate visual comparisons for benchmarking against the DFM simulations illustrate that the algorithms have been implemented to handle upscaling of dual-k transport processes, for low or high diffusion, sorbing or nonsorbing solutes, and fracture or matrix releases. Discrepancies between the particle tracking and DFMs, though relatively small, were noted and additional investigations were conducted to explain and assess the differences. In this way, the robustness of the model was demonstrated. Therefore, these results show that TSPA simulations using the UZ transport abstraction model will be able to propagate uncertainties in the form of parameter distributions through the UZ portion of the TSPA-LA model. After testing the model in a simple particle tracking setup, the complexities of the system were studied in two and three dimensions through comparisons to the T2R3D based process model. These results are also adequate. Good agreement was observed at a variety of infiltration scenarios and diffusion models and parameters. Where differences were uncovered, the FEHM model results yielded earlier breakthrough at the water table than did the process model. The likely impact of this factor in TSPA analyses is small, given that these breakthroughs are at short travel times, which in any event connote a bypassing of the UZ by radionuclides. The exact timing of this breakthrough is relatively unimportant since the differences are within the first 1 year to 100 years of transport.

Note that this validation runs also imply that the model can be used to simulate UZ radionuclide transport behavior under the disruptive event scenarios. These scenarios principally impact the source term, rather than the behavior of the UZ as a transport barrier, so the use of the model under these scenarios is justified.

With regard to the use of this model under a scenario of igneous activity disrupting the UZ flow and transport system, this issue has been treated in *Features, Events, and Processes in UZ Flow and Transport* (BSC 2005 [DIRS 174191]). The impact on the rock properties was excluded on the basis of a low-consequence argument. In essence, the spatial area associated with changes to the rock properties was deemed to be too small to have a significant impact on the rock properties (BSC 2005 [DIRS 174191], Section 6.8.2). By a similar argument, the hydrologic response to igneous activity was determined to be of small spatial extent (BSC 2005 [DIRS 174191], Section 6.8.4), and hence was excluded on the same basis.

In addition, the abstraction model is set up to enable ACMs for f/m interaction through the use of a different set of transfer function curves. For the TSPA-LA model, the dual-k formulation

should be chosen because it was shown in Section 7.2.3.2 (Figure 7-10) to be conservative with respect to the first arrival times at the water table. Finally, the implementation of the AFM in the abstraction model was shown to reproduce the qualitative features of the breakthrough curves documented in the process model reports on which this abstraction is based. In summary, the abstraction model has been compared in the full complexity of the UZ model, and found to be able to represent the system robustly and efficiently for the entire range of parameters and conceptual models required. Therefore, the UZ transport abstraction model is suitable for use in TSPA analyses.

8. CONCLUSIONS

8.1 SUMMARY OF MODELING ACTIVITY

The principal output from this report is an abstraction model for radionuclide transport in the UZ. It is intended for this model to be used directly in the TSPA-LA system model. The code used to implement the model is FEHM V2.23 (LANL 2005 [DIRS 174121]), in the form of a dll callable from GoldSim. Testing of the operation of the dll in a GoldSim model environment has been developed and tested elsewhere (LANL 2003 [DIRS 166306]) and is not repeated here, except to discuss the data structure of the interface between GoldSim and the FEHM dll.

This report pulls together information and data from a variety of sources, creating a simulation model capable of efficiently computing the transport of multiple radionuclides through the UZ. Data sources are listed in Section 4.1, assumptions are discussed in detail in Section 5, and the mathematical formulation and assessment of parameter ranges and distributions are treated in Section 6. The main activity documented in this report is the synthesis of data and models into a simulation tool. The model to be used in TSPA simulations consists of a code (FEHM V2.23 or higher, PC dll) and input files to the code that must be present to run the model within GoldSim. Table 8-2 lists the computer files required to run the base-case model, and a brief description of the purpose of each file. Fixed parameters have been inserted into the appropriate FEHM files. Parameter distributions given in Section 6.5 should be used to generate a table of parameters in a text file, which is read using FEHM's capability of reading in parameters from a separate file and inserting those parameters into the simulation at runtime (see the User Documentation for FEHM V2.21 or higher for details). Thus, this set of files provides the template for the TSPA-LA modelers to set up the UZ transport abstraction model in a multiple-realization GoldSim system model. The table of uncertain parameters itself is not generated in this report: this needs to be done by TSPA system modelers to facilitate parameter correlations and to enable the exploration of parameter sensitivities to be studied systematically at the system level. Table 8-1 lists the UZ transport parameters, which should be presampled and assembled into a table and for FEHM to read at run time in TSPA.

In Section 6.9, several minor issues were discussed that result in either small errors or slight mismatches between the model results presented here and the results that are obtained in the TSPA model. These issues fall into two categories: code issues and input issues. The code issues are known bugs and/or nonoptimal implementations in FEHM V2.23 (LANL 2005 [DIRS 174121]). These issues have been shown to have minimal impact on either the results of this report or the TSPA model (SPR001420050614, BSC 2005 [DIRS 174746]). The input issues are slight discrepancies between the model inputs in this report versus the TSPA abstraction model for reversible and irreversible colloidal species. These issues were shown in Section 6.9.2 to have minimal impact. Therefore, correction of these input issues in the TSPA model can be deferred with negligible consequence to the results.

8.2 MODEL OUTPUTS

8.2.1 Developed Output

Many of the model outputs (FEHM input files to be used by TSPA system modelers) are derived from results of process models or other studies. For a discussion of the uncertainties of those parameters, the reader is referred to the references cited in Table 8-1. Data required to generate the uncertain parameters for TSPA calculations are found in output DTN: MO0506SPAROCKU.000). For those outputs in Table 8-2 listed as being developed in this report, the development of the parameter values is discussed in this report (provided in output DTNs: LA0506BR831371.001 and LA0311BR831229.001). Output DTN: LA0506BR831371.001 is an update to DTN: LA0407BR831371.001 to correct FEHM model parameters so results are consistent with the TSPA model. This update is required so results can be compared directly with the new sensitivity analysis as presented in this document and provided in output DTNs: LA0506BR831371.002 (simulations varying hydrologic properties) and LA0506BR831371.003 (simulations varying gamma in the AFM). Validation simulations are unchanged and are provided in output DTNs: LA0311BR831371.001 (discrete fracture comparison) and LA0311BR831371.002 (T2R3D comparisons). FEHM particle-tracking input files associated with the TSPA-LA uncertainty simulations can be found in DTN: LA0506BR831371.001 along with other associated model grid, zone, and transfer function files.

Table 8-2 shows the two primary output DTNs needed to run the base-case model simulations. The output DTN: LA0311BR831229.001 contains the transfer function curves used in this model, and DTN: LA0506BR831371.001 contains all the files needed to run the model, including files extracted from other sources and files developed in this report.. In addition to the files listed in the table, there may be auxiliary files that the TSPA-LA modeling group must develop and document to complete the process of incorporating the UZ transport abstraction model into GoldSim (BSC 2003 [DIRS 161572]). These files, which are the responsibility of the TSPA-LA modeling group to create, may include files such as batch files to copy files at runtime from one filename to another. They will implement features that are documented in FEHM V2.21 and higher, and are discussed in the code user manual (Zyvoloski et al. 1997 [DIRS 100615]). They will contain no data, so are not required to be documented in this report.

Table 8-1. List of Uncertain Parameters to be Sampled in the TSPA-LA Runs

Uncertain Parameters	Description
Matrix Sorption Coefficient (mL/g)	Matrix sorption coefficient will be presampled based on given distributions for dissolved species in Table 6-7.
Matrix Diffusion Coefficient (m^2/sec)	Matrix water content and effective permeability will first be sampled based on given distribution in Table 6-8. Then, the sampled water content and effective permeability are used in Equation 6.19 for estimating matrix diffusion coefficients.
Fracture Porosity, Fracture Frequency, and Fracture Aperture (m)	Fracture porosity and fracture frequency are sampled based on the distributions presented in Table 6-15, and fracture aperture is derived from these sampled values using Equation 6-26.

Table 8-1. List of Uncertain Parameters to be Sampled in the TSPA-LA Runs

Uncertain Parameters	Description
Colloid K_c	Colloid concentration and colloid K_d are sampled based on given distribution in Tables 6-21 and 6-22. The sampled colloid concentration and K_d are then used in Equation 6-27 for calculating colloid K_c.
Colloid R_{coll}	Colloid R_{coll} is sampled based on given distribution in Table 6-24.

NOTE: Data required to generate the uncertain parameters described in this table are found in output DTN: MO0506SPAROCKU.000.

Table 8-2. Computer Files Necessary to Run the Base-Case UZ Transport Abstraction Model

Computer Files Comprising the UZ Transport Process Model	Qualitative Description and Intended Use	Source Data Tracking Number	Product Output DTN
Files Developed in Other Studies That Feed This Abstraction Model			
fehmn.grid *fehmn.stor*	Numerical model grid files required for UZ transport abstraction model.	LB0305TSPA18FF.001 [DIRS 165625]	N/A
fehmn.zone *fehmn.zone2*	File that indexes each grid node number to a hydrologic zone. Input zone list file for UZ transport abstraction model. *fehmn.zone2* also contains repository zones.	LB0305TSPA18FF.001 [DIRS 165625]	N/A
preqla.ini *preqma.ini* *prequa.ini* *glaqla.ini* *glaqma.ini* *glaqua.ini* *monla.ini* *monma.ini* *monua.ini* *glaqlA_wtrise.ini* *glaqmA_wtrise.ini* *glaquA_wtrise.ini* *monlA_wtrise.ini* *monmA_wtrise.ini* *monuA_wtrise.ini*	Steady state flow fields used to set the fluid flow rates in the UZ transport abstraction model.	LB0305TSPA18FF.001 [DIRS 165625] LB0312TSPA06FF.001 [DIRS 166671]	N/A

Table 8-2. Computer Files Necessary to Run the Base-Case UZ Transport Abstraction Model (Continued)

Computer Files Comprising the UZ Transport Process Model	Qualitative Description and Intended Use	Source Data Tracking Number	Product Output DTN
Files Developed in This Report			
fehm_amr_base.rock	Rock properties for all zones defined in *fehm.zone* – bulk rock density, heat capacity (placeholder, not used in the model), and porosity. File is part of the UZ transport process model.	LB0210THRMLPRP.001 [DIRS 160799]	LA0506BR831371.001
fehm_amr_base.dpdp	Dual permeability model parameters – fracture volume fraction, characteristic distance into the matrix between fractures. File is part of the UZ transport process model.	LB0205REVUZPRP.001 [DIRS 159525] LB0207REVUZPRP.001 [DIRS 159526]	LA0506BR831371.001
fehm_amr_base.mptr. *fehm_amr_base_low.mptr.* *fehm_amr_base_med.mptr.* *fehm_amr_base_high.mptr.*	All solute transport parameters for the multiple radionuclide simulations. File is part of the UZ transport process model.	LA0408AM831341.001 [DIRS 171584] LB0302UZDSCPUI.002 [DIRS 161787] LB0208UZDSCPMI.002 [DIRS 161243] LB0208UZDSCPLI.002 [DIRS 161788] LB0305TSPA18FF.001 [DIRS 165625] LL000122051021.116 [DIRS 142973] SN0306T0504103.005 [DIRS 164132] SN0306T0504103.006 [DIRS 164131] LA0303HV831352.002 [DIRS 163558] LB03023DSSCP9I.001 [DIRS 163044] LB0207REVUZPRP.002 [DIRS 159672] LA0003MCG12213.002 [DIRS 147285] LA0303PR831231.005 [DIRS 166259]	LA0506BR831371.001
repo.zon.xls	Zone lists containing node numbers of repository nodes in each infiltration bin. Used in UZ transport abstraction model as part of radionuclide release model in GoldSim (BSC 2003 [DIRS 161572]) system model.	LL030610323122.029 [DIRS 164513]	LA0506BR831371.001
wt.zone	Zone lists containing node numbers of grid nodes in each collection node at the water table.	LB03023DSSCP9I.001 [DIRS 163044]	LA0506BR831371.001

Table 8-2. Computer Files Necessary to Run the Base-Case UZ Transport Abstraction Model (Continued)

Computer Files Comprising the UZ Transport Process Model	Qualitative Description and Intended Use	Source Data Tracking Number	Product Output DTN
fehm_la.zone2	Zone files containing node numbers in different rock layers and the repository and water table collection bins from repo.zone.xls and wt.zone.	LB0305TSPA18FF.001 [DIRS 165625] repo.zone.xls and wt.zone	LA0506BR831371.001
fracture_pf.doc	File contains developed fracture porosity and frequency distribution data to be used in LA.	LB0205REVUZPRP.001 [DIRS 159525] LB0207REVUZPRP.001 [DIRS 159526]	LA0506BR831371.001
matrix_ekwc.doc	Matrix water content and effective permeability distributions developed for estimating matrix diffusion coefficient.	LB03023DSSCP9I.001 [DIRS 163044] LB0207REVUZPRP.002 [DIRS 159672]	LA0506BR831371.001
uz_tfcurves_nn_3960.in *uz_tfcurves_dualk_nn_3960.in*	Transfer function curves for implementing the RTTF particle-tracking model for upscaling of fracture-matrix interaction process.	N/A, developed output	LA0311BR831229.001
fehm_amr_base.dat, itfc_bf2.txt, itfc_bf3.txt, itfc_ch1.txt, itfc_ch6.txt, itfc_chv.txt, itfc_chz.txt, itfc_pp1.txt, itfc_pp2.txt, itfc_pp3.txt, itfc_pp4.txt, itfc_tsw4.txt, itfc_tsw5.txt, itfc_tsw6.txt, itfc_tsw7.txt, itfc_tsw8.txt, itfc_tsw9.txt	All control parameters for the FEHM simulation. Used as main input file for UZ transport process model.	LA0003MCG12213.002 [DIRS 147285]	LA0506BR831371.001

DTN = data tracking number; FEHM = finite element heat and mass (model); LA = license application; RTTF = residence time transfer function; UZ = unsaturated zone

8.2.2 Output Uncertainty

The calculation of UZ transport uncertainties in the TSPA-LA model will be performed and documented in the TSPA-LA model report because the radionuclide source term is computed using the system model, of which the UZ transport abstraction model is a part. The goal of the present model report is to ensure that a computational tool is set up for TSPA to perform the simulation modeling, and that the uncertainties of parameters in the abstraction model are fully justified and documented. In addition, basic flow and transport parameter and conceptual model uncertainties are explored to assess the sensitivity to these uncertainties. All of these goals have been accomplished, in that the software and computer files needed to perform the modeling have

been completed and sensitivities have been presented. Therefore, parameter and conceptual uncertainties in the UZ transport can be propagated through the TSPA-LA model.

The uncertainties associated with transport in the UZ have been documented in the model report for UZ transport (BSC 2004 [DIRS 164500]), and have been expanded upon in the present model report. Of note is the fact that both parameter and conceptual model uncertainty have been shown to be incorporated into this abstraction, and sensitivities have been explored. The key ACMs discussed in *Radionuclide Transport Models Under Ambient Conditions* (BSC 2004 [DIRS 164500]) and Section 6.7 of this report relate to the treatment of fracture-matrix interactions. Model validation simulations presented in Section 7 suggest strongly that the particle tracking formulation in the abstraction model developed in FEHM replicates the behavior of the process model, and does so in a computationally efficient manner. In addition, simulations using transfer function curves implemented with a dual-k or DFM conceptual model for f/m interactions were shown to yield reasonable results. Thus, both f/m interaction models could conceivably be investigated in TSPA simulations. However, due to the fact that process model validation activities were performed based on a dual-k model, the dual-k transfer functions (file *uz_tfcurves_dualk_nn_3960.in*) should be used in TSPA analyses. The transfer functions based on the DFM conceptual model (file *uz_tfcurves_nn_3960.in*), are provided because the DFM was required to test the implementation of the particle-tracking model through comparison to other numerical models. The DFM representation, though perhaps a more physically realistic scenario for diffusion between the media, should only be used for code validation or sensitivity analyses unless a parallel validation effort of the process model using a DFM formulation is successfully carried out in the future.

Parameter uncertainties leading to different flow model results were examined, and in most instances the sensitivity to these uncertainties was found to range from very small to moderate. Sensitivities to parameters related to the diffusive flux between the fractures and matrix were shown to be larger, but the largest impact is in the choice of the conceptual model describing this diffusive flux.

8.3 HOW THE APPLICABLE ACCEPTANCE CRITERIA ARE ADDRESSED

The pertinent requirements and acceptance criteria for this report are identified in Section 2.2.1.3.7.3 of the *Yucca Mountain Review Plan, Final Report* (NRC 2003 [DIRS 163274]). This section describes how the applicable acceptance criteria identified in Section 4.2 have been addressed in this report. In most cases, the applicable acceptance criteria are not addressed solely by this report; rather, the acceptance criteria are fully addressed when this report is considered in conjunction with other analysis and model reports that describe radionuclide transport in the unsaturated zone. Where a subcriterion includes several components, only some of those components may be addressed. How these components are addressed is summarized below.

Acceptance Criterion 1: System Description and Model Integration Are Adequate.

(1) Total system performance assessment adequately incorporates important design features, physical phenomena, and couplings, and uses consistent and appropriate

assumptions throughout the radionuclide transport in the unsaturated zone abstraction process;

Adequacy of the incorporation of important features and phenomena in the TSPA-LA and of the technical bases for their descriptions is demonstrated by the scope and discussion of the issues addressed. Section 6.4 describes the construction of the UZ transport abstraction model, including the model formulation (Section 6.4.1); physical phenomena such as dispersion (6.4.2), sorption and matrix diffusion (Section 6.4.3); decay/ingrowth (Section 6.4.4); and radionuclide transport via colloids (Section 6.4.5). Consistent and appropriate assumptions are used throughout the abstraction process as illustrated by incorporation of the following factors: UZ radionuclide transport is controlled by UZ flow, which is integrated into the UZ transport abstraction model through the use of steady state flow fields (Section 6.5.1); long-term transients caused by climate change are also incorporated (Section 6.4.8), as are the impacts of water table rise (Section 6.4.8). This report also describes the coupling of the UZ transport abstraction model to the EBS release model (Section 6.4.7) and the SZ transport abstraction model (Section 6.5.16).

(2) The description of the aspects of hydrology, geology, geochemistry, design features, physical phenomena, and couplings that may affect radionuclide transport in the unsaturated zone is adequate. For example, the description includes changes in transport properties in the unsaturated zone, from water-rock interaction. Conditions and assumptions in the total system performance assessment abstraction of radionuclide transport in the unsaturated zone are readily identified, and consistent with the body of data presented in the description;

Adequacy of the description of important features that may affect radionuclide transport in the unsaturated zone is demonstrated by the discussion of the issues addressed, as enumerated above. Assumptions specific to the UZ transport abstraction model are listed in Section 5. In addition, the UZ transport abstraction model incorporates many assumptions and conditions from the coupling to the site-scale UZ flow model. For example, the use of pre-generated steady state flow fields from the site-scale UZ flow model implies that the same hydrogeologic features developed in the flow modeling effort (BSC 2004 [DIRS 169861]) are automatically built into the UZ transport abstraction model. Hydrogeologic features and layering, fluid flow rates and their uncertainties, the role of fractures, and the large-scale flow patterns though the UZ are therefore included in the TSPA-LA abstraction and are consistent with those developed in the flow model.

(3) The abstraction of radionuclide transport in the unsaturated zone uses assumptions, technical bases, data, and models that are appropriate and consistent with other related U.S. Department of Energy abstractions. For example, assumptions used for radionuclide transport in the unsaturated zone are consistent with the abstractions of radionuclide release rates and solubility limits and flow paths in the unsaturated zone (Sections 2.2.1.3.4 and 2.2.1.3.6 of the Yucca Mountain Review Plan, respectively). The descriptions and technical bases provide transparent and traceable support for the abstraction of radionuclide transport in the unsaturated zone;

The basic model formulation employed in the UZ transport abstraction model is consistent with those of other components of the TSPA-LA model. Radionuclide releases from the EBS are treated as aqueous and colloidal species. The UZ transport abstraction model tracks these species through the UZ model as aqueous and colloidal species using consistent assumptions regarding their mobility. This is evidenced by the consistent treatment used to estimate sorption coefficients (Section 6.5.4) in the UZ and SZ transport abstraction models and the consistent treatment of colloid properties in the EBS, UZ, and SZ models (Sections 6.5.12 and 6.5.13). The UZ and SZ transport abstraction models also adopt similar transport mechanisms where applicable: fracture flow and matrix diffusion are treated in a similar fashion in the two models. Thus, the descriptions and technical bases provide transparent and traceable support for the abstraction of radionuclide transport in the unsaturated zone.

(4) Boundary and initial conditions used in the abstraction of radionuclide transport in the unsaturated zone are propagated throughout its abstraction approaches. For example, the conditions and assumptions used to generate transport parameter values are consistent with other geological, hydrological, and geochemical conditions in the total system performance assessment.

Boundary conditions in terms of the extent of the model domain in three-dimensional space is the same as that of the site-scale UZ flow model (see Section 6.5). Regarding the consistency of the UZ transport abstraction model with the site-scale UZ flow model, this occurs automatically by directly incorporating flow model results into the UZ transport abstraction model. In addition, the release of radionuclides to the UZ model is controlled, in part, by the local infiltration patterns across the repository. The spatial dependence of these releases is included in a consistent fashion in the UZ transport abstraction model by using "bins" of similar infiltration rates in the EBS and UZ transport abstraction models (Section 6.5.15).

(5) Sufficient data and technical bases for the inclusion of features, events, and processes related to radionuclide transport in the unsaturated zone in the total system performance assessment abstraction are provided;

Features, events, and processes included in the UZ transport abstraction model are discussed in Section 6.2 of this report.

(6) Guidance in NUREG–1297 and NUREG–1298 (Altman et al. 1988 [DIRS 103597]; Altman et al. 1988 [DIRS 103750]), or other acceptable approaches, is followed for peer review and data qualification.

All input data have been used in accordance with applicable quality assurance procedures developed consistently with the *Quality Assurance Requirements and Description*, which commits to these NUREGs.

Acceptance Criterion 2: Data Are Sufficient for Model Justification.

(1) Geological, hydrological, and geochemical values used in the license application are adequately justified (e.g., flow-path length, sorption coefficients, retardation factors,

colloid concentrations, etc.). Adequate descriptions of how the data were used, interpreted, and appropriately synthesized into the parameters are provided;

Section 6.5 of this model report provides a detailed discussion of the underlying data used to develop parameter uncertainty ranges for all transport parameters. Data uncertainties also are addressed. The sufficiency of the data to support the models is demonstrated by the scope of issues addressed: dispersivity in Section 6.5.2, matrix porosity and rock density in Section 6.5.3, matrix sorption in Section 6.5.4, matrix diffusion in Section 6.5.5, fracture residual saturation and active fracture model gamma parameters in Section 6.5.6, fracture porosity, fracture spacing and fracture aperture in Section 6.5.7, fracture surface retardation in Section 6.5.8, colloid filtration at matrix interface in Section 6.5.9, colloid size exclusion in Section 6.5.10, colloid size distribution in Section 6.5.11, colloid concentration and colloid equilibrium sorption in Section 6.5.12, fraction of colloids traveling unretarded and colloid retardation factor in Section 6.5.13, radionuclide half lives and daughter products in Section 6.5.14, repository radionuclide release bins in Section 6.5.15, and radionuclide collecting bins at UZ/SZ interface in Section 6.5.16. These sections also provide adequately transparent and traceable descriptions of how the data were used, interpreted, and appropriately synthesized in model parameters.

(2) Sufficient data have been collected on the characteristics of the natural system to establish initial and boundary conditions for the total system performance assessment abstraction of radionuclide transport in the unsaturated zone;

Because the UZ transport abstraction model incorporates the flow fields from the site-scale UZ flow model, initial and boundary conditions in three-dimensional space are the same as that of the site-scale UZ flow model (see Section 6.5). Those flow fields are based on sufficient data, including hydrogeologic layering, structural features, rock hydrologic properties, fluid saturations, flow velocities, extent of fracture flow, and large-scale flow patterns. Discussion of the underlying development of the data used to develop the basic characteristics of the natural system is presented in *UZ Flow Models and Submodels* (BSC 2004 [DIRS 169861]) and documents referred to therein.

(3) Data on the geology, hydrology, and geochemistry of the unsaturated zone, including the influence of structural features, fracture distributions, fracture properties, and stratigraphy, used in the total system performance assessment abstraction are based on appropriate techniques. These techniques may include laboratory experiments, site-specific field measurements, natural analogue research, and process-level modeling studies. As appropriate, sensitivity or uncertainty analyses used to support the U.S. Department of Energy total system performance assessment abstraction are adequate to determine the possible need for additional data.

As discussed above, because the UZ transport abstraction model incorporates the flow fields from the site-scale UZ flow model, data on geology, hydrology, and geochemistry of the unsaturated zone, including the influence of structural features, fracture distributions, fracture properties, and stratigraphy, used in the total system performance assessment abstraction are based on appropriate techniques.

Acceptance Criterion 3: Data Uncertainty Is Characterized and Propagated Through the Model Abstraction.

(1) Models use parameter values, assumed ranges, probability distributions, and bounding assumptions that are technically defensible, reasonably account for uncertainties and variabilities, and do not result in an under-representation of the risk estimate;

Section 6.5 of this model report provides a detailed discussion of the development of parameter values, uncertainty ranges, probability distributions, and, where applicable, bounding assumptions, showing that they are technically defensible, reasonably account for uncertainties and variabilities, and do not result in an under-representation of the risk estimate for all transport parameters.Analyses presented in Section 6.6.3 and 6.6.4 illustrate the impact of various flow and transport parameter uncertainties on the breakthrough curves for transport through the UZ model domain.

(2) For those radionuclides where the total system performance assessment abstraction indicates that transport in fractures and matrix in the unsaturated zone is important to waste isolation: (i) estimated flow and transport parameters are appropriate and valid, based on techniques that may include laboratory experiments, field measurements, natural analogue research, and process-level modeling studies conducted under conditions relevant to the unsaturated zone at Yucca Mountain; and (ii) models are demonstrated to adequately reproduce field transport test results. For example, if a sorption coefficient approach is used, the assumptions implicit in that approach are verified;

The techniques used to estimate flow and transport parameters were conducted under conditions relevant to the unsaturated zone at Yucca Mountain, as described in Section 6.5. The method used to validate the UZ transport abstraction model is to benchmark its predictions against the validated UZ transport process model as presented in *Radionuclide Transport Models Under Ambient Conditions* (BSC 2004 [DIRS 164500]). The series of simulations presented in Section 7, along with additional simulations performed to test the performance of the model in the FEHM verification and validation documentation, provide assurance that the UZ transport system is adequately captured in the abstraction model that is the subject of this report. Three classes of comparisons of increasing complexity were made. The least complex showed the validity of the particle tracking method by a comparison with a discrete fracture model in Section 7.2.1. These comparisons tested advective transport between continua (Section 7.2.1.1), diffusion for fracture-dominated flow (Section 7.2.1.2), and diffusion and sorption in the intermediate flow case (Section 7.2.1.3). A more complex comparison between the particle-tracking model and simulations in a two-dimensional cross sectional model in section 7.2.2 showed the ability of the model to replicate the behavior of the comparable process models. This included use of the dual-k and MINC model formulations. Finally, the full complexity of the full three-dimensional UZ transport abstraction model used in TSPA-LA was compared to the abstraction model in Section 7.2.3 and the quality of the agreement is discussed in Section 7.2.3.1. The conclusion that the abstraction

model robustly and efficiently represents the system over the entire range of parameters is explained in Section 7.3.

(4) Uncertainty is adequately represented in parameter development for conceptual models, process-level models, and alternative conceptual models considered in developing the abstraction of radionuclide transport in the unsaturated zone. This may be done either through sensitivity analyses or use of conservative limits;

In the UZ transport abstraction model, uncertainties are represented as uncertain transport parameters (Section 6.5), as well as the use of different steady state flow fields to capture uncertainty in the flow conditions. In a few cases, such as the assumption that there is no sorption onto fracture walls, approaches that are clearly conservative were adopted to treat a process for which insufficient data exists to establish parameter uncertainty ranges (Section 6.5.8). For other flow and transport parameters, sensitivity analyses were conducted to explore the impact of these uncertainties on model results (Section 6.6.3 and 6.6.4). Finally, the impact of conceptual model uncertainty for the diffusion of radionuclides between the fractures and matrix is examined in Section 6.7.

Acceptance Criterion 4: Model Uncertainty Is Characterized and Propagated Through the Model Abstraction.

(1) Alternative modeling approaches of features, events, and processes are considered and are consistent with available data and current scientific understanding, and the results and limitations are appropriately considered in the abstraction;

Most instances of alternative conceptual models of UZ transport have been examined at the process model stage as presented in *Radionuclide Transport Models Under Ambient Conditions* (BSC 2004 [DIRS 164500]) and have not been carried forth into this abstraction model. An exception is the fracture/matrix interaction model, which has been shown to be consistent with site conditions, as discussed in Section 6.4.3.

(2) Conceptual model uncertainties are adequately defined and documented, and effects on conclusions regarding performance are properly assessed;

Uncertainties in alternative models for fracture/matrix interaction are defined, documented and assessed in Section 6.7 and 7.2.3.2.

(3) Consideration of conceptual model uncertainty is consistent with available site characterization data, laboratory experiments, field measurements, natural analogue information and process-level modeling studies; the treatment of conceptual mode uncertainty does not result in an under-representation of the risk estimate;

The UZ transport process model presented in *Radionuclide Transport Models Under Ambient Conditions* (BSC 2004 [DIRS 164500]) contains a discussion of conceptual model uncertainty as it relates to characterization data, laboratory experiments, and field measurements. This abstraction model report implements the key conceptual

model components developed in *Radionuclide Transport Models Under Ambient Conditions* (BSC 2004 [DIRS 164500]).

(4) Appropriate alternative modeling approaches are consistent with available data and current scientific knowledge, and appropriately consider their results and limitations, using tests and analyses that are sensitive to the processes modeled. For example, for radionuclide transport through fractures, the U.S. Department of Energy adequately considers alternative modeling approaches to develop its understanding of fracture distributions and ranges of fracture flow and transport properties in the unsaturated zone.

The UZ transport process model presented in *Radionuclide Transport Models Under Ambient Conditions* (BSC 2004 [DIRS 164500]) contains a discussion of alternative modeling approaches for important model uncertainties in the areas of fracture flow and transport, colloid-facilitated transport, and sorption. This abstraction model report implements the key model assumptions and processes developed in *Radionuclide Transport Models Under Ambient Conditions* (BSC 2004 [DIRS 164500]). In addition, the impact of conceptual model uncertainty for the diffusion of radionuclides between the fractures and matrix is examined in Section 6.7 of this report.

Acceptance Criterion 5: Model Abstraction Output Is Supported by Objective Comparisons.

(1) The models implemented in this total system performance assessment abstraction provide results consistent with output from detailed process-level models and/or empirical observations (laboratory and field testing and/or natural analogues);

The direct comparisons to the UZ transport process model presented in Section 7 show that this total system performance assessment abstraction provide results consistent with output from detailed process-level models.

(2) Outputs of radionuclide transport in the unsaturated zone abstractions reasonably produce or bound the results of corresponding process-level models, empirical observations, or both. The U.S. Department of Energy abstracted models for radionuclide transport in the unsaturated zone are based on the same hydrological, geological, and geochemical assumptions and approximations, shown to be appropriate for closely analogous natural systems or experimental systems;

The satisfactory results of the direct comparisons to the UZ transport process model are presented in Section 7 as discussed above. The use of the same model grid, formulation, and steady state flow fields as the UZ transport process model ensures that this criterion is satisfied.

(3) Well-documented procedures that have been accepted by the scientific community to construct and test the mathematical and numerical models are used to simulate radionuclide transport through the unsaturated zone;

Several leading members of the scientific community, including personnel from the National Laboratories, have participated in the construction and testing of the mathematical and numerical models used to simulate radionuclide transport through the SZ. These scientists use methods based on their education and training. The procedures have been published in peer-reviewed journals and discussed at scientific meetings. Thus, the procedures are well-documented and have been accepted by the scientific community. Moreover, applicable quality assurance procedures and project guidance have been followed to test the UZ transport abstraction model. The process used in Section 7 to benchmark the model results against a similarly constructed numerical model that uses different numerical solution procedures is a scientifically valid, well accepted technique for assuring the correct functioning of the UZ transport abstraction model.

(4) Sensitivity analyses or bounding analyses are provided, to support the total system performance assessment abstraction of radionuclide transport in the unsaturated zone, that cover ranges consistent with site data, field or laboratory experiments and tests, and natural analogue research.

Model sensitivity to a variety of flow and transport parameters are included in this report: infiltration rate, flow conditions, and flow parameters (Sections 6.6.3 and 7.2.3.1); diffusion behavior (Sections 6.6.4, 7.2.1.2, and 7.2.3.2); fracture flow focusing parameters (Sections 6.6.4 and 7.2.3.3); and sorption coefficient (Section 7.2.1.3). A representative case that includes radionuclide species with a variety of transport parameters as well as both colloidal and aqueous species, is also presented (Section 6.6.2). These analyses support the determination that the model uses ranges consistent with available data.

INTENTIONALLY LEFT BLANK

9. INPUTS AND REFERENCES

The following is a list of the references cited in this document. Column 2 represents the unique six-digit numerical identifier (the Document Input Reference System [DIRS] number), which is placed in the text following the reference callout (e.g., BSC 2004 [DIRS 171282]). The purpose of these numbers is to assist the reader in locating a specific reference in the DIRS database. Within the reference list, multiple sources by the same author (e.g., BSC 2002) are sorted alphabetically by title.

9.1 DOCUMENTS CITED

Akindunni, F.F.; Gillham, R.W.; Conant, B.; and Franz, T. 1995. "Modeling of Contaminant Movement Near Pumping Wells: Saturated-Unsaturated Flow with Particle Tracking." Ground Water, 33, (2), 264-274. Worthington, Ohio: National Water Well Association. TIC: 226455. 101378

Altman, W.D.; Donnelly, J.P.; and Kennedy, J.E. 1988. Qualification of Existing Data for High-Level Nuclear Waste Repositories: Generic Technical Position. NUREG-1298. Washington, D.C.: U.S. Nuclear Regulatory Commission. TIC: 200652. 103750

Altman, W.D.; Donnelly, J.P.; and Kennedy, J.E. 1988. Peer Review for High-Level Nuclear Waste Repositories: Generic Technical Position. NUREG-1297. Washington, D.C.: U.S. Nuclear Regulatory Commission. TIC: 200651. 103597

BSC (Bechtel SAIC Company) 2002. Radionuclide Screening. ANL-WIS-MD-000006 REV 01. Las Vegas, Nevada: Bechtel SAIC Company. ACC: MOL.20020923.0177. 160059

BSC 2003. *Analysis of Hydrologic Properties Data.* MDL-NBS-HS-000014 REV 00. Las Vegas, Nevada: Bechtel SAIC Company. ACC: DOC.20030908.0001. 161773

BSC 2004. *Analysis of Hydrologic Properties Data.* ANL-NBS-HS-000042 REV 00. Las Vegas, Nevada: Bechtel SAIC Company. ACC: DOC.20041005.0004. 170038

BSC 2004. *Calibrated Properties Model.* MDL-NBS-HS-000003 REV 02. Las Vegas, Nevada: Bechtel SAIC Company. ACC: DOC.20041006.0004. 169857

BSC 2004. *Conceptual Model and Numerical Approaches for Unsaturated Zone Flow and Transport.* MDL-NBS-HS-000005 REV 01. Las Vegas, Nevada: Bechtel SAIC Company. ACC: DOC.20040922.0006. 170035

BSC 2004. *Drift-Scale Radionuclide Transport.* MDL-NBS-HS-000016 REV 01. Las Vegas, Nevada: Bechtel SAIC Company. ACC: DOC.20040927.0031. 170040

BSC 2004. *Future Climate Analysis.* ANL-NBS-GS-000008 REV 01. Las Vegas, Nevada: Bechtel SAIC Company. ACC: DOC.20040908.0005. 170002

BSC 2004. *Initial Radionuclide Inventories.* ANL-WIS-MD-000020 REV 01. Las Vegas, Nevada: Bechtel SAIC Company. ACC: DOC.20040921.0003. 170022

BSC 2004. *Radionuclide Transport Models Under Ambient Conditions.* MDL-NBS-HS-000008 REV 02. Las Vegas, Nevada: Bechtel SAIC Company. ACC: DOC.20041101.0002. 164500

BSC 2004. *Saturated Zone Colloid Transport.* ANL-NBS-HS-000031 REV 02. Las Vegas, Nevada: Bechtel SAIC Company. ACC: DOC.20041008.0007. 170006

BSC 2004. *Saturated Zone In-Situ Testing.* ANL-NBS-HS-000039 REV 01. Las Vegas, Nevada: Bechtel SAIC Company. ACC: DOC.20041115.0008. 170010

BSC 2004. *Saturated Zone Site-Scale Flow Model.* MDL-NBS-HS-000011 REV 02. Las Vegas, Nevada: Bechtel SAIC Company. ACC: DOC.20041122.0001. 170037

BSC 2004. *Technical Work Plan for: Unsaturated Zone Transport Model Report Integration.* TWP-MGR-HS-000002 REV 00 ICN 01. Las Vegas, Nevada: Bechtel SAIC Company. ACC: DOC.20040816.0001. 171282

BSC 2004. *Thermal Conductivity of the Potential Repository Horizon.* MDL-NBS-GS-000005 REV 01. Las Vegas, Nevada: Bechtel SAIC Company. ACC: DOC.20040928.0006. 169854

BSC 2004. *UZ Flow Models and Submodels.* MDL-NBS-HS-000006 REV 02. Las Vegas, Nevada: Bechtel SAIC Company. ACC: DOC.20041101.0004; DOC.20050629.0003. 169861

BSC 2005. *Features, Events, and Processes in UZ Flow and* Transport. ANL-NBS-MD-000001 REV 04. Las Vegas, Nevada: Bechtel SAIC Company. 174191

BSC 2005. *Drift-Scale Coupled Process (DST and TH Seepage) Models.* MDL-NBS-HS-000015 REV 02. Las Vegas, Nevada: Bechtel SAIC Company. ACC: DOC.20050114.0004. 172232

BSC 2005. *Mountain-Scale Coupled Processes (TH/THC/THM) Models.* MDL-NBS-HS-000007 REV 03. Las Vegas, Nevada: Bechtel SAIC Company. TBV 174101

BSC 2005. *Multiscale Thermohydrologic Model.* ANL-EBS-MD-000049 REV 03. Las Vegas, Nevada: Bechtel SAIC Company. ACC: DOC.20050711.0001. 173944

BSC 2005. *Parameter Sensitivity Analysis for Unsaturated Zone Flow.* ANL-NBS-HS-000049 REV 00. Las Vegas, Nevada: Bechtel SAIC Company. 174116

BSC 2005. *Q-List.* 000-30R-MGR0-00500-000-001. Las Vegas, Nevada: Bechtel SAIC Company. ACC: ENG.20050217.0010. 171190

BSC 2005. *Saturated Zone Flow and Transport Model Abstraction.* MDL-NBS-HS-000021 REV 03. Las Vegas, Nevada: Bechtel SAIC Company. 174012

BSC 2005. *SPR001420050614.* Software Problem Report. Las Vegas, NV: BSC Company. ACC: MOL.20050622.0042. 174746

BSC 2005. *Technical Work Plan for Unsaturated Zone Flow, Drift Seepage and Unsaturated Zone Transport Modeling.* TWP-MGR-HS-000004 REV 01. Las Vegas, Nevada: Bechtel SAIC Company. ACC: DOC.20050523.0003. 173951

BSC 2005. *Total System Performance Assessment Model/Analysis for the License Application.* MDL-WIS-PA-000004 REV 01. Las Vegas, Nevada: Bechtel SAIC Company. 174227

BSC 2005. *Waste Form and In-Drift Colloids-Associated Radionuclide Concentrations: Abstraction and Summary.* MDL-EBS-PA-000004 REV 02. Las Vegas, Nevada: Bechtel SAIC Company. 174290

Canori, G.F. and Leitner, M.M. 2003. *Project Requirements Document.* TER-MGR-MD-000001 REV 02. Las Vegas, Nevada: Bechtel SAIC Company. ACC: DOC.20031222.0006. 166275

Chiang, C.Y.; Wheeler, M.F.; and Bedient, P.D. 1989. "A Modified Method of Characteristics Technique and Mixed Finite Elements Method for Simulation of Groundwater Solute Transport." *Water Resources Research, 25,* (7), 1541-1549. Washington, D.C.: American Geophysical Union. TIC: 226452. 101384

Cordes, C. and Kinzelbach, W. 1992. "Continuous Groundwater Velocity Fields and Path Lines in Linear, Bilinear, and Trilinear Finite Elements." *Water Resources Research, 28,* (11), 2903-2911. Washington, D.C.: American Geophysical Union. TIC: 226449. 101385

CRWMS M&O 2001. *Colloid-Associated Radionuclide Concentration Limits: ANL.* ANL-EBS-MD-000020 REV 00 ICN 01. Las Vegas, Nevada: CRWMS M&O. ACC: MOL.20010216.0003. 154071

Czarnecki, J.B. 1984. *Simulated Effects of Increased Recharge on the Ground-Water Flow System of Yucca Mountain and Vicinity, Nevada-California.* Water-Resources Investigations Report 84-4344. Denver, Colorado: U.S. Geological Survey. ACC: HQS.19880517.1750. 101043

D'Agnese, F.A.; O'Brien, G.M.; Faunt, C.C.; and San Juan, C.A. 1999. *Simulated Effects of Climate Change on the Death Valley Regional Ground-Water Flow System, Nevada and California.* Water-Resources Investigations Report 98-4041. Denver, Colorado: U.S. Geological Survey. TIC: 243555. 120425

Desbarats, A.J. 1990. "Macrodispersion in Sand-Shale Sequences." *Water Resources Research, 26,* (1), 153-163. Washington, D.C.: American Geophysical Union. TIC: 236576. 101386

DOE (U.S. Department of Energy) 1998. *Overview - Viability Assessment of a Repository at Yucca Mountain.* DOE/RW-0508. Washington, D.C.: U.S. Department of Energy, Office of Civilian Radioactive Waste Management. ACC: MOL.19981007.0027. 100547

Fabriol, R.; Sauty, J.P.; and Ouzounian, G. 1993. "Coupling Geochemistry with a Particle Tracking Transport Model." *Journal of Contamination Hydrology, 13,* 117-129. New York, New York: Elsevier. TIC: 222395. 101387

Flint, L.E. 1998. *Characterization of Hydrogeologic Units Using Matrix Properties, Yucca Mountain, Nevada.* Water-Resources Investigations Report 97-4243. Denver, Colorado: U.S. Geological Survey. ACC: MOL.19980429.0512. 100033

Forester, R.M.; Bradbury, J.P.; Carter, C.; Elvidge-Tuma, A.B.; Hemphill, M.L.; Lundstrom, S.C.; Mahan, S.A.; Marshall, B.D.; Neymark, L.A.; Paces, J.B.; Sharpe, S.E.; Whelan, J.F.; and Wigand, P.E. 1999. *The Climatic and Hydrologic History of Southern Nevada During the Late Quaternary.* Open-File Report 98-635. Denver, Colorado: U.S. Geological Survey. TIC: 245717. 109425

Freeze, R.A. and Cherry, J.A. 1979. *Groundwater.* Englewood Cliffs, New Jersey: Prentice-Hall. TIC: 217571. 101173

Grathwohl, P. 2000. *Diffusion in Natural Porous Media: Contaminant Transport, Sorption/Desorption and Dissolution Kinetics.* Boston, Massachusetts: Kluwer Academic Publishers. TIC: 247983. 141512

Hogg, R.V. and Craig, A.T. 1978. *Introduction to Mathematical Statistics.* 4th Edition. New York, New York: Macmillan. TIC: 254311. 163236

Johnson, J.A.; Ravi, V.; and Rumery, J.K. 1994. "Estimation of Solute Concentrations Using the Pathline Counting Method." *Ground Water, 32,* (5), 719-726. Worthington, Ohio: National Water Well Association. TIC: 226453. 101400

Kinzelbach, W. 1988. *The Random Walk Method in Pollutant Transport Simulation.* Groundwater Flow and Quality Modelling. Pages 227-245. Norwell, Massachusetts: D. Reidel Publishing Company. TIC: 224064. 101402

LANL (Los Alamos National Laboratory) 2003. *Validation Test Plan (VTP) for the FEHM Application Version 2.21.* 10086-VTP-2.21-00. Los Alamos, New Mexico: Los Alamos National Laboratory. ACC: MOL.20031031.0264; MOL.20031031.0265. 166306

Latinopoulos, P. and Katsifarakis, K. 1991. "A Boundary Element and Particle Tracking Model for Advective Transport in Zoned Aquifers." *Journal of Hydrology, 124,* 159-176. Amsterdam, The Netherlands: Elsevier. TIC: 226466. 101408

Levy, S.S. 1991. "Mineralogic Alteration History and Paleohydrology at Yucca Mountain, Nevada." High Level Radioactive Waste Management, Proceedings of the Second Annual International Conference, Las Vegas, Nevada, April 28-May 3, 1991. 1, 477-485. La Grange Park, Illinois: American Nuclear Society. TIC: 204272. 100053

Liu, H.H.; Bodvarsson, G.S.; and Zhang, G. 2004. "Scale Dependency of the Effective Matrix Diffusion Coefficient." Vadose Zone Journal, 3, ([1]), 312-315. Madison, Wisconsin: Soil Science Society of America. TIC: 256150. 169948

Liu, H.H.; Doughty, C.; and Bodvarsson, G.S. 1998. "An Active Fracture Model for Unsaturated Flow and Transport in Fractured Rocks." Water Resources Research, 34, (10), 2633-2646. Washington, D.C.: American Geophysical Union. TIC: 243012. 105729

Lu, N. 1994. "A Semianalytical Method of Path Line Computation for Transient Finite-Difference Groundwater Flow Models." *Water Resources Research, 30,* (8), 2449-2459. Washington, D.C.: American Geophysical Union. TIC: 211997. 101413

Maloszewski, P. and Zuber, A. 1991. "Influence of Matrix Diffusion and Exchange Reactions on Radiocarbon Ages in Fissured Carbonate Aquifers." *Water Resources Research, 27,* (8), 1937-1945. Washington, D.C.: American Geophysical Union. TIC: 247494. 146957

Marshall, B.D.; Peterman, Z.E.; and Stuckless, J.S. 1993. "Strontium Isotopic Evidence for a Higher Water Table at Yucca Mountain." *High Level Radioactive Waste Management, Proceedings of the Fourth Annual International Conference, Las Vegas, Nevada, April 26-30, 1993. 2,* 1948-1952. La Grange Park, Illinois: American Nuclear Society. TIC: 208542. 101142

Neretnieks, I. 1980. "Diffusion in the Rock Matrix: An Important Factor in Radionuclide Retardation." *Journal of Geophysical Research, 85,* (B8), 4379-4397. Washington, D.C.: American Geophysical Union. TIC: 221345. 101148

Neuman, S.P. 1984. "Adaptive Eulerian-Lagrangian Finite Element Method for Advection-Dispersion." *International Journal for Numerical Methods in Engineering, 20,* 321-337. New York, New York: John Wiley & Sons. TIC: 226440. 101463

Neuman, S.P. 1990. "Universal Scaling of Hydraulic Conductivities and Dispersivities in Geologic Media." *Water Resources Research, 26,* (8), 1749-1758. Washington, D.C.: American Geophysical Union. TIC: 237977. 101464

NRC (U.S. Nuclear Regulatory Commission) 2003. *Yucca Mountain Review Plan, Final Report.* NUREG-1804, Rev. 2. Washington, D.C.: U.S. Nuclear Regulatory Commission, Office of Nuclear Material Safety and Safeguards. TIC: 254568. 163274

Parrington, J.R.; Knox, H.D.; Breneman, S.L.; Baum, E.M.; and Feiner, F. 1996. *Nuclides and Isotopes, Chart of the Nuclides.* 15th Edition. San Jose, California: General Electric Company and KAPL, Inc. TIC: 233705. 103896

Pollock, D.W. 1988. "Semianalytical Computation of Path Lines for Finite-Difference Models." *Ground Water, 26,* (6), 743-750. Worthington, Ohio: National Water Well Association. TIC: 226464. 101466

Reimus, P.W. 1995. *The Use of Synthetic Colloids in Tracer Transport Experiments in Saturated Rock Fractures.* Ph.D. dissertation. LA-13004-T. Los Alamos, New Mexico: Los Alamos National Laboratory. TIC: 240694. 101474

Reimus, P.W.; Adams, A.; Haga, M.J.; Humphrey, A.; Callahan, T.; Anghel, I.; and Counce, D. 1999. *Results and Interpretation of Hydraulic and Tracer Testing in the Prow Pass Tuff at the C-Holes.* Milestone SP32E7M4. Los Alamos, New Mexico: Los Alamos National Laboratory. TIC: 246377. 126243

Reimus, P.W.; Ware, S.D.; Benedict, F.C.; Warren, R.G.; Humphrey, A.; Adams, A.; Wilson, B.; and Gonzales, D. 2002. *Diffusive and Advective Transport of ^{3}H, ^{14}C, and ^{99}Tc in Saturated, Fractured Volcanic Rocks from Pahute Mesa, Nevada.* LA-13891-MS. Los Alamos, New Mexico: Los Alamos National Laboratory. TIC: 253905. 163008

Robinson, B.A. 1994. "A Strategy for Validating a Conceptual Model for Radionuclide Migration in the Saturated Zone Beneath Yucca Mountain." *Radioactive Waste Management and Environmental Restoration, 19,* (1-3), 73-96. Yverdon, Switzerland: Harwood Academic Publishers. TIC: 222513. 101154

Robinson, B.A.; Li, C.; and Ho, C.K. 2003. "Performance Assessment Model Development and Analysis of Radionuclide Transport in the Unsaturated Zone, Yucca Mountain, Nevada." *Journal of Contaminant Hydrology, 62-63,* 249-268. New York, New York: Elsevier. TIC: 254205. 171674

Rousseau, J.P.; Kwicklis, E.M.; and Gillies, D.C., eds. 1999. *Hydrogeology of the Unsaturated Zone, North Ramp Area of the Exploratory Studies Facility, Yucca Mountain, Nevada.* Water-Resources Investigations Report 98-4050. Denver, Colorado: U.S. Geological Survey. ACC: MOL.19990419.0335. 102097

Schafer-Perini, A.L. and Wilson, J.L. 1991. "Efficient and Accurate Front Tracking for Two-Dimensional Groundwater Flow Models." *Water Resources Research, 27,* (7), 1471-1485. Washington, D.C.: American Geophysical Union. TIC: 226448. 101476

Scheibe, T.D. and Cole, C.R. 1994. "Non-Gaussian Particle Tracking: Application to Scaling of Transport Processes in Heterogeneous Porous Media." *Water Resources Research, 30,* (7), 2027-2039. Washington, D.C.: American Geophysical Union. TIC: 226446. 101477

Sudicky, E.A. and Frind, E.O. 1982. "Contaminant Transport in Fractured Porous Media: Analytical Solutions for a System of Parallel Fractures." *Water Resources Research, 18,* (6), 1634-1642. Washington, D.C.: American Geophysical Union. TIC: 217475. 105043

Tompson, A.F.B. and Gelhar, L.W. 1990. "Numerical Simulation of Solute Transport in Three-Dimensional, Randomly Heterogeneous Porous Media." *Water Resources Research, 26,* (10), 2541-2562. Washington, D.C.: American Geophysical Union. TIC: 224902. 101490

van Genuchten, M.T. 1985. "Convective-Dispersive Transport of Solutes Involved in Sequential First-Order Decay Reactions." *Computers in Geosciences, 11,* (2), 129-147. New York, New York: Pergamon Press. TIC: 245188. 146961

Wang, J.S. 2003. "Scientific Notebooks Referenced in Model Report U0065, Particle Tracking Model and Abstraction of Transport Process, MDL-NBS-HS-000020 REV 00." Letter from J.S. Wang (BSC) to File, December 4, 2003, with attachment. ACC: MOL.20031208.0348. 166070

Wang, J.S. 2003. "Scientific Notebooks Referenced in Model Report U0090, Analysis of Hydrologic Properties Data, MDL-NBS-HS-000014 REV 00" Interoffice correspondence from J.S. Wang (BSC) to File, February 28, 2003, with attachments. ACC: MOL.20030306.0535. 161654

Wolfsberg, A.V. and Freyberg, D.L. 1994. "Efficient Simulation of Single Species and Multispecies Transport in Groundwater with Local Adaptive Grid Refinement." *Water Resources Research, 30,* (11), 2979-2991. Washington, D.C.: American Geophysical Union. TIC: 226450. 101498

Yamashita, R. and Kimura, H. 1990. "Particle-Tracking Technique for Nuclide Decay Chain Transport in Fractured Porous Media." *Journal of Nuclear Science and Technology, 27,* (11), 1041-1049. Tokyo, Japan: Nihon Genshryoku Gakkai. TIC: 236573. 101499

Yeh, G.T. 1990. "A Lagrangian-Eulerian Method with Zoomable Hidden Fine-Mesh Approach to Solving Advective-Dispersion Equations." *Water Resources Research, 26,* (6), 1133-1144. Washington, D.C.: American Geophysical Union. TIC: 224067. 101501

Zheng, C. 1993. "Extension of the Method of Characteristics for Simulation of Solute Transport in Three Dimensions." *Ground Water, 31,* (3), 456-465. Worthington, Ohio: Water Well Publishing Company. TIC: 226465. 101502

Zheng, C. 1994. "Analysis of Particle Tracking Errors Associated with Spatial Discretization." *Ground Water, 32,* (5), 821-828. Dublin, Ohio: Water Well Publishing Company. TIC: 226463. 101503

Zimmerman, R.W.; Chen, G.; Hadgu, T.; and Bodvarsson, G.S. 1993. "A Numerical Dual-Porosity Model with Semianalytical Treatment of Fracture/Matrix Flow." *Water Resources Research, 29,* (7), 2127-2137. Washington, D.C.: American Geophysical Union. TIC: 236571. 100614

Zyvoloski, G.; Dash, Z.; and Kelkar, S. 1992. *FEHMN 1.0: Finite Element Heat and Mass Transfer Code.* LA-12062-MS, Rev. 1. Los Alamos, New Mexico: Los Alamos National Laboratory. ACC: NNA.19910625.0038. 101026

Zyvoloski, G.A.; Robinson, B.A.; Dash, Z.V.; and Trease, L.L. 1997. *User's Manual for the FEHM Application–A Finite-Element Heat- and Mass-Transfer Code.* LA-13306-M. Los Alamos, New Mexico: Los Alamos National Laboratory. TIC: 235999. 100615

9.2 CODES, STANDARDS, REGULATIONS, AND PROCEDURES

10 CFR 63. 2005 Energy: Disposal of High-Level Radioactive Wastes in a Geologic Repository at Yucca Mountain, Nevada. ACC: MOL.20050405.0118. 173273

AP-2.22Q, REV 1, ICN 0. *Classification Analyses and Maintenance of the Q-List.* Washington, D.C.: U.S Department of Energy, Office of Civilian Radioactive Waste Management. ACC: DOC.20030807.0002.

LP-2.29Q-BSC, Rev. 0, ICN 0. *Planning for Science Activities.* Washington, D.C.: U.S. Department of Energy, Office of Civilian Radioactive Waste Management. ACC: DOC.20050114.0001.

LP-SI.11Q-BSC, Rev. 0, ICN 1. *Software Management.* Washington, D.C.: U.S. Department of Energy, Office of Civilian Radioactive Waste Management. ACC: DOC.20041005.0008.

LP-SIII.10Q-BSC, Rev. 0, ICN 1. *Models.* Washington, D.C.: U.S Department of Energy, Office of Civilian Radioactive Waste Management. ACC: DOC.20050623.0001.

9.3 SOURCE DATA, LISTED BY DATA TRACKING NUMBER

LA0002PR831231.003. Probabilities from C-Wells Microsphere Data. Submittal date: 02/17/2000.	144462
LA0002SK831352.003. Colloid Size Distribution and Total Colloid Concentration in INEEL Groundwater Samples. Submittal date: 02/25/2000.	161771
LA0003JC831362.001. Preliminary Matrix Diffusion Coefficients for Yucca Mountain Tuffs. Submittal date: 4/10/2000.	149557
LA0003MCG12213.002. Cumulative Probabilities for Colloid Transport Between One Matrix and Another Calculated from Interpolation of Pore Volume Data from Yucca Mountain Hydrologic (Stratigraphic) Samples. Submittal date: 03/10/2000.	147285
LA0303HV831352.002. Colloid Retardation Factors for the Saturated Zone Fractured Volcanics. Submittal date: 03/31/2003.	163558
LA0303HV831352.003. Fraction of Colloids that Travel Unretarded. Submittal date: 03/31/2003.	165624
LA0303PR831231.005. Simple Calculations for SZ In-Situ Testing AMR. Submittal date: 03/19/2003.	166259
LA0408AM831341.001. Unsaturated Zone Distribution Coefficients (Kds) for U, Np, Pu, Am, Pa, Cs, Sr, Ra, and Th. Submittal date: 08/24/2004.	171584
LB0205REVUZPRP.001. Fracture Properties for UZ Model Layers Developed from Field Data. Submittal date: 05/14/2002.	159525
LB0207REVUZPRP.001. Revised UZ Fault Zone Fracture Properties. Submittal date: 07/03/2002.	159526
LB0207REVUZPRP.002. Matrix Properties for UZ Model Layers Developed from Field and Laboratory Data. Submittal date: 07/15/2002.	159672
LB0208UZDSCPLI.002. Drift-Scale Calibrated Property Sets: Lower Infiltration Data Summary. Submittal date: 08/26/2002.	161788
LB0208UZDSCPMI.002. Drift-Scale Calibrated Property Sets: Mean Infiltration Data Summary. Submittal date: 08/26/2002.	161243
LB0210THRMLPRP.001. Thermal Properties of UZ Model Layers: Data Summary. Submittal date: 10/25/2002.	160799
LB03023DSSCP9I.001. 3-D Site Scale UZ Flow Field Simulations for 9 Infiltration Scenarios. Submittal date: 02/28/2003.	163044

LB0302UZDSCPUI.002. Drift-Scale Calibrated Property Sets: Upper Infiltration Data Summary. Submittal date: 02/05/2003. 161787

LB0305TSPA18FF.001. Eighteen 3-D Site Scale UZ Flow Fields Converted from TOUGH2 to T2FEHM Format. Submittal date: 05/09/2003. 165625

LB0307MR0060R1.007. Ambient Radionuclide Transport - TSPA Deliverable Extractions. Submittal date: 07/19/2003. 164752

LB03093RADTRNS.002. Three Way Transport Model Comparison: Data Summaries. Submittal date: 09/24/2003. 166071

LB0310T2FEHMFF.001. 1-D and 2-D Site Scale UZ Flow Fields Converted from TOUGH2 to T2FEHM Format. Submittal date: 10/20/2003. 166060

LB0312TSPA06FF.001. Six Flow Fields with Raised Water Tables. Submittal date: 12/23/2003. 166671

LB0402THRMLPRP.001. Thermal Properties of UZ Model Layers: Data Summary. Submittal date: 02/20/2004. 168481

LB0506TSPA08FF.001. Eight 3-D Site Scale Sensitivity Study UZ Flow Fields Converted from TOUGH2 to T2FEHM Format. Submittal date: 06/02/2005. 174117

LL000122051021.116. Summary of Analyses of Glass Dissolution Filtrates. Submittal date: 01/27/2000. 142973

LL030610323122.029. Multiscale Thermohydrologic Model Output to TSPA and WAPDEG for the Mean Infiltration Case. Submittal date: 06/27/2003. 164513

LL991109751021.094. Data Associated with the Detection and Measurement of Colloids in Scientific Notebook SN 1644. Submittal date: 01/10/2000. 142910

MO0407SEPFEPLA.000. LA FEP List. Submittal date: 07/20/2004. 170760

SN0206T0503102.005. Thermal Conductivity of the Non-Repository Layers of Yucca Mountain. Submittal date: 06/27/02. 160258

SN0208T0503102.007. Thermal Conductivity of the Potential Repository Horizon Rev 3. Submittal date: 08/26/2002. 160257

SN0306T0502103.006. Data Spreadsheets to Support Parameter Uncertainty Development. Submittal date: 06/05/2003. 163944

SN0306T0504103.005. Revised Groundwater Colloid Mass Concentration Parameters for TSPA (Total System Performance Assessment). Submittal date: 06/30/2003. 164132

SN0306T0504103.006. Revised Sorption Partition Coefficients (Kd Values) for Selected Radionuclides Modeled in the TSPA (Total System Performance Assessment). Submittal date: 06/30/2003. 164131

9.4 OUTPUT DATA, LISTED BY DATA TRACKING NUMBER

LA0311BR831229.001. UZ Transport Abstraction Model, Transfer Function Calculation Files. Submittal date: 11/17/2003.

LA0311BR831371.001. UZ Transport Abstraction Model, Validation Simulations for the Discrete Fracture Comparison Problem. Submittal date: 11/20/2003.

LA0311BR831371.002. UZ Transport Abstraction Model, Validation Simulations for the Comparison to T2R3D. Submittal date: 11/20/2003.

LA0407BR831371.001. UZ Transport Abstraction Model, Transport Parameters and Base Case Simulation Results. Submittal date: 07/27/2004.

LA0506BR831371.001. FEHM Files for Base-Case UZ Transport Abstraction Model Particle Tracking Simulations. Submittal date: 06/21/2005.

LA0506BR831371.002. FEHM Files for Base-Case UZ Transport Abstraction Model Particle Tracking Simulations, Parameter Studies Varying Hydrologic Properties. Submittal date: 06/21/2005.

LA0506BR831371.003. FEHM Files for Base-Case UZ Transport Abstraction Model Particle Tracking Simulations, Parameter Studies Varying Gamma in the AFM Model. Submittal date: 06/21/2005.

MO0506SPAROCKU.000. Rock Unit, Radionuclide, and Colloid Parameters for Particle Tracking. Submittal date: 06/03/2005.

9.5 SOFTWARE CODES

BSC 2003. *Software Code: GoldSim.* V7.50.100. PC. 10344-7.50.100-00. 161572

BSC 2004. *Software Code: GoldSim.* V 8.02. PC, Windows 2000. 10344-8.02-00. 169844

LANL (Los Alamos National Laboratory) 2003. *Software Code: discrete_tf.* V1.1. SUN, SunOS 5.8; PC, Windows 2000 and Linux 7.1. 11033-1.1-00. 165742

LANL 2003. *Software Code: FEHM.* V2.21. SUN, SunOS 5.8; PC, Windows 2000 and Linux 7.1. 10086-2.21-00. 165741

LANL 2003. *Software Code: fehm2post.* V1.0. SUN, SunOS 5.8 and 5.7; PC, Windows 2000 and Redhat Linux 2.4.18. 11031-1.0-00. 165754

LANL 2003. *Software Code: ppptrk.* V1.0. SUN, SunOS 5.8 and 5.7; PC, Windows 2000 and Linux 7.1. 11030-1.0-00. 165753

LANL 2005. *Software Code: FEHM.* V2.23. SUN, Sun OS 5.9. 10086-2.23-01. 174121

LANL 2003. *Software Code: FEHM.* V2.20. SUN, PC. 10086-2.20-00. 161725

LBNL (Lawrence Berkeley National Laboratory) 1999. *Software Code: T2R3D.* V1.4. FORTRAN 77, SUN, DEC/ALPHA. 10006-1.4-00. 146654

LBNL 1999. *Software Code: TOUGH2.* V1.11 MEOS9nTV1.0. MAC, SUN, DEC/Alpha, PC. 10065-1.11MEOS9NTV1.0-00. 113943

LBNL 2002. *Software Code: DCPT.* V2.0. PC, Windows. 10078-2.0-00. 154342

LBNL 2003. *Software Code: WTRISE.* V2.0. PC/WINDOWS 2000/98; DEC ALPHA/OSF1 V5.1. 10537-2.0-00. 163453

APPENDIX A

DERIVATION OF THE DISTRIBUTION OF WATER CONTENT AND EFFECTIVE PERMEABILITY FOR SAMPLING MATRIX DIFFUSION COEFFICIENT

Matrix diffusion is linked through the correlation given by Reimus et al. (2002 [DIRS 163008]) to porosity and permeability. For unsaturated conditions, this relationship is extended to water content and effective permeability. This is done in segments from the output file from rows 61,001 through 122,000; 122,001 through 184,000; and 184,001 through 245,506, and repeated for each of the nine flow fields. Rows 1 through 61,000 are not needed because none of these cells lie within the repository footprint.

Starting with the flow output file for saturation and relative permeability discussed earlier, the file is first sorted on column T to sort out the cells not in the repository footprint. This approximation is made to simplify the procedure and is a reasonable approach since, for the most part, transport is vertically downward. After sorting, the matrix data is copied into a new file. The rock types in column K are compared with the rock types that exist in or beneath the repository horizon. This is done using the following formulas, implemented as formulas in Excel spreadsheets:

Urn = IF(Krn="bf3Md",1,IF(Krn="tr3Md",1,0))

Vrn = IF(Krn="pp2Md",2,IF(Krn="pp1Mz",2,IF(Krn="pp4Mz",2,0)))

Wrn =
IF(Krn="ch2Mz",3,IF(Krn="ch3Mz",3,IF(Krn="ch4Mz",3,IF(Krn="ch5Mz",3,IF(Krn="ch6Mz",3,0)))))

Xrn =
IF(Krn="pcM1z",3,IF(Krn="pcM2z",3,IF(Krn="pcM39",3,IF(Krn="pcM4p",3,IF(Krn="pcM5z",3,IF(Krn="pcM6z",3,0))))))

Yrn = IF(Krn="ch2Mv",4,IF(Krn="ch3Mv",4,IF(Krn="ch4Mv",4,IF(Krn="ch5Mv",4,0))))

Zrn = IF(Krn="tswMv",5,IF(Krn="ch1Mv",5,IF(Krn="ch6Mv",5,IF(Krn="pp3Md",5,0))))

AArn = IF(Krn="tswMz",6,IF(Krn="ch1Mz",6,IF(Krn="bf2Mz",6,0)))

ABrn = IF(Krn="tswM8",7,IF(Krn="pcM38",7,0))

ACrn = IF(Krn="tswM4",8,IF(Krn="tswM6",8,IF(Krn="tswM7",8,0)))

ADrn = IF(Krn="tswM3",9,IF(Krn="tswM5",9,0))

AErn = SUM(U1:AD1)

The sum of the columns in column AE identifies, by number, the rock group from 1 to 9. Table A-1 shows a table of the rock groups:

Table A-1. Crosswalk between Rock Groups and Model Units

Rock Group	Model Units
1	bf3Md, tr3Md
2	pp2Md, pp1Mz, pp4Mz
3	ch2Mz, ch3Mz, ch4Mz, ch5Mz, ch6Mz, pcM1z, pcM2z, pcM39, pcM4p, pcM5z, pcM6z
4	ch2Mv, ch3Mv, ch4Mv, ch5Mv
5	tswMv, ch1Mv, ch6Mv, pp3Md
6	tswMz, ch1Mz, bf2Mz
7	tswM8, pcM38
8	tswM4, tswM6, tswM7
9	tswM3, tswM5

The groupings are based on similarities in porosity from DTN: LB0207REVUZPRP.002 and permeability as found in LB03023DSSCP9I.001, as shown in Table A-2:

Table A-2. Porosity and Permeability of Model Units and Associated Rock Group

Model Unit	Porosity	Permeability m^2	Rock Group
bf3Md	0.175	3.55E-14	1
pp2Md	0.221	1.7E-15	2
pp1Mz	0.297	2.57E-15	2
pp4Mz	0.321	1.02E-15	2
ch6Mz	0.271	8.2E-19	3
pcM39	0.275	6.2E-18	3
pcM1z	0.285	9.3E-20	3
pcM2z	0.322	2.4E-18	3
ch5Mz	0.322	5.2E-18	3
ch4Mz	0.322	5.2E-18	3
ch3Mz	0.322	5.2E-18	3
ch2Mz	0.322	5.2E-18	3
ch5Mv	0.346	4.9E-11	4
ch4Mv	0.346	4.9E-11	4
ch3Mv	0.346	4.9E-11	4
ch2Mv	0.346	4.9E-11	4
tswMv	0.229	2.24E-13	5
pp3Md	0.318	1.26E-13	5
ch1Mv	0.331	1.39E-12	5
tswMz	0.275	3.5E-17	6
ch1Mz	0.285	3.5E-17	6
pcM38	0.043	3E-19	7
tswM8	0.043	7.4E-18	7
tswM7	0.103	7.41E-19	8
tswM6	0.103	7.41E-19	8
tswM4	0.111	2.96E-19	8
tswM5	0.131	8.55E-18	9
tswM3	0.155	2.39E-179	9

The rock type identification files are stored as:

gt upper rock type identification 61001-122000.xls
gt upper rock type identification 122001-184000.xls
gt upper rock type identification 184001-245506.xls

gt mean rock type identification 61001-122000.xls
gt mean rock type identification 122001-184000.xls
gt mean rock type identification 184001-245506.xls

gt lower rock type identification 61001-122000.xls
gt lower rock type identification 122001-184000.xls
gt lower rock type identification 184001-245506.xls

ms upper rock type identification 61001-122000.xls
ms upper rock type identification 122001-184000.xls
ms upper rock type identification 184001-245506.xls

ms mean rock type identification 61001-122000.xls
ms mean rock type identification 122001-184000.xls
ms mean rock type identification 184001-245506.xls

ms lower rock type identification 61001-122000.xls
ms lower rock type identification 122001-184000.xls
ms lower rock type identification 184001-245506.xls

pd upper rock type identification 61001-122000.xls
pd upper rock type identification 122001-184000.xls
pd upper rock type identification 184001-245506.xls

pd mean rock type identification 61001-122000.xls
pd mean rock type identification 122001-184000.xls
pd mean rock type identification 184001-245506.xls

pd lower rock type identification 61001-122000.xls
pd lower rock type identification 122001-184000.xls
pd lower rock type identification 184001-245506.xls

Columns U through AD are deleted and the file is sorted on column U (Rock Type) in descending order. Those with rock type "0" are deleted.

These files are saved as

gt upper sort by rock type 61001-122000.xls
gt upper sort by rock type 122001-184000.xls
gt upper sort by rock type 184001-245506.xls

gt mean sort by rock type 61001-122000.xls
gt mean sort by rock type 122001-184000.xls
gt mean sort by rock type 184001-245506.xls

gt lower sort by rock type 61001-122000.xls
gt lower sort by rock type 122001-184000.xls
gt lower sort by rock type 184001-245506.xls

ms upper sort by rock type 61001-122000.xls
ms upper sort by rock type 122001-184000.xls
ms upper sort by rock type 184001-245506.xls

ms mean sort by rock type 61001-122000.xls
ms mean sort by rock type 122001-184000.xls
ms mean sort by rock type 184001-245506.xls

ms lower sort by rock type 61001-122000.xls
ms lower sort by rock type 122001-184000.xls
ms lower sort by rock type 184001-245506.xls

pd upper sort by rock type 61001-122000.xls
pd upper sort by rock type 122001-184000.xls
pd upper sort by rock type 184001-245506.xls

pd mean sort by rock type 61001-122000.xls
pd mean sort by rock type 122001-184000.xls
pd mean sort by rock type 184001-245506.xls

pd lower sort by rock type 61001-122000.xls
pd lower sort by rock type 122001-184000.xls
pd lower sort by rock type 184001-245506.xls

The results for each climate scenario are compiled into a single file and ordered by column V in descending order. The files are stored as:

gt upper composite by rock type.xls
gt mean composite by rock type.xls
gt lower composite by rock type.xls

ms upper composite by rock type.xls
ms mean composite by rock type.xls
ms lower composite by rock type.xls

pd upper composite by rock type.xls
pd mean composite by rock type.xls
pd lower composite by rock type.xls

Similarities between rock groups 1, 2, 4, 5, and 6 led to making this a single group. The same was also found for groups 7, 8, and 9. This reduces the groupings to 3 composite groups:

1, 2, 4, 5, and 6
3
7, 8, and 9.

The first analysis for the glacial-transition upper climate scenario was conducted on the individual rock groups 1-9. Porosity was randomly sampled because the flow fields and resulting saturations and effective permeabilities are independent of porosity under steady-flow conditions. Porosity sampling was conducted for each model unit according to the mean and standard deviation for the model unit and a minimum and maximum of 9 and 1, respectively, using a beta distribution. The sampling methodology is described on pages 55 through 59 of the report by Wang (2003 [DIRS 166070], SN-LBNL-SCI-236-V1). Once the sampled porosities were generated on separate worksheets in the same file, the porosities were copied and pasted into column T on the main worksheet. Water content for each cell is generated by multiplying column D by column T as follows:

Urn = Drn*Trn

After generating the water content for each model unit, the combined units were assembled and the main worksheet was ordered by rock type (descending order) and secondarily by cell name (ascending order).

Statistics for the water content and effective permeability were assembled from the data based on a volume-weighted average. The cell volumes are given in column L. The total sum of cell volumes are computed as follows:

X1 = SUM(L1:Lre)

Where "re" stands for the last row of data on the worksheet. The statistics for water content are derived from the following:

Yrn = Urn*Lrn/W$1
Zrn = ((Urn-Z$1)^2)*Lrn/W$1
AA1 = SUM(X1:Xre)
AB1 = SQRT(SUM(Y1:Yre))
AC1 = MAX(U1:Ure)
AD1 = MIN(U1:Ure)

where Yrn and Zrn are the sums to determine the volume weighted mean and variance of the water content. AA1 is then the mean water content, AB1 is the standard deviation of water content, AC1 is the maximum water content, and AD1 is the minimum water content.

Statistics for the effective permeability are based on a log-normal distribution. The statistics are derived through the following formulas:

AFrn = LOG(Frn*Srn)*Lrn/W$1
AGrn = ((LOG(Frn*Srn)-AG$1)^2)*Lrn/W$1
AH1 = SUM(AF1:AFre)
AI1 = SQRT(SUM(A1:AGre))

Where AFrn and AGrn are the sums to determine the volume weighted mean and variance of the logarithm of the effective permeability. AH1 is then the mean of the logarithm of the effective permeability, and AI1 is the standard deviation of the logarithm of the effective permeability.

This was carried out for each of the nine flow fields. The files containing the results are stored as:

gt upper group 6-5-4-2-1 diffusion parameters.xls
gt upper group 3 diffusion parameters.xls
gt upper group 9-8-7 diffusion parameters.xls
gt mean group 6-5-4-2-1 diffusion parameters.xls
gt mean group 3 diffusion parameters.xls
gt mean group 9-8-7 diffusion parameters.xls
gt lower group 6-5-4-2-1 diffusion parameters.xls
gt lower group 3 diffusion parameters.xls
gt lower group 9-8-7 diffusion parameters.xls
ms upper group 6-5-4-2-1 diffusion parameters.xls
ms upper group 3 diffusion parameters.xls
ms upper group 9-8-7 diffusion parameters.xls
ms mean group 6-5-4-2-1 diffusion parameters.xls
ms mean group 3 diffusion parameters.xls
ms mean group 9-8-7 diffusion parameters.xls
ms lower group 6-5-4-2-1 diffusion parameters.xls
ms lower group 3 diffusion parameters.xls
ms lower group 9-8-7 diffusion parameters.xls
ps upper group 6-5-4-2-1 diffusion parameters.xls
ps upper group 3 diffusion parameters.xls
ps upper group 9-8-7 diffusion parameters.xls
ps mean group 6-5-4-2-1 diffusion parameters.xls
ps mean group 3 diffusion parameters.xls
ps mean group 9-8-7 diffusion parameters.xls
ps lower group 6-5-4-2-1 diffusion parameters.xls
ps lower group 3 diffusion parameters.xls
ps lower group 9-8-7 diffusion parameters.xls

Summary files for each climate were created. These are stored as:

Summary of matrix diffusion for glacial-transition climate.xls
Summary of matrix diffusion for monsoon climate.xls

Summary of matrix diffusion for present day climate.xls

Averages were conducted across the climate/infiltration scenarios to create categories based on rock type only. Simple arithmetic averages of the results from each climate infiltration scenario were computed for the mean and variance of water content and logarithm of the effective permeability. Composite Distributions for all climate scenarios segregated only by the higher level rock groupings (6-5-4-2-1, 3, 9-8-7) are given in the following file:

Matrix diffusion summary with averages by rock type.xls

And a summary file with only the results is given in:

Matrix diffusion - summary values only.xls

INTENTIONALLY LEFT BLANK

APPENDIX B

DERIVATION OF WATER TABLE COLLECTING BINS

The water table bins were calculated starting with grid information for the unsaturated zone (UZ) flow fields available in DTN: LB03023DSSCP9I.001 [DIRS 163044]. This data contains the cell name and coordinates for each node in the site-scale UZ flow model. Because the number of elements is 245506, the file is split into 4 groups as follows such that the data fits onto an excel worksheet:

Group A
1-62000.xls
62001-124000.xls
124001-186000.xls
186001-245506.xls

The "BT" cells in the site-scale UZ flow model comprise the bottom boundary of the model at the present-day water table. These are cells in the file *186001-245506.xls* from row 57465 to row 59506. The "BT" cell coordinates were put into columns I, J, and K of the following files:

Group B
1-62000 with exact WT picks.xls
62001-124000 with exact WT picks.xls
124001-186000 with exact WT picks.xls
186001-245506 with exact WT picks.xls

Columns L and M were generated using the following relationship:

Lrn = Ern&Frn
Mrn = Irn&Jrn

where the "rn" subscripts stand for "row number". The character strings in columns L and M represent, respectively, a unique x-y coordinate character for the grid nodes and for the "BT" cells. Each grid node was then checked for a match with a "BT" cell. The index for the match was recorded in Column N,

Nrn = MATCH(Lrn,M$1:M$end,0)

where M$end represents the last occupied cell in column M.

The index in column N is then used to extract the local water table elevation in column H as follows:

Hrn = INDEX(K:K,Nrn)

In roughly 10 percent of the cells, no match was found, in which case a value of #N/A was returned. To evaluate a value of the local water table for these cells, columns A through H were copied into a second worksheet in the files listed above. A column was inserted into column A for a sequential number for each cell. Therefore, the local water table resided in column I. The worksheet was sorted on column I to group the cells without local water table values. The cells without local water table values were copied into the following file:

Stragglers.xls

Cells without local water table values were found for each of the following cell ranges:

1-62000
62001-124000
186001-245506

and these cells were kept on separate worksheets in the *Straggles.xls file.*

To identify an appropriate local water table elevation for these cells, the following file was developed:

WT identification for stragglers.xls

Columns A, B, and C from row 3 to row 4086 contain the coordinates of the "BT" cells. Up to 250 x-y coordinates for cells without an exact water table value were put in rows 1 and 2, columns D through IS. Then the square of the distance between each cell and each "BT" cell was computed for each x-y coordinate as follows:

COLrn = (COL$1-$Arn)^2+(COL$2-$Brn)^2

where COL represents a column label and rn the row number. Each column represents the x-y distance from a cell without an exact local water table value to each of the "BT" cells. The minimum distance was determined in row 4087 using the following formula:

COL4087 = MIN(COL3:COL4086)

The index of the "BT" cell associated with the minimum distance was determined in row 4088 as follows:

COL4088 = MATCH(COL4087,COL3:COL4086,0)

And the water table elevation associated with the index is determined in row 4089 as follows:

COL4089 = INDEX($C3:$C4086,COL4088)

These water table elevations were included in the third worksheet of the Group B files.

Files *62001-124000 wt bins.xls*, *124001-186000 wt bins.xls*, and *186001-245506 wt bins.xls* contain the extracted water table collection cells in TOUGH2 columns using conditional if statements and the definition of the collection bin boundary data.

File *62001-124000 wt bins with fehm nodes .xls*, *124001-186000 wt bins with fehm nodes.xls*, and *124001-186000 wt bins with fehm nodes.xls* contain extracted collection bin nodes in finite element heat and mass model grid format.

The final extracted water table collection bins are stored in file *collect_zone* which only contains the fracture nodes as required by FEHM.

All the files used in the extraction of water table collection bins are included in zip file *wtbin.zip*. The file names are listed below in Figure B-1.

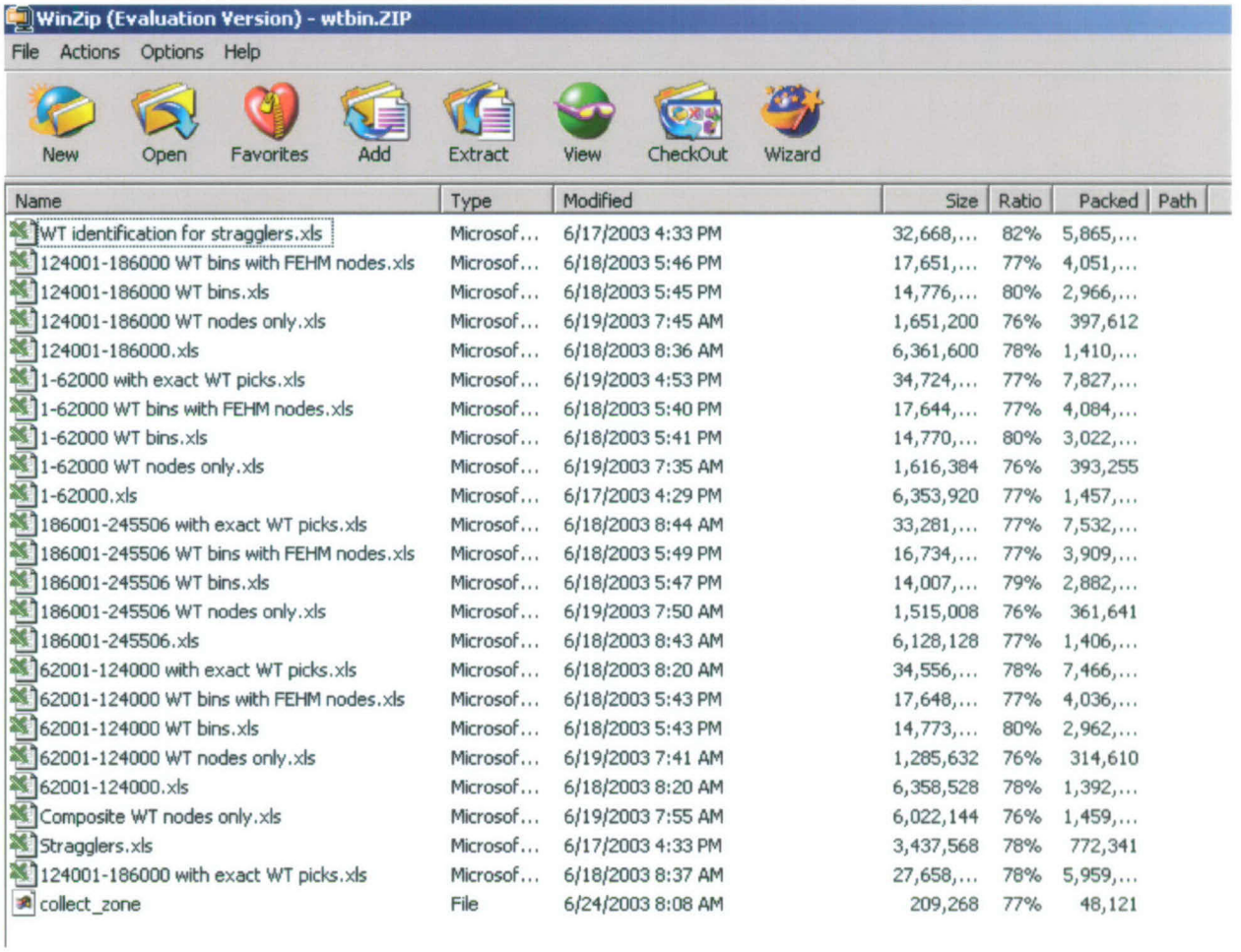

Name	Type	Modified	Size	Ratio	Packed	Path
WT identification for stragglers.xls	Microsof...	6/17/2003 4:33 PM	32,668,...	82%	5,865,...	
124001-186000 WT bins with FEHM nodes.xls	Microsof...	6/18/2003 5:46 PM	17,651,...	77%	4,051,...	
124001-186000 WT bins.xls	Microsof...	6/18/2003 5:45 PM	14,776,...	80%	2,966,...	
124001-186000 WT nodes only.xls	Microsof...	6/19/2003 7:45 AM	1,651,200	76%	397,612	
124001-186000.xls	Microsof...	6/18/2003 8:36 AM	6,361,600	78%	1,410,...	
1-62000 with exact WT picks.xls	Microsof...	6/19/2003 4:53 PM	34,724,...	77%	7,827,...	
1-62000 WT bins with FEHM nodes.xls	Microsof...	6/18/2003 5:40 PM	17,644,...	77%	4,084,...	
1-62000 WT bins.xls	Microsof...	6/18/2003 5:41 PM	14,770,...	80%	3,022,...	
1-62000 WT nodes only.xls	Microsof...	6/19/2003 7:35 AM	1,616,384	76%	393,255	
1-62000.xls	Microsof...	6/17/2003 4:29 PM	6,353,920	77%	1,457,...	
186001-245506 with exact WT picks.xls	Microsof...	6/18/2003 8:44 AM	33,281,...	77%	7,532,...	
186001-245506 WT bins with FEHM nodes.xls	Microsof...	6/18/2003 5:49 PM	16,734,...	77%	3,909,...	
186001-245506 WT bins.xls	Microsof...	6/18/2003 5:47 PM	14,007,...	79%	2,882,...	
186001-245506 WT nodes only.xls	Microsof...	6/19/2003 7:50 AM	1,515,008	76%	361,641	
186001-245506.xls	Microsof...	6/18/2003 8:43 AM	6,128,128	77%	1,406,...	
62001-124000 with exact WT picks.xls	Microsof...	6/18/2003 8:20 AM	34,556,...	78%	7,466,...	
62001-124000 WT bins with FEHM nodes.xls	Microsof...	6/18/2003 5:43 PM	17,648,...	77%	4,036,...	
62001-124000 WT bins.xls	Microsof...	6/18/2003 5:43 PM	14,773,...	80%	2,962,...	
62001-124000 WT nodes only.xls	Microsof...	6/19/2003 7:41 AM	1,285,632	76%	314,610	
62001-124000.xls	Microsof...	6/18/2003 8:20 AM	6,358,528	78%	1,392,...	
Composite WT nodes only.xls	Microsof...	6/19/2003 7:55 AM	6,022,144	76%	1,459,...	
Stragglers.xls	Microsof...	6/17/2003 4:33 PM	3,437,568	78%	772,341	
124001-186000 with exact WT picks.xls	Microsof...	6/18/2003 8:37 AM	27,658,...	78%	5,959,...	
collect_zone	File	6/24/2003 8:08 AM	209,268	77%	48,121	

Figure B-1. Listing of Files Used to Develop the Water Table Binning

INTENTIONALLY LEFT BLANK

APPENDIX C

DERIVATION OF FRACTURE-MATRIX INTERACTION SUBMODEL AND GENERATION OF TRANSFER FUNCTIONS

C1. DERIVATION OF FRACTURE-MATRIX INTERACTION SUBMODEL

The governing equations required for the fracture-matrix interaction submodel is a solute transport system in a domain consisting of parallel flow in a fracture and adjacent matrix, with fracture-matrix solute interaction via molecular diffusion in the rock matrix. This model is, therefore, an extension of the model by Sudicky and Frind (1982 [DIRS 105043]), which assumed the water in the matrix is stagnant. For simplicity, longitudinal dispersion is not considered in either medium, advection is considered only in the z direction, and diffusion is considered only normal to the flow direction. The rationales for these simplifications are as follows. With regard to longitudinal dispersion, this submodel is intended only to capture the impact of diffusion because dispersion is captured separately in the particle-tracking algorithm. Likewise, the advection from fracture to matrix (or the reverse) is implemented in the particle-tracking algorithm separately. Therefore, the remaining processes to be included as part of the transfer functions are advection and diffusion in the z-direction only.

Starting with a derivation of the transport equation for the fracture, a variant of this equation with longitudinal dispersion and decay was presented by Sudicky and Frind (1982 [DIRS 105043], Eq. 1). This derivation is presented here from first principles to demonstrate the means by which terms in the dimensionless groups must be altered to include the effects of the active fracture model (AFM). Taking a control volume in the fracture of width b (half of the full aperture), depth d, and length Δz, the terms of the transient solute mass balance (units of each of these terms are solute mass per time) are:

Accumulation:
$$bd\Delta z\theta_f R_f \frac{(C - C_{prev})}{\Delta t} \qquad \text{(Eq. C-1)}$$

where C_{prev} represents the concentration at the previous time step, θ_f is the volumetric water content in the fracture, and R_f is the fracture retardation factor.

Advection:
$$bd\overline{V}_z(C_{z+\Delta z} - C_z) \qquad \text{(Eq. C-2)}$$

where $\overline{V}_z$ is the Darcy velocity in the fracture, equal to volumetric flow rate divided by the total cross sectional area in the fracture.

Diffusion into Matrix:
$$d\Delta z\theta_m D_m \left.\frac{\partial C_m}{\partial x}\right|_{x=b} \qquad \text{(Eq. C-3)}$$

where D_m is the effective diffusion coefficient in the matrix and θ_m is the matrix volumetric water content. These terms form the overall solute mass balance equation:

$$bd\Delta z\theta_f R_f \frac{(C - C_{prev})}{\Delta t} = -bd\overline{V}_z(C_{z+\Delta z} - C_z) + d\Delta z\theta_m D_m \left.\frac{\partial C_m}{\partial x}\right|_{x=b} \qquad \text{(Eq. C-4)}$$

Dividing by $bd\Delta z\theta_f$, making use of the relation for the fracture interstitial pore-water velocity $V_f = \overline{V}_z / \theta_f$, and taking the limit as Δz and Δt go to 0:

$$R_f \frac{\partial C_f}{\partial t} = -V_f \frac{\partial C_f}{\partial z} + \frac{\theta_m D_m}{\theta_f b} \frac{\partial C_m}{\partial x}\bigg|_{x=b} \quad \text{(Eq. C-5)}$$

Note also that the subscript "f" on the concentration is adopted to denote the fracture.

Given the assumptions listed at the beginning of this derivation, the differential equation governing transport in the matrix is:

$$R_m \frac{\partial C_m}{\partial t} = D_m \frac{\partial^2 C_m}{\partial x^2} - V_m \frac{\partial C_m}{\partial z} \quad \text{(Eq. C-6)}$$

where V_m is the interstitial pore-water velocity in matrix, and D_m is the matrix retardation factor. The initial and boundary conditions for the system are:

$$C_f(z,0) = 0 \quad \text{(Eq. C-7)}$$

$$C_m(x,z,0) = 0 \quad \text{(Eq. C-8)}$$

$$C_f(0,t) = C_{o,f} \quad \text{(Eq. C-9)}$$

$$C_m(x,0,t) = C_{o,m} \quad \text{(Eq. C-10)}$$

$$C_m(b,z,t) = C_f(z,t) \quad \text{(Eq. C-11)}$$

$$\frac{\partial C_m}{\partial x}(B,z,t) = 0 \quad \text{(Eq. C-12)}$$

Here the terms $C_{o,f}$ and $C_{o,m}$ for the fracture and matrix, respectively, are nonzero if mass is being introduced into that medium, and 0 if mass is being introduced in the other medium.

Nondimensionalization of these equations can be accomplished by introducing the following dimensionless variables:

$$\hat{C}_f = C_f / C_o \quad \text{(Eq. C-13)}$$

$$\hat{C}_m = C_m / C_o \quad \text{(Eq. C-14)}$$

$$\hat{z} = z / L \quad \text{(Eq. C-15)}$$

$$\hat{x} = x / B \quad \text{(Eq. C-16)}$$

$$\hat{t} = \frac{V_f t}{R_f L} = \frac{t}{\tau_f R_f} \quad \text{(Eq. C-17)}$$

where L is the length of the flow path. Eq. C-17 uses the definition of $\tau_f = L/V_f$; a corresponding relation is also used for the matrix fluid transport time ($\tau_m = L/V_m$). Note that because the equations are nondimensionalized with respect to transport times through the fracture and matrix, the physical dimensions of the flow path, including the length, is unimportant to the final implementation in the code. Next, substituting Equations C-13 to C-17 into Equations C-5 and C-6:

$$\frac{\partial \hat{C}_f}{\partial \hat{t}} = -\frac{\partial \hat{C}_f}{\partial \hat{z}} + \frac{\theta_m D_m \tau_f}{\theta_f b B} \left. \frac{\partial \hat{C}_m}{\partial \hat{x}} \right|_{\hat{x}=b/B} \quad \text{(Eq. C-18)}$$

$$\frac{\partial \hat{C}_m}{\partial \hat{t}} = \frac{D_m \tau_f R_f}{B^2 R_m} \frac{\partial^2 \hat{C}_m}{\partial \hat{x}^2} - \frac{\tau_f R_f}{\tau_m R_m} \frac{\partial \hat{C}_m}{\partial \hat{z}} \quad \text{(Eq. C-19)}$$

The boundary and initial conditions (Equations C-7 to C-12) are transformed to

$$\hat{C}_f(\hat{z},0) = 0 \quad \text{(Eq. C-20)}$$

$$\hat{C}_m(\hat{x},\hat{z},0) = 0 \quad \text{(Eq. C-21)}$$

$$\hat{C}_f(0,\hat{t}) = 1 \text{ (or 0 if injection is into the matrix)} \quad \text{(Eq. C-22)}$$

$$\hat{C}_m(\hat{x},0,\hat{t}) = 1 \text{ (or 0 if injection is into the fracture)} \quad \text{(Eq. C-23)}$$

$$\hat{C}_m(b/B,\hat{z},\hat{t}) = \hat{C}_f(\hat{z},\hat{t}) \quad \text{(Eq. C-24)}$$

$$\frac{\partial \hat{C}_m}{\partial \hat{x}}(1,\hat{z},\hat{t}) = 0 \quad \text{(Eq. C-25)}$$

The end result is that Equations C-18 and C-19 illustrate that a when nondimensional form of the model equations are produced, the system is fully characterized by three dimensionless parameters (Eq. 6-9 to 6-11 of the main document):

$$p_1 = \frac{D_m \tau_f R_f}{B^2 R_m} \quad \text{(Eq. C-26)}$$

$$p_2 = \frac{D_m \tau_f \theta_m}{b B \theta_f} \quad \text{(Eq. C-27)}$$

$$p_3 = \frac{\tau_f R_f}{\tau_m R_m} \quad \text{(Eq. C-28)}$$

where the retardation factor R_m is related to the sorption coefficient K_d using Eq. 6-2. This derivation shows that a series of transfer function curves generated based on a model with parallel flow in the fractures and matrix can capture the range of behavior of the unsaturated zone transport fracture-matrix interaction submodel as long as the curves span the ranges of the parameters in the vector (p_1, p_2, p_3). The documentation for the finite element heat and mass model (FEHM) V2.21 (LANL 2003 [DIRS 165741]) contains information on the formatting of the input files to invoke this portion of the particle tracking transport model.

C2. GENERATION OF TRANSFER FUNCTIONS

This section describes the process for generating the transfer function curves. This is accomplished through a numerical solution of the model domain depicted in Figure 6-5. As described in Section 6.4.3, both a discrete fracture model (DFM) and a dual permeability model conceptualization is implemented as part of the abstraction. For the DFM, a two-dimensional DFM was set up to perform transport simulations using the advection-dispersion module of FEHM V2.21 (LANL 2003 [DIRS 165741]). The model consists of a regular grid domain consisting of regular spacing of 6 m in the z direction (51 grid points in this direction for a total length of 300 m), and increasing grid spacing into the matrix in the x direction, starting with the first column of nodes of width equal to that of a fracture (22 grid points in this direction). In the model simulations, fracture properties are given to the nodes of the first column, and the remaining nodes are given matrix properties. To ensure that parallel flow occurs in the fracture and matrix in the z direction, a flow permeability barrier is established between the fracture and matrix. Furthermore, for injection into the matrix, water is input and output from the boundary nodes in proportion to the volume of that cell. This model design ensures that flow streamlines remain completely in the z direction. Finally, although the transfer functions being used are for unsaturated transport, there is no requirement that this submodel use unsaturated flow to generate them, as long as the water content values are known. Therefore, for simplicity, these simulations were performed for saturated flow conditions, with the fracture and matrix porosities used instead of water contents. For the dual-k model, a simple grid was constructed with identical spacings in the z direction, but only one matrix cell in the x direction. Aside from the different grid, cell numbering, and application of boundary conditions, the process for generating the breakthrough curves and transfer functions is the same for the dual-k model. Furthermore, the use of these curves in an FEHM particle tracking simulation is completely transparent, requiring only a choice of which transfer function file to use.

In the simulations to generate the transfer functions, parameter p_3 is varied systematically from fracture-dominated to matrix-dominated flow by varying the relative water flux values in the fractures and matrix. Ranges of other parameter values consistent with the span of those parameters required for the UZ transport abstraction model are also selected. Table C-1 lists the variations of each parameter that were used in the formulation of the transfer function curves. Note that for the sorption coefficient K_d, the fact that the range of values only goes to 100 does not imply that the model is incapable of accurately simulating transport behavior for higher

values of K_d. In Section C-4 below, a procedure for normalizing the transfer function curves is described whereby higher values of K_d are properly handled. This procedure allows the code to cover arbitrarily large values of K_d without the need to include transfer function curves that extend to such large values.

A four-dimensional matrix of parameters was established with the parameter values listed in the table, and the transfer function curves for each were computed, for a total of $11 \times 12 \times 3 \times 10 = 3960$ values of the parameter vector (p_1, p_2, p_3).

Table C-1. List of Parameter Values Used to Compute Transfer Function Curves

Parameter	# of Values	List of Values
$F_f = f_f/(f_f + f_m)$	11	0.01, 0.1, 0.2, 0.3, 0.4, 0.5, 0.6, 0.7, 0.8, 0.9, 0.99
D_m	12	1.e-8, 3.e-9, 1.e-9, 3.e-10, 1.e-10, 3.e-11, 1.e-11, 3.e-12, 1.e-12, 3.e-13, 1.e-13, 1.e-20 m^2/s
θ_f	3	0.01, 0.1, 0.5
K_d	10	0., 0.3, 0.5, 1.0, 3.0, 5.0, 10.0, 30.0, 50.0, 100.0 mL/g
Total: 11 × 12 × 3 × 10	3,960	(p_1, p_2, p_3) in Excel spreadsheet *parameter runs.xls*

[a] K_d range of 0-100 does not mean that the model is limited to K_d values of 100 or less. See Section III-4 for details on the normalization procedure for handling higher values of K_d.

Two runs of the model are performed for each parameter set: one where solute mass is injected in the fracture, and another where mass is injected in the matrix. The list of parameter values (p_1, p_2, p_3) are given in the Excel spreadsheet *parameter runs 3960.xls*, along with the underlying FEHM input parameters for each simulation. The code fehm2post V1.0 (LANL 2003 [DIRS 165754]) was used to execute the multiple realizations and to postprocess the results to obtain the transfer functions. The postprocessing itself (executed by fehm2post) was performed using the software discrete_tf V1.1 (LANL 2003 [DIRS 165742]). The resulting output from these runs is then concatenated by hand and the appropriate header information inserted by hand to conform to the input required by FEHM. The file called *uz_tfcurves_nn_3960.in* is the transfer function file for the DFM formulation, whereas the corresponding file for the dual-k formulation is *uz_tfcurves_dualk_nn_3960.in*. These files, along with the excel spreadsheet mentioned above, and the control files required for execution of these runs are available as DTN: LA0311BR831229.001.

C3. DISCUSSION OF FRACTURE-MATRIX SUBMODEL BEHAVIOR

This section explores the behavior of the fracture-matrix submodel for the two alternate formulations, DFM and dual-k. In contrast to the discrete fracture based transfer function model, the dual-k formulation has a single matrix block for each fracture block. All other aspects of the parameterization are kept the same. Figures C-1 and C-2 compare the DFM and dual permeability transport models for a flow situation consisting of 60 percent fracture flow, 40 percent matrix flow, over a range of diffusion coefficients given in Table C-2. Breakthrough curves from the fracture are presented for solute injection into the fracture at the inlet. Also

shown are vertical, dotted red lines representing the limiting behavior expected for fracture transport and no diffusion (dimensionless time of 1) and composite medium behavior for the case of infinitely large diffusion. Composite medium behavior is attained when the time for diffusion across the model domain B is of that same order or smaller than transport time along the flow path. Under these conditions, the transport time through the system reduces to

$$\tau_{comp} = \frac{R_f m_f + R_m m_m}{f_f + f_m} \tag{C-29}$$

where m_f and m_m are the fluid masses in a cell for the fracture and matrix, respectively, and f_f and f_m are the fluid mass fluxes for the fracture and matrix, respectively. Intuitively, Eq. C-29 is derived by picturing a solute molecule traveling with fluid of total flux given by the denominator, with total storage volume (including sorption sites) given by the numerator. The time τ_{comp} is an important characteristic time for this system, and serves as a reference for understanding the behavior and deriving the detailed method for using transfer function, described in the next section.

Table C-2. Diffusion Coefficients Used in Simulations

Curve Label	Diffusion Coefficient (m^2/s)
a	1.e-8
b	1.e-10
c	1.e-11
d	1.e-12
e	1.e-13
f	1.e-20

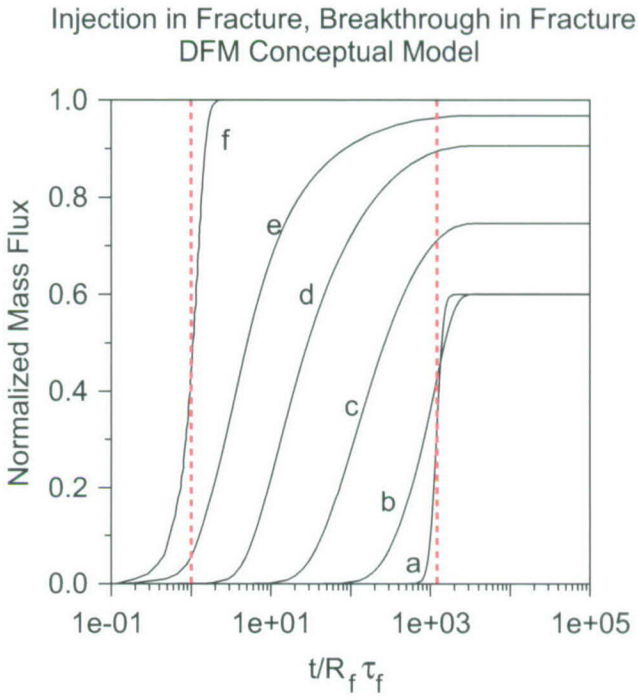

Output DTN: LA0311BR831229.001.

Figure C-1. Transfer Function Computed for the Discrete Fracture Model Formulation: Solute Injection in Fracture, Breakthrough in Fracture, Diffusion Coefficients Given in Table C-2

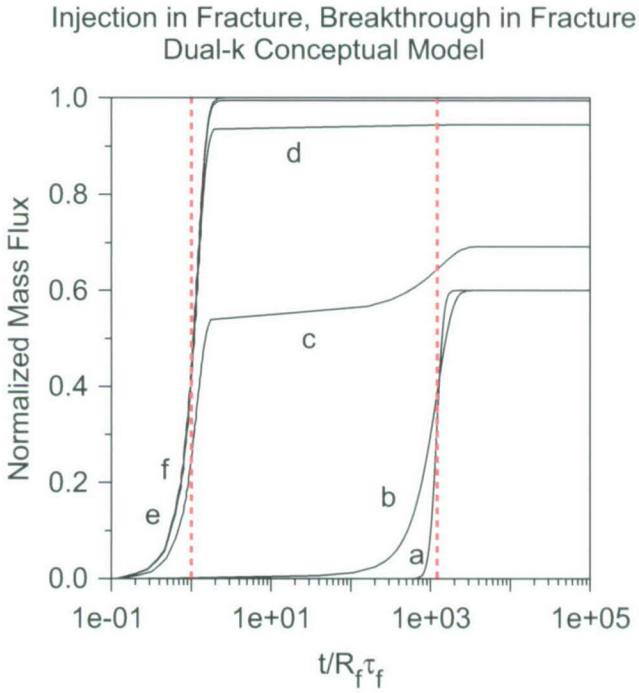

Output DTN: LA0311BR831229.001.

Figure C-2. Transfer Function Computed for the Dual-k Model Formulation: Solute Injection in Fracture, Breakthrough in Fracture, Diffusion Coefficients Given in Table C-2

For each model, the behavior at the extremes of low and high diffusion are similar. For negligible diffusion, transport times approach a dimensionless time of 1, and the normalized mass flux attains a plateau at 1, which is to say that all mass injected in the fracture leaves via the fracture. By contrast, at high diffusion, transport times approach τ_{comp}, and the plateau of normalized mass flux approaches a value of F_f (0.6 in this example), meaning that at this extreme, the probability of mass in the fracture leaving via the fracture equals the fraction of the total flow traveling through the fracture. It is at the intermediate values of diffusion coefficient that the two models diverge. Specifically, the dual-k formulation tends to predict early breakthrough due to rapid transport through the fracture for a significant portion of the mass, compared to the DFM formulation, for which smooth breakthrough curves at progressively longer transport times are predicted for increasing diffusion coefficients. This means that the dual-k formulation ought to predict earlier breakthrough for the first-arriving mass if the parameter ranges of the model are in this intermediate range. Conversely, the models should be similar behavior for high diffusion or low diffusion.

C4. ADDITIONAL IMPLEMENTATION CONSIDERATIONS

This section addresses some additional details concerning the implementation of the transfer function methodology. These considerations concern the nondimensionalization of the transfer function curves, and the method by which the model handles cases in which some parameters are selected that fall at or outside the range of values assumed when generating the transfer function curves.

Figures C-1 and C-2 demonstrated that, in addition to the fracture transport time $R_f\tau_f$ used to nondimensionalize time in the transfer function curves, the composite transport time τ_{comp} is a natural parameter for bracketing the behavior of the f/m interaction submodel. Time in the transfer functions supplied to FEHM is $t/R_f\tau_f$, which contains no information relevant to the extreme of long transport times, which approach τ_{comp}. To make the method more robust, an improved nondimensionalization for time can be made as follows:

$$\bar{t} = \frac{t - R_f\tau_f}{\tau_{comp} - R_f\tau_f} \qquad \text{(Eq. C-30)}$$

Assuming, as is the case for the unsaturated zone transport abstraction model, that $\tau_{comp} >> R_f\tau_f$, Eq. C-30 normalizes the breakthrough times to values in the approximate range of 0 and 1 in Figures C-1 and C-2. Because FEHM reads in time values of $t/R_f\tau_f$, an expression is required for converting these to dimensionless times given by Eq. C-30. This is done by first dividing the top and bottom of Eq. C-30 by $R_f\tau_f$:

$$\bar{t} = \frac{t/R_f\tau_f - 1}{\tau_{comp}/R_f\tau_f - 1} \qquad \text{(Eq.C-31)}$$

The FEHM input time $t/R_f\tau_f$ minus 1 is the numerator, so the requirement is to determine a relation involving the dimensionless parameters (p_1, p_2, p_3) that can be used to express the denominator. For this the following relation is obtained from simple algebra from Equations C-26 to C-28:

$$\frac{p_2 p_3}{p_1} = \left(\frac{\tau_f}{b\theta_f}\right)\left(\frac{\theta_m B}{\tau_m}\right) \qquad \text{(Eq. C-32)}$$

Alternatively, recognizing that $b\theta_f$ and $\theta_m B$ are proportional to the fluid mass in the fracture and matrix, respectively, then this expression reduces to:

$$\frac{p_2 p_3}{p_1} = \frac{f_m}{f_f} \qquad \text{(Eq. C-33)}$$

An equivalent expression using the definition $F_f = f_f/(f_f + f_m)$ is

$$F_f = \frac{p_1}{p_1 + p_2 p_3} \qquad \text{(Eq. C-34)}$$

Returning to the definition of τ_{comp} (Eq. C-29), the following algebraic manipulations can be performed:

$$\tau_{comp} = \frac{R_f m_f + R_m m_m}{f_f + f_m} = F_f\left(R_f\tau_f + R_m\tau_m \frac{f_m}{f_f}\right) = F_f R_f \tau_f \left(1 + \frac{R_m\tau_m}{R_f\tau_f}\frac{p_2 p_3}{p_1}\right) = F_f R_f \tau_f \left(1 + \frac{p_2}{p_1}\right)$$

(Eq. C-35)

This series of steps is conducted using Equations C-30, C-33, and C-28, along with the definitions $F_f = f_f/(f_f + f_m)$, $\tau_f = m_f/f_f$, and $\tau_m = m_m/f_m$. Finally, the denominator $\tau_{comp}/R_f\tau_f - 1$ in Eq. C-31 is obtained through further algebra and the use of Eq. C-34:

$$\tau_{comp}/R_f\tau_f - 1 = \frac{p_2(1 - p_3)}{p_1 + p_2 p_3} \qquad \text{(Eq. C-36)}$$

The important point here is that the transformation of Eq. C-31 can be made by subtracting 1 from the input dimensionless time and dividing by the expression in Eq. C-36. This operation is performed by FEHM upon reading in the transfer function curves. Then, after the normalized time for a particle $\bar{t}$ is obtained in the particle tracking algorithm, Eq. C-30 is used to back out the dimensional value of time of the particle. This approach takes advantage of the self-similarity of the family of curves such as those in Figures C-1 or C-2. That is, even if the parameters (p_1, p_2, p_3) at a given location in the model are not exactly those used to generate

the transfer function, the use of the times $R_f\tau_f$ and τ_{comp} from the model at a given grid cell provide a means for scaling the transfer function accordingly. Also, because a relatively large number of transfer function curves (3960) are used, it is likely that in most instances a curve fairly close to the parameters used in the transfer function will be found.

Despite the effectiveness of this method, there are a few cases for which special consideration needed to be made. This is because of the extraordinarily wide range of parameter values required to be covered in the total system performance assessment for license application model. As a result, the way in which the model handles some of the extreme values of certain parameters is through the use of special rules designed to achieve accuracy. These methods, described below, all call for the adjustment of one or more of the parameters (p_1, p_2, p_3) at a given location in the model so as to yield the desired behavior. Details are given below.

Low Diffusion Coefficient: It is often desirable to lower the diffusion coefficient to extremely low values to examine this end-member case. Furthermore, colloids are low-diffusion species that require accuracy at low values of D_m. The most fool-proof way to do this is to not use the transfer function model all, but instead to simply route the particles through the model with advection and dispersion only. However, if this option is not chosen, the model still must perform properly at the low end of diffusion. The diffusion coefficient only affects parameters p_1 and p_2, so the search algorithm needs to account for the fact that below a minimum value of D_m (10^{-18} m^2/s in the code), the precise values of these parameters are not important. To ensure that the search algorithm locates a curve with the correct value of p_3, p_1, and p_2, are assigned values that were actually used in the generation of the low-diffusion transfer function curves (see Table C-1), so that during the search, p_1 and p_2 are de-emphasized, and p_3 is, in essence, the only parameter considered. In doing so, this approach ensures that the code finds the portion of the parameter space with the correct values for p_3. If this is not done, the least squares method for selecting the correct transfer function curve can sometimes compensate for the extreme parameters chosen by selecting an undesirable part of the parameter space. With the approach just described, the method is forced to select a low-diffusion regime while obtaining the correct ratio of transport times in the fracture and matrix.

High Matrix Sorption: Similar to the case just described, an extremely large value of R_m beyond the range used in the transfer functions causes problems for the search algorithm. When searching for the closest transfer function, the uncorrected method compensates for a large R_m by selecting a fracture-dominated flow case to attain as low a value of p_3 as possible. Similarly, the calculation of p_1 is also affected. Thus, to correct for this case, the maximum value of R_m used in the transfer function curve generation (1000) is used as an upper limit when searching for the correct transfer function curve. However, note that this does *not* mean that the matrix retardation is limited to that value in the particle tracking transport time calculation. Recall that the transfer function curves themselves are normalized using Eq. C-30, which includes τ_{comp}. In contrast to the determination of the closest transfer function curve, the actual value of R_m is used in computing τ_{comp}, which results in a determination of transport time that is scaled by the actual

sorption set in the matrix. Thus the correction is applied only to find an appropriate transfer function curve, and the method for nondimensionalizing those curves ensures that an appropriately large transport time is reproduced for the case of high matrix sorption.

Fracture-Dominated Flow: The parameterization of the transfer function curves is based on a model that has some flow within both the fracture and matrix. When the flow is fracture dominated ($F_f > 0.99$), the details of the actual fraction of flow should be unimportant, since advective transport in the matrix should be negligible. However, without correction for cases where $F_f > 0.99$, the algorithm for finding the transfer function will inappropriately attempt to select curves with high R_m to compensate for the fact that transfer functions with extremely large F_f are not included. To correct for this problem, the code makes use of the following rearranged form of Eq. C-30:

$$p_3 = \frac{p_1}{p_2}\frac{(1-F_f)}{F_f} \qquad \text{(Eq. C-37)}$$

When $F_f > 0.99$, the code uses 0.99 and the values of p_1 and p_2 to compute p_3 for the purposes of selecting the transfer function curve. This assures that a fracture-dominated transfer function is chosen with appropriate values for the other diffusion and sorption parameters.

Matrix-Dominated Flow: For this extreme, it is desirable to bypass the transfer function method altogether, since the transport time is trivially found to be $R_m\tau_m$. Allowing the transfer function algorithm to be used for this case causes problems because the normalization procedure implicitly assumes that the matrix transport time is longer than the fracture transport time. To cover the special case of essentially no flow in the fracture, the transport time is assigned a value of τ_{comp}, which reduces to $R_m\tau_m$ under these conditions.

C5. ADAPTING THE ACTIVE FRACTURE MODEL FOR TRANSPORT

The AFM of the report by Liu et al. (1998 [DIRS 105729]) is formulated on the basis that only a fraction of the fractures flow. This requires that adjustments be applied to the interface area and the mean spacing between flowing fractures. These adjusted parameters can then be used in the UZ transport abstraction model calculations. Examining the individual terms of the mass balance for the fracture derived in Section C-1, the accumulation term (Eq. C-1) is unchanged by the AFM, because it is based on the storage volume in the fracture, as well as sorption parameters. Storage volumes in the dual-k flow fields are fully defined by the fracture volume fractions and the fluid saturations in the fracture continuum. Fluid saturations are model output from the flow simulations, and no further correction for transport is required for the accumulation term. Likewise, the Darcy velocity in the advection term (Eq. C-2) is fully defined by the flux through the fracture continuum, so no AFM corrections are required for advection either. The diffusion term (Equation C-3) consists of a flux $\theta_m D_m \left.\frac{\partial C_m}{\partial x}\right|_{x=b}$ times an interfacial area, which on geometrical grounds for the simple geometry of the transfer function model is

$d\Delta z$. This interfacial area term, according to the AFM, should be reduced to account for the fact that not all fractures are flowing. (Liu et al. 1998 [DIRS 105729], Eq. 12), gives the following reduction factor for correcting the advective flux term [note: nomenclature from the report by Liu et al. (1998 [DIRS 105729]) is used in this equation]:

$$R = \left(\frac{A_{fm,a}}{A_{fm}}\right)\left(\frac{n_{f,a}}{n_f}\right)\left(\frac{d}{d_a}\right) \quad \text{(Eq. C-38)}$$

Although (Liu et al. 1998 [DIRS 105729]) refer to R as the F-M interface area reduction factor, it is clear from their derivation that the term represents the ratio of the fluxes for the uncorrected and corrected cases, correcting for both the interface area and the transport length scale associated with the distance between the flowing fractures (the third term on the right hand side of this equation). Therefore, in the FEHM simulations, AFM-based adjustments should be applied to both the interface area and the spacing B. The term d/d_a is the adjustment to the fracture spacing, and is accounted for by adjusting the spacing B in the FEHM transport simulations using the following relation (Liu et al. 1998 [DIRS 105729], Eq. 17):

$$\frac{d}{d_a} = S_e^{\gamma} \quad \text{(Eq. C-39)}$$

Thus, the geometric spacing is divided by S_e^{γ} to obtain the spacing between flowing fractures. The interface-area portion of the adjustment consists of the first two terms on the right hand side of Eq. C-38, the first to account for the reduction in wetted area within an individual fracture, and the second to account for the reduction in area associated with a smaller number of wetted fractures. This term can be related to the AFM parameters using Equations 13 and 14 of the report by Liu et al. (1998 [DIRS 105729]):

$$\left(\frac{A_{fm,a}}{A_{fm}}\right)\left(\frac{n_{f,a}}{n_f}\right) = S_e^{1-\gamma} S_e^{\gamma} = S_e \quad \text{(Eq. C-40)}$$

To implement this area reduction term in FEHM, the geometrically defined aperture b is divided by S_e. The adjustment to b is for convenience, and actually arises from the need to adjust the interface area in the fracture transport equation. These adjustment factors have been incorporated into FEHM so that for given AFM model parameters, B and b, input as geometrically defined parameters, are converted to hydrologic parameters for use in the transfer function methodology.

Addendum Cover Page

Complete only applicable items.

QA: QA

1. Total Pages: 192

2. Addendum to (Title):

Particle Tracking Model and Abstraction of Transport Processes

3. DI (including Revision and Addendum No.):

MDL-NBS-HS-000020 REV02 AD01

	Printed Name	Signature	Date
4. Originator	Bruce Robinson		08/16/2007
5. Independent Technical Reviewer	Marsh Lavenue		8/17/07
6. Checker	June Fabryka-Martin		8/17/07
7. QCS/Lead Lab QA Reviewer	Charles D. Beach		8-17-07
8. Responsible Manager/Lead	Clifford Ho		8/17/07
9. Responsible Manager	Stephanie Kuzio		8/17/07

12. Remarks

Change History

13. Revision and Addendum No.	14. Description of Change
REV02 AD01	Update of parameter uncertainty distributions, rerun of Validation runs using new version of code, new representative case model analyses and sensitivity runs.

CONTENTS

Page

ACRONYMS AND ABBREVIATIONS xv

1. PURPOSE 1-1

2. QUALITY ASSURANCE 2-1

3. USE OF SOFTWARE 3-1
   3.1 SOFTWARE TRACKED BY CONFIGURATION MANAGEMENT 3-1
   3.2 EXEMPT SOFTWARE 3-2

4. INPUTS 4-1
   4.1 DIRECT INPUT 4-1
      4.1.1 Unsaturated Zone Flow Parameters 4-4
      4.1.2 Fracture Frequency and Fracture Porosity 4-5
      4.1.3 Matrix Porosity 4-6
      4.1.4 Matrix Diffusion Coefficient 4-6
      4.1.5 Matrix Sorption Coefficient 4-10
      4.1.6 Fracture Dispersivity 4-10
      4.1.7 Radionuclide Sorption onto Colloids 4-11
      4.1.8 Colloid Filtration and Size Exclusion 4-12
      4.1.9 Colloid Retardation in Transport Through Fractures 4-12
   4.2 CRITERIA 4-13
   4.3 CODES, STANDARDS, AND REGULATIONS 4-14

5. ASSUMPTIONS 5-1

6. MODEL DISCUSSION 6-1
   6.1 MODELING OBJECTIVES AND APPROACH 6-1
   6.2 FEATURES, EVENTS, AND PROCESSES INCLUDED IN THE MODEL 6-1
   6.3 THE UNSATURATED ZONE TRANSPORT ABSTRACTION MODEL 6-1
   6.4 THE NUMERICAL REPRESENTATION OF THE UNSATURATED ZONE TRANSPORT ABSTACTION MODEL 6-1
   6.5 UNSATURATED ZONE TRANSPORT ABSTRACTION MODEL INPUTS 6-1
      6.5.1 Pregenerated Flow Fields 6-1
      6.5.2 Dispersivity 6-2
      6.5.3 Matrix Porosity and Rock Density 6-2
      6.5.4 Matrix Sorption Coefficient (mL/g) 6-5
      6.5.5 Matrix Diffusion Coefficient (m^2/s) 6-5
         6.5.5.1 Correlation between Tortuosity, Porosity, and Permeability 6-6
         6.5.5.2 Tortuosity for Unsaturated Media 6-7
         6.5.5.3 Free-Water Diffusion Coefficients 6-7
         6.5.5.4 Uncertainty Treatment for Matrix Diffusion Coefficient 6-10

CONTENTS (Continued)

Page

6.5.6 Fracture Residual Saturation and Active Fracture Model Gamma Parameters (Unitless) ... 6-10
6.5.7 Fracture Porosity, Fracture Spacing (m), and Fracture Aperture (m) ... 6-11
6.5.8 Fracture Surface Retardation Factor (Unitless) ... 6-11
6.5.9 Colloid Filtration at Matrix Interface ... 6-11
6.5.10 Colloid Size Exclusion ... 6-12
6.5.11 Colloid-Size Distribution ... 6-12
6.5.12 Colloid Concentration and Colloid K_c ... 6-12
6.5.13 Fractions of Colloids Traveling Unretarded and Colloid Retardation Factor ... 6-14
6.5.14 Radionuclide Half Lives (Years) and Daughter Products ... 6-14
6.5.15 Repository Radionuclide Release Bins ... 6-15
6.5.16 Radionuclide Collecting Bins at Unsaturated Zone/Saturated Zone Interface ... 6-19
6.6 REPRESENTATIVE-CASE MODEL ... 6-19
6.6.1 Overview ... 6-19
6.6.2 Representative-Case Model Results ... 6-23
6.6.2.1 Statistics of Travel Time and Exit Location ... 6-23
6.6.2.2 Radionuclide Breakthrough Curves ... 6-30
6.6.2.3 Fracture versus Matrix Release ... 6-35
6.6.3 Sensitivity to Flow Parameter Uncertainty ... 6-36
6.6.4 Sensitivity to AFM and Diffusion Parameter Uncertainty ... 6-36
6.7 EVALUATION OF ALTERNATIVE MODELS AND MODEL UNCERTAINTY ... 6-37
6.8 DESCRIPTION OF BARRIER CAPABILITY ... 6-37
6.8.1 Analyses of Barrier Capability ... 6-37
6.8.2 Barrier Capability Simulations and Uncertainty Analyses ... 6-37
6.8.2.1 Travel Time Statistics ... 6-40
6.8.2.2 Barrier Capability Analyses Using the Decay Fraction ... 6-52
6.9 OTHER TSPA IMPLEMENTATION CONSIDERATIONS ... 6-70

7. VALIDATION ... 7-1
7.1 CONFIDENCE BUILDING DURING MODEL DEVELOPMENT TO ESTABLISH THE SCIENTIFIC BASIS AND ACCURACY FOR INTENDED USE ... 7-1
7.2 POSTDEVELOPMENT MODEL VALIDATION TO SUPPORT THE SCIENTIFIC BASIS OF THE MODEL ... 7-1
7.2.1 COMPARISONS WITH DISCRETE FRACTURE MODEL ... 7-1
7.2.1.1 Test of Advective Transport Between Continua ... 7-3
7.2.1.2 Comparisons with Diffusion for Fracture-Dominated Flow ... 7-4
7.2.1.3 Comparisons with Diffusion and Sorption for Intermediate Flow Case ... 7-5
7.2.1.4 Summary of Validation Tests for a Discrete Fracture Model ... 7-10

CONTENTS (Continued)

Page

7.2.2 Comparison with the Dual-k and MINC Model Formulations on a Two-Dimensional Cross-Section Model 7-10
7.2.3 Comparison with T2R3D Process Model for the Three-Dimensional System 7-11
7.2.3.1 Comparisons of FEHM and T2R3D for the Dual-k Conceptual Model 7-13
7.2.3.2 Influence of Diffusion Coefficient and f/m Interaction Alternative Conceptual Model 7-14
7.2.3.3 Tests of the Active Fracture Model Implementation 7-16
7.3 SUMMARY OF VALIDATION ACTIVITIES 7-17

8. CONCLUSIONS 8-1
8.1 SUMMARY OF MODELING ACTIVITY 8-1
8.2 MODEL OUTPUTS 8-18
8.2.1 Developed Output 8-18
8.2.2 Other Outputs 8-19
8.3 HOW THE APPLICABLE ACCEPTANCE CRITERIA ARE ADDRESSED 8-20

9. INPUTS AND REFERENCES 9-1
9.1 DOCUMENTS CITED 9-1
9.2 CODES, STANDARDS, REGULATIONS, AND PROCEDURES 9-3
9.3 SOURCE DATA, LISTED BY DATA TRACKING NUMBER 9-4
9.4 OUTPUT DATA, LISTED BY DATA TRACKING NUMBER 9-5
9.5 SOFTWARE CODES 9-6

APPENDIX A MATRIX DIFFUSION COEFFICIENTS A-1

APPENDIX B DERIVATION OF WATER TABLE COLLECTING BINS B-1

APPENDIX C DERIVATION OF FRACTURE-MATRIX INTERACTION SUBMODEL AND GENERATION OF TRANSFER FUNCTIONS C-1

APPENDIX D SUPPLEMENTARY UNSATURATED ZONE TRANSPORT SIMULATION RESULTS D-1

INTENTIONALLY LEFT BLANK

FIGURES

Page

4-1. Plot of Measured $Log_{10}(\tau)$ versus Porosity for the Qualified and Unqualified Data 4-8

4-2. Plot of Measured $Log_{10}(\tau)$ versus Log_{10}(Permeability, m^2) for the Qualified and Unqualified Data 4-9

4-3. Plot of Measured $Log_{10}(\tau)$ versus Predicted $Log_{10}(\tau)$ for the Qualified and Unqualified Data 4-9

6-14. Repository Nodes Colored by Percolation Bin for the Glacial-Transition, 10th Percentile Flow Field 6-17

6.6.2-1. Contour Maps of (a) the Minimum Travel Time, (b) the Mean Travel Time, and (c) the Maximum Travel Time for Particles Released at All Repository Nodes under Glacial-Transition, 10th Percentile Infiltration Scenario, and Conservative Species without Decay and Matrix Diffusion 6-24

6.6.2-2. Contour Maps of Mean Displacement (in meters) of Particles (a) in the *x* Direction, and (b) in the *y* Direction for Particles Released at All Repository Nodes under Glacial Transition, 10th Percentile Infiltration Scenario and Conservative Species. 6-26

6.6.2-3. Comparison of Particle Release Locations (Left) and Exit Locations in Terms of Percolation Bin Assignment (middle) or Mean Travel Time (right) for the Glacial-Transition, 10th percentile Infiltration Scenario 6-28

6.6.2-4. Comparison of the Bin-Averaged Log Travel Time for Particles Released at All Repository Nodes for Three Climate Conditions (a) Present-Day, b) Monsoon, and c) Glacial-Transition) and Four Infiltration Scenarios, and Conservative Species without Decay and Matrix Diffusion 6-29

6.6.2-5 Normalized Cumulative Breakthrough Curves of 14 Radionuclides with Simple Decay for the Glacial-Transition 10th Percentile Infiltration Condition and Representative Parameter Values 6-32

6.6.2-6. Normalized Cumulative Breakthrough Curves of 6 Irreversible Fast Colloids and 6 Irreversible Slow Colloids for the Glacial-Transition 10th Percentile Infiltration Condition and Representative Parameter Values 6-33

6.6.2-7. Normalized Cumulative Breakthrough Curves of 4 Radionuclides (^{235}U, ^{233}U, ^{236}U, and ^{230}Th) with One Decay Chain for the Glacial-Transition 10th Percentile Infiltration Condition and Representative Parameter Values 6-34

6.6.2-8. Comparison of Normalized Cumulative Breakthrough Curves of ^{99}Tc for Particles Released at Fracture Node or Matrix Node for the Glacial-Transition, 10th Percentile Infiltration Scenario, Representative Parameter Values 6-36

6.8.2-1. Comparison of Mean Travel Time of ^{99}Tc as a Function of Matrix Diffusion Coefficient under Glacial-Transition Climate Conditions for the dual-k Model 6-41

6.8.2-2. Comparison of Mean Travel Time of ^{99}Tc as a Function of Matrix Diffusion Coefficient under Glacial-Transition Climate Conditions for the DFM Model 6-42

6.8.2-3. Mean Travel Time of ^{237}Np as a Function of Matrix Diffusion Coefficient and Sorption Coefficient for the Glacial-Transition Climate Condition, dual-k Model, Northern Release Location 6-44

FIGURES (Continued)

Page

6.8.2-4. Mean Travel Time of ^{237}Np as a Function of Matrix Diffusion Coefficient and Sorption Coefficient for the Glacial-Transition Climate Condition, dual-k Model, Southern Release Location 6-45
6.8.2-5. Mean Travel Time of ^{237}Np as a Function of Matrix Diffusion Coefficient and Sorption Coefficient for the Glacial-Transition Climate Condition, DFM Model, Northern Release Location 6-46
6.8.2-6. Mean Travel Time of ^{237}Np as a Function of Matrix Diffusion Coefficient and Sorption Coefficient for the Glacial-Transition Climate Condition, DFM Model, Southern Release Location 6-47
6.8.2-7. Mean Travel Time of ^{240}Pu as a Function of Matrix Diffusion Coefficient and Sorption Coefficient for the Glacial-Transition Climate Condition, dual-k Model, Northern Release Location 6-49
6.8.2-8. Mean Travel Time of ^{240}Pu as a Function of Matrix Diffusion Coefficient and Sorption Coefficient for the Glacial-Transition Climate Condition, dual-k Model, Southern Release Location 6-50
6.8.2-9. Mean Travel Time of ^{240}Pu as a Function of Matrix Diffusion Coefficient and Sorption Coefficient for the Glacial-Transition Climate Condition, DFM Model, Northern Release Location 6-51
6.8.2-10. Mean Travel Time of ^{240}Pu as a Function of Matrix Diffusion Coefficient and Sorption Coefficient for the Glacial-Transition Climate Condition, DFM Model, Southern Release Location 6-52
6.8.2-11. Normalized ^{99}Tc Concentration (Decay Fraction, Computed from Travel Time Distributions) as a Function of Matrix Diffusion Coefficient for Glacial-Transition Climate Condition, dual-k Model, (a) Northern Release Location, (b) Southern Release Location 6-54
6.8.2-12. Normalized ^{99}Tc Concentration (Decay Fraction, Computed from Travel Time Distributions) as a Function of Matrix Diffusion Coefficient for Glacial-Transition Climate Condition, DFM Model, (a) Northern Release Location, (b) Southern Release Location 6-55
6.8.2-13. Normalized ^{14}C Concentration (Decay Fraction, Computed from Travel Time Distributions) as a Function of Matrix Diffusion Coefficient for Glacial-Transition Climate Condition, dual-k Model, (a) Northern Release Location, (b) Southern Release Location 6-56
6.8.2-14. Normalized ^{14}C Concentration (Decay Fraction, Computed from Travel Time Distributions) as a Function of Matrix Diffusion Coefficient for Glacial-Transition Climate Condition, DFM Model, (a) Northern Release Location, (b) Southern Release Location 6-57
6.8.2-15. Normalized ^{237}Np Concentration (Decay Fraction, Computed from Travel Time Distributions) as a Function of Matrix Diffusion Coefficient and Sorption Coefficient for the Glacial-Transition Climate Conditions, dual-k Model, Northern Release Location 6-58

FIGURES (Continued)

Page

6.8.2-16. Normalized ^{237}Np Concentration (Decay Fraction, Computed from Travel Time Distributions) as a Function of Matrix Diffusion Coefficient and Sorption Coefficient for the Glacial-Transition Climate Conditions, dual-k Model, Southern Release Location 6-59
6.8.2-17. Normalized ^{237}Np Concentration (Decay Fraction, Computed from Travel Time Distributions) as a Function of Matrix Diffusion Coefficient and Sorption Coefficient for the Glacial-Transition Climate Conditions, DFM Model, Northern Release Location 6-60
6.8.2-18. Normalized ^{237}Np Concentration (Decay Fraction, Computed from Travel Time Distributions) as a Function of Matrix Diffusion Coefficient and Sorption Coefficient for the Glacial-Transition Climate Conditions, DFM Model, Southern Release Location 6-61
6.8.2-19. Normalized ^{240}Pu Concentration (Decay Fraction, Computed from Travel Time Distributions) as a Function of Matrix Diffusion Coefficient and Sorption Coefficient for the Glacial-Transition Climate Conditions, dual-k Model, Northern Release Location 6-63
6.8.2-20. Normalized ^{240}Pu Concentration (Decay Fraction, Computed from Travel Time Distributions) as a Function of Matrix Diffusion Coefficient and Sorption Coefficient for the Glacial-Transition Climate Conditions, dual-k Model, Southern Release Location 6-64
6.8.2-21. Normalized ^{240}Pu Concentration (Decay Fraction, Computed from Travel Time Distributions) as a Function of Matrix Diffusion Coefficient and Sorption Coefficient for the Glacial-Transition Climate Conditions, DFM Model, Northern Release Location 6-65
6.8.2-22. Normalized ^{240}Pu Concentration (Decay Fraction, Computed from Travel Time Distributions) as a Function of Matrix Diffusion Coefficient and Sorption Coefficient for the Glacial-Transition Climate Conditions, DFM Model, Southern Release Location 6-66
6.8.2-23. Mean Travel Time of $Ic^{240}Pu$ as a Function of Colloid Retardation Factor for the Glacial-Transition Climate Condition 6-68
6.8.2-24. Normalized Concentration of $Ic^{240}Pu$ (Decay Fraction, Computed from Travel Time Distributions) as a Function of Colloid Retardation Factor for the Glacial-Transition Climate Condition 6-69

7-1. Particle-Tracking Abstraction Model Behavior for Advective Transport Between the Fracture and Matrix Continua: No Diffusion or Sorption, Solute Injected into the Fracture, Compared to Theoretical Results 7-3
7-2. Comparison of Discrete Fracture Model and Particle-Tracking Abstraction Model: Non-Sorbing Solute Injected into the Fracture for Different Values of Diffusion Coefficient 7-4
7-3. Comparison of Discrete Fracture Model and Particle-Tracking Abstraction Model: Non-Sorbing Solute Injected into the Fracture for Different Values of Diffusion Coefficient 7-5

FIGURES (Continued)

Page

7-4. Comparison of Discrete Fracture Model and Particle-Tracking Abstraction Model: Sorbing Solute Injected into the Fracture for Different Values of Diffusion Coefficient 7-6

7-5. Comparison of Discrete Fracture Model and Particle-Tracking Abstraction Model: Sorbing Solute Injected into the Fracture for Different Values of Sorption Coefficient 7-7

7-6. Comparison of Discrete Fracture Model and Particle-Tracking Abstraction Model: Sorbing Solute Injected into the Fracture for Different Values of Sorption Coefficient 7-8

7-7. Comparison of Discrete Fracture Model and Particle-Tracking Abstraction Model: Non-Sorbing Solute Injected into the Matrix for Different Values of Diffusion Coefficient 7-9

7-8. Comparison of Discrete Fracture Model and Particle-Tracking Abstraction Model: Non-Sorbing Solute Injected into the Fracture for Different Numbers of Grid Cells in the Flow Path 7-10

7-9. Comparison of Particle-Tracking Model with T2R3D Models for a Two-Dimensional, Mountain-Scale Model: with (and without) Diffusion, for dual-k and DFM Formulations for the f/m Interaction Model, Present-Day Mean Infiltration, Representative Parameter Values, and Present-Day Water Table 7-11

7-10. Comparison of Breakthrough Curves for ^{99}Tc for T2R3D and the Unsaturated Zone Transport Abstraction Model: Simulations for Different Present-Day Infiltration Rate Scenarios (Lower, Mean, and Upper), Representative Parameter Values, and Present-Day Water Table 7-13

7-11. Comparison of Breakthrough Curves for ^{99}Tc for T2R3D and the Unsaturated Zone Transport Abstraction Model: Present-Day Mean Infiltration Scenario, Diffusion in FEHM Ranging from No Diffusion to High Values, Representative Parameter Values, and Present-Day Water Table 7-14

7-12. Breakthrough Curves for ^{99}Tc Using the Unsaturated Zone Transport Abstraction Model to Investigate the Role f/m Interaction Conceptual Model: Simulations for Different Glacial-Transition Infiltration Rate Scenarios (10%, 30%, 50%, and 90%), Representative Parameter Values, and Glacial-Transition Water Table 7-15

7-13. Breakthrough Curves for Conservative Solute Using the Unsaturated Zone Transport Abstraction Model to Investigate the Role of AFM γ Parameter: dual-k ACM, Simulation for Different Values of Gamma in Rock Units Beneath the Repository, Present-Day Mean Infiltration, Representative Parameter Values, and Present-Day Water Table 7-16

7-14. Breakthrough Curves for Conservative Solute Using the Unsaturated Zone Transport Abstraction Model to Investigate the Role of AFM γ Parameter: Discrete Fracture ACM, Simulation for Different Values of Gamma in Rock Units Beneath the Repository, Present-Day Mean Infiltration, Representative Parameter Values, and Present-Day Water Table 7-17

FIGURES (Continued)

Page

A-1. Cumulative Probability Distribution for the Normalized Residuals of Tortuosity A-12

B-1. List of Files Used to Develop the Water Table Binning B-1

D.1-1. Comparison of Mean Travel Times for Different Infiltration Scenarios of Under Present-Day Climate Conditions, and Representative Parameter Values D-2

D.1-2. Comparison of Mean Travel Times for Different Infiltration Scenarios of Monsoon Climate Conditions, Representative Parameter Values D-3

D.1-3. Comparison of Mean Travel Times for Different Infiltration Scenarios of Glacial-Transition Climate Conditions, Representative Parameter Values D-4

D.2-1. Normalized Cumulative Breakthrough Curves of Decay Chain $^{243}Am \rightarrow {}^{239}Pu \rightarrow {}^{235}U \rightarrow {}^{231}Pa$ for the Glacial-Transition, 10th Percentile Infiltration Condition, Representative Parameter Values, Northern and Southern Release Nodes D-5

D.2-2. Normalized Cumulative Breakthrough Curves of Decay Chain $^{239}Pu \rightarrow {}^{235}U \rightarrow {}^{231}Pa$ for the Glacial-Transition, 10th Percentile Infiltration Condition, Representative Parameter Values, Northern and Southern Release Nodes D-6

D.2-3. Normalized Cumulative Breakthrough Curves of Decay Chain $^{241}Am \rightarrow {}^{237}Np \rightarrow {}^{233}U \rightarrow {}^{229}Th$ for the Glacial-Transition, 10th Percentile Infiltration Condition, Representative Parameter Values, Northern and Southern Release Nodes D-6

D.2-4. Normalized Cumulative Breakthrough Curves of Decay Chain $^{237}Np \rightarrow {}^{233}U \rightarrow {}^{229}Th$ for the Glacial-Transition, 10th Percentile Infiltration Condition, Representative Parameter Values, Northern and Southern Release Nodes D-7

D.2-5. Normalized Cumulative Breakthrough Curves of Decay Chain $^{242}Pu \rightarrow {}^{238}U \rightarrow {}^{234}U \rightarrow {}^{230}Th \rightarrow {}^{226}Ra$ for the Glacial-Transition, 10th Percentile Infiltration Condition, Representative Parameter Values, Northern and Southern Release Nodes D-7

D.2-6. Normalized Cumulative Breakthrough Curves of Decay Chain $^{240}Pu \rightarrow {}^{236}U \rightarrow {}^{232}Th$ for the Glacial-Transition, 10th Percentile Infiltration Condition, Representative Parameter Values, Northern and Southern Release Nodes D-8

D.2-7. Normalized Cumulative Breakthrough Curves of Decay Chain $^{238}Pu \rightarrow {}^{234}U \rightarrow {}^{230}Th \rightarrow {}^{226}Ra$ for the Glacial-Transition, 10th Percentile Infiltration Condition, Representative Parameter Values, Northern and Southern Release Nodes D-8

D.2-8. Normalized Cumulative Breakthrough Curves of Decay Chain $^{238}U \rightarrow {}^{234}U \rightarrow {}^{230}Th \rightarrow {}^{226}Ra$ for the Glacial-Transition, 10th Percentile Infiltration Condition, Representative Parameter Values, Northern and Southern Release Nodes D-9

D.2-9. Normalized Cumulative Breakthrough Curves of Decay Chain $^{234}U \rightarrow {}^{230}Th \rightarrow {}^{226}Ra$ for the Glacial-Transition, 10th Percentile Infiltration Condition, Representative Parameter Values, Northern and Southern Release Nodes D-9

INTENTIONALLY LEFT BLANK

TABLES

		Page
3-1.	Qualified Software Used in This Report	3-1
3-2.	Exempt Software	3-2
4-1.	Transport Input Parameters for the Unsaturated Zone Transport Abstraction Model	4-2
4.2-1.	Condition Reports Addressed in this Addendum	4-13
6-1.	List of Steady State Flow Field Names for the TSPA Model and the Original Data Source	6-1
6-5.	Matrix Porosities Used in the Unsaturated Zone Transport Abstraction Model	6-3
6-6.	Matrix Rock Density Values	6-4
6.5.5-1.	Average Tortuosities	6-7
6.5.5-2.	Free-Water Diffusion Coefficients	6-7
6.5.5-3.	Representative Values of Matrix Diffusion Coefficients	6-8
6-21.	Colloid Concentration Distribution	6-12
6-22.	Radionuclide Sorption Coefficient (mL/g) onto Colloids	6-12
6-25.	List of Radionuclides Simulated in Compliance Model	6-14
6-26.	Definition of Repository Release Bins	6-18
6.6.1-1.	Selected Parameter Values for Representative-Case Unsaturated Zone Model	6-20
6.8.2-1	Diffusion Coefficient Values as a Function of CDF Interval for 11 Cases Used in Sensitivity Analysis	6-39
6.8.2-2	K_d Values as a Function of CDF Interval for 11 Cases Used in Sensitivity Analysis	6-40
7-1.	Parameter Values for Discrete Fracture Model Test Suite	7-2
8-1.	Unsaturated Zone Transport Abstraction Model Input Files	8-2
8-2.	Unsaturated Zone Transport Epistemically Uncertain Input Parameters Found in TSPA Model GoldSim-Generated UZ_PARAMS_MULTI_LA_COMPLIANCE Files	8-5
A-1.	Hydrological Properties and Tortuosities of the Model Units between the Repository and the Water Table	A-4
A-2.	Rock Group 1 Tortuosities	A-5
A-3.	Rock Group 2 Tortuosities	A-5
A-4.	Rock Group 3 Tortuosities	A-6
A-5.	Rock Group Average Tortuosities	A-6
A-6.	Radioelements, Aqueous Species, and Available Diffusion Data	A-7
A-7.	(a) Atomic Radii; (b) Estimated Radii of Radionuclide Molecular Species, Analogue Molecular Species, and Correction Factors to Estimate Molar Ionic Conductivities for the Radionuclide Molecular Species from Values for the Analogue Molecular Species	A-9

TABLES (Continued)

Page

A-8. Free-Water Diffusion Coefficients A-10

C-1. List of Parameter Values Used to Compute Transfer Function Curves C-2

ACRONYMS AND ABBREVIATIONS

ACM	alternative conceptual model
AFM	active fracture model
CDF	cumulative distribution function
CML	carboxylate modified polystyrene latex
CR	condition report
DFM	discrete fracture model
dll	dynamic link library
dual-k	dual permeability
EBS	Engineered Barrier System
FEHM	finite-element heat and mass model
f/m	fracture/matrix
QA	quality assurance
TDMS	Technical Data Management System
TSPA	total system performance assessment
TSPA-LA	total system performance assessment for the license application
TSw	Topopah Spring welded unit
TWP	technical work plan
UZ	unsaturated zone
YMP	Yucca Mountain Project

INTENTIONALLY LEFT BLANK

1. PURPOSE

The purpose of this addendum is to document changes made to the abstraction model being used in total system performance assessment (TSPA) model calculations for radionuclide transport in the unsaturated zone (UZ). This is required to update parameter distributions and inputs, to update the validation of the model to the current version of the software, and to present new model calculation results. The activities in this addendum are based on work plans outlined in *Technical Work Plan for: Unsaturated Zone Flow, Drift Seepage and Unsaturated Zone Transport Modeling* (BSC 2006 [DIRS 177465]). The following is a list of items from the technical work plan (TWP) (BSC 2006 [DIRS 177465] Section 1, Item 8) and the corresponding disposition of the work in this addendum or elsewhere:

- *Update matrix diffusion in the unsaturated zone transport abstraction model.* This activity was accomplished by generating two sets of transfer function curves for the matrix diffusion submodel (Appendix C), one assuming the dual-k (dual-permeability) conceptual model and the other assuming the discrete fracture conceptual model. For the purposes of performing sensitivity analyses, both of these submodels are invoked in the sensitivity analyses presented in Section 6.8. For the purposes of defining the unsaturated zone transport model for the TSPA compliance model, the dual-k model is used exclusively due to its approved validation status.

- *Update FEHM software to address specific technical issues.* The code changes, up to and including the current version of FEHM[1] (V. 2.24-01 STN: 10086-2.24-01-00 [DIRS 179419]), have addressed all issues outlined in the TWP (BSC 2006 [DIRS 177465]), including correcting a specific issue related to Neptunium transport, problems with occasional negative travel times in a cell, inflexible assignment of particles leading to TSPA model oscillations, and updates to the logic for specifying external flow-field files.

- *Develop abstraction approach for colloid filtration as a kinetic process.* Work associated with the revision to the colloid transport model to incorporate kinetics effects was performed and documented as part of the Performance Margin Analysis and appears in *Total System Performance Assessment Model /Analysis for the License Application* (SNL 2007 [DIRS 178871]).

- *Integrate software into abstraction model to allow dynamic sampling of future water table rise during execution of TSPA, and define the distribution of water table elevations.* This work was performed and documented as part of the Performance Margin Analysis and appears in *Total System Performance Assessment Model /Analysis for the License Application* (SNL 2007 [DIRS 178871]).

[1] FEHM = finite-element heat and mass model.

- *Revise method for computing effective matrix diffusion coefficients to account for averaging of spatial variability over the domain.* The TWP (BSC 2006 [DIRS 177465]) specified two alternative approaches for performing this work. The method presented in Section 6.5.5 was used to fulfill this part of the work. This method retains the approach of dividing the domain into rock groups of similar diffusion properties and assigns diffusion coefficients based on an analysis of a correlation between rock properties and diffusion coefficients. Differences in diffusion coefficients for each radioelement due to molecular size and speciation differences are also included in the analysis.

- *Revise software to allow a user-defined minimum number of particles per time step.* FEHM software was updated to address this issue (see second bulleted item above).

- *Address data qualification issues associated with data used to develop the correlation of matrix diffusion coefficients to permeability and moisture content.* This issue, documented in CR 7260, is resolved in the qualification activity presented in Section 4.1.4.

- *Revise representative case analyses, sensitivity analyses, and validation cases to reflect software modifications and model and parameter changes.* Representative-case analyses are presented in Section 6.6, sensitivity analyses are presented in Section 6.8, and validation results are presented in Section 7.

Based on this list of activities, deviations from the TWP include the following items:

- This work is documented as an addendum rather than a revision. This deviation has no impact on the model or associated analyses.

- Some of the work specified in the TWP, such as the diffusion model (specifically the use of the discrete fracture model (DFM)), the colloid transport model (incorporation of kinetics effects), and the water table rise models, has been performed and documented in the Performance Margin Analysis and is included in *Total System Performance Assessment Model /Analysis for the License Application* (SNL 2007 [DIRS 178871]). Work specified in the TWP that has not been performed includes the implementation of a kinetic model for colloid filtration and the implementation of a matrix diffusion model in which the diffusion coefficient varies at each node, as a function of the rock and fluid properties at that node. For these two deviations, it was decided that changes implemented in the Performance Margin Analysis provided a better, more-defensible approach to the topics of matrix diffusion and colloid transport. Therefore, these activities were bypassed in favor of better approaches.

- The TWP (BSC 2006 [DIRS 177465]) referred to a particular version of the FEHM computer code, which has changed subsequent to the writing of the TWP. This represents a change to the code numbering only, rather than a meaningful change to the content of the work. Thus, this deviation has no impact on the model or associated analyses.

This addendum provides updated parameter distributions for the matrix diffusion coefficients, colloid transport parameters, the active fracture model gamma parameter, and other rock properties, along with updated data sources for these parameters, plus the flow fields used in the model. The addendum also presents validation model runs for FEHM V 2.24-01 to be used in the TSPA for the license application (TSPA-LA) model, thus presenting new model calculations and uncertainty analyses. Along with these new validation runs, several code and model input fixes were made and, in the case of the code fixes, documented in the software documentation for FEHM. Finally, new output DTNs are prepared that are direct inputs to the TSPA-LA model. These files are described in Section 8.

INTENTIONALLY LEFT BLANK

2. QUALITY ASSURANCE

Development of this addendum has been determined to be subject to the Yucca Mountain Project (YMP) Quality Assurance (QA) Program, as indicated in *Technical Work Plan for: Unsaturated Zone Flow, Drift Seepage and Unsaturated Zone Transport Modeling* (BSC 2006 [DIRS 177465], Section 8.1). Approved QA procedures identified in the TWP (BSC 2006 [DIRS 177465], Section 4) were used to conduct and document the activities described in this report. As this activity was transitioned to the Lead Laboratory QA Program, the corresponding Lead Laboratory procedures were used. The methods used to control the electronic management of data (BSC 2006 [DIRS 177465], Section 8.4) during the analysis and documentation activities are described in IM-PRO-002, *Control of the Electronic Management of Information.* The model activities and associated calculations herein were conducted and documented following SCI-PRO-006, *Models.*

INTENTIONALLY LEFT BLANK

3. USE OF SOFTWARE

3.1 SOFTWARE TRACKED BY CONFIGURATION MANAGEMENT

The computer codes used directly in this addendum are summarized in Table 3-1. The computer software code on which the UZ transport abstraction model is based is FEHM V. 2.24-01 (STN: 10086-2.24-01-00 [DIRS 179419]). This software was developed for use in this and other YMP applications and has been tailored for this application through the formal software development process. The validation simulations presented in Section 7 demonstrate that the software is appropriate for use in simulating unsaturated zone radionuclide transport, and the use of the software in this addendum is within its validation range. The qualification status of this and other software is indicated in the electronic Document Input Reference System (DIRS) database. All software was obtained from Software Configuration Management and is appropriate for the application. Qualified codes were used only within the range of validation. Computer files for this report are located in data tracking numbers and identified in the respective discussions in Section 6; the outputs are listed in Section 8.2. In addition, FEHM V. 2.24 (STN: 10086-2.24-00 [DIRS 178965]) (the version of the FEHM code used to generate the transfer function curves) was fully qualified and acceptable for generating the transfer function curves, in advance of the V. 2.24-01 being qualified. Also included in Table 3-1 is fehm2post V. 1.0 (STN: 11031-1.0-01 [DIRS 181225]), which is unchanged from the previous version but included to correct an incorrect software tracking number in the parent report. All other specified software in this category remains unchanged.

Table 3-1. Qualified Software Used in This Report

Software Title/Version (v)	Software Tracking Number	Platform/Operating System	Code Usage	DIRS
FEHM V. 2.24	10086-2.24-00	PC/Windows 2000 and XP SUN/OS 5.9	Generation of transfer function curves	[DIRS 178965]
FEHM V. 2.24-01	10086-2.24-01-00	PC/Windows 2000, 2003, and SUN/OS 5.9	Simulation of particle tracking base-case runs; abstraction model simulations	[DIRS 179419]
PARTICLE_STAT V. 1.0	11241-1.0-00	SUN/OS 5.9	Code to postprocess particle-tracking results	[DIRS 181317]

Table 3-1. Qualified Software Used in This Report (Continued)

Software Title/Version (v)	Software Tracking Number	Platform/Operating System	Code Usage	DIRS
fehm2post V. 1.0	11031-1.0-01	SUN/OS 5.9	Executes multiple FEHM simulations along with pre- and postprocessing runs; used to execute the individual simulations and generation of transfer function curves used in the TSPA-LA UZ transport abstraction model	[DIRS 181225]
DISCRETE_TF V. 1.1	11033-1.1-00	SUN/OS 5.9	Postprocessing of discrete fracture model results to convert results to transfer functions	[DIRS 165742]
ppptrk V. 1.0	11030-1.0-01.	SUN, SunOS 5.9	Postprocessing of particle-tracking results to obtain breakthrough curves for the validation runs	[DIRS 181269]

NOTE: FEHM = finite-element heat and mass (model).

3.2 EXEMPT SOFTWARE

Commercial off-the-shelf software used in support of this report is listed in Table 3-2.

Table 3-2. Exempt Software

Software Name and Version (V)	Software Tracking Number	Description	Computer and Platform Identification
Microsoft Excel 2003	N/A	This standard spreadsheet package was used to perform simple spreadsheet calculations using built-in formulas and functions.	IBM PC, Windows 2000 and XP Operating System
Techplot 360	N/A	The commercial software, Techplot 360, was used for plotting the results of breakthrough curve simulations. Only built-in standard functions in this software were used. No software routines or macros were used with this software to prepare this report. The output was visually checked for correctness.	IBM PC, Windows 2000 and XP Operating Systems

4. INPUTS

4.1 DIRECT INPUT

Data and parameters used in this report as direct inputs to the unsaturated zone transport abstraction model include:

- Numerical grid for the unsaturated zone transport abstraction model (Table 8-1)
- Unsaturated zone flow field for the prevailing climate (Table 6-1)
- Unsaturated zone rock properties (Table 4-1)
  - Matrix porosity
  - Fracture porosity and fracture frequency
  - Active fracture model (AFM) γ parameter
  - Fracture residual saturation
  - Rock density.

- Unsaturated zone radionuclide transport parameters (Table 4-1)
  - Fracture dispersivity
  - Matrix diffusion coefficient
  - Matrix sorption coefficient
  - Colloid size distribution
  - Colloid size-exclusion factors at fracture-matrix interface
  - Colloid filtration factors at matrix interfaces
  - Colloid concentration
  - Radionuclide sorption coefficient onto colloid
  - Colloid retardation factor.

- Repository radionuclide release bins (Section 6.5.15)

- Radionuclide half-lives (Table 4-1).

The parameters listed in Table 4-1 are inputs to the unsaturated zone transport abstraction model. The values of those parameters affect the strength of the transport mechanism to which those parameters are related. The values of the parameters vary from layer to layer, as do the distributions. Rock properties (rock density, fracture porosity, spacing, aperture, AFM γ parameter, and fracture residual saturation) are used as inputs to the unsaturated zone transport abstraction model. The validity and uncertainty of those parameters are discussed in the corresponding parameter source documents listed in Table 4-1. The influence of these parameter uncertainties on system performance will be studied in TSPA multiple-realization runs.

Radionuclide transport properties are used in FEHM for simulating the transport processes of radionuclides in the unsaturated fracture media from the repository downward to the water table.

Colloid size distribution, concentration, sorption coefficient, size exclusion, filtration factors, and retardation factors are input parameters to FEHM for simulating colloid-facilitated radionuclide transport in fractured media. Those data are functions of colloid and rock properties and vary from layer to layer.

The uncertainty and validity of each parameter are addressed in the corresponding documents listed in the parameter source column in Table 4-1 and are also discussed in subsequent sections.

Table 4-1. Transport Input Parameters for the Unsaturated Zone Transport Abstraction Model

Parameter Name (Section Discussed)	Parameter Source	DTN	Parameter Value(s)	Units	Distribution (or single value if fixed)
Matrix porosity	BSC 2004 [DIRS 170038]	LB0207REVUZPRP.002 [DIRS 159672], *hydropropos_fin.xls*	Varies from layer to layer	None	Fixed
Rock density	BSC 2004 [DIRS 170038]	LB0207REVUZPRP.002 [DIRS 159672], *hydropropos_fin.xls*	Varies from layer to layer	kg/m^3	Single value
Fracture porosity	BSC 2004 [DIRS 170038]	LB0205REVUZPRP.001 [DIRS 159525], *FRACTURE_PROPERTY.xls* LB0207REVUZPRP.001 [DIRS 159526], *faultprops_2002.xls*	Varies from layer to layer	None	Beta distribution; layers are grouped together based on similar rock properties
Fracture frequency	BSC 2004 [DIRS 170038]	LB0205REVUZPRP.001 [DIRS 159525], *FRACTURE_PROPERTY.xls* LB0207REVUZPRP.001 [DIRS 159526], *faultprops_2002.xls*	Varies from layer to layer	m^{-1}	Log-normal distribution
Active fracture model gamma parameter	SNL 2007 [DIRS 175177]; BSC 2004 [DIRS 170035]; BSC 2004 [DIRS 169861]	LB0611MTSCHP10.001 [DIRS 178586], *CalibratedMountainScaleParameters_R218For10Case.doc* and LB0212C14INFIL.002 [DIRS 179300], *C14_SD12_age.xls*	Single value for all rock units at or below the repository	None	Uniform distribution
Fracture residual saturation	BSC 2004 [DIRS 169857]	LB0207REVUZPRP.001 [DIRS 159526], *faultprops_2002.xls*	0.01	None	Fixed

Table 4-1. Transport Input Parameters for the Unsaturated Zone Transport Abstraction Model (Continued)

Parameter Name (Section Discussed)	Parameter Source	DTN	Parameter Value(s)	Units	Distribution (or single value if fixed)
Matrix diffusion coefficient	Lide 1992 [DIRS 166224] Slater 1965 [DIRS 179613] SNL 2007 [DIRS 177418] Sato et al. 1996 [DIRS 163213] Cutter 1989 [DIRS 178861] Baes and Mesmer 1986 [DIRS 100702] Reimus et al. 2007 [DIRS 179246] Bird et al. 1960 [DIRS 103524] SNL 2007 [DIRS 175177]	MO0005PORWATER.000 [DIRS 150930] LB0208UZDSCPMI.001 [DIRS 161285] LB0611MTSCHP10.001 [DIRS 178586] LB0207REVUZPRP.002 [DIRS 159672] LB06123DPDUZFF.001 [DIRS 178587]	Parameter values are sampled at run time	m^2/s	Normal distribution for log of diffusive tortuosity. Diffusion coefficient is the product of diffusive tortuosity and free water diffusion coefficient. Free water diffusion coefficient is taken to be fixed, with no uncertainty.
Matrix sorption coefficient	SNL 2007 [DIRS 177396]	LA0408AM831341.001 [DIRS 171584] LB0701PAKDSESN.001 [DIRS 179299]	Sorption coefficients sampled based on the given distribution	mL/g	Distribution type varies with radioelement
Colloid concentration distribution	SNL 2007 [DIRS 177423]	MO0701PAGROUND.000 [DIRS 179310], *DTN_Groundwater_REV03.doc*	Concentration will be sampled based on the given distribution	mg/L	Cumulative distribution
Radionuclide sorption coefficient onto colloid	SNL 2007 [DIRS 177423]	MO0701PASORPTN.000 [DIRS 180391], *DTN_Kds_Pu_Am_Th_Pa_Cs_REV03.doc*, Table 1-3 MO0701PAKDSUNP.000 [DIRS 180392], *DTN_Kds_U_Np_Sn_Ra_REV03.doc*, Table 1-2	Values will be sampled based on the given distribution	mL/g	Uniform distribution parameter range depends on the type of radionuclides
Colloid size distribution	N/A	LL000122051021.116 [DIRS 142973]	Parameter values are sampled at run time	None	Cumulative distribution
Colloid filtration factors	N/A	LA0003MCG12213.002 [DIRS 147285], Table S00163_002	Cumulative probabilities of a particle being filtered at matrix interface; varies from layer to layer	None	Fixed values but varies with layers

Table 4-1. Transport Input Parameters for the Unsaturated Zone Transport Abstraction Model (Continued)

Parameter Name (Section Discussed)	Parameter Source	DTN	Parameter Value(s)	Units	Distribution (or single value if fixed)
Colloid size-exclusion factors	N/A	LA0003MCG12213.002 [DIRS 147285], Table S00163_001	Probability of a colloid being excluded at fracture-matrix interface; varies from layer to layer	None	Fixed values but vary from layer to layer
Fractions of colloid traveling unretarded	BSC 2004 [DIRS 170006]	LA0303HV831352.003 [DIRS 165624], *Unretarded_fraction.txt*	Varies with transport time	None	Fractions of colloids traveling unretarded are given
Colloid retardation factor	BSC 2004 [DIRS 170006]	LA0303HV831352.002 [DIRS 163558], *Volcanics_retardation.xls*	Sampled statistical values	None	Cumulative distribution
Fracture dispersivity	SNL 2007 [DIRS 177394]	LA0303PR831231.005 [DIRS 166259], *AMR_Simple_Calcs.xls*, Table 28	10	m	Fixed
Radionuclide half-lives	Parrington et al. 1996 [DIRS 103896] and Singh 2002 [DIRS 164741]	N/A: Accepted data	Varies for each radionuclide	yr	Fixed value for each radionuclide

4.1.1 Unsaturated Zone Flow Parameters

The unsaturated zone flow data set provides the hydrologic properties needed to calculate the flowing fracture spacing based on the AFM (Liu et al. 1998 [DIRS 105729], Equation 17). The ratio of the geometric fracture spacing to the flowing fracture spacing is equated to the normalized fracture water saturation raised to an exponent that is the active fracture parameter (Liu et al. 1998 [DIRS 105729], Equation 17). The fracture residual saturation is a uniform value of 0.01 for all climate and infiltration scenarios as given in DTN: LB0207REVUZPRP.001 [DIRS 159526]. Because the flow model computes water flux using the normalized water saturation (SNL 2007 [DIRS 175177], Appendix A), the uniform value with no uncertainty is appropriate. The AFM gamma parameter is inferred, rather than obtained directly, from a measured input (see Section 6.5.6 for an explanation of the rationale for the selection of the parameter distribution for gamma).

Justification for the Use of Information from BSC 2004 [DIRS 169861] for Developing the AFM γ Parameter Uncertainty Distribution

Revision 2 of *UZ Flow Models and Submodels* (BSC 2004 [DIRS 169861]) is an historical document that has been revised (SNL 2007 [DIRS 175177]) to accommodate revisions to the infiltration rate that serves as the boundary condition for the unsaturated zone flow model. This discussion provides justification for using specific information from the historical reference (BSC 2004 [DIRS 169861]) as direct input for specifying the uncertainty distribution for the AFM γ parameter.

As part of the validation process for the unsaturated zone flow model, *UZ Flow Models and Submodels* (BSC 2004 [DIRS 169861], Section 7.5) presented an analysis that examined the sensitivity of the model in simulating ^{14}C ages[2] measured in wells USW UZ-1 and USW SD-12 to changes in the gamma parameter. The simulation results (BSC 2004 [DIRS 169861], Figures 7.5-1 and 7.5-2) show that parameter values of 0.4 and 0.6 provide equally good matches to the data for depths at or below the repository horizon. The analysis was conducted with a version of the present-day flow field that was available at the time that analysis was conducted. Since that time, the unsaturated zone flow model has been changed. Nevertheless, this analysis is being cited in the present model for the purpose of establishing the degree to which the gamma parameter is constrained by ^{14}C measurements.

The specific application of this analysis from an historical source is to compare the simulation results for different values of the gamma parameter, rather than a more-quantitative prediction of the behavior of the system. Such a comparison should still be valid, even though the previous and updated unsaturated zone flow models are different in detail. As long as the basic hydrologic conditions and parameters are similar for the previous and updated models, it is expected that the sensitivity analysis results (simulated ^{14}C profiles that are insensitive to the gamma parameter) would have been reproduced with the updated model, had those simulations been performed in *UZ Flow Models and Submodels* (SNL 2007 [DIRS 175177]). The most important parameter to compare when assessing the degree of similarity of the models is the infiltration rate. The mean infiltration rate over the repository footprint from the previous present-day mean flow field used in *UZ Flow Models and Submodels* (BSC 2004 [DIRS 169861]) was 4.7 mm/yr (BSC 2004 [DIRS 170007], Table 6-10). For comparing to the updated flow field, this addendum considers the median percolation rate for the present-day, 10th percentile flow field of 3.93 mm/yr from Table 6-26 in Section 6.5.15 below. A difference of this magnitude is unlikely to change the comparison of simulation results significantly because similar hydrologic behavior is expected in unsaturated, fractured tuff for infiltration rates in the same general range. Therefore, the comparison results from the historical reference (BSC 2004 [DIRS 169861]) may be used as direct input for specifying the uncertainty distribution for the AFM γ parameter. The analysis leading to the assignment of the parameter uncertainty distribution is presented in Section 6.5.6.

4.1.2 Fracture Frequency and Fracture Porosity

Analysis of Hydrologic Properties Data (BSC 2004 [DIRS 170038], Table 6-5; DTN: LB0205REVUZPRP.001 [DIRS 159525]) provides data for the mean and standard deviation of fracture frequency and fracture porosity for the hydrologic units in and beneath the repository. Fracture frequency is determined from qualified fracture property data developed from field data (BSC 2004 [DIRS 170038], Section 6.1.2). These include detailed line survey fracture data (collected from the Exploratory Studies Facility North and South Ramps, Main Drift, and Enhanced Characterization of the Repository Block Cross Drift, providing spatially varying frequency, length, and fracture dips and strikes) and fracture frequency data from boreholes. A combination of fracture porosity data derived from gas tracer tests in the

[2] "^{14}C ages" refers to the results of radiometric dating using the naturally occurring isotope carbon-14 (^{14}C) to determine the age of carbonaceous materials up to about 60,000 years.

Exploratory Studies Facility, fracture frequency data, fracture aperture estimates, and the geometry of fracture networks is used to develop representative fracture porosities for the unsaturated zone model layers (BSC 2004 [DIRS 170038], Section 6.1.3). Fracture aperture is calculated within this report based on two direct input parameters: fracture porosity and fracture frequency. Section 6.5.7 of the parent report provides a complete discussion of the uncertainty treatment for fracture frequency and fracture porosity. Fracture frequency data in the repository host rock provide estimates for the standard deviation of fracture frequency in some, but not all, of the model units. Data from units having standard deviations are used to develop uncertainty data for those without such data by determining the standard deviation based on the data, and assuming that the ratio of the standard deviation to the mean for the remaining units is equal to the value determined for units for which data are available.

4.1.3 Matrix Porosity

Matrix water content is needed to determine the advective transport velocity from the water flux provided by the flow model. Water content is the product of the porosity and the water saturation. Water saturation is an output of the flow model. Matrix porosity is also used by the flow model, although steady-state flow fields are insensitive to this parameter. The data sets for matrix porosity are obtained from the hydrologic property set (DTN: LB0207REVUZPRP.002 [DIRS 159672]).

4.1.4 Matrix Diffusion Coefficient

Site-specific diffusion cell data were used to develop a correlation between the matrix diffusion coefficient and the porosity and permeability of the rock matrix under saturated conditions, as discussed by Reimus et al. (2007 [DIRS 179246]). The diffusing species, ^{3}HHO, Br^{-}, and I^{-}, were used in the experiments to define the correlation. Samples of welded and nonwelded volcanic tuffs were taken from Pahute Mesa and the C-holes near Yucca Mountain. The ranges in porosity and permeability of samples from Pahute Mesa and C-holes are approximately 0.05 to 0.4 and 10^{-18} m^2 to 10^{-14} m^2, respectively. The porosity and permeability of rock units in and below the repository horizon are in approximately the same range (porosity ranges from 0.04 to 0.35 (DTN: LB0207REVUZPRP.002 [DIRS 159672]) and permeability from 10^{-19} m^2 to 10^{-12} m^2 (DTNs: LB0611MTSCHP10.001 [DIRS 178586] and LB06123DPDUZFF.001 [DIRS 178587]). The highest predictability in determining a value of the tortuosity occurs when both matrix porosity and log permeability are known, with log permeability as the more important predictive variable. Modifications of the correlation expression in Section 6.5.5.1 (Equation 6.5.5-1) account for unsaturated conditions by substituting water content and effective permeability, the unsaturated properties equivalent to porosity and permeability. A portion of the data set used by Reimus et al. (2007 [DIRS 179246]) for developing the correlation consists of qualified data in DTN: LA0303PR831362.001 [DIRS 165641] (output DTN of SNL 2007 [DIRS 177394]; see justification below concerning the unqualified data).

Data for matrix porosity and permeability are used to evaluate matrix diffusion. Matrix porosity is taken from the hydrologic parameter set presented in *Analysis of Hydrologic Properties Data* (BSC 2004 [DIRS 170038], Table 6-6; DTN: LB0207REVUZPRP.002 [DIRS 159672]). Matrix permeability is taken from the mountain-scale calibrated property sets (DTNs: LB0611MTSCHP10.001 [DIRS 178586] and LB06123DPDUZFF.001 [DIRS 178587]).

These permeability values are calibrated against water saturation and water potential values for the most probable infiltration case.

In-situ hydrologic conditions are evaluated using DTN: LB0208UZDSCPMI.001 [DIRS 161285] for capillary pressure in the unsaturated zone. This DTN provides site-specific capillary pressure as measured in the unsaturated zone at Yucca Mountain.

Site-specific information on the rock volumes for each unsaturated zone model unit expected below the repository is taken from DTN: LB06123DPDUZFF.001 [DIRS 178587]. This provides the best estimate of spatial stratigraphic data in the unsaturated zone, based on the observed stratigraphy.

The remaining information used to determine matrix diffusion coefficients, the Nernst-Einstein equation, Stokes-Einstein equation, molar ionic conductivities, and atomic radii is considered established fact.

Justification of Unqualified Matrix Diffusion Data Given by Reimus et al. (2007 [DIRS 179246])

The data evaluated here are a mixture of qualified and unqualified data that were used previously without presenting justification, as identified in CR 7260.

Data Set for Justification: Reimus, P.W.; Callahan T.J.; Ware, S.D.; Haga, M.J.; and Counce, D.A. 2007 [DIRS 179246]. "Matrix Diffusion Coefficients in Volcanic Rocks at the Nevada Test Site: Influence of Matrix Porosity, Matrix Permeability, and Fracture Coating Minerals." *Journal of Contaminant Hydrology*.

Description of Use: Reimus et al. (2007 [DIRS 179246]) developed a correlation among tortuosity τ, permeability k, and porosity ϕ, based on measurements of rock samples from the Nevada Test Site. Diffusion measurements were conducted using bromide, iodide, and tritium as tracers. The correlation based on the diffusion data is to be used in TSPA dose calculations to assign matrix diffusion coefficients for aqueous radioelements in the unsaturated zone radionuclide transport computations.

Extent to which the Data Demonstrate the Properties of Interest: The property of interest is the matrix diffusion coefficient, or more exactly, the ratio of the matrix diffusion coefficient to the free-water diffusion coefficient, D_m / D^*, also known as the tortuosity.

Method of Justification and Criteria: Corroboration with qualified data is used for justification of these data. Of the 40 data points used in the development of the correlation in Equation 6.5.5-1, six of the values are qualified in DTN: LA0303PR831362.001 [DIRS 165641]. To justify use of the unqualified data, the qualified and unqualified data will show a similar range in the $\log_{10}(\tau)$ when plotted against variations in ϕ and $\log_{10}(k)$. For each data set, the $\log_{10}(\tau)$ will be reasonably explained by the derived correlation. This will be demonstrated by comparison of a fit of the measured $\log_{10}(\tau)$ values from the correlation against the predicted values from the correlation with a line representing a perfect correlation

(i.e., predicted values equal measured values). The variations in these fits should be smaller than the variations in the underlying data.

Evaluation Results: Figures 4-1 and 4-2 demonstrate that the qualified and unqualified data lie within the same range for variations in porosity and permeability. Furthermore, the plot of the measured and predicted values of $\log_{10}(\tau)$ in Figure 4-3 shows that the best fit lines for the qualified and unqualified data lie well within the range of scatter in the qualified data. Therefore, the unqualified data are justified for use in the development of a correlation for matrix diffusion coefficients.

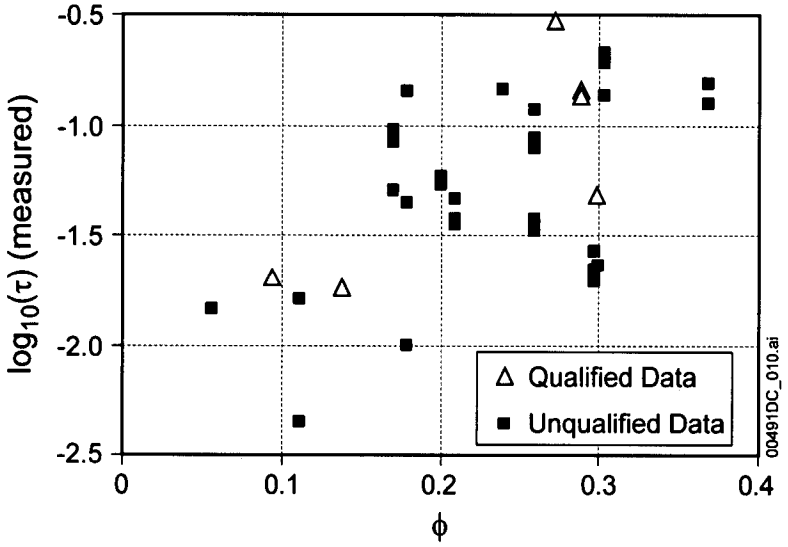

Source: Reimus et al. 2007 [DIRS 179246].

Output DTN: LB0702PAUZMTDF.001.

Figure 4-1. Plot of Measured $\text{Log}_{10}(\tau)$ versus Porosity for the Qualified and Unqualified Data

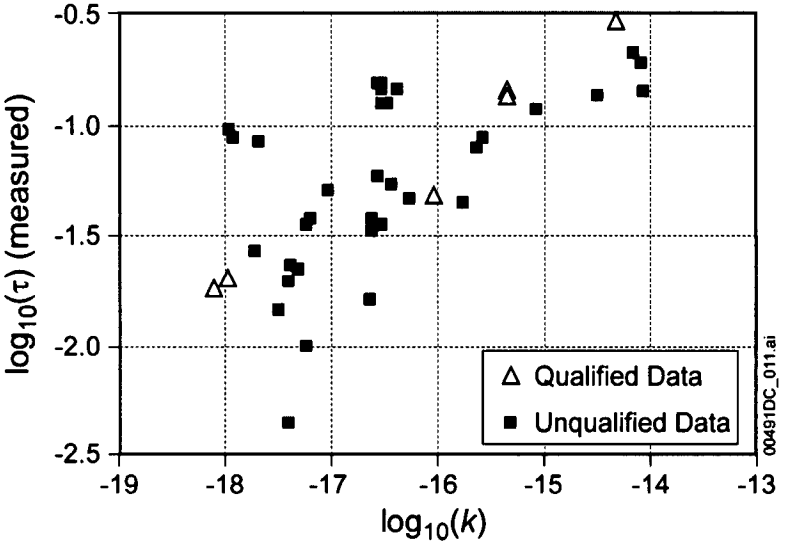

Source: Reimus et al. 2007 [DIRS 179246].

Output DTN: LB0702PAUZMTDF.001.

Figure 4-2. Plot of Measured $Log_{10}(\tau)$ versus Log_{10}(Permeability, m^2) for the Qualified and Unqualified Data

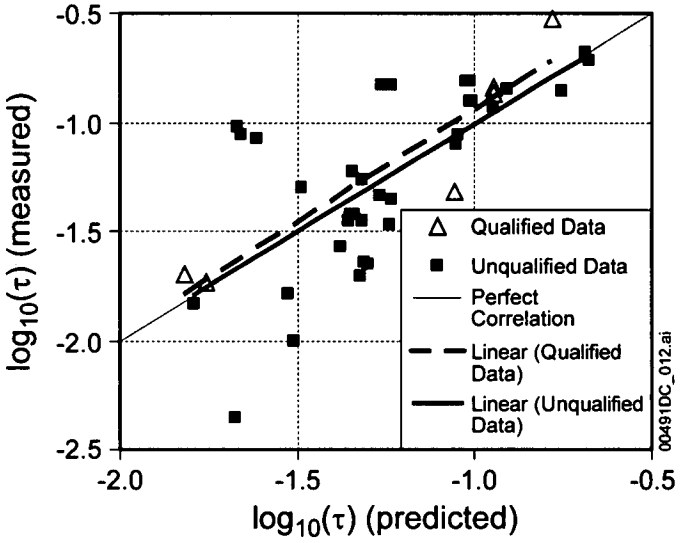

Source: Reimus et al. 2007 [DIRS 179246].

Output DTN: LB0702PAUZMTDF.001.

Figure 4-3. Plot of Measured $Log_{10}(\tau)$ versus Predicted $Log_{10}(\tau)$ for the Qualified and Unqualified Data

The remaining inputs used for matrix diffusion coefficients are for the free-water diffusion coefficients. These inputs are (1) the molar ionic conductivities presented by Lide (1992 [DIRS 166224]), which are considered established fact; (2) speciation results from *Dissolved Concentration Limits of Elements with Radioactive Isotopes* (SNL 2007 [DIRS 177418]), which are qualified; (3) *The Hydrolysis of Cations* (Baes and Mesmer 1986 [DIRS 100702]) for aqueous speciation of cesium, tin, and technetium; (4) *Fresh Water Systems* (Cutter 1989 [DIRS 178861]) for the aqueous speciation of selenium, which are considered established fact; (5) parameters used in the Nernst-Einstein equation (Equation (A-7)) and Stokes-Einstein equation (Equation (A-8)) from Lide (1992 [DIRS 166224]), which are considered established fact; and (6) atomic radii given by Slater (1965 [DIRS 179613]), which are considered established fact.

The free-water diffusion coefficient for TcO_4^- is from Sato et al. (1996 [DIRS 163213] Table 2). This datum may be justified by comparison with diffusion coefficients for the aqueous species analogues MnO_4^- and ReO_4^-. Based on information from Lide (1992 [DIRS 166224]), the free-water diffusion coefficients for MnO_4^- and ReO_4^- are 1.63×10^{-9} m^2/s and 1.46×10^{-9} m^2/s, respectively. The positions of manganese and rhenium in the periodic table of elements suggests that the diffusion coefficient for TcO_4^- should be approximately the average of these values. The average of the diffusion coefficients for MnO_4^- and ReO_4^- is 1.55×10^{-9} m^2/s. The diffusion coefficient reported by Sato et al. (1996 [DIRS 163213], Table 2) for TcO_4^- is 1.95×10^{-9} m^2/s. Therefore, the analogue diffusion coefficient values lie within 21% of the value reported by Sato et al. (1996 [DIRS 163213], Table 2) and all analogue values are well within the uncertainty of the measurement, 0.56×10^{-9} m^2/s, reported by Sato et al. (1996 [DIRS 163213], Table 2).

4.1.5 Matrix Sorption Coefficient

The sorption coefficients for radionuclides onto the matrix rock are developed in *Radionuclide Transport Models Under Ambient Conditions* (SNL 2007 [DIRS 177396]). These sorption coefficient distributions, obtained from DTNs: LA0408AM831341.001 [DIRS 171584] and LB0701PAKDSESN.001 [DIRS 179299], are used in this addendum to assign values for use in the representative case simulations and the sensitivity calculations presented in Section 6. The justifications for the uncertainty distributions themselves can be found in *Radionuclide Transport Models Under Ambient Conditions* (SNL 2007 [DIRS 177396]) and the referenced DTNs.

4.1.6 Fracture Dispersivity

The fracture dispersivity is set at a fixed value of 10 m. There are few data available on dispersivity distributions at Yucca Mountain site. Neuman (1990 [DIRS 101464]) showed that field dispersivity varied with the scale of study. Field tracer tests at the C-holes at Yucca Mountain also showed that, on a 100-m scale, field dispersivity had a range of approximately 3 m to 63 m (SNL 2007 [DIRS 177394], Table 6.3-3). The 10-m value is toward the lower end of the values from field studies available in DTN: LA0303PR831231.005 [DIRS 166259].

With respect to tracer test under unsaturated conditions, none of the field tests conducted either at the Busted Butte or Alcove 8/Niche 3 site provided definitive information on either the longitudinal or transverse dispersion. For example, *Radionuclide Transport Models Under*

Ambient Conditions (SNL 2007 [DIRS 177396], Section 7.2.4.1.4, Table 7-12) showed that the Busted Butte Phase 2C data are consistent with a longitudinal dispersivity for the fractures of 0.1 m; transverse dispersivity was set to 0 for these simulations. Results of these simulations indicated that these low values of the longitudinal and transverse dispersivities are consistent with the data, but that further analysis to refine the dispersivity estimates was unwarranted due to the uncertainties associated with the sample collection system and its effect on the measured breakthrough curves. The transport distance for this tracer analysis was approximately 0.6 m, making this a relatively small-scale test compared to the entire transport distance through the unsaturated zone. In *Radionuclide Transport Models Under Ambient Conditions* (SNL 2007 [DIRS 177396], Section 7.3.3.3), analyses of tracer responses from the Alcove 8/Niche 3 fault test (characteristic transport distance on the order of 20 m) indicated that assuming dispersivity values significantly larger than 0 made it more difficult to match the breakthrough curve data for the two tracers injected. In this case, matrix diffusion is the predominant mechanism affecting the transport, and hydrodynamic dispersion is taken to exert a relatively minor influence on the results.

The influence of dispersion on radionuclide transport is not expected to be important because the spreading of radionuclides due to matrix diffusion effects has a much greater impact on transport times than longitudinal dispersion over the expected range of longitudinal dispersivities. Although the impact of dispersivity should be very small, the value chosen should be conservative, as higher dispersivity tends to spread the radionuclide plume and reduce the peak value. While it can be argued that, for a decaying species, higher dispersivity can allow a greater fraction of the mass to arrive downstream before decaying, the point here is that in comparison to diffusion and large scale heterogeneities, dispersivity effects have a very small influence on the breakthrough curves. This justifies using a fixed value for dispersivity rather than treating it as a stochastic parameter.

4.1.7 Radionuclide Sorption onto Colloids

Colloid transport is represented through radionuclide attachment to colloids that are either reversible or irreversible. For reversible attachment, the degree of partitioning onto colloids is a function of both the colloid concentration and the sorption coefficient for a given radioelement onto the colloid (Section 6.5.12 of the parent report). The groundwater colloid concentration distribution that was developed for use in the TSPA-LA model was based on data from 79 groundwater samples collected in the vicinity of Yucca Mountain and 11 samples collected from the Idaho National Laboratory. Inclusion of the Idaho National Laboratory groundwater colloid data was deemed appropriate for inclusion in the data analysis among the groundwater data from the Yucca Mountain area because the climate in Idaho Falls is similarly arid and the field sampling and analytical techniques used at both locations were similar (SNL 2007 [DIRS 177423]). For this parameter, the distributions for two ionic strength conditions are presented, one for ionic strength less than 0.05 M; the other for ionic strength $\geq$ 0.05 M (DTN: MO0701PAGROUND.000 [DIRS 179310]). However, only the lower ionic strength distribution will be used for TSPA because the lower ionic strength distribution results in greater colloid concentrations leading to greater colloid-facilitated radionuclide transport.

Sorption partition coefficients (K_d values) have been developed for selected radionuclides onto smectite and iron corrosion product colloids (DTNs: MO0701PASORPTN.000 [DIRS 180391]; MO0701PAKDSUNP.000 [DIRS 180392]). Smectite is representative of defense high-level waste glass degradation product colloids and natural groundwater colloids. Colloidal constituents may act as pseudocolloids that sorb radionuclides and subsequently be transported from the Engineered Barrier System (EBS) by seepage waters moving through the repository. The K_d values for the radioelements plutonium, americium, thorium, protactinium, cesium, and tin are drawn from YMP-supported experimental work, government publications, and the open literature.

For irreversible attachment, the parameter K_c is set to a fixed value of 10^{20} (unitless) that practically ensures radioelements remain permanently attached to the colloid (Section 6.5.12 of the parent report).

4.1.8 Colloid Filtration and Size Exclusion

Colloid size exclusion is treated in the model for colloid movement from fractures into the rock matrix. Size exclusion is treated on the basis of effective colloid and matrix pore diameters, where a colloid is excluded from entry into a pore that is smaller than the colloid. The matrix pore size distributions for different rock types were developed from moisture retention curve measurements on rock matrix samples taken from 16 different hydrogeologic units between the repository host rock and the water table at Yucca Mountain (DTN: LA0003MCG12213.002 [DIRS 147285]). The pore-size distribution data for each hydrogeologic unit were compared to the average effective colloid diameter of 0.1 μm, giving the expected fraction of colloids excluded from entering the rock matrix in that unit.

Colloid filtration is treated in the model for colloid transport between successive rock matrix hydrogeologic units. This is based on physical straining, in which filtration will occur if a colloid attempts to pass though a pore with an effective diameter that is smaller than the colloid effective diameter. Pore size distributions are based on the data discussed above. Colloid size distribution data are available from colloid measurements generated from high-level waste glass corrosion using a dynamic light-scattering method (DTN: LL000122051021.116 [DIRS 142973], CRWMS M&O 2001 [DIRS 154071], Section 6.3; see also DTN: LL991109751021.094 [DIRS 142910], MOL.20000124.0207, pp. 32 and 34).

4.1.9 Colloid Retardation in Transport Through Fractures

Colloid retardation in transport through fractures in volcanic tuffs has been investigated in field tests conducted in the saturated zone at Yucca Mountain (BSC 2004 [DIRS 170006], Section 6.4). These retardation factors represent the chemical and physical filtration of colloids in the saturated zone. The field measurements were conducted using fluorescent carboxylate modified polystyrene latex (CML) microspheres ranging in diameter from 280 nm to 830 nm. Results from laboratory fracture experiments conducted using silica, montmorillonite, and clinoptilolite colloids in addition to CML microspheres suggest that colloid filtration and retardation parameters derived from CML microsphere responses in field tracer tests should be conservative if used to predict natural inorganic colloid transport in fractured systems. The retardation factors have been derived in terms of a cumulative probability distribution

representing the uncertainty in retardation factors applied to colloid transport through fractures (DTN: LA0303HV831352.002 [DIRS 163558]). The application of these results to the unsaturated zone is based on the similar geologic units (fractured volcanic rocks) and transport processes at the scale governing colloid transport processes. Furthermore, colloid transport in the unsaturated zone is expected to be less favorable than in the saturated zone, possibly due to precipitation of secondary salts (e.g., $CaCO_3$) or the presence of water films that reduce effective fracture size. Thus, ignoring these potential factors, the model is a conservative representation of colloid transport in the unsaturated zone. In addition to colloid retardation, a fraction of unretarded colloid transport is developed based on the attachment rates derived from the colloid transport field test data (DTN: LA0303HV831352.003 [DIRS 165624]). This distribution is tied to the transport time distributions experienced by the colloids (BSC 2004 [DIRS 170006], Section 6.6). Rather than incorporating the full distribution as a function of transport time, a single conservative value for unretarded colloid transport is used, as discussed in Section 6.5.13 of the parent report.

4.2 CRITERIA

There is no change to the list of acceptance criteria that apply to the parent report or this addendum. Section 8.3 provides an updated accounting of how the work documented in this addendum addresses the acceptance criteria.

In addition, the work documented in this addendum addresses a series of condition reports (CRs) that were written against the parent report. Table 4.2-1 lists, provides a brief description of these CRs, and gives their resolutions and locations of information regarding their resolution.

Table 4.2-1. Condition Reports Addressed in this Addendum

Condition Report Number	Title	Description	Resolution
6035	Uncorrected Errors in FEHM 2.23	The three problems identified in this CR were: 1) Neptunium released to the unsaturated zone rock matrix exits the unsaturated zone at an excessive rate. 2) Code incorrectly obtains a negative travel time in a cell. 3) Inflexible particle assignment during the simulation results in model oscillations.	Each of these issues was resolved and fixed in FEHM V2.24-01.
7138	RIT Action Item Associated with AMR MDL-NBS-HS-000020, Particle Tracking Model and Abstraction of Transport Process	Although numerous calculations are presented for a global source term in which all of the repository locations are a source for radionuclide releases, there are no example calculations for point-source releases.	Point-source calculations are provided in Sections 6.6 and 6.8 of this addendum.

Table 4.2-1.Condition Reports Addressed in this Addendum (Continued)

Condition Report Number	Title	Description	Resolution
7225	Inconsistencies in Definition of Repository Cells in the UZ Model	Two sets of repository cells for the UZ model had been identified in the TDMS at the time this CR was written, and these cell listings were not identical. There was no rationale for having two different definitions for the repository in the UZ model.	In the current analyses, the two representations of the repository used the same definition of the outer boundary of the repository, but, because of different intended uses of the repository region, the node lists for the two reports are still slightly different. This is acceptable because in this addendum, the purpose is to supply TSPA with a set of nodes from which to release radionuclides in the UZ model (see Section 6.5.15). In the flow-modeling report, the purpose is to define the "repository footprint" in order to assess the mean percolation flux through the footprint. These are different requirements, and the slight differences in the repository node lists that are still present reflect these different requirements. Therefore, this CR has been addressed.
7248	Non-Compliance with LP-SIII.10Q-BSC for Documenting Use of Software	In the parent report, the STN for the fehm2post software was incorrectly cited	STN is correctly cited in this addendum for the fehm2post software.
7260	Matrix Diffusion in the UZ and SZ	Data used to develop the correlation of diffusion coefficient with permeability and water content consisted of three separate data sets, only one of which was qualified at the time the CR was written. Therefore, this correlation cannot be considered qualified.	Section 4.1.4 of this addendum presents the qualification of the unqualified diffusion data for its intended use.

NOTE: CR = condition report; STN = software tracking number; SZ = saturated zone; TDMS = Technical Data Management System; TSPA = total system performance assessment; UZ = unsaturated zone.

4.3 CODES, STANDARDS, AND REGULATIONS

No change.

5. ASSUMPTIONS

No change.

INTENTIONALLY LEFT BLANK

6. MODEL DISCUSSION

6.1 MODELING OBJECTIVES AND APPROACH

No change.

6.2 FEATURES, EVENTS, AND PROCESSES INCLUDED IN THE MODEL

No change.

6.3 THE UNSATURATED ZONE TRANSPORT ABSTRACTION MODEL

No change.

6.4 THE NUMERICAL REPRESENTATION OF THE UNSATURATED ZONE TRANSPORT ABSTACTION MODEL

No change.

6.5 UNSATURATED ZONE TRANSPORT ABSTRACTION MODEL INPUTS

In this addendum, the introductory material of this section is unchanged from the parent report. In this section, changes from the parent report are identified below the individual third level heading.

6.5.1 Pregenerated Flow Fields

The basic process for integrating flow field information into the TSPA simulation of unsaturated zone transport is unchanged from that described in the parent report. However, the flow-field references themselves have changed and are described below. To implement the flow fields, FEHM-compatible flow fields are generated from the original steady-state flow fields developed in *UZ Flow Models and Submodels* (SNL 2007 [DIRS 175177], Sections 6.6 and 8.6. In the TSPA model, these flow fields, developed in several DTNs, are renamed in a manner that facilitates the sampling of the flow fields and the transition of the flow field at times specified for climate change. Table 6-1 shows the indexing between the original file names and the name required in the TSPA compliance model.

Table 6-1. List of Steady State Flow Field Names for the TSPA Model and the Original Data Source

Description	TSPA Name	Original Name in Source DTN	Source DTN
Present-day climate, 10% infiltration scenario	*ff1100.ini*	*pd10.ini*	LB0612PDFEHMFF.001 [DIRS 179296]
Present-day climate, 30% infiltration scenario	*ff1200.ini*	*pd30.ini*	
Present-day climate, 50% infiltration scenario	*ff1300.ini*	*pd50.ini*	
Present-day climate, 90% infiltration scenario	*ff1400.ini*	*pd90.ini*	

Table 6-1. List of Steady State Flow Field Names for the TSPA Model and the Original Data Source (Continued)

Description	TSPA Name	Original Name in Source DTN	Source DTN
Monsoon climate, 10% infiltration scenario	*ff2100.ini*	*mo10wtrise.ini*	LB0701MOFEHMFF.001 [DIRS 179297]
Monsoon climate, 30% infiltration scenario	*ff2200.ini*	*mo30wtrise.ini*	
Monsoon climate, 50% infiltration scenario	*ff2300.ini*	*mo50wtrise.ini*	
Monsoon climate, 90% infiltration scenario	*ff2400.ini*	*mo90wtrise.ini*	
Glacial-transition climate, 10% infiltration scenario	*ff3100.ini*	*gt10wtrise.ini*	LB0701GTFEHMFF.001 [DIRS 179160]
Glacial-transition climate, 30% infiltration scenario	*ff3200.ini*	*gt30wtrise.ini*	
Glacial-transition climate, 50% infiltration scenario	*ff3300.ini*	*gt50wtrise.ini*	
Glacial-transition climate, 90% infiltration scenario	*ff3400.ini*	*gt90wtrise.ini*	
Post-10k-yr flow field, infiltration from modified 10% map	*ff4100.ini*	*post10kWTRISEpkdq1.ini*	LB0702PAFEM10K.002 [DIRS 179507]
Post-10k-yr flow field, infiltration from modified 30% map	*ff4200.ini*	*post10kWTRISEpkdq2.ini*	
Post-10k-yr flow field, infiltration from modified 50% map	*ff4300.ini*	*post10kWTRISEpkdq3.ini*	
Post-10k-yr flow field, infiltration from modified 90% map	*ff4400.ini*	*post10kWTRISEpkdq4.ini*	

6.5.2 Dispersivity

No changes.

6.5.3 Matrix Porosity and Rock Density

Matrix porosity is used to calculate the matrix pore volume associated with each matrix block. The pore volume data are then multiplied by the corresponding water saturation data to determine the fluid volume in a cell.

Matrix porosity and rock density values combined with rock sorption coefficient and water saturation are used for calculating matrix retardation factors used in simulating the sorption effect on radionuclide transport.

Values of matrix porosity are from the Technical Data Management System (TDMS) (DTN: LB0207REVUZPRP.002 [DIRS 159672]; output DTN: MO0704PAFEHMBR.001) and are listed in Table 6-5.

Table 6-5. Matrix Porosities Used in the Unsaturated Zone Transport Abstraction Model

Matrix Layer	Matrix Porosity	Input Description	Input Source	Type of Uncertainty
tcwM1	2.41×10^{-1}	Matrix porosity values are used in determining matrix pore volume, simulating matrix diffusion effects, and calculating matrix sorption retardation factors.	Source DTN: LB0207REVUZPRP .002 [DIRS 159672]; Output DTN: MO0704PAFEHMB R.001 *"FEHM Model and Input"*	Fixed values for each layer but varies from layer to layer
tcwM2	8.80×10^{-2}			
tcwM3	2.00×10^{-1}			
ptnM1	3.87×10^{-1}			
ptnM2	4.28×10^{-1}			
ptnM3	2.33×10^{-1}			
ptnM4	4.13×10^{-1}			
ptnM5	4.98×10^{-1}			
ptnM6	4.90×10^{-1}			
tswM1	5.41×10^{-2}			
tswM2	1.57×10^{-1}			
tswM3	1.55×10^{-1}			
tswM4	1.11×10^{-1}			
tswM5	1.31×10^{-1}			
tswM6	1.03×10^{-1}			
tswM7	1.03×10^{-1}			
tswM8	4.27×10^{-2}			
tswMz	2.75×10^{-1}			
tswMv	2.29×10^{-1}			
ch1Mz	2.85×10^{-1}			
ch1Mv	3.31×10^{-1}			
ch2Mv	3.46×10^{-1}			
ch3Mv	3.46×10^{-1}			
ch4Mv	3.46×10^{-1}			
ch5Mv	3.46×10^{-1}			
ch2Mz	3.22×10^{-1}			
ch3Mz	3.22×10^{-1}			
ch4Mz	3.22×10^{-1}			
ch5Mz	3.22×10^{-1}			
ch6Mz	2.71×10^{-1}			
ch6Mv	2.53×10^{-1}			
pp4Mz	3.21×10^{-1}			
pp3Md	3.18×10^{-1}			
pp2Md	2.21×10^{-1}			
pp1Mz	2.97×10^{-1}			
bf3Md	1.75×10^{-1}			
bf2Mz	2.34×10^{-1}			
tr3Md	1.75×10^{-1}			
tr2Mz	2.34×10^{-1}			
pcM38	4.27×10^{-2}			

Table 6-5. Matrix Porosities Used in the Unsaturated Zone Transport Abstraction Model (Continued)

Matrix Layer	Matrix Porosity	Input Description	Input Source	Type of Uncertainty
pcM39	2.75×10^{-1}			
pcM1z	2.85×10^{-1}			
pcM2z	3.22×10^{-1}			
pcM5z	3.22×10^{-1}			
pcM6z	2.71×10^{-1}			
pcM4p	3.21×10^{-1}			

Rock density values are from the TDMS (DTN: LB0207REVUZPRP.002 [DIRS 159672]; output DTN: MO0704PAFEHMBR.001) and are listed in Table 6-6. These densities are bulk rock densities.

Table 6-6. Matrix Rock Density Values

Matrix Layer	Rock Density (kg/m^3)	Rock Type	Input Description	Input Source	Type of Uncertainty
tcwM1	1.93×10^3	–	Rock density data are used by FEHM in the calculation of matrix sorption retardation factors. These densities are bulk rock densities.	Source DTN: LB0207REVUZPRP.002 [DIRS 159672] Output DTN: MO0704PAFEHMBR.001 *"FEHM Model and Input"*	Fixed values for each layer but varies from layer to layer
tcwM2	2.28×10^3	–			
tcwM3	1.97×10^3	–			
ptnM1	1.45×10^3	–			
ptnM2	1.32×10^3	–			
ptnM3	1.84×10^3	–			
ptnM4	1.40×10^3	–			
ptnM5	1.13×10^3	–			
ptnM6	1.21×10^3	–			
tswM1	2.38×10^3	–			
tswM2	2.15×10^3	–			
tswM3	2.12×10^3	D			
tswM4	2.25×10^3	D			
tswM5	2.22×10^3	D			
tswM6	2.29×10^3	D			
tswM7	2.29×10^3	D			
tswM8/pcM38	2.29×10^3	D			
tswMz/pcM39	1.72×10^3	Z			
tswMv	1.74×10^3	V			
ch1Mz/pcM1z	1.67×10^3	Z			
ch1Mv	1.53×10^3	V			
ch2Mv	1.47×10^3	V			
ch3Mv	1.47×10^3	V			
ch4Mv	1.47×10^3	V			
ch5Mv	1.47×10^3	V			
ch2Mz/pcM2z	1.60×10^3	Z			
ch3Mz	1.60×10^3	Z			
ch4Mz	1.60×10^3	Z			
ch5Mz/pcM5z	1.60×10^3	Z			

Table 6-6. Matrix Rock Density Values (Continued)

Matrix Layer	Rock Density (kg/m^3)	Rock Type	Input Description	Input Source	Type of Uncertainty
ch6Mz/pcM6z	1.78×10^3	Z			
ch6Mv	1.89×10^3	V			
pp4Mz/pcM4p	1.63×10^3	Z			
pp3Md	1.76×10^3	D			
pp2Md	1.99×10^3	D			
pp1Mz	1.69×10^3	Z			
bf3Md	2.11×10^3	D			
bf2Mz	1.83×10^3	Z			
tr3Md	2.11×10^3	D			
tr2Mz	1.83×10^3	Z			
Fault Zone Rock Density Data					
tcwFf	2.198×10^3	–			
ptnFf	1.577×10^3	–			
tswFf	2.125×10^3	D			
chnFf	1.550×10^3	Z			

NOTES: Layers defining the perched water units (pc) are assigned porosity values that are the same as those of the corresponding model unit that they replace.

The fault zone rock density values are selected to be near the middle of the range of the values of the individual sublayers for TSw and CHn. The values for TCw and PTn are placeholders that do not affect the model because these portions of the faults lie above the repository.

D = Devitrified, Z = Zeolitic, V = Vitric; DTN = data tracking number; FEHM = finite-element heat and mass (model).

6.5.4 Matrix Sorption Coefficient (mL/g)

The sorption coefficients for radionuclides onto the matrix rock have been updated to include additional radionuclides not considered in the parent report. The new treatment for radionuclide sorption onto rock is treated in *Radionuclide Transport Models Under Ambient Conditions* (SNL 2007 [DIRS 177396]).

6.5.5 Matrix Diffusion Coefficient (m^2/s)

In this section, there is an update to the corresponding section in the parent report that necessitates a renumbering of the tables and equations. The numbering convention within this section of the addendum is designed so that the numbering scheme is independent of the numbering in the remainder of the document.

A matrix diffusion coefficient is a constant of proportionality between aqueous solute mass flux (solute mass flow rate per unit wetted area) and the aqueous solute concentration gradient (gradient of the solute mass per unit water volume) for diffusive transport in the rock matrix. The matrix diffusion coefficient accounts for the diffusive properties of the solute in water as well as the geometrical effects of the rock matrix pore structure and the hydrological conditions of the rock. The matrix diffusion coefficient is expressed in units of length squared per unit time.

It has been shown that matrix diffusion combined with matrix sorption can play an important role in slowing the movement of radionuclides in fractured rocks (Sudicky and Frind 1982 [DIRS 105043]). A matrix diffusion coefficient is used in FEHM for simulating the effect of matrix diffusion on radionuclide transport in the fractured media. Values of matrix diffusion coefficient affect the strength of fracture-matrix interaction due to diffusion of radionuclides.

Each matrix diffusion coefficient, D_m, is constructed from two independent parameters, the tortuosity, τ, and the free-water diffusion coefficient, D^*, through the relationship, $D_m = \tau D^*$. The tortuosity coefficient parameters are given in Table 6.5.5-1 and the free-water diffusion coefficient parameters are given in Table 6.5.5.-2. Therefore, in Equation 6.5.5-1, $\log_{10}(D_m / D^*)$ is the logarithm of the tortuosity. The range of tortuosity values is subdivided into three subranges called tortuosity rock groups, based on the tortuosity characteristics of the rock types in the unsaturated zone. These rock groups are defined by tortuosity characteristics, with tortuosity rock group 1 having tortuosity greater than 0.05, tortuosity rock group 2 having tortuosity between 0.05 and 0.016, and tortuosity rock group 3 having tortuosity less than 0.016. There is one free-water diffusion coefficient for each radioelement. The free-water diffusion coefficients are distinguished by radioelement (rather than radionuclide) because the same diffusion coefficient is used for different isotopes of a given radioelement. The free-water diffusion coefficients and matrix diffusion coefficients have the same units, meters squared per second, and the tortuosities are dimensionless.

6.5.5.1 Correlation between Tortuosity, Porosity, and Permeability

Experimental data for diffusion in rock matrix for volcanic rock from the Yucca Mountain area (Reimus et al. 2007 [DIRS 179246]) have been used to correlate the matrix diffusion coefficient, divided by the free-water diffusion coefficient, with porosity and permeability for saturated conditions. A correlation for the tortuosity as a function of porosity and permeability has been proposed by Reimus et al. (2007 [DIRS 179246], Equation 2),

$$\log_{10}(D_m / D^*) = 1.42 + 1.91\phi + 0.19\log_{10}(k) \qquad \text{(Eq. 6.5.5-1)}$$

where D_m is the matrix diffusion coefficient, D^* is the free water diffusion coefficient, ϕ is the matrix porosity, and k is the matrix permeability in m^2. The tortuosity, τ, is the ratio D_m / D^*. The correlation coefficient (R^2) is 0.542 (Reimus et al. 2007 [DIRS 179246], Equation 2) and the standard error is 0.29 (Reimus et al. 2007 [DIRS 179246], following Equation 2). The standard error of a correlation is the standard deviation of the data points as they are distributed around the regression line. This correlation is based on diffusion cell measurements for bromide, iodide, and tritium made on volcanic tuff rock matrix from the Yucca Mountain region. The dataset includes qualified and unqualified data that were previously used without specific justification for using unqualified data, as identified in CR 7260. The correlation differs from that previously implemented in the parent report in that the diffusion coefficient is normalized by the free-water diffusion coefficient. This normalization helps to remove the effects of molecular size and ionic charge from the correlation.

6.5.5.2 Tortuosity for Unsaturated Media

The experimental data were taken for saturated conditions. In the unsaturated zone, the analogous quantities to porosity and permeability are water content and effective permeability. These are appropriate because the water content and effective permeability for the unsaturated system are in fact the porosity and permeability of a saturated system if the pore space occupied by air in the unsaturated system were transformed into mineral. Therefore, in Equation 6.5.5-1 porosity is replaced by water content and permeability is replaced by effective permeability for unsaturated conditions. See Appendix A for derivation of effective water content and effective permeability. Tortuosities were computed for each model unit from Equations A-1 through A-6 (Appendix A) using a capillary pressure of 1.25×10^5 Pa.

The individual rock units are grouped based on similar characteristics for tortuosity as shown in Tables A-2 through A-4 (Appendix A). These rock groups are defined by tortuosity characteristics with tortuosity rock group 1 having tortuosity greater than 0.05, tortuosity rock group 2 having tortuosity between 0.05 and 0.016, and tortuosity rock group 3 having tortuosity less than 0.016. The tortuosities for the various units are averaged on a volume-weighted basis and the volume-weighted tortuosities for the three tortuosity rock groups are given in Table 6.5.5-1.

Table 6.5.5-1. Average Tortuosities

Tortuosity Rock Group	Tortuosity
1	7.01×10^{-2}
2	2.67×10^{-2}
3	1.45×10^{-2}

Output DTN: LB0702PAUZMTDF.001.

6.5.5.3 Free-Water Diffusion Coefficients

Free-water diffusion coefficients for the various aqueous chemical forms of the radioelements may be estimated directly in some cases, but in other cases must be estimated using a chemical analogue. Appendix A provides a detailed procedure for computing free-water diffusion coefficient, and results for the radioelements of interest are listed in Table 6.5.5-2.

Table 6.5.5-2. Free-Water Diffusion Coefficients

Element	D* (m^2/s)	Element	D* (m^2/s)
Americium	9.49×10^{-10}	Radium	8.89×10^{-10}
Carbon	1.18×10^{-9}	Selenium	1.04×10^{-9}
Chlorine	2.03×10^{-9}	Tin	1.55×10^{-9}
Cesium	2.06×10^{-9}	Strontium	7.91×10^{-10}
Iodine	2.05×10^{-9}	Technetium	1.95×10^{-9}
Neptunium	6.18×10^{-10}	Thorium	5.97×10^{-10}
Protactinium	6.04×10^{-10}	Uranium	6.64×10^{-10}
Plutonium	1.30×10^{-9}		

Output DTN: LB0702PAUZMTDF.001.

Once both the tortuosity and free-water diffusion coefficients are available, the matrix diffusion coefficients for all radioelements in three rock groups can be computed using $D_m = \tau D^*$. Table 6.5.5-3 lists representative values of the matrix diffusion coefficients using the free-water diffusion coefficients from Table 6.5.5-2 and the average value of the tortuosity from Table 6.5.5-1.

Table 6.5.5-3. Representative Values of Matrix Diffusion Coefficients

Key	Radionuclide in Tortuosity Rock Groups	D_m (m^2/s)	Comments
-11	Am in Tortuosity Rock Group 1	6.718×10^{-11}	The values for Key -11 to -45 are computed from Table 2-5 and Table 2-8 of output DTN: LB0702PAUZMTDF.001, Unsaturated Zone Matrix Diffusion Coefficients.
-12	Am in Tortuosity Rock Group 2	2.554×10^{-11}	
-13	Am in Tortuosity Rock Group 3	1.372×10^{-11}	
-14	C in Tortuosity Rock Group 1	8.354×10^{-11}	
-15	C in Tortuosity Rock Group 2	3.176×10^{-11}	
-16	C in Tortuosity Rock Group 3	1.706×10^{-11}	
-17	Cl in Tortuosity Rock Group 1	1.437×10^{-10}	
-18	Cl in Tortuosity Rock Group 2	5.464×10^{-11}	
-19	Cl in Tortuosity Rock Group 3	2.934×10^{-11}	
-20	Cs in Tortuosity Rock Group 1	1.458×10^{-10}	
-21	Cs in Tortuosity Rock Group 2	5.545×10^{-11}	
-22	Cs in Tortuosity Rock Group 3	2.978×10^{-11}	
-23	I in Tortuosity Rock Group 1	1.451×10^{-10}	
-24	I in Tortuosity Rock Group 2	5.518×10^{-11}	
-25	I in Tortuosity Rock Group 3	2.963×10^{-11}	
-26	Np in Tortuosity Rock Group 1	4.375×10^{-11}	
-27	Np in Tortuosity Rock Group 2	1.663×10^{-11}	
-28	Np in Tortuosity Rock Group 3	8.933×10^{-12}	
-29	Pa in Tortuosity Rock Group 1	4.276×10^{-11}	
-30	Pa in Tortuosity Rock Group 2	1.626×10^{-11}	
-31	Pa in Tortuosity Rock Group 3	8.730×10^{-12}	
-32	Pu in Tortuosity Rock Group 1	9.203×10^{-11}	
-33	Pu in Tortuosity Rock Group 2	3.499×10^{-11}	

Table 6.5.5-3. Representative Values of Matrix Diffusion Coefficients (Continued)

Key	Radionuclide in Tortuosity Rock Groups	D_m (m^2/s)	Comments
-34	Pu in Tortuosity Rock Group 3	1.879×10^{-11}	
-35	Ra in Tortuosity Rock Group 1	6.294×10^{-11}	
-36	Ra in Tortuosity Rock Group 2	2.393×10^{-11}	
-37	Ra in Tortuosity Rock Group 3	1.285×10^{-11}	
-38	Se in Tortuosity Rock Group 1	7.363×10^{-11}	
-39	Se in Tortuosity Rock Group 2	2.799×10^{-11}	
-40	Se in Tortuosity Rock Group 3	1.503×10^{-11}	
-41	Sn in Tortuosity Rock Group 1	1.097×10^{-10}	
-42	Sn in Tortuosity Rock Group 2	4.172×10^{-11}	
-43	Sn in Tortuosity Rock Group 3	2.240×10^{-11}	
-44	Sr in Tortuosity Rock Group 1	5.600×10^{-11}	
-45	Sr in Tortuosity Rock Group 2	2.129×10^{-11}	
-46	Sr in Tortuosity Rock Group 3	1.143×10^{-11}	
-47	Tc in Tortuosity Rock Group 1	1.380×10^{-11}	
-48	Tc in Tortuosity Rock Group 2	5.248×10^{-11}	
-49	Tc in Tortuosity Rock Group 3	2.819×10^{-11}	
-50	Th in Tortuosity Rock Group 1	4.226×10^{-11}	
-51	Th in Tortuosity Rock Group 2	1.607×10^{-11}	
-52	Th in Tortuosity Rock Group 3	8.629×10^{-12}	
-53	U in Tortuosity Rock Group 1	4.701×10^{-11}	
-54	U in Tortuosity Rock Group 2	1.787×10^{-11}	
-55	U in Tortuosity Rock Group 3	9.598×10^{-12}	

Output DTN: MO0705TRANSTAT.000.

NOTE: Due to round-off issue, values may be slightly different than those obtained when applying the equation, $D_m = \tau D^*$. Values in this table are computed in the spreadsheet *Dm.xls* in output DTN: MO0705TRANSTAT.000. These slight differences have no influence on the conclusions reached in this report.

Radionuclides listed = americium (Am), carbon (C), chlorine (Cl), cesium (Cs), iodine (I), neptunium (Np), protactinium (Pa), plutonium (Pl), radium (Ra), selenium (Se), tin (Sn), strontium (Sm), technetium (Tc), thorium (Th), and uranium (U).

6.5.5.4 Uncertainty Treatment for Matrix Diffusion Coefficient

This section summarizes the uncertainty treatment for matrix diffusion coefficient; the detailed justification for the approach is developed in Section A.4. The method for assigning the uncertainty in matrix diffusion coefficient starts by assuming that uncertainties in the effective water content, effective permeability, and the free-water diffusion coefficient are small compared to uncertainty reflected in the laboratory measurements of tortuosity. The standard deviation associated with Equation 6.5.5-1 (the standard error of 0.29) is then used to provide a basis for assigning a normal distribution of uncertainty in tortuosity. In particular, uncertainty in the log of tortuosity for each tortuosity rock group is taken to follow a normal distribution, with mean equal to the value given in Table 6.5.5-1 and a normalized standard deviation (standard deviation divided by the mean) of 0.29. The distribution and the normalized standard deviation are applied to each tortuosity rock group, and the diffusion coefficient is computed by multiplying the stochastically determined value of tortuosity by the fixed value of the free-water diffusion coefficient. The justification for using this uncertainty distribution is provided in Section A.4.

6.5.6 Fracture Residual Saturation and Active Fracture Model Gamma Parameters (Unitless)

Fracture residual saturation and AFM γ parameter values are used by FEHM to calculate the fracture spacing based on the AFM (Liu et al. 1998 [DIRS 105729]).

Analyses in *Conceptual Model and Numerical Approaches for Unsaturated Zone Flow and Transport* (BSC 2004 [DIRS 170035], Section 7.4.1; DTN: LB0212C14INFIL.002 [DIRS 179300]) indicate that a value of the AFM γ parameter less than or equal to 0.4 in the Topopah Spring welded unit (TSw) provides an acceptable fit to the ^{14}C ages measured in wells USW UZ-1 and USW SD-12. This range reflects the degree to which this parameter can be varied in a series of one-dimensional simulations and still result in mountain-scale model simulations that match the observed data. The numerical simulations show that, for values of the AFM γ parameter greater than 0.4, the simulated ^{14}C concentration deviates from the data. A similar set of three-dimensional model simulations presented in *UZ Flow Models and Submodels* (BSC 2004 [DIRS 169861]) show that parameter values of 0.4 and 0.6 provide equally good matches to the data for depths at or below the repository horizon. The justification for citing this comparison for the purpose of developing the uncertainty distribution for the AFM γ parameter is provided in Section 4.1.1. Analyses of mineral coating data presented in *Conceptual Model and Numerical Approaches for Unsaturated Zone Flow and Transport* (BSC 2004 [DIRS 170035], Section 7.4.2) show that the model is consistent with gamma values in this range.

Potential limitations in using ^{14}C to set the gamma parameter are:

- Possible inadequacy of the use of gas ^{14}C as an approximation of the liquid ^{14}C age, which is the value the model uses for comparison
- Uncertainty in infiltration rate at the wells used for the simulations
- Model structural errors such as inappropriate use of one-dimensional models or inexact flow patterns in the three-dimensional simulations.

Similarly, the use of hydrogenic calcite fracture-coating data for this purpose also has limitations. The coatings observable today are the cumulative result of over ten million years of calcite precipitation and dissolution, subjected to shifts in the geothermal gradient and numerous climate cycles. The uncertainties and approximations involved in modeling fracture coatings prevent use of this model for bounding parameter values with precision, given the uncertainties in the prevailing conditions over the extended time periods over which the coatings were formed.

Given these potential limitations, it would be inappropriate to assume that the gamma parameter is tightly constrained by the available information. A reasonable upper bound, given these limitations, is 0.6, which is the highest value demonstrated in past analyses to be consistent with the ^{14}C simulations. To constrain the lower bound, note first that the one-dimensional ^{14}C simulations do not rule out values as low as 0. However, 0 would imply that every fracture in the system flows, and that no preferential flow through the network exists. Simulated transport rates would be slowest for a value of 0 because the active (effective) interface area between fracture and matrix would then be maximized, as demonstrated in Section 6.6.4 of the parent report. This extreme is not thought to be credible, given the body of evidence in favor of preferential flow under unsaturated conditions through a relatively small subset of the total number of fractures (Liu et al. 1998 [DIRS 105729]). As 0.4 appears to provide a good match to the ^{14}C data, and 0.6 is the upper bound, a range that extends down to 0.2 provides an overall range that is equally distributed above and below the nominal value of 0.4. With no additional information available to define this parameter uncertainty distribution, the parameter will be sampled from a uniform distribution from 0.2 to 0.6. This range is consistent with the available data, and maintains the model within a range in which preferential flow through a subset of fractures will occur for all realizations.

For fracture residual saturation, a constant value of 0.01 is used for all layers (DTN: LB0207REVUZPRP.001 [DIRS 159526]).

6.5.7 Fracture Porosity, Fracture Spacing (m), and Fracture Aperture (m)

The development of parameter distributions for these parameters is unchanged from the parent report. The data now appear in output DTN: LA0701PANS02BR.003.

6.5.8 Fracture Surface Retardation Factor (Unitless)

No change.

6.5.9 Colloid Filtration at Matrix Interface

The development of parameter distributions for these parameters is unchanged from the parent report. The data now appear in output DTN: LA0701PANS02BR.003.

6.5.10 Colloid Size Exclusion

The development of parameter distributions for these parameters is unchanged from the parent report. The data now appear output DTN: LA0701PANS02BR.003.

6.5.11 Colloid-Size Distribution

The development of parameter distributions for these parameters is unchanged from the parent report. The data now appear in output DTN: LA0701PANS02BR.003.

6.5.12 Colloid Concentration and Colloid K_c

The basic equations associated with the use of the colloid concentration and colloid K_c in the TSPA model is unchanged from the parent report. The data sources, and the parameter values in some cases, have undergone changes, leading to the need to publish the following new versions of Tables 6-21 and 6-22.

Table 6-21. Colloid Concentration Distribution

Colloid Concentration (mg/L)	Cumulative Probability	Comment
0.001 to 0.1	0.50	Ionic strength less than 0.05 M. Data are used in the estimation of reversible colloid K_c
0.1 to 1.0	0.75	
1.0 to 10	0.90	
10 to 50	0.98	
50 to 200	1	
10^{-6}	1	Ionic strength ≥ 0.05 M
Type of Uncertainty		The cumulative distribution data listed in this table will be used to generate random colloid concentrations at TSPA-LA runtime to address the influence of colloid concentration uncertainty of radionuclide transport
Input Description		This parameter is used along with sorption coefficient onto colloids to determine the partitioning coefficient of radionuclides onto colloids

Source: SNL 2007 [DIRS 177423], Section 6.3.2.4, Table 6-4; DTN: MO0701PAGROUND.000 [DIRS 179310].

Output DTN: LA0701PANS02BR.003.

TSPA-LA = total system performance assessment for the license application.

Table 6-22. Radionuclide Sorption Coefficient (mL/g) onto Colloids

Radionuclide	Colloid	K_d Value Range (mL/g) with pH	K_d Value Intervals (mL/g)	K_d Value Cumulative Probabilities
Plutonium	FeCP*	10^4 to 10^6	1×10^4 to 5×10^4 5×10^4 to 1×10^5 1×10^5 to 5×10^5 5×10^5 to 1×10^6	0.4 0.7 0.9 1.0
	Smectite	10^3 to 10^5	1×10^3 to 5×10^3 5×10^3 to 1×10^4 1×10^4 to 5×10^4 5×10^4 to 1×10^5	0.45 0.80 0.95 1.00

Table 6-22. Radionuclide Sorption Coefficient (mL/g) onto Colloids (Continued)

Radionuclide	Colloid	K_d Value Range (mL/g) with pH	K_d Value Intervals (mL/g)	K_d Value Cumulative Probabilities
Americium Thorium Protactinium	FeCP	10^5 to 10^7	1×10^5 to 5×10^5 5×10^5 to 1×10^6 1×10^6 to 5×10^6 5×10^6 to 1×10^7	0.15 0.35 0.90 1.00
	Smectite	10^4 to 10^7	1×10^4 to 5×10^4 5×10^4 to 1×10^5 1×10^5 to 5×10^5 5×10^5 to 1×10^6 1×10^6 to 5×10^6 5×10^6 to 1×10^7	0.07 0.17 0.40 0.60 0.92 1.00
Cesium	FeCP	10^0 to 10^1	1×10^0 to 5×10^0 5×10^0 to 1×10^1	0.27 1.00
	Smectite	5×10^1 to 5×10^3	5×10^1 to 1×10^2 1×10^2 to 5×10^2 5×10^2 to 1×10^3 1×10^3 to 5×10^3	0.05 0.40 0.70 1.00
Tin	FeCP	10^2 to 10^6	10^2 to 10^6	Log Uniform
	Smectite	10^5 to 10^6	10^5 to 10^6	Log Uniform

Sources: DTNs: MO0701PASORPTN.000 [DIRS 180391] for plutonium, americium, thorium, protactinium, and cesium; MO0701PAKDSUNP.000 [DIRS 180392] for tin.

NOTE: FeCP = iron oxide corrosion products.

Colloid concentrations should be sampled from the same distribution for the EBS, unsaturated zone, and saturated zone components of the TSPA model because measurements have been made only under saturated groundwater conditions and the resulting uncertainty distribution does not distinguish concentration of colloids in the EBS, unsaturated zone, and saturated zone. Because of the limited information available, and differences in mineralogic and geochemical conditions in these domains, it is recommended that colloid concentration be sampled independently in each domain, rather than correlating the parameters within a given realization. However, because of this uncertainty, and the fact that correlating these concentrations could lead to a wider range of dose response in the TSPA model, a sensitivity study using the TSPA model is recommended in which colloid concentrations are 100% correlated between the EBS, unsaturated zone, and saturated zone components of the TSPA model.

Sorption coefficients for radionuclides on smectite colloids should be sampled from the same distributions for the EBS, unsaturated zone, and saturated zone components of the TSPA model because no other site-specific data are available to refine the model. Because of the limited information available, and the likelihood of significant differences in geochemical conditions in the three domains, it is recommended that the sorption coefficients be sampled independently in each domain, rather than correlating the parameters within a given realization. Independent sampling for radionuclide sorption onto smectite colloids between the unsaturated zone and saturated zone components of the TSPA model is supported by the fact that factors controlling sorption onto colloids in these three environments are believed to be relatively independent (see the discussion of conditions for radionuclide sorption onto tuff in the unsaturated versus saturated zones in SNL 2007 [DIRS 177396], Appendix B2). Because of the uncertainties in this

approach, the following sensitivities for unsaturated zone and EBS transport are recommended to be performed using the TSPA model:

- Correlate the K_d values on smectite colloids for americium and protactinium with a correlation coefficient of 0.75, with no correlation used for americium and thorium. These selections are based on the correlations presented in *Radionuclide Transport Models Under Ambient Conditions* (SNL 2007 [DIRS 177396], Table B-2) for sorption of these radionuclides onto tuff.

- Correlate K_d values on smectite colloids 100% between the EBS and unsaturated zone components of the TSPA model to investigate the uncertainty in the sorption behavior between these two domains.

6.5.13 Fractions of Colloids Traveling Unretarded and Colloid Retardation Factor

The development of parameter distributions for these parameters is unchanged from the parent report. The data now appear in output DTN: LA0701PANS02BR.003.

Colloid retardation factors should be sampled from the same distribution for the unsaturated zone and saturated zone components of the TSPA model because measurements have been made only under saturated groundwater conditions and the resulting uncertainty distribution does not distinguish between retardation under saturated and unsaturated conditions. It is recommended that sampling should be performed without correlating the colloid retardation factors in each domain because mineralogic and geochemical conditions influencing colloid retardation may differ in the unsaturated zone and saturated zone. However, because correlating the retardation factors may lead to a wider range of dose response in the TSPA model, a sensitivity study using the TSPA model is recommended in which colloid retardation factors are 100% correlated between the unsaturated zone and saturated zone.

6.5.14 Radionuclide Half Lives (Years) and Daughter Products

The following is the new version of Table 6-25 for the TSPA compliance model, which incorporates a new list of species to be simulated since the writing of the parent report.

Table 6-25. List of Radionuclides Simulated in Compliance Model

No.	Species	Half Life (yr)	Daughter Index
1	^{14}C	5.715×10^3	—
2	^{135}Cs (rev)	2.3×10^6	—
3	^{137}Cs (rev)	30.07	—
4	^{129}I	1.57×10^7	—
5	^{90}Sr	28.78	—
6	^{99}Tc	2.13×10^5	—
7	^{243}Am (rev)	7.37×10^3	10
8	Ic ^{243}Am	7.37×10^3	11
9	If ^{243}Am	7.37×10^3	12
10	^{239}Pu (rev)	2.410×10^4	13
11	Ic ^{239}Pu	2.410×10^4	13

Table 6-25. List of Radionuclides Simulated in Compliance Model (Continud)

No.	Species	Half Life (yr)	Daughter Index
12	If ^{239}Pu	2.410×10^{4}	13
13	^{235}U	7.04×10^{8}	14
14	^{231}Pa (rev)	3.28×10^{4}	—
15	^{241}Am (rev)	4.327×10^{2}	18
16	Ic ^{241}Am	4.327×10^{2}	18
17	If ^{241}Am	4.327×10^{2}	18
18	^{237}Np	2.14×10^{6}	19
19	^{233}U	1.592×10^{5}	20
20	^{229}Th (rev)	7.3×10^{3}	—
21	^{240}Pu (rev)	6.56×10^{3}	24
22	Ic ^{240}Pu	6.56×10^{3}	24
23	If ^{240}Pu	6.56×10^{3}	24
24	^{236}U	2.342×10^{7}	25
25	^{232}Th (rev)	1.40×10^{10}	—
26	^{232}U	69.8	—
27	^{242}Pu (rev)	3.75×10^{5}	33
28	Ic ^{242}Pu	3.75×10^{5}	33
29	If ^{242}Pu	3.75×10^{5}	33
30	^{238}Pu (rev)	87,7	34
31	Ic ^{238}Pu	87.7	34
32	If ^{238}Pu	87.7	34
33	^{238}U	4.47×10^{9}	34
34	^{234}U	2.46×10^{5}	35
35	^{230}Th (rev)	7.54×10^{4}	36
36	^{226}Ra	1.599×10^{3}	—
37	^{36}Cl	3.01×10^{5}	—
38	^{79}Se	2.95×10^{5}	—
39	^{126}Sn (rev)	2.50×10^{5}	—

Source: Parrington et al. 1996 [DIRS 103896] half-lives for all radionuclides except ^{79}Se, which comes from Singh 2002 [DIRS 164741].

Output DTN: LA0701PANS02BR.003.

NOTE: The designations "Ic" and "If" refer to colloid-facilitated transport of the corresponding species, and the term "(rev)" refers to a species for which reversible sorption onto colloids is simulated.

6.5.15 Repository Radionuclide Release Bins

Radionuclides will be released from nodes corresponding to the repository, which is located in the Topopah Spring middle nonlithophysal (Tmn) and lower lithophysal (Tll) hydrogeologic units (UZ model layers tsw34 and tsw35). These nodes were grouped into bins (zones) that shared common percolation rate ranges, to be compatible with a conceptual model for radionuclide release in which releases are a strong function of the percolation rates at the repository horizon. This would help to categorize release points according to high or low percolation rates. Five bins were chosen based on the cumulative probability of percolation for the 12 flow fields (three different climate periods, present-day, monsoon, and glacial-transition with each climate period categorized by four infiltration scenarios, 10%, 30%, 50%, and 90%).

The definition of the five bins, and the percolation rate ranges associated with each, is listed in Table 6-26.

The new process is described in output DTN: LA0702PANS02BR.001, in which, a separate FEHM zone2 file is developed for each flow field. This was done to facilitate an analysis of the degree of similarity of the bins for the different flow fields. A series of steps were conducted for each flow field, leading to the final list of nodes for each bin. In each of the twelve Excel workbooks in output DTN: LA0702PANS02BR.001, there are four spreadsheets, one for each of the following steps in the process: (1) Identify the FEHM node number for the new repository node list that corresponds to the column in the original grid containing that node[3]; (2) Eliminate the nodes that are not repository nodes and include an additional column containing the matrix node corresponding to each fracture repository model; (3) For each of the 12 flow fields, sort the nodes from lowest percolation rate to highest, using the flux from the PTn to the TSw in that column of the grid as a surrogate for the flux at the repository itself; and (4) Divide the nodes into five bins that share common percolation rate ranges, using the same cumulative probability intervals for these bins as were used in the parent report.

Output DTN: LA0702PANS02BR.001, file *compare_bins.xls*, presents an analysis of the degree of similarity or difference of the results of the binning process depending on which flow field is analyzed. The results indicate that the bins for the 12 flow fields are quite similar to one another. In other words, if a bin is identified for a particular node in the glacial-transition, 10th percentile flow field (denoted as GT10, with the number "10" indicating that the flow field corresponds to the 10th percentile infiltration map), it is very often identified as the same bin for the other flow fields. When they are different, they almost always differ by only one bin, that is, a 3 in GT10 becomes a 4 in another flow field, or a 2 becomes a 1. This result indicates that it is an acceptable approximation to use bins from one flow field for all infiltration scenarios and climate states. Furthermore, if the post-10k-yr flow fields are similar to the ones developed so far, the bins should remain similar for these as well. Therefore, for the compliance model, *fehmn.zone2_GT10%* from the DTN should be used to define the bins for all simulations. Figure 6-14 shows a representation of the repository nodes colored by percolation bin for the glacial-transition, 10th percentile flow field.

[3] This spreadsheet contains all columns in the three-dimensional model, only a fraction of which are within the footprint of the repository.

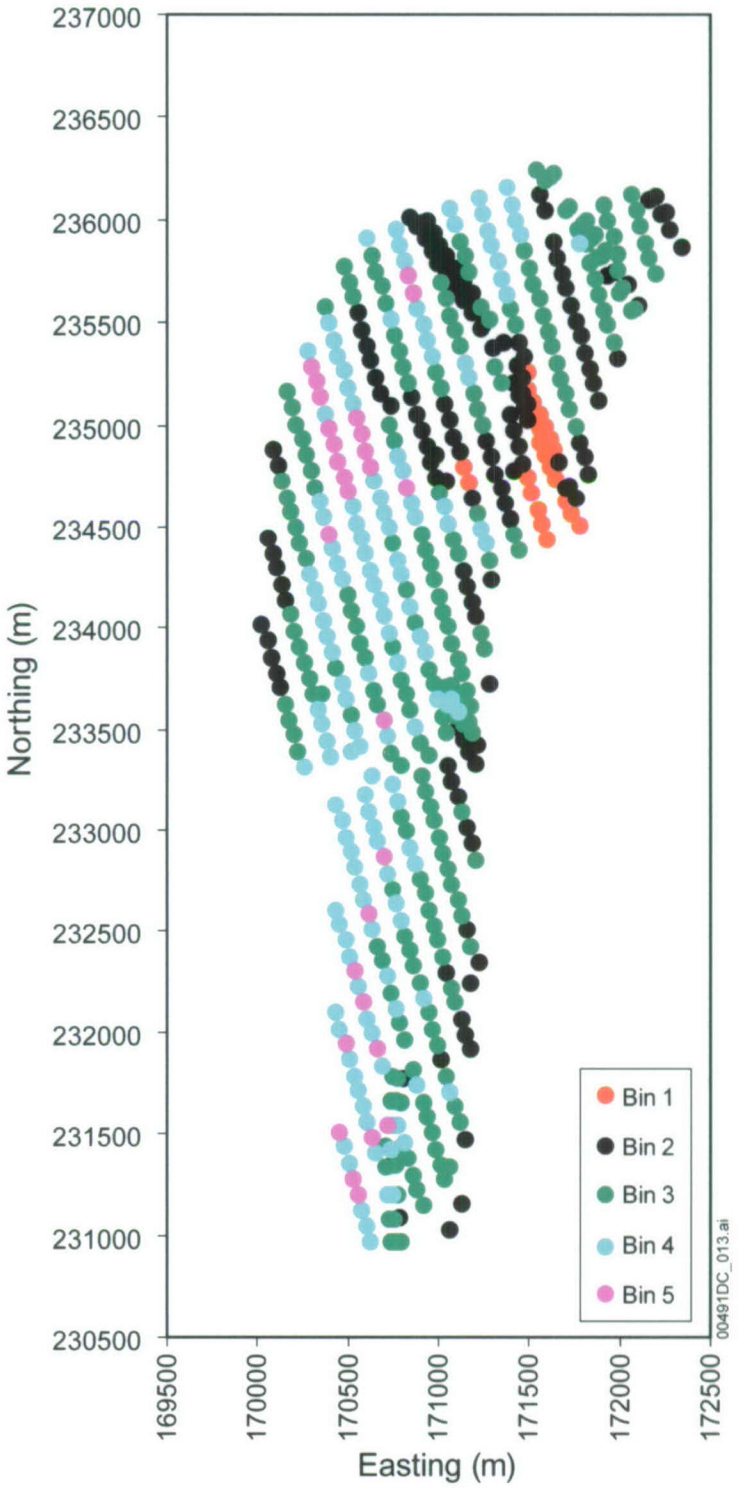

Output DTN: LA0702PANS02BR.001.

Figure 6-14. Repository Nodes Colored by Percolation Bin for the Glacial-Transition, 10th Percentile Flow Field

Table 6-26. Definition of Repository Release Bins

Range of Cumulative Probability (range of nodes when sorted from lowest to highest percolation flux)	Bin1	Bin2	Bin3	Bin4	Bin5	Median Percolation Flux (flux of node 280 when sorted from lowest to highest percolation flux)
	0 to 0.05 (1 to 28)	0.05 to 0.30 (29 to 168)	0.30 to 0.70 (169 to 392)	0.70 to 0.95 (393 to 532)	0.95 to 1.00 (533 to 560)	
Range of Percolation Flux (mm/yr) for Present-day climate, 10% infiltration scenario	0.13 to 0.57	0.57 to 2.83	2.83 to 4.92	4.92 to 6.43	6.43 to 8.10	3.93
Present-day climate, 30% infiltration scenario	0.34 to 1.70	1.70 to 7.73	7.73 to 12.23	12.23 to 15.27	15.27 to 19.00	10.04
Present-day climate, 50% infiltration scenario	0.60 to 2.26	2.26 to 11.87	11.87 to 17.09	17.09 to 21.02	21.02 to 26.56	14.77
Present-day climate, 90% infiltration scenario	1.32 to 4.94	4.94 to 29.33	29.33 to 40.35	40.35 to 47.17	47.17 to 58.74	35.27
Monsoon climate, 10% infiltration scenario	0.43 to 1.22	1.22 to 6.52	6.52 to 9.21	9.21 to 11.11	11.11 to 14.61	7.97
Monsoon climate, 30% infiltration scenario	0.55 to 2.33	2.33 to 12.05	12.05 to 18.99	18.99 to 24.99	24.99 to 31.17	15.62
Monsoon climate, 50% infiltration scenario	0.53 to 2.70	2.70 to 13.06	13.06 to 23.06	23.06 to 31.96	31.96 to 49.90	19.02
Monsoon climate, 90% infiltration scenario	3.08 to 11.94	11.94 to 80.32	80.32 to 109.82	109.82 to 127.58	127.58 to 159.63	96.68
Glacial-transition climate, 10% infiltration scenario	0.15 to 0.82	0.82 to 4.55	4.55 to 14.06	14.06 to 26.16	26.16 to 36.19	8.97
Glacial-transition climate, 30% infiltration scenario	0.43 to 2.88	2.88 to 15.99	15.99 to 31.97	31.97 to 44.51	44.51 to 54.89	24.02

Table 6-26. Definition of Repository Release Bins (Continued)

Range of Cumulative Probability (range of nodes when sorted from lowest to highest percolation flux)	Bin1	Bin2	Bin3	Bin4	Bin5	Median Percolation Flux (flux of node 280 when sorted from lowest to highest percolation flux)
	0 to 0.05 (1 to 28)	0.05 to 0.30 (29 to 168)	0.30 to 0.70 (169 to 392)	0.70 to 0.95 (393 to 532)	0.95 to 1.00 (533 to 560)	
Glacial-transition climate, 50% infiltration scenario	0.45 to 3.10	3.10 to 18.90	18.90 to 45.87	45.87 to 63.40	63.40 to 79.89	32.58
Glacial-transition climate, 90% infiltration scenario	1.20 to 6.93	6.93 to 50.96	50.96 to 84.51	84.51 to 105.74	105.74 to 136.06	70.12

NOTE: For percolation values, see Output DTN: LA0702PANS02BR.001.

6.5.16 Radionuclide Collecting Bins at Unsaturated Zone/Saturated Zone Interface

There are no changes to this section, compared with the parent report, except that the output DTN is LA0702PANS02BR.001.

6.6 REPRESENTATIVE-CASE MODEL

In this section and subsections, there is a significant update to the corresponding section in Revision 2 that necessitates a renumbering of the tables, figures, and equations. The numbering convention within this addendum section is designed such that the numbering scheme is independent of the numbering in the remainder of the document.

6.6.1 Overview

In this addendum, the representative case is taken to be a series of simulations using either median or mean values of radionuclide transport parameters. For comparisons examining the impact of climate and flow scenarios on the model results, the full set of flow fields are used. For many other simulations, such as the breakthrough curve results, the glacial-transition, 10th percentile flow field is used for illustrative purposes. However, none of the results from these runs will be used directly by TSPA. Rather, this simulation activity illustrates the possible transport behavior of radionuclides within the unsaturated zone for representative flow conditions and transport parameter values. In TSPA-LA, the abstracted model will be used with different parameter combinations to study the uncertainty of parameters and flow fields on radionuclide transport through the unsaturated zone and its impacts on system performance. However, the representative case represents typical behavior of the unsaturated zone transport abstraction model for the purposes of understanding the role of the unsaturated zone in the overall repository transport system. Then, in Section 6.8.2, sensitivity analyses are presented to illustrate the impact of uncertainties in key parameters on the capability of the unsaturated zone as a barrier to radionuclide transport.

The simulations presented in this addendum for both the representative case and the barrier capability and uncertainty analyses of Section 6.8.2 were carried out using FEHM V. 2.24-01 [DIRS 179419]. Data used in these simulations are the radionuclides in Table 6-25 and the representative parameter values listed in Table 6.6.1-1. These values are selected typically as the median values within the uncertainty distribution. For studies in which the impact of flow conditions are examined, the flow fields used in the simulations represent three climate conditions (present-day, glacial transition, and monsoon), each of which has four different percolation scenarios (10th, 30th, 50th, and 90th percentile). The objective of these representative-case simulations is to study the movement of radionuclides released from the EBS into unsaturated fractured geological media downward to the water table under conditions that represent the nominal behavior of the unsaturated zone. Large-scale issues such as the influence of flow rates and flow patterns, and the influence of release location and percolation bin are presented in Section 6.6.2.1. Then, Section 6.6.2.2 presents representative breakthrough curves at the water table for all radionuclides, including an analysis of the important decay chains in the model. Finally, Section 6.6.2.3 investigates the impact of whether the releases occur in the fracture versus matrix continuum.

Table 6.6.1-1. Selected Parameter Values for Representative-Case Unsaturated Zone Model

Key	Parameter Type	Value	Comments
Aperture (m) 2b, Output DTN: LA0701PANS02BR.003, *Table 1.doc*			
-1	Group 1 Units	7.94×10^{-3}	
-2	Group 2 Units	1.43×10^{-2}	
-3	Group 3 Units	2.64×10^{-3}	
-4	Group 4 Units	4.85×10^{-3}	
-5	Group 5 Units	4.00×10^{-3}	
-6	Group 6 Units	5.75×10^{-3}	
-7	Group 7 Units	4.48×10^{-3}	
-8	Group 8 Units	2.64×10^{-3}	
-9	Group 9 Units	7.16×10^{-3}	
Gamma Parameter, all units			
-10	Gamma Parameter	0.6	Median value is 0.4, but calculations in this addendum used 0.6, the value used in the parent report
D_m: Mean Values (m^2/s) from Table 6.5.5-3			
-11	Am in Tortuosity Rock Group 1	6.718×10^{-11}	
-12	Am in Tortuosity Rock Group 2	2.554×10^{-11}	
-13	Am in Tortuosity Rock Group 3	1.372×10^{-11}	
-14	C in Tortuosity Rock Group 1	8.354×10^{-11}	
-15	C in Tortuosity Rock Group 2	3.176×10^{-11}	
-16	C in Tortuosity Rock Group 3	1.706×10^{-11}	
-17	Cl in Tortuosity Rock Group 1	1.437×10^{-10}	
-18	Cl in Tortuosity Rock Group 2	5.464×10^{-11}	
-19	Cl in Tortuosity Rock Group 3	2.934×10^{-11}	
-20	Cs in Tortuosity Rock Group 1	1.458×10^{-10}	
-21	Cs in Tortuosity Rock Group 2	5.545×10^{-11}	
-22	Cs in Tortuosity Rock Group 3	2.978×10^{-11}	

Table 6.6.1-1. Selected Parameter Values for Representative-Case Unsaturated Zone Model (Continued)

Key	Parameter Type	Value	Comments
D_m: Mean Values (m^2/s) from Table 6.5.5-3 (Continued)			
-23	I in Tortuosity Rock Group 1	1.451×10^{-10}	
-24	I in Tortuosity Rock Group 2	5.518×10^{-11}	
-25	I in Tortuosity Rock Group 3	2.963×10^{-11}	
-26	Np in Tortuosity Rock Group 1	4.375×10^{-11}	
-27	Np in Tortuosity Rock Group 2	1.663×10^{-11}	
-28	Np in Tortuosity Rock Group 3	8.933×10^{-12}	
-29	Pa in Tortuosity Rock Group 1	4.276×10^{-11}	
-30	Pa in Tortuosity Rock Group 2	1.626×10^{-11}	
-31	Pa in Tortuosity Rock Group 3	8.730×10^{-12}	
-32	Pu in Tortuosity Rock Group 1	9.203×10^{-11}	
-33	Pu in Tortuosity Rock Group 2	3.499×10^{-11}	
-34	Pu in Tortuosity Rock Group 3	1.879×10^{-11}	
-35	Ra in Tortuosity Rock Group 1	6.294×10^{-11}	
-36	Ra in Tortuosity Rock Group 2	2.393×10^{-11}	
-37	Ra in Tortuosity Rock Group 3	1.285×10^{-11}	
-38	Se in Tortuosity Rock Group 1	7.363×10^{-11}	
-39	Se in Tortuosity Rock Group 2	2.799×10^{-11}	
-40	Se in Tortuosity Rock Group 3	1.503×10^{-11}	
-41	Sn in Tortuosity Rock Group 1	1.097×10^{-10}	
-42	Sn in Tortuosity Rock Group 2	4.172×10^{-11}	
-43	Sn in Tortuosity Rock Group 3	2.240×10^{-11}	
-44	Sr in Tortuosity Rock Group 1	5.600×10^{-11}	
-45	Sr in Tortuosity Rock Group 2	2.129×10^{-11}	
-46	Sr in Tortuosity Rock Group 3	1.143×10^{-11}	
-47	Tc in Tortuosity Rock Group 1	1.380×10^{-10}	
-48	Tc in Tortuosity Rock Group 2	5.248×10^{-11}	
-49	Tc in Tortuosity Rock Group 3	2.819×10^{-11}	
-50	Th in Tortuosity Rock Group 1	4.226×10^{-11}	
-51	Th in Tortuosity Rock Group 2	1.607×10^{-11}	
-52	Th in Tortuosity Rock Group 3	8.629×10^{-12}	
-53	U in Tortuosity Rock Group 1	4.701×10^{-11}	
-54	U in Tortuosity Rock Group 2	1.787×10^{-11}	
-55	U in Tortuosity Rock Group 3	9.598×10^{-12}	
Representative Value Sorption Coefficients (K_d: mL/g) from SNL 2007 [DIRS 177396]; DTNs: LA0408AM831341.001 [DIRS 171584] and LB0701PAKDSESN.001 [DIRS 179299]			
-56	Am in Rock Group 1	5,500	
-57	Am in Rock Group 2	5,500	
-58	Am in Rock Group 3	400	
-59	C in Rock Group 1	0	
-60	C in Rock Group 2	0	
-61	C in Rock Group 3	0	
-62	Cl in Rock Group 1	0	
-63	Cl in Rock Group 2	0	

Table 6.6.1-1. Selected Parameter Values for Representative-Case Unsaturated Zone Model (Continued)

Key	Parameter Type	Value	Comments
Representative Value Sorption Coefficients (K_d: mL/g) from SNL 2007 [DIRS 177396]; DTNs: LA0408AM831341.001 [DIRS 171584] and LB0701PAKDSESN.001 [DIRS 179299] (Continued)			
-64	Cl in Rock Group 3	0	
-65	Cs in Rock Group 1	5,000	
-66	Cs in Rock Group 2	8	
-67	Cs in Rock Group 3	2	
-68	I in Rock Group 1	0	
-69	I in Rock Group 2	0	
-70	I in Rock Group 3	0	
-71	Np in Rock Group 1	0.5	
-72	Np in Rock Group 2	0.5	
-73	Np in Rock Group 3	1	
-74	Pa in Rock Group 1	5,500	
-75	Pa in Rock Group 2	5,500	
-76	Pa in Rock Group 3	5,500	
-77	Pu in Rock Group 1	100	
-78	Pu in Rock Group 2	70	
-79	Pu in Rock Group 3	100	
-80	Ra in Rock Group 1	3,000	
-81	Ra in Rock Group 2	550	
-82	Ra in Rock Group 3	325	
-83	Se in Rock Group 1	14.3	
-84	Se in Rock Group 2	14.0	
-85	Se in Rock Group 3	8.6	
-86	Sn in Rock Group 1	707	
-87	Sn in Rock Group 2	3,162	
-88	Sn in Rock Group 3	707	
-89	Sr in Rock Group 1	1,025	
-90	Sr in Rock Group 2	40	
-91	Sr in Rock Group 3	25	
-92	Tc in Rock Group 1	0	
-93	Tc in Rock Group 2	0	
-94	Tc in Rock Group 3	0	
-95	Th in Rock Group 1	15,500	
-96	Th in Rock Group 2	5,500	
-97	Th in Rock Group 3	5,500	
-98	U in Rock Group 1	0.5	
-99	U in Rock Group 2	0.2	
-100	U in Rock Group 3	0.2	

Table 6.6.1-1. Selected Parameter Values for Representative-Case Unsaturated Zone Model (Continued)

Key	Parameter Type	Value	Comments
Sorption Partition Coefficient (L/kg) onto Colloids			
-101	Am	0.075	Example calculation for Am on smectite: Median C_{coll} = 0.1 mg/L = 0.1 × 10^{-6} kg/L from Table 6-21 Median $K_{d,coll}$ = 7.5 × 10^{5} mL/g = 7.5 × 10^{5} L/kg (interpolated from Table 6-22) K_c = 0.1 × 10^{-6}kg/L*7.5e5 L/kg = .075
-102	Cs	6.67 × 10^{-5}	
-103	Pa	0.075	
-104	Pu	0.0005714	
-105	Sn	0.0316	
-106	Th	0.075	
-107	Retardation factor	26	Does not apply to the If (irreversible fast colloids). Value from Table 6-24 of this addendum.

NOTES: The key values represent a file input location for a distribution of values that are sampled to represent the uncertainty parameters in runs for TSPA-LA.
Radionuclides listed = americium (Am), carbon (C), chlorine (Cl), cesium (Cs), iodine (I), neptunium (Np), protactinium (Pa), plutonium (Pl), radium (Ra), selenium (Se), tin (Sn), strontium (Sm), technetium (Tc), thorium (Th), and uranium (U).

6.6.2 Representative-Case Model Results

6.6.2.1 Statistics of Travel Time and Exit Location

In this addendum, the statistics of the simulated travel time and exit location (defined as the coordinate location at which mass reaches the water table) for conservative particles released at repository site are presented. For this purpose, a dissolved species without decay or matrix diffusion was chosen to examine fluid flow properties of the unsaturated zone. In the parent report, composite breakthrough curves were reported from a uniform distribution of particles across the entire repository domain. This approach yielded a breakthrough curve result that mixed spatial variability and uncertainty in a complex way, potentially masking the behavior of the unsaturated zone model. In this addendum, particles are released at each individual node and then the statistics of travel time and of exiting locations are computed based on all particles released at the node. Organizing the simulations in this way, information on the spatial variability across the repository is retained, thereby allowing for an exploration of the dependence of travel time statistics on the release location. In addition, the dependence on travel time statistics and exit locations of the bin classification with respect to percolation rate at the repository (e.g., see Figure 6-14 and Table 6-26) can be examined.

Preliminary calculations suggested that for examining the mean travel time and mean exit location, about 2,000 particles were sufficient, whereas a stable value for the variance of the travel time and exiting locations required about 5,000 particles. To ensure convergence for both types of analyses, 10,000 particles were used at each simulation. Thus, for each of the 12 flow fields, 560 model runs were performed in which 10,000 particles were released at each repository node. Results were postprocessed using software routine PARTICLE_STAT V1.0 [DIRS 181317] to generate the results presented herein.

The unsaturated zone base-case simulations presented in this report are for three climate conditions (present-day, glacial-transition, and monsoon), each of which has four different infiltration scenarios (10th, 30th, 50th, and 90th percentile infiltration scenarios). Simulations for glacial-transition and monsoon climate conditions use a raised water table elevation of 850 m.

Figure 6.6.2-1 illustrates statistics of the travel time for the glacial-transition, 10th percentile infiltration scenario. This mean travel time map shows a dramatic spatial variability in which releases in the northern repository region yield much shorter travel times than releases in the southern region. This result is due to the presence of an unaltered, vitric Calico Hills unit beneath the repository in the southern region. In contrast, the northern release yields fracture flow from the repository horizon to the water table, with Calico Hills units altered to low-matrix-permeability rocks in which fracture flow and/or lateral diversion occurs.

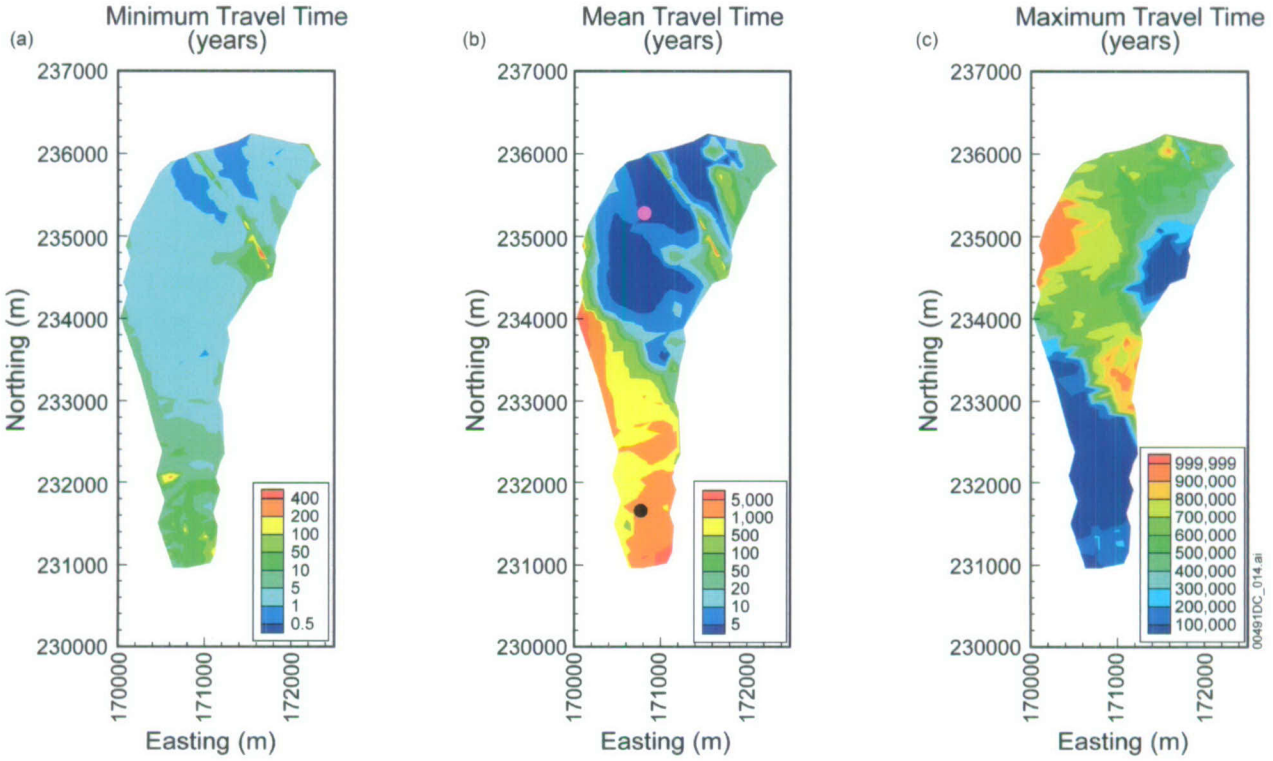

Output DTN: MO0705TRANSTAT.000.

NOTE: The pink (Northern) and black (Southern) points in (b) are the individual release locations used in this study.

Figure 6.6.2-1. Contour Maps of (a) the Minimum Travel Time, (b) the Mean Travel Time, and (c) the Maximum Travel Time for Particles Released at All Repository Nodes under Glacial-Transition, 10th Percentile Infiltration Scenario, and Conservative Species without Decay and Matrix Diffusion

Figure 6.6.2-1 also shows contour maps of the minimum travel time (first arrival) among the 10,000 particles across the repository horizon, as well as a contour map for the maximum travel time. Like the mean travel times, the minimum travel time in the southern region is larger than that in the northern region. However, the maximum travel time in the southern region is smaller

than that in the northern region. In other words, the spread of travel times is greater for the northern release locations. This result is due to the different transport mechanisms at work in the two regions. For an area dominated by fracture flow, slow matrix transport spreads the arrival times over a greater range than for a system in which only matrix flow and transport occurs.

For the 10,000 particles released from each repository node, the vast majority have reached the water table by the end of the simulation time of 1,000,000 years. For these particles, one can compute the mean position and spreading of these particles at water table (irrespective of the arrival times of the particles). In this analysis, the mean displacement, from the repository release point to the location at the water table, is computed in each of the horizontal directions. Thus, the mean displacement is an indication of the trajectory of the particle pathways from different release locations. Figure 6.6.2-2 shows the mean shifts in the x and y directions and the variability in these shifts as a function of the location of release from a repository node for the glacial-transition, 10th percentile infiltration scenario. Each location in the figures represents a release location of 10,000 particles from a given computational grid cell in the repository region. The figure clearly demonstrates that the x-component of the mean velocity in the flow paths from the repository to the water table is always positive, indicating that particles migrate toward the east from the release location to the water table. The figure also shows that the mean travel distance in the x direction decreases as the release location moves from the western area to the eastern area, an indication that the most releases will exit the unsaturated system from the eastern boundary of the repository footprint. The right-hand figure shows that displacement in the y direction is almost always slightly positive (i.e., northerly) for releases in the southern region (i.e., south of a Northing coordinate of 234400 m), while in the northern region particles move toward the south, except in the several fault zones where particles have a small displacement toward the north. In addition, the mean displacement in the y direction is relatively small (less than 300 m) in the southern region but may reach as large as 1,000 m in the northern region.

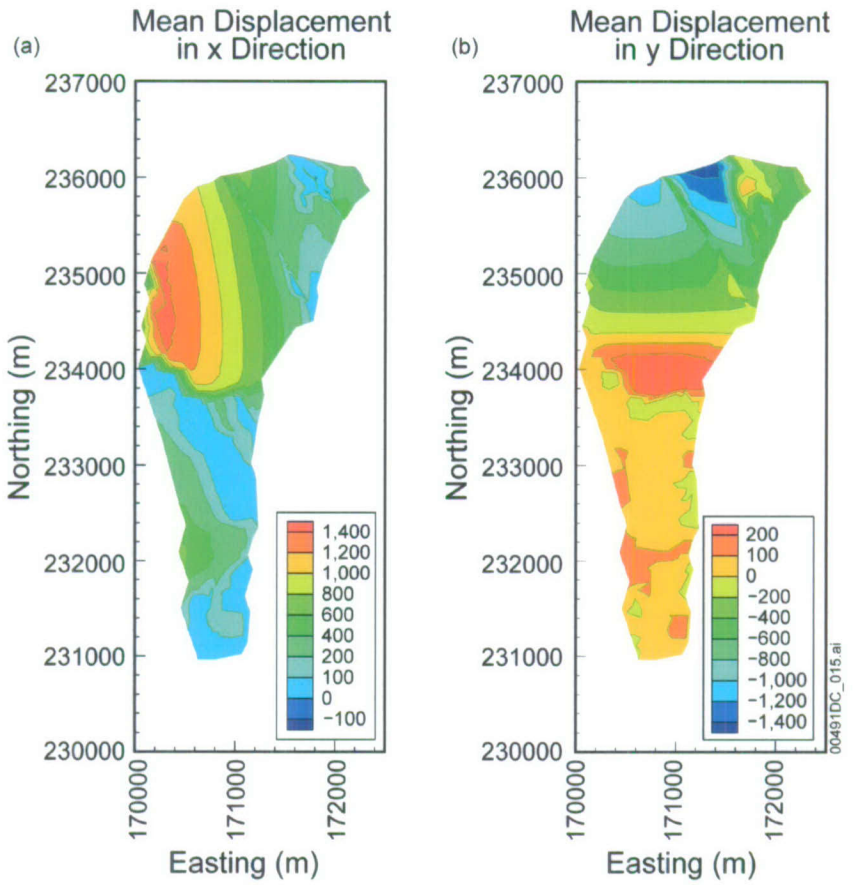

Output DTN: MO0705TRANSTAT.000.

Figure 6.6.2-2. Contour Maps of Mean Displacement (in meters) of Particles (a) in the *x* Direction, and (b) in the *y* Direction for Particles Released at All Repository Nodes under Glacial Transition, 10th Percentile Infiltration Scenario and Conservative Species.

Another method for displaying these results is to plot the mean particle arrival location at the water table as individual points colored by either bin classification or the mean travel time. Figure 6.6.2-3 shows the percolation bin assignments for each repository node (left), and mean arrival locations at the water table colored by bin (middle figure) and the travel time (right figure) for the glacial-transition, 10th percentile infiltration scenario. Note that each dot in the figures represents a release location of 10,000 particles, and the resulting mean arrival location represents the mean position of the 10,000 particles released. For the northern release locations, the trends are for lateral diversion to yield arrivals that coincide with several fault zones, including the Drill Hole Wash Fault and Pagany Wash Fault (for the locations of these faults, see SNL 2007 [DIRS 175177], Figure 6.1-1). These results are consistent with a model of vertical transport to the perching horizons beneath the repository, followed by lateral diversion to fault zones, and vertical transport down the faults. In contrast, the paths followed by particles originating from southern release locations are essentially vertical. The plot in which the locations are colored based on travel time (the right plot) shows that the particles with shortest mean travel time (less than 10 years) reach the water table in the fault zones. These pathways represent releases over a broad region (not just releases into the fault itself) that are diverted laterally in the perching horizon and eventually reach the fault zones. As a result of lateral

diversion, the shortest mean travel times (< 10 yrs) are coincidentally associated with the repository area with the lowest percolation flux (Bin 1, < 1 mm/yr) because of its location relative to the Drill Hole Wash fault zone.

Similar figures to those presented thus far have been plotted for all flow fields associated with the three climate scenarios. Results presented in Appendix D show that travel times correlate with the percolation flux (a function of the climate and infiltration models), as expected. However, other analyses (documented in Output DTN: MO0705TRANSTAT.000) indicate that the spatial variability of travel time and the mean displacements in both the x and y directions are very similar for different flow scenarios, implying that the infiltration scenarios result in different rates of migration, but similar flow directions.

Figure 6.6.2-4 presents the travel times to the water table (plotted as mean log (10-based) travel time) for releases from the repository, categorized by percolation bin assignment. The plotted travel times are the averages of all travel times associated with repository release nodes within a given percolation bin, for the four infiltration scenarios for the present-day (left figure), monsoon (middle figure), and glacial-transition (right figure) climate states. The expected trend of longer travel times for the 10th percentile case, compared to the 30th, 50th, and 90th percentile cases, are clearly reflected in these simulations. However, note that a smaller bin number, which corresponds to a smaller percolation rate at the repository horizon, often results in smaller travel times, despite the lower water flux at that location. In fact, for several of these flow fields, including all of the present-day flow fields, there is a *positive* correlation between percolation rate at the repository and travel time, i.e., travel times from percolation bin 5 result in *longer* travel times despite the higher percolation rates at the repository horizon. This counterintuitive result indicates that the local percolation flux does not play as important a role in the travel time as do other factors.

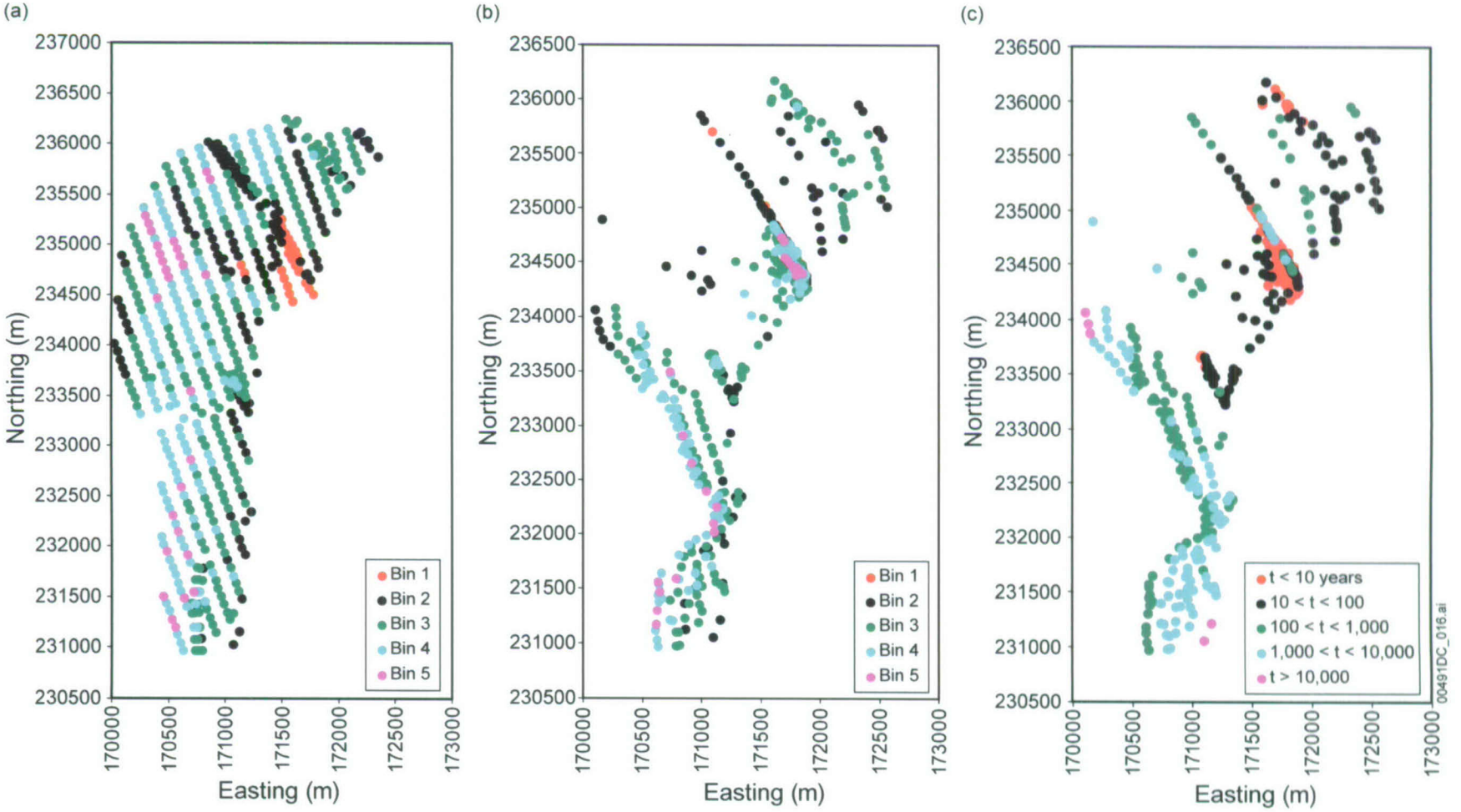

Output DTN: MO0705TRANSTAT.000.

NOTE: For this scenario, upper percolation rates for each bin are Bin 1 = 0.82, Bin 2 = 4.55, Bin 3 = 14.06, Bin 4 = 26.16, and Bin 5 = 36.19 mm/yr (Table 6-26). The figure on the right shows the exit locations plotted with mean travel time of a conservative species without decay and matrix diffusion.

Figure 6.6.2-3. Comparison of Particle Release Locations (Left) and Exit Locations in Terms of Percolation Bin Assignment (middle) or Mean Travel Time (right) for the Glacial-Transition, 10th percentile Infiltration Scenario

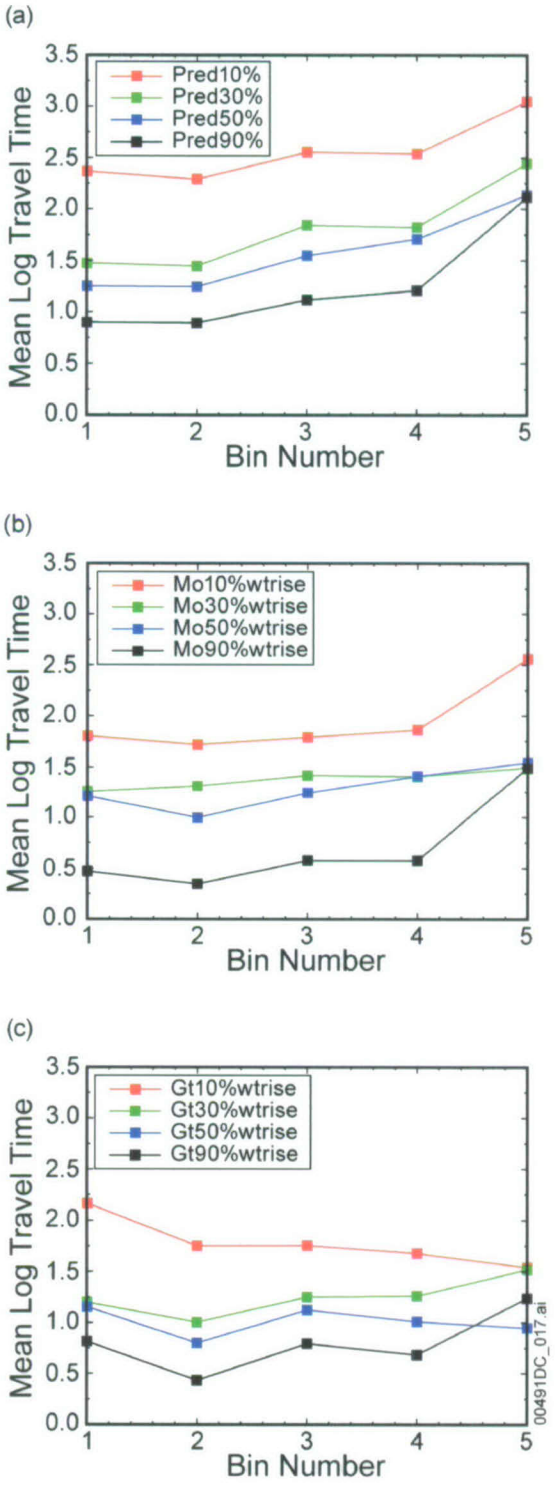

Output DTN: MO0705TRANSTAT.000.

Figure 6.6.2-4. Comparison of the Bin-Averaged Log Travel Time for Particles Released at All Repository Nodes for Three Climate Conditions (a) Present-Day, b) Monsoon, and c) Glacial-Transition) and Four Infiltration Scenarios, and Conservative Species without Decay and Matrix Diffusion

Furthermore, it was pointed out in Section 6.5.15 that the bins for the 12 flow fields are quite similar to one another. It turns out that other factors such as the hydrogeologic conditions beneath the repository actually drive the results: the location of the release point (north versus south) with respect to the underlying hydrogeologic strata and faults is the controlling factor in determining the travel time to the water table. Therefore, while percolation bin may have an important impact on radionuclide releases predicted in other parts of the TSPA model, such as the radionuclide release rate from the engineered barrier system, it is relatively unimportant as a factor controlling the travel times through the unsaturated zone.

6.6.2.2 Radionuclide Breakthrough Curves

This section presents breakthrough curves for different radionuclides from the specified release location to the water table. In the figures of this section and others in which the term "normalized" is used, the simulation consists of a pulse input of particles, with the breakthrough curve plot representing the cumulative number of particles reaching the water table, normalized by the total number of particles injected. Therefore, if all particles released from the repository reach the water table, the breakthrough curve value will reach unity. Under the conditions of steady-state flow, this integral plot represents the mass flux (normalized by the input mass flux) that would have been obtained if a constant mass flux had been input, even though the actual input was a pulse. For these simulations, the representative-case parameter values specified in Table 6.6.1-1 are used.

In TSPA, radionuclides released from the near field environment will migrate from individual point sources, the location of which is determined randomly based on the engineered barrier system (EBS) radionuclide release model. If multiple waste packages fail, then the releases will occur from several point sources. However, as long as only a few waste packages fail in a given realization, then the unsaturated zone model behavior will depend on the local conditions from a few point sources. Therefore, it is important to examine the behavior under such conditions. Given the results of the previous section, the repository behavior can be characterized, to first order, by examining breakthrough curves from two locations: one in the northern region, and one in the southern region. This simplification, for the purposes of demonstrating unsaturated zone behavior, captures the primary dependence of the model in terms of hydrogeologic variability, in that one region with predominantly fracture transport (the northern release location) and one region with an interval with matrix-dominated transport (the southern release location) are selected. The northern node (grid cell number 39713) is located at Nevada State Plane coordinates (m) (170810, 235280), and the southern node (grid cell number 104432) is located at Nevada State Plane coordinates (m) (170770, 231660). In Section 6.6.2.3, releases into the matrix are simulated. For those studies, the matrix grid cells at these same locations are selected. The locations of the two release locations are plotted in the mean travel time plot of Figure 6.6.2-1: the pink dot represents the northern release location, and the black dot represents the southern release location.

Figure 6.6.2-5 shows the normalized cumulative breakthrough curves for all species modeled as simple decay radionuclides (^{14}C, ^{135}Cs, ^{137}Cs, ^{129}I, ^{90}Sr, ^{99}Tc, ^{231}Pa, ^{229}Th, ^{232}Th, ^{232}U, ^{226}Ra, ^{36}Cl, ^{79}Se, and ^{126}Sn). The upper figure presents breakthrough curves for the northern release location, while the lower figure shows the breakthrough curves for the southern release location. These and other results for this representative case are for the glacial-transition, 10th percentile

infiltration scenario. Due to pervasive fracture transport along the entire flow path, arrival times for all species are much shorter for particles released from the northern location, compared to those released from the southern location. The first arrival at the water table from the northern location is within a year, versus about 400 years from the southern location. Because of the longer travel time through the matrix units, cumulative arrivals at the water table are negligible for radionuclides released from the southern location, for either relatively short-lived or strongly sorbing radionuclides, including ^{137}Cs, ^{90}Sr, ^{231}Pa, ^{229}Th, ^{232}Th, ^{232}U, ^{226}Ra, and ^{126}Sn. However, significant proportions of all 14 radioactive species reach the water table for releases from the northern location. This result illustrates the model's prediction that the unsaturated zone serves as a significant barrier to radionuclide migration for sorbed species released in the southern region, whereas for the northern region, the unsaturated zone provides a limited barrier to radionuclide migration even for sorbing species (for parameter values selected for this representative case). A more-complete examination of the uncertainties of key parameters and their influence on the unsaturated zone as a barrier to radionuclide migration is presented in Section 6.8.2. Finally, the breakthrough curves for nonsorbing radionuclides with long half lives (^{129}I, ^{99}Tc, and ^{36}Cl), reach normalized breakthrough values close to unity for both release locations. The unsaturated zone provides virtually no barrier to radionuclide migration for these species.

Comparisons of breakthrough curves for 12 colloidal species (Ic and If species of ^{243}Am, ^{239}Pu, ^{241}Am, ^{240}Pu, ^{242}Pu, and ^{238}Pu) released from both the locations are illustrated in Figure 6.6.2-6. The simulation results show that, as expected, radionuclides that are irreversibly attached to "fast" colloids (If species), which are not affected by matrix diffusion and retardation, have the shortest breakthrough times. At the northern location, within about 10 years after release, over 90% of the irreversible fast colloids travel through the unsaturated zone. Radionuclides that are irreversibly attached to "slow" colloids (Ic species), which undergo retardation due to colloid attachment/detachment processes, move more slowly than their corresponding fast colloid counterparts. The transport time of the irreversible slow colloids depends on the colloid retardation factor, a parameter that is explored more fully in Section 6.8.2. Compared to the fast colloids released at the northern location, the first arrival times for the southern release location are about one order of magnitude larger, due to the thickness of the interval of unfractured rock governed by slower matrix transport. The cumulative breakthroughs for most of these irreversible fast colloids in the northern location are close to unity (except for Ic^{238}Pu and Ic^{241}Am), whereas for the southern location, the cumulative breakthrough is significantly reduced for many radionuclides. The exceptions are If ^{242}Pu, Ic ^{242}Pu, and If ^{240}Pu, which reach the water table with a normalized breakthrough approaching unity (greater than 0.8), even for the southern release location. In summary, most of the Ic and If colloidal species have very limited reduction due to decay in the unsaturated zone from the northern release location, whereas a larger proportion of the radionuclides decay in the unsaturated zone before reaching the water table for the southern release location.

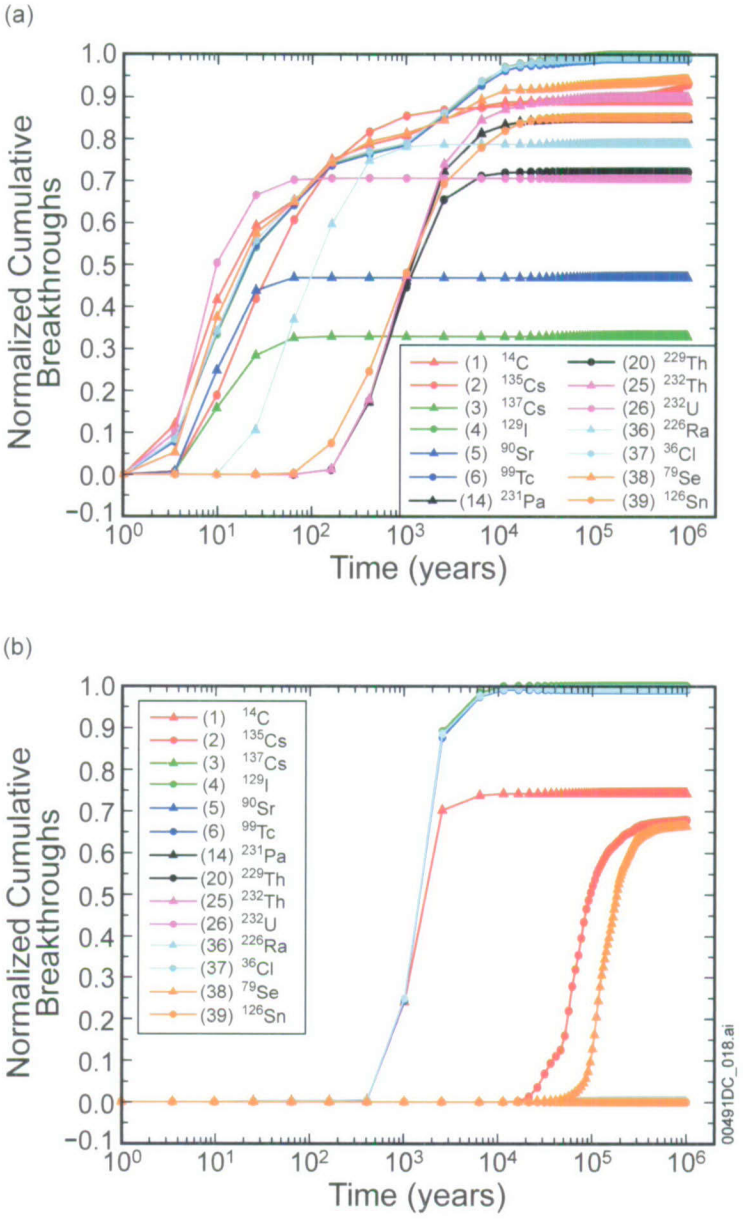

Output DTN: MO0705TRANSTAT.000.

NOTE: Northern Release Location (top) and Southern Release Location (bottom).

Figure 6.6.2-5 Normalized Cumulative Breakthrough Curves of 14 Radionuclides with Simple Decay for the Glacial-Transition 10th Percentile Infiltration Condition and Representative Parameter Values

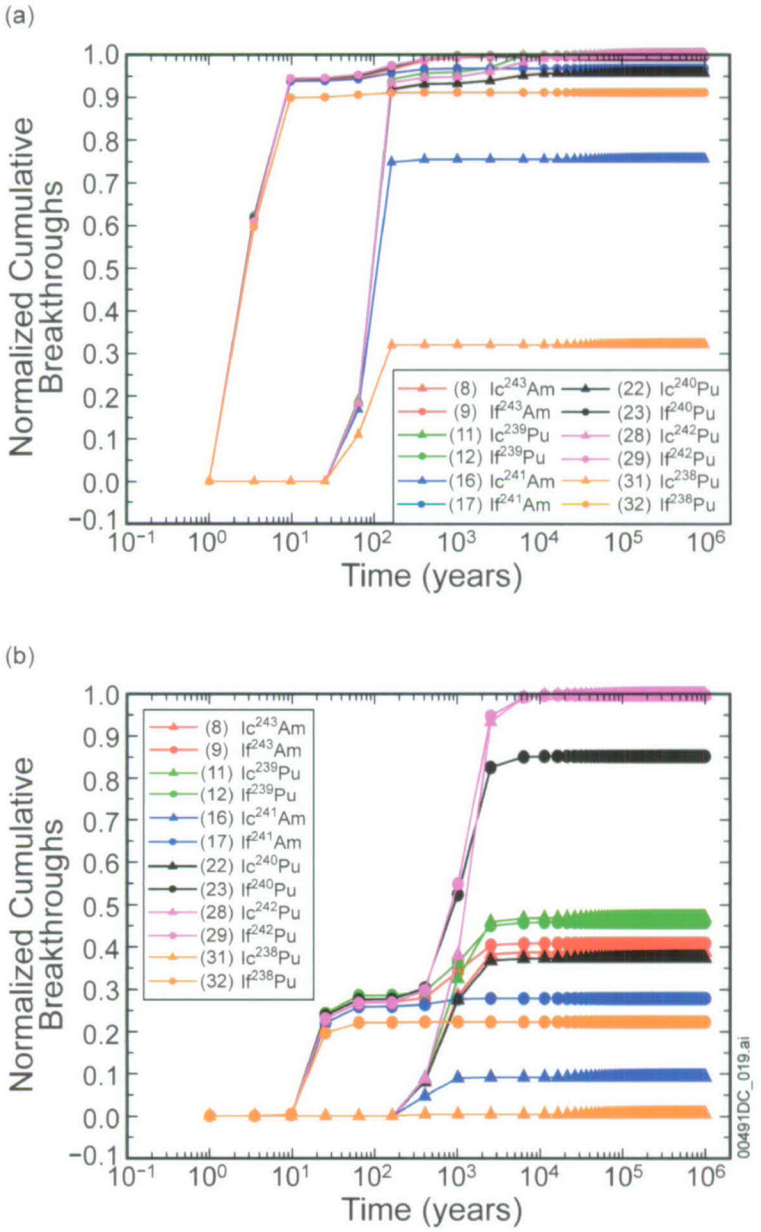

Output DTN: MO0705TRANSTAT.000.

NOTE: Northern Release Location (top) and Southern Release Location (bottom).

Figure 6.6.2-6. Normalized Cumulative Breakthrough Curves of 6 Irreversible Fast Colloids and 6 Irreversible Slow Colloids for the Glacial-Transition 10th Percentile Infiltration Condition and Representative Parameter Values

Figure 6.6.2-7 presents normalized breakthrough curves for radionuclide ^{235}U, ^{233}U, ^{236}U, and ^{230}Th and their daughter products ^{231}Pa, ^{229}Th, ^{232}Th, and ^{226}Ra, respectively for the two release locations. In these simulations, 10,000 particles are released for each parent species, and the daughter species are formed from the decay, with no source term at the repository. At the northern location, the first arrival time is only about a year for ^{235}U, ^{233}U, and ^{236}U, and about 100 years for ^{230}Th. Only ^{230}Th has an appreciable level of breakthrough of daughter product ^{226}Ra; none of the daughter products of ^{235}U, ^{233}U, and ^{236}U reach the water table, due to their high

sorption coefficients and long half lives of the parent species. For the southern location, the first arrival time is much longer for the parent species, and for this release location, no daughter products and no ^{230}Th, reaches the water table.

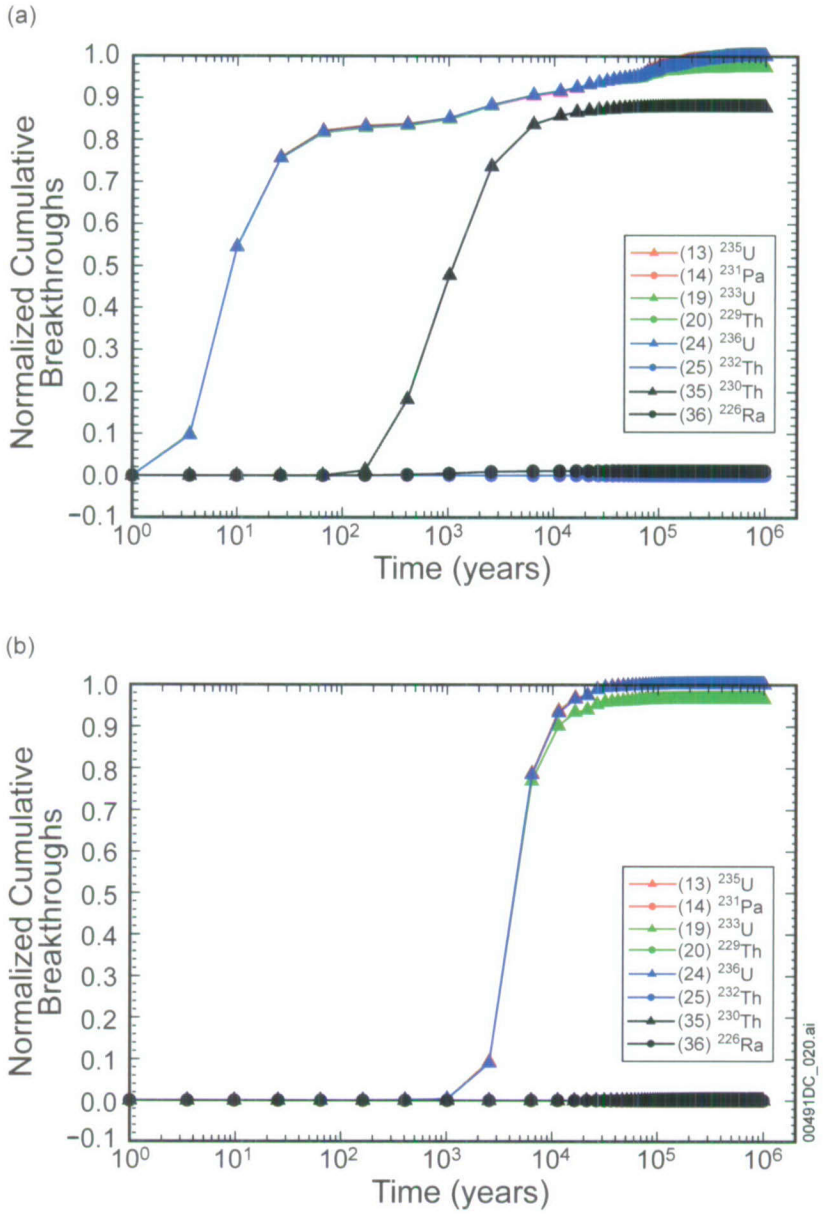

Output DTN: MO0705TRANSTAT.000.

NOTE: Northern Release Location (top) and Southern Release Location (bottom).

Figure 6.6.2-7. Normalized Cumulative Breakthrough Curves of 4 Radionuclides (^{235}U, ^{233}U, ^{236}U, and ^{230}Th) with One Decay Chain for the Glacial-Transition 10th Percentile Infiltration Condition and Representative Parameter Values

Additional breakthrough curve plots are presented in Appendix D for other decay chains.

6.6.2.3 Fracture versus Matrix Release

In TSPA, radionuclides can enter the unsaturated zone transport model in either the fracture or matrix domain, depending on the nature of the hydrodynamic and transport conditions in the EBS. The results presented so far were based on the assumption that radionuclides are released at fracture node. This section examines the relative behavior of fracture versus matrix releases at the same location within the repository (north or south). Figure 6.6.2-8 compares the normalized breakthrough curves for fracture versus matrix release for ^{99}Tc released at the northern (upper figure) or southern (lower figure) release locations. For the northern release location, nearly 50% of mass released into the fracture reach the water table within about 20 years, compared to about 5,000 years for 50% arrival for the matrix releases. For the southern release location, the first arrival times are longer due to matrix transport, even for the fracture releases. However, the same phenomenon (delayed arrivals for matrix releases) is evident. When mass is released into the matrix of the TSw at the repository horizon, local matrix percolation rates are so low that for radionuclides to escape the unsaturated zone, they must first diffuse to a nearby flowing fracture. Thus, the additional transport time is due to the slow rate of the diffusion process transporting radionuclides to the fracture. This process will be governed by the diffusion coefficient, spacing between flowing fractures, and, for sorbing species, sorption coefficient.

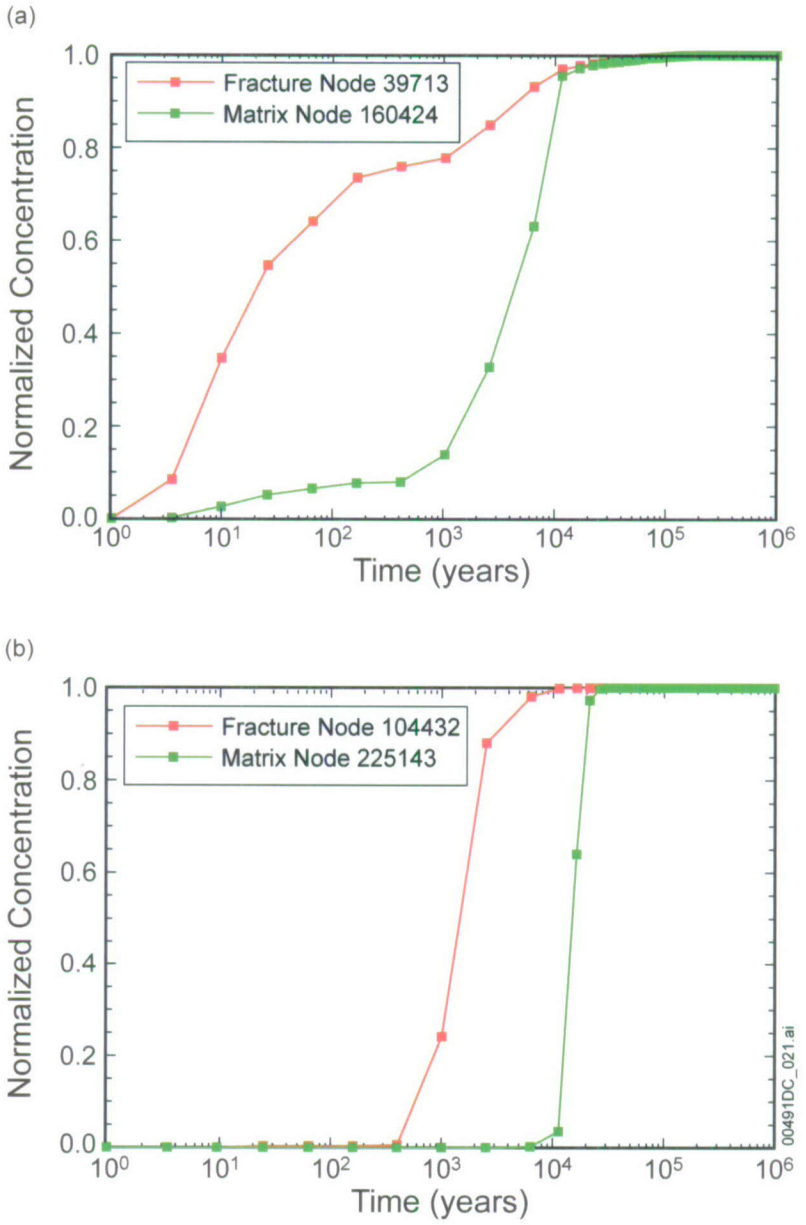

Output DTN: MO0705TRANSTAT.000.

NOTE: Northern Release Location (top) and Southern Release Location (bottom).

Figure 6.6.2-8. Comparison of Normalized Cumulative Breakthrough Curves of ^{99}Tc for Particles Released at Fracture Node or Matrix Node for the Glacial-Transition, 10th Percentile Infiltration Scenario, Representative Parameter Values

6.6.3 Sensitivity to Flow Parameter Uncertainty

No change.

6.6.4 Sensitivity to AFM and Diffusion Parameter Uncertainty

No change.

6.7 EVALUATION OF ALTERNATIVE MODELS AND MODEL UNCERTAINTY

No change.

6.8 DESCRIPTION OF BARRIER CAPABILITY

No change to this introductory section. Changes from the parent report are identified below the third-level heading in the subsections below.

6.8.1 Analyses of Barrier Capability

No change.

6.8.2 Barrier Capability Simulations and Uncertainty Analyses

The degree to which the unsaturated zone acts as a barrier to radionuclide transport must be assessed with a full accounting of the uncertainties of key transport parameters and processes. To augment the analyses presented in Section 6.6, this section explores conceptual and parameter uncertainty from the standpoint of their impacts on the predicted unsaturated zone transport barrier capability for various radionuclides.

Because the actual role of the unsaturated zone in the repository system as a whole must be assessed within the total-system model, simulations involving only the unsaturated zone submodel must be synthesized using a "figure of merit" that serves as a proxy for unsaturated zone performance. Two metrics of unsaturated zone barrier performance are used in the analyses below. The first is the mean travel time of a radionuclide from the repository to the water table. While this travel time will be a function of the individual radionuclides through their transport parameters, it also serves as a measure of unsaturated zone travel times for other radionuclides with similar transport characteristics. The second metric takes into consideration the half life of the individual radionuclide. The decay fraction, abbreviated using the nomenclature "C/C_0" in this addendum, is defined by

$$C / C_0 = \int_0^\infty f(t) e^{-kt} dt \qquad \text{(Eq. 6.8.2-1)}$$

where f(t) is the travel time distribution to the water table for a radionuclide in the absence of decay, and k is the radioactive decay rate constant, which is related to the half life by the relationship $t_{1/2} = \ln(2)/k$. Physically, C/C_0 is the fraction of the releases of a radionuclide from the repository that reaches the water table before decaying, and as such, provides a radionuclide-specific measure of unsaturated zone performance as a barrier to radionuclide migration. It is especially suitable to assess the barrier with respect to the long term, peak dose regulatory criterion because it integrates over all travel times, not just those in the first 10,000 years. In contrast, the mean travel time is a metric that can be compared to the regulatory time period of 10,000 years to assess whether the unsaturated zone barrier alone will retard a radionuclide beyond that regulatory cutoff time.

The travel-time distribution depends on a number of factors, including sorption coefficient K_d, and matrix diffusion coefficient D_m. In this section on barrier capability, simulations covering the uncertainty ranges of these key parameters have been conducted for several selected species, including conservative species ^{99}Tc and ^{14}C, weakly sorbing species ^{237}Np, and strongly sorbing species ^{240}Pu. The effect of release locations (northern versus southern node), transport conceptual models (dual permeability, commonly abbreviated as dual-k, versus discrete fracture model, or DFM), and transport parameters (D_m and K_d), as well as infiltration rate is explored. In each simulation, 10,000 particles are released from one node and the travel time of each particle to the water table is recorded. Based on these travel time data, either the mean travel time or the value of C/C_0 of Equation 6.8.2-1, are computed with the PARTICLE_STAT [DIRS 181317] postprocessing software.

To ensure that simulations span the entire range of uncertainty for each parameter of interest, a common method was developed that accommodates an arbitrary uncertainty distribution. In this study, parameter values are sampled from the cumulative distribution function (CDF) for that parameter, in equal intervals of 0.1 on the CDF axis. The exception to this approach is for the low and high ends of the CDF, which can be asymptotic at the 0 and 1 ends of the distribution, such as for the case of a normal distribution. Instead, the low and high ends are defined by values that represent minus and plus three standard deviations from the mean for a normal distribution (i.e., 0.00135 and 0.99865). For distributions that have well-defined minima and maxima, these two end members are sufficiently close to 0 and 1 to provide an effective end member, and the choice of these values accommodates the normal distributions used for many uncertainty distributions such as the diffusion coefficients. Therefore, for each of the species examined in these calculations, 11 values of D_m for each of these "keys" as listed in Table 6.8.2-1 were chosen in such a way that the values of their corresponding cumulative density function of $\log(D_m)$ are 0.00135, 0.1, 0.2, 0.3, 0.4, 0.5, 0.6, 0.7, 0.8, 0.9, and 0.99865. Similarly, 11 values of sorption coefficient K_d are listed in Table 6.8.2-2.

Table 6.8.2-1 Diffusion Coefficient Values (m^2/s) as a Function of CDF Interval for 11 Cases Used in Sensitivity Analysis

Key	Element	CDF Interval										
		0.00135	0.1	0.2	0.3	0.4	0.5	0.6	0.7	0.8	0.9	0.99865
-14	C in Group 1	1.13×10^{-11}	3.55×10^{-11}	4.76×10^{-11}	5.89×10^{-11}	7.05×10^{-11}	8.35×10^{-11}	9.89×10^{-11}	1.19×10^{-10}	1.47×10^{-10}	1.97×10^{-10}	6.19×10^{-10}
-15	C in Group 2	4.28×10^{-12}	1.35×10^{-11}	1.81×10^{-11}	2.24×10^{-11}	2.68×10^{-11}	3.18×10^{-11}	3.76×10^{-11}	4.51×10^{-11}	5.57×10^{-11}	7.47×10^{-11}	2.35×10^{-10}
-16	C in Group 3	2.30×10^{-12}	7.25×10^{-12}	9.72×10^{-12}	1.20×10^{-11}	1.44×10^{-11}	1.71×10^{-11}	2.02×10^{-11}	2.42×10^{-11}	2.99×10^{-11}	4.01×10^{-11}	1.26×10^{-10}
-26	Np in Group 1	5.90×10^{-12}	1.86×10^{-11}	2.49×10^{-11}	3.08×10^{-11}	3.69×10^{-11}	4.38×10^{-11}	5.18×10^{-11}	6.21×10^{-11}	7.67×10^{-11}	1.03×10^{-10}	3.24×10^{-10}
-27	Np in Group 2	2.24×10^{-12}	7.07×10^{-12}	9.48×10^{-12}	1.17×10^{-11}	1.40×10^{-11}	1.66×10^{-11}	1.97×10^{-11}	2.36×10^{-11}	2.92×10^{-11}	3.91×10^{-11}	1.23×10^{-10}
-28	Np in Group 3	1.21×10^{-12}	3.80×10^{-12}	5.09×10^{-12}	6.29×10^{-12}	7.54×10^{-12}	8.93×10^{-12}	1.06×10^{-11}	1.27×10^{-11}	1.57×10^{-11}	2.10×10^{-11}	6.62×10^{-11}
-32	Pu in Group 1	1.24×10^{-11}	3.91×10^{-11}	5.25×10^{-11}	6.48×10^{-11}	7.77×10^{-11}	9.20×10^{-11}	1.09×10^{-10}	1.31×10^{-10}	1.61×10^{-10}	2.17×10^{-10}	6.82×10^{-10}
-33	Pu in Group 2	4.72×10^{-12}	1.49×10^{-11}	1.99×10^{-11}	2.47×10^{-11}	2.95×10^{-11}	3.50×10^{-11}	4.14×10^{-11}	4.97×10^{-11}	6.14×10^{-11}	8.23×10^{-11}	2.59×10^{-10}
-34	Pu in Group 3	2.53×10^{-12}	7.99×10^{-12}	1.07×10^{-11}	1.32×10^{-11}	1.59×10^{-11}	1.88×10^{-11}	2.23×10^{-11}	2.67×10^{-11}	3.30×10^{-11}	4.42×10^{-11}	1.39×10^{-10}
-47	Tc in Group 1	1.86×10^{-11}	5.87×10^{-11}	7.87×10^{-11}	9.73×10^{-11}	1.17×10^{-10}	1.38×10^{-10}	1.63×10^{-10}	1.96×10^{-10}	2.42×10^{-10}	3.25×10^{-10}	1.02×10^{-9}
-48	Tc in Group 2	7.08×10^{-12}	2.23×10^{-11}	2.99×10^{-11}	3.70×10^{-11}	4.43×10^{-11}	5.25×10^{-11}	6.22×10^{-11}	7.45×10^{-11}	9.21×10^{-11}	1.24×10^{-10}	3.89×10^{-10}
-49	Tc in Group 3	3.80×10^{-12}	1.20×10^{-11}	1.61×10^{-11}	1.99×10^{-11}	2.38×10^{-11}	2.82×10^{-11}	3.34×10^{-11}	4.00×10^{-11}	4.94×10^{-11}	6.63×10^{-11}	2.09×10^{-10}

Output DTN: MO0705TRANSTAT.000.

NOTES: Values rounded to two places after the decimal. The groups in the list of elements refer to the three tortuosity rock groups used to characterize diffusion. CDF = cumulative distribution function, C = carbon, Np = neptunium, Pu = plutonium, Tc = technetium.

Table 6.8.2-2 K_d Values (L/kg) as a Function of CDF Interval for 11 Cases Used in Sensitivity Analysis

Key	Element	CDF Interval										
		0.00135	0.1	0.2	0.3	0.4	0.5	0.6	0.7	0.8	0.9	0.99865
-71	Np in Group 1	0.00	0.10	0.20	0.30	0.40	0.50	1.60	2.70	3.80	4.90	5.99
-72	Np in Group 2	0.00	0.10	0.20	0.30	0.40	0.50	1.60	2.70	3.80	4.90	5.99
-73	Np in Group 3	0.00	0.20	0.40	0.60	0.60	1.00	1.40	1.80	2.20	2.60	2.99
-77	Pu in Group 1	10.24	28.00	46.00	64.00	82.00	100.00	120.00	140.00	160.00	180.00	199.73
-78	Pu in Group 2	10.16	22.00	34.00	46.00	58.00	70.003	96.00	122.00	148.00	174.00	199.65
-79	Pu in Group 3	10.24	28.00	46.00	64.00	80.00	100.00	120.00	140.00	160.00	180.00	199.73

Output DTN: MO0705TRANSTAT.000.

NOTE: CDF = cumulative distribution function, Np = neptunium, Pu = plutonium.

6.8.2.1 Travel Time Statistics

Figure 6.8.2-1 shows the mean log travel time (in years) of ^{99}Tc as a function of diffusion coefficient D_m for particles released at northern and southern locations. The diffusion coefficient values are those sampled across the entire range of values in the uncertainty distribution, and are given in Table 6.8.2-1. Separate simulations are presented for all four flow fields of the glacial-transition climate condition, using the dual-k diffusion model. Consistent with previous results, the mean travel time decreases significantly with the infiltration rate for both release locations. There is roughly an order-of-magnitude uncertainty in travel times over the range of infiltration rates in the model. With respect to diffusion coefficient, the mean travel time increases with the matrix diffusion coefficient for the northern release node, while for the southern node, the travel time is virtually independent of D_m. For the southern release location, matrix diffusion does have an impact in the fracture-dominated TSw, but the effect is masked by the longer travel times within the matrix-dominated Calico Hills units. Under matrix-dominated flow and transport conditions, the travel times are a function of the flow velocity in the matrix, and fractures play no role in providing a short-circuit pathway. Therefore, diffusion is irrelevant under these conditions. For this reason, the travel times are longer from the southern release location, and are virtually independent of diffusion coefficient.

Figure 6.8.2-2 plots the similar comparison for the DFM model. The trends are similar to those in Figure 6.8.2-1 for the dual-k model, but the travel times are slightly longer for the DFM model for the northern release location. This is due to the DFM model's effect of reducing the earliest arrivals compared to the dual-k model. Since the diffusion model has very little impact on overall transport times for the southern release location, the travel times are very insensitive to the choice of diffusion conceptual model as well (as seen from a comparison of the right figures of Figures 6.8.2-1 and 6.8.2-2). Very similar results are found for ^{14}C (not shown), in keeping with the fact that these two radionuclides are both nonsorbing species.

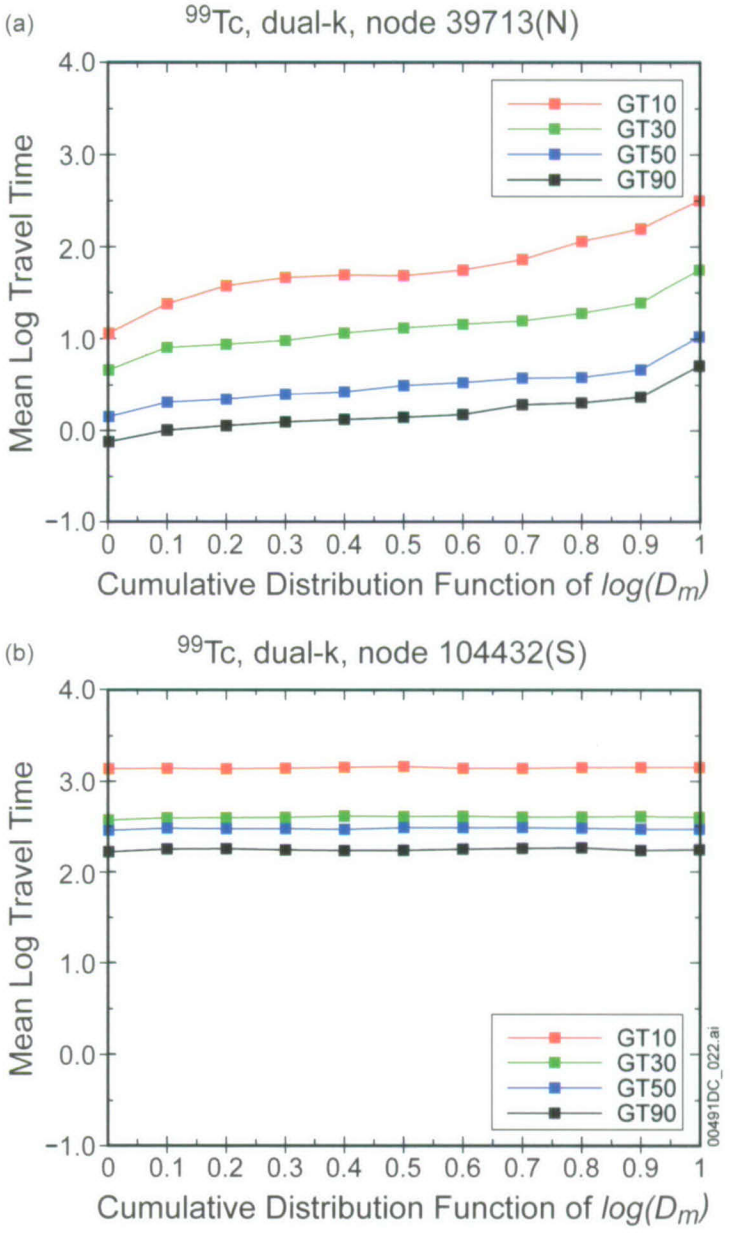

Output DTN: MO0705TRANSTAT.000.

NOTE: a) Northern release location, b) Southern release location.

Figure 6.8.2-1. Comparison of Mean Travel Time of ^{99}Tc as a Function of Matrix Diffusion Coefficient under Glacial-Transition Climate Conditions for the dual-k Model

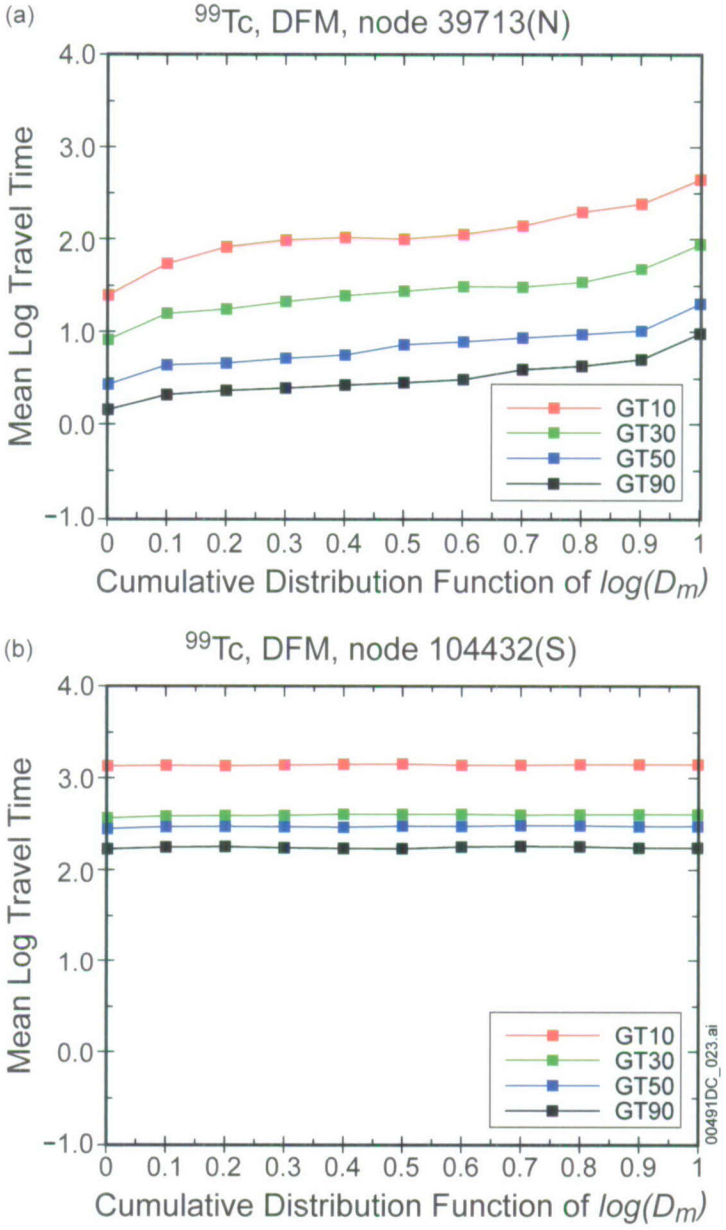

Output DTN: MO0705TRANSTAT.000.

NOTE: a) Northern release location, b) Southern release location.

Figure 6.8.2-2. Comparison of Mean Travel Time of ^{99}Tc as a Function of Matrix Diffusion Coefficient under Glacial-Transition Climate Conditions for the DFM Model

For sorbing species, both diffusion coefficient and sorption coefficient have an influence on the travel time to the water table. In the analyses that follow, the values in Tables 6.8.2-1 and 6.8.2-2 are used to create a matrix of simulations that span the entire uncertainty ranges of both D_m and K_d. For each simulation, consisting of a separate pair of D_m and K_d values, the mean travel time is computed, and the results are displayed in contour plots of travel time, with CDFs of K_d and D_m as the axes. Figure 6.8.2-3 and 6.8.2-4 show the mean travel times for the weakly sorbing species ^{237}Np released at the northern (6.8.2-3) and southern (6.8.2-4) nodes under four

different flow fields (glacial-transition, 10-, 30-, 50-, and 90-percentile infiltration rates), simulated using the dual-k model. Figures 6.8.2-5 and 6.8.2-6 present analogous results for DFM model. These comparisons reveal the following results:

- For the northern release location, mean travel times range from very short (approximately one year) for the highest infiltration scenario, to greater than 100 years (but still short compared to the long half life of ^{237}Np)
- The travel times from the northern release location are a function of both K_d and D_m
- The DFM conceptual model leads to significantly longer travel times for this weakly sorbing radionuclide
- The releases from the southern location are much longer than those in the north, and the travel times depend, to first order, on the K_d, but are virtually insensitive to D_m.
- Releases from the southern location are insensitive to the choice of conceptual model (dual-k versus DFM).

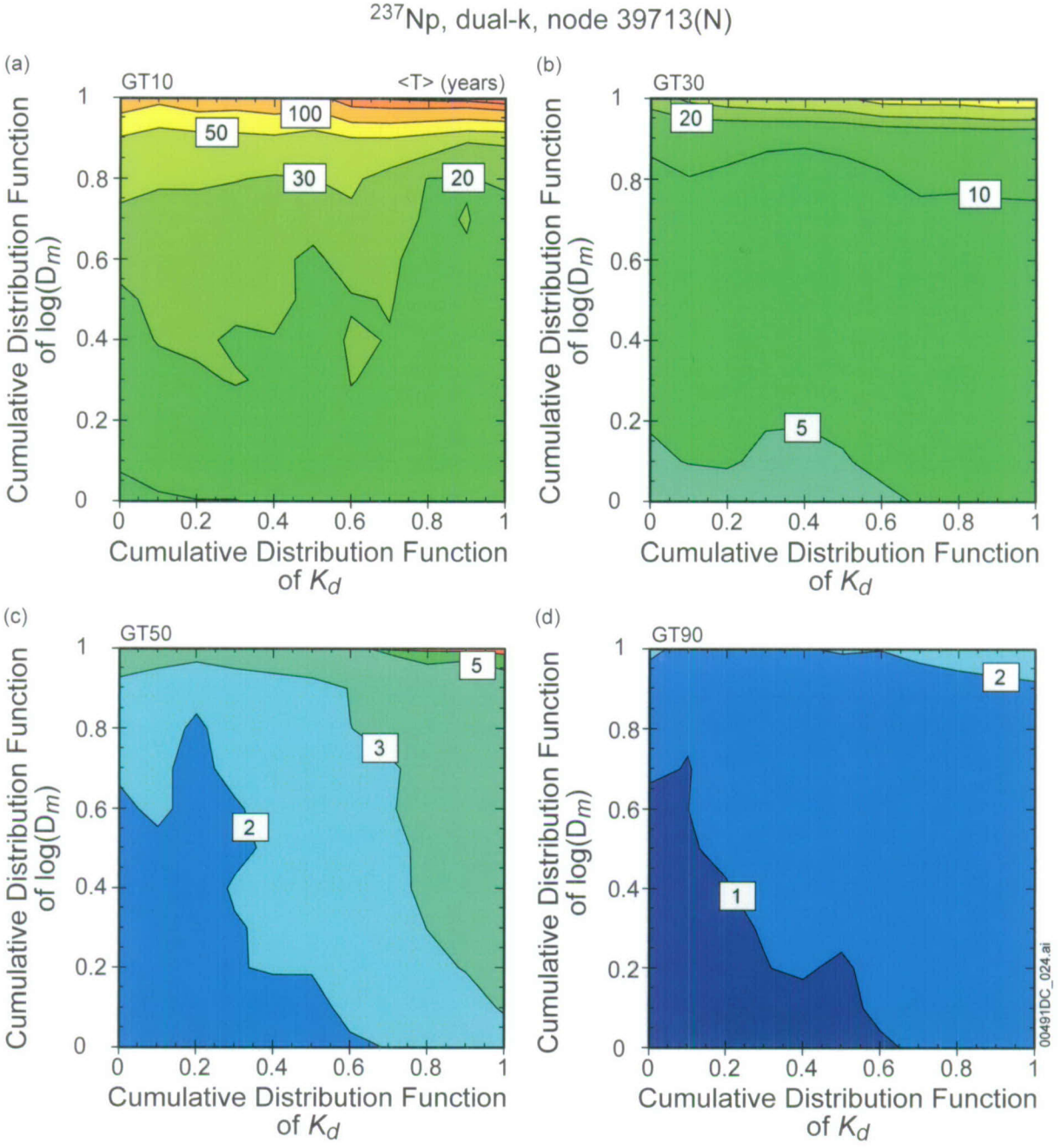

Output DTN: MO0705TRANSTAT.000.

Figure 6.8.2-3. Mean Travel Time of ^{237}Np as a Function of Matrix Diffusion Coefficient and Sorption Coefficient for the Glacial-Transition Climate Condition, dual-k Model, Northern Release Location

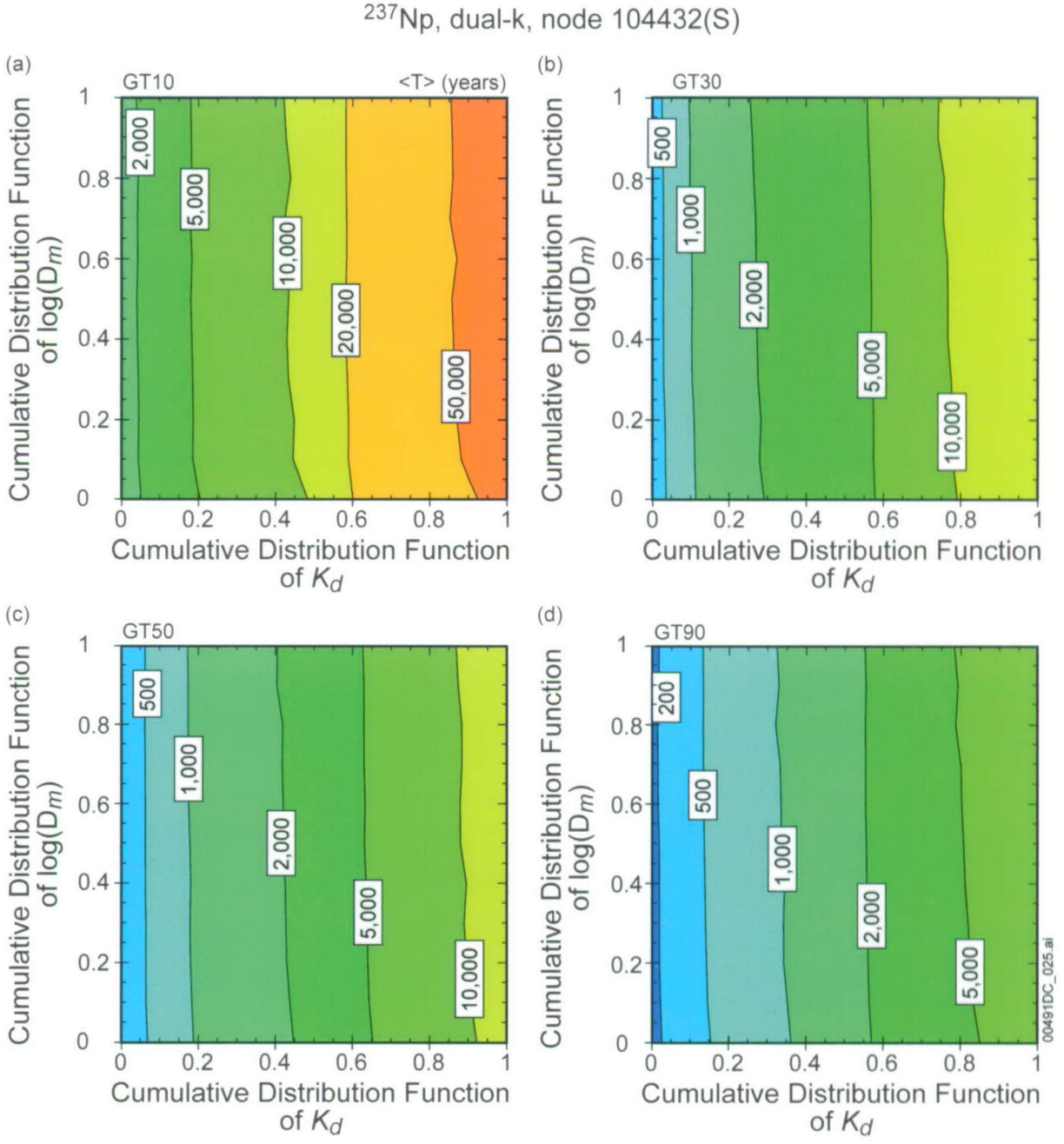

Output DTN: MO0705TRANSTAT.000.

Figure 6.8.2-4. Mean Travel Time of ^{237}Np as a Function of Matrix Diffusion Coefficient and Sorption Coefficient for the Glacial-Transition Climate Condition, dual-k Model, Southern Release Location

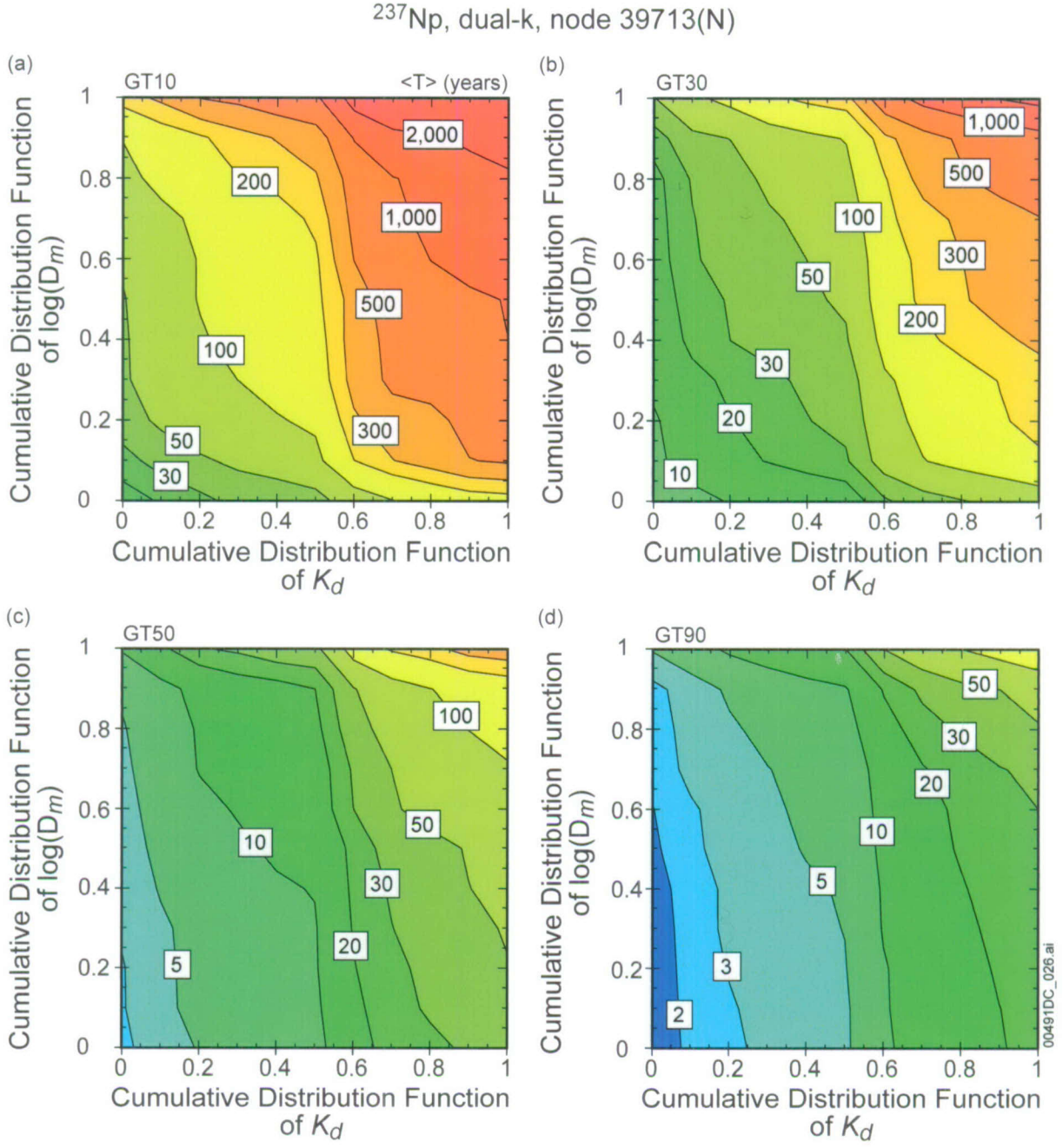

Output DTN: MO0705TRANSTAT.000.

Figure 6.8.2-5. Mean Travel Time of ^{237}Np as a Function of Matrix Diffusion Coefficient and Sorption Coefficient for the Glacial-Transition Climate Condition, DFM Model, Northern Release Location

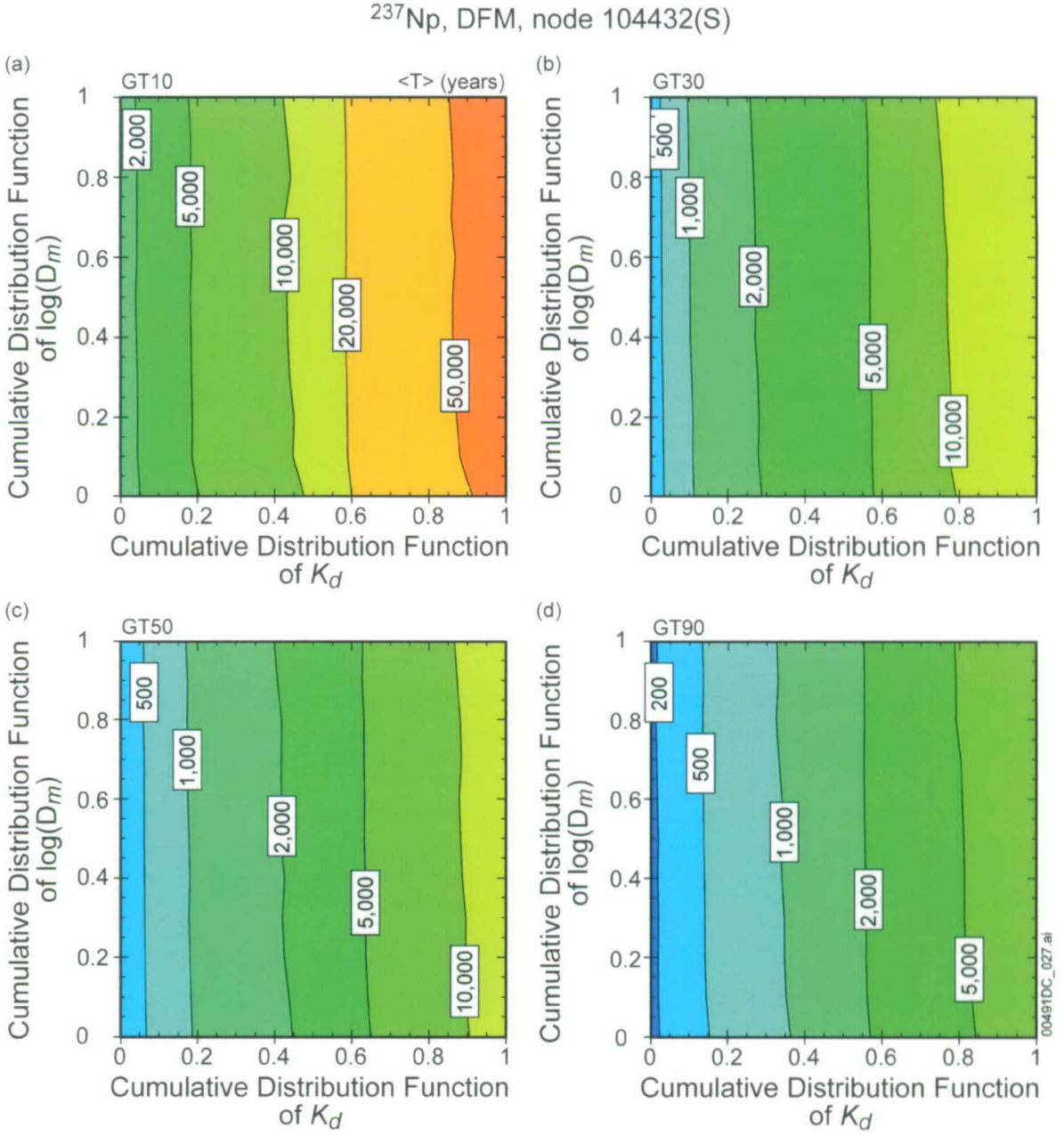

Output DTN: MO0705TRANSTAT.000.

Figure 6.8.2-6. Mean Travel Time of ^{237}Np as a Function of Matrix Diffusion Coefficient and Sorption Coefficient for the Glacial-Transition Climate Condition, DFM Model, Southern Release Location

The interplay between diffusion and sorption for transport through units with fracture-dominated flow is reflected in these results. Greater diffusion leads to both diffusion- and sorption-related delays in the transport time. This leads to larger travel times for larger values of either K_d or D_m, as well as for the DFM model case, which leads to an enhancement in the contact of radionuclides with the matrix rock. However, for the southern release, all of these effects are

masked by the significant travel time delays associated with slow matrix transport and sorption in the Calico Hills unit.

An analogous set of comparisons for the mean travel time for the strongly sorbing ^{240}Pu (reversibly sorbed species) is illustrated in Figures 6.8.2-7, 6.8.2-8, 6.8.2-9, and 6.8.2-10. Overall trends similar to those discussed for ^{237}Np are observed for this strongly sorbing species, but the travel time disparity between the northern and southern release locations is more striking. A matrix-dominated transport layer in the flow path has an extremely beneficial impact on travel time when combined with strong sorption. In addition, the selection of the DFM conceptual model has a more dramatic effect of increasing travel times for the northern release location. This result is due to the increased contact of radionuclide mass with the matrix in the DFM model.

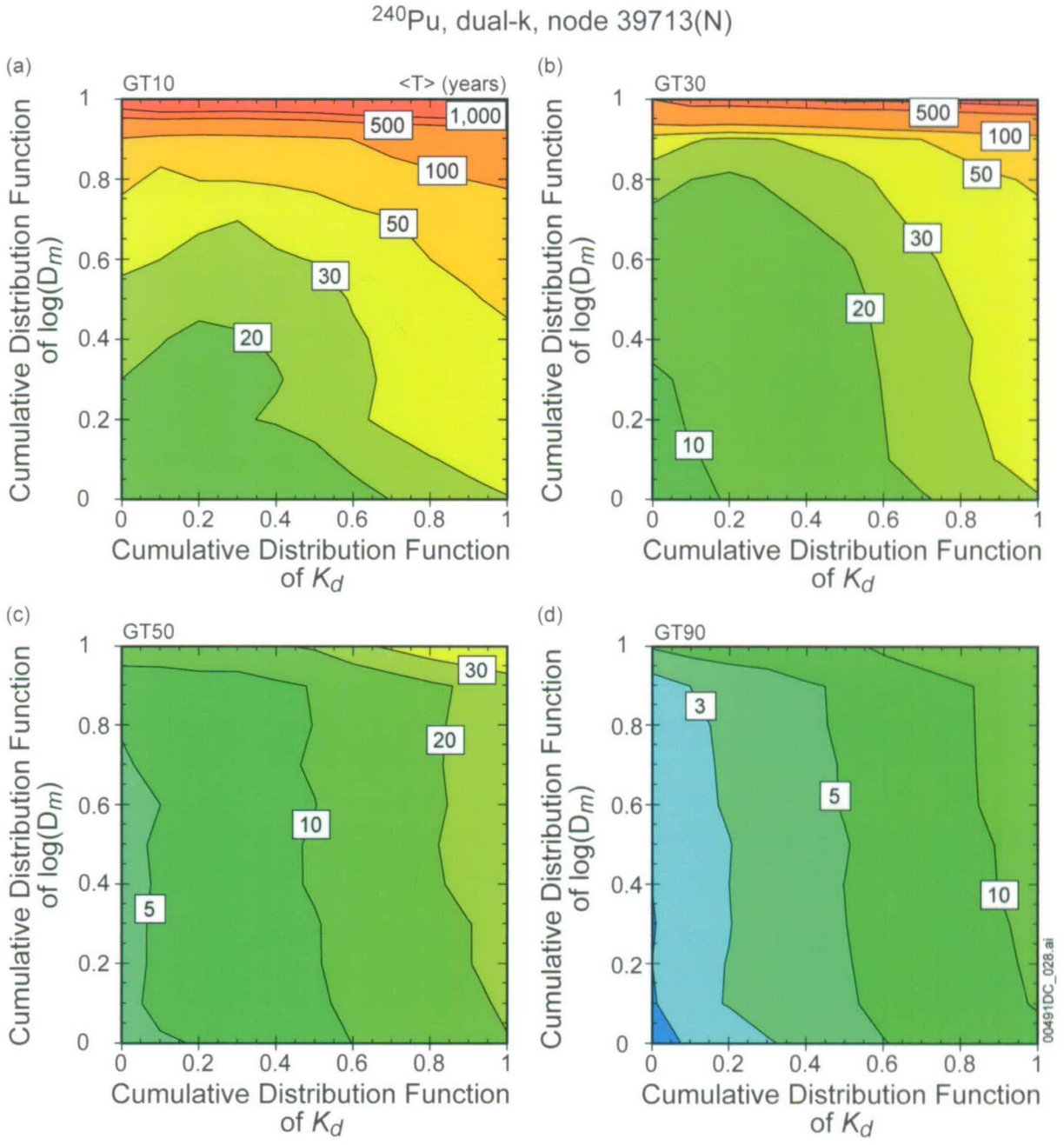

Output DTN: MO0705TRANSTAT.000.

Figure 6.8.2-7. Mean Travel Time of ^{240}Pu as a Function of Matrix Diffusion Coefficient and Sorption Coefficient for the Glacial-Transition Climate Condition, dual-k Model, Northern Release Location

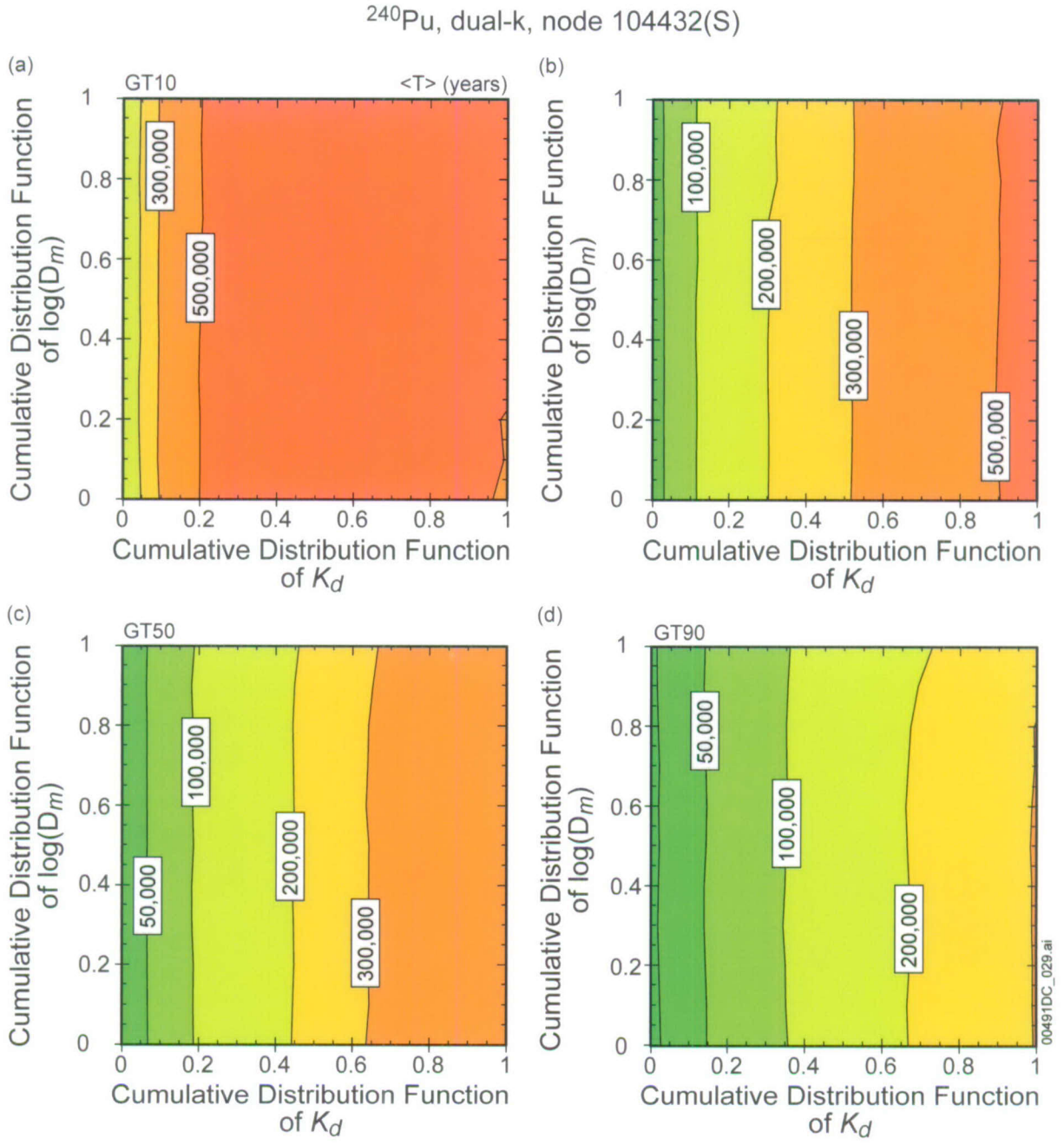

Output DTN: MO0705TRANSTAT.000.

Figure 6.8.2-8. Mean Travel Time of ^{240}Pu as a Function of Matrix Diffusion Coefficient and Sorption Coefficient for the Glacial-Transition Climate Condition, dual-k Model, Southern Release Location

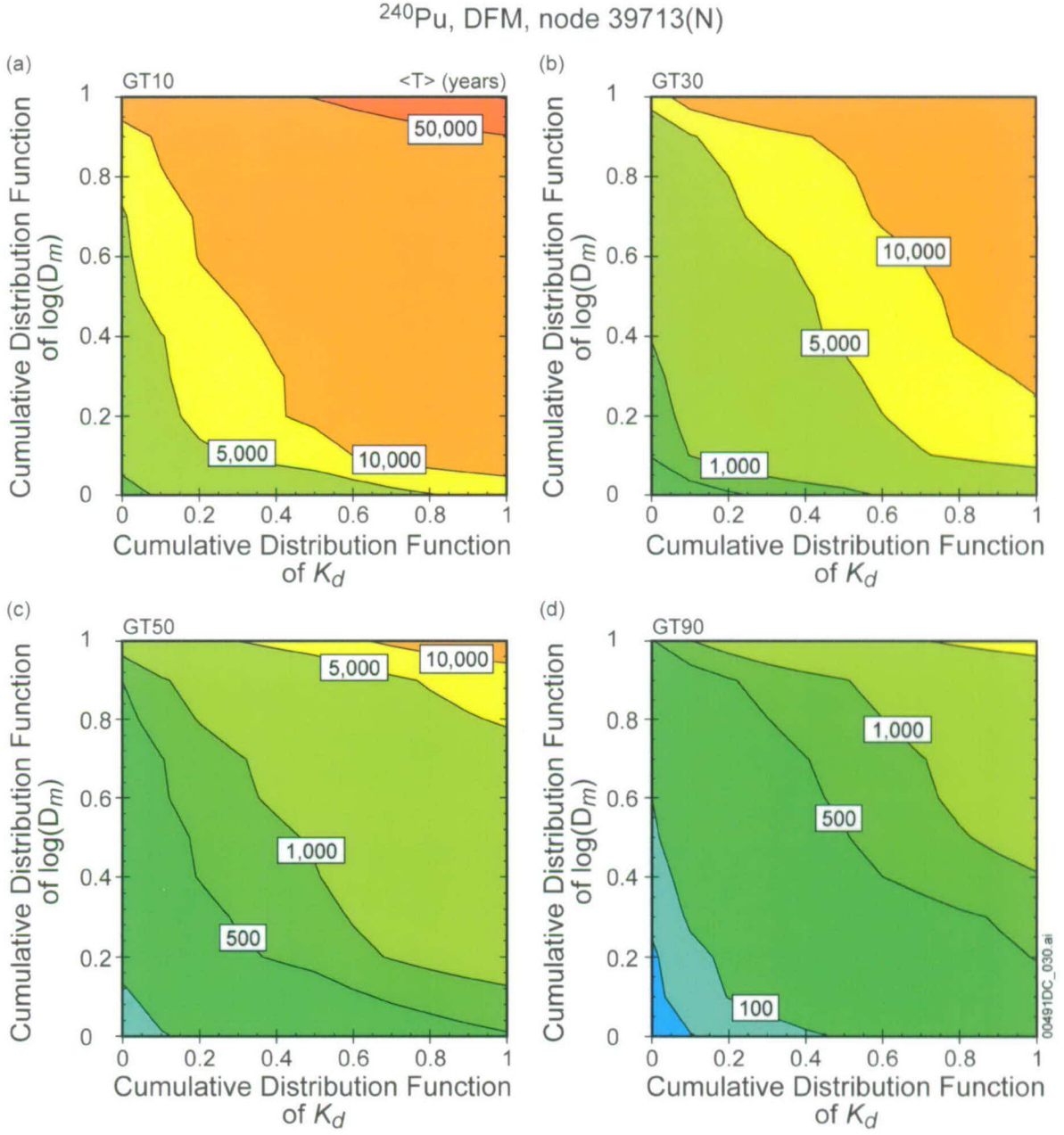

Output DTN: MO0705TRANSTAT.000.

Figure 6.8.2-9. Mean Travel Time of ^{240}Pu as a Function of Matrix Diffusion Coefficient and Sorption Coefficient for the Glacial-Transition Climate Condition, DFM Model, Northern Release Location

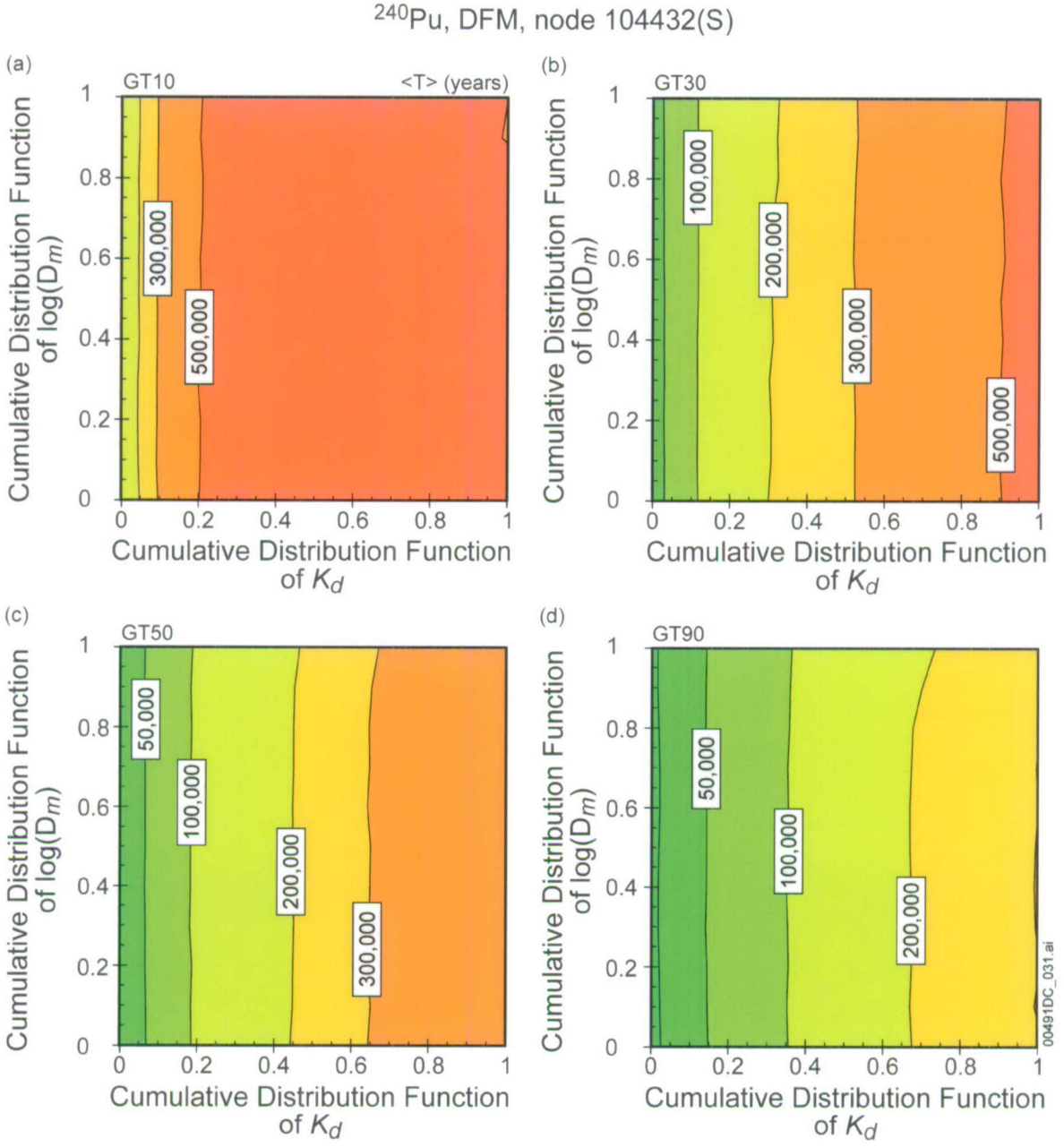

Output DTN: MO0705TRANSTAT.000.

Figure 6.8.2-10. Mean Travel Time of ^{240}Pu as a Function of Matrix Diffusion Coefficient and Sorption Coefficient for the Glacial-Transition Climate Condition, DFM Model, Southern Release Location

6.8.2.2 Barrier Capability Analyses Using the Decay Fraction

The analyses presented earlier used the mean travel time as a metric. In this section, the results are cast in terms of the effectiveness of the barrier as measured by the decay fraction C/C_0. The barrier capability is calculated from the travel time distribution using Equation 6.8.2-1. As with the previous analysis for mean travel time, the analysis is performed for a number of species

released either at the northern or southern release points under the four glacial-transition flow fields, simulated using both the dual-k model DFM models. For nonsorbing species, simple line plots are used, whereas for cases in which both D_m and K_d are varied (sorbing species ^{237}Np and ^{240}Pu), the matrix of 11 D_m values and 11 K_d values are used, and the results are displayed as contour plots.

Figures 6.8.2-11 and 6.8.2-12 plot C/C_0 for species ^{99}Tc for the northern and southern nodes. Due to the long half life and relatively short travel times for ^{99}Tc, this species essentially all reaches the water table without decay, yielding C/C_0 values close to unity. These results indicate that in all cases examined here more than 90% of ^{99}Tc reaches the water table. Different models have a slight impact on C/C_0 for the northern release, but they do not have a noticeable effect on C/C_0 for the southern release.

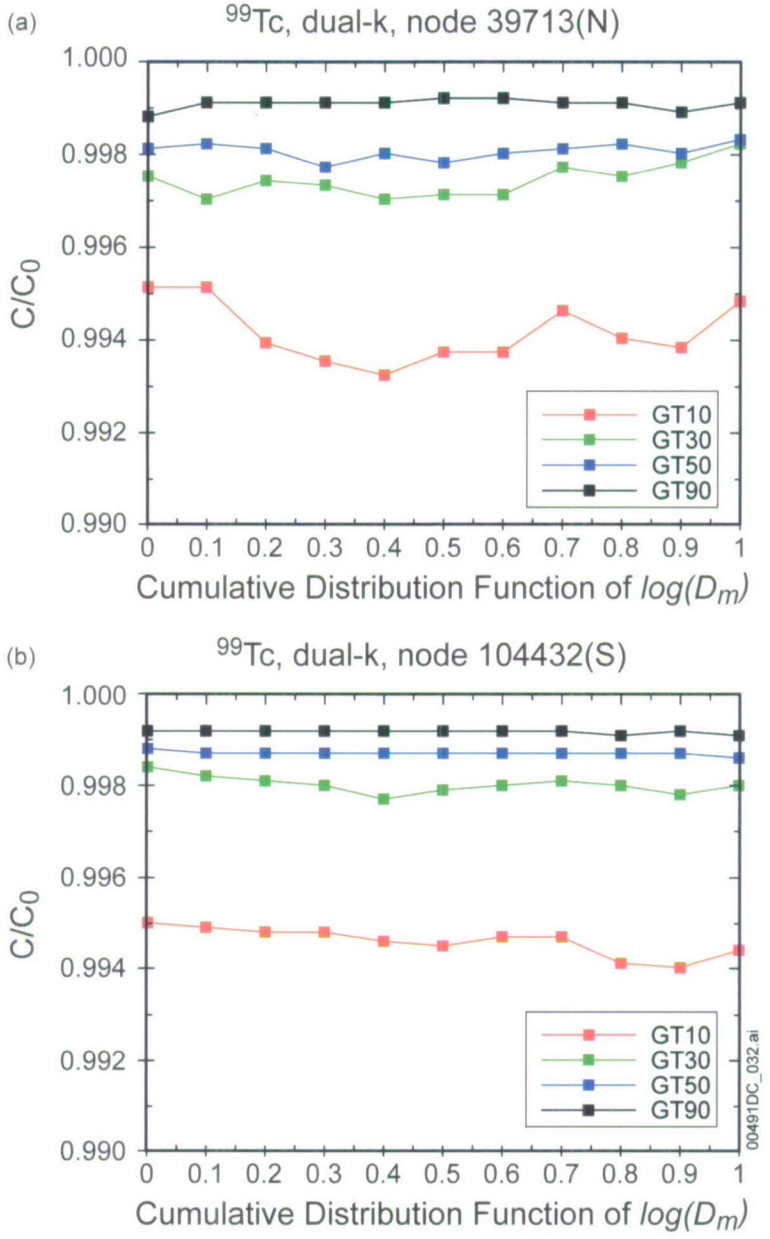

Output DTN: MO0705TRANSTAT.000.

Figure 6.8.2-11. Normalized ^{99}Tc Concentration (Decay Fraction, Computed from Travel Time Distributions) as a Function of Matrix Diffusion Coefficient for Glacial-Transition Climate Condition, dual-k Model, (a) Northern Release Location, (b) Southern Release Location

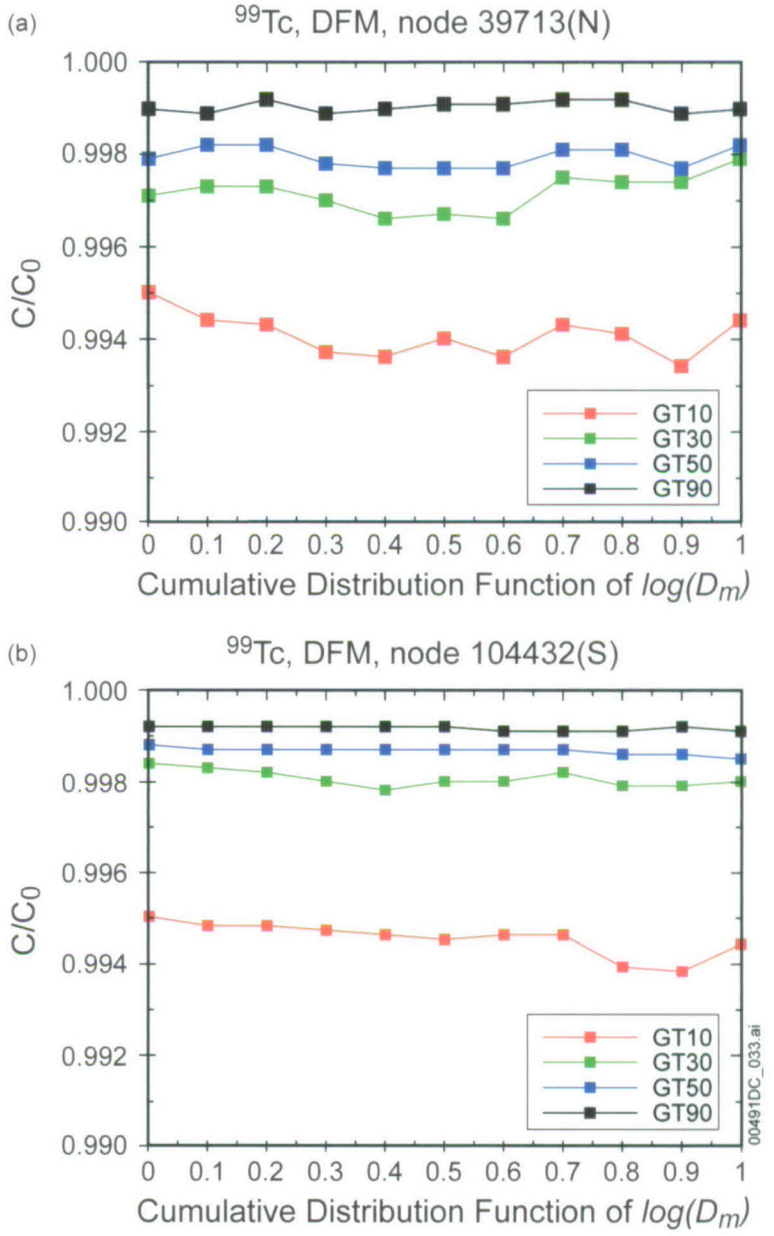

Output DTN: MO0705TRANSTAT.000.

Figure 6.8.2-12. Normalized ^{99}Tc Concentration (Decay Fraction, Computed from Travel Time Distributions) as a Function of Matrix Diffusion Coefficient for Glacial-Transition Climate Condition, DFM Model, (a) Northern Release Location, (b) Southern Release Location

Similar comparisons for a nonsorbing species ^{14}C are illustrated in Figures 6.8.2-13 and 6.8.2-14. Although the general patterns are similar to those of ^{99}Tc, the shorter half life results in more-substantial reduction in arrivals due to radioactive decay, especially for the 10th percentile flow case. However, the influence of diffusion coefficient uncertainty on the decay fraction is significant only for the 10th percentile flow field with the northern release location, but very minor for other flow fields with the northern release location and for all flow fields with the southern release location. Furthermore, the impact of the choice of diffusion model (dual-k

versus DFM) is relatively small for both release locations, but more important for the northern location than the southern location. As explained previously, the influence of diffusion in general is more predominant for the release location in which fracture transport dominates, and this conclusion applies to these C/C_0 results as well.

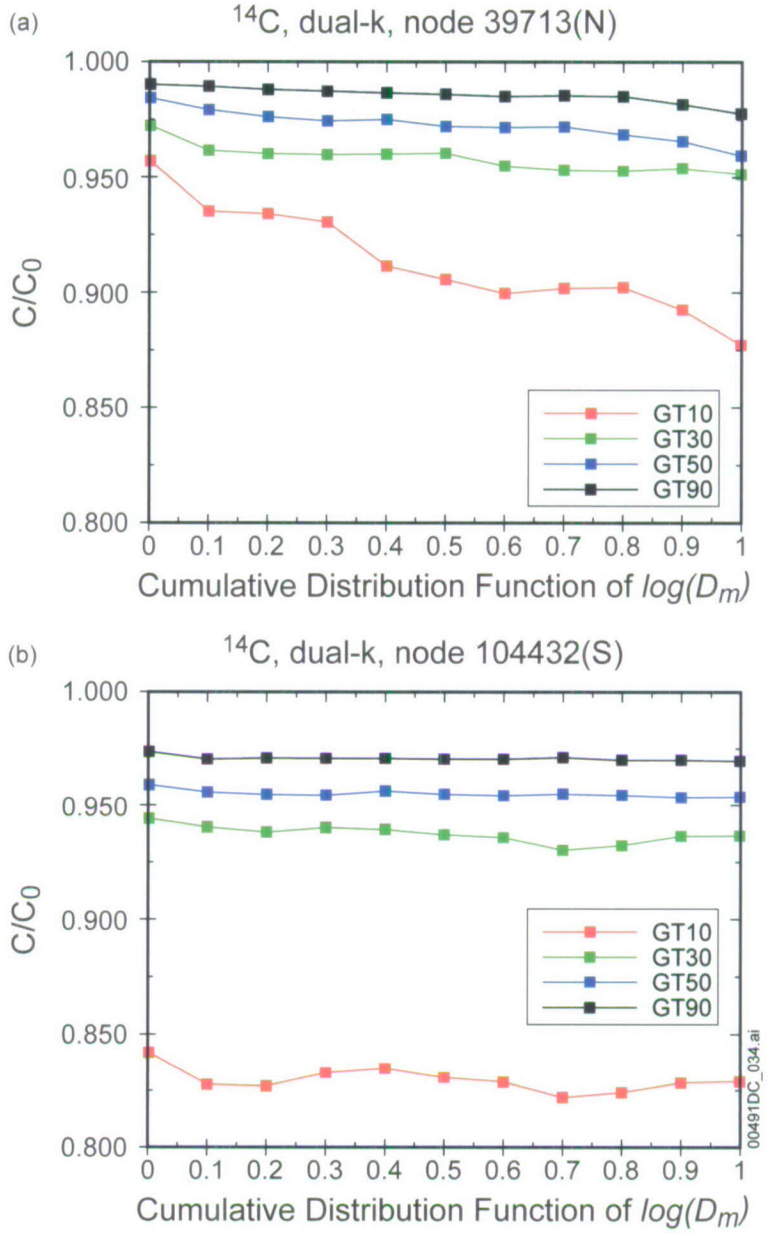

Output DTN: MO0705TRANSTAT.000.

Figure 6.8.2-13. Normalized ^{14}C Concentration (Decay Fraction, Computed from Travel Time Distributions) as a Function of Matrix Diffusion Coefficient for Glacial-Transition Climate Condition, dual-k Model, (a) Northern Release Location, (b) Southern Release Location

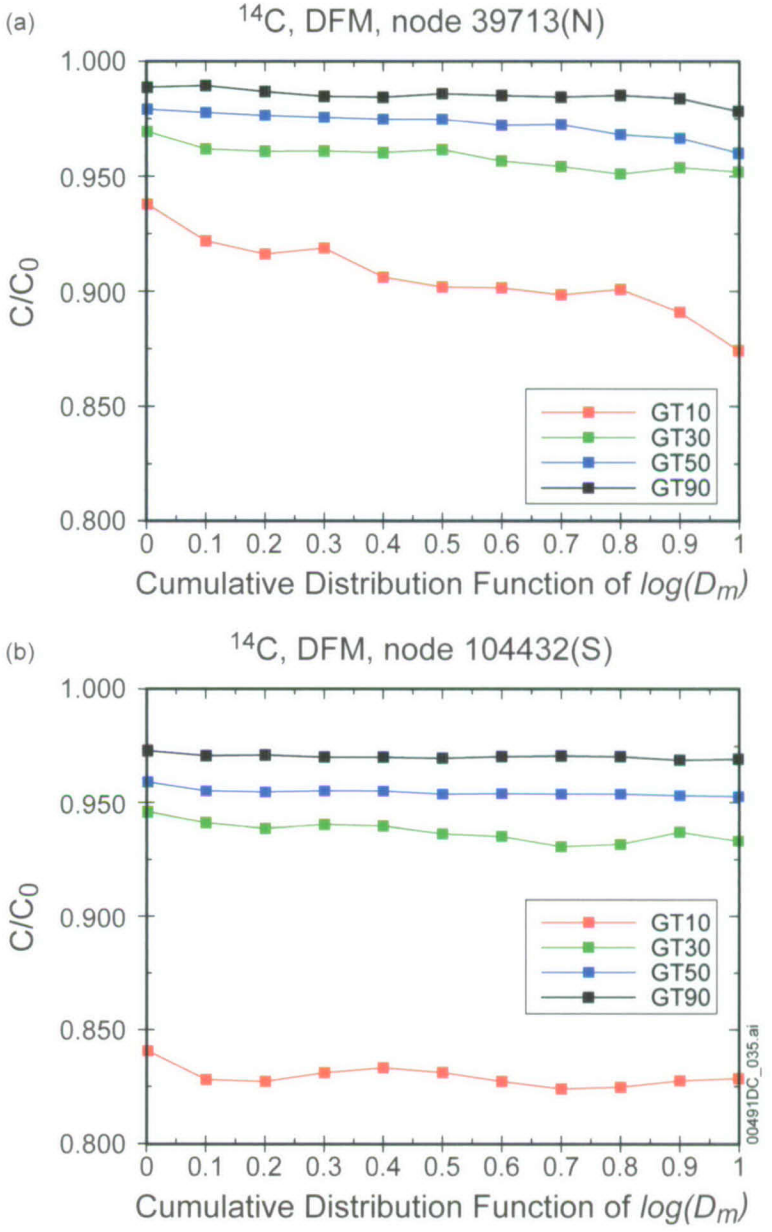

Output DTN: MO0705TRANSTAT.000.

Figure 6.8.2-14. Normalized ^{14}C Concentration (Decay Fraction, Computed from Travel Time Distributions) as a Function of Matrix Diffusion Coefficient for Glacial-Transition Climate Condition, DFM Model, (a) Northern Release Location, (b) Southern Release Location

Similar to the contour plots of mean travel time presented earlier, contour maps of C/C_0 for ^{237}Np are compared in Figures 6.8.2-15, 6.8.2-16, 6.8.2-17, and 6.8.2-18. These figures show that, although there are some variations of C/C_0 due to different models, parameter values D_m and K_d, and release locations, more than 90% of ^{237}Np will eventually reach the water table under any of the scenarios selected. Sorption is quite weak for ^{237}Np, and, in comparison to the half life, travel times are relatively short, leading to decay fractions close to unity.

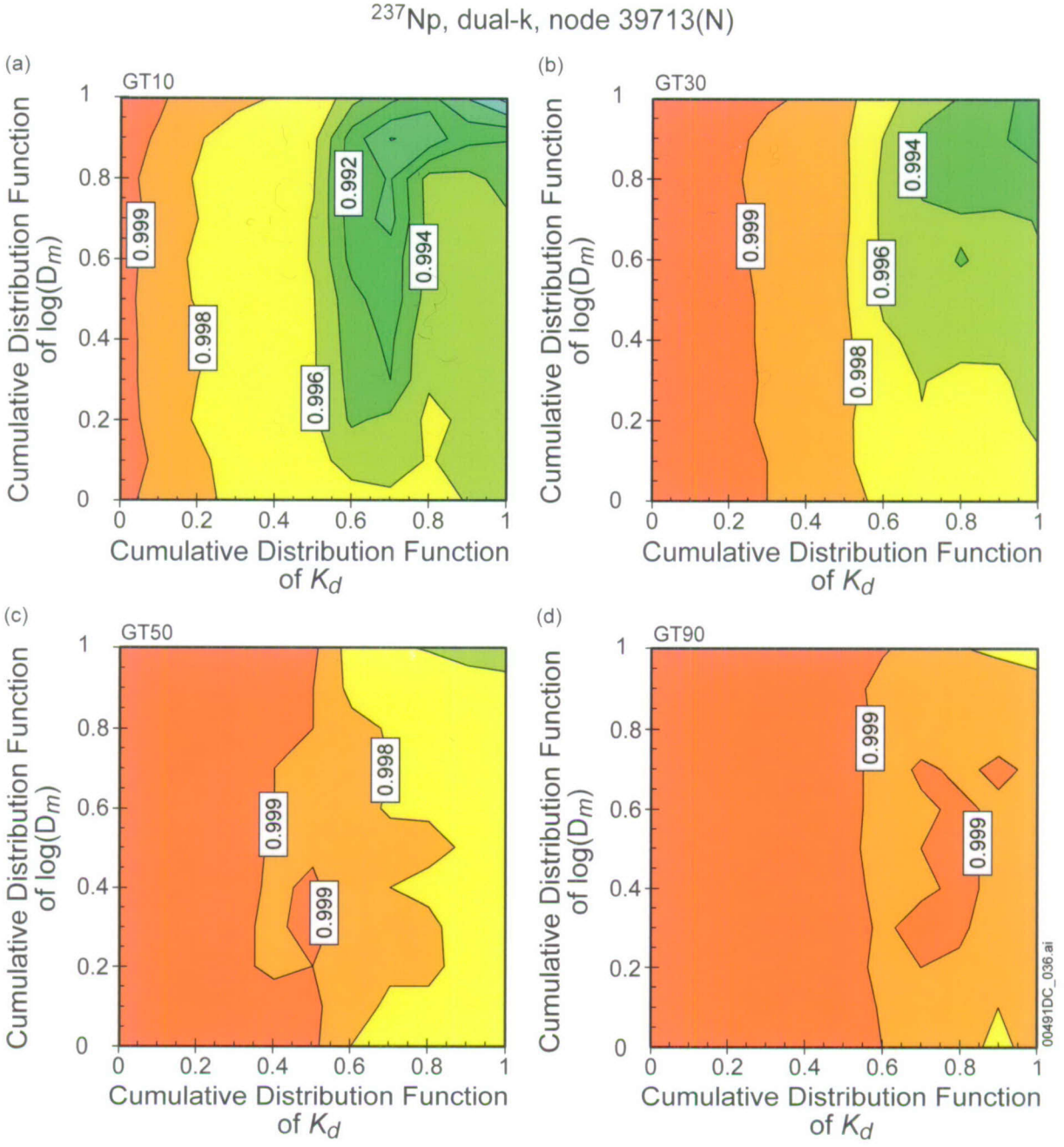

Output DTN: MO0705TRANSTAT.000.

Figure 6.8.2-15. Normalized ^{237}Np Concentration (Decay Fraction, Computed from Travel Time Distributions) as a Function of Matrix Diffusion Coefficient and Sorption Coefficient for the Glacial-Transition Climate Conditions, dual-k Model, Northern Release Location

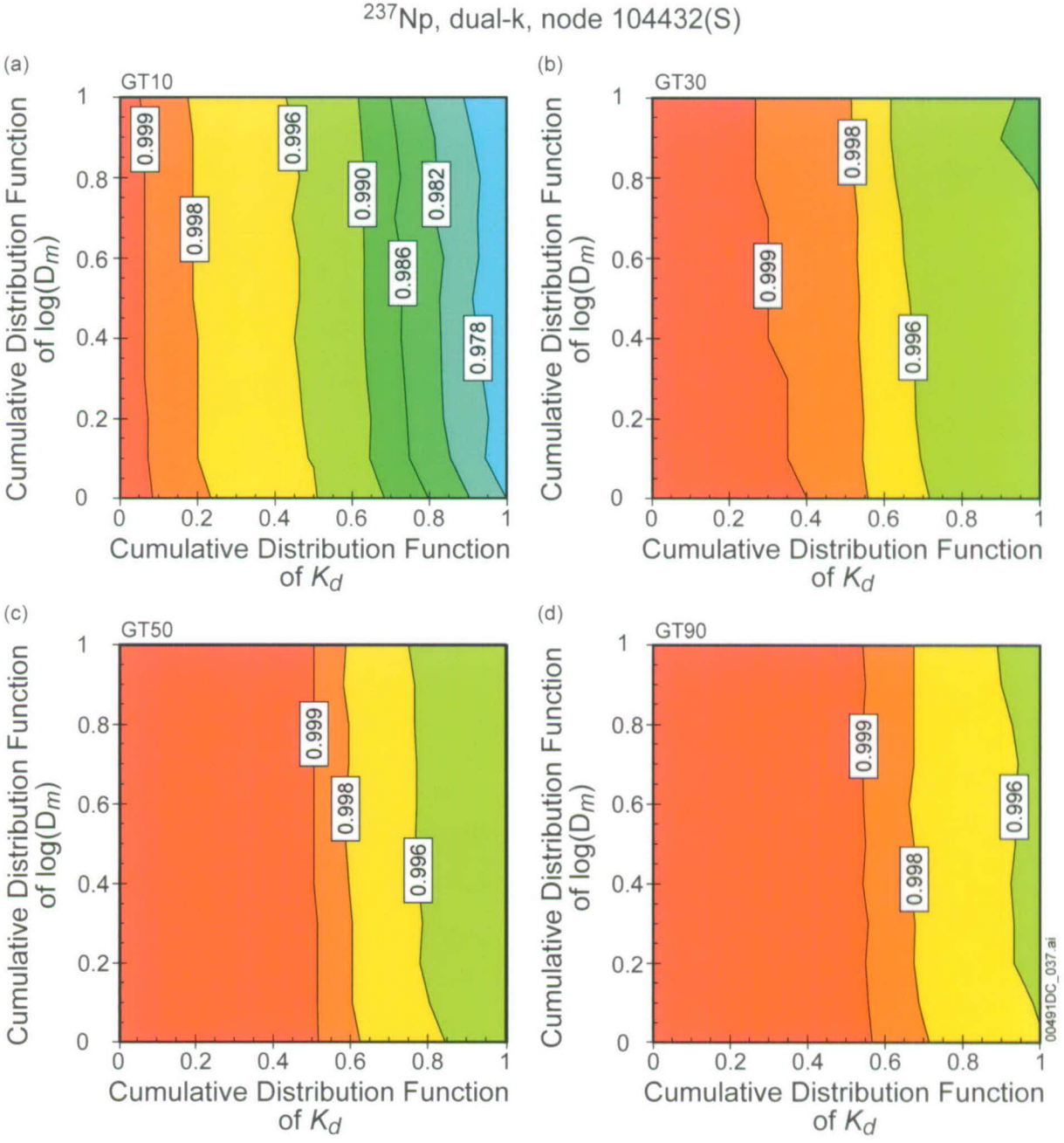

Output DTN: MO0705TRANSTAT.000.

Figure 6.8.2-16. Normalized ^{237}Np Concentration (Decay Fraction, Computed from Travel Time Distributions) as a Function of Matrix Diffusion Coefficient and Sorption Coefficient for the Glacial-Transition Climate Conditions, dual-k Model, Southern Release Location

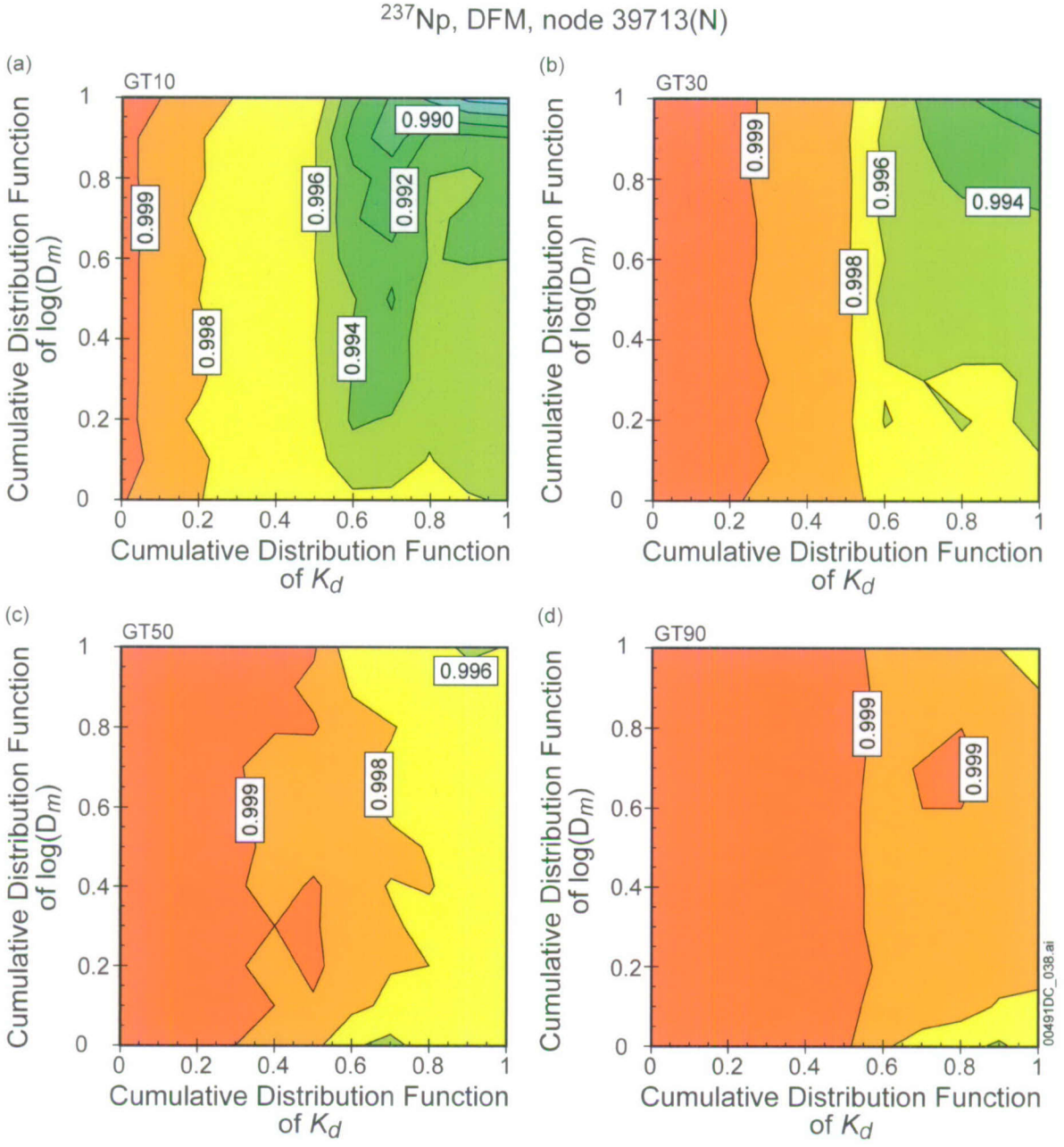

Output DTN: MO0705TRANSTAT.000.

Figure 6.8.2-17. Normalized ^{237}Np Concentration (Decay Fraction, Computed from Travel Time Distributions) as a Function of Matrix Diffusion Coefficient and Sorption Coefficient for the Glacial-Transition Climate Conditions, DFM Model, Northern Release Location

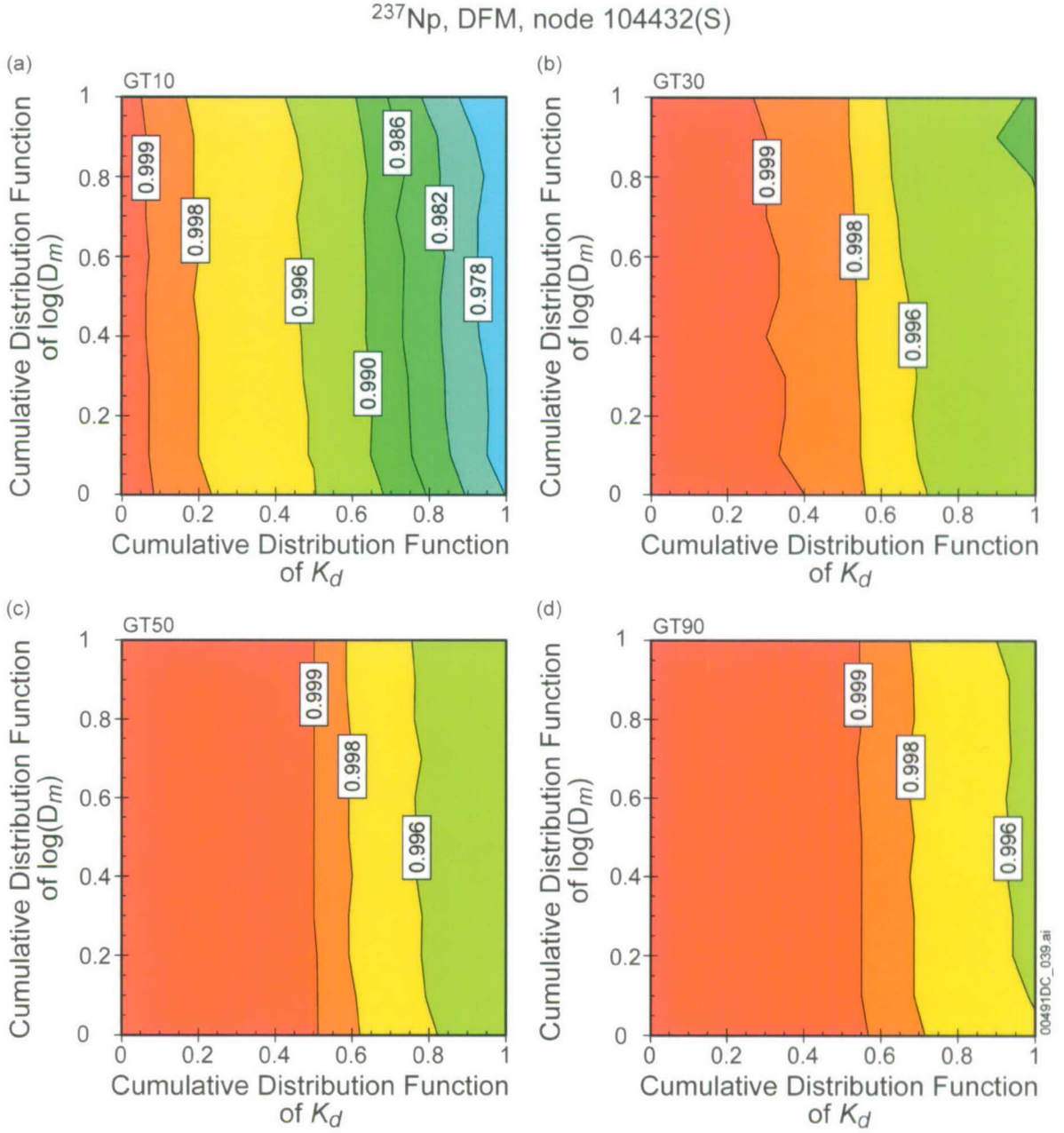

Output DTN: MO0705TRANSTAT.000.

Figure 6.8.2-18. Normalized ^{237}Np Concentration (Decay Fraction, Computed from Travel Time Distributions) as a Function of Matrix Diffusion Coefficient and Sorption Coefficient for the Glacial-Transition Climate Conditions, DFM Model, Southern Release Location

A similar set of plots for ^{240}Pu are presented in Figures 6.8.2-19, 6.8.2-20, 6.8.2-21, and 6.8.2-22. From the plots for the southern release location, it is apparent that the unsaturated zone in the southern region is an effective barrier for ^{240}Pu, as only less than 0.1% of ^{240}Pu will reach the water table even under the most unfavorable combination of parameter values. This is due to the long travel time in this region (matrix transport and strong sorption) and short half-life (6.56×10^3 years) of ^{240}Pu. In addition, in the southern region, the values of C/C_0 simulated

using both the dual-k model and DFM model are very close, reflecting the relative importance of the matrix flow component over transport in the fractured units. However, in the northern region, the contour maps of C/C_0 from the dual-k model and the DFM model are much different. For example, using the DFM model under flow field GT10, the unsaturated zone is predicted to be an effective barrier if both K_d and D_m are large, while at the same conditions with the dual-k model, nearly 80% of ^{240}Pu is predicted to reach the water table, unless the D_m is very high. This result shows that under certain conditions (fracture-dominated transport) and for certain species (strongly sorbing species with half-lives up to thousands of years, rather than millions of years), the predicted performance of the unsaturated zone barrier depends strongly on the choice of conceptual model for diffusion.

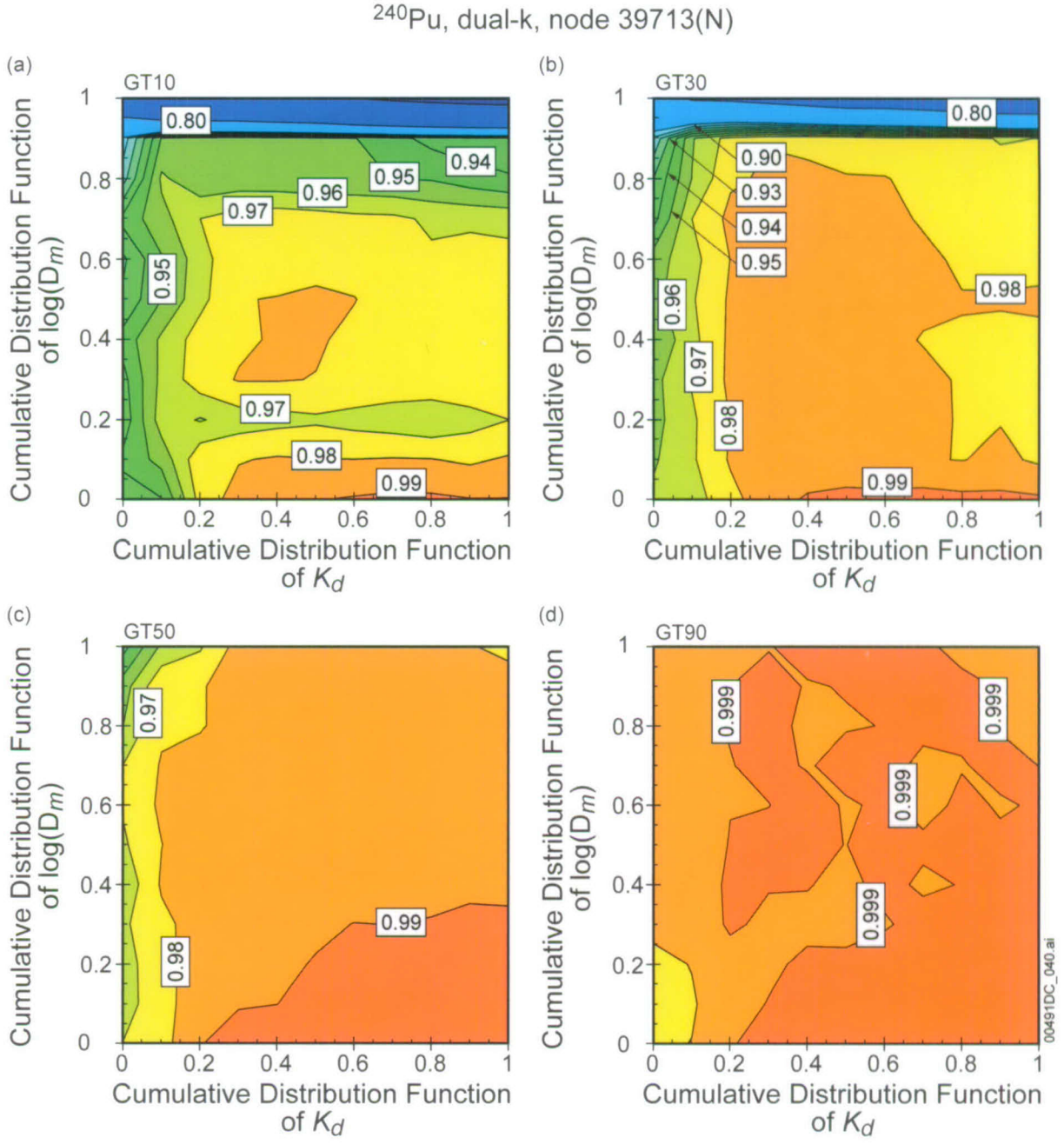

Output DTN: MO0705TRANSTAT.000.

Figure 6.8.2-19. Normalized ^{240}Pu Concentration (Decay Fraction, Computed from Travel Time Distributions) as a Function of Matrix Diffusion Coefficient and Sorption Coefficient for the Glacial-Transition Climate Conditions, dual-k Model, Northern Release Location

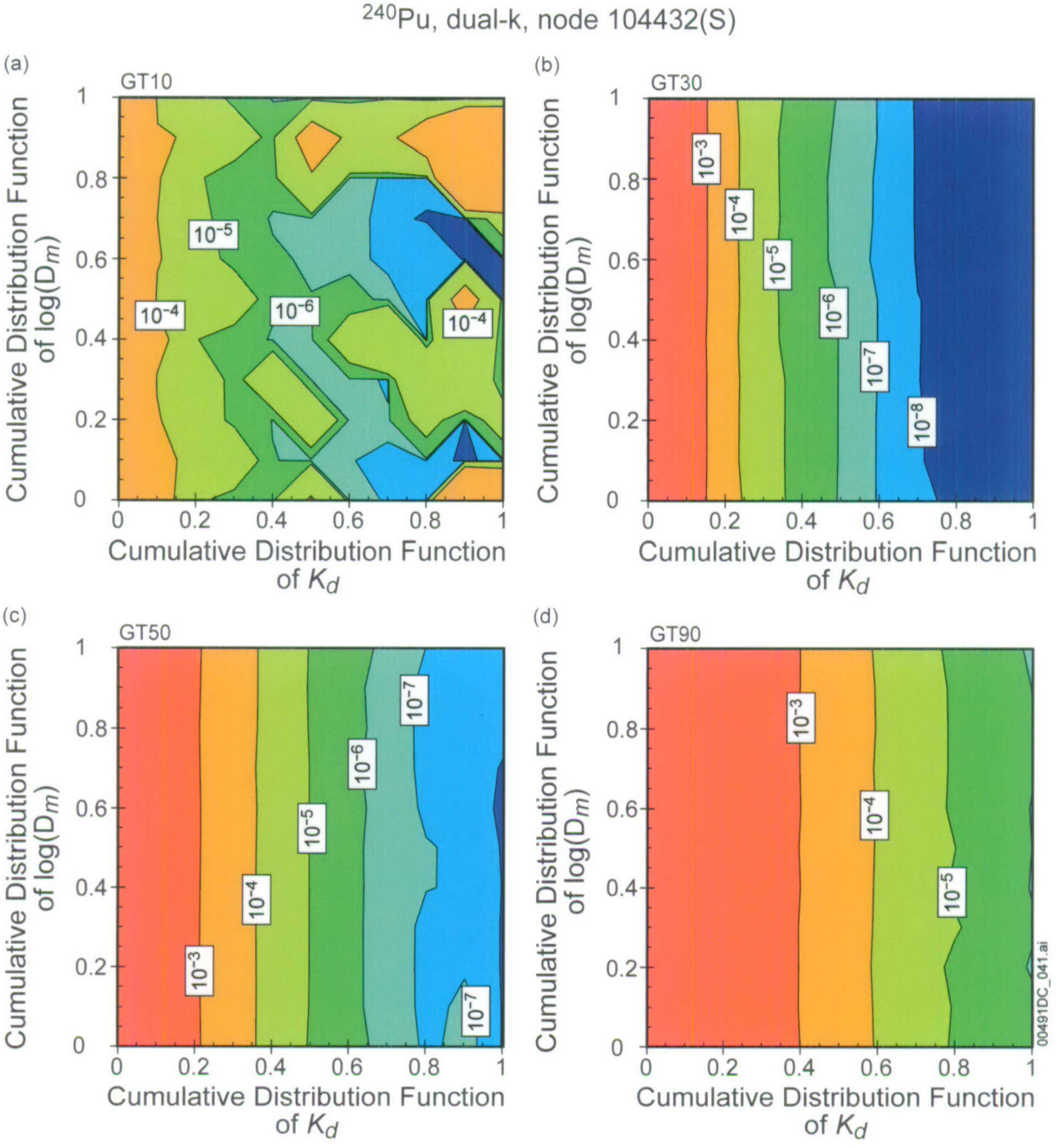

Output DTN: MO0705TRANSTAT.000.

Figure 6.8.2-20. Normalized ^{240}Pu Concentration (Decay Fraction, Computed from Travel Time Distributions) as a Function of Matrix Diffusion Coefficient and Sorption Coefficient for the Glacial-Transition Climate Conditions, dual-k Model, Southern Release Location

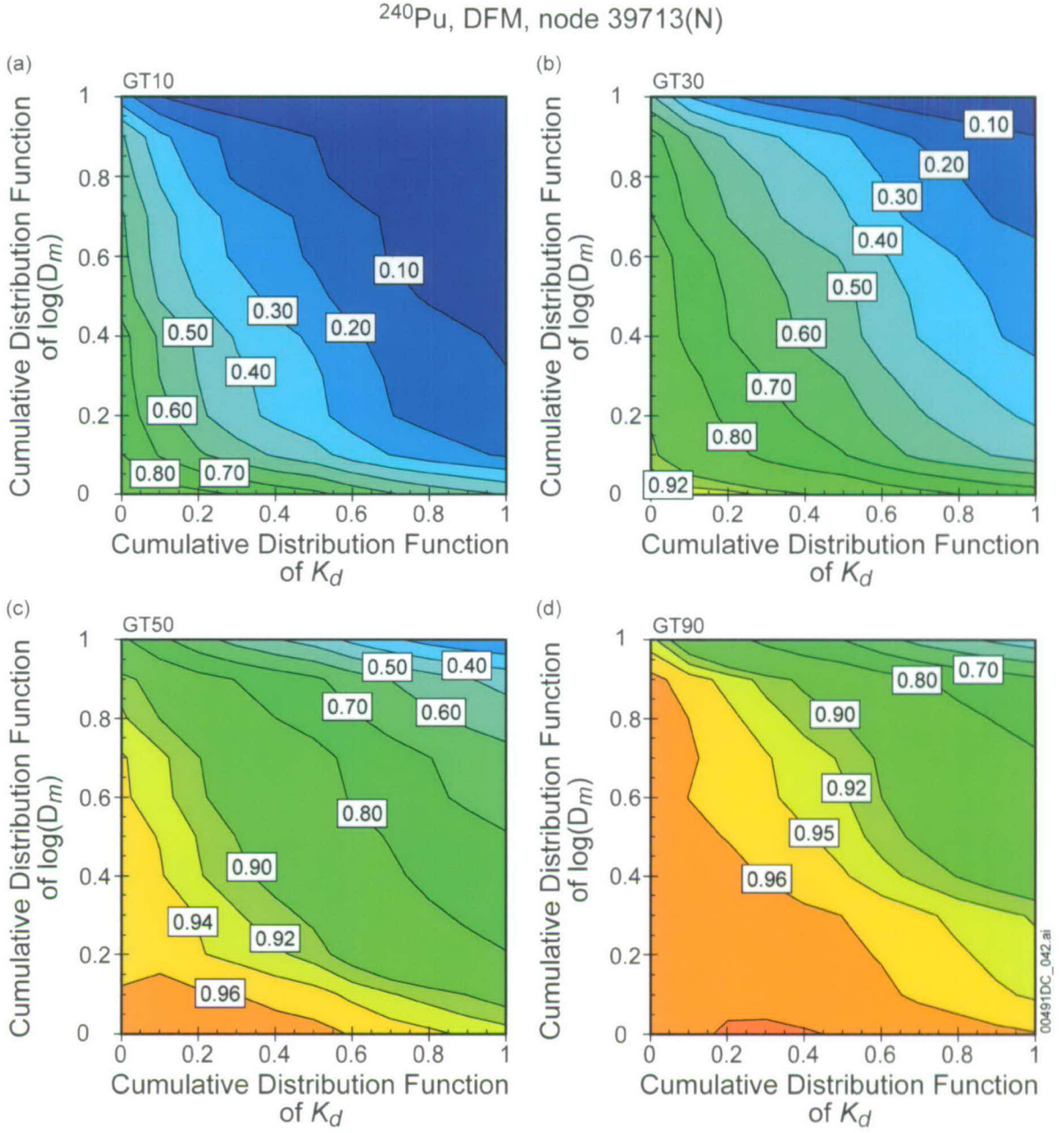

Output DTN: MO0705TRANSTAT.000.

Figure 6.8.2-21. Normalized ^{240}Pu Concentration (Decay Fraction, Computed from Travel Time Distributions) as a Function of Matrix Diffusion Coefficient and Sorption Coefficient for the Glacial-Transition Climate Conditions, DFM Model, Northern Release Location

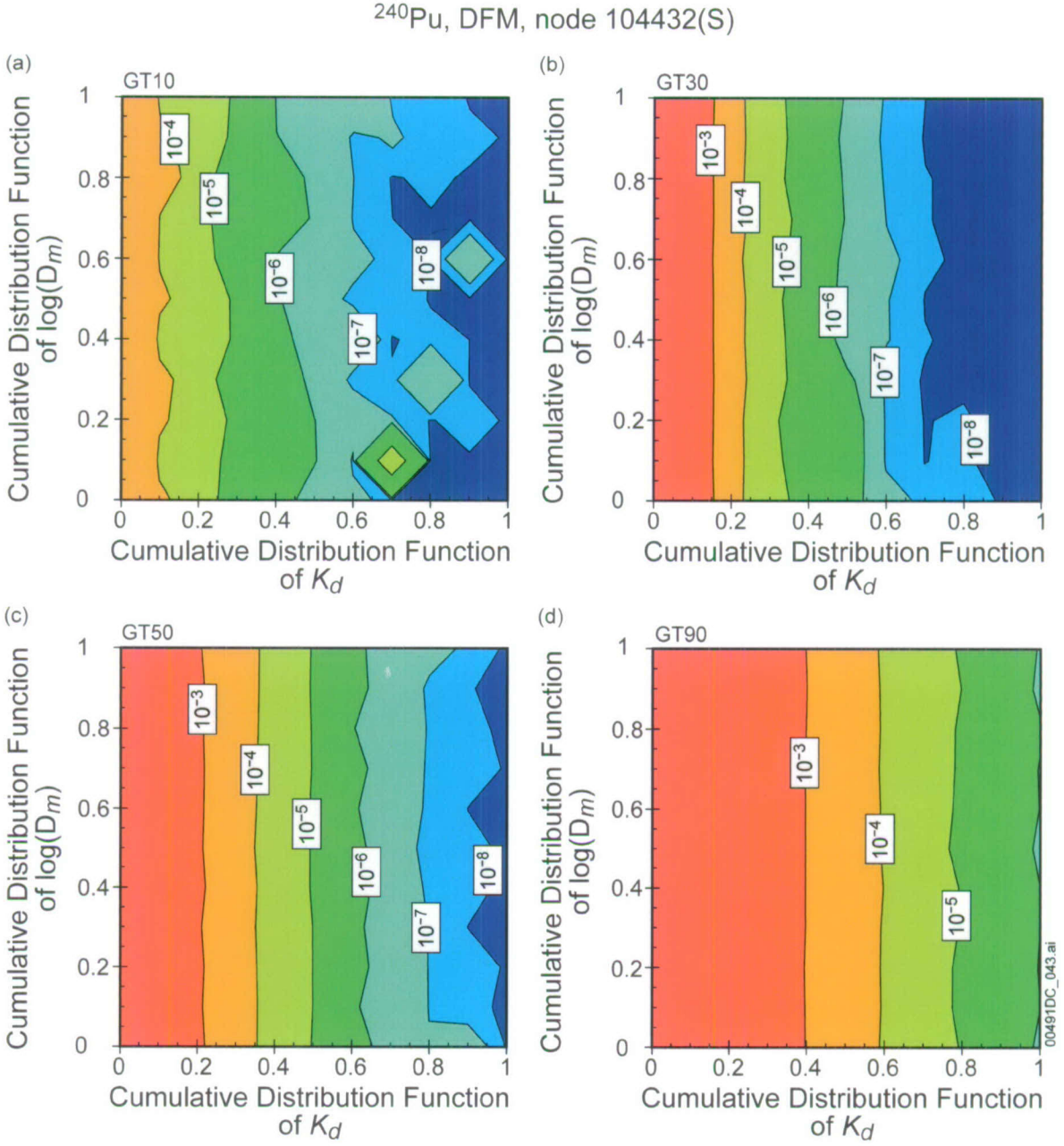

Output DTN: MO0705TRANSTAT.000.

Figure 6.8.2-22. Normalized ^{240}Pu Concentration (Decay Fraction, Computed from Travel Time Distributions) as a Function of Matrix Diffusion Coefficient and Sorption Coefficient for the Glacial-Transition Climate Conditions, DFM Model, Southern Release Location

The final set of analyses examines the influence of uncertainty in the value of the colloid retardation factor R_{coll} for the irreversible Ic species of ^{240}Pu. Using the same method of sampling from the uncertainty distribution in equal intervals of the cumulative distribution function, the 11 values of R_{coll}, spanning the range from 0 to 1 in intervals of 0.1, are 6, 6, 8.115, 13.384, 19.692, 26, 37.327, 48.653, 59.98, 429.99, and 800 (output DTN: MO0705TRANSTAT.000). Figure 6.8.2-23 shows the results of the mean travel time as

a function of R_{coll} for the four glacial-transition flow fields, for the northern (left) and southern (right) release locations. Similar plots for the decay fraction C/C_0 are shown in Figure 6.8.2-24. For the northern release location, travel times are larger for either lower fluid flow rates or larger values of R_{coll}. The southern release location, with its interval of matrix-dominated transport, has generally larger travel times and a smaller impact of fracture retardation of colloids, since this effect "competes with" the matrix transport time for importance. For either release location, the decay fraction is close to unity for this species of ^{240}Pu except for the highest values of R_{coll} in the uncertainty distribution. For other Ic species with shorter half lives, a larger effect of R_{coll} uncertainty on the decay fraction would be expected.

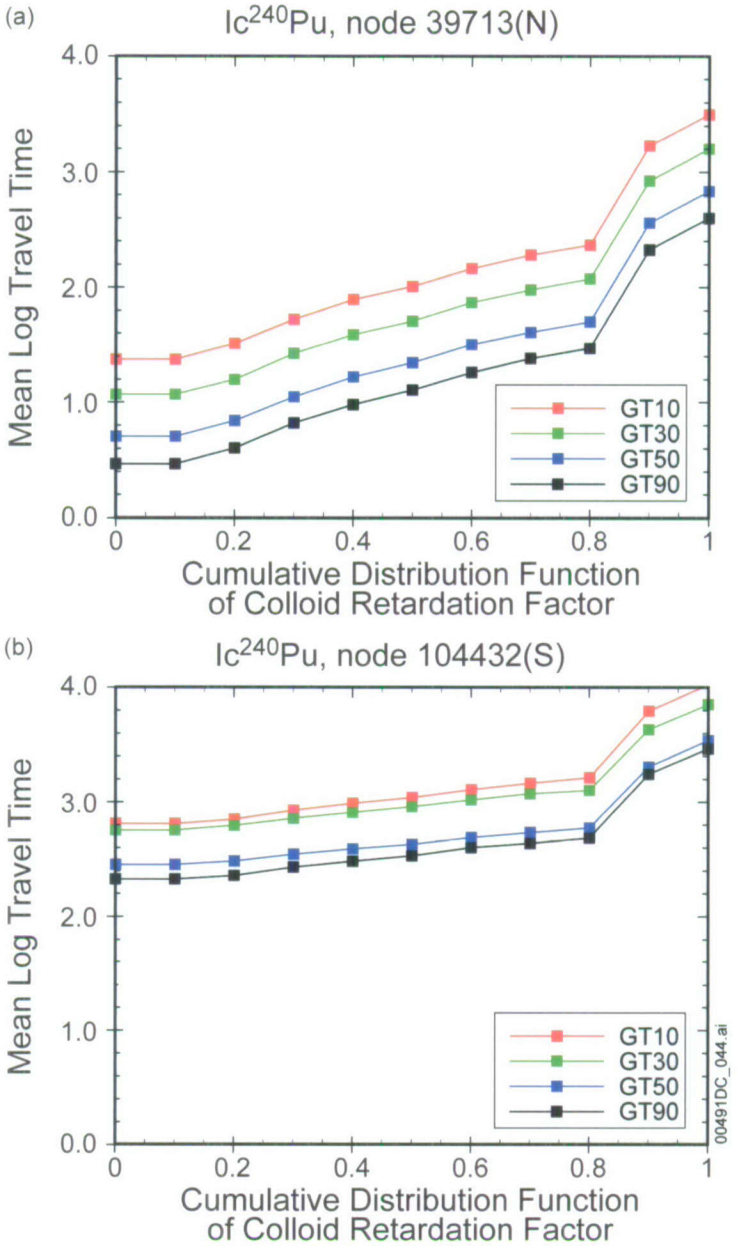

Output DTN: MO0705TRANSTAT.000.

Figure 6.8.2-23. Mean Travel Time of $Ic^{240}Pu$ as a Function of Colloid Retardation Factor for the Glacial-Transition Climate Condition

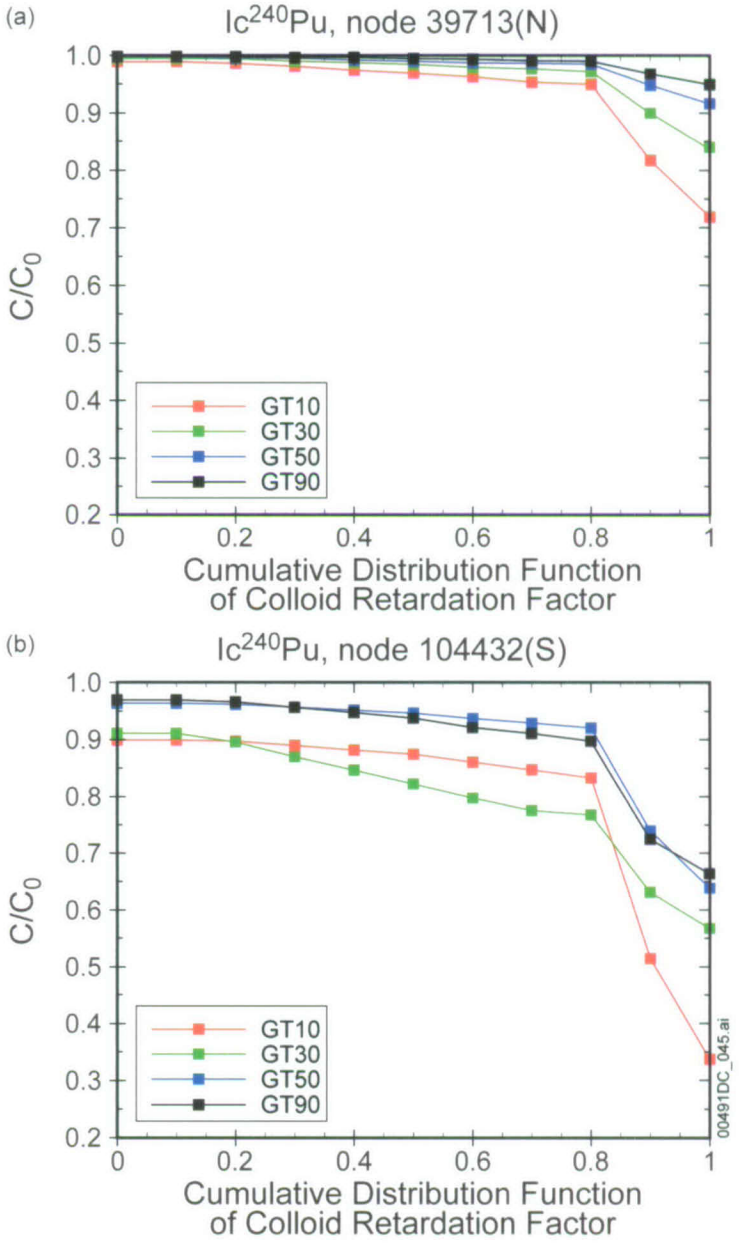

Output DTN: MO0705TRANSTAT.000.

Figure 6.8.2-24. Normalized Concentration of $Ic^{240}Pu$ (Decay Fraction, Computed from Travel Time Distributions) as a Function of Colloid Retardation Factor for the Glacial-Transition Climate Condition

In conclusion, the relative importance of conceptual and parameter uncertainties must be treated separately for each radionuclide, and the analysis techniques applied herein provide insights into the behavior of species in the TSPA model. However, the actual predicted performance of the unsaturated zone barrier system within the repository total system must be examined in the TSPA model itself.

6.9 OTHER TSPA IMPLEMENTATION CONSIDERATIONS

In the parent report, this section described several issues with previous versions of the FEHM computer code and with inconsistencies in colloid parameter inputs used in the particle tracking model and the TSPA model. All of these issues have been addressed and resolved. Code issues are treated in the software documentation for FEHM V. 2.24-01. The input inconsistencies involved the lack of colloid size-exclusion factors for fault zones and the lack of colloid retardation factors for reversible sorbed radionuclides. These issues have been corrected in this version of the particle tracking model; the parameter distributions are provided in output DTN: LA0701PANS02BR.003.

7. VALIDATION

Several changes have been made to this section:

- Figures 7-1 to 7-14 and associated output DTN number have changed because they were produced with new code FEHM V. 2.24-01, but the discussions of these results have not changed, with the exception of Figure 7-12, which is discussed in Section 7.2.3.2
- In Section 7.2.1, the software references have been updated
- In Section 7.2.3, a paragraph has been added to discuss the issue of using previously developed flow fields for validation purposes.

7.1 CONFIDENCE BUILDING DURING MODEL DEVELOPMENT TO ESTABLISH THE SCIENTIFIC BASIS AND ACCURACY FOR INTENDED USE

No change.

7.2 POSTDEVELOPMENT MODEL VALIDATION TO SUPPORT THE SCIENTIFIC BASIS OF THE MODEL

No change to this introductory section.

7.2.1 COMPARISONS WITH DISCRETE FRACTURE MODEL

The references to software have been updated, but the content of this section is identical to that of the parent report.

A DFM, in which transport in a dual-permeability medium is simulated directly, is an excellent test case of the transport model employed in the unsaturated zone abstraction model. In the most general case, water moves in both media, as well as between the media, and solute communicates between the media as it moves through the system via molecular diffusion and advection. First, a test case for the advective movement between the fracture and matrix in such a system is presented. Then, parallel flow and transport in the two media are tested, with solute introduced into either the fracture or the matrix. To investigate the ability of the model to span a range of hydrologic conditions, a fracture-dominated flow situation (essentially 100% fracture flow) and a case with a 60/40 fracture/matrix (f/m) flow split are used for testing. Figure 6-5 of the parent report represents the model system simulated with a DFM. Transport between the media occurs via molecular diffusion, so that the breakthrough curve at the outlet of such a model is a function of the relative and absolute velocities and of the degree of diffusive communication of solute between the media. Geometric, flow, and transport parameters, listed in Table 7-1 for this suite of tests, are selected to be representative of transport conditions in the unsaturated zone at Yucca Mountain, but do not constitute an actual model of the system, merely a testing setup to enable comparisons to be made. Therefore, data sources for these values are not required. Nevertheless, because the parameters are in general in the range likely to be encountered in TSPA-LA model analyses, the model comparisons provide a good test of the correct functioning of the model.

Table 7-1. Parameter Values for Discrete Fracture Model Test Suite

Parameter	Symbol	Value	
		Case 2 (Sect. 7.2.1.2)	Case 3 (Sect. 7.2.1.3)
Flow Path Length (m)	L	300	300
Fracture Half-Spacing (m)	B	0.5	0.5
Fracture Half-Aperture (m)	b	0.5×10^{-3}	0.5×10^{-3}
Fracture Saturation (unitless)	θ_f	0.2	0.2
Matrix Water Content (unitless)	θ_m	0.4	0.4
Fracture Water Flux (kg/s)	f_f	1.583×10^{-5} (99% of total)	9.49×10^{-6} (60% of total)
Matrix Water Flux (kg/s)	f_m	1.583×10^{-7} (1% of total)	6.336×10^{-6} (40% of total)
Diffusion Coefficient (m^2/s)	D_m	10^{-30}, 10^{-12}, $1. 10^{-11}$, 10^{-10}, 10^{-9}	10^{-30}, 10^{-12}, $1. 10^{-11}$, 10^{-10}, 10^{-9}
Matrix Sorption Coefficient (mL/g)	K_d	0	0 or 5

For this entire set of simulations, a two-dimensional DFM with these parameters was simulated using FEHM V. 2.24-01 in a manner similar to that used to generate the transfer functions (Appendix C of the parent report). The software routine fehm2post V. 1.0 was used to execute the runs and perform postprocessing, and the resulting breakthrough curves at the outlet were processed using the software routine DISCRETE_TF V. 1.1 (STN: 11033-1.1-00 [DIRS 165742]). For the simulations using the particle-tracking model, a simple one-dimensional pathway is constructed consisting of ten dual-permeability cells (twenty total). The flow conditions (water contents, volumes, flow rates, etc.) were built into an FEHM restart flow field file by hand. These conditions, along with the grid files and the main FEHM input file, are read directly into the code and the transport particle-tracking solution is obtained for the input flow field. This process was chosen to make this test as similar as possible to the way the code is to be used in TSPA calculations, in which flow fields are read in directly and transport is computed. Results are then postprocessed using software routine ppptrk V. 1.0 (STN: 11030-1.0-01 [DIRS 181269]).

7.2.1.1 Test of Advective Transport Between Continua

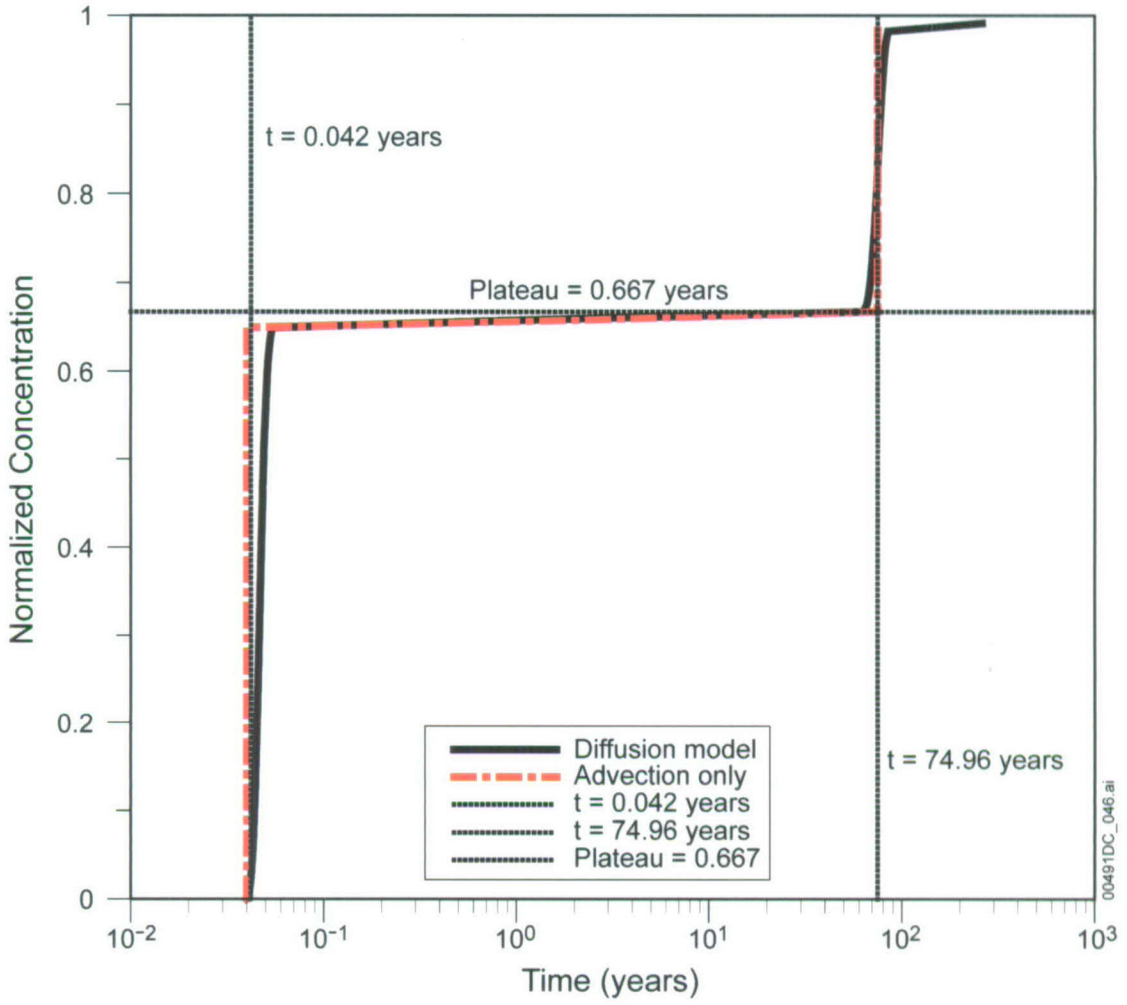

Output DTN: MO0705PAVALSIM.000.

Figure 7-1. Particle-Tracking Abstraction Model Behavior for Advective Transport Between the Fracture and Matrix Continua: No Diffusion or Sorption, Solute Injected into the Fracture, Compared to Theoretical Results

7.2.1.2 Comparisons with Diffusion for Fracture-Dominated Flow

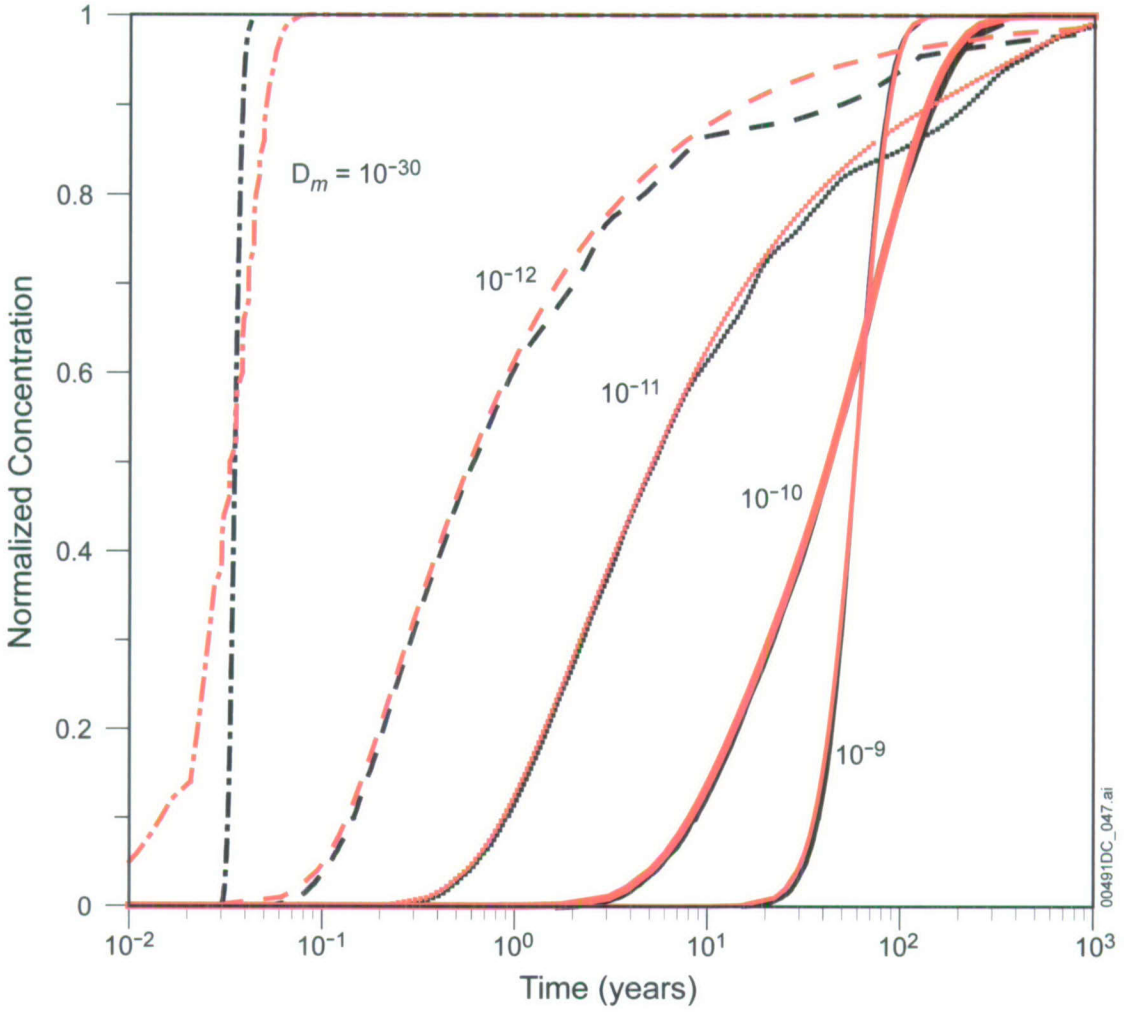

Output DTN: MO0705PAVALSIM.000.

NOTE: f_f = 0.99. Black = Particle Tracking; Red = Discrete Fracture Model.

Figure 7-2. Comparison of Discrete Fracture Model and Particle-Tracking Abstraction Model: Non-Sorbing Solute Injected into the Fracture for Different Values of Diffusion Coefficient

7.2.1.3 Comparisons with Diffusion and Sorption for Intermediate Flow Case

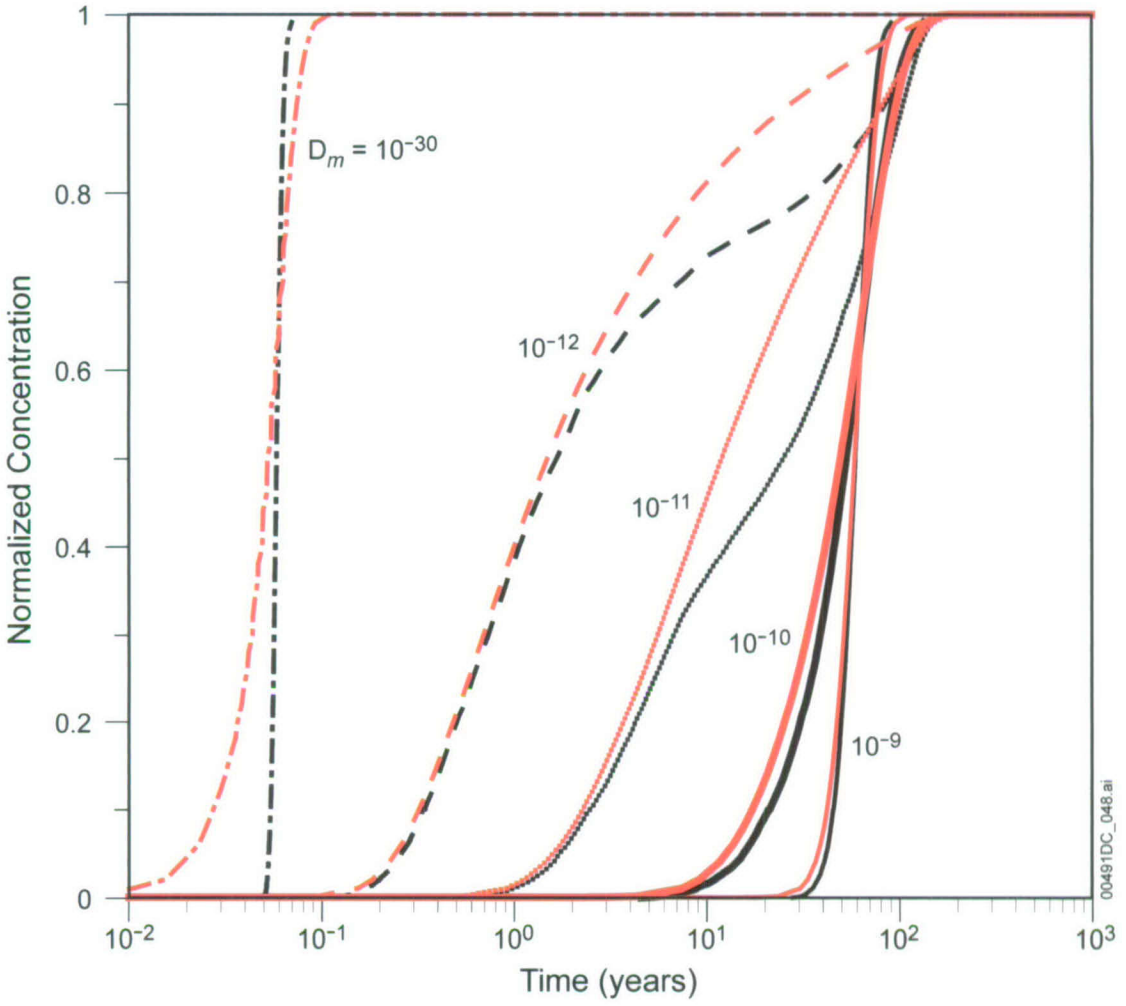

Output DTN: MO0705PAVALSIM.000.

NOTE: f_f = 0.6. Black lines = particle tracking; red lines = discrete fracture model

Figure 7-3. Comparison of Discrete Fracture Model and Particle-Tracking Abstraction Model: Non-Sorbing Solute Injected into the Fracture for Different Values of Diffusion Coefficient

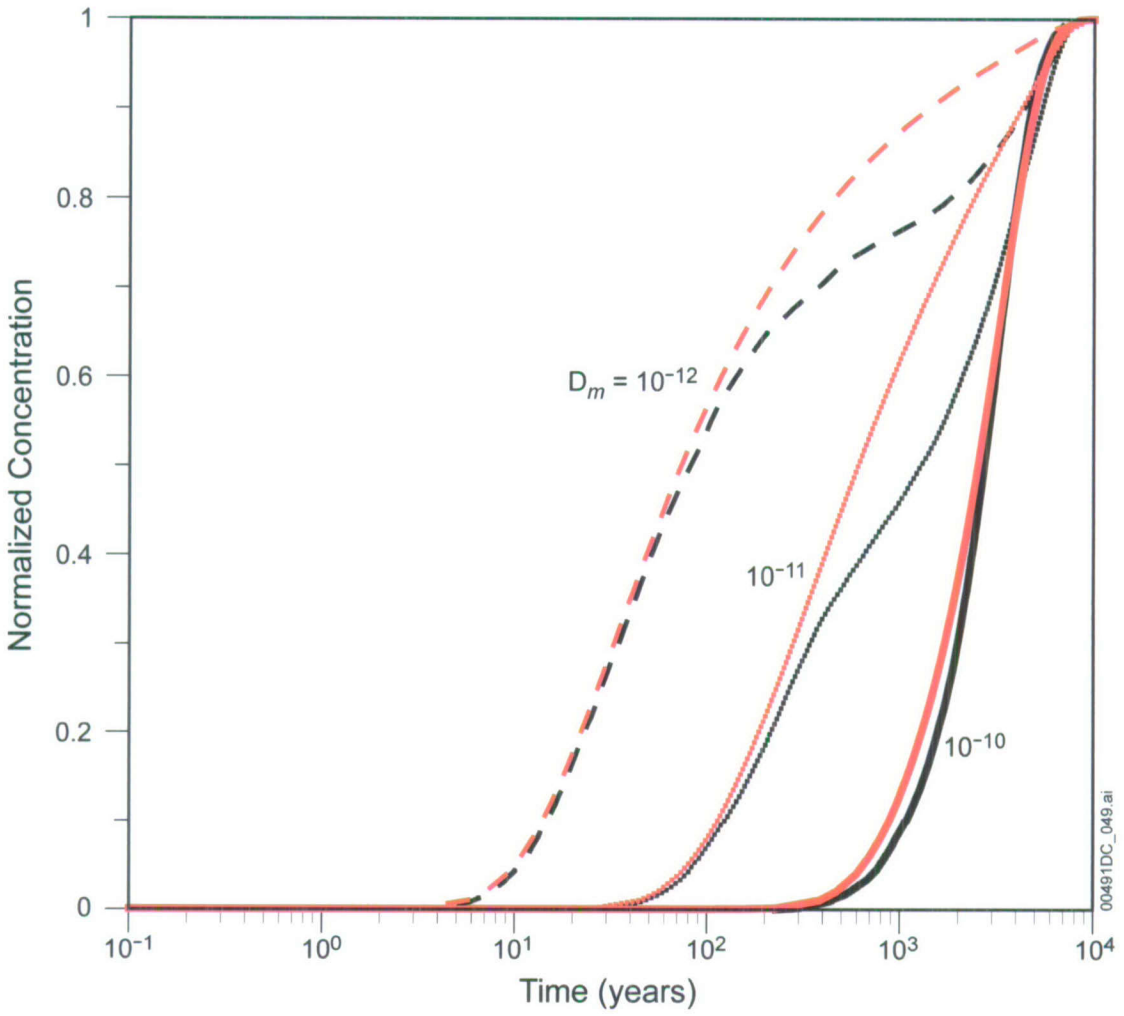

Output DTN: MO0705PAVALSIM.000.

NOTE: K_d = 5, black lines = particle tracking; red lines = discrete fracture model.

Figure 7-4. Comparison of Discrete Fracture Model and Particle-Tracking Abstraction Model: Sorbing Solute Injected into the Fracture for Different Values of Diffusion Coefficient

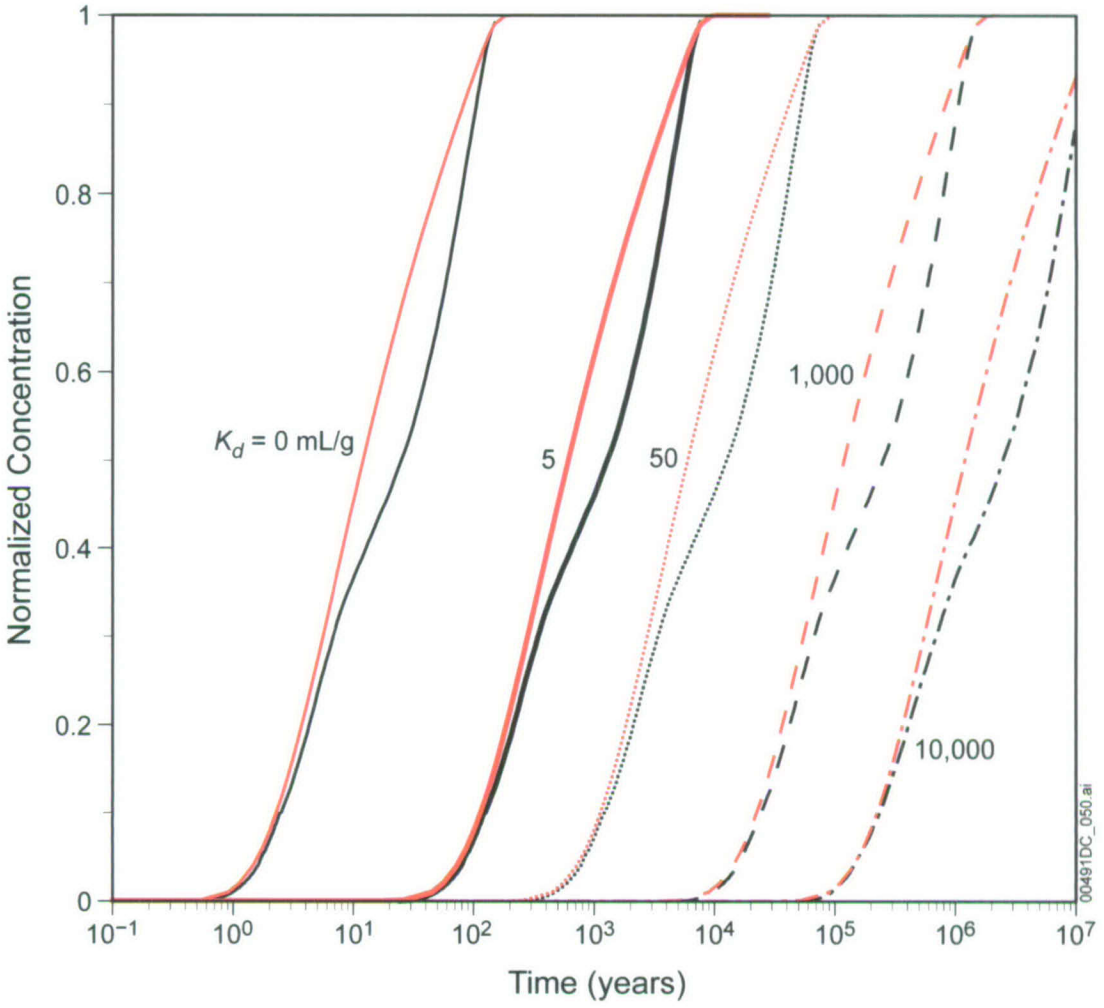

Output DTN: MO0705PAVALSIM.000.

NOTE: $D_m = 10^{-11}$, black lines = particle tracking; red lines = discrete fracture model.

Figure 7-5. Comparison of Discrete Fracture Model and Particle-Tracking Abstraction Model: Sorbing Solute Injected into the Fracture for Different Values of Sorption Coefficient

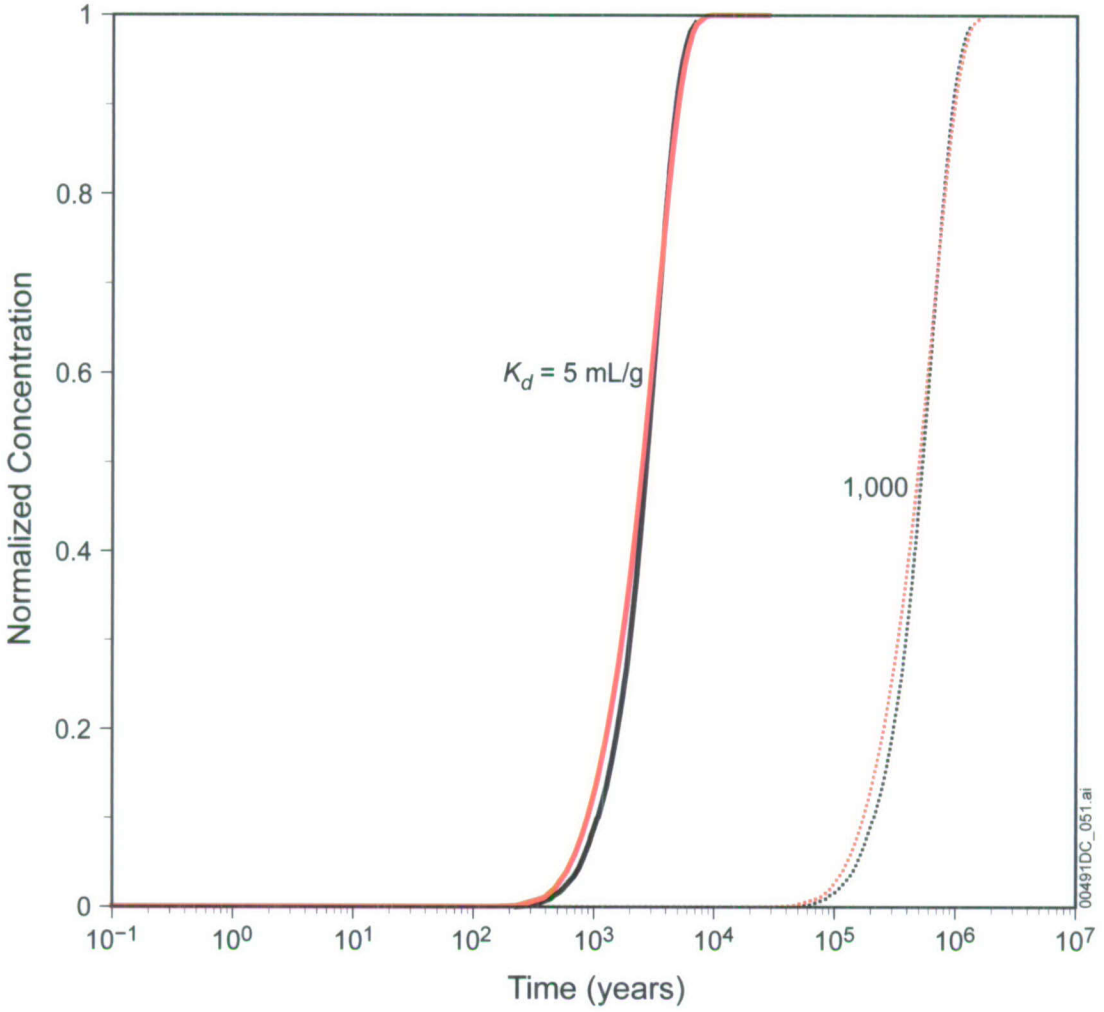

Output DTN: MO0705PAVALSIM.000.

NOTE: D_m = 10^{-10}, black lines = particle tracking; red lines = discrete fracture model.

Figure 7-6. Comparison of Discrete Fracture Model and Particle-Tracking Abstraction Model: Sorbing Solute Injected into the Fracture for Different Values of Sorption Coefficient

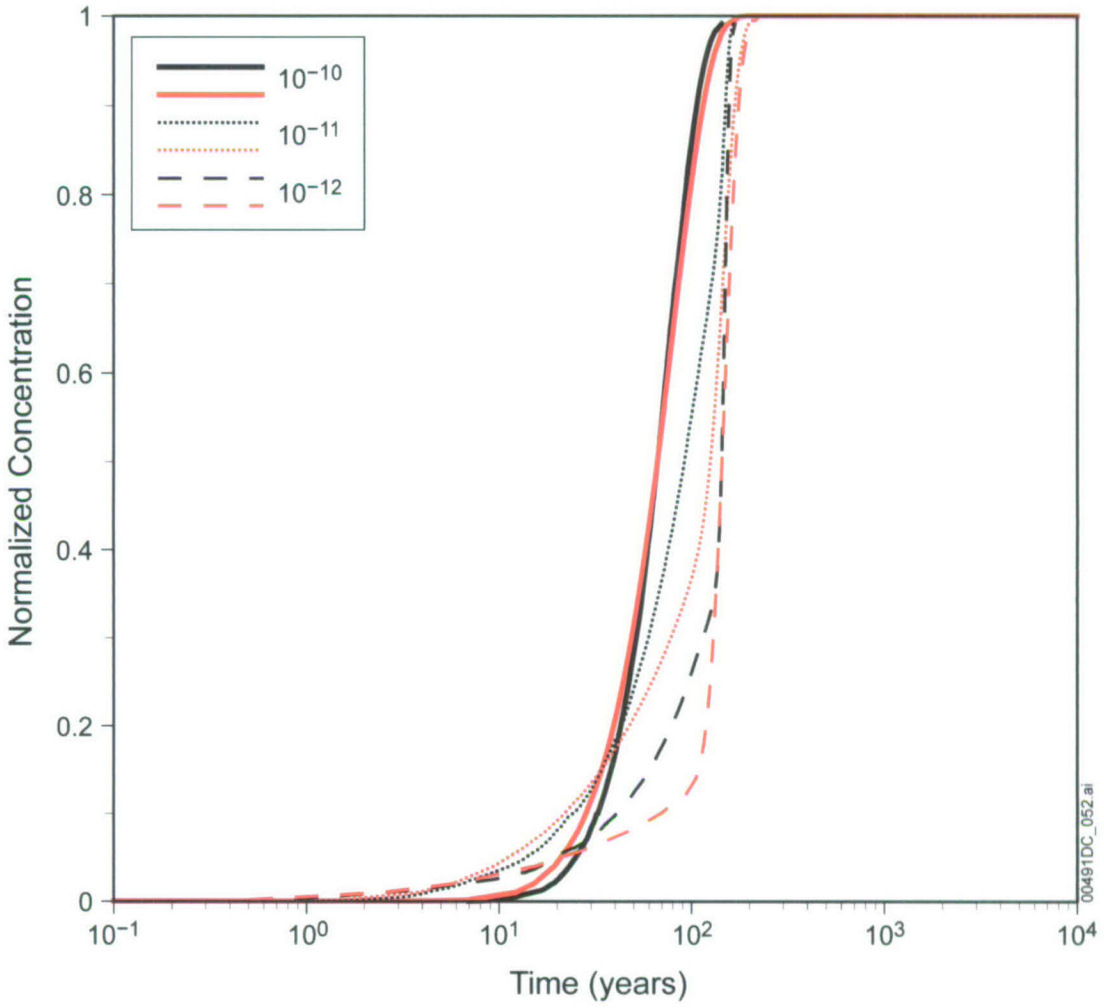

Output DTN: MO0705PAVALSIM.000.

NOTE: Solute injection into matrix. Black lines = particle tracking; red lines = discrete fracture model.

Figure 7-7. Comparison of Discrete Fracture Model and Particle-Tracking Abstraction Model: Non-Sorbing Solute Injected into the Matrix for Different Values of Diffusion Coefficient

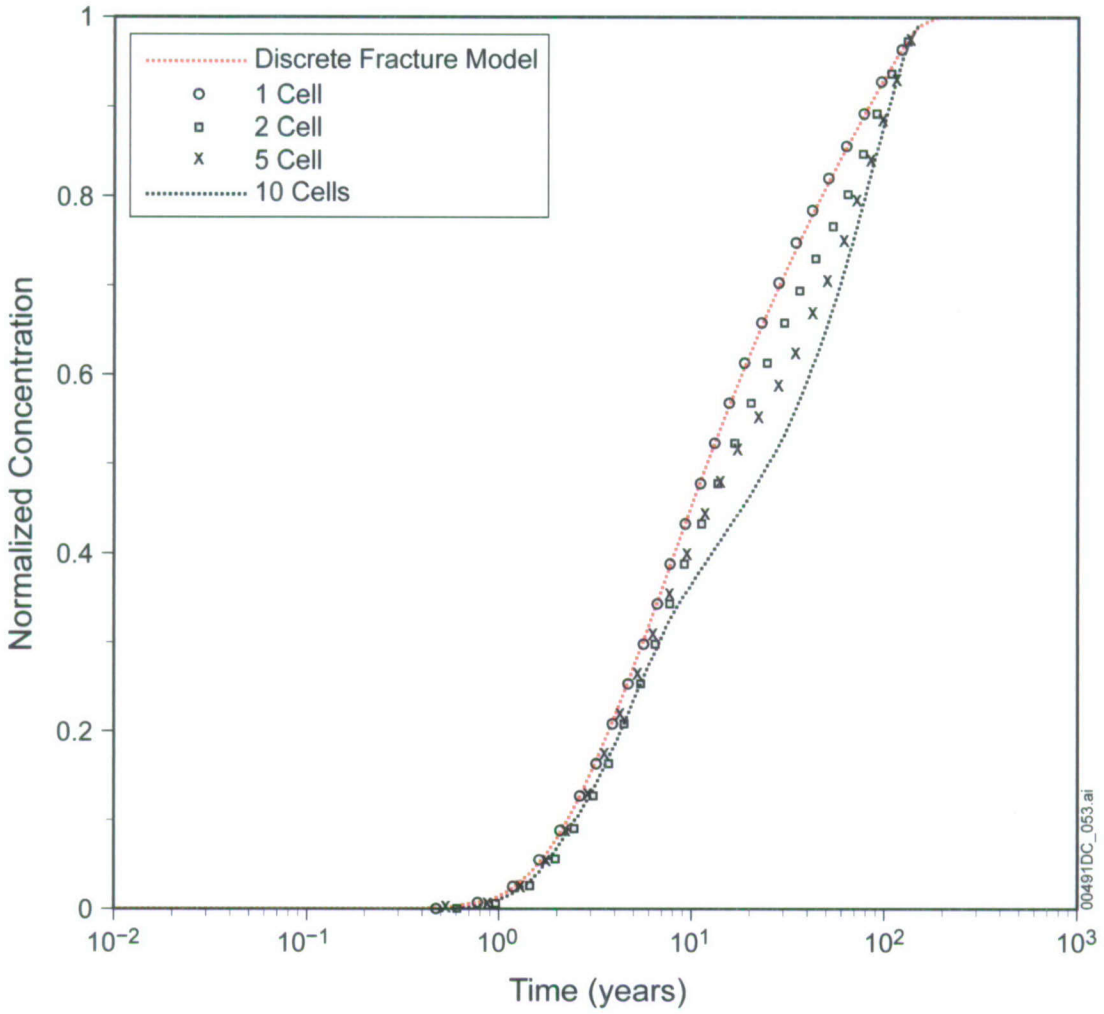

Output DTN: MO0705PAVALSIM.000.

NOTE: Grid resolution test of particle tracking algorithm, $D_m = 10^{-11}$.

Figure 7-8. Comparison of Discrete Fracture Model and Particle-Tracking Abstraction Model: Non-Sorbing Solute Injected into the Fracture for Different Numbers of Grid Cells in the Flow Path

7.2.1.4 Summary of Validation Tests for a Discrete Fracture Model

No change.

7.2.2 Comparison with the Dual-k and MINC Model Formulations on a Two-Dimensional Cross-Section Model

No change to the text of this section. Figure 7-9 is the new figure generated in the validation of the model.

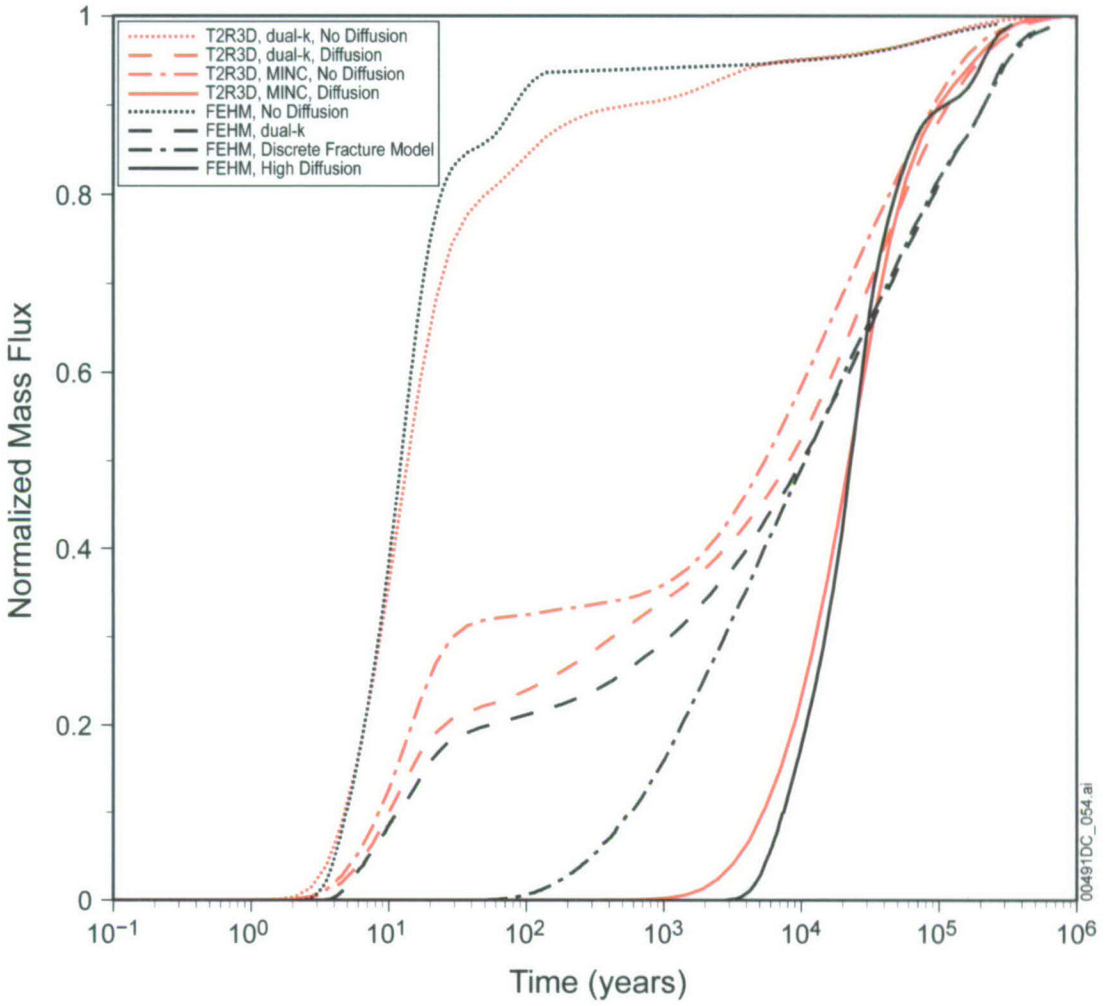

Source: DTN: LB03093RADTRNS.002 [DIRS 166071] (T2R3D simulations).

Output DTN: MO0705PAVALSIM.000.

Figure 7-9. Comparison of Particle-Tracking Model with T2R3D Models for a Two-Dimensional, Mountain-Scale Model: with (and without) Diffusion, for dual-k and DFM Formulations for the f/m Interaction Model, Present-Day Mean Infiltration, Representative Parameter Values, and Present-Day Water Table

7.2.3 Comparison with T2R3D Process Model for the Three-Dimensional System

For simulations in which FEHM is compared to the process model code T2R3D (Figures 7-10, 7-11, 7-12, 7-13, and 7-14), flow fields from a previous version of the flow model are used (DTN: LA0311BR831371.002 [DIRS 169182], an Output DTN of the parent report) because these process model results are available for this purpose. This approach requires justification that for the purposes of model validation, the previously developed flow fields provide an adequate basis for comparison. To justify this, first direct correspondence of each new flow field to one considered in the previous modeling effort is impossible due to the many changes the model has undergone since the infiltration model has been revised. Also, considering the complexity of the three-dimensional flow model, the large variability of percolation rates throughout the model domain for each flow field, and the large range of spatially averaged

infiltration rates across the collection of flow fields listed in Table 6-1 of this addendum, model comparison criteria for validation purposes must be flexible. As long as the FEHM and T2R3D models being directly compared are based on the same flow and transport conditions and parameters, and the overall transport system previously simulated reasonably replicates the conditions of the current TSPA model over a range of conditions, then the use of the older flow fields for validation purposes is acceptable.

The main differences between the flow fields developed recently and those available at the time of the validation runs are the mean infiltration rate and the spatial variability of the local percolation rate. Despite these differences, the mean infiltration rates from the older flow fields span a considerable portion of the range of repository percolation rates of the new flow fields (DTN: LB0701GTFEHMFF.001 [DIRS 179160]), as is demonstrated by comparing the range of mean infiltration rates under present-day climate conditions of 0.4 to 11.6 mm/yr from Table 6-10 in *Simulation of Net Infiltration for Present-Day and Potential Future Climates* (BSC 2004 [DIRS 170007]) to the range of median percolation rates of 3.93 to 35.27 mm/yr from Table 6-26 in this addendum. Beyond the mean or median values, the spatial variability of infiltration and percolation rates also overlap in the two sets of flow fields, as can be seen by comparing the ranges associated with each percolation bin in Table 6-26 to the net infiltration minimum and maximum values in *Simulation of Net Infiltration for Present-Day and Potential Future Climates* (BSC 2004 [DIRS 170007], Table 6-10). Similar comparisons for the monsoon and glacial-transition climate states yield a similar result. Lastly, the basic flow and transport processes simulated in the newer model are the same as those used in the past, and the transport results presented in Section 6.8 are similar to those in the previous model, in terms of the median travel time and range of travel times reflected in the breakthrough curves. Thus, the new model, though different in detail, is fundamentally similar to past models. Therefore, the use of older process model results (based on an older flow field developed with a previous version of the infiltration model) for the purposes of validating the abstraction model is justified.

7.2.3.1 Comparisons of FEHM and T2R3D for the Dual-k Conceptual Model

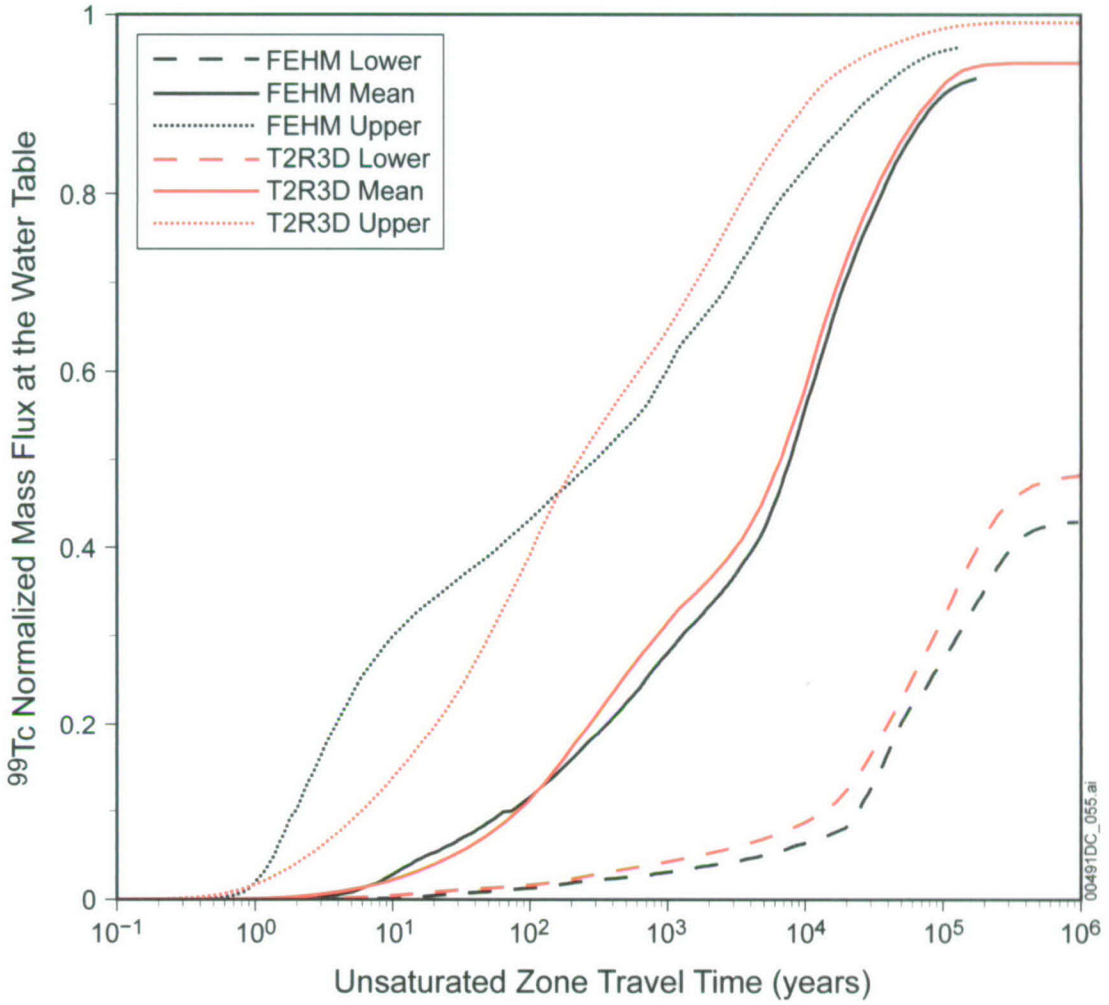

Sources: SNL 2007 [DIRS 177396] (T2R3D simulations); DTN: LB0307MR0060R1.007 [DIRS 164752].

Output DTN: MO0705PAVALSIM.000.

Figure 7-10. Comparison of Breakthrough Curves for ^{99}Tc for T2R3D and the Unsaturated Zone Transport Abstraction Model: Simulations for Different Present-Day Infiltration Rate Scenarios (Lower, Mean, and Upper), Representative Parameter Values, and Present-Day Water Table

7.2.3.2 Influence of Diffusion Coefficient and f/m Interaction Alternative Conceptual Model

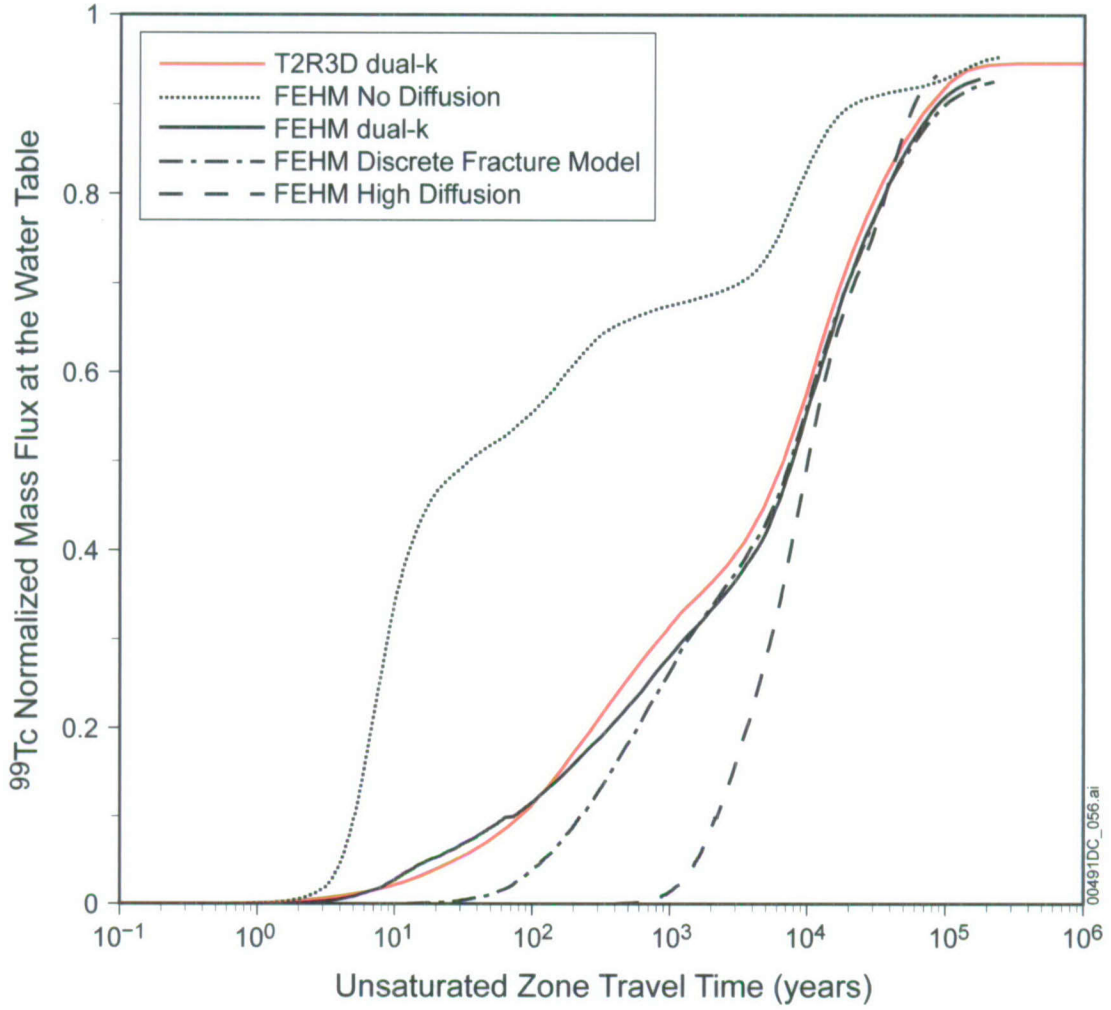

Sources: SNL 2007 [DIRS 177396] (T2R3D simulations); DTN: LB0307MR0060R1.007 [DIRS 164752].

Output DTN: MO0705PAVALSIM.000.

Figure 7-11. Comparison of Breakthrough Curves for ^{99}Tc for T2R3D and the Unsaturated Zone Transport Abstraction Model: Present-Day Mean Infiltration Scenario, Diffusion in FEHM Ranging from No Diffusion to High Values, Representative Parameter Values, and Present-Day Water Table

The influence of f/m conceptual model is explored more fully in Figure 7-12, a comparison, using only the FEHM particle-tracking model, of the dual-k and DFM alternative conceptual models (ACMs) for all of the flow scenarios. The simulation is using input files from output DTN: MO0704PAFEHMBR.001. The flow fields are from DTN: LB0701GTFEHMFF.001 [DIRS 179160]. The choice of ACM is particularly sensitive for the higher (50% and 90%) infiltration scenarios, whereas differences become progressively more subtle for the lower (30% and 10%) infiltration scenarios. As the fluid velocity is reduced, the characteristic diffusional distance into the matrix increases. For this situation, the dual-k model becomes more like the DFM in the sense that concentration gradients in the latter are not nearly as steep. With respect

to the abstraction model, these comparisons have reasonable qualitative explanations. This result illustrates that the abstraction model can propagate conceptual model uncertainties for f/m interactions through the TSPA-LA model.

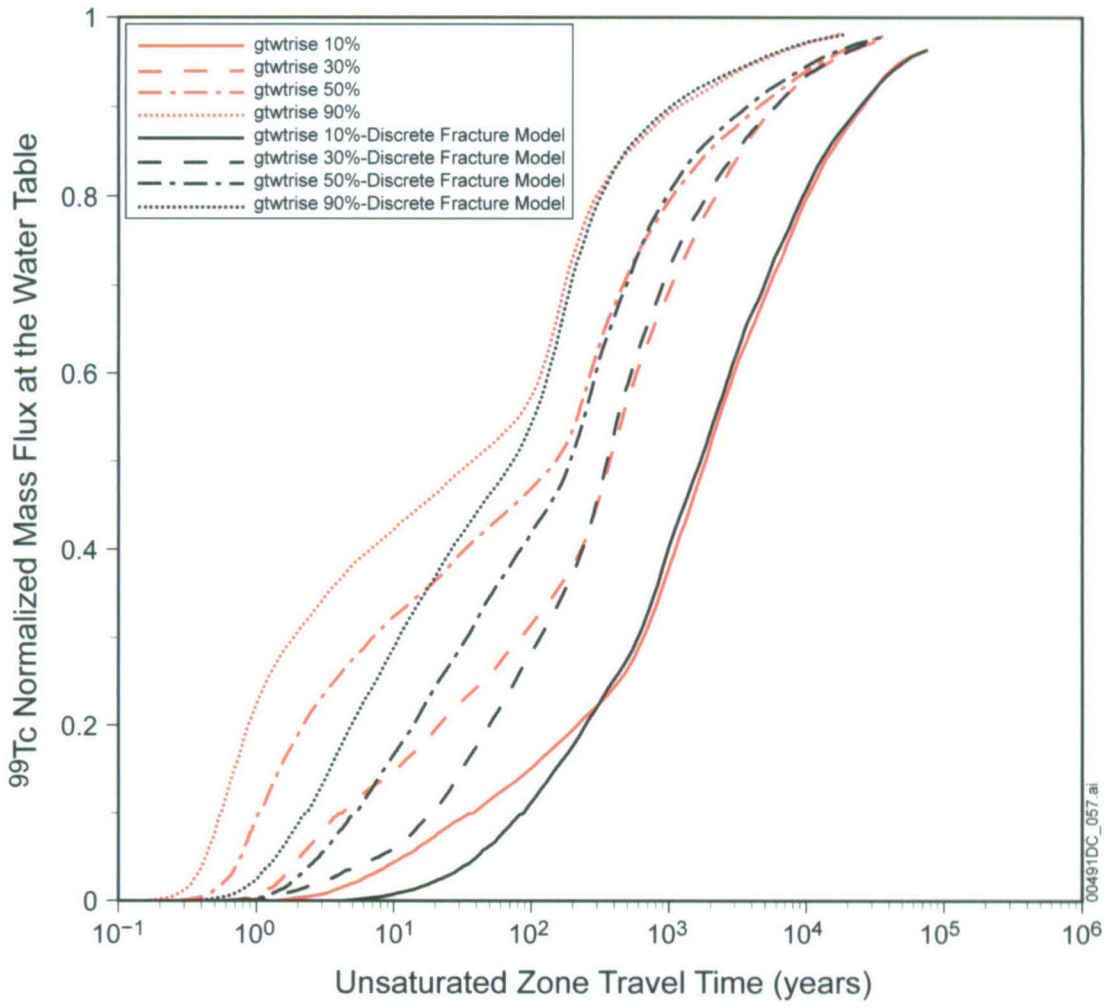

Output DTN: MO0705PAVALSIM.000.

Figure 7-12. Breakthrough Curves for ^{99}Tc Using the Unsaturated Zone Transport Abstraction Model to Investigate the Role f/m Interaction Conceptual Model: Simulations for Different Glacial-Transition Infiltration Rate Scenarios (10%, 30%, 50%, and 90%), Representative Parameter Values, and Glacial-Transition Water Table

7.2.3.3 Tests of the Active Fracture Model Implementation

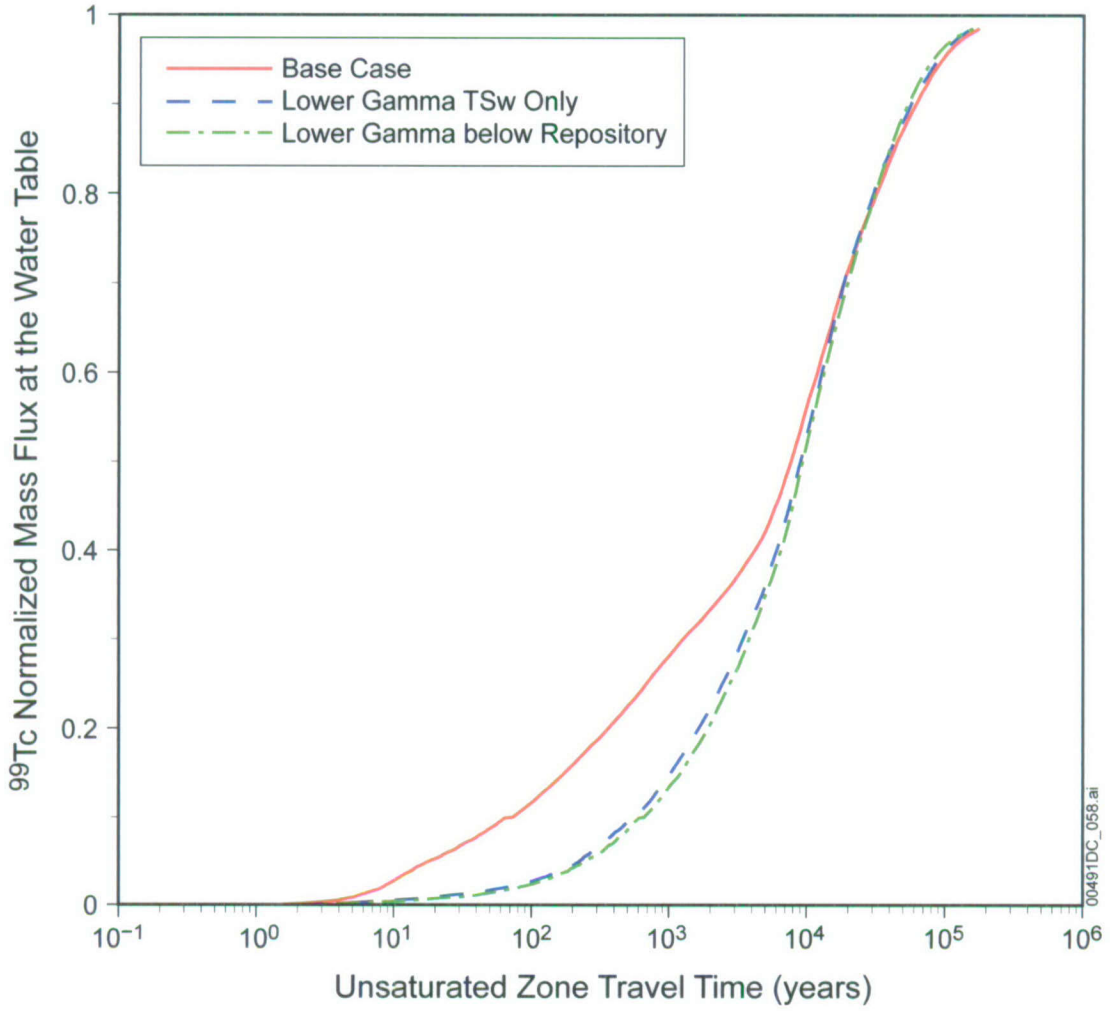

Output DTN: MO0705PAVALSIM.000.

Figure 7-13. Breakthrough Curves for Conservative Solute Using the Unsaturated Zone Transport Abstraction Model to Investigate the Role of AFM γ Parameter: dual-k ACM, Simulation for Different Values of Gamma in Rock Units Beneath the Repository, Present-Day Mean Infiltration, Representative Parameter Values, and Present-Day Water Table

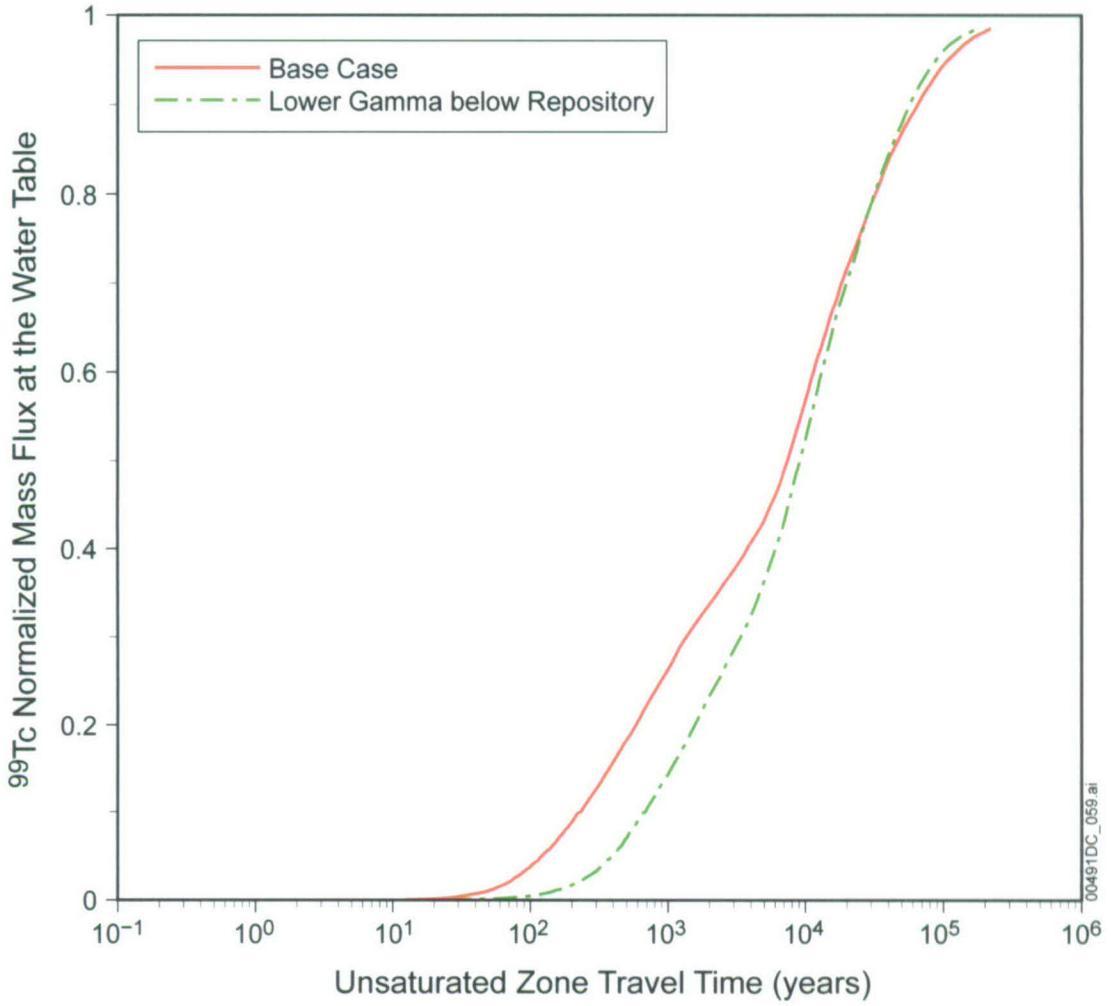

Output DTN: MO0705PAVALSIM.000.

Figure 7-14. Breakthrough Curves for Conservative Solute Using the Unsaturated Zone Transport Abstraction Model to Investigate the Role of AFM γ Parameter: Discrete Fracture ACM, Simulation for Different Values of Gamma in Rock Units Beneath the Repository, Present-Day Mean Infiltration, Representative Parameter Values, and Present-Day Water Table

7.3 SUMMARY OF VALIDATION ACTIVITIES

No change.

INTENTIONALLY LEFT BLANK

8. CONCLUSIONS

8.1 SUMMARY OF MODELING ACTIVITY

The principal output from this addendum is an abstraction model for radionuclide transport in the unsaturated zone. It is intended for this model to be used directly in the TSPA-LA system model. The code used to implement the model is FEHM V. 2.24-01, in the form of a dynamic link library (dll) callable from GoldSim V. 9.60.100 (STN: 10344.9.60-01 [DIRS 181903]). The operation of the dll in a GoldSim model environment has been developed and tested in the software documentation and is not repeated here, except to discuss the data structure of the interface between GoldSim and the FEHM dll. In addition, the work was conducted in part to address several condition reports related to code bug fixes and enhancements identified during the course of using the model in TSPA analyses. These condition reports and their resolutions are discussed in Section 4.2.

This addendum and the accompanying parent report pulls together information and data from a variety of sources, creating a simulation model capable of efficiently computing the transport of multiple radionuclides through the unsaturated zone. Current data sources are listed in Section 4.1, and the mathematical formulation and assessment of parameter ranges and distributions are treated in Section 6. The direct feed to TSPA documented in this report is the synthesis of data and models into a simulation tool. The model to be used in TSPA simulations consists of a code (FEHM V. 2.24-01, PC dll) and input files to the code that must be present to run the model within GoldSim. Table 8-1 lists the computer files required to run the base-case model, and a brief description of the purpose of each file. Fixed parameters have been inserted into the appropriate FEHM files. Parameter distributions given in Section 6.5 are used to generate a table of parameters in a text file, which is read using FEHM's capability of reading in parameters from a separate file and inserting those parameters into the simulation at runtime. Thus, this set of files provides the template for the TSPA-LA modelers to set up the unsaturated zone transport abstraction model in a multiple-realization GoldSim system model. The table of uncertain parameters is not generated in this report: TSPA system modelers must do this to facilitate parameter correlations and to enable the exploration of parameter sensitivities to be studied systematically at the system level. Table 8-2 lists the unsaturated zone transport parameters, which should be presampled and assembled into a table for FEHM to read at run time in TSPA.

Table 8-1. Unsaturated Zone Transport Abstraction Model Input Files

Parameter Name	Parameter Definition	Uncertainty Description	Parameter Value (s)	DTN/Title
fehmn.files	FEHM model input setup file containing file names for model run	File	See DTN	Output DTN: MO0704PAFEHMBR.001: FEHM Model and Input. Identical to file in LB0612PDFEHMFF.001 [DIRS 179296] and applicable to TSPA model runs under all climate scenarios
fehmn.grid	FEHM grid file: grid node coordinates	File	See DTN	Output DTN: MO0704PAFEHMBR.001: FEHM Model and Input. Identical to file in LB0612PDFEHMFF.001 [DIRS 179296] and applicable to TSPA model runs under all climate scenarios
fehmn.stor	FEHM geometric storage coefficient data (and accompanying cell connection information)	File	See DTN	Output DTN: MO0704PAFEHMBR.001: FEHM Model and Input. Identical to file in LB0612PDFEHMFF.001 [DIRS 179296] and applicable to TSPA model runs under all climate scenarios
fehmn.zone	FEHM zone identification files for grid nodes: this file indexes each grid node number to a hydrologic zone. Input zone list file for UZ transport abstraction model	File	See DTN	Output DTN: MO0704PAFEHMBR.001: FEHM Model and Input. Identical to file in LB0612PDFEHMFF.001 [DIRS 179296] and applicable to TSPA model runs under all climate scenarios
fehmn.zone2 (file is called *fehmn.zone2_GT10%* in the DTN)	FEHM zone identification files for grid nodes: Zone file containing node numbers in different rock layers and the repository and water table collection bins	File	See DTN	Output DTN: LA0702PANS02BR.001: Repository and Water Table Bins, file *fehmn.zone2_GT10%* - applicable to all infiltration scenarios and climate states

Table 8-1. Unsaturated Zone Transport Abstraction Model Input Files (Continued)

Parameter Name	Parameter Definition	Uncertainty Description	Parameter Value (s)	DTN/Title
FEHM ".ini" files: *ff1100.ini, ff1200.ini, ff1300.ini, ff1400.ini,* *ff2100.ini, ff2200.ini, ff2300.ini, ff2400.ini* *ff3100.ini, ff3200.ini, ff3300.ini, ff3400.ini* *ff4100.ini, ff4200.ini, ff4300.ini, ff4400.ini* (Note: corresponding file names of the files as they exist in the DTNs are listed in the "DTN/Title" entry)	Steady-state flow fields used to set the fluid flow rates in the UZ transport abstraction model	File	See DTN	LB0612PDFEHMFF.001 [DIRS 179296]: Flow-Field Conversions from TOUGH2 to FEHM Format for Present-Day 10-, 30-, 50-, and 90-Percentile Infiltration Maps, files *pd10.ini, pd30.ini, pd50.ini, pd90.ini* LB0701MOFEHMFF.001 [DIRS 179297]: Flow-Field Conversions from TOUGH2 to FEHM Format for Monsoon Climate10th-, 30th-, 50th-, and 90th-Percentile Infiltration Maps, files *mo10wtrise.ini. mo30wtrise.ini, mo50 wtrise.ini*, and *mo90wtrise.ini* LB0701GTFEHMFF.001 [DIRS 179160]: Flow-Field Conversions from TOUGH2 to FEHM Format for Glacial Transition Climate 10th-, 30th-, 50th-, and 90th-Percentile Infiltration Maps, files *gt10wtrise.ini, gt30wtrise.ini, gt50wtrise.ini, gt90wtrise.ini* LB0702PAFEM10K.002 [DIRS 179507]: Flow Field Conversions to FEHM Format for Post 10,000 Year Peak Dose Fluxes in the Unsaturated Zone for Four Selected Infiltration Rates, files *post10kWTRISEpkdq1.ini, post10kWTRISEpkdq2.ini, post10kWTRISEpkdq3.ini, post10kWTRISEpkdq4.ini*
fehm_TSPA.rock	Matrix porosity and rock density file: rock properties for all zones defined in fehmn.zone	File	See DTN	Output DTN: MO0704PAFEHMBR.001: FEHM Model and Input
fehm_TSPA.dpdp	Fracture porosity and fracture spacing data for model layers and fault zones	File	See DTN	Output DTN: MO0704PAFEHMBR.001: FEHM Model and Input
fehm_TSPA_10kyr.mptr *fehm_TSPA_1Myr.mptr* *fehm_TSPA_10kyr_ign.mptr* *fehm_TSPA_1Myr_ign.mptr*	Particle tracking input file containing the specification of the species, daughter products, and other transport inputs	File	See DTN	Output DTN: MO0704PAFEHMBR.001: FEHM Model and Input, file *fehm_TSPA.mptr*[a]
uz_tfcurves_dualk_nn_4680.in	Transfer function curves for implementing the RTTF particle tracking model for upscaling of fracture-matrix interaction process: dual permeability submodel	File	See DTN	MO0704PAPTTFBR.002: Particle Tracking Transfer Functions

Table 8-1. Unsaturated Zone Transport Abstraction Model Input Files (Continued)

Parameter Name	Parameter Definition	Uncertainty Description	Parameter Value (s)	DTN/Title
uz_tfcurves_nn_4680.in	Transfer function curves for implementing the RTTF particle tracking model for upscaling of fracture-matrix interaction process: discrete fracture submodel	File	See DTN	MO0704PAPTTFBR.002: Particle Tracking Transfer Functions
fehm_TSPA_gs_10kyr.dat *fehm_TSPA_gs_1Myr.dat*	All control parameters for the FEHM simulation. Used as main input file for UZ transport abstraction model	File	See DTN	Output DTN: MO0704PAFEHMBR.001: FEHM Model and Input, file *fehm_TSPA_template.dat*[1]
itfc_bf2.txt	Colloid transport probabilities for filtration at matrix interfaces, Unit BF2	File	See DTN	Output DTN: MO0704PAFEHMBR.001: FEHM Model and Input
itfc_bf3.txt	Colloid transport probabilities for filtration at matrix interfaces, Unit BF3	File	See DTN	Output DTN: MO0704PAFEHMBR.001: FEHM Model and Input
itfc_ch1.txt	Colloid transport probabilities for filtration at matrix interfaces, Unit CH1	File	See DTN	Output DTN: MO0704PAFEHMBR.001: FEHM Model and Input
itfc_ch6.txt	Colloid transport probabilities for filtration at matrix interfaces, Unit CH6	File	See DTN	Output DTN: MO0704PAFEHMBR.001: FEHM Model and Input
itfc_chv.txt	Colloid transport probabilities for filtration at matrix interfaces, Unit CHV	File	See DTN	Output DTN: MO0704PAFEHMBR.001: FEHM Model and Input
itfc_chz.txt	Colloid transport probabilities for filtration at matrix interfaces, Unit CHZ	File	See DTN	Output DTN: MO0704PAFEHMBR.001: FEHM Model and Input
itfc_pp1.txt	Colloid transport probabilities for filtration at matrix interfaces, Unit PP1	File	See DTN	Output DTN: MO0704PAFEHMBR.001: FEHM Model and Input
itfc_pp2.txt	Colloid transport probabilities for filtration at matrix interfaces, Unit PP2	File	See DTN	Output DTN: MO0704PAFEHMBR.001: FEHM Model and Input
itfc_pp3.txt	Colloid transport probabilities for filtration at matrix interfaces, Unit PP3	File	See DTN	Output DTN: MO0704PAFEHMBR.001: FEHM Model and Input
itfc_pp4.txt	Colloid transport probabilities for filtration at matrix interfaces, Unit PP4	File	See DTN	Output DTN: MO0704PAFEHMBR.001: FEHM Model and Input
itfc_tsw4.txt	Colloid transport probabilities for filtration at matrix interfaces, Unit TSW4	File	See DTN	Output DTN: MO0704PAFEHMBR.001: FEHM Model and Input
itfc_tsw5.txt	Colloid transport probabilities for filtration at matrix interfaces, Unit TSW5	File	See DTN	Output DTN: MO0704PAFEHMBR.001: FEHM Model and Input
itfc_tsw6.txt	Colloid transport probabilities for filtration at matrix interfaces, Unit TSW6	File	See DTN	Output DTN: MO0704PAFEHMBR.001: FEHM Model and Input
itfc_tsw7.txt	Colloid transport probabilities for filtration at matrix interfaces, Unit TSW7	File	See DTN	Output DTN: MO0704PAFEHMBR.001: FEHM Model and Input

Table 8-1. Unsaturated Zone Transport Abstraction Model Input Files (Continued)

Parameter Name	Parameter Definition	Uncertainty Description	Parameter Value (s)	DTN/Title
itfc_tsw8.txt	Colloid transport probabilities for filtration at matrix interfaces, Unit TSW8	File	See DTN	Output DTN: MO0704PAFEHMBR.001: FEHM Model and Input
itfc_tsw9.txt	Colloid transport probabilities for filtration at matrix interfaces, Unit TSW9	File	See DTN	Output DTN: MO0704PAFEHMBR.001: FEHM Model and Input
UZ_PARAMS_MULTI_LA_ COMPLIANCE[b]	Table of epistemically uncertain parameters generated within the TSPA model and input to the FEHM UZ transport abstraction model at runtime	File	N/A: Table generated within the TSPA model and supplied to FEHM at runtime	N/A: Table generated within the TSPA model and supplied to FEHM at runtime

[a] The input files listed in the "Parameter Name" entry are created by the TSPA group using the DTN file listed in the "DTN/Title" entry as a starting point. Slight modifications to that file will be made to handle specific simulation length and scenario situations. These changes will be documented by the TSPA group.

[b] File name added for completeness; not included in this report. The form of the file is described in Section 8.2.1, and its contents are described in Table 8-2.

Table 8-2. Unsaturated Zone Transport Epistemically Uncertain Input Parameters Found in TSPA Model GoldSim-Generated UZ_PARAMS_MULTI_LA_COMPLIANCE Files

Parameter Name (#)	Parameter Definition	Uncertainty Description	Parameter Value(s)	DTN/Title
fa_group1_UZP (1)	Aperture for Rock Group 1 (chnFf)	Stochastic	See DTN	Output DTN: LA0701PANS02BR.003: UZ Transport Parameters
fa_group2_UZP (2)	Aperture for Rock Group 2 (tswFf)	Stochastic	See DTN	Output DTN: LA0701PANS02BR.003: UZ Transport Parameters
fa_group3_UZP (3)	Aperture for Rock Group 3 (various units)	Stochastic	See DTN	Output DTN: LA0701PANS02BR.003: UZ Transport Parameters
fa_group4_UZP (4)	Aperture for Rock Group 4 (various units)	Stochastic	See DTN	Output DTN: LA0701PANS02BR.003: UZ Transport Parameters
fa_group5_UZP (5)	Aperture for Rock Group 5 (various units)	Stochastic	See DTN	Output DTN: LA0701PANS02BR.003: UZ Transport Parameters
fa_group6_UZP (6)	Aperture for Rock Group 6 (various units)	Stochastic	See DTN	Output DTN: LA0701PANS02BR.003: UZ Transport Parameters
fa_group7_UZP (7)	Aperture for Rock Group 7 (various units)	Stochastic	See DTN	Output DTN: LA0701PANS02BR.003: UZ Transport Parameters
fa_group8_UZP (8)	Aperture for Rock Group 8 (various units)	Stochastic	See DTN	Output DTN: LA0701PANS02BR.003: UZ Transport Parameters

Table 8-2. Unsaturated Zone Transport Epistemically Uncertain Input Parameters Found in TSPA Model GoldSim-Generated UZ_PARAMS_MULTI_LA_COMPLIANCE Files (Continued)

Parameter Name (#)	Parameter Definition	Uncertainty Description	Parameter Value(s)	DTN/Title
fa_group9_UZP (9)	Aperture for Rock Group 9 (tswF3)	Stochastic	See DTN	Output DTN: LA0701PANS02BR.003: UZ Transport Parameters
Gamma_UZP (10)	Gamma Parameter, all units	Stochastic	See DTN	Output DTN: LA0701PANS02BR.003: UZ Transport Parameters
UZDC_Am_RG1_out (11)	Matrix Diffusion Coefficient, Am, Tortuosity Rock Group 1	Stochastic	See DTN	Parameter developed in this Addendum from statistical data descriptors in DTN: LB0702PAUZMTDF.001 Unsaturated Zone Matrix Diffusion Coefficients
UZDC_Am_RG2_out (12)	Matrix Diffusion Coefficient, Am, Tortuosity Rock Group 2	Stochastic	See DTN	Parameter developed in this Addendum from statistical data descriptors in DTN: LB0702PAUZMTDF.001 Unsaturated Zone Matrix Diffusion Coefficients
UZDC_Am_RG3_out (13)	Matrix Diffusion Coefficient, Am, Tortuosity Rock Group 3	Stochastic	See DTN	Parameter developed in this Addendum from statistical data descriptors in DTN: LB0702PAUZMTDF.001 Unsaturated Zone Matrix Diffusion Coefficients
UZDC_C_RG1_out (14)	Matrix Diffusion Coefficient, C, Tortuosity Rock Group 1	Stochastic	See DTN	Parameter developed in this Addendum from statistical data descriptors in DTN: LB0702PAUZMTDF.001 Unsaturated Zone Matrix Diffusion Coefficients
UZDC_C_RG2_out (15)	Matrix Diffusion Coefficient, C, Tortuosity Rock Group 2	Stochastic	See DTN	Parameter developed in this Addendum from statistical data descriptors in DTN: LB0702PAUZMTDF.001 Unsaturated Zone Matrix Diffusion Coefficients
UZDC_C_RG3_out (16)	Matrix Diffusion Coefficient, C, Tortuosity Rock Group 3	Stochastic	See DTN	Parameter developed in this Addendum from statistical data descriptors in DTN: LB0702PAUZMTDF.001 Unsaturated Zone Matrix Diffusion Coefficients
UZDC_Cl_RG1_out (17)	Matrix Diffusion Coefficient, Cl, Tortuosity Rock Group 1	Stochastic	See DTN	Parameter developed in this Addendum from statistical data descriptors in DTN: LB0702PAUZMTDF.001 Unsaturated Zone Matrix Diffusion Coefficients
UZDC_Cl_RG2_out (18)	Matrix Diffusion Coefficient, Cl, Tortuosity Rock Group 2	Stochastic	See DTN	Parameter developed in this Addendum from statistical data descriptors in DTN: LB0702PAUZMTDF.001 Unsaturated Zone Matrix Diffusion Coefficients

Table 8-2. Unsaturated Zone Transport Epistemically Uncertain Input Parameters Found in TSPA Model GoldSim-Generated UZ_PARAMS_MULTI_LA_COMPLIANCE Files (Continued)

Parameter Name (#)	Parameter Definition	Uncertainty Description	Parameter Value(s)	DTN/Title
UZDC_Cl_RG3_out (19)	Matrix Diffusion Coefficient, Cl, Tortuosity Rock Group 3	Stochastic	See DTN	Parameter developed in this Addendum from statistical data descriptors in DTN: LB0702PAUZMTDF.001 Unsaturated Zone Matrix Diffusion Coefficients
UZDC_Cs_RG1_out (20)	Matrix Diffusion Coefficient, Cs, Tortuosity Rock Group 1	Stochastic	See DTN	Parameter developed in this Addendum from statistical data descriptors in DTN: LB0702PAUZMTDF.001 Unsaturated Zone Matrix Diffusion Coefficients
UZDC_Cs_RG2_out (21)	Matrix Diffusion Coefficient, Cs, Tortuosity Rock Group 2	Stochastic	See DTN	Parameter developed in this Addendum from statistical data descriptors in DTN: LB0702PAUZMTDF.001 Unsaturated Zone Matrix Diffusion Coefficients
UZDC_Cs_RG3_out (22)	Matrix Diffusion Coefficient, Cs, Tortuosity Rock Group 3	Stochastic	See DTN	Parameter developed in this Addendum from statistical data descriptors in DTN: LB0702PAUZMTDF.001 Unsaturated Zone Matrix Diffusion Coefficients
UZDC_I_RG1_out (23)	Matrix Diffusion Coefficient, I, Tortuosity Rock Group 1	Stochastic	See DTN	Parameter developed in this Addendum from statistical data descriptors in DTN: LB0702PAUZMTDF.001 Unsaturated Zone Matrix Diffusion Coefficients
UZDC_I_RG2_out (24)	Matrix Diffusion Coefficient, I, Tortuosity Rock Group 2	Stochastic	See DTN	Parameter developed in this Addendum from statistical data descriptors in DTN: LB0702PAUZMTDF.001 Unsaturated Zone Matrix Diffusion Coefficients
UZDC_I_RG3_out (25)	Matrix Diffusion Coefficient, I, Tortuosity Rock Group 3	Stochastic	See DTN	Parameter developed in this Addendum from statistical data descriptors in DTN: LB0702PAUZMTDF.001 Unsaturated Zone Matrix Diffusion Coefficients
UZDC_Np_RG1_out (26)	Matrix Diffusion Coefficient, Np, Tortuosity Rock Group 1	Stochastic	See DTN	Parameter developed in this Addendum from statistical data descriptors in DTN: LB0702PAUZMTDF.001 Unsaturated Zone Matrix Diffusion Coefficients
UZDC_Np_RG2_out (27)	Matrix Diffusion Coefficient, Np, Tortuosity Rock Group 2	Stochastic	See DTN	Parameter developed in this Addendum from statistical data descriptors in DTN: LB0702PAUZMTDF.001 Unsaturated Zone Matrix Diffusion Coefficients

Table 8-2. Unsaturated Zone Transport Epistemically Uncertain Input Parameters Found in TSPA Model GoldSim-Generated UZ_PARAMS_MULTI_LA_COMPLIANCE Files (Continued)

Parameter Name (#)	Parameter Definition	Uncertainty Description	Parameter Value(s)	DTN/Title
UZDC_Np_RG3_out (28)	Matrix Diffusion Coefficient, Np, Tortuosity Rock Group 3	Stochastic	See DTN	Parameter developed in this Addendum from statistical data descriptors in DTN: LB0702PAUZMTDF.001 Unsaturated Zone Matrix Diffusion Coefficients
UZDC_Pa_RG1_out (29)	Matrix Diffusion Coefficient, Pa, Tortuosity Rock Group 1	Stochastic	See DTN	Parameter developed in this Addendum from statistical data descriptors in DTN: LB0702PAUZMTDF.001 Unsaturated Zone Matrix Diffusion Coefficients
UZDC_Pa_RG2_out (30)	Matrix Diffusion Coefficient, Pa, Tortuosity Rock Group 2	Stochastic	See DTN	Parameter developed in this Addendum from statistical data descriptors in DTN: LB0702PAUZMTDF.001 Unsaturated Zone Matrix Diffusion Coefficients
UZDC_Pa_RG3_out (31)	Matrix Diffusion Coefficient, Pa, Tortuosity Rock Group 3	Stochastic	See DTN	Parameter developed in this Addendum from statistical data descriptors in DTN: LB0702PAUZMTDF.001 Unsaturated Zone Matrix Diffusion Coefficients
UZDC_Pu_RG1_out (32)	Matrix Diffusion Coefficient, Pu, Tortuosity Rock Group 1	Stochastic	See DTN	Parameter developed in this Addendum from statistical data descriptors in DTN: LB0702PAUZMTDF.001 Unsaturated Zone Matrix Diffusion Coefficients
UZDC_Pu_RG2_out (33)	Matrix Diffusion Coefficient, Pu, Tortuosity Rock Group 2	Stochastic	See DTN	Parameter developed in this Addendum from statistical data descriptors in DTN: LB0702PAUZMTDF.001 Unsaturated Zone Matrix Diffusion Coefficients
UZDC_Pu_RG3_out (34)	Matrix Diffusion Coefficient, Pu, Tortuosity Rock Group 3	Stochastic	See DTN	Parameter developed in this Addendum from statistical data descriptors in DTN: LB0702PAUZMTDF.001 Unsaturated Zone Matrix Diffusion Coefficients
UZDC_Ra_RG1_out (35)	Matrix Diffusion Coefficient, Ra, Tortuosity Rock Group 1	Stochastic	See DTN	Parameter developed in this Addendum from statistical data descriptors in DTN: LB0702PAUZMTDF.001 Unsaturated Zone Matrix Diffusion Coefficients
UZDC_Ra_RG2_out (36)	Matrix Diffusion Coefficient, Ra, Tortuosity Rock Group 2	Stochastic	See DTN	Parameter developed in this Addendum from statistical data descriptors in DTN: LB0702PAUZMTDF.001 Unsaturated Zone Matrix Diffusion Coefficients

Table 8-2. Unsaturated Zone Transport Epistemically Uncertain Input Parameters Found in TSPA Model GoldSim-Generated UZ_PARAMS_MULTI_LA_COMPLIANCE Files (Continued)

Parameter Name (#)	Parameter Definition	Uncertainty Description	Parameter Value(s)	DTN/Title
UZDC_Ra_RG3_out (37)	Matrix Diffusion Coefficient, Ra, Tortuosity Rock Group 3	Stochastic	See DTN	Parameter developed in this Addendum from statistical data descriptors in DTN: LB0702PAUZMTDF.001 Unsaturated Zone Matrix Diffusion Coefficients
UZDC_Se_RG1_out (38)	Matrix Diffusion Coefficient, Se, Tortuosity Rock Group 1	Stochastic	See DTN	Parameter developed in this Addendum from statistical data descriptors in DTN: LB0702PAUZMTDF.001 Unsaturated Zone Matrix Diffusion Coefficients
UZDC_Se_RG2_out (39)	Matrix Diffusion Coefficient, Se, Tortuosity Rock Group 2	Stochastic	See DTN	Parameter developed in this Addendum from statistical data descriptors in DTN: LB0702PAUZMTDF.001 Unsaturated Zone Matrix Diffusion Coefficients
UZDC_Se_RG3_out (40)	Matrix Diffusion Coefficient, Se, Tortuosity Rock Group 3	Stochastic	See DTN	Parameter developed in this Addendum from statistical data descriptors in DTN: LB0702PAUZMTDF.001 Unsaturated Zone Matrix Diffusion Coefficients
UZDC_Sn_RG1_out (41)	Matrix Diffusion Coefficient, Sn, Tortuosity Rock Group 1	Stochastic	See DTN	Parameter developed in this Addendum from statistical data descriptors in DTN: LB0702PAUZMTDF.001 Unsaturated Zone Matrix Diffusion Coefficients
UZDC_Sn_RG2_out (42)	Matrix Diffusion Coefficient, Sn, Tortuosity Rock Group 2	Stochastic	See DTN	Parameter developed in this Addendum from statistical data descriptors in DTN: LB0702PAUZMTDF.001 Unsaturated Zone Matrix Diffusion Coefficients
UZDC_Sn_RG3_out (43)	Matrix Diffusion Coefficient, Sn, Tortuosity Rock Group 3	Stochastic	See DTN	Parameter developed in this Addendum from statistical data descriptors in DTN: LB0702PAUZMTDF.001 Unsaturated Zone Matrix Diffusion Coefficients
UZDC_Sr_RG1_out (44)	Matrix Diffusion Coefficient, Sr, Tortuosity Rock Group 1	Stochastic	See DTN	Parameter developed in this Addendum from statistical data descriptors in DTN: LB0702PAUZMTDF.001 Unsaturated Zone Matrix Diffusion Coefficients
UZDC_Sr_RG2_out (45)	Matrix Diffusion Coefficient, Sr, Tortuosity Rock Group 2	Stochastic	See DTN	Parameter developed in this Addendum from statistical data descriptors in DTN: LB0702PAUZMTDF.001 Unsaturated Zone Matrix Diffusion Coefficients

Table 8-2. Unsaturated Zone Transport Epistemically Uncertain Input Parameters Found in TSPA Model GoldSim-Generated UZ_PARAMS_MULTI_LA_COMPLIANCE Files (Continued)

Parameter Name (#)	Parameter Definition	Uncertainty Description	Parameter Value(s)	DTN/Title
UZDC_Sr_RG3_out (46)	Matrix Diffusion Coefficient, Sr, Tortuosity Rock Group 3	Stochastic	See DTN	Parameter developed in this Addendum from statistical data descriptors in DTN: LB0702PAUZMTDF.001 Unsaturated Zone Matrix Diffusion Coefficients
UZDC_Tc_RG1_out (47)	Matrix Diffusion Coefficient, Tc, Tortuosity Rock Group 1	Stochastic	See DTN	Parameter developed in this Addendum from statistical data descriptors in DTN: LB0702PAUZMTDF.001 Unsaturated Zone Matrix Diffusion Coefficients
UZDC_Tc_RG2_out (48)	Matrix Diffusion Coefficient, Tc, Tortuosity Rock Group 2	Stochastic	See DTN	Parameter developed in this Addendum from statistical data descriptors in DTN: LB0702PAUZMTDF.001 Unsaturated Zone Matrix Diffusion Coefficients
UZDC_Tc_RG3_out (49)	Matrix Diffusion Coefficient, Tc, Tortuosity Rock Group 3	Stochastic	See DTN	Parameter developed in this Addendum from statistical data descriptors in DTN: LB0702PAUZMTDF.001 Unsaturated Zone Matrix Diffusion Coefficients
UZDC_Th_RG1_out (50)	Matrix Diffusion Coefficient, Th, Tortuosity Rock Group 1	Stochastic	See DTN	Parameter developed in this Addendum from statistical data descriptors in DTN: LB0702PAUZMTDF.001 Unsaturated Zone Matrix Diffusion Coefficients
UZDC_Th_RG2_out (51)	Matrix Diffusion Coefficient, Th, Tortuosity Rock Group 2	Stochastic	See DTN	Parameter developed in this Addendum from statistical data descriptors in DTN: LB0702PAUZMTDF.001 Unsaturated Zone Matrix Diffusion Coefficients
UZDC_Th_RG3_out (52)	Matrix Diffusion Coefficient, Th, Tortuosity Rock Group 3	Stochastic	See DTN	Parameter developed in this Addendum from statistical data descriptors in DTN: LB0702PAUZMTDF.001 Unsaturated Zone Matrix Diffusion Coefficients
UZDC_U_RG1_out (53)	Matrix Diffusion Coefficient, U, Tortuosity Rock Group 1	Stochastic	See DTN	Parameter developed in this Addendum from statistical data descriptors in DTN: LB0702PAUZMTDF.001 Unsaturated Zone Matrix Diffusion Coefficients
UZDC_U_RG2_out (54)	Matrix Diffusion Coefficient, U, Tortuosity Rock Group 2	Stochastic	See DTN	Parameter developed in this Addendum from statistical data descriptors in DTN: LB0702PAUZMTDF.001 Unsaturated Zone Matrix Diffusion Coefficients

Table 8-2. Unsaturated Zone Transport Epistemically Uncertain Input Parameters Found in TSPA Model GoldSim-Generated UZ_PARAMS_MULTI_LA_COMPLIANCE Files (Continued)

Parameter Name (#)	Parameter Definition	Uncertainty Description	Parameter Value(s)	DTN/Title
UZDC_U_RG3_out (55)	Matrix Diffusion Coefficient, U, Tortuosity Rock Group 3	Stochastic	See DTN	Parameter developed in this Addendum from statistical data descriptors in DTN: LB0702PAUZMTDF.001 Unsaturated Zone Matrix Diffusion Coefficients
KdAm_Zeo_UZP (56)	Matrix Sorption Coefficient, Am, Zeolitic units	Stochastic	See DTN	Parameter developed in SNL 2007 [DIRS 177396] from statistical data descriptors in DTN: LA0408AM831341.001 [DIRS 171584] Unsaturated Zone Distribution Coefficients (K_ds) FOR U, Np, Pu, Am, Pa, Cs, Sr, Ra, and Th
KdAm_Devit_UZP (57)	Matrix Sorption Coefficient, Am, Devitrified units	Stochastic	See DTN	Parameter developed in SNL 2007 [DIRS 177396] from statistical data descriptors in DTN: LA0408AM831341.001 [DIRS 171584] Unsaturated Zone Distribution Coefficients (K_ds) for U, Np, Pu, Am, Pa, Cs, Sr, Ra, and Th
KdAm_Vit_UZP (58)	Matrix Sorption Coefficient, Am, Vitric units	Stochastic	See DTN	Parameter developed in SNL 2007 [DIRS 177396] from statistical data descriptors in DTN: LA0408AM831341.001 [DIRS 171584] Unsaturated Zone Distribution Coefficients (K_ds) for U, Np, Pu, Am, Pa, Cs, Sr, Ra, and Th
KdC_Zeo_UZP (59)	Matrix Sorption Coefficient, C, Zeolitic units	Constant	0.	Justification provided in SNL 2007 [DIRS 177396]
KdC_Devit_UZP (60)	Matrix Sorption Coefficient, C, Devitrified units	Constant	0.	Justification provided in SNL 2007 [DIRS 177396]
KdC_Vit_UZP (61)	Matrix Sorption Coefficient, C, Vitric units	Constant	0.	Justification provided in SNL 2007 [DIRS 177396]
KdCl_Zeo_UZP (62)	Matrix Sorption Coefficient, Cl, Zeolitic units	Constant	0.	Justification provided in SNL 2007 [DIRS 177396]
KdCl_Devit_UZP (63)	Matrix Sorption Coefficient, Cl, Devitrified units	Constant	0.	Justification provided in SNL 2007 [DIRS 177396]
KdCl_Vit_UZP (64)	Matrix Sorption Coefficient, Cl, Vitric units	Constant	0.	Justification provided in SNL 2007 [DIRS 177396]

Table 8-2. Unsaturated Zone Transport Epistemically Uncertain Input Parameters Found in TSPA Model GoldSim-Generated UZ_PARAMS_MULTI_LA_COMPLIANCE Files (Continued)

Parameter Name (#)	Parameter Definition	Uncertainty Description	Parameter Value(s)	DTN/Title
KdCs_Zeo_UZP (65)	Matrix Sorption Coefficient, Cs, Zeolitic units	Stochastic	See DTN	Parameter developed in SNL 2007 [DIRS 177396] from statistical data descriptors in DTN: LA0408AM831341.001 [DIRS 171584] Unsaturated Zone Distribution Coefficients (K_ds) for U, Np, Pu, Am, Pa, Cs, Sr, Ra, and Th
KdCs_Devit_UZP (66)	Matrix Sorption Coefficient, Cs, Devitrified units	Stochastic	See DTN	Parameter developed in SNL 2007 [DIRS 177396] from statistical data descriptors in DTN: LA0408AM831341.001 [DIRS 171584] Unsaturated Zone Distribution Coefficients (K_ds) for U, Np, Pu, Am, Pa, Cs, Sr, Ra, and Th
KdCs_Vit_UZP (67)	Matrix Sorption Coefficient, Cs, Vitric units	Stochastic	See DTN	Parameter developed in SNL 2007 [DIRS 177396] from statistical data descriptors in DTN: LA0408AM831341.001 [DIRS 171584] Unsaturated Zone Distribution Coefficients (K_ds) for U, Np, Pu, Am, Pa, Cs, Sr, Ra, and Th
Kdl_Zeo_UZP (68)	Matrix Sorption Coefficient, I, Zeolitic units	Constant	0.	Justification provided in SNL 2007 [DIRS 177396]
Kdl_Devit_UZP (69)	Matrix Sorption Coefficient, I, Devitrified units	Constant	0.	Justification provided in SNL 2007 [DIRS 177396]
Kdl_Vit_UZP (70)	Matrix Sorption Coefficient, I, Vitric units	Constant	0.	Justification provided in SNL 2007 [DIRS 177396]
KdNp_Zeo_UZP (71)	Matrix Sorption Coefficient, Np, Zeolitic units	Stochastic	See DTN	Parameter developed in SNL 2007 [DIRS 177396] from statistical data descriptors in DTN: LA0408AM831341.001 [DIRS 171584] Unsaturated Zone Distribution Coefficients (K_ds) for U, Np, Pu, Am, Pa, Cs, Sr, Ra, and Th
KdNp_Devit_UZP (72)	Matrix Sorption Coefficient, Np, Devitrified units	Stochastic	See DTN	Parameter developed in SNL 2007 [DIRS 177396] from statistical data descriptors in DTN: LA0408AM831341.001 [DIRS 171584] Unsaturated Zone Distribution Coefficients (K_ds) for U, Np, Pu, Am, Pa, Cs, Sr, Ra, and Th

Table 8-2. Unsaturated Zone Transport Epistemically Uncertain Input Parameters Found in TSPA Model GoldSim-Generated UZ_PARAMS_MULTI_LA_COMPLIANCE Files (Continued)

Parameter Name (#)	Parameter Definition	Uncertainty Description	Parameter Value(s)	DTN/Title
KdNp_Vit_UZP (73)	Matrix Sorption Coefficient, Np, Vitric units	Stochastic	See DTN	Parameter developed in SNL 2007 [DIRS 177396] from statistical data descriptors in DTN: LA0408AM831341.001 [DIRS 171584] Unsaturated Zone Distribution Coefficients (K_ds) for U, Np, Pu, Am, Pa, Cs, Sr, Ra, and Th
KdPa_Zeo_UZP (74)	Matrix Sorption Coefficient, Pa, Zeolitic units	Stochastic	See DTN	Parameter developed in SNL 2007 [DIRS 177396] from statistical data descriptors in DTN: LA0408AM831341.001 [DIRS 171584] Unsaturated Zone Distribution Coefficients (K_ds) for U, Np, Pu, Am, Pa, Cs, Sr, Ra, and Th
KdPa_Devit_UZP (75)	Matrix Sorption Coefficient, Pa, Devitrified units	Stochastic	See DTN	Parameter developed in SNL 2007 [DIRS 177396] from statistical data descriptors in DTN: LA0408AM831341.001 [DIRS 171584] Unsaturated Zone Distribution Coefficients (K_ds) for U, Np, Pu, Am, Pa, Cs, Sr, Ra, and Th
KdPa_Vit_UZP (76)	Matrix Sorption Coefficient, Pa, Vitric units	Stochastic	See DTN	Parameter developed in SNL 2007 [DIRS 177396] from statistical data descriptors in DTN: LA0408AM831341.001 [DIRS 171584] Unsaturated Zone Distribution Coefficients (K_ds) for U, Np, Pu, Am, Pa, Cs, Sr, Ra, and Th
KdPu_Zeo_UZP (77)	Matrix Sorption Coefficient, Pu, Zeolitic units	Stochastic	See DTN	Parameter developed in SNL 2007 [DIRS 177396] from statistical data descriptors in DTN: LA0408AM831341.001 [DIRS 171584] Unsaturated Zone Distribution Coefficients (K_ds) for U, Np, Pu, Am, Pa, Cs, Sr, Ra, and Th
KdPu_Devit_UZP (78)	Matrix Sorption Coefficient, Pu, Devitrified units	Stochastic	See DTN	Parameter developed in SNL 2007 [DIRS 177396] from statistical data descriptors in DTN: LA0408AM831341.001 [DIRS 171584] Unsaturated Zone Distribution Coefficients (K_ds) for U, Np, Pu, Am, Pa, Cs, Sr, Ra, and Th

Table 8-2. Unsaturated Zone Transport Epistemically Uncertain Input Parameters Found in TSPA Model GoldSim-Generated UZ_PARAMS_MULTI_LA_COMPLIANCE Files (Continued)

Parameter Name (#)	Parameter Definition	Uncertainty Description	Parameter Value(s)	DTN/Title
KdPu_Vit_UZP (79)	Matrix Sorption Coefficient, Pu, Vitric units	Stochastic	See DTN	Parameter developed in SNL 2007 [DIRS 177396] from statistical data descriptors in DTN: LA0408AM831341.001 [DIRS 171584] Unsaturated Zone Distribution Coefficients (K_ds) for U, Np, Pu, Am, Pa, Cs, Sr, Ra, and Th
KdRa_Zeo_UZP (80)	Matrix Sorption Coefficient, Ra, Zeolitic units	Stochastic	See DTN	Parameter developed in SNL 2007 [DIRS 177396] from statistical data descriptors in DTN: LA0408AM831341.001 [DIRS 171584] Unsaturated Zone Distribution Coefficients (K_ds) for U, Np, Pu, Am, Pa, Cs, Sr, Ra, and Th
KdRa_Devit_UZP (81)	Matrix Sorption Coefficient, Ra, Devitrified units	Stochastic	See DTN	Parameter developed in SNL 2007 [DIRS 177396] from statistical data descriptors in DTN: LA0408AM831341.001 [DIRS 171584] Unsaturated Zone Distribution Coefficients (K_ds) for U, Np, Pu, Am, Pa, Cs, Sr, Ra, and Th
KdRa_Vit_UZP (82)	Matrix Sorption Coefficient, Ra, Vitric units	Stochastic	See DTN	Parameter developed in SNL 2007 [DIRS 177396] from statistical data descriptors in DTN: LA0408AM831341.001 [DIRS 171584] Unsaturated Zone Distribution Coefficients (K_ds) for U, Np, Pu, Am, Pa, Cs, Sr, Ra, and Th
KdSe_Zeo_UZP (83)	Matrix Sorption Coefficient, Se, Zeolitic units	Stochastic	See DTN	Parameter developed in SNL 2007 [DIRS 177396] from statistical data descriptors in LB0701PAKDSESN.001 [DIRS 179299] Unsaturated Zone Sorption Coefficients for Selenium and Tin
KdSe_Devit_UZP (84)	Matrix Sorption Coefficient, Se, Devitrified units	Stochastic, or a constant of 0 in the TSw units	See DTN	Parameter developed in SNL 2007 [DIRS 177396] from statistical data descriptors in LB0701PAKDSESN.001 [DIRS 179299] Unsaturated Zone Sorption Coefficients for Selenium and Tin

Table 8-2. Unsaturated Zone Transport Epistemically Uncertain Input Parameters Found in TSPA Model GoldSim-Generated UZ_PARAMS_MULTI_LA_COMPLIANCE Files (Continued)

Parameter Name (#)	Parameter Definition	Uncertainty Description	Parameter Value(s)	DTN/Title
KdSe_Vit_UZP (85)	Matrix Sorption Coefficient, Se, Vitric units	Stochastic	See DTN	Parameter developed in SNL 2007 [DIRS 177396] from statistical data descriptors in LB0701PAKDSESN.001 [DIRS 179299] Unsaturated Zone Sorption Coefficients for Selenium and Tin
KdSn_Zeo_UZP (86)	Matrix Sorption Coefficient, Sn, Zeolitic units	Stochastic	See DTN	Parameter developed in SNL 2007 [DIRS 177396] from statistical data descriptors in LB0701PAKDSESN.001 [DIRS 179299] Unsaturated Zone Sorption Coefficients for Selenium and Tin
KdSn_Devit_UZP (87)	Matrix Sorption Coefficient, Sn, Devitrified units	Stochastic	See DTN	Parameter developed in SNL 2007 [DIRS 177396] from statistical data descriptors in LB0701PAKDSESN.001 [DIRS 179299] Unsaturated Zone Sorption Coefficients for Selenium and Tin
KdSn_Vit_UZP (88)	Matrix Sorption Coefficient, Sn, Vitric units	Stochastic	See DTN	Parameter developed in SNL 2007 [DIRS 177396] from statistical data descriptors in LB0701PAKDSESN.001 [DIRS 179299] Unsaturated Zone Sorption Coefficients for Selenium and Tin
KdSr_Zeo_UZP (89)	Matrix Sorption Coefficient, Sr, Zeolitic units	Stochastic	See DTN	Parameter developed in SNL 2007 [DIRS 177396] from statistical data descriptors in DTN: LA0408AM831341.001 [DIRS 171584] Unsaturated Zone Distribution Coefficients (K_ds) for U, Np, Pu, Am, Pa, Cs, Sr, Ra, and Th
KdSr_Devit_UZP (90)	Matrix Sorption Coefficient, Sr, Devitrified units	Stochastic	See DTN	Parameter developed in SNL 2007 [DIRS 177396] from statistical data descriptors in DTN: LA0408AM831341.001 [DIRS 171584] Unsaturated Zone Distribution Coefficients (K_ds) for U, Np, Pu, Am, Pa, Cs, Sr, Ra, and Th
KdSr_Vit_UZP (91)	Matrix Sorption Coefficient, Sr, Vitric units	Stochastic	See DTN	Parameter developed in SNL 2007 [DIRS 177396] from statistical data descriptors in DTN: LA0408AM831341.001 [DIRS 171584] Unsaturated Zone Distribution Coefficients (K_ds) for U, Np, Pu, Am, Pa, Cs, Sr, Ra, and Th

Table 8-2. Unsaturated Zone Transport Epistemically Uncertain Input Parameters Found in TSPA Model GoldSim-Generated UZ_PARAMS_MULTI_LA_COMPLIANCE Files (Continued)

Parameter Name (#)	Parameter Definition	Uncertainty Description	Parameter Value(s)	DTN/Title
KdTc_Zeo_UZP (92)	Matrix Sorption Coefficient, Tc, Zeolitic units	Constant	0.	Justification provided in SNL 2007 [DIRS 177396]
KdTc_Devit_UZP (93)	Matrix Sorption Coefficient, Tc, Devitrified units	Constant	0.	Justification provided in SNL 2007 [DIRS 177396]
KdTc_Vit_UZP (94)	Matrix Sorption Coefficient, Tc, Vitric units	Constant	0.	Justification provided in SNL 2007 [DIRS 177396]
KdTh_Zeo_UZP (95)	Matrix Sorption Coefficient, Th, Zeolitic units	Stochastic	See DTN	Parameter developed in SNL 2007 [DIRS 177396] from statistical data descriptors in DTN: LA0408AM831341.001 [DIRS 171584] Unsaturated Zone Distribution Coefficients (K_ds) for U, Np, Pu, Am, Pa, Cs, Sr, Ra, and Th
KdTh_Devit_UZP (96)	Matrix Sorption Coefficient, Th, Devitrified units	Stochastic	See DTN	Parameter developed in SNL 2007 [DIRS 177396] from statistical data descriptors in DTN: LA0408AM831341.001 [DIRS 171584] Unsaturated Zone Distribution Coefficients (K_ds) for U, Np, Pu, Am, Pa, Cs, Sr, Ra, and Th
KdTh_Vit_UZP (97)	Matrix Sorption Coefficient, Th, Vitric units	Stochastic	See DTN	Parameter developed in SNL 2007 [DIRS 177396] from statistical data descriptors in DTN: LA0408AM831341.001 [DIRS 171584] Unsaturated Zone Distribution Coefficients (K_ds) for U, Np, Pu, Am, Pa, Cs, Sr, Ra, and Th
KdU_Zeo_UZP (98)	Matrix Sorption Coefficient, U, Zeolitic units	Stochastic	See DTN	Parameter developed in SNL 2007 [DIRS 177396] from statistical data descriptors in DTN: LA0408AM831341.001 [DIRS 171584] Unsaturated Zone Distribution Coefficients (K_ds) for U, Np, Pu, Am, Pa, Cs, Sr, Ra, and Th

Table 8-2. Unsaturated Zone Transport Epistemically Uncertain Input Parameters Found in TSPA Model GoldSim-Generated UZ_PARAMS_MULTI_LA_COMPLIANCE Files (Continued)

Parameter Name (#)	Parameter Definition	Uncertainty Description	Parameter Value(s)	DTN/Title
KdU_Devit_UZP (99)	Matrix Sorption Coefficient, U, Devitrified units	Stochastic	See DTN	Parameter developed in SNL 2007 [DIRS 177396] from statistical data descriptors in DTN: LA0408AM831341.001 [DIRS 171584] Unsaturated Zone Distribution Coefficients (K_ds) for U, Np, Pu, Am, Pa, Cs, Sr, Ra, and Th
KdU_Vit_UZP (100)	Matrix Sorption Coefficient, U, Vitric units	Stochastic	See DTN	Parameter developed in SNL 2007 [DIRS 177396] from statistical data descriptors in DTN: LA0408AM831341.001 [DIRS 171584] Unsaturated Zone Distribution Coefficients (K_ds) for U, Np, Pu, Am, Pa, Cs, Sr, Ra, and Th
Colloidal_Kc_Am_UZP (101)	Sorption Partition Coefficient onto Colloids, Am	Stochastic	See DTN	Output DTN: LA0701PANS02BR.003: UZ Transport Parameters
Colloidal_Kc_Cs_UZP (102)	Sorption Partition Coefficient onto Colloids, Cs	Stochastic	See DTN	Output DTN: LA0701PANS02BR.003: UZ Transport Parameters
Colloidal_Kc_Pa_UZP (103)	Sorption Partition Coefficient onto Colloids, Pa	Stochastic	See DTN	Output DTN: LA0701PANS02BR.003: UZ Transport Parameters
Colloidal_Kc_Pu_UZP (104)	Sorption Partition Coefficient onto Colloids, Pu	Stochastic	See DTN	Output DTN: LA0701PANS02BR.003: UZ Transport Parameters
Colloidal_Kc_Sn_UZP (105)	Sorption Partition Coefficient onto Colloids, Sn	Stochastic	See DTN	Output DTN: LA0701PANS02BR.003: UZ Transport Parameters
Colloidal_Kc_Th_UZP (106)	Sorption Partition Coefficient onto Colloids, Th	Stochastic	See DTN	Output DTN: LA0701PANS02BR.003: UZ Transport Parameters
Rc_UZP (107)	Retardation Factor for Colloidal Species traveling retarded (both reversible species and irreversible species referred to as "Ic" species)	Stochastic	See DTN	Output DTN: LA0701PANS02BR.003: UZ Transport Parameters

8.2 MODEL OUTPUTS

8.2.1 Developed Output

Model Files: Many of the model outputs (FEHM input files to be used by TSPA system modelers) are derived from results of process models or other studies. The references cited in Table 8-1 provide a discussion of the development of those files. Data files required to perform the TSPA calculations are found in output DTNs: MO0704PAFEHMBR.001, LA0702PANS02BR.001, and MO0704PAPTTFBR.002. All input files referred to are inputs to the FEHM computer code.

In the TSPA analysis, the FEHM code is linked dynamically to the computer code GoldSim, the platform used to implement the systems model. With regard to the FEHM ".ini" files that contain the flow field information needed to simulate unsaturated zone transport, both this addendum and the parent report discuss only the simulation of unsaturated zone transport using flow fields for present-day, monsoon, and glacial-transition climates in the first 10,000 years. However, the incorporation of the post-10k-yr flow fields is achieved using the identical process. That is, the flow fields developed from the unsaturated zone flow modeling effort are converted to FEHM-compatible flow fields and provided to the FEHM TSPA model for unsaturated zone transport in the form of an *.ini* file, as before. The details of this process, including the use of the post-10k-yr flow fields, will be developed and presented in the TSPA model report.

The definitions for the unsaturated zone transport abstraction model input files are provided in the "Parameter Definition" column of Table 8-1. When used in TSPA, these file names can be changed to accommodate local file system paths and naming conventions, with the exception of only file *fehmn.files*, which must be named as indicated. This file contains file names that the model run uses, and FEHM expects to find a file with that name in the local directory. Other input files also refer to additional files containing input data. If these file names are changed, that change must be reflected at the place in the input file where the file is referenced.

One required additional file not included here is named *fehmn.gold.* This file contains parameters (such as the number of parameters passed from the TSPA model to the FEHM dll) specifying the interface between FEHM and GoldSim for the TSPA model. Because this file is inherently part of the GoldSim model rather than the unsaturated zone transport abstraction model itself, it is more logical to develop it within the TSPA model report, rather than here.

Transport Parameters: The unsaturated zone transport epistemically uncertain input parameters are given in Table 8-2. The development of most of the parameter values is discussed in this addendum or in the parent report (provided in output DTNs: LA0701PANS02BR.003 and LB0702PAUZMTDF.001.

Although *Radionuclide Transport Models Under Ambient Conditions* (SNL 2007 [DIRS 177396]) provides the parameter values for sorption coefficients of radionuclides onto rock, they are included in Table 8-2 because this table defines the interface between the TSPA GoldSim model and the FEHM unsaturated zone transport abstraction model. Therefore, even though the sorption coefficients are developed elsewhere, they are included in Table 8-2 to fully specify and document the interface. The development of sorption coefficient uncertainty

distributions is described in *Radionuclide Transport Models Under Ambient Conditions* (SNL 2007 [DIRS 177396]), and data are provided in DTNs: LA0408AM831341.001 [DIRS 171584] and LB0701PAKDSESN.001 [DIRS 179299].

The entries in Table 8-2 refer to the parameter as it is passed from the GoldSim model to FEHM in *UZ_PARAMS_LA_COMPLIANCE*. The form of this table is an ASCII file of parameter vectors. For the compliance model, each line contains a space- or tab-delimited list of 107 parameters, and the file contains one row of such values for each realization. Therefore, the rows are realizations and the columns are parameters. The numbers provided in parentheses in the "Parameter Name" column of Table 8-2 refer to the column number of that particular parameter. The FEHM input file, *fehm_TSPA.mptr*, is developed with this indexing system, so any changes to the structure of the table (e.g., changing the number or order of parameters) will require an accompanying change to *fehm_TSPA.mptr*.

8.2.2 Other Outputs

Validation simulations are updated to test this version of FEHM and are provided in output DTN: MO0705PAVALSIM.000. FEHM particle-tracking input files associated with the TSPA-LA uncertainty simulations can be found in DTN: MO0705TRANSTAT.000, Output Uncertainty

The calculation of unsaturated zone transport uncertainties in the TSPA-LA model will be performed and documented in the TSPA-LA model report because the radionuclide source term is computed using the system model, of which the unsaturated zone transport abstraction model is a part. The goal of both the addendum and the parent report is twofold: to ensure that (1) a computational tool is set up for TSPA to perform the simulation modeling and (2) the uncertainties of parameters in the abstraction model are fully justified and documented. In addition, basic flow and transport parameter and conceptual model uncertainties are explored to assess the sensitivity to these uncertainties. All of these goals have been accomplished, in that the software and computer files needed to perform the modeling have been completed and sensitivities have been presented. Therefore, parameter and conceptual uncertainties in the unsaturated zone transport can be propagated through the TSPA-LA model.

The uncertainties associated with transport in the unsaturated zone have been documented in the model report for unsaturated zone transport (SNL 2007 [DIRS 177396]), expanded upon in the parent report, and augmented in this addendum. Of note is the fact that both parameter and conceptual model uncertainty have been shown to be incorporated into this abstraction, and sensitivities have been explored. Validation model runs have been rerun for this addendum, and the documented results illustrate that the model is valid for its intended use.

Representative-case model results were presented in Section 6.6.2. These results illustrated the spatial variability of the model results (travel times, breakthrough curves, arrival locations at the water table), showing the strong dependence of the results on release location. Transport from northern release locations exhibit fracture-dominated transport, lateral diversion and transport to the water table via faults, and relatively short travel times. In contrast, for southern release locations, an interval of the Calico Hills unit exhibiting matrix-dominated transport leads to generally longer travel times and pathways that are predominantly vertical. The selection of the

flow field (which varies according to the infiltration scenario chosen) also has an important influence on the calculation of travel times, as illustrated by the travel time contours of Appendix D.1. However, the general flow patterns are independent of infiltration scenario, as illustrated by the similarity of the patterns reflected in the figures of Appendix D.1.

Sensitivity analyses focused on the capability of the unsaturated zone to perform as a barrier to migration of radionuclides to the water table. The mean travel time and the decay fraction C/C_0 are two metrics used for this purpose. For nonsorbing species, diffusion coefficient and flow scenario have an impact on these two metrics, but if these radionuclides have long half lives, such as ^{99}Tc, the unsaturated zone provides very minimal barrier to radionuclide migration over the ranges of uncertainty in diffusion and flow rate. Similarly, the selection of the diffusion conceptual model (dual-k versus DFM) is also relatively unimportant for ^{99}Tc, as neither model predicts a significant barrier for this radionuclide and others like it (nonsorbing, long-half-life radionuclides). For sorbing species, contour plots of the mean travel time or C/C_0 were constructed spanning the ranges of diffusion coefficient and K_d given by the uncertainty distributions of these parameters. For more strongly sorbed species, the impact of diffusion coefficient and diffusion conceptual model becomes more important. There is interplay between diffusion and sorption for the northern release locations, which exhibit fracture-dominated transport. For the southern release locations, the intervening layer of matrix-dominated transport makes travel times and barrier capability dependent only on the sorption coefficient, and the diffusion model and parameters become relatively unimportant. Lastly, the range of colloid retardation factors for the irreversibly sorbed species (Ic) is such that the resulting transport behavior ranges from minimal barrier to effective barrier, depending on the retardation factor and the half life of the species.

Finally, the relative importance of conceptual and parameter uncertainties must be treated separately for each radionuclide; the analysis techniques applied herein provide insights into the behavior of species in the TSPA model. However, the actual predicted performance of the unsaturated zone barrier system within the repository total system must be examined in the TSPA model itself.

8.3 HOW THE APPLICABLE ACCEPTANCE CRITERIA ARE ADDRESSED

There is no change to the list of acceptance criteria that apply to the parent report or this addendum. The summary below places the work performed in this addendum in the context of the acceptance criteria by identifying which criteria are better satisfied by the specific work element. The nomenclature for identifying the acceptance criterion from the parent report is to identify the criterion number, followed by the item number within that acceptance criterion. For example, Acceptance Criterion 1, Item 4 refers first to the first acceptance criterion "System Description and Model Integration Are Adequate," and then to the fourth item, which is on boundary and initial conditions.

Acceptance Criterion 1, Item 4: The development of repository percolation bins containing the repository nodes (Section 6.5.15) is an updated version of these percolation bins that provides a boundary condition for radionuclide releases that reflects the current unsaturated zone flow models. This work was conducted in part to address CR 7225.

Acceptance Criterion 2, Item 1: The work conducted to revise the treatment of matrix diffusion coefficient parameter development and uncertainty distributions (Section 6.5.5) and to qualify previously unqualified data (Section 4.1.4) addresses this acceptance criterion item. This work was conducted in part to address CR 7260.

Acceptance Criterion 4, Item 2: The work conducted to study the impact of conceptual uncertainty in the matrix diffusion submodel addresses this acceptance criterion. Analyses illustrating the impact of conceptual model (dual-k versus DFM) on unsaturated zone performance are presented in Section 6.8.

Acceptance Criterion 5, Items 1 and 2: The abstraction model runs comparing the results to the process models and other numerical models (Section 7) address these acceptance criteria.

Acceptance Criterion 5, Item 4: The sensitivity analyses presented in Sections 6.6 and 6.8 address this acceptance criterion. This work was conducted in part to address CR 7138.

INTENTIONALLY LEFT BLANK

9. INPUTS AND REFERENCES

The following is a list of the references cited in this addendum. Column 2 represents the unique six-digit numerical identifier (the Document Input Reference System [DIRS] number), which is placed in the text following the reference callout (e.g., SNL 2007 [DIRS 177396]). The purpose of these numbers is to assist the reader in locating a specific reference in the DIRS database. Within the reference list, multiple sources by the same author (e.g., SNL 2007) are sorted alphabetically by title.

9.1 DOCUMENTS CITED

100702 Baes, C.F., Jr. and Mesmer, R.E. 1986. *The Hydrolysis of Cations.* Malabar, Florida: Krieger Publishing Company. TIC: 223481.

103524 Bird, R.B.; Stewart, W.E.; and Lightfoot, E.N. 1960. *Transport Phenomena.* New York, New York: John Wiley & Sons. TIC: 208957.

170038 BSC (Bechtel SAIC Company) 2004. *Analysis of Hydrologic Properties Data.* ANL-NBS-HS-000042 REV 00. Las Vegas, Nevada: Bechtel SAIC Company. ACC: DOC.20041005.0004.

169857 BSC 2004. *Calibrated Properties Model.* MDL-NBS-HS-000003 REV 02. Las Vegas, Nevada: Bechtel SAIC Company. ACC: DOC.20041006.0004.

170035 BSC 2004. *Conceptual Model and Numerical Approaches for Unsaturated Zone Flow and Transport.* MDL-NBS-HS-000005 REV 01. Las Vegas, Nevada: Bechtel SAIC Company. ACC: DOC.20040922.0006.

170006 BSC 2004. *Saturated Zone Colloid Transport.* ANL-NBS-HS-000031 REV 02. Las Vegas, Nevada: Bechtel SAIC Company. ACC: DOC.20041008.0007; DOC.20051215.0005.

170007 BSC 2004. *Simulation of Net Infiltration for Present-Day and Potential Future Climates.* MDL-NBS-HS-000023 REV 00. Las Vegas, Nevada: Bechtel SAIC Company. ACC: DOC.20041109.0004.

169861 BSC 2004. *UZ Flow Models and Submodels.* MDL-NBS-HS-000006 REV 02. Las Vegas, Nevada: Bechtel SAIC Company. ACC: DOC.20041101.0004; DOC.20050629.0003.

169734 BSC 2004. *Yucca Mountain Site Description.* TDR-CRW-GS-000001 REV 02 ICN 01. Two volumes. Las Vegas, Nevada: Bechtel SAIC Company. ACC: DOC.20040504.0008.

177465 BSC 2006. *Technical Work Plan for: Unsaturated Zone Flow, Drift Seepage and Unsaturated Zone Transport Modeling.* TWP-MGR-HS-000004 REV 04. Las Vegas, Nevada: Bechtel SAIC Company. ACC: DOC.20060824.0001.

154071 CRWMS M&O 2001. *Colloid-Associated Radionuclide Concentration Limits: ANL.* ANL-EBS-MD-000020 REV 00 ICN 01. Las Vegas, Nevada: CRWMS M&O. ACC: MOL.20010216.0003.

178861 Cutter, G.A. 1989. "Freshwater Systems." *Chapter 10 of Occurrence and Distribution of Selenium.* Ihnat, M., ed. Boca Raton, Florida: CRC Press. TIC: 259080.

106109 Howard, J.H., III 1977. "Geochemistry of Selenium: Formation of Ferroselite and Selenium Behavior in the Vicinity of Oxidizing Sulfide and Uranium Deposits." *Geochimica et Cosmochimica Acta, 41,* 1665-1678. New York, New York: Pergamon Press. TIC: 239142.

166224 Lide, D.R., ed. 1992. *CRC Handbook of Chemistry and Physics.* 73rd Edition. Boca Raton, Florida: CRC Press. TIC: 255239.

105729 Liu, H.H.; Doughty, C.; and Bodvarsson, G.S. 1998. "An Active Fracture Model for Unsaturated Flow and Transport in Fractured Rocks." Water Resources Research, 34, (10), 2633-2646. Washington, D.C.: American Geophysical Union. TIC: 243012.

101464 Neuman, S.P. 1990. "Universal Scaling of Hydraulic Conductivities and Dispersivities in Geologic Media." *Water Resources Research, 26,* (8), 1749-1758. Washington, D.C.: American Geophysical Union. TIC: 237977.

103896 Parrington, J.R.; Knox, H.D.; Breneman, S.L.; Baum, E.M.; and Feiner, F. 1996. *Nuclides and Isotopes, Chart of the Nuclides.* 15th Edition. San Jose, California: General Electric Company and KAPL, Inc. TIC: 233705.

179246 Reimus, P.W.; Callahan T.J.; Ware, S.D.; Haga, M.J.; and Counce, D.A. 2007. "Matrix Diffusion Coefficients in Volcanic Rocks at the Nevada Test Site: Influence of Matrix Porosity, Matrix Permeability, and Fracture Coating Minerals." *Journal of Contaminant Hydrology.* TIC: 259170.

163213 Sato, H.; Yui, M.; and Yoshikawa, H. 1996. "Ionic Diffusion Coefficients of Cs^{+}, Pb^{2+}, Sm^{3+}, Ni^{2+}, SeO_4^{2-} and TcO_4^{-} in Free Water Determined from Conductivity Measurements." *Journal of Nuclear Science and Technology, 33,* (12), 950-955. Tokyo, Japan: Atomic Energy Society of Japan. TIC: 254307.

164741 Singh, B. 2002. "Nuclear Data Sheets for A = 79." *Nuclear Data Sheets, 96,* (1), 1-240. San Diego, California: Elsevier. TIC: 254728.

179613 Slater, J.C. 1965. *Quantum Theory of Molecules and Solids, Symmetry and Energy Bands in Crystals.* International Series in Pure and Applied Physics. Volume 2. New York, New York: McGraw-Hill. TIC: 259171.

179545 SNL (Sandia National Laboratories) 2007. *Calibrated Unsaturated Zone Properties.* ANL-NBS-HS-000058 REV 00. Las Vegas, Nevada: Sandia National Laboratories. ACC: DOC.20070530.0013.

177418 SNL 2007. *Dissolved Concentration Limits of Elements with Radioactive Isotopes.* ANL-WIS-MD-000010 REV 06. Las Vegas, Nevada: Sandia National Laboratories.

177404 SNL 2007. *Drift-Scale THC Seepage Model.* MDL-NBS-HS-000001 REV 05. Las Vegas, Nevada: Sandia National Laboratories.

177412 SNL 2007. *Engineered Barrier System: Physical and Chemical Environment.* ANL-EBS-MD-000033 REV 06. Las Vegas, Nevada: Sandia National Laboratories.

177396 SNL 2007. *Radionuclide Transport Models Under Ambient Conditions.* MDL-NBS-HS-000008 REV 02 AD 01. Las Vegas, Nevada: Sandia National Laboratories. ACC: DOC.20041101.0002; DOC.20050823.0003; DOC.20070718.0003.

177394 SNL 2007. *Saturated Zone In-Situ Testing.* ANL-NBS-HS-000039 REV 02. Las Vegas, Nevada: Sandia National Laboratories. ACC: DOC.20070608.0004.

178871 SNL 2007. *Total System Performance Assessment Model /Analysis for the License Application.* MDL-WIS-PA-000005 REV 00. Las Vegas, Nevada: Sandia National Laboratories.

175177 SNL 2007. *UZ Flow Models and Submodels.* MDL-NBS-HS-000006 REV 03. Las Vegas, Nevada: Sandia National Laboratories.

177423 SNL 2007. *Waste Form and In-Drift Colloids-Associated Radionuclide Concentrations: Abstraction and Summary.* MDL-EBS-PA-000004 REV 03. Las Vegas, Nevada: Sandia National Laboratories.

105043 Sudicky, E.A. and Frind, E.O. 1982. "Contaminant Transport in Fractured Porous Media: Analytical Solutions for a System of Parallel Fractures." *Water Resources Research, 18,* (6), 1634-1642. Washington, D.C.: American Geophysical Union. TIC: 217475.

100610 van Genuchten, M.T. 1980. "A Closed-Form Equation for Predicting the Hydraulic Conductivity of Unsaturated Soils." *Soil Science Society of America Journal, 44,* (5), 892-898. Madison, Wisconsin: Soil Science Society of America. TIC: 217327.

9.2 CODES, STANDARDS, REGULATIONS, AND PROCEDURES

IM-PRO-002, *Control of the Electronic Management of Information*

SCI-PRO-006, *Models*

9.3 SOURCE DATA, LISTED BY DATA TRACKING NUMBER

147285 LA0003MCG12213.002. Cumulative Probabilities for Colloid Transport Between One Matrix and Another Calculated from Interpolation of Pore Volume Data from Yucca Mountain Hydrologic (Stratigraphic) Samples. Submittal date: 03/10/2000.

163558 LA0303HV831352.002. Colloid Retardation Factors for the Saturated Zone Fractured Volcanics. Submittal date: 03/31/2003.

165624 LA0303HV831352.003. Fraction of Colloids that Travel Unretarded. Submittal date: 03/31/2003.

166259 LA0303PR831231.005. Simple Calculations for SZ In-Situ Testing AMR. Submittal date: 03/19/2003.

165641 LA0303PR831362.001. Model Interpretations of C-Wells Diffusion Cell Experiments. Submittal date: 04/02/2003.

169182 LA0311BR831371.002. UZ Transport Abstraction Model, Validation Simulations for the Comparison to T2R3D. Submittal date: 11/20/2003.

171584 LA0408AM831341.001. Unsaturated Zone Distribution Coefficients (K_ds) for U, Np, Pu, Am, Pa, Cs, Sr, Ra, and Th. Submittal date: 08/24/2004.

159525 LB0205REVUZPRP.001. Fracture Properties for UZ Model Layers Developed from Field Data. Submittal date: 05/14/2002.

159526 LB0207REVUZPRP.001. Revised UZ Fault Zone Fracture Properties. Submittal date: 07/03/2002.

159672 LB0207REVUZPRP.002. Matrix Properties for UZ Model Layers Developed from Field and Laboratory Data. Submittal date: 07/15/2002.

161285 LB0208UZDSCPMI.001. Drift-Scale Calibrated Property Sets: Mean Infiltration Supporting Files. Submittal date: 08/27/2002.

179300 LB0212C14INFIL.002. 1-D Simulation and Sensitivity Analyses of Groundwater Age by Matching to C14 Age Data: 2. Data Summaries. Submittal date: 12/19/2002.

164752 LB0307MR0060R1.007. Ambient Radionuclide Transport - TSPA Deliverable Extractions. Submittal date: 07/19/2003.

166071 LB03093RADTRNS.002. Three Way Transport Model Comparison: Data Summaries. Submittal date: 09/24/2003.

178586 LB0611MTSCHP10.001. Mountain Scale Calibrated Property Set for the 10-Percentile Infiltration Map. Submittal date: 11/28/2006.

178587 LB06123DPDUZFF.001. 3-D UZ Flow Fields for Present-Day Climate of 10th-, 30th-, 50th- and 90th -percentile infiltration Maps. Submittal date: 12/19/2006.

179296 LB0612PDFEHMFF.001. Flow-Field Conversions from TOUGH2 to FEHM Format for Present Day 10-, 30-, 50-, and 90-Percentile Infiltration Maps. Submittal date: 12/19/2006.

179160 LB0701GTFEHMFF.001. Flow-Field Conversions from TOUGH2 to FEHM Format for Glacial Transition Climate 10th-, 30th-, 50th-, and 90th-Percentile Infiltration Maps. Submittal date: 01/05/2007.

179297 LB0701MOFEHMFF.001. Flow-Field Conversions from TOUGH2 to FEHM Format for Monsoon Climate 10th-, 30th-, 50th-, and 90th-Percentile Infiltration Maps. Submittal date: 01/05/2007.

179299 LB0701PAKDSESN.001. Unsaturated Zone Sorption Coefficients for Selenium and Tin. Submittal date: 01/31/2007.

179283 LB0701PAWFINFM.001 Weighting Factors for Infiltration Maps. Submittal date: 01/25/2007.

179507 LB0702PAFEM10K.002. Flow-Field Conversions to FEHM Format for Post 10,000 Year Peak Dose Fluxes in the Unsaturated Zone for Four Selected Infiltration Rates. Submittal date: 02/15/2007.

142973 LL000122051021.116. Summary of Analyses of Glass Dissolution Filtrates. Submittal date: 01/27/2000.

142910 LL991109751021.094. Data Associated with the Detection and Measurement of Colloids in Scientific Notebook SN 1644. Submittal date: 01/10/2000.

150930 MO0005PORWATER.000. Perm-Sample Pore Water Data. Submittal date: 05/04/2000.

179310 MO0701PAGROUND.000. Groundwater Colloid Concentration Parameters. Submittal date: 01/18/2007.

180391 MO0701PASORPTN.000. Colloidal Sorption Coefficients for Pu, Am, Th, Cs, and Pa. Submittal date: 04/17/2007.

180392 MO0701PAKDSUNP.000. Colloidal K_ds for U, Np, Ra and Sn. Submittal date: 04/17/2007.

9.4 OUTPUT DATA, LISTED BY DATA TRACKING NUMBER

LA0701PANS02BR.003. UZ Transport Parameters. Submittal date: 04/23/2007.

LA0702PANS02BR.001. Repository and Water Table Bins. Submittal date: 04/16/2007.

LB0702PAUZMTDF.001. Unsaturated Zone Matrix Diffusion Coefficients. Submittal date: 05/10/2007.

MO0704PAFEHMBR.001. FEHM Model and Input. Submittal date: 04/26/2007.

MO0704PAPTTFBR.002. Particle Tracking Transfer Functions. Submittal date: 04/12/2007.

MO0705PAVALSIM.000. UZ Transport Abstraction Model, Validation Simulations for the Discrete Fracture Comparison Problem and Comparison to T2R3D. Submittal date: 05/08/2007.

MO0705TRANSTAT.000. UZ Radionuclide Transport Travel Time Statistics and Sensitivity Analysis. Submittal date: 05/15/2007.

9.5 SOFTWARE CODES

165742 DISCRETE_TF V. 1.1. 2003. SUN OS, Windows 2000, Red Hat Linux 7.1. STN: 11033-1.1-00.

178965 FEHM V. 2.24. 2006. 5.9/2.4.21/WINXP/WIN 2000. STN: 10086-2.24-00.

179419 FEHM V. 2.24-01. 2007. WIN2003, 2000, & XP, Red Hat Linux 2.4.21, OS 5.9. STN: 10086-2.24-01-00.

181225 fehm2post V. 1.0. 2005. SUNOS 5.9. STN: 11031-1.0-01.

181903 Goldsim V. 9.60.100. 2007. WIN 2000, 2003, XP. STN: 10344-9.60-01

181317 PARTICLE_STAT V. 1.0. 2007. SUN OS 5.9. STN: 11241-1.0-00.

181269 ppptrk V. 1.0. 2005. SUNOS 5.9. STN: 11030-1.0-01.

APPENDIX A
MATRIX DIFFUSION COEFFICIENTS

A1. INTRODUCTION

Appendix A in the parent report (titled "Derivation of the Distribution of Water Content and Effective Permeability for Sampling Matrix Diffusion Coefficient") is no longer used in the analysis and is replaced by the appendix given herein.

A matrix diffusion coefficient is a constant of proportionality between aqueous solute mass flux (solute mass flow rate per unit wetted area) and the aqueous solute concentration gradient (gradient of the solute mass per unit water volume) for diffusive transport in the rock matrix. The matrix diffusion coefficient accounts for the diffusive properties of the solute in water as well as the geometrical effects of the rock matrix pore structure and the hydrological conditions of the rock. The matrix diffusion coefficient is expressed in units of length squared per unit of time.

Each matrix diffusion coefficient, D_m, is constructed from two independent parameters, the tortuosity, τ, and the free-water diffusion coefficient, D^*, through the relationship, $D_m = \tau D^*$. Therefore, $\log_{10}(D_m / D^*)$ is the logarithm of the tortuosity. The range of tortuosity values is subdivided into three subranges, called tortuosity rock groups, based on the tortuosity characteristics of the rock types in the unsaturated zone. These tortuosity rock groups are defined by tortuosity characteristics, with tortuosity rock group 1 having tortuosity greater than 0.05, tortuosity rock group 2 having tortuosity between 0.05 and 0.016, and tortuosity rock group 3 having tortuosity less than 0.016. There is one free-water diffusion coefficient for each radioelement. The free-water diffusion coefficients are distinguished by radioelement (rather than radionuclide) because the same diffusion coefficient is used for different isotopes of a given radioelement. The free-water diffusion coefficients and matrix diffusion coefficients have the same units, meters squared per second, and the tortuosities are dimensionless.

A.1 CORRELATION FOR TORTUOSITY AS A FUNCTION OF POROSITY AND PERMEABILITY

Experimental data for diffusion in the rock matrix for volcanic rock from the Yucca Mountain area (Reimus et al. 2007 [DIRS 179246]) have been used to correlate the matrix diffusion coefficient, divided by the free-water diffusion coefficient, with porosity and permeability for saturated conditions. A correlation for the tortuosity as a function of porosity and permeability has been proposed by Reimus et al. (2007 [DIRS 179246], Equation 2),

$$\log_{10}(D_m / D^*) = 1.42 + 1.91\phi + 0.19\log_{10}(k) \qquad \text{(Eq. A-1)}$$

where D_m is the matrix diffusion coefficient, D^* is the free water diffusion coefficient, ϕ is the matrix porosity, and k is the matrix permeability in m^2. The tortuosity, τ, is the ratio D_m / D^*. The correlation coefficient (R^2) is 0.542 (Reimus et al. 2007 [DIRS 179246], Equation 2) and the standard error is 0.29 (Reimus et al. 2007 [DIRS 179246], following Equation 2). The standard error of a correlation is the standard deviation of the data points as they are distributed around the regression line. This correlation is based on diffusion cell measurements for bromide, iodide, and tritium made on volcanic tuff rock matrix from the Yucca Mountain region. The dataset includes both qualified and unqualified data that were previously used without specific

justification for using unqualified data, as identified in CR 7260. The justification for the use of these data is presented in Section 4.1.4. The correlation differs from that previously implemented in the parent report in that the diffusion coefficient is normalized by the free-water diffusion coefficient. This normalization helps to remove the effects of molecular size and ionic charge from the correlation.

A.2 TORTUOSITY FOR UNSATURATED CONDITIONS

The experimental data were taken for saturated conditions. In the unsaturated zone, the analogous quantities to porosity and permeability are water content and effective permeability. These are appropriate because the water content and effective permeability for the unsaturated system are in fact the porosity and permeability of a saturated system if the pore space occupied by air in the unsaturated system were transformed into mineral. Therefore, in Equation A-1, which is the same as Equation 6.5.5-1 in Section 6.5.5, porosity is replaced by water content and permeability is replaced by effective permeability for unsaturated conditions.

The methodology for evaluating matrix diffusion coefficients uses the fact that the measured capillary pressure is relatively constant in the unsaturated zone between the repository and the water table. This can be seen from *Calibrated Unsaturated Zone Properties* (SNL 2007 [DIRS 179545], Figure 6-6) and *UZ Flow Models and Submodels* (SNL 2007 [DIRS 175177], Figure 6.2-4), with the exception of a sharp reduction in capillary pressure in limited perched water regions typically located at or near the base of the TSw. Using unsaturated zone capillary pressure data from DTN: LB0208UZDSCPMI.001 [DIRS 161285], a total of eight data points from four boreholes were selected from the interval of 1,100 m (roughly the elevation of the repository) to the water table elevation of roughly 730 m. These data points, obtained from DTN: LB0208UZDSCPMI.001 [DIRS 161285], *in_situ-pcap.xls*, worksheet "trend uncert plot", were reduced in output DTN LB0702PAUZMTDF.001, file *Tortuosities by model unit.xls*, worksheet "Pc data," to obtain a mean value of the capillary pressure of 1.25 bars, or 1.25×10^5 Pascals (Pa), and a standard deviation of 0.526 bars. Using the approximation of a constant capillary pressure will result in an underestimation of diffusion coefficients in the perched water zones as compared with more exact methods, but these zones are only a small portion of the unsaturated zone between the repository and the water table.

The effects of climate variations on the matrix diffusion coefficient in the unsaturated zone were considered in Section 6.5.5 of the parent report. Because of the low sensitivity to climate, the effects of climate variations on matrix diffusion were combined so that the diffusion coefficient was a function only of the rock group (Table 6-8 in the parent report). Based on these findings, the small changes to matrix diffusion resulting from climate change/climate uncertainty are not included in the current method for estimating matrix diffusion. This approach limits the use of the matrix diffusion coefficients to natural hydrologic conditions (e.g., the matrix diffusion method given here is not appropriate for estimating matrix diffusion coefficients under conditions of thermal dry-out).

To estimate D_m using Equation A-1, parameters k_m and θ_m are derived using the van Genuchten equation for capillary pressure as a function of effective water saturation (van Genuchten 1980 [DIRS 100610]; SNL 2007 [DIRS 175177], Appendix A):

$$P_c = \frac{1}{\alpha}\left(S_e^{-1/m} - 1\right)^{1-m} \quad \text{(Eq. A-2)}$$

where P_c is the capillary pressure (Pa), α is the van Genuchten capillary strength parameter (Pa^{-1}), m is the van Genuchten pore size distribution index, and S_e is the effective water saturation, which equals $(S - S_r)/(1 - S_r)$, where S is the water saturation and S_r is the residual water saturation.

Equation A-2 may be inverted for the effective water saturation:

$$S_e = \left[1 + (\alpha P_c)^{1/(1-m)}\right]^{-m} \quad \text{(Eq. A-3)}$$

and the water saturation is then:

$$S = S_e(1 - S_r) + S_r \quad \text{(Eq. A-4)}$$

The water content, θ, is then:

$$\theta = \phi S \quad \text{(Eq. A-5)}$$

where ϕ is the porosity.

The effective permeability, k_m (m^2), is given by (van Genuchten 1980 [DIRS 100610]; SNL 2007 [DIRS 175177], Appendix A):

$$k_m = k S_e^{1/2}\left[1 - \left(1 - S_e^{1/m}\right)^m\right]^2 \quad \text{(Eq. A-6)}$$

where k is the permeability (m^2).

The calculations for water content and effective permeability are presented in output DTN: LB0702PAUZMTDF.001, file *Tortuosities by Model Unit.xls*, worksheet "Matrix Properties." In Columns K through M, the components of Equation A-3 are computed to give the effective water saturation. Similarly, in columns O through R, the components of Equation A-6 are computed to give the relative permeability, $k_r = k_m / k$. Equations A-4 and A-5 are used in column U to compute the water content, and the base-10 log of the effective permeability is given in column W.

The parameters α, m, and k are given for each rock type (or model unit) in DTN: LB0611MTSCHP10.001 [DIRS 178586], with the exception of the perched water zones. This dataset is one of four parameter sets developed for the unsaturated zone, based on the calibration of the flow model to the four infiltration scenarios (the 10th-, 30th-, 50th-, and

90th-percentile scenarios). For the purpose of assigning hydrologic parameters to develop the tortuosities for diffusion, the most probable flow model parameters must be selected. It is expected that DTN: LB0611MTSCHP10.001 [DIRS 178586] will be the most probable case of the four in the TSPA analyses (see the analysis results provided in DTN: LB0701PAWFINFM.001 [DIRS 179283]). The parameters ϕ and S_r are given in DTN: LB0207REVUZPRP.002 [DIRS 159672], including the perched water zones, which were assigned the same values as the corresponding matrix units without perched water. Data for α, m, and k for the perched water zones was taken from DTN: LB06123DPDUZFF.001 [DIRS 178587]. Tortuosities were computed for each model unit from Equations A-1 through A-6 using a capillary pressure of 1.25×10^5 Pa. The parameter values and the resulting tortuosities (τ) are given in Table A-1. The calculations for tortuosity are presented in output DTN: LB0702PAUZMTDF.001, file *Tortuosities by Model Unit.xls*, worksheet "Tortuosity." The tortuosity is computed from water content and base 10 log of the effective permeability in columns B and C. The formula for the tortuosity, given in Equation A-1, is in column D.

Table A-1. Hydrological Properties and Tortuosities of the Model Units between the Repository and the Water Table

UZ Model Unit[a]	ϕ[b]	S_r[b]	α[c] (Pa^{-1})	m[c]	K[c] (m^2)	τ
tsw33	0.1554	0.1231	7.26×10^{-6}	0.283	1.86×10^{-17}	1.65×10^{-2}
tsw34	0.1106	0.1903	2.55×10^{-6}	0.317	3.16×10^{-18}	1.45×10^{-2}
tsw35	0.1307	0.1233	4.45×10^{-6}	0.216	1.09×10^{-17}	1.49×10^{-2}
tsw3[67]	0.1026	0.2038	2.51×10^{-6}	0.442	3.16×10^{-18}	1.59×10^{-2}
tsw38	0.0427	0.4177	1.88×10^{-6}	0.286	3.79×10^{-18}	1.15×10^{-2}
tsw39z	0.2751	0.3563	4.61×10^{-6}	0.059	3.50×10^{-17}	2.19×10^{-2}
tsw39v	0.2295	0.1322	4.72×10^{-5}	0.293	1.49×10^{-13}	3.65×10^{-2}
ch1z	0.2849	0.3832	2.12×10^{-7}	0.349	3.50×10^{-17}	6.48×10^{-2}
ch1v	0.3309	0.0582	1.20×10^{-4}	0.24	2.21×10^{-12}	4.28×10^{-2}
ch[2-5]v	0.3458	0.0618	3.36×10^{-4}	0.158	1.55×10^{-12}	2.86×10^{-2}
ch[2-5]z	0.3216	0.2584	2.25×10^{-6}	0.257	5.20×10^{-18}	3.72×10^{-2}
ch6z	0.2712	0.3587	1.56×10^{-7}	0.499	8.20×10^{-19}	3.15×10^{-2}
ch6v	0.2530	0.1739	1.72×10^{-5}	0.147	3.92×10^{-13}	9.42×10^{-2}
pp4	0.3212	0.2866	6.31×10^{-6}	0.474	3.01×10^{-17}	4.21×10^{-2}
pp3	0.3180	0.0791	1.72×10^{-5}	0.407	9.24×10^{-14}	7.50×10^{-2}
pp2	0.2210	0.0994	4.84×10^{-6}	0.309	1.68×10^{-15}	6.07×10^{-2}
pp1	0.2972	0.2962	3.16×10^{-5}	0.272	5.01×10^{-17}	1.43×10^{-2}
bf3	0.1752	0.1127	3.20×10^{-5}	0.193	1.00×10^{-14}	2.61×10^{-2}
bf2	0.2341	0.2117	1.18×10^{-7}	0.617	8.10×10^{-17}	6.45×10^{-2}
pc38[d]	0.0427	0.4177	1.88×10^{-6}	0.286	3.00×10^{-19}	7.09×10^{-3}
pc39[d]	0.2751	0.3563	4.61×10^{-6}	0.059	6.20×10^{-18}	1.58×10^{-2}
pc1z[d]	0.2849	0.3832	2.12×10^{-7}	0.349	9.30×10^{-20}	2.10×10^{-2}
pc[2,5]z[d]	0.3216	0.2584	2.25×10^{-6}	0.257	2.40×10^{-18}	3.21×10^{-2}

Table A-1. Hydrological Properties and Tortuosities of the Model Units between the Repository and the Water Table (Continued)

UZ Model Unit[a]	ϕ[b]	S_r[b]	α[c] (Pa^{-1})	m[c]	K[c] (m^2)	τ
pc6z[d]	0.2712	0.3587	1.56×10^{-7}	0.499	1.10×10^{-19}	2.15×10^{-2}
pc4p[d]	0.3212	0.2866	6.31×10^{-6}	0.474	7.70×10^{-19}	2.10×10^{-2}

Sources: [a] BSC 2004 [DIRS 170038], Table 6-1.
[b] DTN: LB0207REVUZPRP.002 [DIRS 159672].
[c] DTN: LB0611MTSCHP10.001 [DIRS 178586].
[d] DTN: LB06123DPDUZFF.001 [DIRS 178587]; SNL 2007 [DIRS 175177], Section 6.2.3.

Output DTN: LB0702PAUZMTDF.001 (units in the saturated zone have been deleted).

Individual rock units are grouped based on similar characteristics for tortuosity as shown in Tables A-2 through A-4. These tortuosity rock groups are defined by tortuosity characteristics with tortuosity rock group 1 having tortuosity greater than 0.05, tortuosity rock group 2 having tortuosity between 0.05 and 0.016, and tortuosity rock group 3 having tortuosity less than 0.016.

Table A-2. Rock Group 1 Tortuosities

Model Unit	Tortuosity
ch1z	6.48×10^{-2}
ch6v	9.42×10^{-2}
pp3	7.50×10^{-2}
pp2	6.07×10^{-2}
bf2	6.45×10^{-2}

Output DTN: LB0702PAUZMTDF.001.

Table A-3. Rock Group 2 Tortuosities

Model Unit	Tortuosity
tsw33	1.65×10^{-2}
tsw39z	2.19×10^{-2}
tsw39v	3.65×10^{-2}
ch1v	4.28×10^{-2}
ch[2-5]z	3.72×10^{-2}
ch[2-5]v	2.86×10^{-2}
ch6z	3.15×10^{-2}
pp4	4.21×10^{-2}
bf3	2.61×10^{-2}
pc1z	2.10×10^{-2}
pc[2,5]z	3.21×10^{-2}
pc6z	2.15×10^{-2}
pc4p	2.10×10^{-2}

Output DTN: LB0702PAUZMTDF.001.

Table A-4. Rock Group 3 Tortuosities

Model Unit	Tortuosity
tsw34	1.45×10^{-2}
tsw35	1.49×10^{-2}
tsw3[6,7]	1.59×10^{-2}
tsw38	1.15×10^{-2}
pp1	1.43×10^{-2}
pc38	7.09×10^{-3}
pc39	1.58×10^{-2}

Output DTN: LB0702PAUZMTDF.001.

The tortuosities for the various units are averaged on a volume-weighted basis for the model unit grid cells listed in Tables A-2 through A-4 between Nevada State Plan, NAD 27 Easting coordinates 170110 m and 172280 m and between Nevada State Plan, NAD 27 Northing coordinates 230960 m and 236220 m (DTN: LB0612PDFEHMFF.001 [DIRS 179296], file *RepoCell_LA_2006.mck*). These are the extreme values for Easting and Northing coordinates of the waste emplacement drifts. The grid coordinates and volumes are available in DTN: LB06123DPDUZFF.001 [DIRS 178587]. The volume-weighted tortuosities for the three rock groups are given in Table A-5.

Table A-5. Rock Group Average Tortuosities

Rock Group	Tortuosity
1	7.01×10^{-2}
2	2.67×10^{-2}
3	1.44×10^{-2}

Output DTN: LB0702PAUZMTDF.001.

A.3 FREE-WATER DIFFUSION COEFFICIENTS

Free-water diffusion coefficients for the various aqueous chemical forms of the radioelements may be estimated directly in some cases, but in other cases must be estimated using a chemical analogue. Table A-6 presents the radioelements, expected dominant chemical form in UZ waters, and indicates if a direct estimate of the free-water diffusion coefficient measurement is available. In Table A-6 each radioelement has one identified dominant aqueous species except for americium, which has two. For species that are pH dependent, a pH of 8.3 was used based on information from *Drift-Scale THC Seepage Model* (SNL 2007 [DIRS 177404], Table 6.2-1; DTN: MO0005PORWATER.000 [DIRS 150930]). This is the higher value found for the TSw hydrogeologic unit, ranging from 7.7 to 8.31 (SNL 2007 [DIRS 177404], Table 6.2-1), and the rounded value of 8.3 was used because of higher pH values generally found in deeper units of the unsaturated zone (BSC 2004 [DIRS 169734], pp. 5-18 to 5-19). Values of pH ranging from 7.6 to 8.3 in the TSw are also reported in *Engineered Barrier System: Physical and Chemical Environment* (SNL 2007 [DIRS 177412]). Many of the species in Table A-6 were taken from Section 6 of *Dissolved Concentration Limits of Radioactive Elements* (SNL 2007 [DIRS 177418]). The speciation diagrams used as input from that report were generated using qualified inputs and software; therefore, the speciation results may be considered qualified

inputs. These species are shown in Table A-6. For selenium, Cutter (1989 [DIRS 178861], p. 254) shows that aqueous selenium occurs predominantly as selenite (SeO_3^{2-}) and selenate (SeO_4^{2-}) in natural groundwaters and drinking waters. The predominance of either selenite or selenate varies with its location. Howard (1975 [DIRS 106109], p. 1,671) concludes that selenite is the predominant species in the presence of iron and sulfur. The repository host rock consists of about 1% iron as Fe_2O_3 (BSC 2004 [DIRS 169734], p. 3-28), and sulfate is a major component of the natural water (SNL 2007 [DIRS 177404], Table 6.2-1). In any case, there is only a 3% difference in the free-water diffusion coefficients estimated for selenite as compared with selenate (Table A-8); therefore, the selection of selenite as the predominant species is adequate for its intended use. There is uncertainty about the chemical form of iodine in unsaturated zone pore waters. In this analysis, a species thought to be nonsorbing, I^-, has been selected, rather than iodate (IO_3^-). This selection is made on the grounds that the nonsorbing I^- species is the more conservative choice for repository performance predictions.

Table A-6. Radioelements, Aqueous Species, and Available Diffusion Data

Radioelement	Aqueous Species	Source of Information for Aqueous Species	Direct Estimate Available for Free-Water Diffusion Coefficient	Source of Measurement/Analogue Data
Americium	$AmCO_3^+$	SNL 2007 [DIRS 177418], Figure 6.9-2	no	Lide 1992 [DIRS 166224], p. 5-111 /analogue Na^+
Americium	$Am(CO_3)_2^-$	SNL 2007 [DIRS 177418], Figure 6.9-2	no	Lide 1992 [DIRS 166224], p. 5-111 /analogue $B(C_6H_5)_4^-$
Carbon	HCO_3^-	DTN: MO0005PORWATER.000 [DIRS 150930]	yes	Lide 1992 [DIRS 166224], p. 5-111
Chlorine	Cl^-	DTN: MO0005PORWATER.000 [DIRS 150930]	yes	Lide 1992 [DIRS 166224], p. 5-111
Cesium	Cs^+	Baes and Mesmer 1986 [DIRS 100702], p. 73	yes	Lide 1992 [DIRS 166224], p. 5-111
Iodine	I^-	A halogen chemically analogous to Cl^- and F^- reported in DTN: MO0005PORWATER.000 [DIRS 150930]	yes	Lide 1992 [DIRS 166224], p. 5-111
Neptunium	$NpO_2CO_3^-$	SNL 2007 [DIRS 177418], Figure 6.6-4	no	Lide 1992 [DIRS 166224], p. 5-111 /analogue $B(C_6H_5)_4^-$
Protactinium	$PaO_2CO_3^-$	SNL 2007 [DIRS 177418], Table 6.11-1	no	Lide 1992 [DIRS 166224], p. 5-111 /analogue $B(C_6H_5)_4^-$
Plutonium	PuO_2CO_3	SNL 2007 [DIRS 177418], Figure 6.4-15	no	Estimated using Stokes-Einstein equation (Equation A-8)
Radium	Ra^{2+}	SNL 2007 [DIRS 177418], Section 6.12	yes	Lide 1992 [DIRS 166224], p. 5-111
Selenium	SeO_3^{2-}	Cutter 1989 [DIRS 178861], p. 254	no	Lide 1992 [DIRS 166224], p. 5-112 /analogue SeO_4^{2-}

Table A-6. Radioelements, Aqueous Species, and Available Diffusion Data (Continued)

Radioelement	Aqueous Species	Source of Information for Aqueous Species	Direct Estimate Available for Free-Water Diffusion Coefficient	Source of Measurement/Analogue Data
Tin	$Sn(OH)_4$	Baes and Mesmer 1986 [DIRS 100702], Figure 15.6	no	Estimated using Stokes-Einstein equation (Equation A-8)
Strontium	Sr^{2+}	An alkaline earth element and chemical analog to radium given in SNL 2007 [DIRS 177418], Section 6.12	yes	Lide 1992 [DIRS 166224], p. 5-111
Technetium	TcO_4^-	Baes and Mesmer 1986 [DIRS 100702], p. 261)	yes	Sato et al. 1996 [DIRS 163213], Table 2
Thorium	$Th(OH)_3CO_3^-$	SNL 2007 [DIRS 177418], Figure 6.4-13	no	Lide 1992 [DIRS 166224], p. 5-111 /analogue $B(C_6H_5)_4^-$
Uranium	$(UO_2)(CO_3)_3^{4-}$	SNL 2007 [DIRS 177418], Figure 6.3-2	no	Lide 1992 [DIRS 166224], p. 5-111 /analogue $[Fe(CN)_6]^{4-}$

Output DTN: LB0702PAUZMTDF.001.

All of the free-water diffusion coefficients that have a direct estimate available, as identified in Table A-6, are computed from measured values of the molar ionic conductivity using the Nernst-Einstein equation (Lide 1992 [DIRS 166224], p. 5-111):

$$D^* = \left(\frac{RT}{F^2}\right)\left(\frac{\lambda}{|n|}\right) \qquad \text{(Eq. A-7)}$$

where D^* is the free-water diffusion coefficient, R is the gas constant, T is the absolute temperature, F is the Faraday constant, n is the charge of the ion, and λ is the molar ionic conductivity at infinite dilution. The value of RT/F^2 at 25°C is given by Lide (1992 [DIRS 166224], p. 5-111) to be 2.6629×10^{-7} mol/(S-s), where S denotes siemans, or reciprocal ohms. Seven of the 15 radioelement aqueous species have measured values of λ.

Values of λ are estimated for chemical forms where measured values are not available, using the closest analogue that has a measured value of λ. The analogues, identified in Table A-6, were determined by using a species with a measured value of λ having the same charge and a molecular size that is as close as possible to the identified species. The estimated values of the molar ionic conductivity have been corrected for molecular size because ionic conductivity is expected to be inversely proportional to the molecular radius as in the Stokes-Einstein equation (see Equation (A-8) below). The correction accounts for the differences in molecular radii between the analog molecular form and the estimated molecular form. Atomic radii are used to estimate the molecular volumes by summing the atomic volumes of the constituent atoms (see Table A-7). The atomic volumes are computed assuming a spherical form for the atoms and using the equation $V = (4/3)\pi r^3$, where V is the atomic volume and r is the radius. Again,

assuming a spherical form, the molecular volume is then used to compute a molecular radius by inverting the equation for volume into an equation for radius. A correction to the ionic conductivity is computed from the ratio of analogue molecular radius to the molecular radius of the identified species. The molar ionic conductivity for americium is the average for the two molecular forms identified in Table A-6, as shown in Table A-8.

Table A-7. (a) Atomic Radii; (b) Estimated Radii of Radionuclide Molecular Species, Analogue Molecular Species, and Correction Factors to Estimate Molar Ionic Conductivities for the Radionuclide Molecular Species from Values for the Analogue Molecular Species

(a)

Element	Atomic Radius (nm)*
Americium	0.175
Boron	0.085
Carbon	0.070
Iron	0.140
Hydrogen	0.025
Nitrogen	0.065
Sodium	0.180
Neptunium	0.175
Oxygen	0.060
Protactinium	0.180
Plutonium	0.175
Selenium	0.115
Tin	0.145
Thorium	0.180
Uranium	0.175

Output DTN: LB0702PAUZMTDF.001.

NOTES: *From Slater 1965 [DIRS 179613].

(b)

Aqueous Species	Molecular Radius (nm)	Selected Analogue	Molecular Radius (nm)	Correction Factor
$AmCO_3^+$	0.185	Na^+	0.180	0.972
$Am(CO_3)_2^-$	0.194	$B(C_6H_5)_4^-$	0.209	1.077
$NpO_2CO_3^-$	0.189	$B(C_6H_5)_4^-$	0.209	1.105
$PaO_2CO_3^-$	0.194	$B(C_6H_5)_4^-$	0.209	1.081
PuO_2CO_3	0.189	N/A	N/A	N/A
SeO_3^{2-}	0.129	$(1/2)SeO_4^{2-}$	0.134	1.032
$Sn(OH)_4$	0.158	N/A	N/A	N/A
$Th(OH)_3CO_3^-$	0.196	$B(C_6H_5)_4^-$	0.209	1.068
$(UO_2)(CO_3)_3^{4-}$	0.206	$(1/4)[Fe(CN)_6]^{4-}$	0.186	0.903

Output DTN: LB0702PAUZMTDF.001.

N/A = analogue information not applicable for uncharged species.

The molar ionic conductivities in Table A-8 are from the sources given in Table A-6 or are estimated by applying the correction factors in Table A-7. The resulting free-water diffusion coefficients are given in Table A-8. The expected molecular forms for tin and plutonium in water, $Sn(OH)_4$ and PuO_2CO_3, are not ionic. Therefore, the diffusion coefficients were estimated using the Stokes-Einstein equation (Bird et al. 1960 [DIRS 103524], p. 514):

$$D^* = \frac{kT}{3\pi\mu d_m} \quad \text{(Eq. A-8)}$$

where k is Boltzmann's constant, T is the absolute temperature, μ is the viscosity of water, and d_m is the molecular diameter. The values of the parameters are $k = 1.38 \times 10^{-23}$ JK^{-1} (Lide et al. 1992 [DIRS 166224], p. 1-1), $T = 298$ K, and $\mu = 9 \times 10^{-4}$ Pa-s (output DTN: LB0702PAUZMTDF.001, file *Viscosity of Water.xls*, interpolated from viscosity data from Lide et al. (1992 [DIRS 166224], p. 6-10). The approach discussed above for estimating the molecular radius is also used to estimate molecular radii for $Sn(OH)_4$ and PuO_2CO_3 (see Table A-7), which is used in Equation A-8 to compute the free-water diffusion coefficients, given in Table A-8.

Table A-8. Free-Water Diffusion Coefficients

Radio-Element	Dominant Chemical Form	λ (m^2 - S/mol)	λ Correction Factor	λ (m^2 - S/mol), Corrected	Free-Water Diffusion Coefficient (m^2/s)
Americium	$AmCO_3^+$	5.01×10^{-3}	0.972	4.87×10^{-3}	1.30×10^{-9}
Americium	$Am(CO_3)_2^-$	2.10×10^{-3}	1.077	2.26×10^{-3}	6.02×10^{-10}
Americium average					9.49×10^{-10}
Carbon	HCO_3^-	4.45×10^{-3}	1.000	4.45×10^{-3}	1.18×10^{-9}
Chlorine	Cl^-	7.63×10^{-3}	1.000	7.63×10^{-3}	2.03×10^{-9}
Cesium	Cs^+	7.72×10^{-3}	1.000	7.72×10^{-3}	2.06×10^{-9}
Iodine	I^-	7.68×10^{-3}	1.000	7.68×10^{-3}	2.05×10^{-9}
Neptunium	$NpO_2CO_3^-$	2.10×10^{-3}	1.105	2.32×10^{-3}	6.18×10^{-10}
Protactinium	$PaO_2CO_3^-$	2.10×10^{-3}	1.081	2.27×10^{-3}	6.04×10^{-10}
Plutonium	PuO_2CO_3	N/A	N/A	N/A	1.30×10^{-9}
Radium	Ra^{2+}	6.68×10^{-3}	1.000	6.68×10^{-3}	8.89×10^{-10}
Selenium	SeO_3^{2-}	7.57×10^{-3}	1.032	7.81×10^{-3}	1.04×10^{-9}
Tin	$Sn(OH)_4$	N/A	N/A	N/A	1.55×10^{-9}
Strontium	Sr^{2+}	5.94×10^{-3}	1.000	5.94×10^{-3}	7.91×10^{-10}
Technetium	TcO_4^-	7.34×10^{-3}	1.000	7.34×10^{-3}	1.95×10^{-9}
Thorium	$Th(OH)_3CO_3^-$	2.10×10^{-3}	1.068	2.24×10^{-3}	5.97×10^{-10}
Uranium	$(UO_2)(CO_3)_3^{4-}$	1.10×10^{-2}	0.903	9.97×10^{-3}	6.64×10^{-10}

Output DTN: LB0702PAUZMTDF.001.

N/A = analogue information not applicable for uncharged species.

A.4. Uncertainty Treatment for Matrix Diffusion Coefficients

The use of large grid elements in the UZ transport model representing a "point" in space may result in a spatially averaged value of the diffusion coefficient for a grid element that is close to the population mean of the laboratory data. This assumes a spatial correlation length for the diffusion coefficient that is small relative to the size of a model grid element. Furthermore, if radioelement concentrations are spatially limited (e.g., release from a limited set of waste packages), then averaging over the entire grid element may overestimate the volume of rock directly involved in the transport process. In this case the effective diffusion coefficient may not be well-represented by a volume average over the entire grid element. The case of limited access of the radioelements to the entire volume of the rock may also be applicable to the propagation of a radioelement concentration front, and the diffusion coefficient is most important in determining the propagation of this transient front in transport calculations. Nevertheless, it is likely that correlation lengths for water content and effective permeability are not comparable to length scales representative of grid elements in the model and that some uncertainty reduction occurs from scale-up.

No fundamental or empirical solution to the problem of scale effects on uncertainty for matrix diffusion coefficients exists for the conditions relevant to transient solute concentration fronts moving through fractured rock. The approach here is to suppress the uncertainty associated with effective water content, effective permeability, and free-water diffusion coefficient while retaining the uncertainty found in the laboratory experiments for tortuosity. Water content and effective permeability uncertainties are suppressed because saturation changes tend to offset the effects of variations in porosity and permeability on water content and effective permeability. This occurs for water content, which is the product of porosity and water saturation, because porosity and pore size are typically correlated. This correlation results in lower water saturations at the prevailing capillary pressures for areas of higher porosity. Effective permeability, which is the product of permeability and relative permeability, behaves similarly because of a similar correlation between permeability and pore size. Uncertainty in free-water diffusion coefficients is smaller than uncertainties in tortuosity. Therefore, the uncertainties associated with the laboratory-measured tortuosities relative to the correlation (Equation A-1) are the only uncertainties included in the stochastic sampling of diffusion coefficients.

The differences between the predicted values using Equation A-1 and measured values for the diffusion coefficients are called the residuals. The basis for calculating residuals is the correlation line derived by Reimus et al. (2007 [DIRS 179246], Equation 2) for a subset of measured diffusion coefficients from which repeat measurements were excluded. The subset was restricted to results from experiments in which rock permeability and porosity were also measured. The normalized residuals are the residuals divided by the standard deviation for the correlation in Equation (A-1), or $NR = \{\log_{10}(\tau_p) - \log_{10}(\tau_o)\}/SD$, where NR is the normalized residual, $\log_{10}(\tau_p)$ is the predicted value from Equation A-1, $\log_{10}(\tau_o)$ is the experimentally observed value, and SD is the standard deviation of the observed values relative to the correlation line. This represents the uncertainty in the matrix diffusion coefficient because this coefficient is defined as the product of the free-water diffusion coefficient (a constant parameter) times the tortuosity (a stochastic parameter). Therefore, the normalized residuals for the matrix diffusion coefficient are the same as for the tortuosity coefficient. Assigning rank order

empirical cumulative probability values, P, to the normalized residuals gives a curve that may be compared against a standard normal cumulative probability distribution, a normal distribution with a mean of 0 and a standard deviation of 1, computed using the Excel function NORMSINV(P). This is shown in Figure A-1.

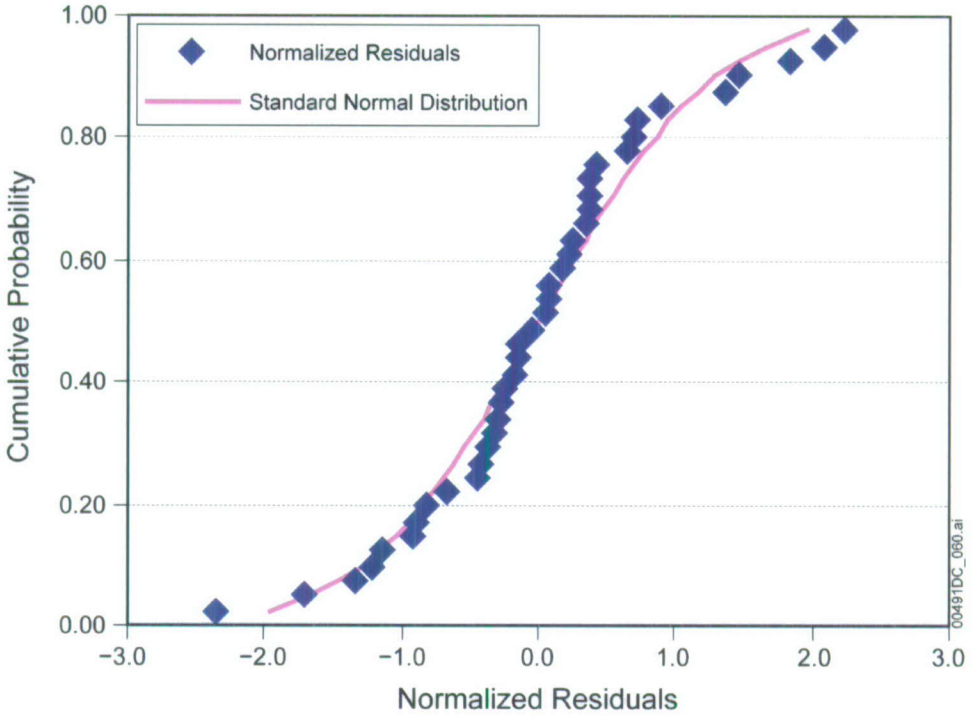

Output DTN: LB0702PAUZMTDF.001.

Figure A-1. Cumulative Probability Distribution for the Normalized Residuals of Tortuosity

Therefore, the distribution of the residuals of $\log_{10}(\tau)$, normalized by the standard deviation, is approximated by a normal distribution with a mean of zero and a standard deviation of one. This uncertainty distribution is used for stochastic sampling of the matrix diffusion coefficient in TSPA.

APPENDIX B
DERIVATION OF WATER TABLE COLLECTING BINS

B1. INTRODUCTION

The final extracted water table collection bins are stored in file *wt.zone* which only contains the fracture nodes as required by FEHM. All files used in the extraction of water table collection bins are included in *wtbin.zip* and are listed in Figure B-1.

Name	Size	Type	Modified
wt.zone	205 KB	ZONE File	7/24/2003 10:24 AM
wtbin	70,255 KB	WinZip File	7/15/2003 11:51 AM

Name	Size	Type	Modified
wt.zone	205 KB	ZONE File	7/24/2003 10:24 AM
wtbin	70,255 KB	WinZip File	7/15/2003 11:51 AM

WinZip - wtbin.zip

File Actions View Jobs Options Help

New Open Favorites Add Extract Encrypt View CheckOut Wizard View Style

Name	Type	Modified	Size	Ratio	Packed	Path
WT identification for stragglers.xls	Microsoft Ex...	6/17/2003 4:33 PM	32,668,...	82%	5,865,...	
124001-186000 WT bins with FEHM nodes.xls	Microsoft Ex...	6/18/2003 5:46 PM	17,651,...	77%	4,051,...	
124001-186000 WT bins.xls	Microsoft Ex...	6/18/2003 5:45 PM	14,776,...	80%	2,966,...	
124001-186000 WT nodes only.xls	Microsoft Ex...	6/19/2003 7:45 AM	1,651,200	76%	397,612	
124001-186000.xls	Microsoft Ex...	6/18/2003 8:36 AM	6,361,600	78%	1,410,...	
1-62000 with exact WT picks.xls	Microsoft Ex...	6/19/2003 4:53 PM	34,724,...	77%	7,827,...	
1-62000 WT bins with FEHM nodes.xls	Microsoft Ex...	6/18/2003 5:40 PM	17,644,...	77%	4,084,...	
1-62000 WT bins.xls	Microsoft Ex...	6/18/2003 5:41 PM	14,770,...	80%	3,022,...	
1-62000 WT nodes only.xls	Microsoft Ex...	6/19/2003 7:35 AM	1,616,384	76%	393,255	
1-62000.xls	Microsoft Ex...	6/17/2003 4:29 PM	6,353,920	77%	1,457,...	
186001-245506 with exact WT picks.xls	Microsoft Ex...	6/18/2003 8:44 AM	33,281,...	77%	7,532,...	
186001-245506 WT bins with FEHM nodes.xls	Microsoft Ex...	6/18/2003 5:49 PM	16,734,...	77%	3,909,...	
186001-245506 WT bins.xls	Microsoft Ex...	6/18/2003 5:47 PM	14,007,...	79%	2,882,...	
186001-245506 WT nodes only.xls	Microsoft Ex...	6/19/2003 7:50 AM	1,515,008	76%	361,641	
186001-245506.xls	Microsoft Ex...	6/18/2003 8:43 AM	6,128,128	77%	1,406,...	
62001-124000 with exact WT picks.xls	Microsoft Ex...	6/18/2003 8:20 AM	34,556,...	78%	7,466,...	
62001-124000 WT bins with FEHM nodes.xls	Microsoft Ex...	6/18/2003 5:43 PM	17,648,...	77%	4,036,...	
62001-124000 WT bins.xls	Microsoft Ex...	6/18/2003 5:43 PM	14,773,...	80%	2,962,...	
62001-124000 WT nodes only.xls	Microsoft Ex...	6/19/2003 7:41 AM	1,285,632	76%	314,610	
62001-124000.xls	Microsoft Ex...	6/18/2003 8:20 AM	6,358,528	78%	1,392,...	
Composite WT nodes only.xls	Microsoft Ex...	6/19/2003 7:55 AM	6,022,144	76%	1,459,...	
Stragglers.xls	Microsoft Ex...	6/17/2003 4:33 PM	3,437,568	78%	772,341	
Water Table Binning.doc	Microsoft W...	6/19/2003 6:21 PM	25,088	86%	3,426	
124001-186000 with exact WT picks.xls	Microsoft Ex...	6/18/2003 8:37 AM	27,658,...	78%	5,959,...	

Selected 0 files, 0 bytes Total 24 files, 323,878KB

00491DC_061.ai

Output DTN: MO0705PAVALSIM.000.

Figure B-1. List of Files Used to Develop the Water Table Binning

INTENTIONALLY LEFT BLANK

APPENDIX C
DERIVATION OF FRACTURE-MATRIX INTERACTION SUBMODEL AND GENERATION OF TRANSFER FUNCTIONS

C1. DERIVATION OF FRACTURE-MATRIX INTERACTION SUBMODEL

No Change.

C2. GENERATION OF TRANSFER FUNCTIONS

This section describes the process for generating the transfer function curves. This is accomplished through a numerical solution of the model domain depicted in Figure 6-5. As described in Section 6.4.3 of the parent report, both a discrete fracture model (DFM) and a dual permeability (dual-k) model conceptualization are implemented as part of the abstraction. For the DFM, a two-dimensional model was set up to perform transport simulations using the advection-dispersion module of FEHM V2.24 [DIRS 178965]. The model consists of a regular grid domain consisting of regular spacing of 6 m in the z direction (51 grid points in this direction for a total length of 300 m) and increasing grid spacing into the matrix in the x direction, starting with the first column of nodes of width equal to that of a fracture (22 grid points in this direction). In the model simulations, fracture properties are given to the nodes of the first column, and the remaining nodes are given matrix properties. To ensure that parallel flow occurs in the fracture and matrix in the z direction, a flow permeability barrier is established between the fracture and matrix. Furthermore, for injection into the matrix, water is input and output from the boundary nodes in proportion to the volume of that cell. This model design ensures that flow streamlines remain completely in the z direction. Finally, although the transfer functions being used are for unsaturated transport, there is no requirement that this submodel use unsaturated flow to generate them, as long as the water content values are known. Therefore, for simplicity, these simulations were performed for saturated flow conditions, with the fracture and matrix porosities used instead of water contents. For the dual-k model, a simple grid was constructed with identical spacings in the z direction, but only one matrix cell in the x direction. Aside from the different grid, cell numbering, and application of boundary conditions, the process for generating the breakthrough curves and transfer functions is the same for the dual-k model. Furthermore, the use of these curves in an FEHM particle-tracking simulation is completely transparent, requiring only a choice of which transfer function file to use.

In the simulations to generate the transfer functions, parameter p_3 is varied systematically from fracture-dominated to matrix-dominated flow by varying the relative water flux values in the fractures and matrix. Ranges of other parameter values consistent with the span of those parameters required for the UZ transport abstraction model are also selected. Table C-1 lists the variations of each parameter that were used in the formulation of the transfer function curves. For the sorption coefficient K_d, the fact that the range of values only goes to 100 does not imply that the model is incapable of accurately simulating transport behavior for higher values of K_d. In Section C-4 of the parent report, a procedure for normalizing the transfer function curves is described whereby higher values of K_d are properly handled. This procedure allows the code to cover arbitrarily large values of K_d without the need to include transfer function curves that extend to such large values.

A four-dimensional matrix of parameters was established with the parameter values listed in the table, and the transfer function curves for each were computed, for a total of $13 \times 12 \times 3 \times 10 = 4{,}680$ values of the parameter vector, (p_1, p_2, p_3).

Table C-1. List of Parameter Values Used to Compute Transfer Function Curves

Parameter	Description	Number of Values	List of Values
$F_f = f_f/(f_f + f_m)$	Fracture Flux Fraction	13	0.01, 0.1, 0.2, 0.3, 0.4, 0.5, 0.6, 0.7, 0.8, 0.9, 0.99, 0.999, 0.9999
D_m	Matrix Diffusion Coefficient	12	10^{-8}, 3×10^{-9}, 10^{-9}, 3×10^{-10}, 10^{-10}, 3×10^{-11}, 10^{-11}, 3×10^{-12}, 10^{-12}, 3×10^{-13}, 10^{-13}, 10^{-20} m^2/s
θ_f	Fracture Volume Fraction	3	0.01, 0.1, 0.5
K_d	Sorption Coefficient	10	0, 0.3, 0.5, 1, 3, 5, 10, 30, 50, 100 mL/g
Total: 13 × 12 × 3 × 10		4,680	(p_1, p_2, p_3) in *parameter runs.xls*

Output DTN: MO0704PAPTTFBR.002.

Two runs of the model are performed for each parameter set: one where solute mass is injected in the fracture and another where mass is injected in the matrix. The list of parameter values (p_1, p_2, p_3) is given in the file *parameter runs 4680.xls*, along with the underlying FEHM input parameters for each simulation. The code fehm2post V. 1.0 [DIRS 181225] was used to execute the multiple realizations and to postprocess the results to obtain the transfer functions. The postprocessing itself (executed by fehm2post) was performed using the software DISCRETE_TF V. 1.1. The resulting output from these runs is then concatenated by hand and the appropriate header information inserted by hand to conform to the input required by FEHM. The transfer function file for the DFM formulation is *uz_tfcurves_nn_4680.in*, whereas the corresponding file for the dual-k formulation is *uz_tfcurves_dualk_nn_4680.in*. These files, along with the Excel spreadsheet mentioned earlier, and the control files required for execution of these runs are available as output DTN: MO0704PAPTTFBR.002.

C3. DISCUSSION OF FRACTURE-MATRIX SUBMODEL BEHAVIOR

No change.

C4. ADDITIONAL IMPLEMENTATION CONSIDERATIONS

Changes here consist only of a minor update to Fracture-Dominated Flow section. No changes from the parent report occur in the rest of this section, so the unaffected portion of the section is not included in this addendum. Equations are numbered as in the parent report.

Fracture-Dominated Flow: The parameterization of the transfer function curves is based on a model that has some flow within both the fracture and matrix. When the flow is fracture dominated ($F_f > 0.9999$), the details of the actual fraction of flow should be unimportant, since advective transport in the matrix should be negligible. However, without correction for cases where $F_f > 0.9999$, the algorithm for finding the transfer function will inappropriately attempt to select curves with high values of the matrix retardation coefficient, R_m, to compensate for the fact that transfer functions with extremely large F_f are not included. To correct this problem, the code uses the following rearranged form of Equation C-30:

$$p_3 = \frac{p_1}{p_2}\frac{(1-F_f)}{F_f} \qquad \text{(Eq. C-37)}$$

When $F_f > 0.9999$, the code uses 0.9999 and the values of p_1 and p_2 to compute p_3 for the purposes of selecting the transfer function curve. This assures that a fracture-dominated transfer function is chosen with appropriate values for the other diffusion and sorption parameters.

C5. ADAPTING THE ACTIVE FRACTURE MODEL FOR TRANSPORT

No change.

INTENTIONALLY LEFT BLANK

APPENDIX D
SUPPLEMENTARY UNSATURATED ZONE TRANSPORT SIMULATION RESULTS

D.1 TRAVEL TIME PLOTS FOR OTHER FLOW FIELDS

This section presents, without discussion, simulation results analogous to those presented in Section 6.6.2.1 examining the travel time for mass released from various release locations, for all flow scenarios and climate conditions, to augment those presented in the main body of this addendum.

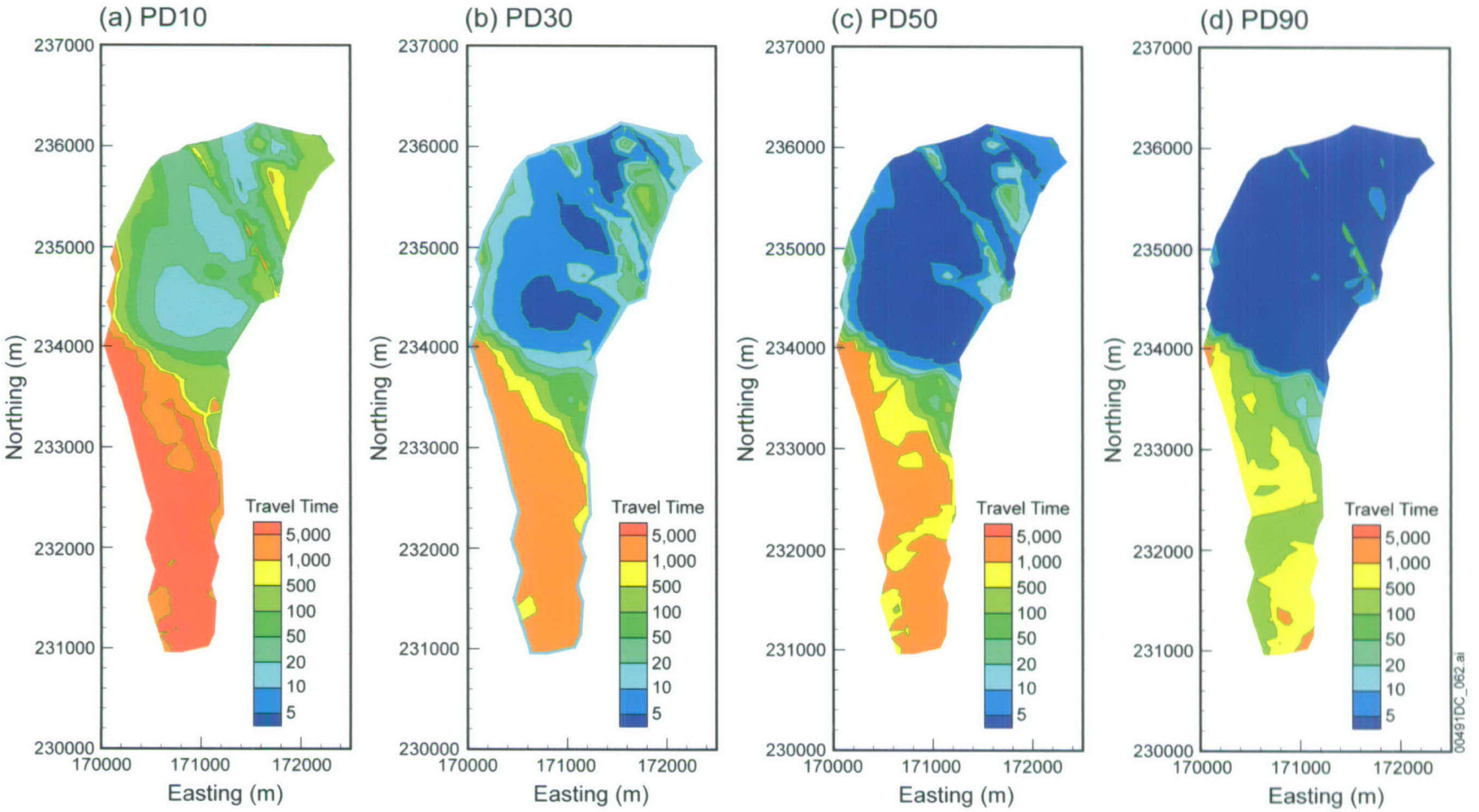

Output DTN: MO0705TRANSTAT.000.

NOTE: Travel times are in years.

Figure D.1-1. Comparison of Mean Travel Times for Different Infiltration Scenarios of Under Present-Day Climate Conditions, and Representative Parameter Values

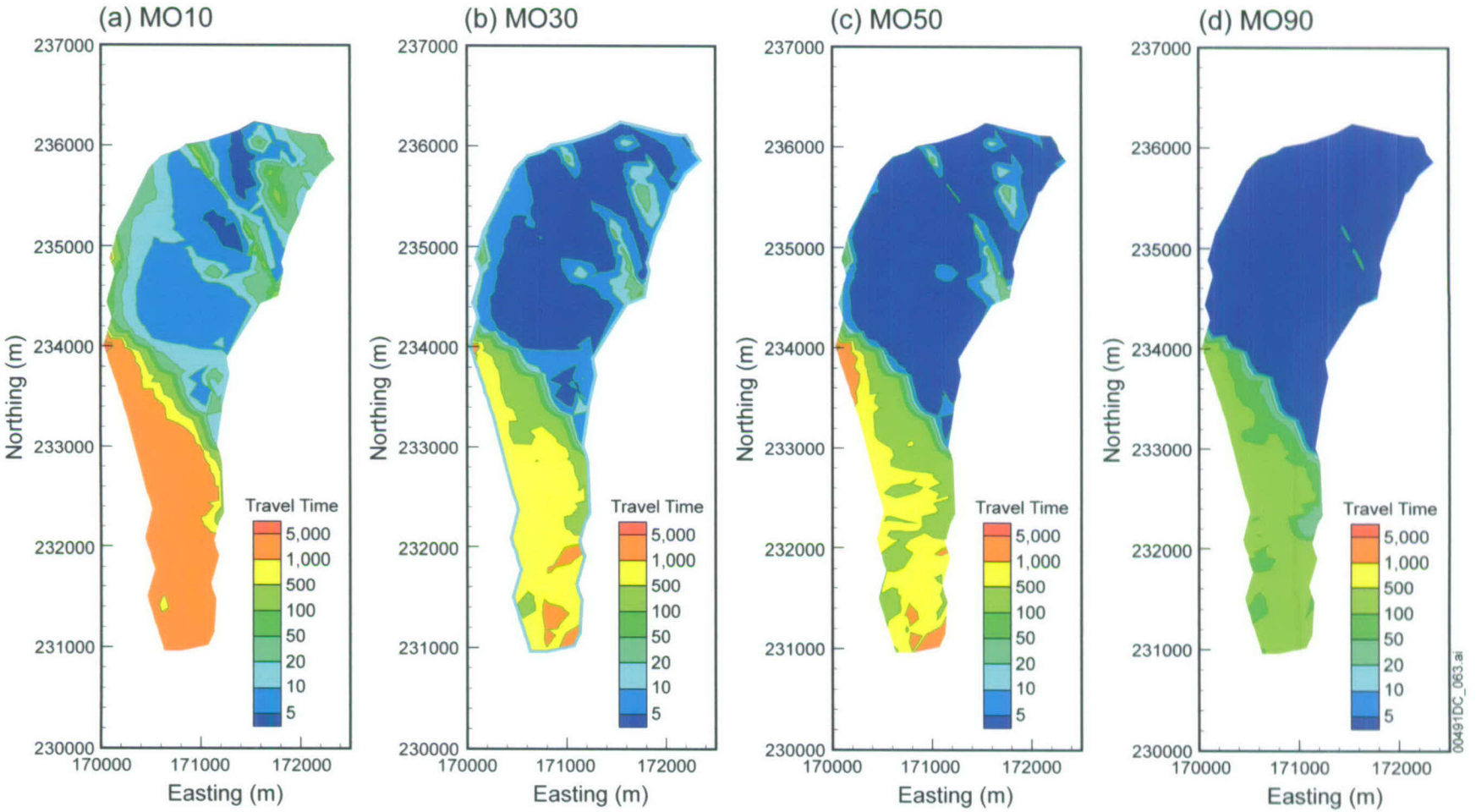

Output DTN: MO0705TRANSTAT.000.

NOTE: Travel times are in years.

Figure D.1-2. Comparison of Mean Travel Times for Different Infiltration Scenarios of Monsoon Climate Conditions, Representative Parameter Values

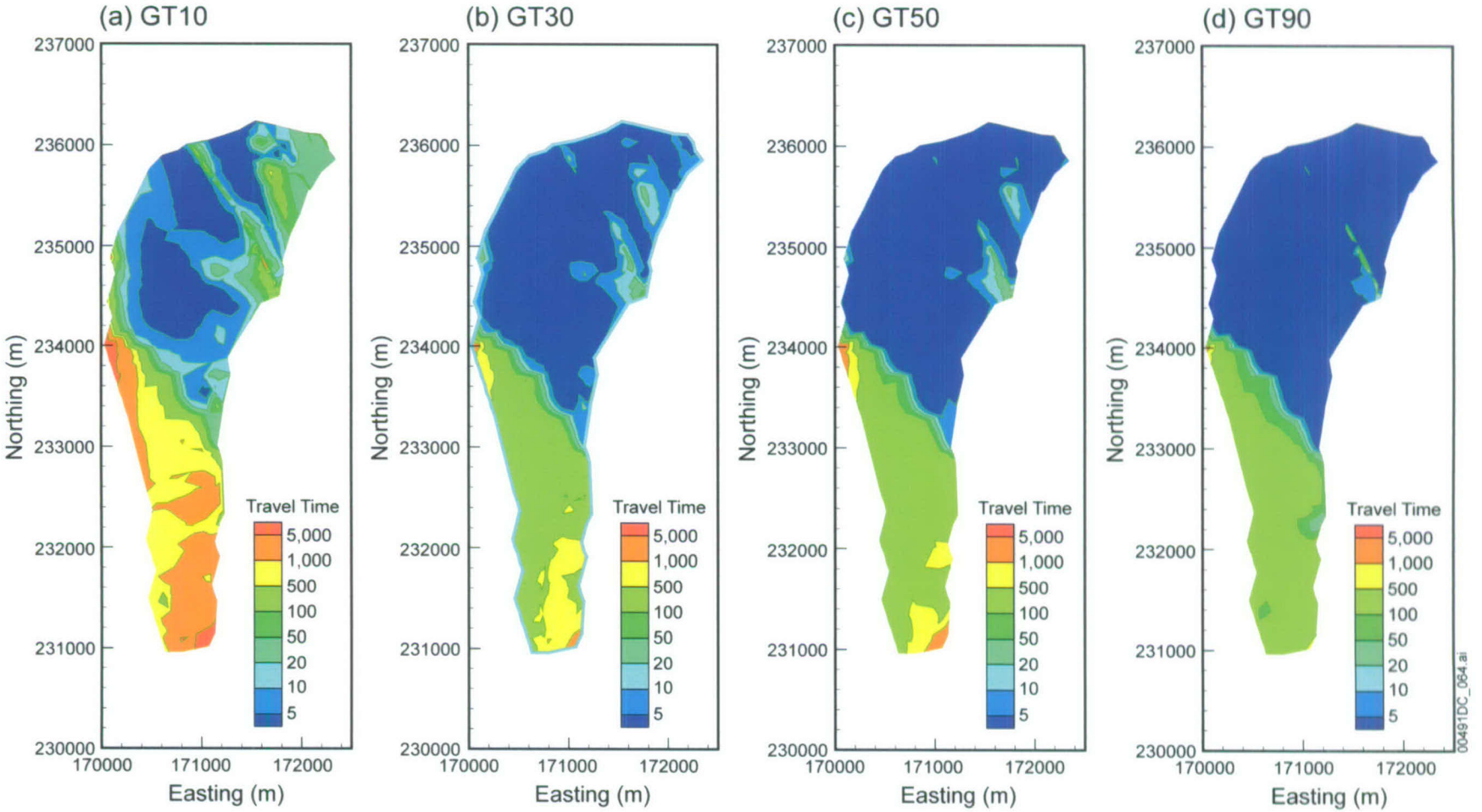

Output DTN: MO0705TRANSTAT.000.

NOTE: Travel times are in years.

Figure D.1-3. Comparison of Mean Travel Times for Different Infiltration Scenarios of Glacial-Transition Climate Conditions, Representative Parameter Values

D.2 ADDITIONAL BREAKTHROUGH CURVES

This section presents, without discussion, additional breakthrough curve simulation results for decay chains not presented in Section 6.6.2.2. In all cases, only the parent species is introduced at the repository, and the breakthrough curves of the parent and daughters at the water table are recorded. In some plots, a portion of the decay chain is simulated to illustrate the behavior of that species as the source term at the repository. In the TSPA model, the sources of each radionuclide can occur either as the source at the repository or within the natural system due to decay of a parent radionuclide.

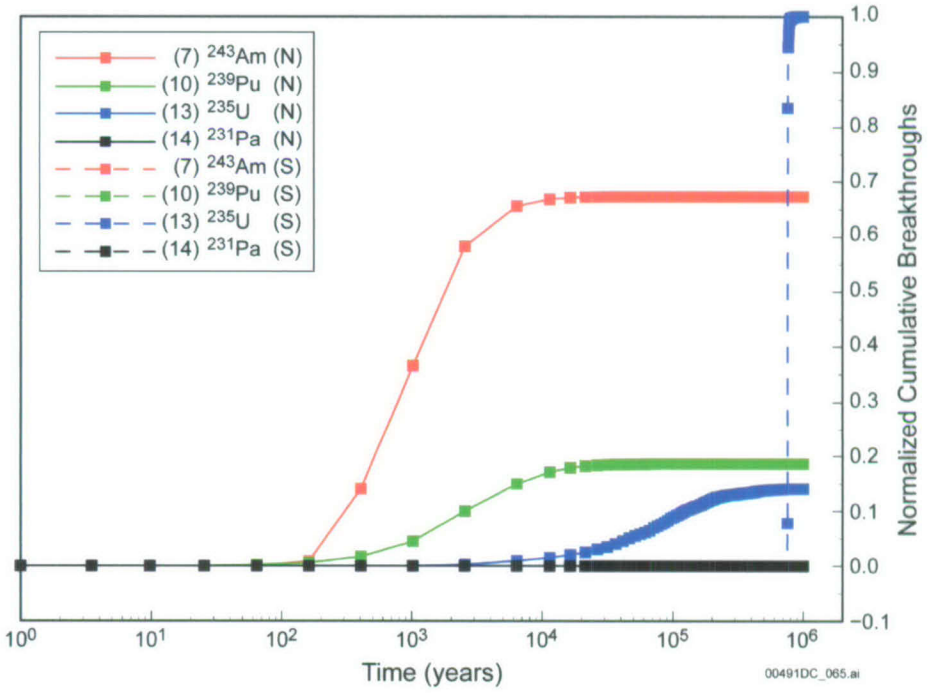

Output DTN: MO0705TRANSTAT.000.

Figure D.2-1. Normalized Cumulative Breakthrough Curves of Decay Chain $^{243}Am \rightarrow {}^{239}Pu \rightarrow {}^{235}U \rightarrow {}^{231}Pa$ for the Glacial-Transition, 10th Percentile Infiltration Condition, Representative Parameter Values, Northern and Southern Release Nodes

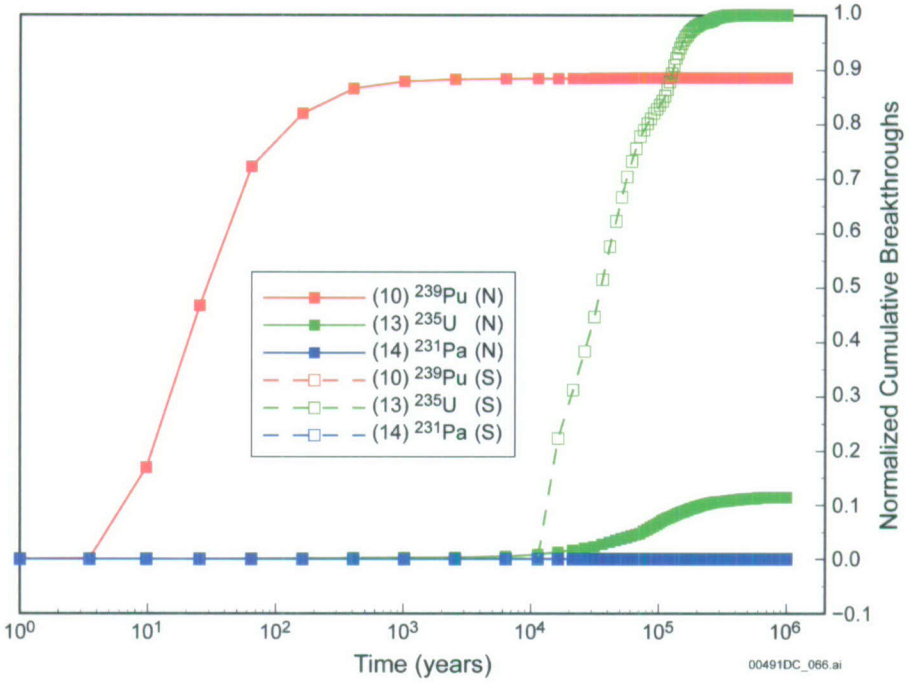

Output DTN: MO0705TRANSTAT.000.

Figure D.2-2. Normalized Cumulative Breakthrough Curves of Decay Chain $^{239}Pu \rightarrow {}^{235}U \rightarrow {}^{231}Pa$ for the Glacial-Transition, 10th Percentile Infiltration Condition, Representative Parameter Values, Northern and Southern Release Nodes

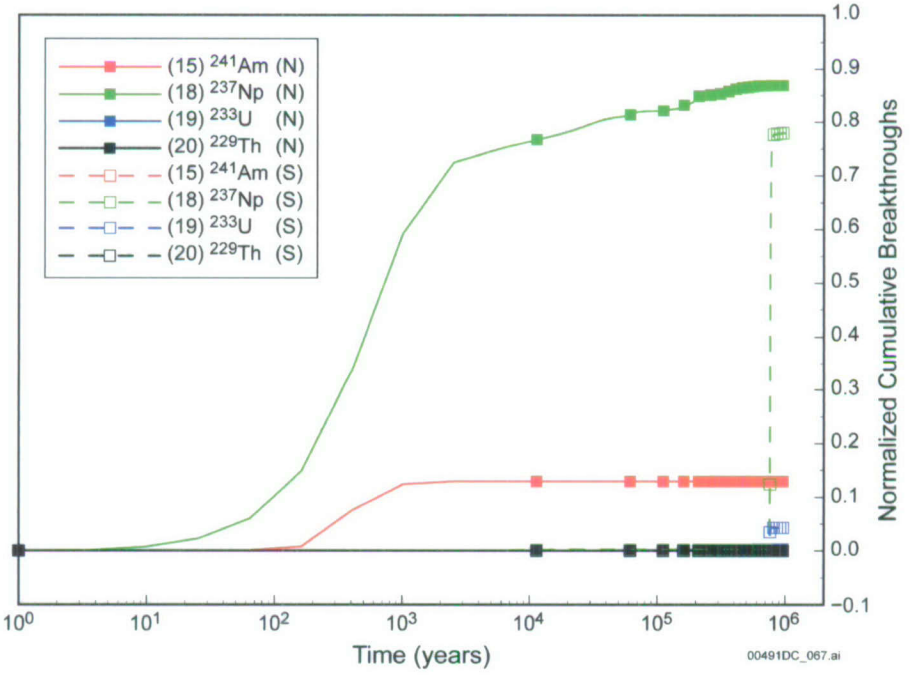

Output DTN: MO0705TRANSTAT.000.

Figure D.2-3. Normalized Cumulative Breakthrough Curves of Decay Chain $^{241}Am \rightarrow {}^{237}Np \rightarrow {}^{233}U \rightarrow {}^{229}Th$ for the Glacial-Transition, 10th Percentile Infiltration Condition, Representative Parameter Values, Northern and Southern Release Nodes

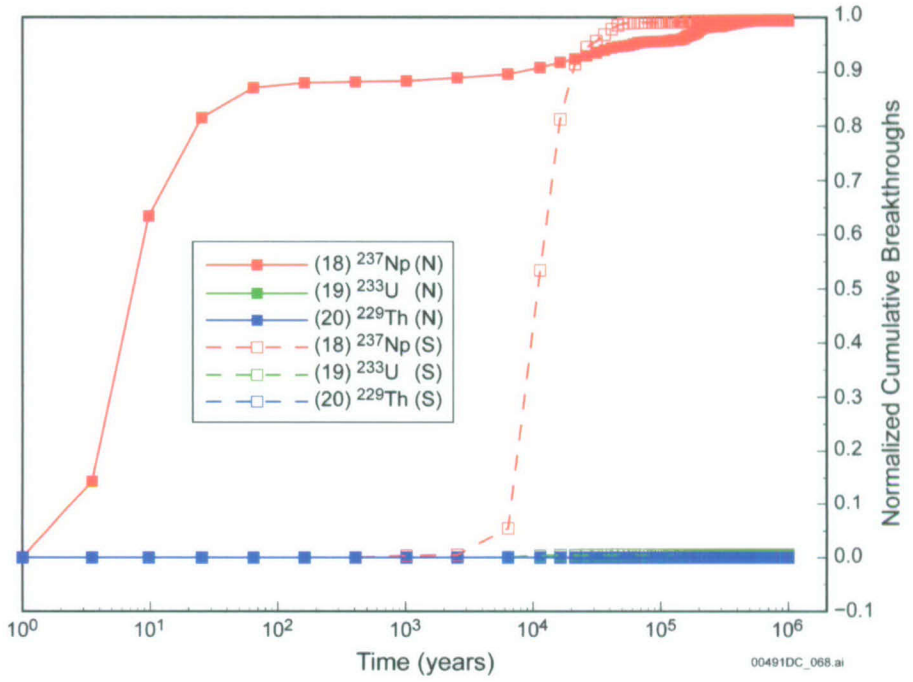

Output DTN: MO0705TRANSTAT.000.

Figure D.2-4. Normalized Cumulative Breakthrough Curves of Decay Chain $^{237}Np \rightarrow {}^{233}U \rightarrow {}^{229}Th$ for the Glacial-Transition, 10th Percentile Infiltration Condition, Representative Parameter Values, Northern and Southern Release Nodes

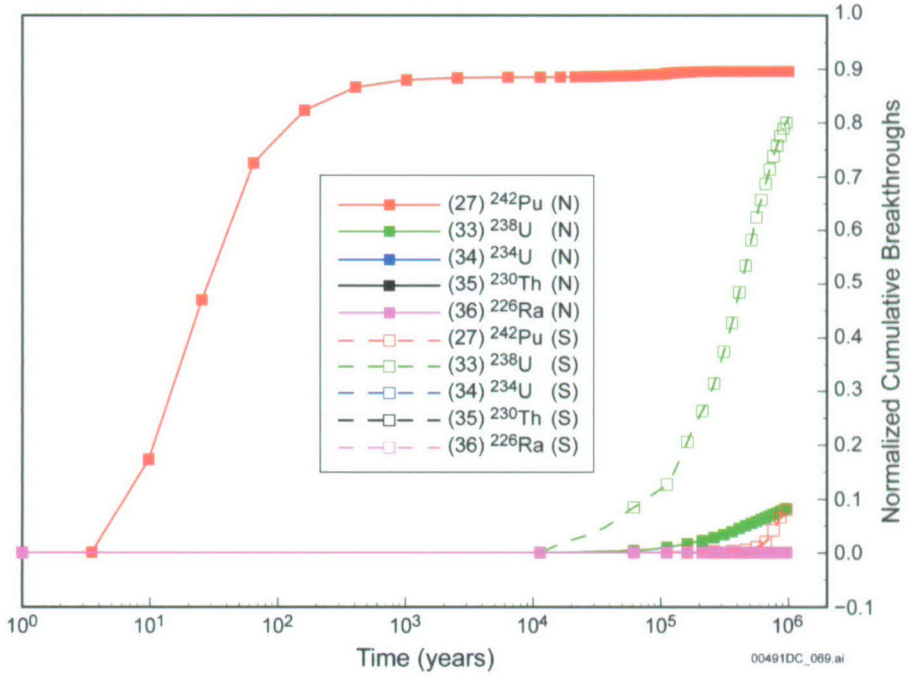

Output DTN: MO0705TRANSTAT.000.

Figure D.2-5. Normalized Cumulative Breakthrough Curves of Decay Chain $^{242}Pu \rightarrow {}^{238}U \rightarrow {}^{234}U \rightarrow {}^{230}Th \rightarrow {}^{226}Ra$ for the Glacial-Transition, 10th Percentile Infiltration Condition, Representative Parameter Values, Northern and Southern Release Nodes

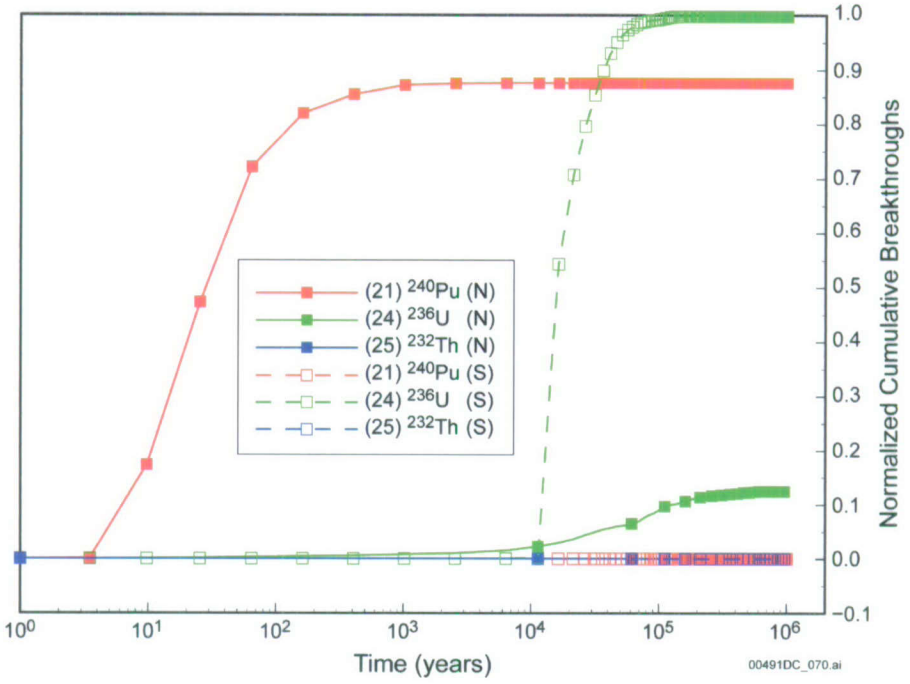

Output DTN: MO0705TRANSTAT.000.

Figure D.2-6. Normalized Cumulative Breakthrough Curves of Decay Chain $^{240}Pu \rightarrow {}^{236}U \rightarrow {}^{232}Th$ for the Glacial-Transition, 10th Percentile Infiltration Condition, Representative Parameter Values, Northern and Southern Release Nodes

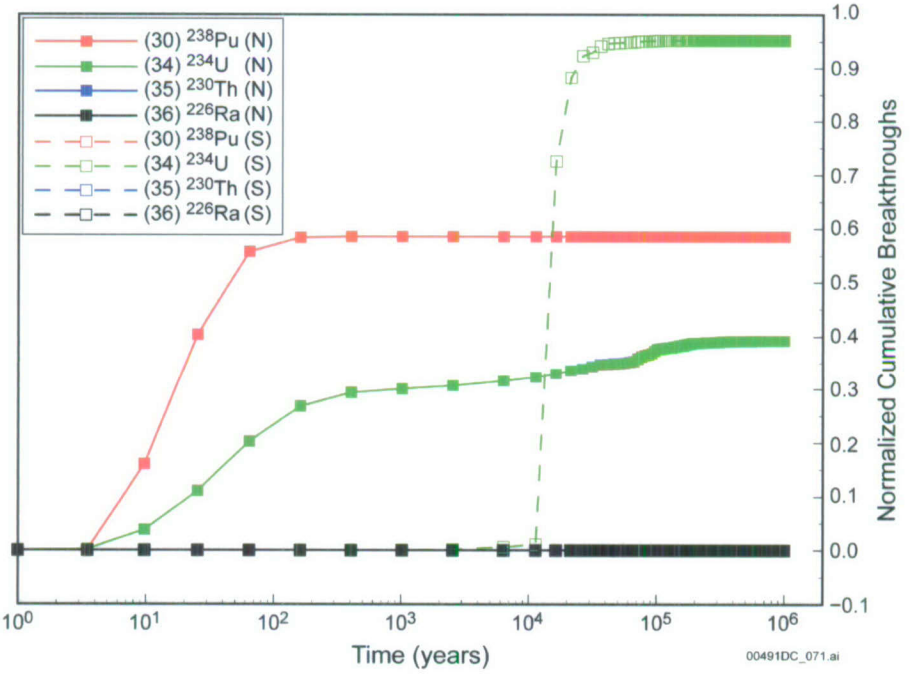

Output DTN: MO0705TRANSTAT.000.

Figure D.2-7. Normalized Cumulative Breakthrough Curves of Decay Chain $^{238}Pu \rightarrow {}^{234}U \rightarrow {}^{230}Th \rightarrow {}^{226}Ra$ for the Glacial-Transition, 10th Percentile Infiltration Condition, Representative Parameter Values, Northern and Southern Release Nodes

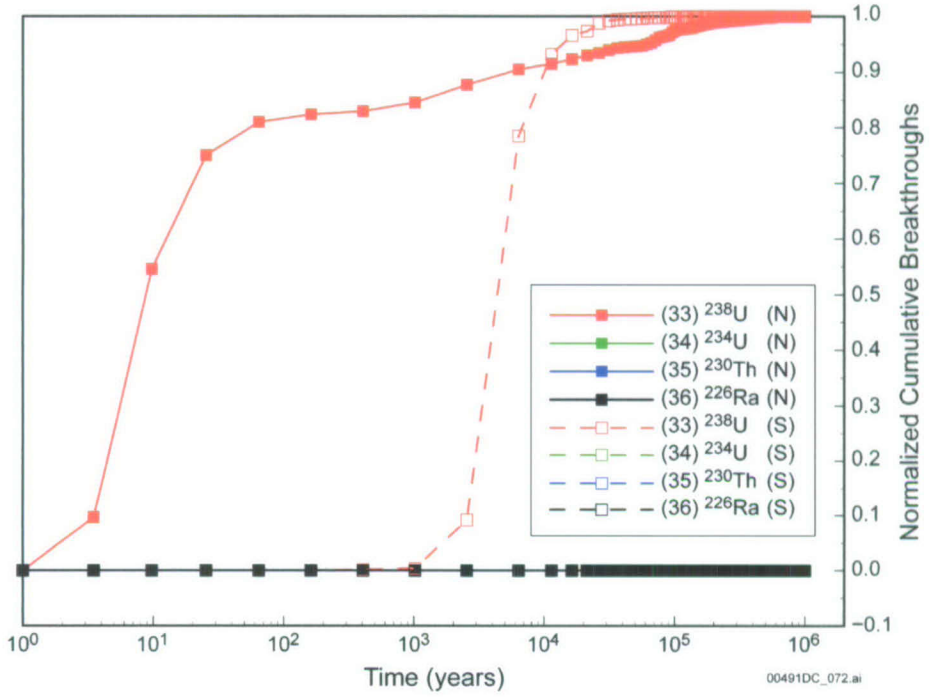

Output DTN: MO0705TRANSTAT.000.

Figure D.2-8. Normalized Cumulative Breakthrough Curves of Decay Chain $^{238}U \rightarrow {}^{234}U \rightarrow {}^{230}Th \rightarrow {}^{226}Ra$ for the Glacial-Transition, 10th Percentile Infiltration Condition, Representative Parameter Values, Northern and Southern Release Nodes

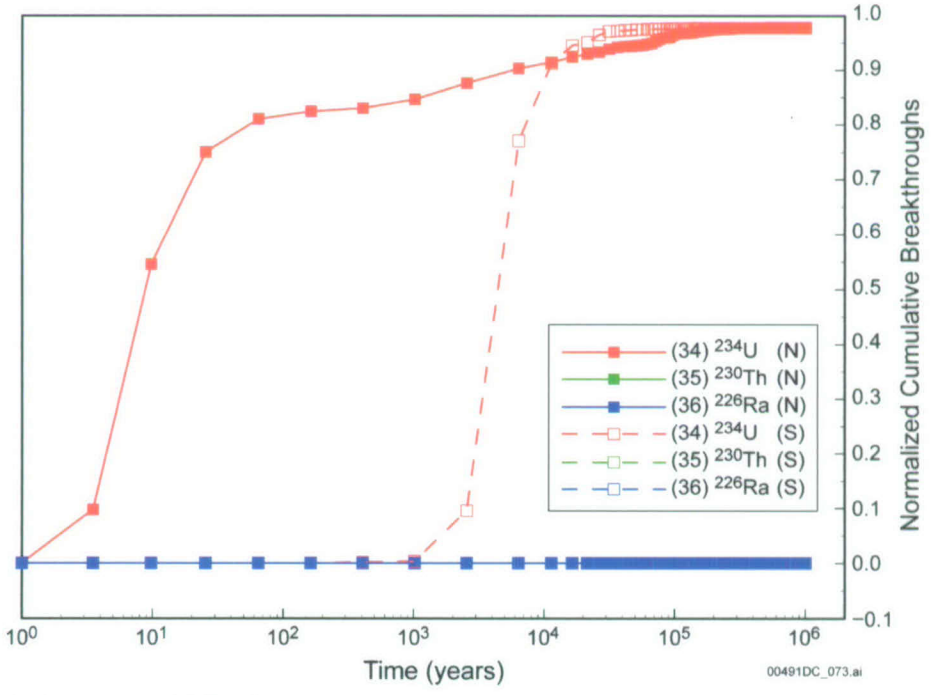

Output DTN: MO0705TRANSTAT.000.

Figure D.2-9. Normalized Cumulative Breakthrough Curves of Decay Chain $^{234}U \rightarrow {}^{230}Th \rightarrow {}^{226}Ra$ for the Glacial-Transition, 10th Percentile Infiltration Condition, Representative Parameter Values, Northern and Southern Release Nodes

INTENTIONALLY LEFT BLANK

Addendum Cover Page

Complete only applicable items.

QA: QA

1. Total Pages: 86

2. Addendum to (Title):
Particle Tracking Model and Abstraction of Transport Processes

3. DI (including Revision and Addendum No.):
MDL-NBS-HS-000020 REV 02 AD 02

	Printed Name	Signature	Date
4. Originator	Bruce Robinson		01/24/2008
5. Independent Technical Reviewer	Mel Marietta		1/24/08
6. Checker	Barry Lester		1/24/08
7. QCS/Lead Lab QA Reviewer	Sounia Kassabian-Darnell		01/24/08
8. Responsible Manager/Lead	Ming Zhu		1/24/08
9. Responsible Manager	Kathryn Knowles		1/24/08

12. Remarks

Change History

13. Revision and Addendum No.	14. Description of Change
REV02 AD 02	Illustrative model runs are presented for a different southern release location than the one used in AD 01, and with corrected input files for the colloid filtration model input. These changes are required to address CR-11572 and CR-11594.

CONTENTS

Page

ACRONYMS AND ABBREVIATIONS xi

1[b]. PURPOSE 1-1

2[b]. QUALITY ASSURANCE 2-1

3[b]. USE OF SOFTWARE 3-1
3.1[b] SOFTWARE TRACKED BY CONFIGURATION MANAGEMENT 3-1
3.2[b] EXEMPT SOFTWARE 3-1

4[b]. INPUTS 4-1
4.1[b] DIRECT INPUT 4-1
4.1.1[b] Unsaturated Zone Flow Parameters 4-1
4.1.2[b] Fracture Frequency and Fracture Porosity 4-1
4.1.3[b] Matrix Porosity 4-1
4.1.4[b] Matrix Diffusion Coefficient 4-1
4.1.5[b] Matrix Sorption Coefficient 4-1
4.1.6[b] Fracture Dispersivity 4-1
4.1.7[b] Radionuclide Sorption onto Colloids 4-1
4.1.8[b] Colloid Filtration and Size Exclusion 4-1
4.1.9[b] Colloid Retardation in Transport through Fractures 4-1
4.2[b] CRITERIA 4-1
4.3[b] CODES, STANDARDS, AND REGULATIONS 4-3

5[b]. ASSUMPTIONS 5-1

6[b]. MODEL DISCUSSION 6-1
6.1[b] MODELING OBJECTIVES AND APPROACH 6-1
6.2[b] FEATURES, EVENTS, AND PROCESSES INCLUDED IN THE MODEL 6-1
6.3[b] THE UNSATURATED ZONE TRANSPORT ABSTRACTION MODEL 6-1
6.4[b] THE NUMERICAL REPRESENTATION OF THE UNSATURATED ZONE TRANSPORT ABSTACTION MODEL 6-1
6.5[b] UNSATURATED ZONE TRANSPORT ABSTRACTION MODEL INPUTS 6-1
6.5.1[b] Pregenerated Flow Fields 6-1
6.5.2[b] Dispersivity 6-1
6.5.3[b] Matrix Porosity and Rock Density 6-1
6.5.4[b] Matrix Sorption Coefficient (mL/g) 6-1
6.5.5[b] Matrix Diffusion Coefficient (m^2/s) 6-2
6.5.5.1[b] Correlation between Tortuosity, Porosity, and Permeability 6-2

CONTENTS (Continued)

Page

6.5.5.2[b] Tortuosity for Unsaturated Media 6-2
6.5.5.3[b] Free-Water Diffusion Coefficients 6-2
6.5.5.4[b] Uncertainty Treatment for Matrix Diffusion Coefficient 6-2
6.5.6[b] Fracture Residual Saturation and Active Fracture Model Gamma Parameters (Unitless) 6-2
6.5.7[b] Fracture Porosity, Fracture Spacing (m), and Fracture Aperture (m) 6-2
6.5.8[b] Fracture Surface Retardation Factor (Unitless) 6-2
6.5.9[b] Colloid Filtration at Matrix Interface 6-2
6.5.10[b] Colloid Size Exclusion 6-2
6.5.11[b] Colloid-Size Distribution 6-2
6.5.12[b] Colloid Concentration and Colloid K_c 6-3
6.5.13[b] Fractions of Colloids Traveling Unretarded and Colloid Retardation Factor 6-3
6.5.14[b] Radionuclide Half-Lives (Years) and Daughter Products 6-3
6.5.15[b] Repository Radionuclide Release Bins 6-3
6.5.16[b] Radionuclide Collecting Bins at Unsaturated Zone/Saturated Zone Interface 6-3
6.6[b] REPRESENTATIVE-CASE MODEL 6-3
6.6.1[b] Overview 6-3
6.6.2[b] Representative-Case Model Results 6-3
6.6.2.1[b] Statistics of Travel Time and Exit Location 6-3
6.6.2.2[b] Radionuclide Breakthrough Curves 6-4
6.6.2.3[b] Fracture versus Matrix Release 6-9
6.6.3[b] Sensitivity to Flow Parameter Uncertainty 6-11
6.6.4[b] Sensitivity to AFM and Diffusion Parameter Uncertainty 6-11
6.7[b] EVALUATION OF ALTERNATIVE MODELS AND MODEL UNCERTAINTY 6-11
6.8[b] DESCRIPTION OF BARRIER CAPABILITY 6-11
6.8.1[b] Analyses of Barrier Capability 6-11
6.8.2[b] Barrier Capability Simulations and Uncertainty Analyses 6-11
6.8.2.1[b] Travel Time Statistics 6-11
6.8.2.2[b] Barrier Capability Analyses Using the Decay Fraction 6-23
6.9[b] OTHER TSPA IMPLEMENTATION CONSIDERATIONS 6-38

7[b]. VALIDATION 7-1
7.1[b] CONFIDENCE BUILDING DURING MODEL DEVELOPMENT TO ESTABLISH THE SCIENTIFIC BASIS AND ACCURACY FOR INTENDED USE 7-1
7.2[b] POSTDEVELOPMENT MODEL VALIDATION TO SUPPORT THE SCIENTIFIC BASIS OF THE MODEL 7-1

CONTENTS (Continued)

Page

7.2.1[b] Comparisons with Discrete Fracture Model 7-1
7.2.1.1[b] Test of Advective Transport between Continua 7-1
7.2.1.2[b] Comparisons with Diffusion for Fracture-Dominated Flow 7-1
7.2.1.3[b] Comparisons with Diffusion and Sorption for Intermediate Flow Case 7-1
7.2.1.4[b] Summary of Validation Tests for a Discrete Fracture Model 7-1
7.2.2[b] Comparison with the Dual-k and MINC Model Formulations on a Two-Dimensional Cross-Section Model 7-1
7.2.3[b] Comparison with T2R3D Process Model for the Three-Dimensional System 7-1
7.2.3.1[b] Comparisons of FEHM and T2R3D for the Dual-k Conceptual Model 7-1
7.2.3.2[b] Influence of Diffusion Coefficient and f/m Interaction Alternative Conceptual Model 7-2
7.2.3.3[b] Tests of the Active Fracture Model Implementation 7-2
7.3[b] SUMMARY OF VALIDATION ACTIVITIES 7-2

8[b]. CONCLUSIONS 8-1
8.1[b] SUMMARY OF MODELING ACTIVITY 8-1
8.2[b] MODEL OUTPUTS 8-1
8.2.1[b] Developed Output 8-1
8.2.2[b] Other Outputs 8-1
8.3[b] HOW THE APPLICABLE ACCEPTANCE CRITERIA ARE ADDRESSED 8-1

9[b]. INPUTS AND REFERENCES 9-1
9.1[b] DOCUMENTS CITED 9-1
9.2[b] CODES, STANDARDS, REGULATIONS, AND PROCEDURES 9-1
9.3[b] SOURCE DATA, LISTED BY DATA TRACKING NUMBER 9-1
9.4[b] OUTPUT DATA, LISTED BY DATA TRACKING NUMBER 9-1
9.5[b] SOFTWARE CODES 9-1

APPENDIX A[b]: MATRIX DIFFUSION COEFFICIENTS A-1

APPENDIX B[b]: DERIVATION OF WATER TABLE COLLECTING BINS B-1

APPENDIX C[b]: DERIVATION OF FRACTURE–MATRIX INTERACTION SUBMODEL AND GENERATION OF TRANSFER FUNCTIONS C-1

APPENDIX D[b]: SUPPLEMENTARY UNSATURATED ZONE TRANSPORT SIMULATION RESULTS D-1

INTENTIONALLY LEFT BLANK

FIGURES

Page

6.6.2-1[b]. Contour Maps of (a) the Minimum Travel Time, (b) the Mean Travel Time, and (c) the Maximum Travel Time for Particles Released at All Repository Nodes under Glacial-Transition, 10th Percentile Infiltration Scenario, and Conservative Species without Decay and Matrix Diffusion 6-4

6.6.2-5[b]. Normalized Cumulative Breakthrough Curves of 14 Radionuclides with Simple Decay for the Glacial-Transition 10th Percentile Infiltration Condition and Representative Parameter Values 6-6

6.6.2-6[b]. Normalized Cumulative Breakthrough Curves of Six Irreversible Fast Colloids and Six Irreversible Slow Colloids for the Glacial-Transition 10th Percentile Infiltration Condition and Representative Parameter Values 6-7

6.6.2-7[b]. Normalized Cumulative Breakthrough Curves of Four Radionuclides (^{235}U, ^{233}U, ^{236}U, and ^{230}Th) with One Decay Chain for the Glacial-Transition 10th Percentile Infiltration Condition and Representative Parameter Values 6-8

6.6.2-8[b]. Comparison of Normalized Cumulative Breakthrough Curves of ^{99}Tc for Particles Released at Fracture Node or Matrix Node for the Glacial-Transition, 10th Percentile Infiltration Scenario, Representative Parameter Values 6-10

6.8.2-1[b]. Comparison of Mean Travel Time of ^{99}Tc as a Function of Matrix Diffusion Coefficient under Glacial-Transition Climate Conditions for the dual-k Model 6-12

6.8.2-2[b]. Comparison of Mean Travel Time of ^{99}Tc as a Function of Matrix Diffusion Coefficient under Glacial-Transition Climate Conditions for the DFM 6-13

6.8.2-3[b]. Mean Travel Time of ^{237}Np as a Function of Matrix Diffusion Coefficient and Sorption Coefficient for the Glacial-Transition Climate Condition, dual-k Model, Northern Release Location 6-15

6.8.2-4[b]. Mean Travel Time of ^{237}Np as a Function of Matrix Diffusion Coefficient and Sorption Coefficient for the Glacial-Transition Climate Condition, dual-k Model, Southern Release Location 6-16

6.8.2-5[b]. Mean Travel Time of ^{237}Np as a Function of Matrix Diffusion Coefficient and Sorption Coefficient for the Glacial-Transition Climate Condition, DFM, Northern Release Location 6-17

6.8.2-6[b]. Mean Travel Time of ^{237}Np as a Function of Matrix Diffusion Coefficient and Sorption Coefficient for the Glacial-Transition Climate Condition, DFM, Southern Release Location 6-18

6.8.2-7[b]. Mean Travel Time of ^{240}Pu as a Function of Matrix Diffusion Coefficient and Sorption Coefficient for the Glacial-Transition Climate Condition, dual-k Model, Northern Release Location 6-19

6.8.2-8[b]. Mean Travel Time of ^{240}Pu as a Function of Matrix Diffusion Coefficient and Sorption Coefficient for the Glacial-Transition Climate Condition, dual-k Model, Southern Release Location 6-20

FIGURES (Continued)

Page

6.8.2-9[b]. Mean Travel Time of ^{240}Pu as a Function of Matrix Diffusion Coefficient and Sorption Coefficient for the Glacial-Transition Climate Condition, DFM, Northern Release Location 6-21

6.8.2-10[b]. Mean Travel Time of ^{240}Pu as a Function of Matrix Diffusion Coefficient and Sorption Coefficient for the Glacial-Transition Climate Condition, DFM, Southern Release Location 6-22

6.8.2-11[b]. Normalized ^{99}Tc Concentration (Decay Fraction, Computed from Travel Time Distributions) as a Function of Matrix Diffusion Coefficient for Glacial-Transition Climate Condition, dual-k Model, (a) Northern Release Location, (b) Southern Release Location 6-24

6.8.2-12[b]. Normalized ^{99}Tc Concentration (Decay Fraction, Computed from Travel Time Distributions) as a Function of Matrix Diffusion Coefficient for Glacial-Transition Climate Condition, DFM, (a) Northern Release Location, (b) Southern Release Location 6-25

6.8.2-13[b]. Normalized ^{14}C Concentration (Decay Fraction, Computed from Travel Time Distributions) as a Function of Matrix Diffusion Coefficient for Glacial-Transition Climate Condition, dual-k Model, (a) Northern Release Location, (b) Southern Release Location 6-26

6.8.2-14[b]. Normalized ^{14}C Concentration (Decay Fraction, Computed from Travel Time Distributions) as a Function of Matrix Diffusion Coefficient for Glacial-Transition Climate Condition, DFM, (a) Northern Release Location, (b) Southern Release Location 6-27

6.8.2-15[b]. Normalized ^{237}Np Concentration (Decay Fraction, Computed from Travel Time Distributions) as a Function of Matrix Diffusion Coefficient and Sorption Coefficient for the Glacial-Transition Climate Conditions, dual-k Model, Northern Release Location 6-28

6.8.2-16[b]. Normalized ^{237}Np Concentration (Decay Fraction, Computed from Travel Time Distributions) as a Function of Matrix Diffusion Coefficient and Sorption Coefficient for the Glacial-Transition Climate Conditions, dual-k Model, Southern Release Location 6-29

6.8.2-17[b]. Normalized ^{237}Np Concentration (Decay Fraction, Computed from Travel Time Distributions) as a Function of Matrix Diffusion Coefficient and Sorption Coefficient for the Glacial-Transition Climate Conditions, DFM, Northern Release Location 6-30

6.8.2-18[b]. Normalized ^{237}Np Concentration (Decay Fraction, Computed from Travel Time Distributions) as a Function of Matrix Diffusion Coefficient and Sorption Coefficient for the Glacial-Transition Climate Conditions, DFM, Southern Release Location 6-31

6.8.2-19[b]. Normalized ^{240}Pu Concentration (Decay Fraction, Computed from Travel Time Distributions) as a Function of Matrix Diffusion Coefficient and Sorption Coefficient for the Glacial-Transition Climate Conditions, dual-k Model, Northern Release Location 6-33

FIGURES (Continued)

Page

6.8.2-20[b]. Normalized ^{240}Pu Concentration (Decay Fraction, Computed from Travel Time Distributions) as a Function of Matrix Diffusion Coefficient and Sorption Coefficient for the Glacial-Transition Climate Conditions, dual-k Model, Southern Release Location 6-34

6.8.2-21[b]. Normalized ^{240}Pu Concentration (Decay Fraction, Computed from Travel Time Distributions) as a Function of Matrix Diffusion Coefficient and Sorption Coefficient for the Glacial-Transition Climate Conditions, DFM, Northern Release Location 6-35

6.8.2-22[b]. Normalized ^{240}Pu Concentration (Decay Fraction, Computed from Travel Time Distributions) as a Function of Matrix Diffusion Coefficient and Sorption Coefficient for the Glacial-Transition Climate Conditions, DFM, Southern Release Location 6-36

6.8.2-23[b]. Mean Travel Time of $Ic^{240}Pu$ as a Function of Colloid Retardation Factor for the Glacial-Transition Climate Condition 6-37

6.8.2-24[b]. Normalized Concentration of $Ic^{240}Pu$ (Decay Fraction, Computed from Travel Time Distributions) as a Function of Colloid Retardation Factor for the Glacial-Transition Climate Condition 6-38

D.2-1[b]. Normalized Cumulative Breakthrough Curves of Decay Chain $^{243}Am \rightarrow {}^{239}Pu \rightarrow {}^{235}U \rightarrow {}^{231}Pa$ for the Glacial-Transition, 10th Percentile Infiltration Condition, Representative Parameter Values, Northern and Southern Release Nodes D-1

D.2-2[b]. Normalized Cumulative Breakthrough Curves of Decay Chain $^{239}Pu \rightarrow {}^{235}U \rightarrow {}^{231}Pa$ for the Glacial-Transition, 10th Percentile Infiltration Condition, Representative Parameter Values, Northern and Southern Release Nodes D-2

D.2-3[b]. Normalized Cumulative Breakthrough Curves of Decay Chain $^{241}Am \rightarrow {}^{237}Np \rightarrow {}^{233}U \rightarrow {}^{229}Th$ for the Glacial-Transition, 10th Percentile Infiltration Condition, Representative Parameter Values, Northern and Southern Release Nodes D-3

D.2-4[b]. Normalized Cumulative Breakthrough Curves of Decay Chain $^{237}Np \rightarrow {}^{233}U \rightarrow {}^{229}Th$ for the Glacial-Transition, 10th Percentile Infiltration Condition, Representative Parameter Values, Northern and Southern Release Nodes D-4

D.2-5[b]. Normalized Cumulative Breakthrough Curves of Decay Chain $^{242}Pu \rightarrow {}^{238}U \rightarrow {}^{234}U \rightarrow {}^{230}Th \rightarrow {}^{226}Ra$ for the Glacial-Transition, 10th Percentile Infiltration Condition, Representative Parameter Values, Northern and Southern Release Nodes D-5

D.2-6[b]. Normalized Cumulative Breakthrough Curves of Decay Chain $^{240}Pu \rightarrow {}^{236}U \rightarrow {}^{232}Th$ for the Glacial-Transition, 10th Percentile Infiltration Condition, Representative Parameter Values, Northern and Southern Release Nodes D-6

FIGURES (Continued)

Page

D.2-7[b]. Normalized Cumulative Breakthrough Curves of Decay Chain $^{238}Pu \rightarrow {}^{234}U \rightarrow {}^{230}Th \rightarrow {}^{226}Ra$ for the Glacial-Transition, 10th Percentile Infiltration Condition, Representative Parameter Values, Northern and Southern Release Nodes D-7

D.2-8[b]. Normalized Cumulative Breakthrough Curves of Decay Chain $^{238}U \rightarrow {}^{234}U \rightarrow {}^{230}Th \rightarrow {}^{226}Ra$ for the Glacial-Transition, 10th Percentile Infiltration Condition, Representative Parameter Values, Northern and Southern Release Nodes D-8

D.2-9[b]. Normalized Cumulative Breakthrough Curves of Decay Chain $^{234}U \rightarrow {}^{230}Th \rightarrow {}^{226}Ra$ for the Glacial-Transition, 10th Percentile Infiltration Condition, Representative Parameter Values, Northern and Southern Release Nodes D-9

ACRONYMS AND ABBREVIATIONS

AFM	active fracture model
CR	condition report
DFM	discrete fracture model
dual-k	dual permeability
FEPs	features, events, and processes
TSPA	total system performance assessment
TSw	Topopah Spring welded unit
TWP	technical work plan
UZ	unsaturated zone

INTENTIONALLY LEFT BLANK

1[b]. PURPOSE

The purpose of this addendum (Addendum 02) is to document new model simulations for the unsaturated zone (UZ) radionuclide transport abstraction model, performed to address two condition reports (CRs): CR-11572, Issue with Decay Chain Transport in UZ Transport Abstraction Model, and CR-11594, Issue with Colloid Infiltration Input in MDL-NBS-HS-000020. CR-11572 deals with the manner in which decay chains perform in the UZ transport abstraction model. None of the model parameters and distributions of the UZ transport abstraction model being used in the total system performance assessment (TSPA) model are changed in this addendum. The only changes to analyses performed in Addendum 01 of the parent report are to certain illustrative calculations demonstrating the behavior of the UZ barrier. Specifically, a different release location was selected for radionuclides to illustrate the behavior for releases in the southern portion of the repository to avoid placing the particles directly in a node designated as a fault node. In this condition report, it was noted that due to the way fault nodes are parameterized, particle placement in fault nodes leads to anomalous model behavior for some decay chains. As described more fully in Section 4.2[b], this situation is caused by the manner in which the code behaves for the fault nodes, which are treated as a continuum model with low porosity and sorption. A small percentage of the release points (about 7%) are fault nodes, which led to an unrepresentative set of model simulations in Addendum 01. In order to illustrate the behavior of the model for a more representative situation, a different release location was selected and used in this addendum. For CR-11594, the error identified was in the computer input files for some of the illustrative calculations of unsaturated zone behavior presented in Addendum 01 of the parent report. The error incorrectly set a model input flag for some of the colloidal species, resulting in some of the species inadvertently not including colloid filtration. This error was not propagated to the TSPA model so the corrections affect only Addendum 01 of the parent report. The results in the current addendum now properly reflect the behavior of the unsaturated zone simulated by the TSPA model.

The activities in this addendum are based on work plans outlined in *Technical Work Plan for: Unsaturated Zone Flow, Drift Seepage and Unsaturated Zone Transport Modeling* (BSC 2006 [DIRS 177465]). Although the exact set of calculations is not mentioned in the technical work plan (TWP), the analyses presented herein are called for by the following items listed in the TWP (BSC 2006 [DIRS 177465] Section 1, Items 8 and 11):

- *Revise representative case analyses, sensitivity analyses, and validation cases to reflect software modifications and model and parameter changes.* Representative-case analyses are presented in Section 6.6 and sensitivity analyses are presented in Section 6.8.

- *Provide technical support to Post Closure Activities in analyses, checking, and review of administrative change notices (ACNs) in response to CRs.* The analyses provided herein are performed to address CR-11572 and CR-11594.

Based on this list of activities, deviations from the TWP include the following items:

- This work is documented as an addendum rather than a revision. This deviation has no impact on the model or associated analyses.

- The TWP (BSC 2006 [DIRS 177465]) referred to a particular version of the FEHM computer code, which has changed subsequent to the writing of the TWP. This represents a change to the code numbering only, rather than a meaningful change to the content of the work. This change, conducted in advance of the writing of Addendum 01 of the parent report, does not change the qualification status of the software. Thus, this deviation has no impact on the model or associated analyses.

This addendum contains updated modeling results relative to Revision 02 of the parent report and Addendum 01 of the same report. The documentation is structured such that this addendum contains only information that is new or has been updated and thus supersedes information presented in the parent report or Addendum 01. Information on topics that are not addressed in this addendum remains unchanged from the parent report and Addendum 01 of the parent report. Consequently, a complete understanding of the technical work associated with this report requires access to this addendum, the parent report, and Addendum 01 of the parent report. Section numbers, table numbers, and figure numbers (and associated cross-references) within this addendum contain the designator "[b]" to distinguish them from the numbers in the previous revisions. Cross-references within this report that do not contain the designator "[b]" refer to sections, tables, or figures in the parent report or Addendum 01 of the parent report.

2[b]. QUALITY ASSURANCE

No change.

INTENTIONALLY LEFT BLANK

3[b]. USE OF SOFTWARE

3.1[b] SOFTWARE TRACKED BY CONFIGURATION MANAGEMENT

No change.

3.2[b] EXEMPT SOFTWARE

No change.

INTENTIONALLY LEFT BLANK

4[b]. INPUTS

4.1[b] DIRECT INPUT

No change.

4.1.1[b] Unsaturated Zone Flow Parameters

No change.

4.1.2[b] Fracture Frequency and Fracture Porosity

No change.

4.1.3[b] Matrix Porosity

No change.

4.1.4[b] Matrix Diffusion Coefficient

No change.

4.1.5[b] Matrix Sorption Coefficient

No change.

4.1.6[b] Fracture Dispersivity

No change.

4.1.7[b] Radionuclide Sorption onto Colloids

No change.

4.1.8[b] Colloid Filtration and Size Exclusion

No change.

4.1.9[b] Colloid Retardation in Transport through Fractures

No change.

4.2[b] CRITERIA

There is no change to the list of acceptance criteria that apply to the parent report, Addendum 01, or this addendum. Section 8.3 of Addendum 01 provides an updated accounting of how the work documented in this addendum addresses the acceptance criteria; there is no change to this description in the current addendum. The work documented in this addendum addresses issues identified in two condition reports, CR-11572 (Issue with Decay Chain Transport in UZ

Transport Abstraction Model) and CR-11594 (Issue with Colloid Infiltration Input in MDL-NBS-HS-00020). CR-11572 focuses on the manner in which decay chains perform in the UZ transport abstraction model. In Addendum 01 of the parent report, radionuclide transport of simple decay species and decay chains are simulated for releases across the repository footprint. Illustrative calculations are also performed at two specific release locations: one in the northern repository region, and one in the southern repository region. Some anomalous behavior was being simulated for certain daughter products of decay chains for the southern release location used in those simulations. For example, in Appendix D.2, Figure D.2-1 of Addendum 01 of the parent report, the breakthrough of ^{235}U from the southern release location resulting from input as ^{243}Am is much later in time than for the same release location when ^{235}U is input directly into the model, or if it is input as ^{239}Pu, the intermediate nuclide between ^{243}Am and ^{235}U. One would not expect this delay in the breakthrough curve. Note that the corresponding issue does not occur for the northern release location; here the results are reasonable. One other decay chain simulation is affected as well: ^{237}Np in Figure D.2-3 of Addendum 01 of the parent report, when the source is ^{241}Am. The parent species, as well as simple decay species, are unaffected, and the results are reasonable.

A closer look at the simulation for the southern release location indicates that the node selected for the southern release location is within a zone designated in the model as a fault node. In these zones, the transport properties are parameterized by assuming that the fracture continuum is a continuum with fracture-like properties but no diffusion into the rock matrix. This set of circumstances appears to lead to the anomalously long travel time of the daughter species to the water table. For information purposes, note that of the 560 repository nodes, 39 are fault nodes (about 7%) in which this behavior might be expected to occur. The anomalous behavior does not occur for situations in which the daughter is released directly: the issue appears only for releases into a fault node, and for this circumstance only for the daughter species when the mass is injected as the parent species. In addition, the northern release location, which is not at a node parameterized as a fault, exhibits reasonable behavior for both simple decay species and all decay chains, including the ones being cited here as problematic. To address CR-11572, this addendum presents new results for a different southern release location, one not identified as a fault node in the model.

In CR-11594, an issue was identified with the input in the FEHM file that controls the species that are simulated as colloidal species in Addendum 01 of the parent report. In the file *fehm_tspa_template.dat* in output DTN: MO0704PAFEHMBR.001, there is an array of input flags for the so-called "itfc" macro in the input file that is not correctly set. The input designates, for each species, whether or not the filtration model option for colloidal species is invoked (1 means filtration is invoked, 0 means it is not invoked). This input is set for all species, but is only a meaningful input for the so-called "Ic" and "If" colloidal species in the particle tracking model. It was found that in output DTN: MO0704PAFEHMBR.001, this input is an array of 43 values, rather than the 39 values required for the current version of this model. The discrepancy stems from a previous iteration in the model development when four additional colloidal species were temporarily added to the input files. When it was decided that these species were not needed, they were removed from the main particle tracking input file (*fehm_tspa.mptr*), but this array in *fehm_tspa_template.dat* was incorrectly left as the 43-species version.

Note that this error was not propagated into the TSPA model calculations from the parent report or this addendum. Therefore, there is no impact of this error to any of the model calculations in the TSPA model. However, this incorrect input was applied to illustrative calculations presented in Addendum 01 of the parent report, and compiled in output DTN: MO0705TRANSTAT.000. In those calculations, due to the use of the old input array, four colloidal species are inadvertently set to not invoke the colloid filtration model. These species are: $If^{240}Pu$, $Ic^{242}Pu$, $If^{242}Pu$, $If^{238}Pu$. All aqueous species are unaffected, and the eight remaining "Ic" and "If" species are properly assigned to undergo filtration. This error principally affects Figure 6.6.2-6 of Addendum 01. For the southern release location (bottom plot of that figure), the three breakthrough curves that rise to the level of 0.8 or above will, after correcting the error, plateau at lower values (see Figure 6.6.2-6[b] of the current addendum), similar to the majority of the other species in the plot. One other species, $If^{238}Pu$, plateaus at a low value due to decay, but correcting the error will reduce it still further. The simulation for the top plot also has this problem, but the effects are much more muted. For this release location, there is generally a lack of filtration due to the fact that the pathways are dominated by fracture transport, and the filtration process only occurs at the interfaces of matrix units. Thus, even though the error is present for the northern release simulation, its impact is minor. Even though the error has no impact for many species, and a minor impact for many others, the flaw in the input file was present for most of the calculations in Addendum 01 of the parent report. Therefore, the process of correcting the error was to purge it from all input files in output DTN: MO0705TRANSTAT.000. This effect, plus the desire to choose a different southern release point to address CR-11572, resulted in the rerunning of many more simulations than those that were actually affected significantly by the error.

4.3[b] CODES, STANDARDS, AND REGULATIONS

No change.

INTENTIONALLY LEFT BLANK

5[b]. ASSUMPTIONS

No change.

INTENTIONALLY LEFT BLANK

6[b]. MODEL DISCUSSION

6.1[b] MODELING OBJECTIVES AND APPROACH

No change.

6.2[b] FEATURES, EVENTS, AND PROCESSES INCLUDED IN THE MODEL

This section has the following changes from the parent report:

The list of features, events, and processes (FEPs) relevant to this report is now documented in DTN: MO0706SPAFEPLA.001 [DIRS 181613] (file: *FEPs_be.mdb*). In addition, FEP 2.2.09.01.0B (Microbial activity in the UZ) is now classified as excluded, rather than included. There are no other changes to this section.

6.3[b] THE UNSATURATED ZONE TRANSPORT ABSTRACTION MODEL

No change.

6.4[b] THE NUMERICAL REPRESENTATION OF THE UNSATURATED ZONE TRANSPORT ABSTACTION MODEL

No change.

6.5[b] UNSATURATED ZONE TRANSPORT ABSTRACTION MODEL INPUTS

In this addendum, the introductory material of this section is unchanged from the parent report or Addendum 01. In this section, changes from the parent report and Addendum 01 are identified below the individual third-level heading.

6.5.1[b] Pregenerated Flow Fields

No change.

6.5.2[b] Dispersivity

No change.

6.5.3[b] Matrix Porosity and Rock Density

No change.

6.5.4[b] Matrix Sorption Coefficient (mL/g)

No change.

6.5.5[b] Matrix Diffusion Coefficient (m^2/s)

No change to the existing discussion in Addendum 01 of the parent report. However, for clarity and transparency, in the current addendum it is noted that the matrix diffusion model is applied to all nodes except those designated as fault nodes. The fracture continuum within the fault zone is treated as a continuum with low porosity and no matrix diffusion, to accentuate the fracture transport characteristics prevalent in faults in the unsaturated zone. In addition, sorption within this continuum is assumed.

6.5.5.1[b] Correlation between Tortuosity, Porosity, and Permeability

No change.

6.5.5.2[b] Tortuosity for Unsaturated Media

No change.

6.5.5.3[b] Free-Water Diffusion Coefficients

No change.

6.5.5.4[b] Uncertainty Treatment for Matrix Diffusion Coefficient

No change.

6.5.6[b] Fracture Residual Saturation and Active Fracture Model Gamma Parameters (Unitless)

No change.

6.5.7[b] Fracture Porosity, Fracture Spacing (m), and Fracture Aperture (m)

No change.

6.5.8[b] Fracture Surface Retardation Factor (Unitless)

No change.

6.5.9[b] Colloid Filtration at Matrix Interface

No change.

6.5.10[b] Colloid Size Exclusion

No change.

6.5.11[b] Colloid-Size Distribution

No change.

6.5.12[b] Colloid Concentration and Colloid K_c

No change.

6.5.13[b] Fractions of Colloids Traveling Unretarded and Colloid Retardation Factor

No change.

6.5.14[b] Radionuclide Half-Lives (Years) and Daughter Products

No change.

6.5.15[b] Repository Radionuclide Release Bins

No change.

6.5.16[b] Radionuclide Collecting Bins at Unsaturated Zone/Saturated Zone Interface

No change.

6.6[b] REPRESENTATIVE-CASE MODEL

In this section and subsections, there was a significant update to the corresponding section in the parent report that necessitated a renumbering of the tables, figures, and equations in Addendum 01. The numbering convention within this addendum section adheres to that of Addendum 01 of the parent report.

6.6.1[b] Overview

The description of model runs provided in Addendum 01 is applicable for this addendum. The model runs in this addendum differ from Addendum 01 only in the location of the southern release location, and in providing updated figures for model input files, which eliminates the input error described in CR-11594. A different location was selected to avoid difficulties that arise due to the injection of particles at a node designated as a fault zone. In Addendum 01 of the parent report, a fault node was selected for the southern release location. To provide a more representative set of results for the southern release location that avoids the problem described earlier, a different node was selected. Therefore, in the results that follow, new figures are provided in which this new southern release location is used. When the accompanying text discussing these figures is unchanged from the previous addendum, this is noted, rather than reproducing the text in the current addendum.

6.6.2[b] Representative-Case Model Results

6.6.2.1[b] Statistics of Travel Time and Exit Location

No change to the text in this section. Note that the results of Figure 6.6.2-1[b] are unchanged from those presented in Figure 6.6.2-1 of Addendum 01, but the point plotted to locate the southern release location has changed in the current addendum. To visualize the location of the southern release location for Addendum 01, see Figure 6.6.2-1 of Addendum 01.

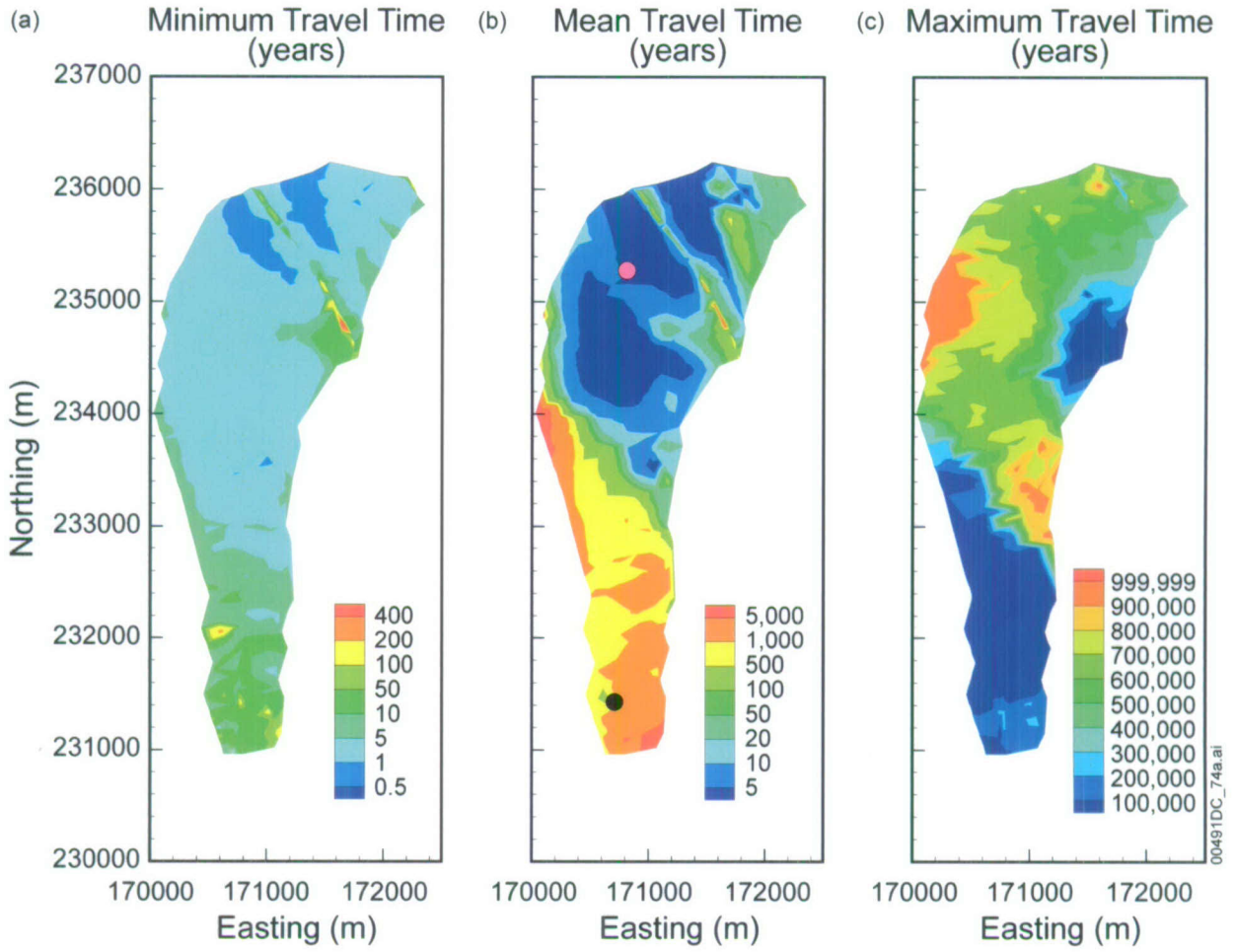

Output DTN: MO0705TRANSTAT.000, files: *MO0705TRANSTAT.000\TravelTime_2_WT\gt10wtrise\time_meanVar.wmf* and *MO0705TRANSTAT.000\TravelTime_2_WT\gt10wtrise\time_mean\time_minmax.wmf.*

NOTE: The pink (northern) and black (southern) points in (b) are the individual release locations used in this study.

Figure 6.6.2-1[b]. Contour Maps of (a) the Minimum Travel Time, (b) the Mean Travel Time, and (c) the Maximum Travel Time for Particles Released at All Repository Nodes under Glacial-Transition, 10th Percentile Infiltration Scenario, and Conservative Species without Decay and Matrix Diffusion

6.6.2.2[b] Radionuclide Breakthrough Curves

The plots for the southern release location in this section and subsequent subsections have been rerun in this addendum using a different node location (grid cell number 104159), located at Nevada State Plane coordinates (m) (170710, 231430). This node is in the same percolation bin (Bin 3) as the node selected in the previous addendum, but is a node not designated as a fault node. By selecting this node, the problems identified in CR-11572 are avoided for these illustrative simulations. In addition, the error identified in CR-11594 associated with the input for the colloidal species for some of the model runs is corrected in these runs. These errors had no effect on aqueous species. For the filtration submodel for the colloidal species, the new

model runs are presented for the corrected input files. Since this error was not propagated to the TSPA model, the current figures properly reflect the behavior of the TSPA model.

Figure 6.6.2-5[b] shows the normalized cumulative breakthrough curves for all species modeled as simple decay radionuclides (^{14}C, ^{135}Cs, ^{137}Cs, ^{129}I, ^{90}Sr, ^{99}Tc, ^{231}Pa, ^{229}Th, ^{232}Th, ^{232}U, ^{226}Ra, ^{36}Cl, ^{79}Se, and ^{126}Sn). The upper figure presents breakthrough curves for the northern release location, while the lower figure shows the breakthrough curves for the southern release location. These results are different than the corresponding results in Addendum 01 for the southern location, but the conclusions reached are still valid.

Comparisons of breakthrough curves for 12 colloidal species (Ic and If species of ^{243}Am, ^{239}Pu, ^{241}Am, ^{240}Pu, ^{242}Pu, and ^{238}Pu) released from both the locations are illustrated in Figure 6.6.2-6[b]. The simulation results show that, as expected, radionuclides that are irreversibly attached to "fast" colloids (If species), which are not affected by matrix diffusion and retardation, have the shortest breakthrough times. At the northern location, within about 10 years after release, over 90% of the irreversible fast colloids travel through the unsaturated zone. Radionuclides that are irreversibly attached to "slow" colloids (Ic species), which undergo retardation due to colloid attachment/detachment processes, move more slowly than their corresponding fast colloid counterparts. The transport time of the irreversible slow colloids depends on the colloid retardation factor, a parameter that is explored more fully in Section 6.8.2[b]. Compared to the fast colloids released at the northern location, the first arrival times for the southern release location are about one order of magnitude larger, due to the thickness of the interval of unfractured rock governed by slower matrix transport. The cumulative breakthroughs for most of these irreversible fast colloids in the northern location are close to unity (except for $Ic^{238}Pu$ and $Ic^{241}Am$), whereas for the southern location, the cumulative breakthrough is significantly reduced for all radionuclides due to a combination of filtration at the interfaces of matrix units and radioactive decay. The filtration mechanism is more pronounced for the southern release location due to the prevalence of matrix-dominated flow in the south. In summary, most of the Ic and If colloidal species have very limited reduction due to decay in the unsaturated zone from the northern release location, whereas a larger proportion of the radionuclides decay or are subject to colloid filtration in the unsaturated zone before reaching the water table for the southern release location.

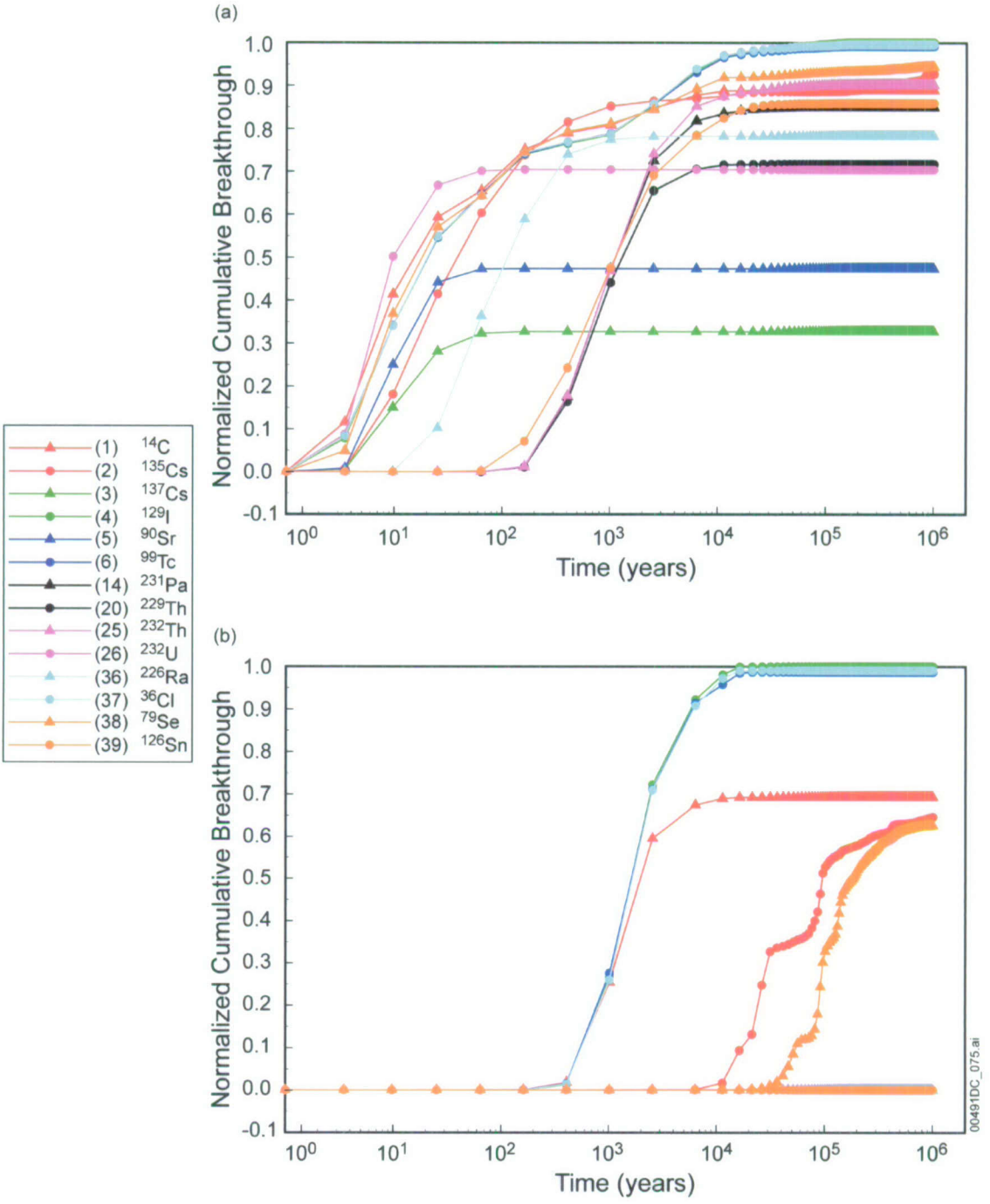

Output DTN: MO0705TRANSTAT.000, files: *MO0705TRANSTAT.000\Breakthroughs\simpleDecay\simpleDecay_north.wmf* (top) and *MO0705TRANSTAT.000\Breakthroughs\simpleDecay\simpleDecay_south.wmf* (bottom).

NOTE: (a) northern release location, (b) southern release location.

Figure 6.6.2-5[b]. Normalized Cumulative Breakthrough Curves of 14 Radionuclides with Simple Decay for the Glacial-Transition 10th Percentile Infiltration Condition and Representative Parameter Values

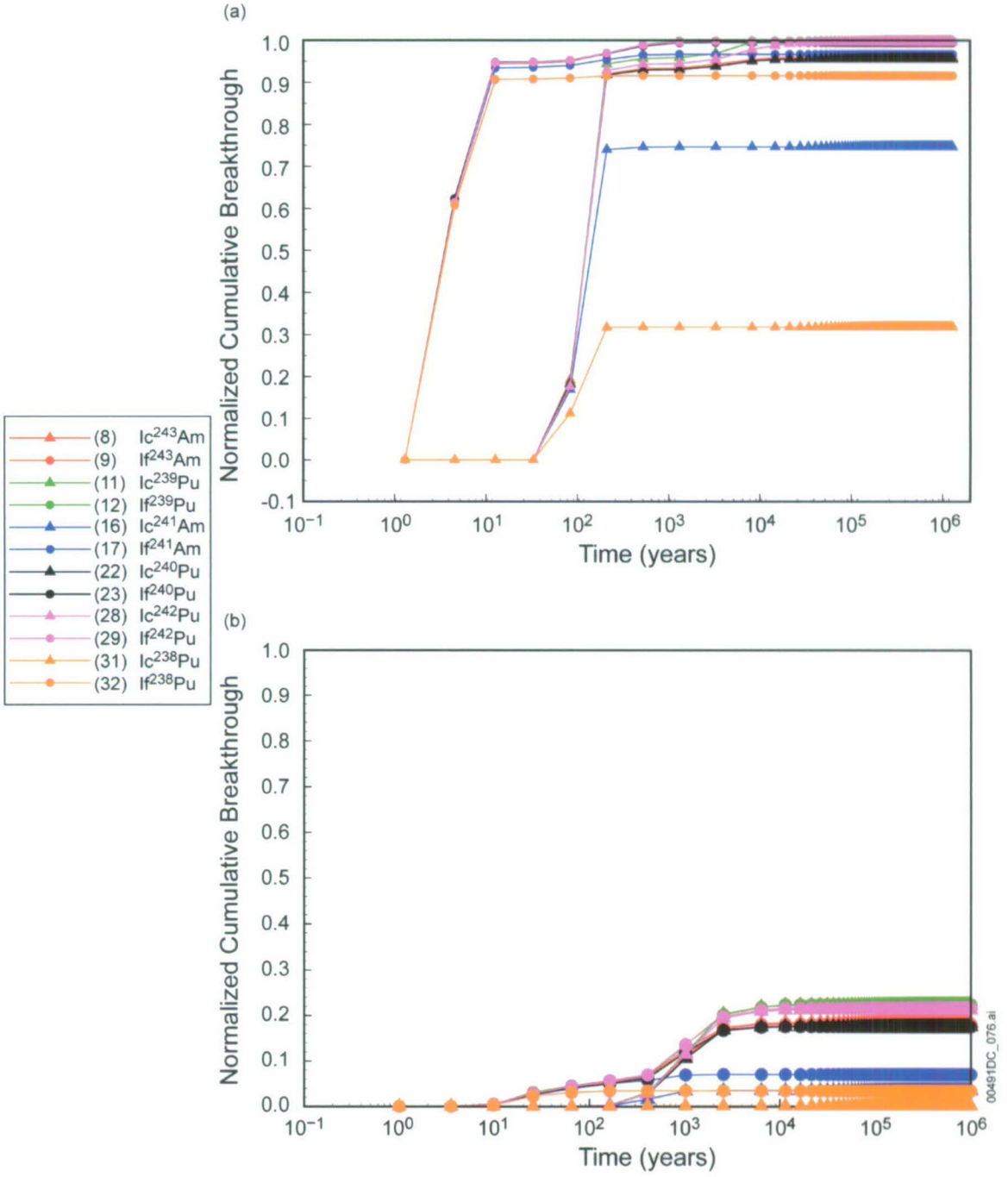

Output DTN: MO0705TRANSTAT.000, files: *MO0705TRANSTAT.000\Breakthroughs\ic_if\icif_north.wmf* (top) and *MO0705TRANSTAT.000\Breakthroughs\ic_if\icif_south.wmf* (bottom).

NOTE: (a) northern release location, (b) southern release location.

Figure 6.6.2-6[b]. Normalized Cumulative Breakthrough Curves of Six Irreversible Fast Colloids and Six Irreversible Slow Colloids for the Glacial-Transition 10th Percentile Infiltration Condition and Representative Parameter Values

Figure 6.6.2-7[b] presents normalized breakthrough curves for radionuclides ^{235}U, ^{233}U, ^{236}U, and ^{230}Th and their daughter products ^{231}Pa, ^{229}Th, ^{232}Th, and ^{226}Ra, respectively, for the two release locations. These results are essentially the same as in Addendum 01 of this report.

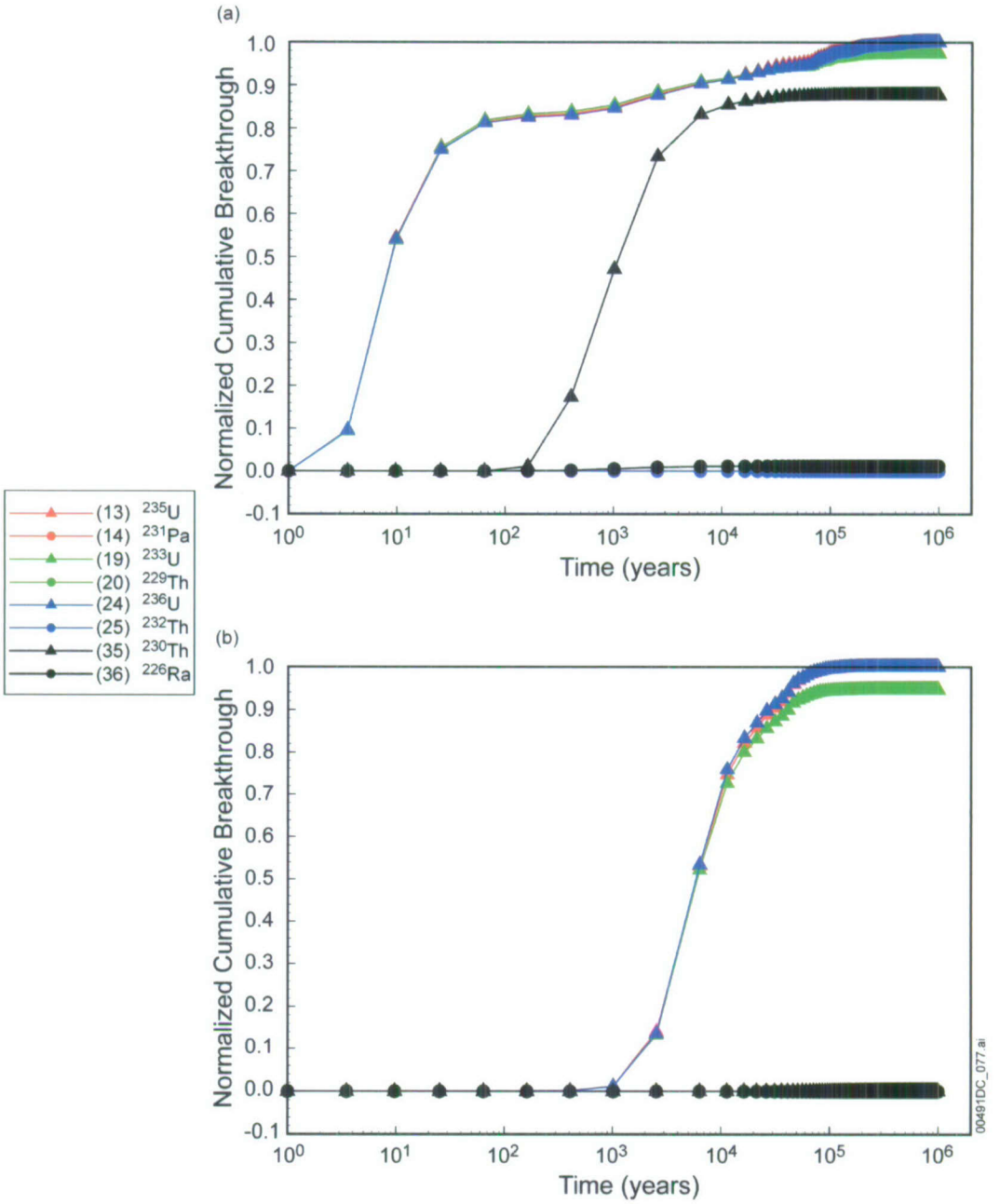

Output DTN: MO0705TRANSTAT.000, files: *MO0705TRANSTAT.000\Breakthroughs\onechain\onechain_north.wmf* (top) and *MO0705TRANSTAT.000\Breakthroughs\onechain\onechain_south.wmf* (bottom).

NOTE: (a) northern release location, (b) southern release location.

Figure 6.6.2-7[b]. Normalized Cumulative Breakthrough Curves of Four Radionuclides (^{235}U, ^{233}U, ^{236}U, and ^{230}Th) with One Decay Chain for the Glacial-Transition 10th Percentile Infiltration Condition and Representative Parameter Values

Additional breakthrough curve plots are presented in Appendix D[b] for other decay chains.

6.6.2.3[b] Fracture versus Matrix Release

Figure 6.6.2-8[b] compares the normalized breakthrough curves for fracture versus matrix release for ^{99}Tc released at the northern (upper figure) or southern (lower figure) release locations. For the northern release location, nearly 50% of mass released into the fracture reaches the water table within about 20 years, compared to about 5,000 years for 50% arrival for the matrix releases. For the southern release location, the breakthrough curves are very similar regardless of whether the releases are in the fracture or the matrix. When mass is released into the matrix of the TSw at the repository horizon, local matrix percolation rates are so low that for radionuclides to escape the unsaturated zone, they must first diffuse to a nearby flowing fracture. Thus, the additional transport time is due to the slow rate of the diffusion process transporting radionuclides to the fracture. For the northern release location, the increase in travel time is pronounced for the matrix releases because the time required for back-diffusion into the fractures in the TSw is much longer than the subsequent fracture transport to the water table. In contrast, for the southern release location, the back-diffusion time is relatively short compared to the subsequent transport time through the matrix in the Calico Hills, resulting in similar breakthrough curves for the fracture and matrix releases. Overall, this process will be governed by the diffusion coefficient, spacing between flowing fractures, and, for sorbing species, sorption coefficient.

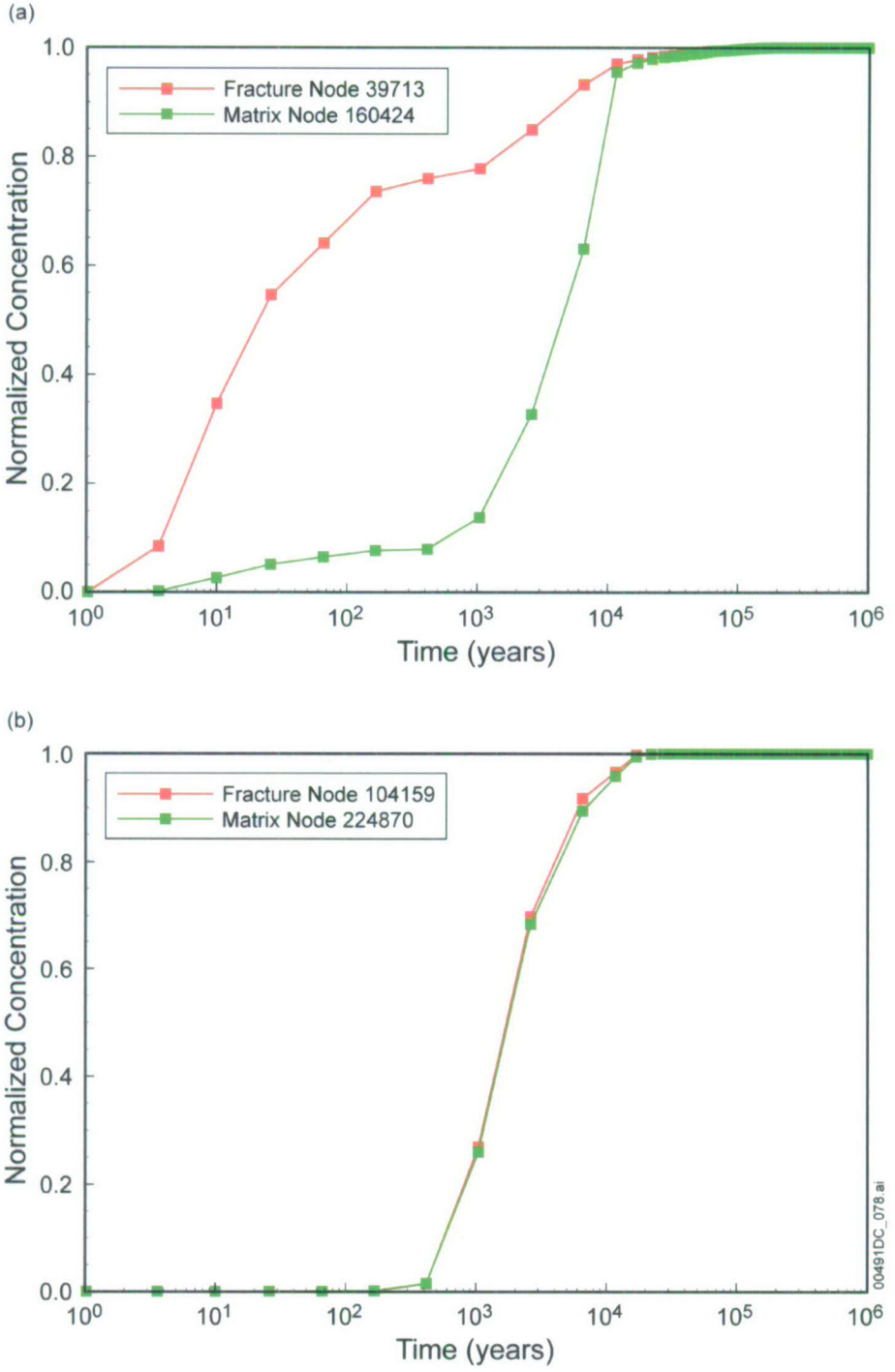

Output DTN: MO0705TRANSTAT.000, files: *MO0705TRANSTAT.000\Sensitivity\fracture_matrix_release\compare_FM_release_dualk_north.wmf* (top) and *MO0705TRANSTAT.000\Sensitivity\fracture_matrix_release\compare_FM_release_dualk_south.wmf* (bottom).

NOTE: (a) northern release location, (b) southern release location.

Figure 6.6.2-8[b]. Comparison of Normalized Cumulative Breakthrough Curves of ^{99}Tc for Particles Released at Fracture Node or Matrix Node for the Glacial-Transition, 10th Percentile Infiltration Scenario, Representative Parameter Values

6.6.3[b] Sensitivity to Flow Parameter Uncertainty

No change.

6.6.4[b] Sensitivity to AFM and Diffusion Parameter Uncertainty

No change.

6.7[b] EVALUATION OF ALTERNATIVE MODELS AND MODEL UNCERTAINTY

No change.

6.8[b] DESCRIPTION OF BARRIER CAPABILITY

No change to this introductory section. Changes from the parent report or Addendum 01 are identified below the third-level heading in the subsections below.

6.8.1[b] Analyses of Barrier Capability

No change.

6.8.2[b] Barrier Capability Simulations and Uncertainty Analyses

No change.

6.8.2.1[b] Travel Time Statistics

Figure 6.8.2-1[b] shows the mean log travel time (in years) of ^{99}Tc as a function of diffusion coefficient D_m for particles released at northern and southern locations. These results are imperceptibly different than those presented in Addendum 01 of the parent report.

Figure 6.8.2-2[b] plots the similar comparison for the discrete fracture model (DFM). These results are imperceptibly different than those presented in Addendum 01 of the parent report.

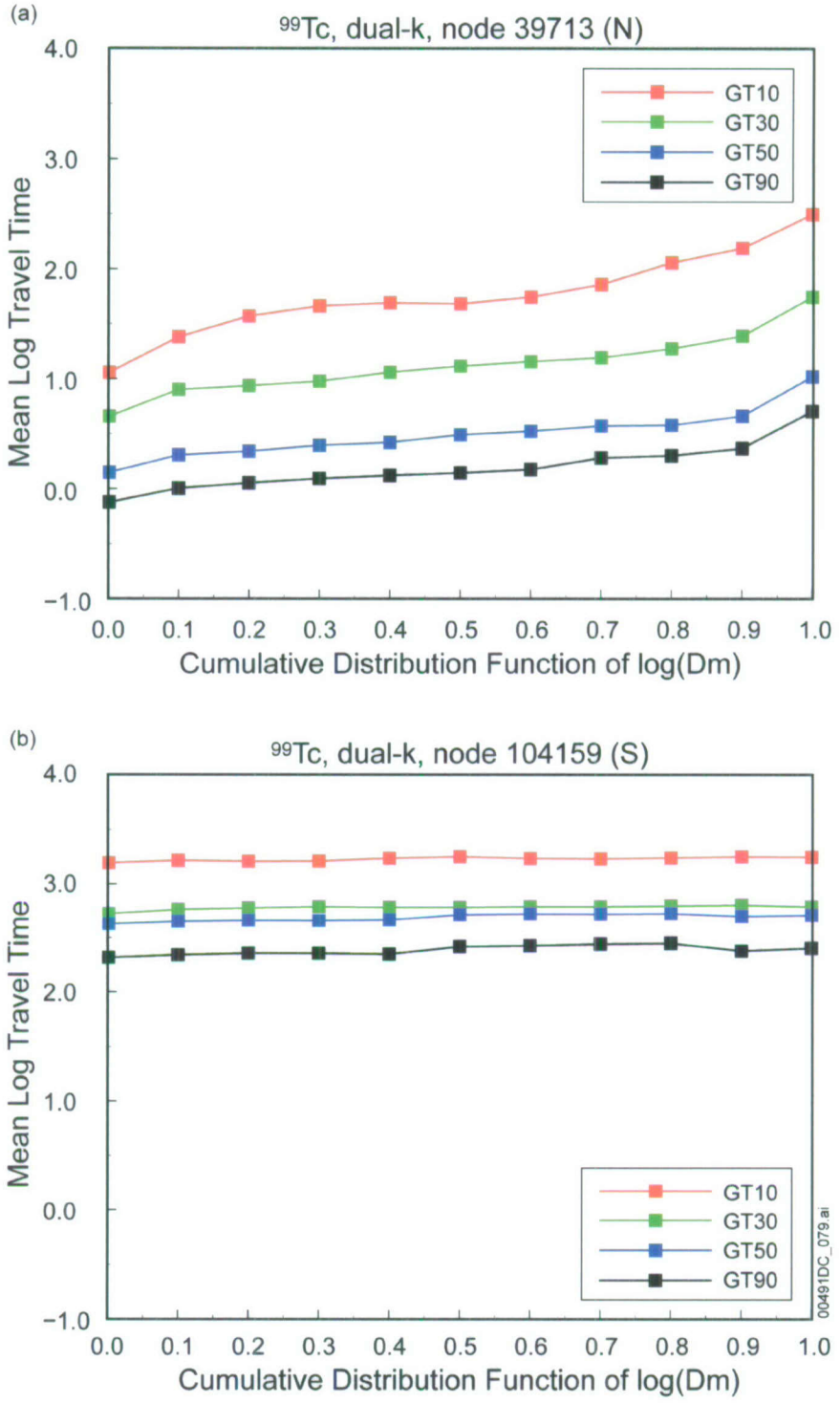

Output DTN: MO0705TRANSTAT.000, file: *MO0705TRANSTAT.000\Sensitivity\conservative\dualk\tc_time.wmf.*

NOTE: (a) northern release location, (b) southern release location.

Figure 6.8.2-1[b]. Comparison of Mean Travel Time of ^{99}Tc as a Function of Matrix Diffusion Coefficient under Glacial-Transition Climate Conditions for the dual-k Model

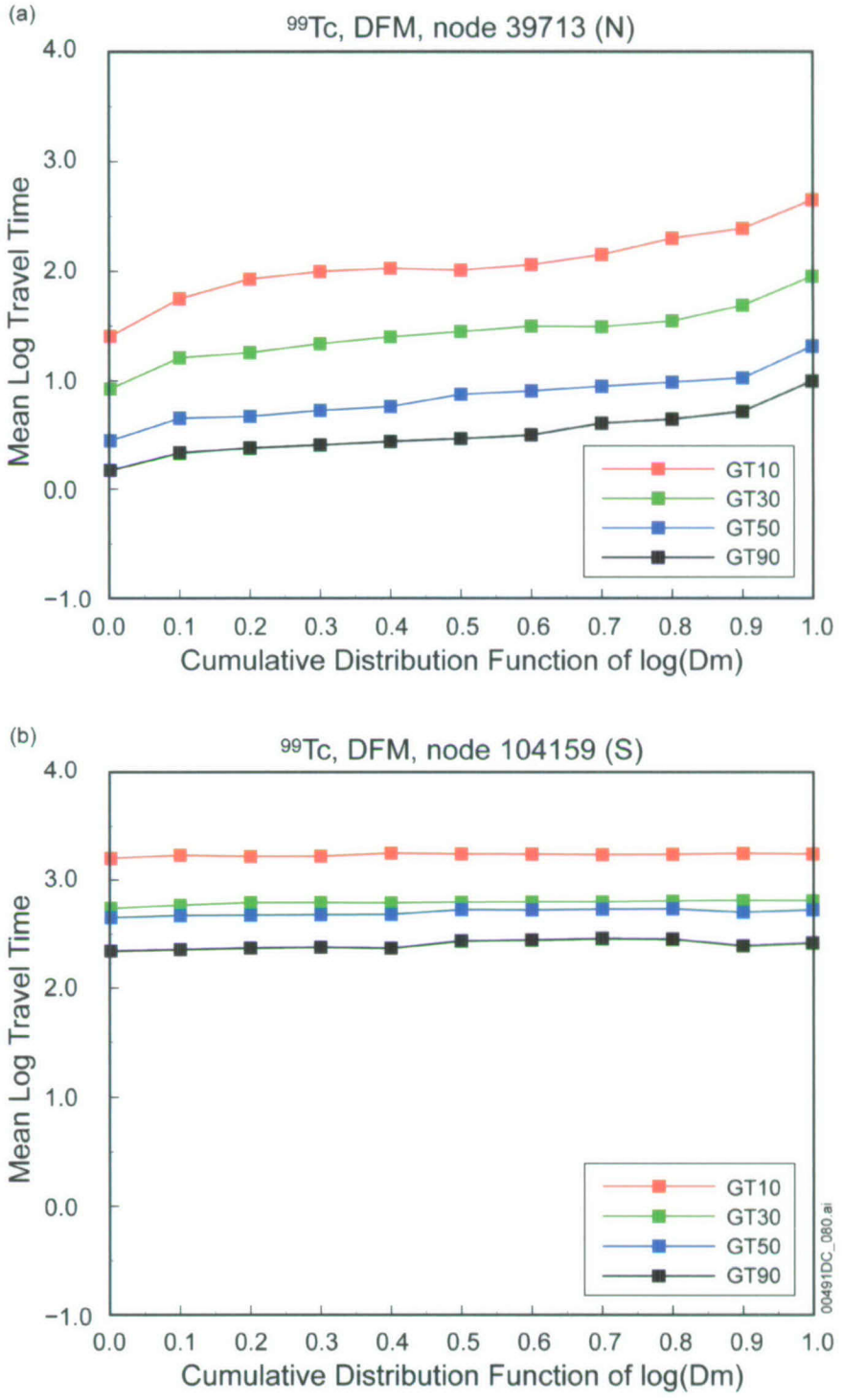

Output DTN: MO0705TRANSTAT.000, file: *MO0705TRANSTAT.000\Sensitivity\conservative\DFM\tc_time.wmf* .

NOTE: (a) northern release location, (b) southern release location.

Figure 6.8.2-2[b]. Comparison of Mean Travel Time of ^{99}Tc as a Function of Matrix Diffusion Coefficient under Glacial-Transition Climate Conditions for the DFM

For sorbing species, both diffusion coefficient and sorption coefficient have an influence on the travel time to the water table. In the analyses that follow, a matrix of simulations is performed that span the entire uncertainty ranges of both D_m and K_d. For each simulation, consisting of a separate pair of D_m and K_d values, the mean travel time is computed, and the results are displayed in contour plots of travel time, with cumulative distribution functions of K_d and D_m as the axes. Figures 6.8.2-3[b] and 6.8.2-4[b] show the mean travel times for the weakly sorbing species ^{237}Np released at the northern (Figure 6.8.2-3[b]) and southern (Figure 6.8.2-4[b]) nodes under four different flow fields (glacial-transition, 10-, 30-, 50-, and 90-percentile infiltration rates), simulated using the dual-k model. Figures 6.8.2-5[b] and 6.8.2-6[b] present analogous results for the DFM. These results are slightly different than the corresponding figures in Addendum 01 of the parent report, but the conclusions reached in that document are still valid.

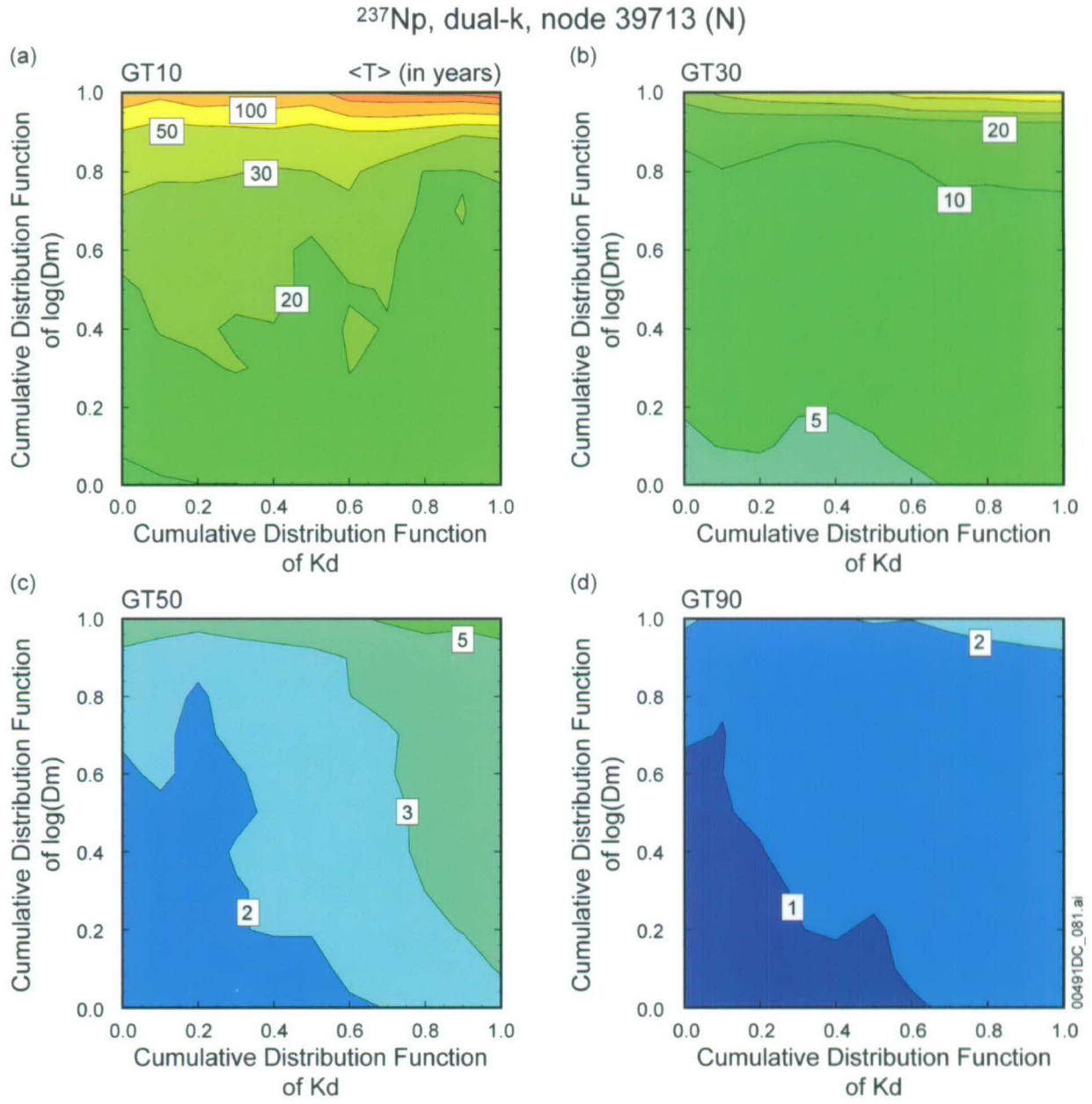

Output DTN: MO0705TRANSTAT.000, file: *MO0705TRANSTAT.000\Sensitivity\weak_sorbing\237Np_time_dualk_north.wmf.*

Figure 6.8.2-3[b]. Mean Travel Time of ^{237}Np as a Function of Matrix Diffusion Coefficient and Sorption Coefficient for the Glacial-Transition Climate Condition, dual-k Model, Northern Release Location

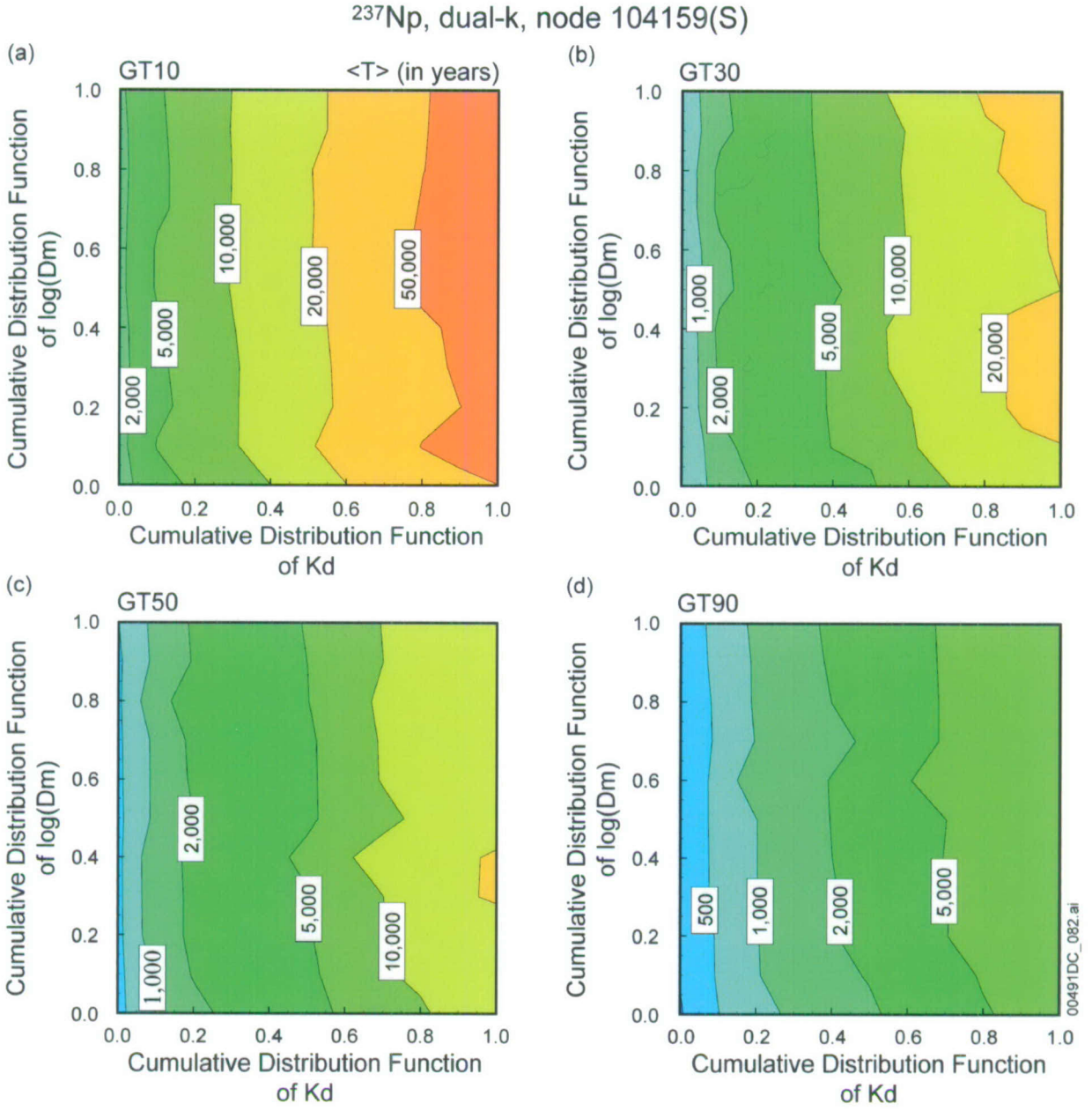

Output DTN: MO0705TRANSTAT.000, file: *MO0705TRANSTAT.000\Sensitivity\weak_sorbing\237Np_time_dualk_south.wmf.*

Figure 6.8.2-4[b]. Mean Travel Time of ^{237}Np as a Function of Matrix Diffusion Coefficient and Sorption Coefficient for the Glacial-Transition Climate Condition, dual-k Model, Southern Release Location

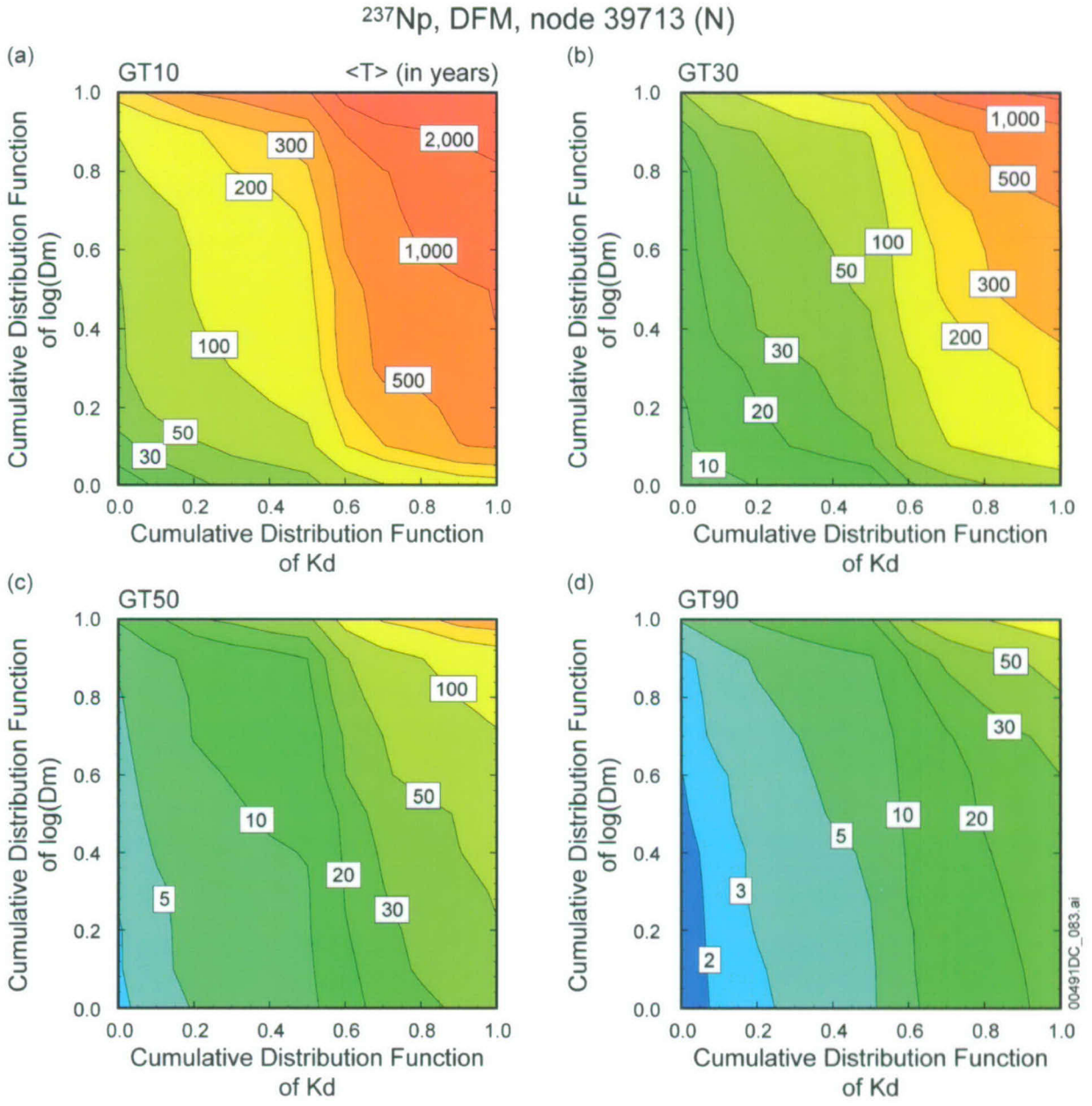

Output DTN: MO0705TRANSTAT.000, file: *MO0705TRANSTAT.000\Sensitivity\weak_sorbing\237Np_time_DFM_north.wmf.*

Figure 6.8.2-5[b]. Mean Travel Time of ^{237}Np as a Function of Matrix Diffusion Coefficient and Sorption Coefficient for the Glacial-Transition Climate Condition, DFM, Northern Release Location

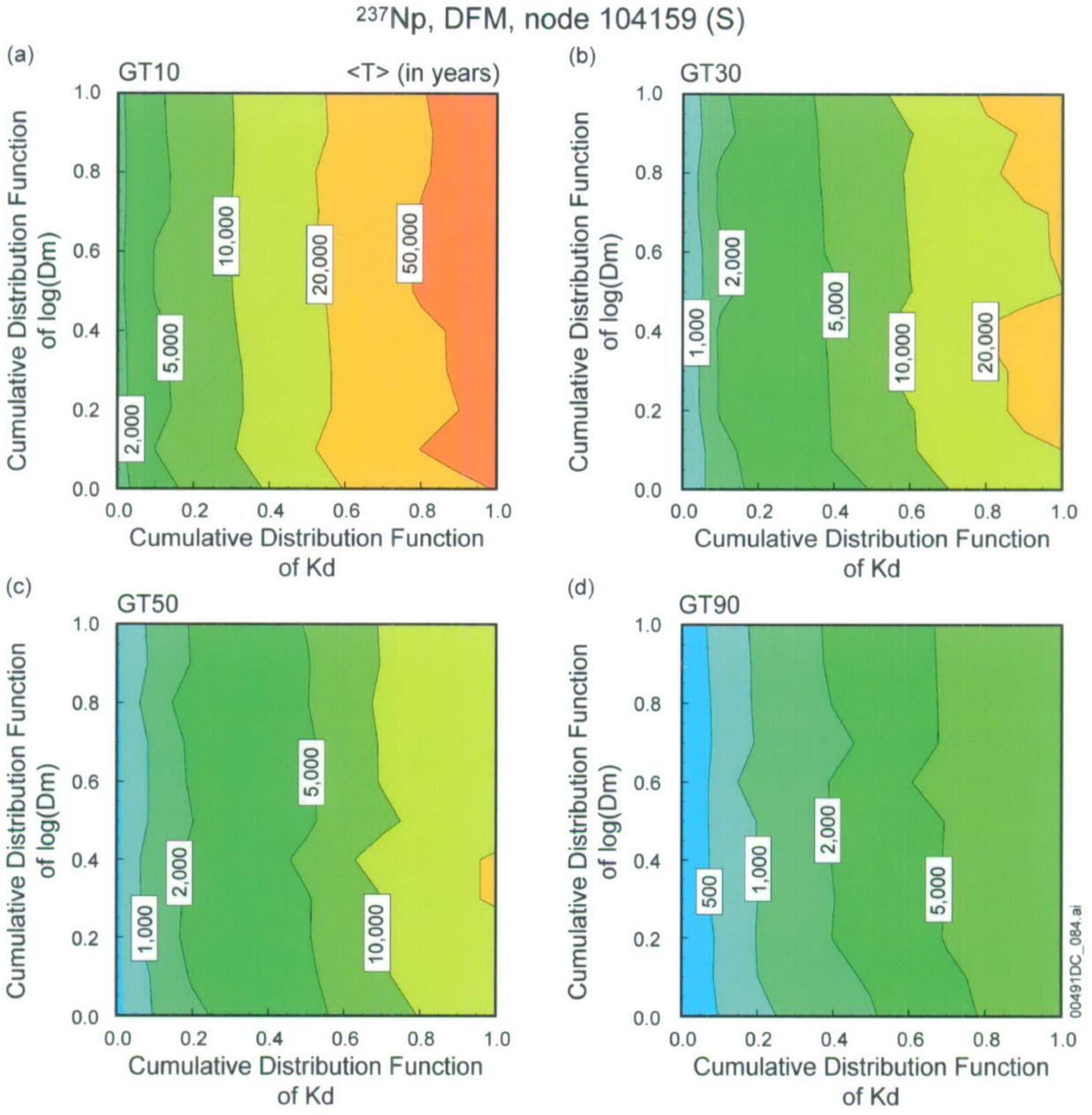

Output DTN: MO0705TRANSTAT.000, file: *MO0705TRANSTAT.000\Sensitivity\weak_sorbing\237Np_time_DFM_south.wmf.*

Figure 6.8.2-6[b]. Mean Travel Time of ^{237}Np as a Function of Matrix Diffusion Coefficient and Sorption Coefficient for the Glacial-Transition Climate Condition, DFM, Southern Release Location

An analogous set of comparisons for the mean travel time for the strongly sorbing ^{240}Pu (reversibly sorbed species) is illustrated in Figures 6.8.2-7[b], 6.8.2-8[b], 6.8.2-9[b], and 6.8.2-10[b]. These results are different than the corresponding results in Addendum 01 for the southern location, but the conclusions reached are still valid.

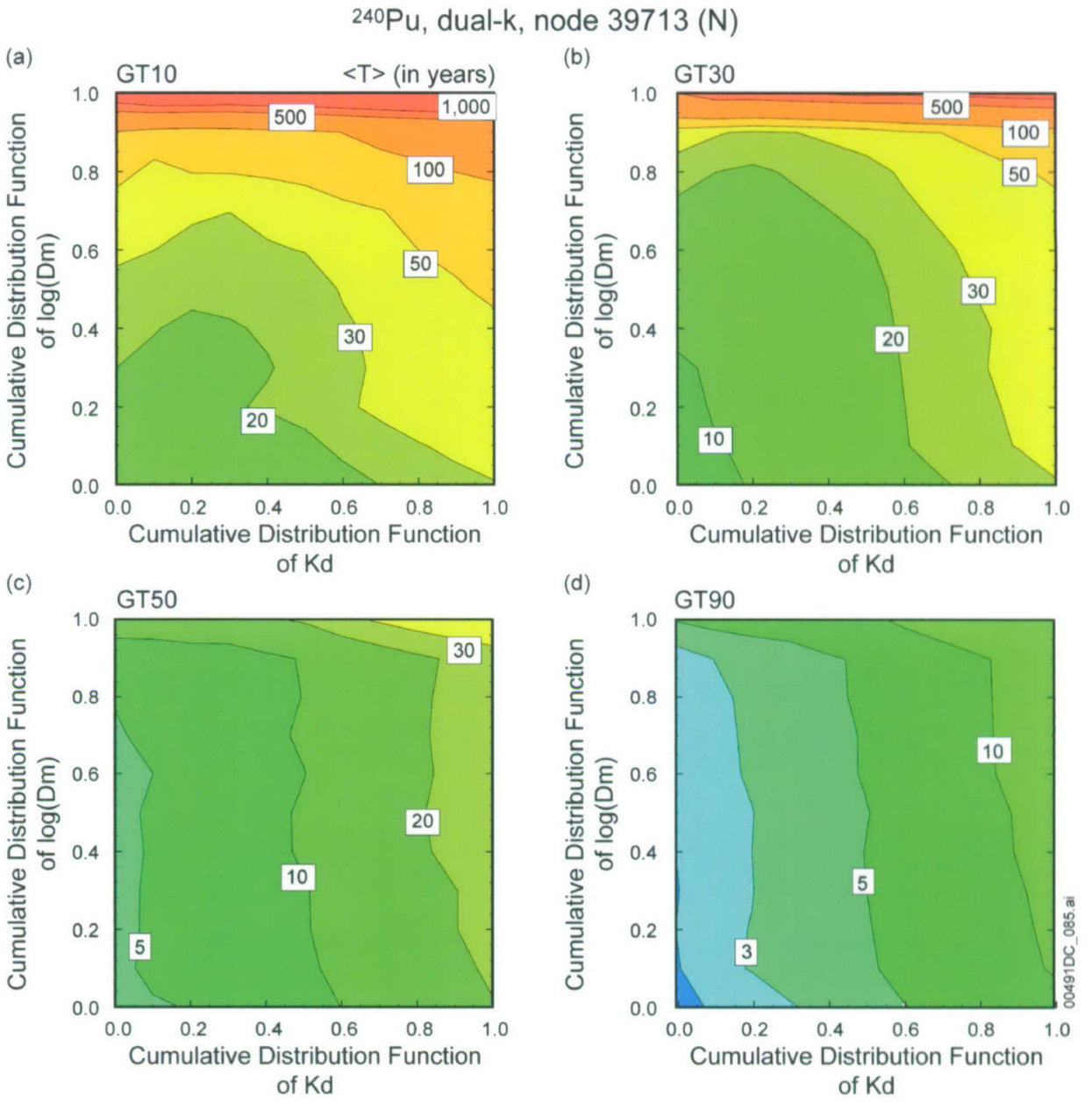

Output DTN: MO0705TRANSTAT.000, file: *MO0705TRANSTAT.000\Sensitivity\strong_sorbing\240Pu_time_dualk_north.wmf*.

Figure 6.8.2-7[b]. Mean Travel Time of ^{240}Pu as a Function of Matrix Diffusion Coefficient and Sorption Coefficient for the Glacial-Transition Climate Condition, dual-k Model, Northern Release Location

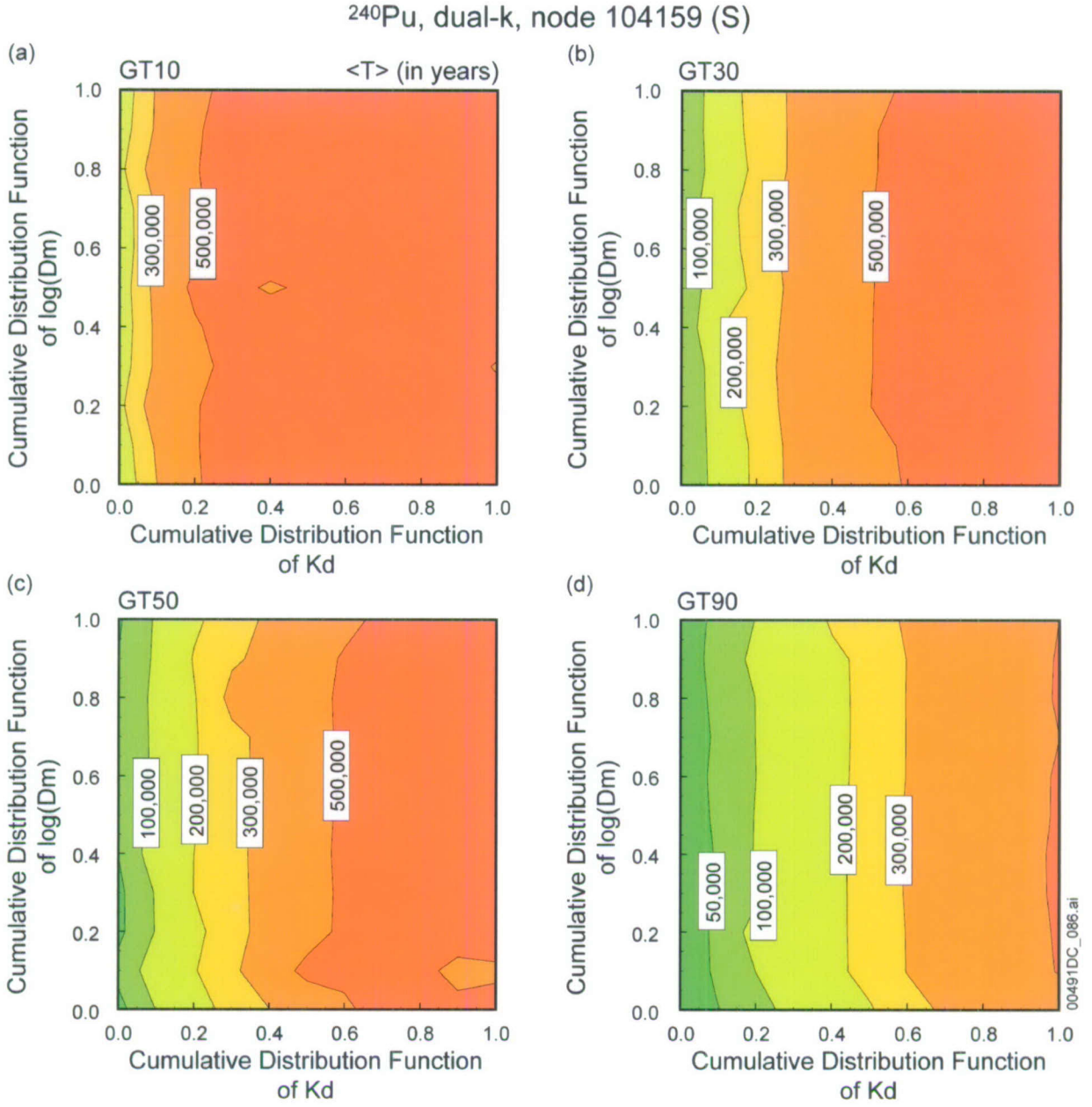

Output DTN: MO0705TRANSTAT.000, file: *MO0705TRANSTAT.000\Sensitivity\strong_sorbing\240Pu_time_dualk_south.wmf.*

Figure 6.8.2-8[b]. Mean Travel Time of ^{240}Pu as a Function of Matrix Diffusion Coefficient and Sorption Coefficient for the Glacial-Transition Climate Condition, dual-k Model, Southern Release Location

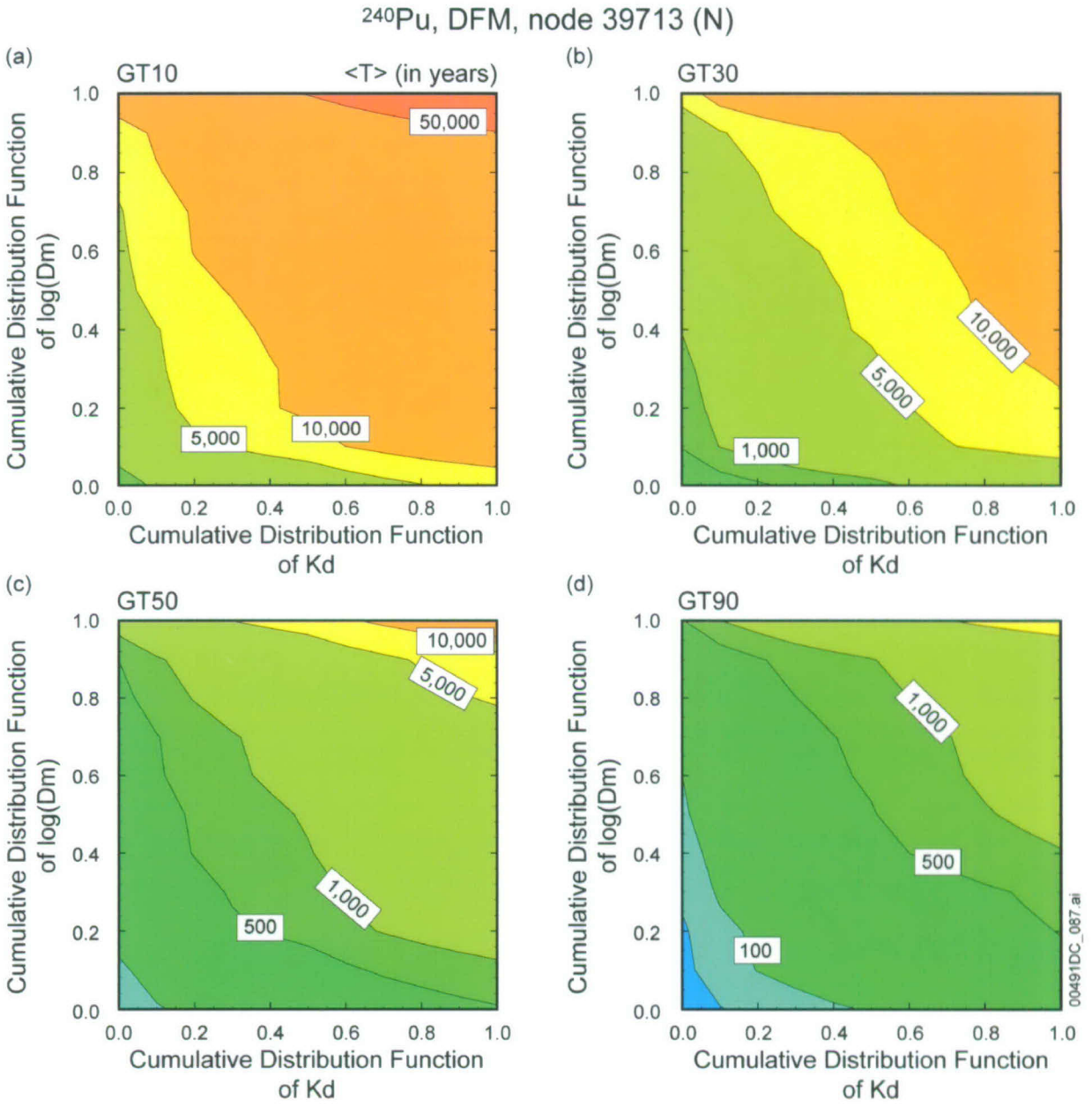

Output DTN: MO0705TRANSTAT.000, file: *MO0705TRANSTAT.000\Sensitivity\strong_sorbing\240Pu_time_DFM_north.wmf.*

Figure 6.8.2-9[b]. Mean Travel Time of ^{240}Pu as a Function of Matrix Diffusion Coefficient and Sorption Coefficient for the Glacial-Transition Climate Condition, DFM, Northern Release Location

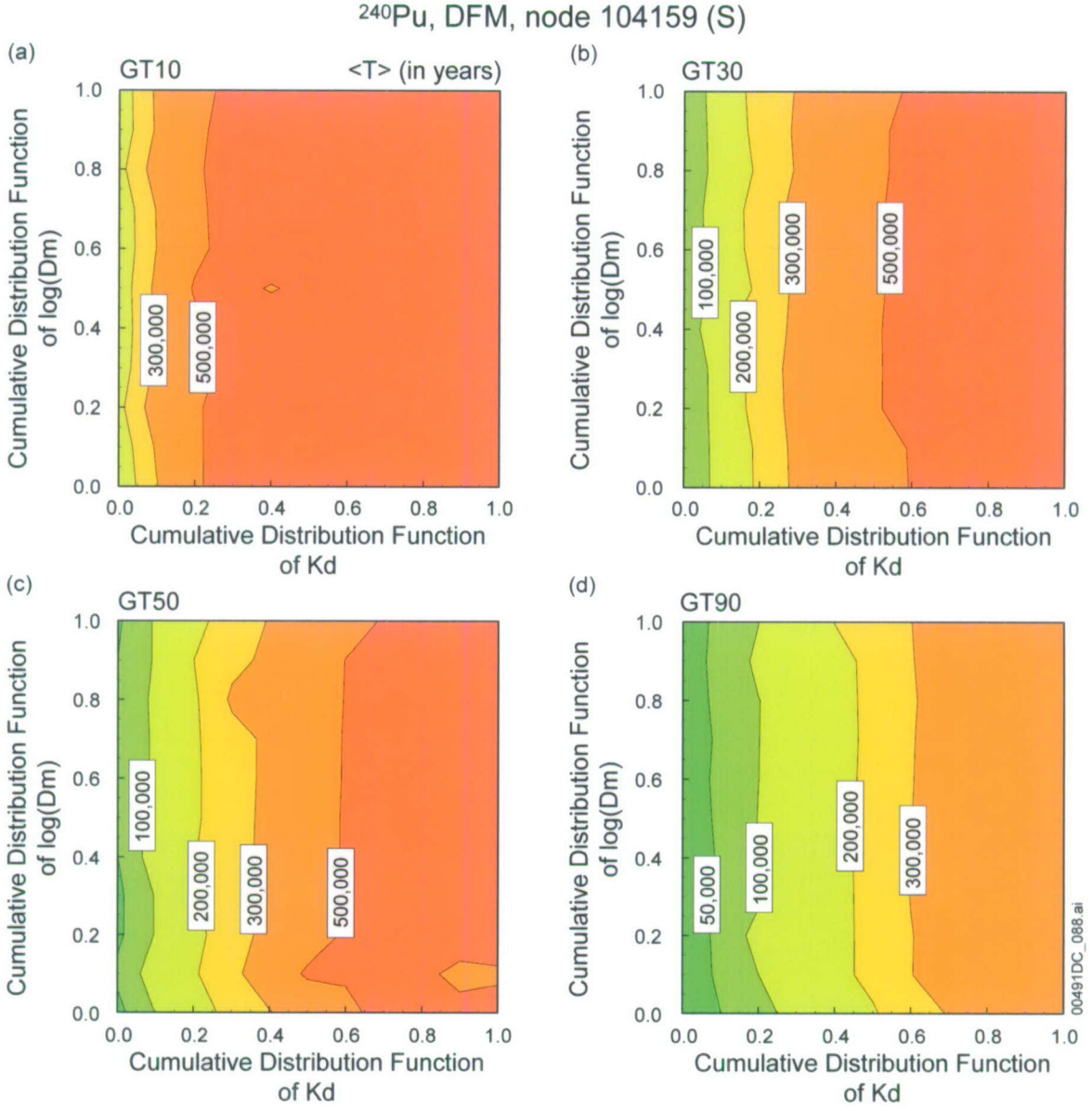

Output DTN: MO0705TRANSTAT.000, file: *MO0705TRANSTAT.000\Sensitivity\strong_sorbing\240Pu_time_DFM_south.wmf.*

Figure 6.8.2-10[b]. Mean Travel Time of ^{240}Pu as a Function of Matrix Diffusion Coefficient and Sorption Coefficient for the Glacial-Transition Climate Condition, DFM, Southern Release Location

6.8.2.2[b] Barrier Capability Analyses Using the Decay Fraction

The analyses presented earlier used the mean travel time as a metric. In this section, the results are cast in terms of the effectiveness of the barrier as measured by the decay fraction C/C_0. The barrier capability is calculated from the travel time distribution using Equation 6.8.2-1 of Addendum 01. As with the previous analysis for mean travel time, the analysis is performed for a number of species released either at the northern or southern release points under the four glacial-transition flow fields, simulated using both the dual-k model and the DFM. For nonsorbing species, simple line plots are used, whereas for cases in which both D_m and K_d are varied (sorbing species ^{237}Np and ^{240}Pu), the matrix of 11 D_m values and 11 K_d values are used, and the results are displayed as contour plots.

Figures 6.8.2-11[b] and 6.8.2-12[b] plot C/C_0 for species ^{99}Tc for the northern and southern nodes. These results are different than the corresponding results in Addendum 01 for the southern location, but the conclusions reached are still valid. In all cases examined here, more than approximately 99.1% of ^{99}Tc reaches the water table.

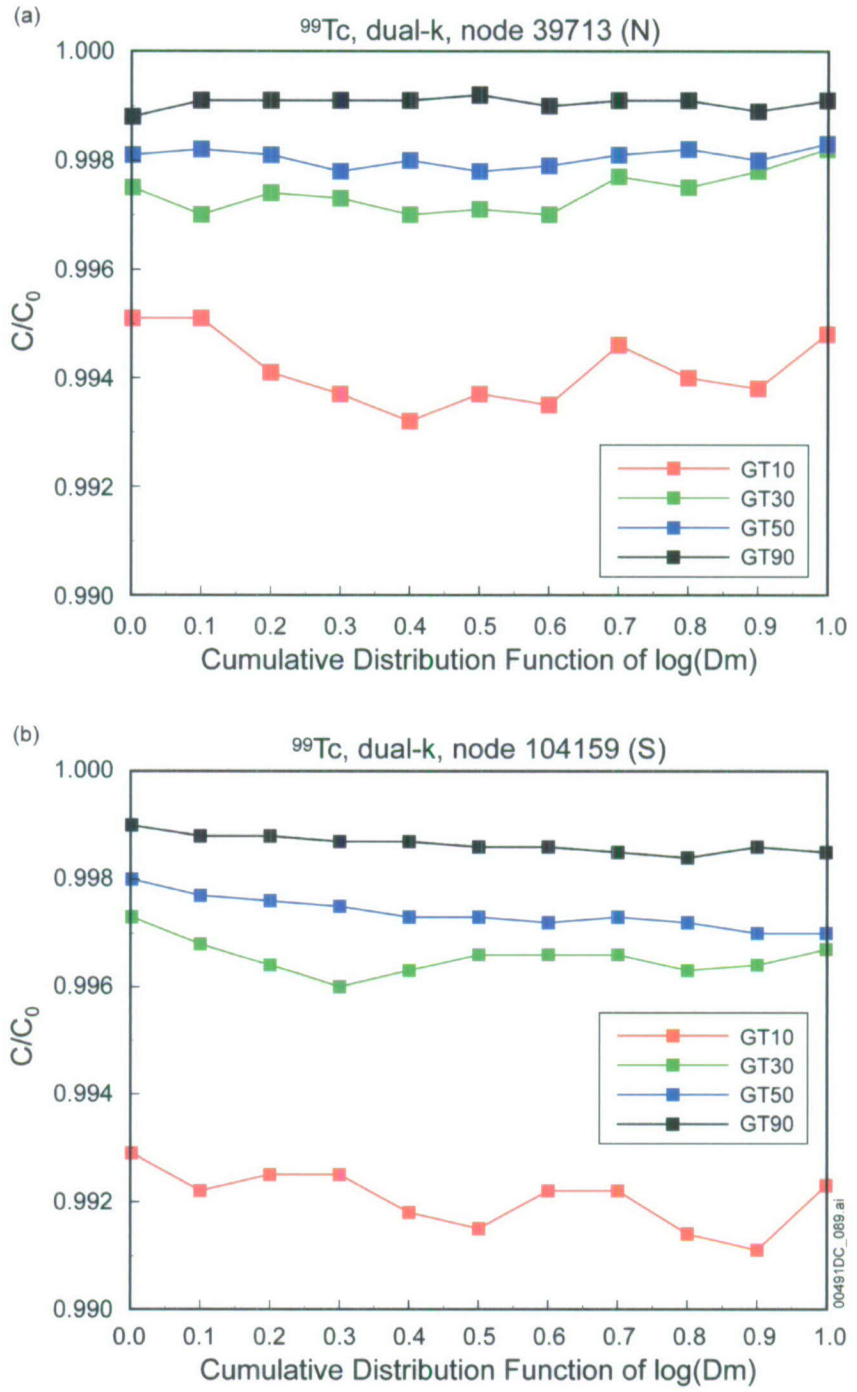

Output DTN: MO0705TRANSTAT.000, file: *MO0705TRANSTAT.000\Sensitivity\conservative\dualk\Tc_cRatio.wmf.*

Figure 6.8.2-11[b]. Normalized ^{99}Tc Concentration (Decay Fraction, Computed from Travel Time Distributions) as a Function of Matrix Diffusion Coefficient for Glacial-Transition Climate Condition, dual-k Model, (a) Northern Release Location, (b) Southern Release Location

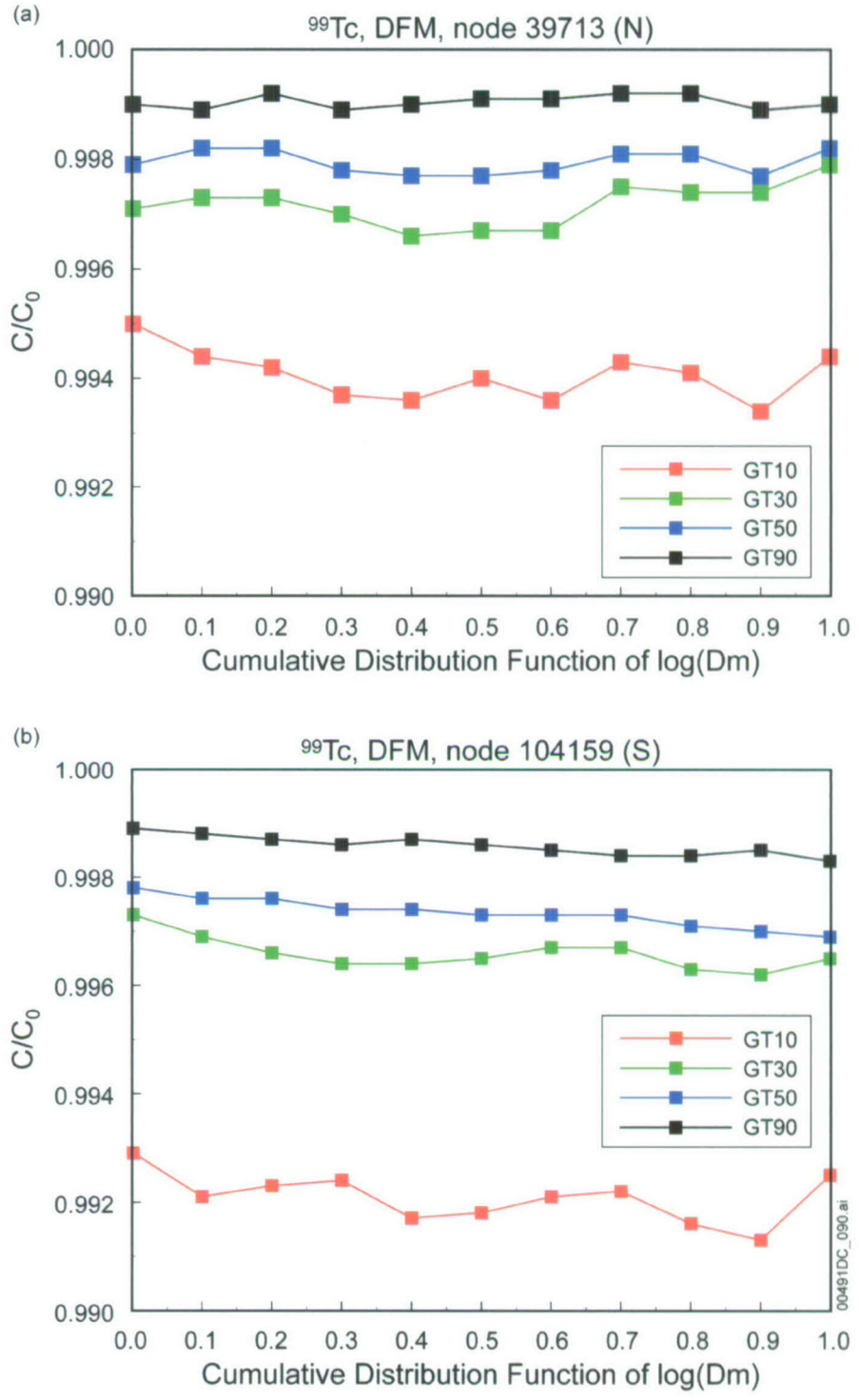

Output DTN: MO0705TRANSTAT.000, file: *MO0705TRANSTAT.000\Sensitivity\conservative\DFM\Tc_cratio.wmf.*

Figure 6.8.2-12[b]. Normalized ^{99}Tc Concentration (Decay Fraction, Computed from Travel Time Distributions) as a Function of Matrix Diffusion Coefficient for Glacial-Transition Climate Condition, DFM, (a) Northern Release Location, (b) Southern Release Location

Similar comparisons for a nonsorbing species ^{14}C are illustrated in Figures 6.8.2-13[b] and 6.8.2-14[b]. These results are different than the corresponding results in Addendum 01 for the southern location, but the conclusions reached are still valid.

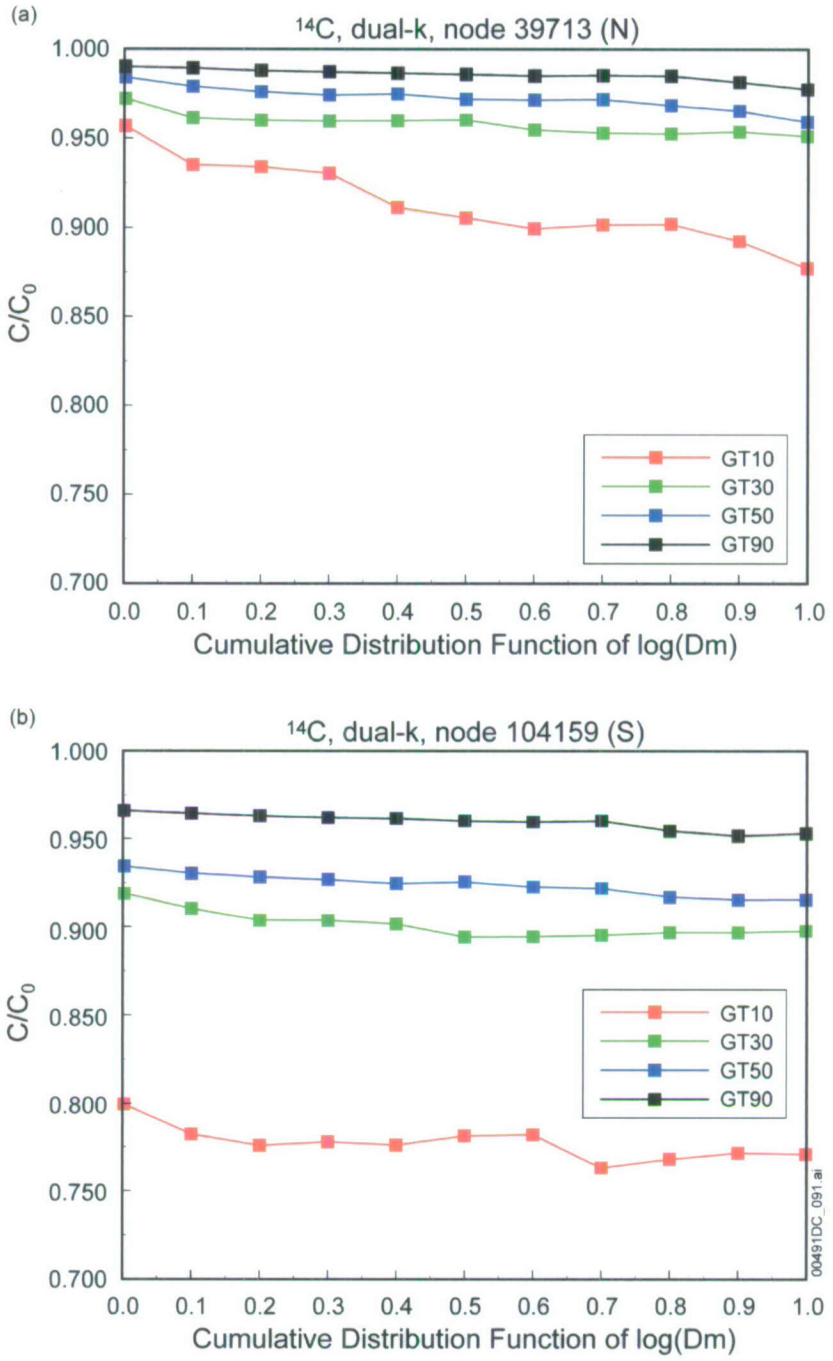

Output DTN: MO0705TRANSTAT.000, file: *MO0705TRANSTAT.000\Sensitivity\conservative\dualk\c_cratio.wmf.*

Figure 6.8.2-13[b]. Normalized ^{14}C Concentration (Decay Fraction, Computed from Travel Time Distributions) as a Function of Matrix Diffusion Coefficient for Glacial-Transition Climate Condition, dual-k Model, (a) Northern Release Location, (b) Southern Release Location

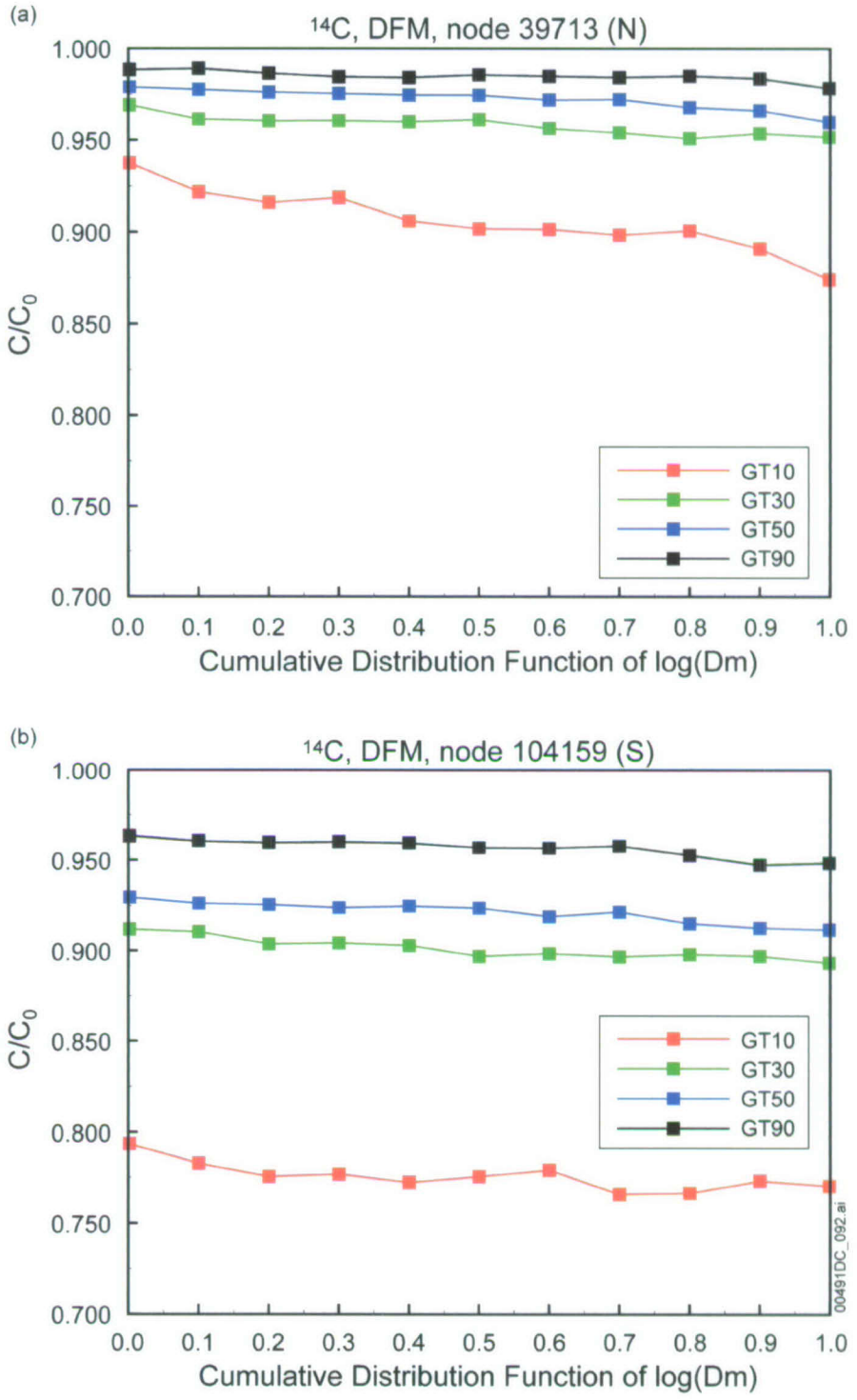

Output DTN: MO0705TRANSTAT.000, file: *MO0705TRANSTAT.000\Sensitivity\conservative\DFM\c_cratio.wmf.*

Figure 6.8.2-14[b]. Normalized ^{14}C Concentration (Decay Fraction, Computed from Travel Time Distributions) as a Function of Matrix Diffusion Coefficient for Glacial-Transition Climate Condition, DFM, (a) Northern Release Location, (b) Southern Release Location

Similar to the contour plots of mean travel time presented earlier, contour maps of C/C_0 for ^{237}Np are compared in Figures 6.8.2-15[b], 6.8.2-16[b], 6.8.2-17[b], and 6.8.2-18[b]. These results are different than the corresponding results in Addendum 01 for the southern location, but the conclusions reached are still valid.

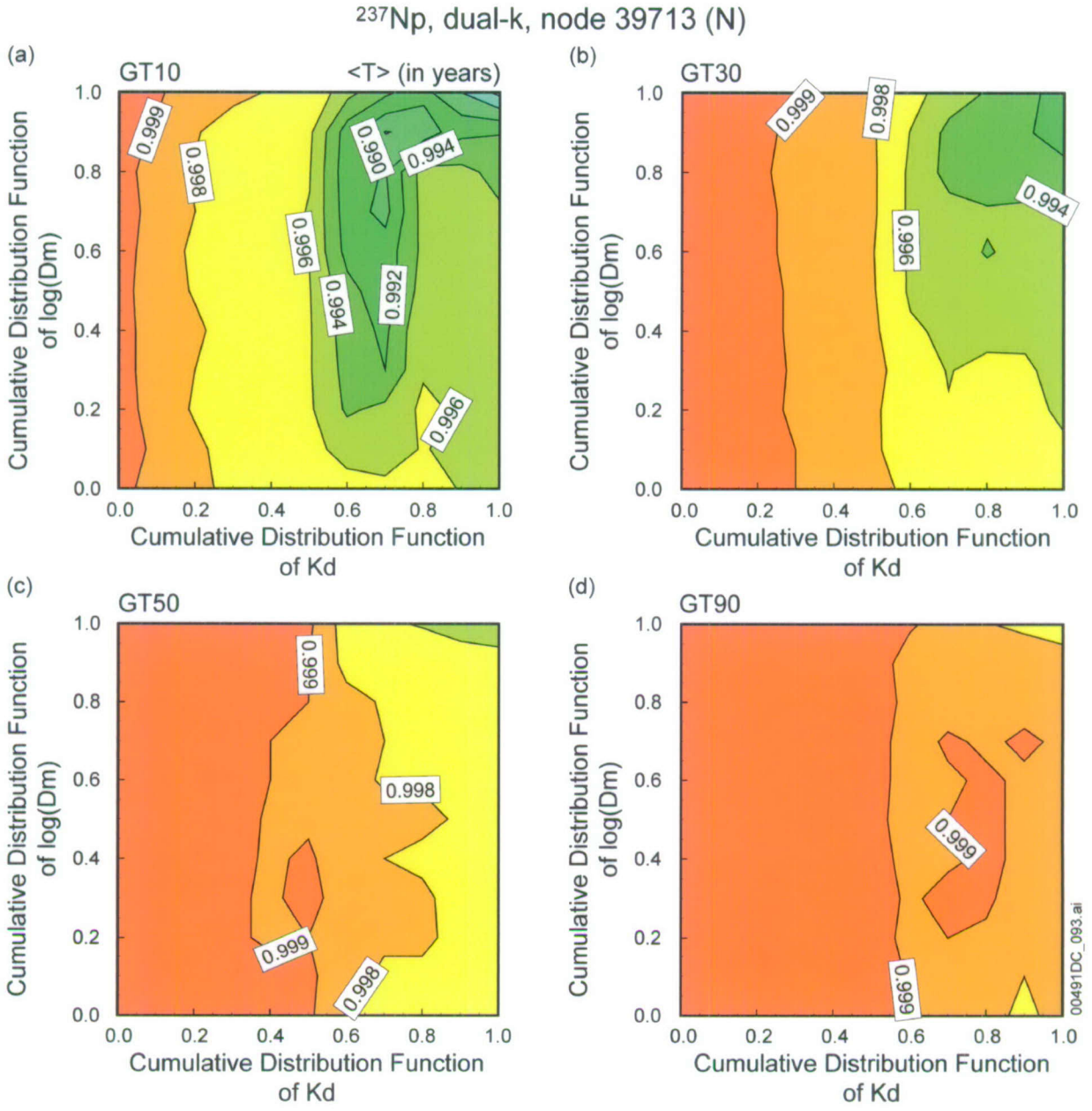

Output DTN: MO0705TRANSTAT.000, file: *MO0705TRANSTAT.000\Sensitivity\weak_sorbing\237Np_CC0_dualk_north.wmf*.

Figure 6.8.2-15[b]. Normalized ^{237}Np Concentration (Decay Fraction, Computed from Travel Time Distributions) as a Function of Matrix Diffusion Coefficient and Sorption Coefficient for the Glacial-Transition Climate Conditions, dual-k Model, Northern Release Location

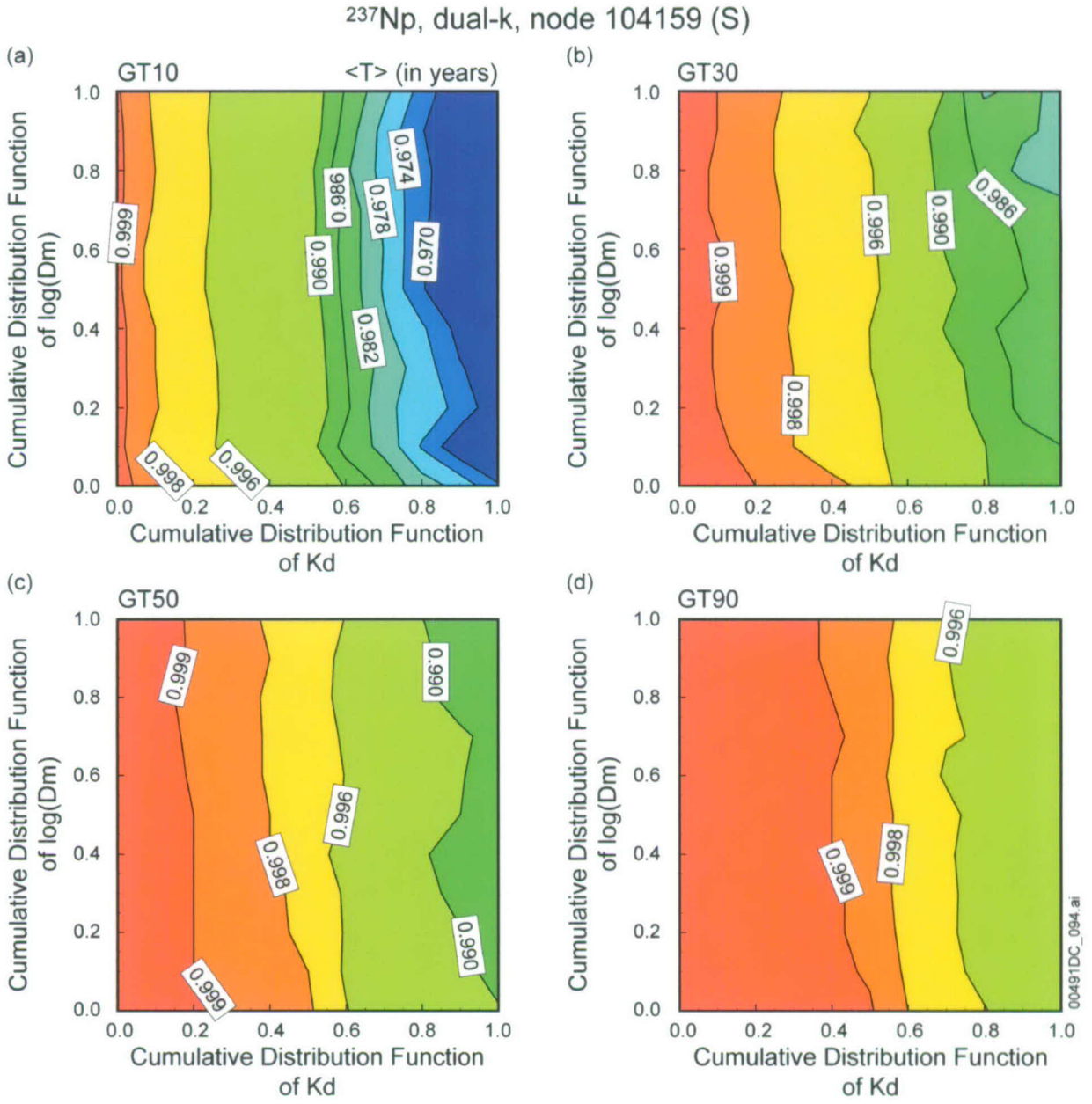

Output DTN: MO0705TRANSTAT.000, file: *MO0705TRANSTAT.000\Sensitivity\weak_sorbing\237Np_CC0_dualk_south.wmf*.

Figure 6.8.2-16[b]. Normalized ^{237}Np Concentration (Decay Fraction, Computed from Travel Time Distributions) as a Function of Matrix Diffusion Coefficient and Sorption Coefficient for the Glacial-Transition Climate Conditions, dual-k Model, Southern Release Location

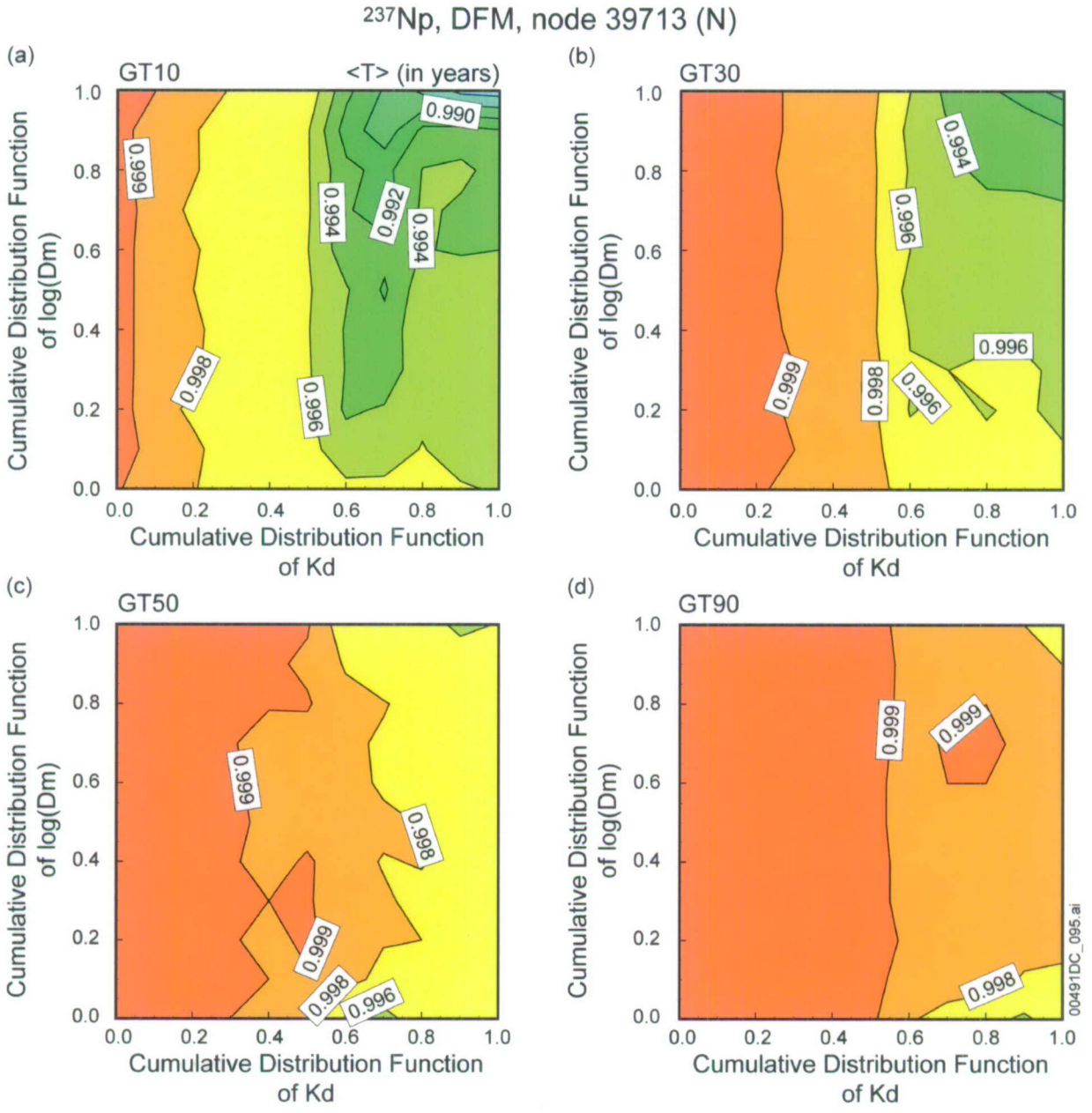

Output DTN: MO0705TRANSTAT.000, file: *MO0705TRANSTAT.000\Sensitivity\weak_sorbing\237Np_CC0_DFM_north.wmf*.

Figure 6.8.2-17[b]. Normalized ^{237}Np Concentration (Decay Fraction, Computed from Travel Time Distributions) as a Function of Matrix Diffusion Coefficient and Sorption Coefficient for the Glacial-Transition Climate Conditions, DFM, Northern Release Location

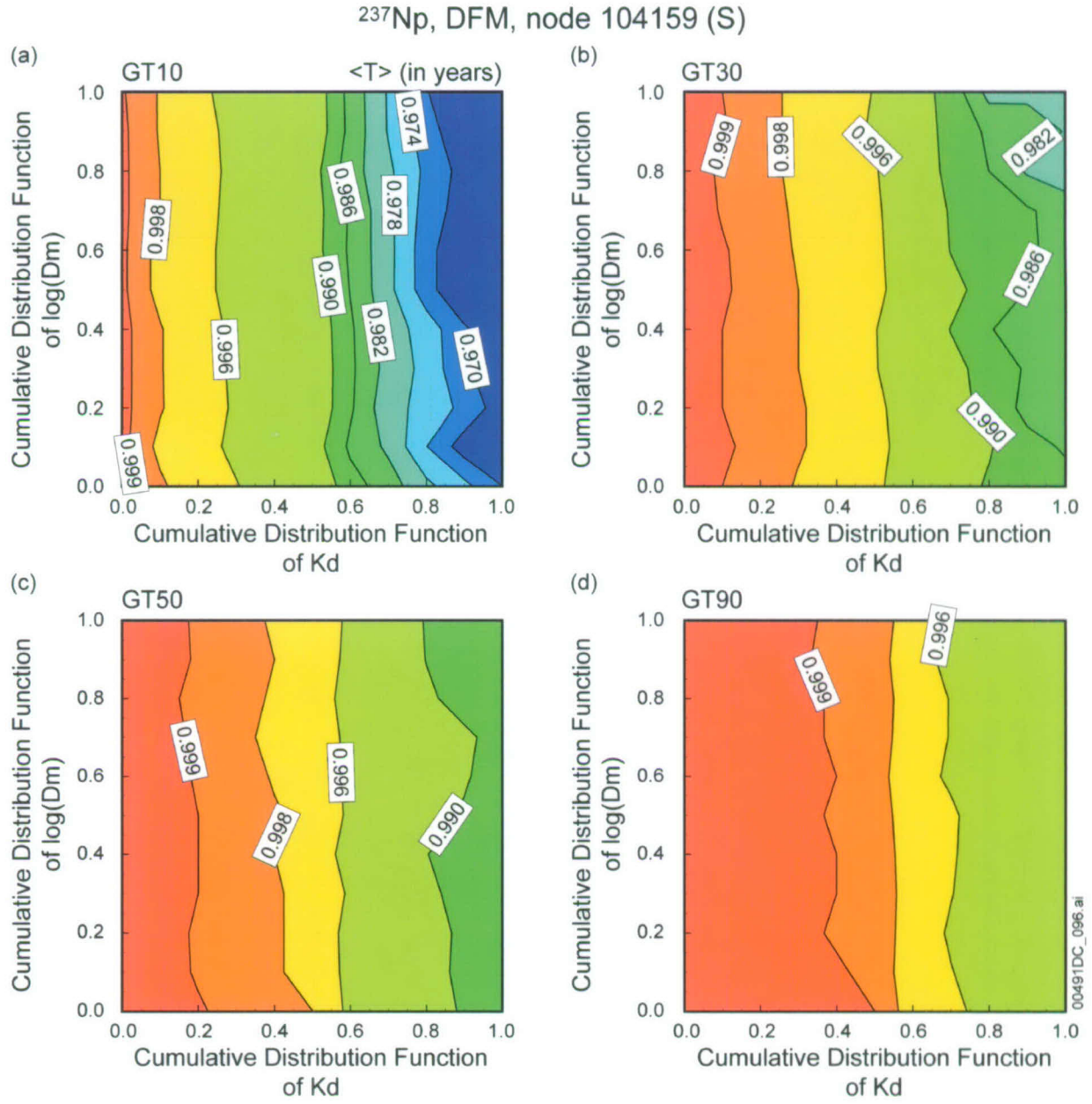

Output DTN: MO0705TRANSTAT.000, file: *MO0705TRANSTAT.000\Sensitivity\weak_sorbing\237Np_CC0_DFM_south.wmf.*

Figure 6.8.2-18[b]. Normalized ^{237}Np Concentration (Decay Fraction, Computed from Travel Time Distributions) as a Function of Matrix Diffusion Coefficient and Sorption Coefficient for the Glacial-Transition Climate Conditions, DFM, Southern Release Location

A similar set of plots for ^{240}Pu are presented in Figures 6.8.2-19[b], 6.8.2-20[b], 6.8.2-21[b], and 6.8.2-22[b]. From the plots for the southern release location, it is apparent that the unsaturated zone in the southern region is an effective barrier for ^{240}Pu, as only less than about 1% of ^{240}Pu will reach the water table even under the most unfavorable combination of parameter values. This is due to the long travel time in this region (matrix transport and strong sorption) and short half-life (6.56×10^3 years) of ^{240}Pu. In addition, in the southern region, the values of C/C_0 simulated using both the dual-k model and the DFM are similar, reflecting the relative importance of the matrix flow component over transport in the fractured units. However, in the northern region, the contour maps of C/C_0 from the dual-k model and the DFM are much different. For example, using the DFM under flow field GT10, the unsaturated zone is predicted to be an effective barrier if both K_d and D_m are large, while at the same conditions with the dual-k model, nearly 80% of ^{240}Pu is predicted to reach the water table, unless the D_m is very high. This result shows that under certain conditions (fracture-dominated transport) and for certain species (strongly sorbing species with half-lives up to thousands of years, rather than millions of years), the predicted performance of the unsaturated zone barrier depends strongly on the choice of conceptual model for diffusion.

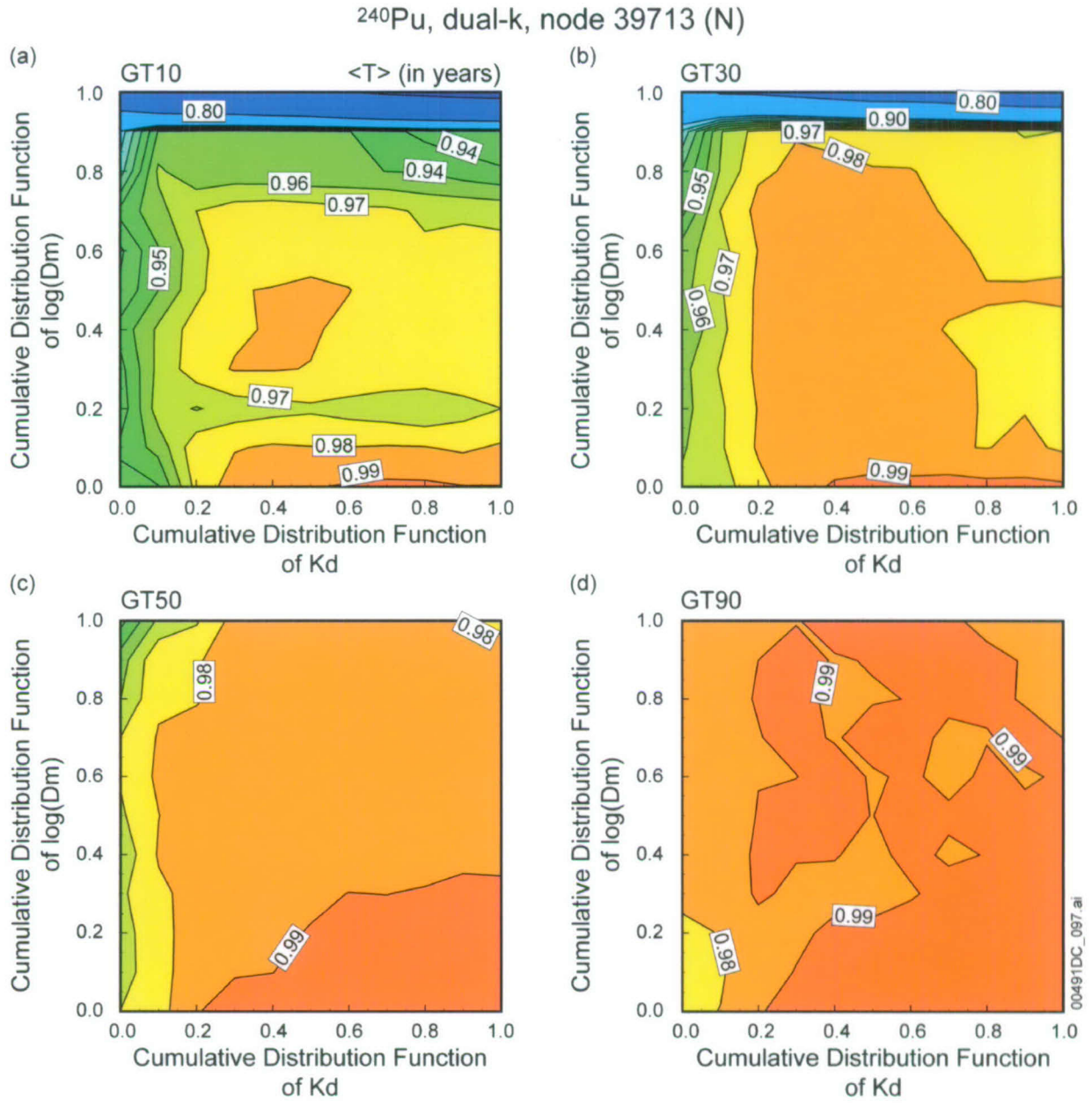

Output DTN: MO0705TRANSTAT.000, file: *MO0705TRANSTAT.000\Sensitivity\strong_sorbing\240Pu_CC0_dualk_north.wmf.*

Figure 6.8.2-19[b]. Normalized ^{240}Pu Concentration (Decay Fraction, Computed from Travel Time Distributions) as a Function of Matrix Diffusion Coefficient and Sorption Coefficient for the Glacial-Transition Climate Conditions, dual-k Model, Northern Release Location

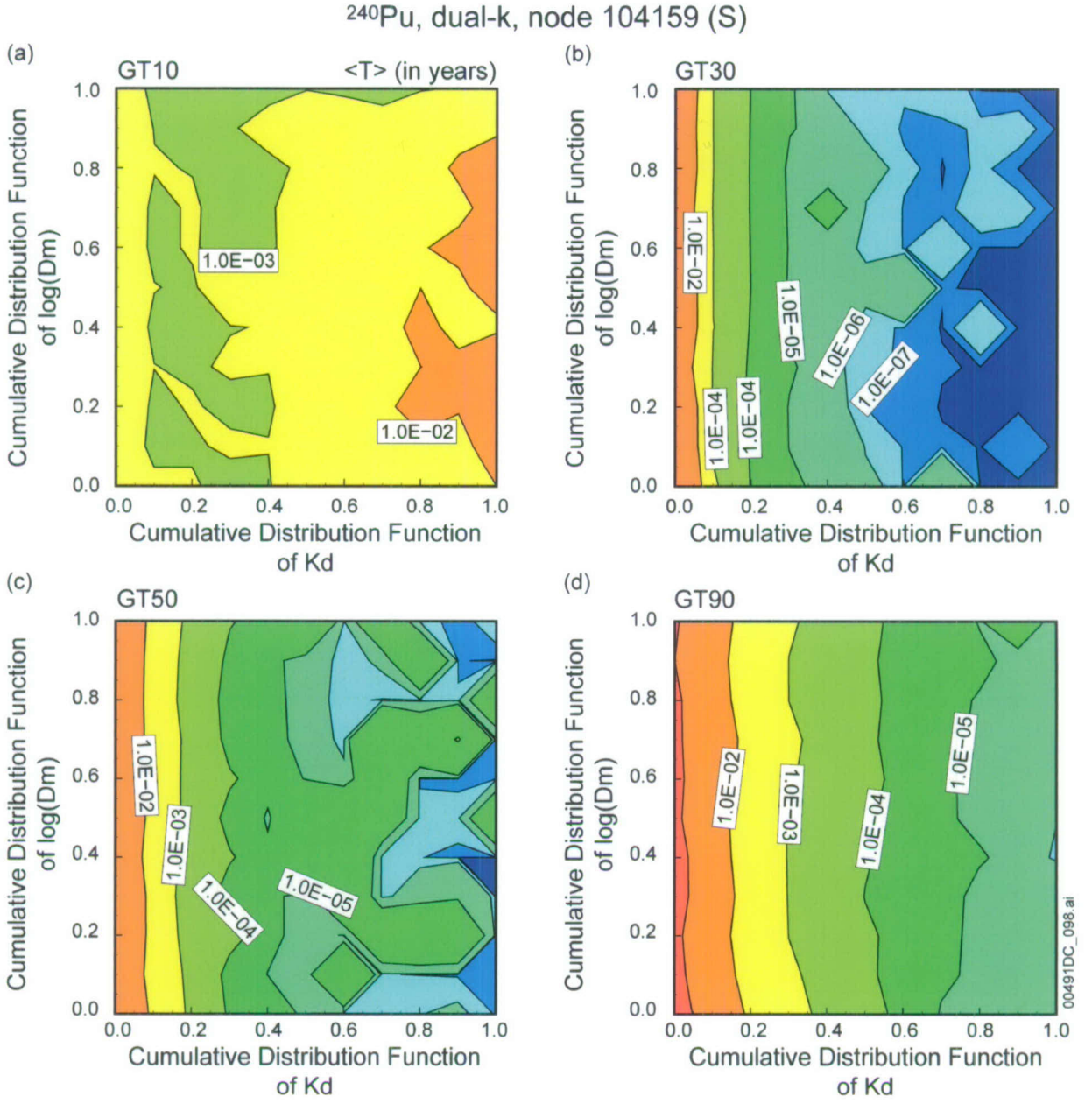

Output DTN: MO0705TRANSTAT.000, file: *MO0705TRANSTAT.000\Sensitivity\strong_sorbing\240Pu_CC0_dualk_south.wmf.*

Figure 6.8.2-20[b]. Normalized ^{240}Pu Concentration (Decay Fraction, Computed from Travel Time Distributions) as a Function of Matrix Diffusion Coefficient and Sorption Coefficient for the Glacial-Transition Climate Conditions, dual-k Model, Southern Release Location

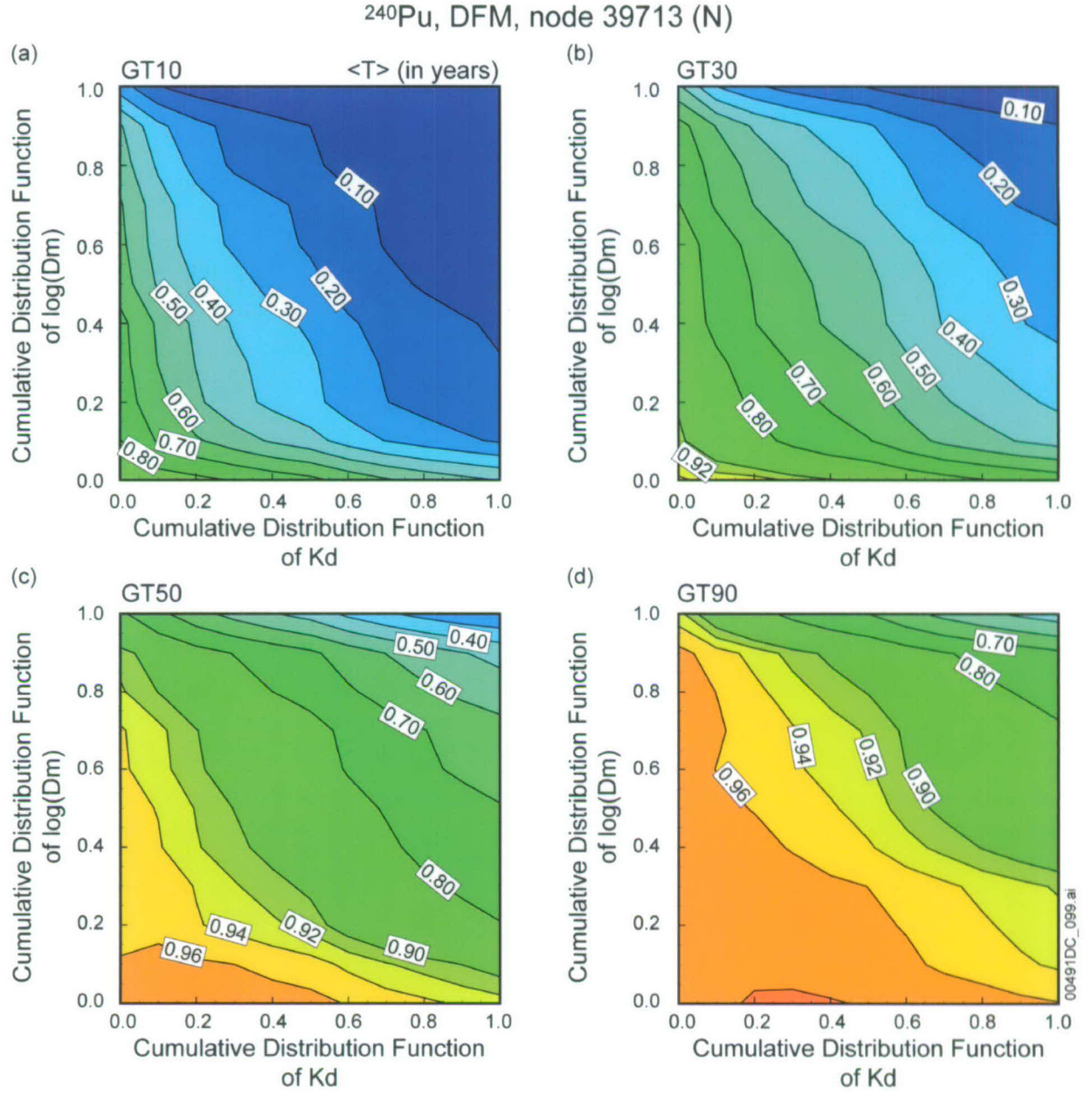

Output DTN: MO0705TRANSTAT.000, file: *MO0705TRANSTAT.000\Sensitivity\strong_sorbing\240Pu_CC0_DFM_north.wmf*.

Figure 6.8.2-21[b]. Normalized ^{240}Pu Concentration (Decay Fraction, Computed from Travel Time Distributions) as a Function of Matrix Diffusion Coefficient and Sorption Coefficient for the Glacial-Transition Climate Conditions, DFM, Northern Release Location

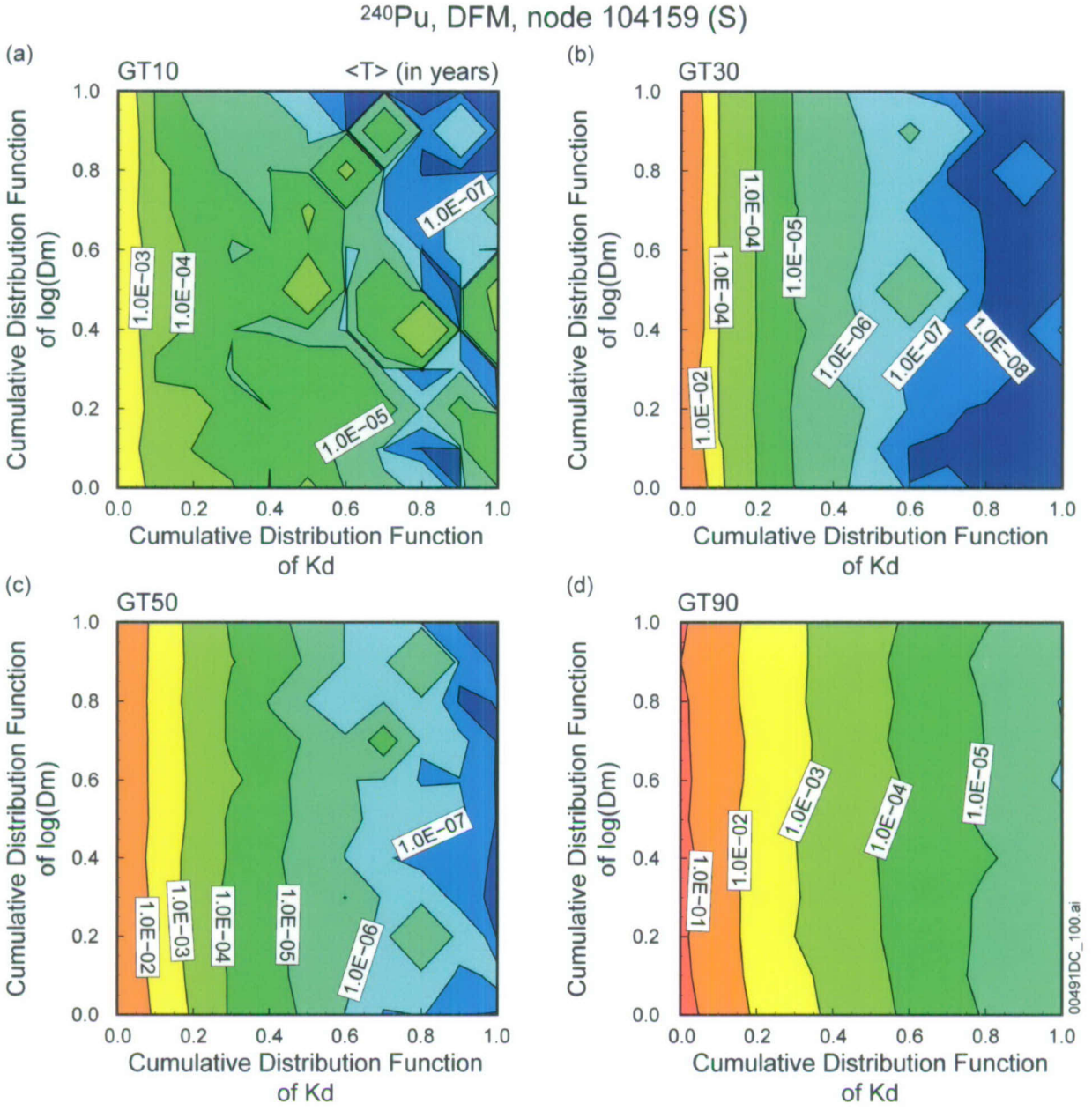

Output DTN: MO0705TRANSTAT.000, file: *MO0705TRANSTAT.000\Sensitivity\strong_sorbing\240Pu_CC0_DFM_south.wmf.*

Figure 6.8.2-22[b]. Normalized ^{240}Pu Concentration (Decay Fraction, Computed from Travel Time Distributions) as a Function of Matrix Diffusion Coefficient and Sorption Coefficient for the Glacial-Transition Climate Conditions, DFM, Southern Release Location

The final set of analyses examines the influence of uncertainty in the value of the colloid retardation factor R_{coll} for the irreversible Ic species of ^{240}Pu. Figure 6.8.2-23[b] shows the results of the mean travel time as a function of R_{coll} for the four glacial-transition flow fields, for the northern (top) and southern (bottom) release locations. Similar plots for the decay fraction C/C_0 are shown in Figure 6.8.2-24[b]. These results are slightly different than the corresponding

figures in Addendum 01 of the parent report, but the conclusions reached in that document are still valid.

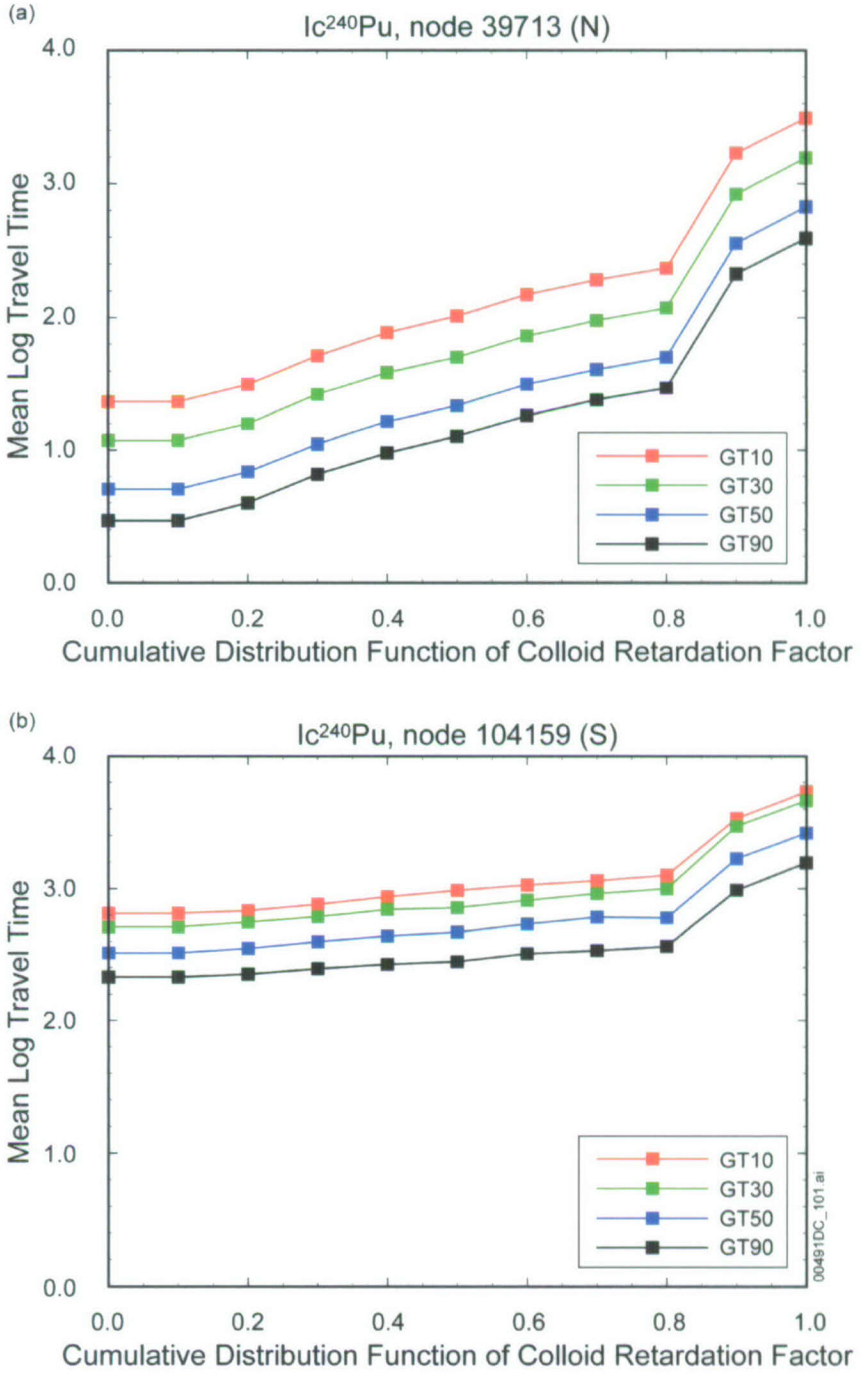

Output DTN: MO0705TRANSTAT.000, file: *MO0705TRANSTAT.000\Sensitivity\strong_sorbing\240IC_time_RC.wmf.*

Figure 6.8.2-23[b]. Mean Travel Time of $Ic^{240}Pu$ as a Function of Colloid Retardation Factor for the Glacial-Transition Climate Condition

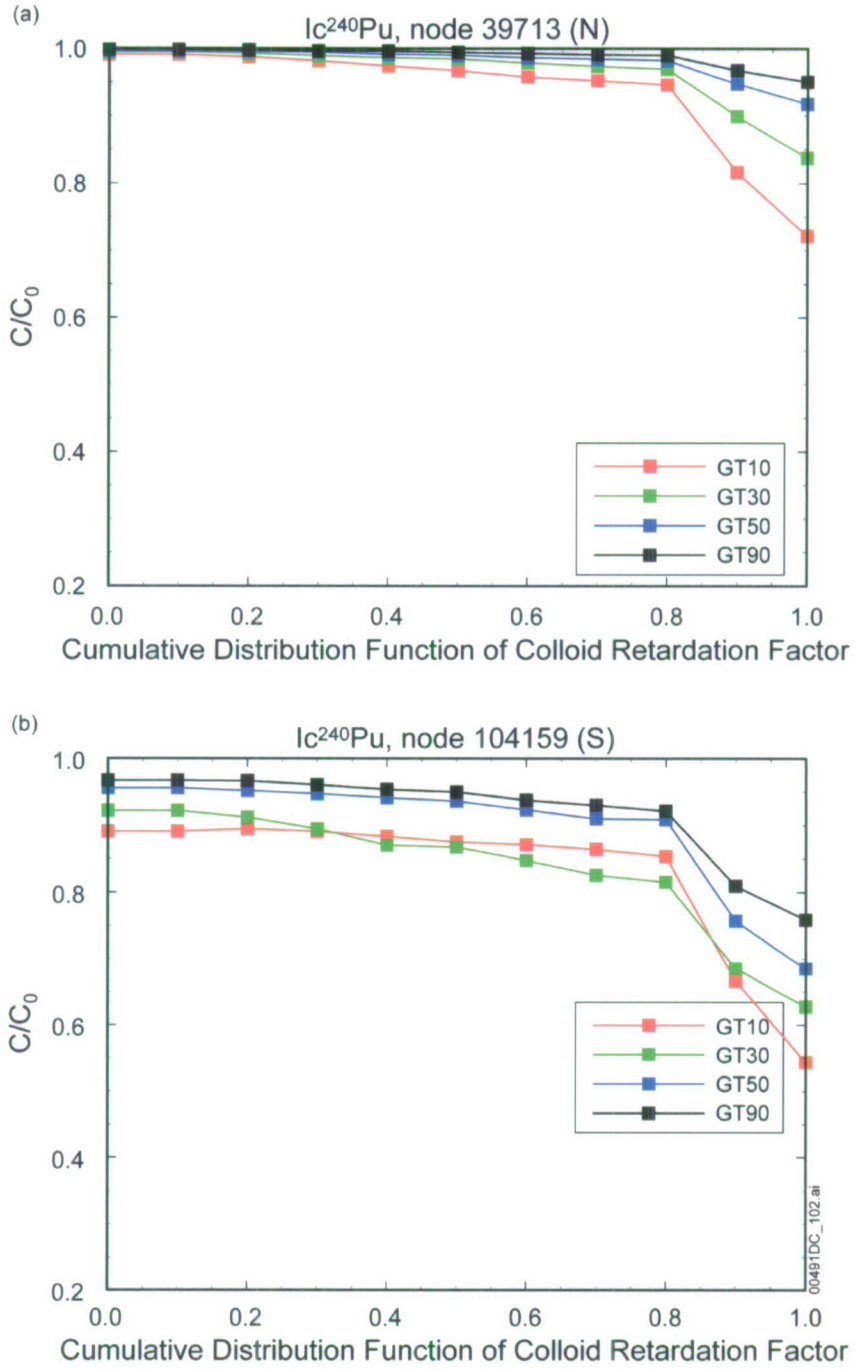

Output DTN: MO0705TRANSTAT.000, file: *MO0705TRANSTAT.000\Sensitivity\strong_sorbing\240IC_CC0_RC.wmf.*

Figure 6.8.2-24[b]. Normalized Concentration of $Ic^{240}Pu$ (Decay Fraction, Computed from Travel Time Distributions) as a Function of Colloid Retardation Factor for the Glacial-Transition Climate Condition

6.9[b] OTHER TSPA IMPLEMENTATION CONSIDERATIONS

No change.

7[b]. VALIDATION

No change.

7.1[b] CONFIDENCE BUILDING DURING MODEL DEVELOPMENT TO ESTABLISH THE SCIENTIFIC BASIS AND ACCURACY FOR INTENDED USE

No change.

7.2[b] POSTDEVELOPMENT MODEL VALIDATION TO SUPPORT THE SCIENTIFIC BASIS OF THE MODEL

No change.

7.2.1[b] Comparisons with Discrete Fracture Model

No change.

7.2.1.1[b] Test of Advective Transport between Continua

No change.

7.2.1.2[b] Comparisons with Diffusion for Fracture-Dominated Flow

No change.

7.2.1.3[b] Comparisons with Diffusion and Sorption for Intermediate Flow Case

No change.

7.2.1.4[b] Summary of Validation Tests for a Discrete Fracture Model

No change.

7.2.2[b] Comparison with the Dual-k and MINC Model Formulations on a Two-Dimensional Cross-Section Model

No change.

7.2.3[b] Comparison with T2R3D Process Model for the Three-Dimensional System

No change.

7.2.3.1[b] Comparisons of FEHM and T2R3D for the Dual-k Conceptual Model

No change.

7.2.3.2[b] Influence of Diffusion Coefficient and f/m Interaction Alternative Conceptual Model

No change.

7.2.3.3[b] Tests of the Active Fracture Model Implementation

No change.

7.3[b] SUMMARY OF VALIDATION ACTIVITIES

No change.

8[b]. CONCLUSIONS

8.1[b] SUMMARY OF MODELING ACTIVITY

No fundamental conclusions made in the parent report are changed as a result of the simulations presented in this addendum. For most of these simulations, the changes in the simulations as a result of addressing CR-11572 and CR-11594 do not require changes in the discussions of Addendum 01. In the few cases in which a change in the discussion is required, the discussion in this addendum supersedes that in Addendum 01. With respect to the issue of how the fault zones are treated, the more representative southern release location (outside of a fault zone) was used in these revised simulations. Nevertheless, for releases into fault zones, the TSPA model treats those releases in a manner that does lead to anomalous behavior for some decay chains (CR-11572). An assessment of the impact of this behavior on the TSPA results is presented in Appendix P, Section P21, of *Total System Performance Assessment Model/Analysis for the License Application* (SNL 2008 [DIRS 183478]). The conclusion of that impact assessment is that "the overall impact of the error on the mean annual dose for all modeling cases is categorized to be small (< 5 percent)."

8.2[b] MODEL OUTPUTS

8.2.1[b] Developed Output

No change.

8.2.2[b] Other Outputs

No change.

8.3[b] HOW THE APPLICABLE ACCEPTANCE CRITERIA ARE ADDRESSED

No change.

INTENTIONALLY LEFT BLANK

9[b]. INPUTS AND REFERENCES

The following is a list of the references cited in this addendum. Column 1 represents the unique six-digit numerical identifier (the Document Input Reference System [DIRS] number), which is placed in the text following the reference callout (e.g., SNL 2008 [DIRS 183478]). The purpose of these numbers is to assist the reader in locating a specific reference in the DIRS database.

9.1[b] DOCUMENTS CITED

177465 BSC (Bechtel SAIC Company) 2006. *Technical Work Plan for: Unsaturated Zone Flow, Drift Seepage and Unsaturated Zone Transport Modeling.* TWP-MGR-HS-000004 REV 04. Las Vegas, Nevada: Bechtel SAIC Company. ACC: DOC.20060824.0001.

183478 SNL (Sandia National Laboratories) 2008. *Total System Performance Assessment Model /Analysis for the License Application.* MDL-WIS-PA-000005 REV 00 AD 01. Las Vegas, Nevada: Sandia National Laboratories.

9.2[b] CODES, STANDARDS, REGULATIONS, AND PROCEDURES

No change.

9.3[b] SOURCE DATA, LISTED BY DATA TRACKING NUMBER

181613 MO0706SPAFEPLA.001. FY 2007 LA FEP List and Screening. Submittal date: 06/20/2007.

9.4[b] OUTPUT DATA, LISTED BY DATA TRACKING NUMBER

MO0704PAFEHMBR.001. FEHM Model and Input. Submittal date: 01/10/2008.

MO0705TRANSTAT.000. UZ Radionuclide Transport Travel Time Statistics and Sensitivity Analysis. Submittal date: 01/18/2008.

9.5[b] SOFTWARE CODES

No change.

INTENTIONALLY LEFT BLANK

APPENDIX A[b]
MATRIX DIFFUSION COEFFICIENTS

No Change.

APPENDIX B[b]
DERIVATION OF WATER TABLE COLLECTING BINS

No change.

APPENDIX C[b]
DERIVATION OF FRACTURE–MATRIX INTERACTION SUBMODEL AND GENERATION OF TRANSFER FUNCTIONS

No Change.

APPENDIX D[b]
SUPPLEMENTARY UNSATURATED ZONE TRANSPORT SIMULATION RESULTS

D.1[b] TRAVEL TIME PLOTS FOR OTHER FLOW FIELDS

No change.

D.2[b] ADDITIONAL BREAKTHROUGH CURVES

This section presents the same decay chain simulation cases as in Addendum 01, except that the location of the southern release point has been changed to avoid inserting particles into a node designated as a fault node.

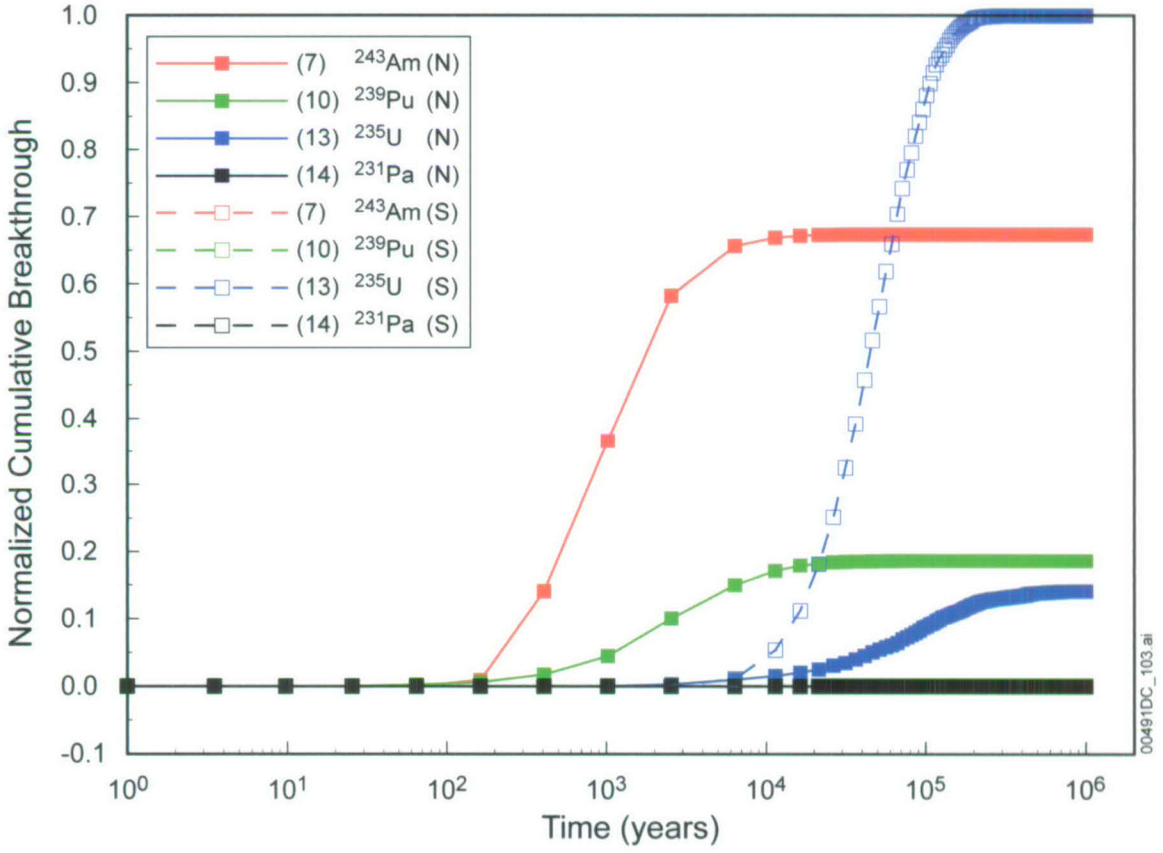

Output DTN: MO0705TRANSTAT.000, file: *MO0705TRANSTAT.000\Breakthroughs\243am\243Am_239Pu_235U_231Pa.wmf*.

Figure D.2-1[b]. Normalized Cumulative Breakthrough Curves of Decay Chain $^{243}Am \rightarrow {}^{239}Pu \rightarrow {}^{235}U \rightarrow {}^{231}Pa$ for the Glacial-Transition, 10th Percentile Infiltration Condition, Representative Parameter Values, Northern and Southern Release Nodes

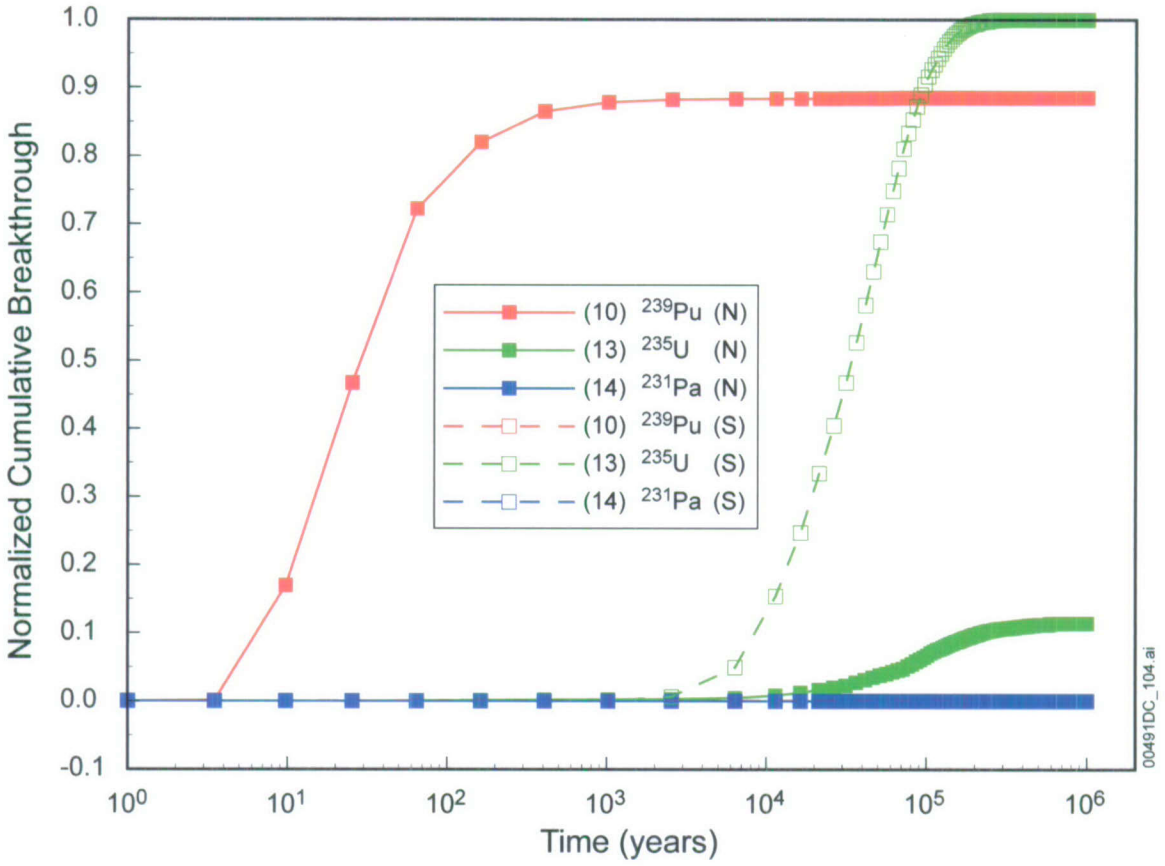

Output DTN: MO0705TRANSTAT.000, file: *MO0705TRANSTAT.000\Breakthroughs\239pu\239Pu_235U_231Pa.wmf.*

Figure D.2-2[b]. Normalized Cumulative Breakthrough Curves of Decay Chain ^{239}Pu→ ^{235}U → ^{231}Pa for the Glacial-Transition, 10th Percentile Infiltration Condition, Representative Parameter Values, Northern and Southern Release Nodes

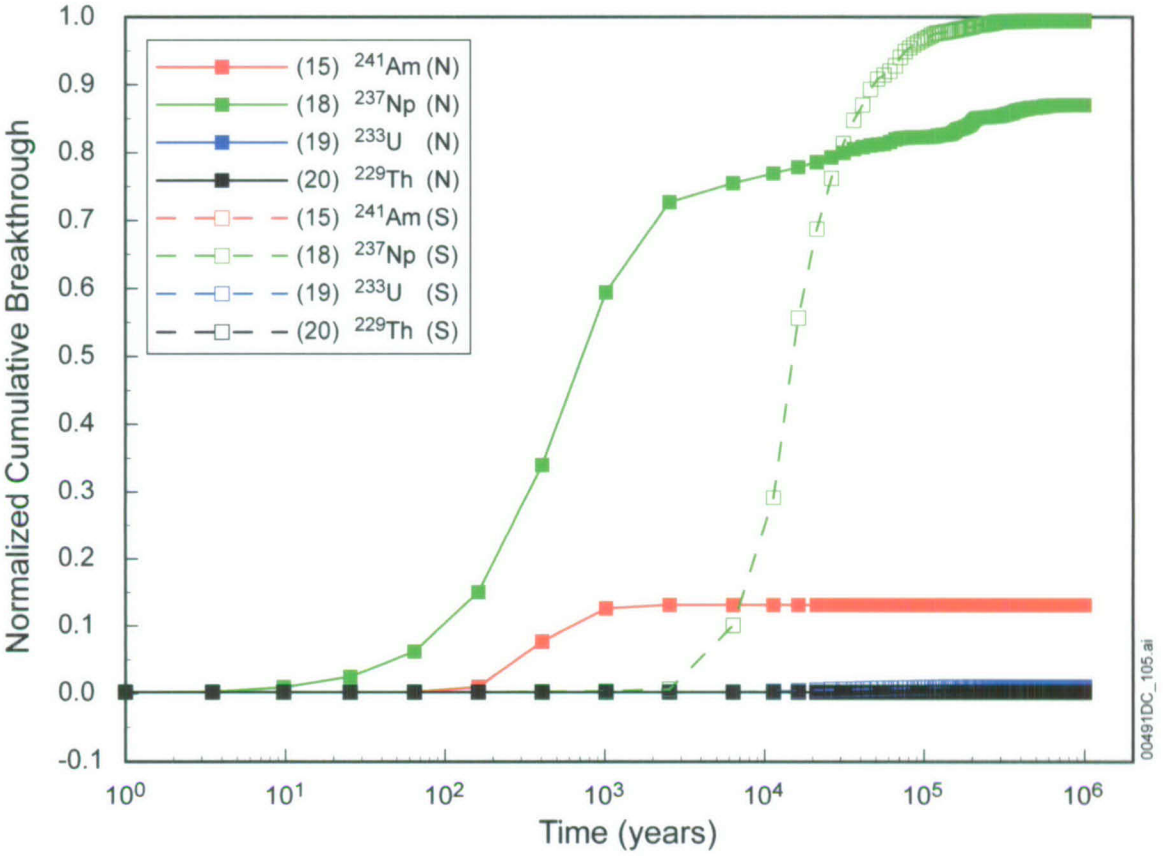

Output DTN: MO0705TRANSTAT.000, file: *MO0705TRANSTAT.000\Breakthroughs\241am\241Am_237Np_233U_229Th.wmf.*

Figure D.2-3[b]. Normalized Cumulative Breakthrough Curves of Decay Chain $^{241}Am \rightarrow {}^{237}Np \rightarrow {}^{233}U \rightarrow {}^{229}Th$ for the Glacial-Transition, 10th Percentile Infiltration Condition, Representative Parameter Values, Northern and Southern Release Nodes

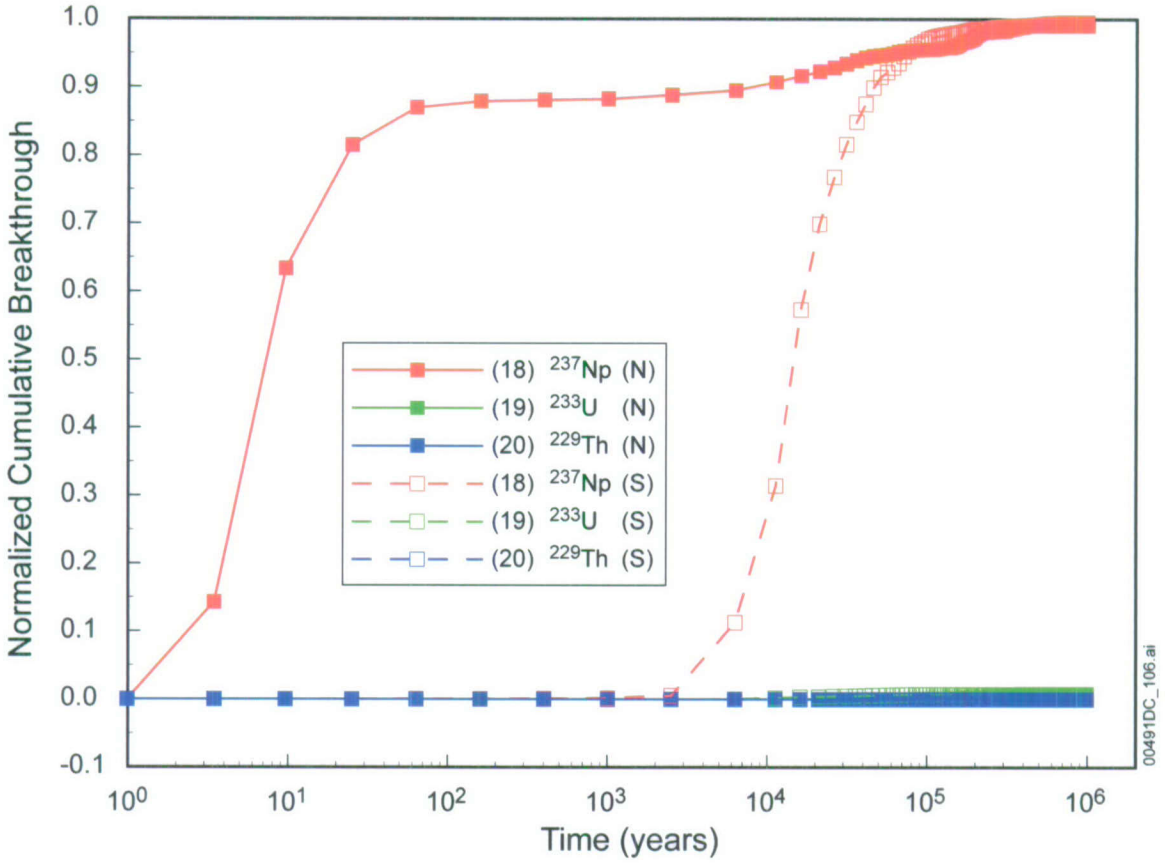

Output DTN: MO0705TRANSTAT.000, file: *MO0705TRANSTAT.000\Breakthroughs\237np\237Np_233U_229Th.wmf.*

Figure D.2-4[b]. Normalized Cumulative Breakthrough Curves of Decay Chain ^{237}Np→ ^{233}U → ^{229}Th for the Glacial-Transition, 10th Percentile Infiltration Condition, Representative Parameter Values, Northern and Southern Release Nodes

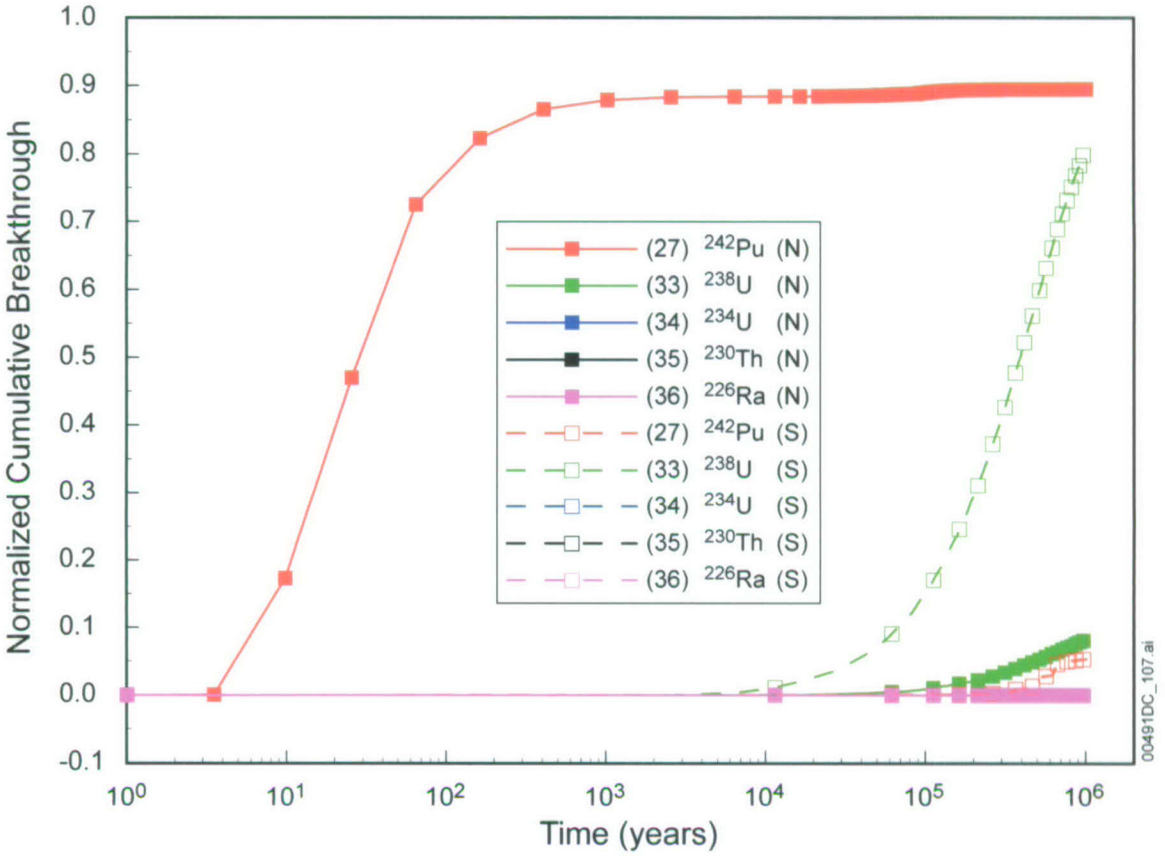

Output DTN: MO0705TRANSTAT.000, file: *MO0705TRANSTAT.000\Breakthroughs\242pu\242Pu_238U_234U_230Th_226Ra.wmf.*

Figure D.2-5[b]. Normalized Cumulative Breakthrough Curves of Decay Chain ^{242}Pu→ ^{238}U → ^{234}U → ^{230}Th→ ^{226}Ra for the Glacial-Transition, 10th Percentile Infiltration Condition, Representative Parameter Values, Northern and Southern Release Nodes

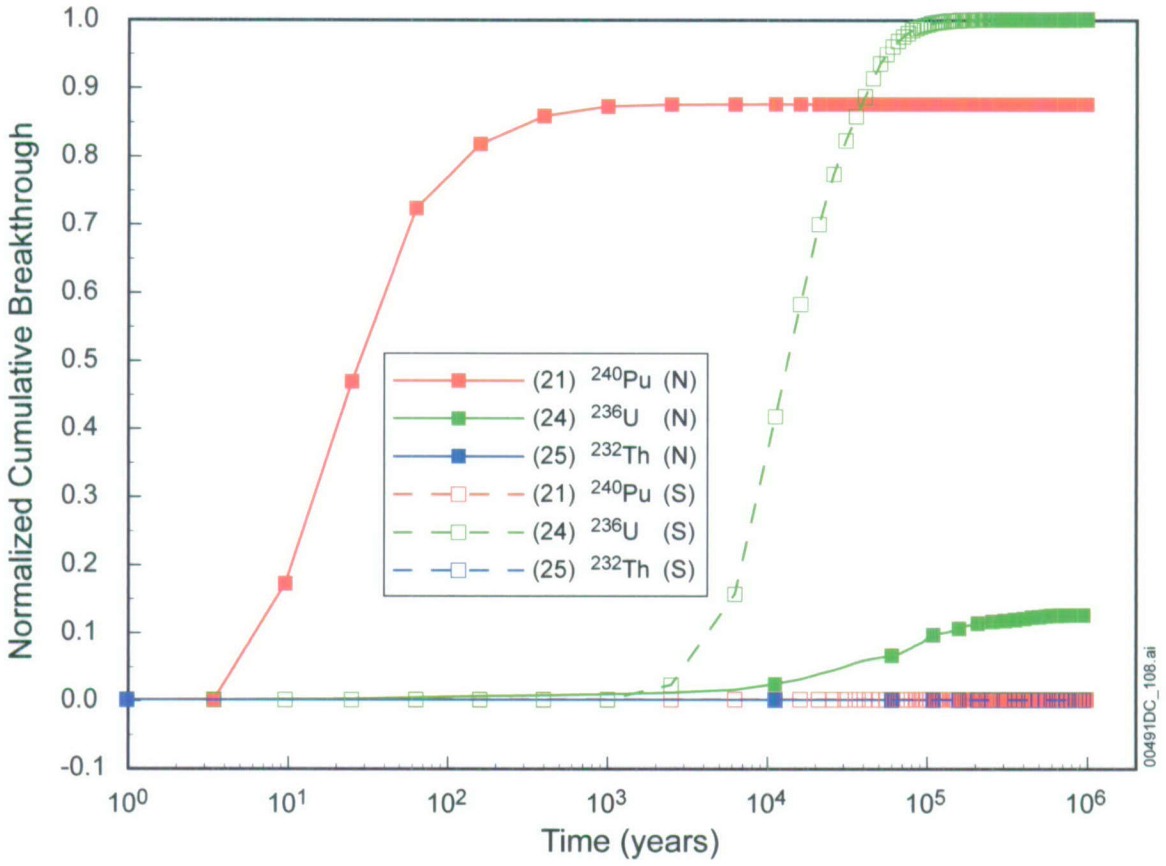

Output DTN: MO0705TRANSTAT.000, file: *MO0705TRANSTAT.000\Breakthroughs\240pu\240Pu_236U_232Th.wmf.*

Figure D.2-6[b]. Normalized Cumulative Breakthrough Curves of Decay Chain ^{240}Pu → ^{236}U→ ^{232}Th for the Glacial-Transition, 10th Percentile Infiltration Condition, Representative Parameter Values, Northern and Southern Release Nodes

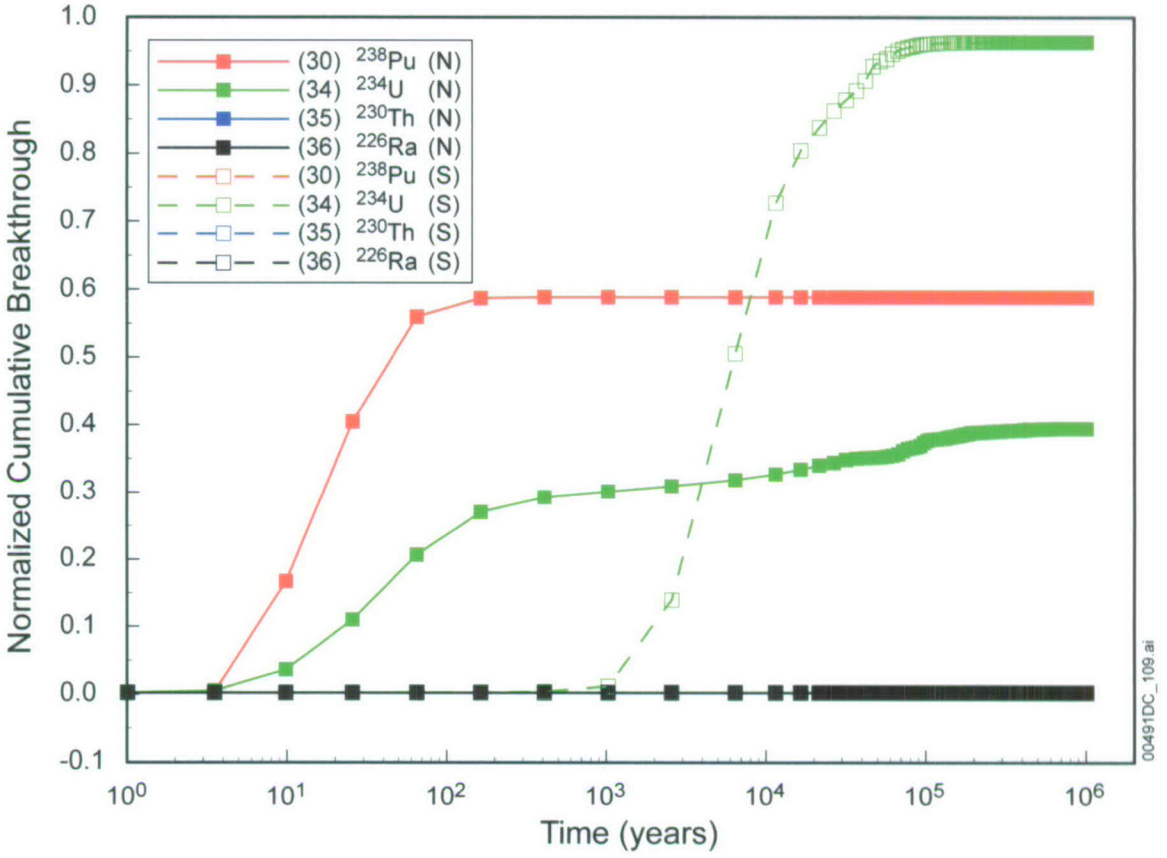

Output DTN: MO0705TRANSTAT.000, file: *MO0705TRANSTAT.000\Breakthroughs\238pu\238Pu_234U_230Th_226Ra.wmf.*

Figure D.2-7[b]. Normalized Cumulative Breakthrough Curves of Decay Chain $^{238}Pu \rightarrow {}^{234}U \rightarrow {}^{230}Th \rightarrow {}^{226}Ra$ for the Glacial-Transition, 10th Percentile Infiltration Condition, Representative Parameter Values, Northern and Southern Release Nodes

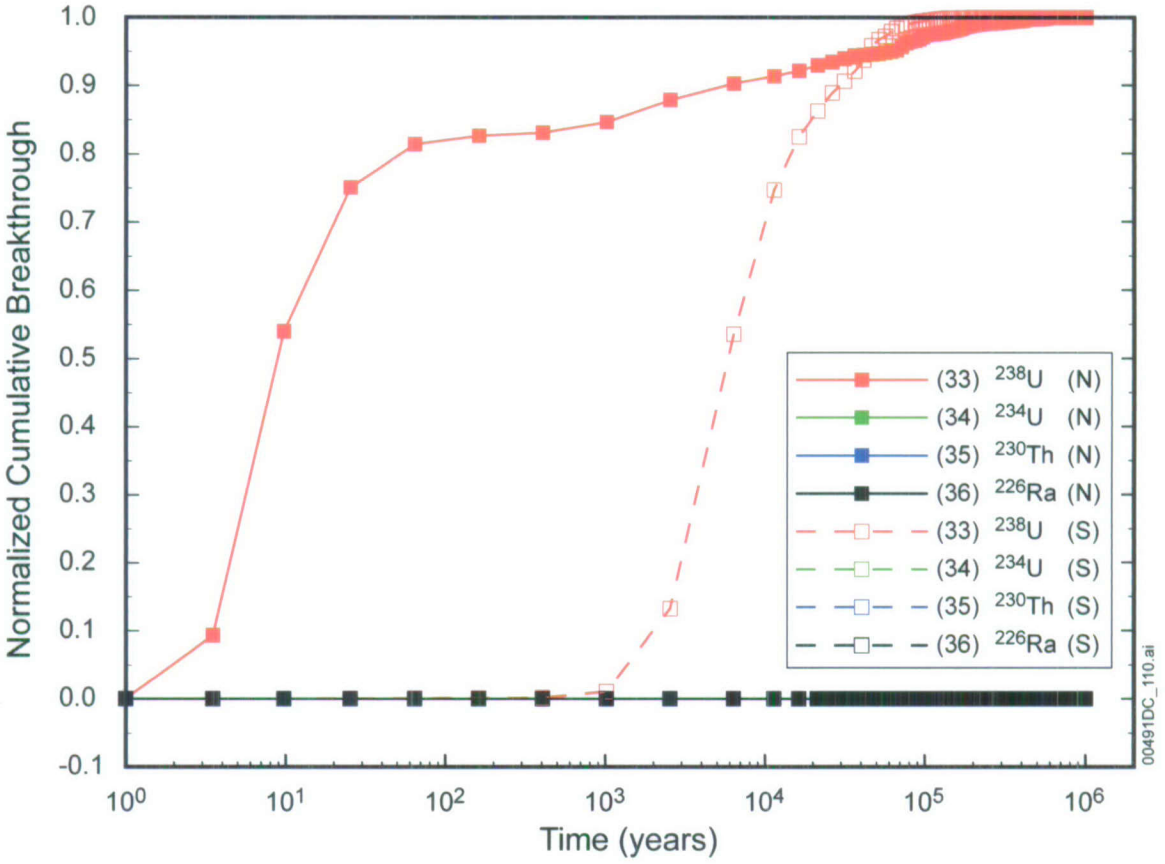

Output DTN: MO0705TRANSTAT.000, file: *MO0705TRANSTAT.000\Breakthroughs\238u\238U_234U_230Th_226Ra.wmf*.

Figure D.2-8[b]. Normalized Cumulative Breakthrough Curves of Decay Chain ^{238}U → ^{234}U→ ^{230}Th →^{226}Ra for the Glacial-Transition, 10th Percentile Infiltration Condition, Representative Parameter Values, Northern and Southern Release Nodes

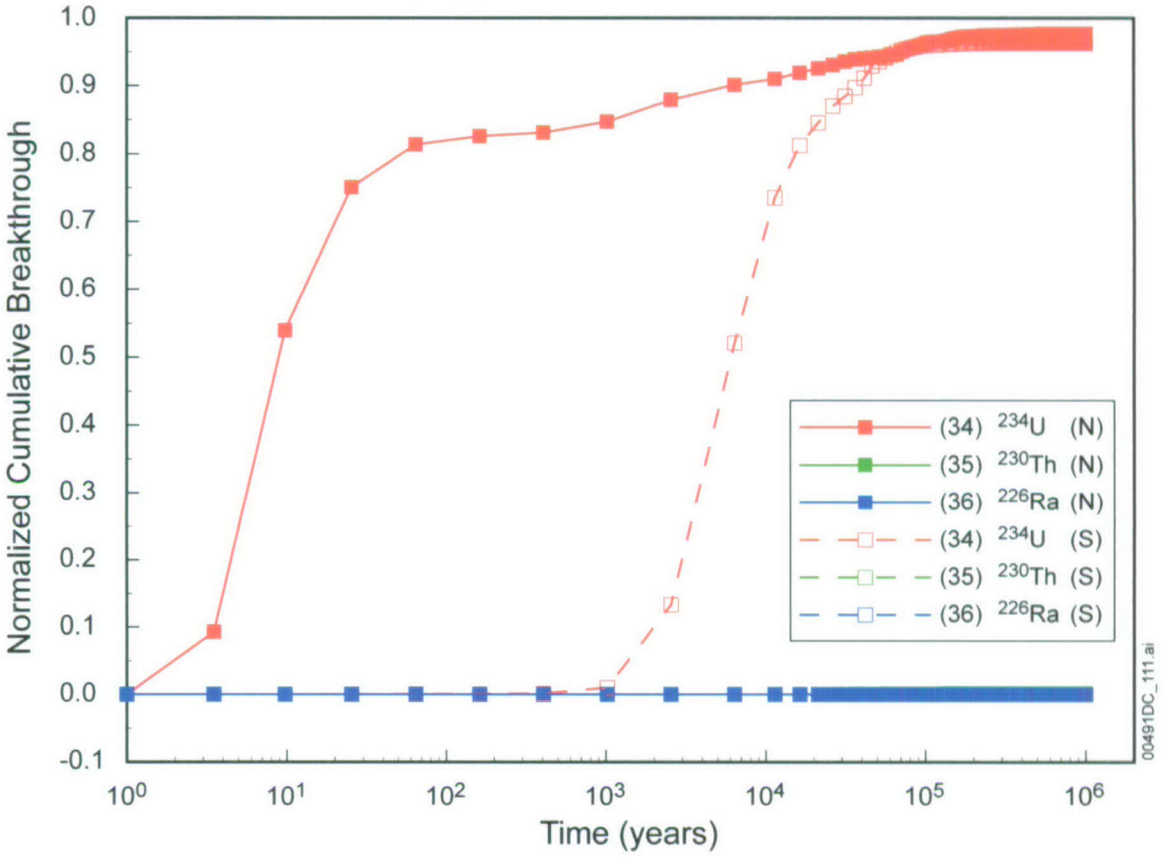

Output DTN: MO0705TRANSTAT.000, file: *MO0705TRANSTAT.000\Breakthroughs\234u\234U_230Th_226Ra.wmf.*

Figure D.2-9[b]. Normalized Cumulative Breakthrough Curves of Decay Chain $^{234}U \rightarrow {}^{230}Th \rightarrow {}^{226}Ra$ for the Glacial-Transition, 10th Percentile Infiltration Condition, Representative Parameter Values, Northern and Southern Release Nodes

INTENTIONALLY LEFT BLANK